HYDROGEN EXCHANGE PATHWAYS BETWEEN ARENES AND DIHYDROARENES: AN EXPERIMENTAL AND MECHANISTIC MODELING STUDY OF HIGH TEMPERATURE HYDROGEN TRANSFER PATHWAYS.

Tom Autrey, Emily Alborn-Cleveland, Don M. Camaioni and James A Franz.
Pacific Northwest Laboratory Richland WA 99352

Introduction

One of the major areas of interest in thermal hydroliquefaction involves the mechanisms of hydrogen shuttling by aromatic/hydroaromatic donor solvents to coal structure, engendering the scission of thermally-stable alkylaromatic linkages. Derbyshire et al.[1] and McMillen and Malhotra[2] were among the first to recognize that hydrogen donor solvents can play an active role in the scission of thermally stable C-C bonds in coal structures. At least two "conventional" hydrogen-transfer pathways, hydrogen atoms (HA) and reverse radical disproportionation (RRD), and two "unconventional" hydrogen transfer pathways, radical hydrogen-transfer (RHT)[3] and addition-transfer-elimination,[4] could play a role in the shuttling of hydrogen from donor solvent to the ipso positions of substituted aromatic linkages in coal structures. It is unreasonable to assume that any one of these pathways is responsible for all solvent-engendered bond scission. Depending on the reaction conditions, one pathway may be more dominate than the others, or several of them could contribute simultaneously. A quantitative understanding of competing hydrogen-transfer pathways between aromatic structures can yield valuable information regarding the efficient cleavage of bonds in coal structures during hydroliquefaction. It is the goal of this work to quantify the importance of the conventional hydrogen-transfer pathways and make qualitative predictions regarding the unconventional pathways.

(1)	ArH · -> Ar + H ·	
	H · + ArR -> ArHR ·	HA
(2)	ArH_2 + ArR -> ArH · + ArHR ·	RRD
(3)	ArH · + ArR -> ArH-ArR ·	Addition
	ArH-ArR · -> · Ar-ArRH	Transfer
	Ar-ArRH -> Ar + ArHR ·	Elimination
(4)	ArH. + ArR -> Ar + ArHR.	RHT

We have undertaken mechanistic kinetic modeling (MKM) studies and experimental thermolysis studies of model compounds to quantify the importance of individual hydrogen-transfer pathways involved in the scission of alkyl-arene C-C bonds in diarylmethanes as a function of donor solvent composition.[5] In this paper, we report the role of hydrogen-transfer pathways in the aromatic/hydroaromatic solvent mixtures naphthalene/dihydronaphthalene ($Nap/NapH_2$), phenanthrene/dihydrophenanthrene ($Phen/PhenH_2$), anthracene/diydroanthracene (An/AnH_2), and cyclohexadiene/benzene (Ph/PhH_2) for promoting bond scission in a family of diarylmethanes (Ar-R)-diphenylmethane ($PhCH_2$-Ph), 1-benzylnaphthalene ($PhCH_2$-Nap), 9-benzylphenanthrene ($PhCH_2$-Phen) and 9-benzylanthracene ($PhCH_2$-An).

The results of this work will 1) show the significance of the role of free hydrogen atoms and 2) question the necessity of invoking the radical hydrogen-transfer pathway in promoting c-c bond scission in alkylarenes.

Results and Discussion

One of the advantages of MKM is the ability to quantify individual reaction pathways that compete from the same intermediate or yield the same products. It is a challenging experimental task to separate the amount of alkylarene bond scission by competing RRD and HA pathways This difficulty has led to ambiguous results regarding the role of solvent-induced bond scission. MKM permits "computer labeling" studies to quantify each competing pathway.

The activation barriers for the two conventional hydrogen-transfer pathways, HA and RRD, can be estimated to within a few kcal/mol because of the "product" like or "reactant" like nature of the transition state. On the other hand, there is no a priori means to estimate the intrinsic activation barriers for the two unconventional hydrogen-transfer pathways, ATE and RHT. Theoretical approaches and rigorously-designed experiments must be undertaken to quantitatively evaluate the feasibility of competing unconventional hydrogen transfer pathways.[6]

The Model. A mechanistic model composed of the free radical hydrogen-transfer pathways, initiation, termination, hydrogen scission, abstraction, addition, and reverse radical disproportionation, was developed for each mixed-solvent system and diarylmethane substrate (Scheme I). Arrhenius rate parameters were derived from the literature values of the thermochemical estimates of the heat of formation (ΔHf) of the products, reactants, and intermediate radicals.[7] We utilized the regimen of Malhotra and McMillen[3a] and Manka and Stein[8] to calculate the temperature-dependant rate for each individual reaction step. For concise introduction, we separate our model in three sections, 1) initiation and termination events, 2) efficient utilization of solvent and bond scission by HA and RRD pathways, and 3) inefficient utilization of solvent.

The initiation pathway utilized in this modeling study is the RRD between the dihydroarene and arene solvent molecules. Only radical disproportionation was considered as a termination event in our model since solvent derived radical coupling products have been shown to be unstable at temperatures above 350°C.[9]

Efficient solvent utilization pathways are defined as pathways leading to the scission of C-C bonds by RRD and H atom pathways. The rate determining step of the two-step HA pathway is scission from the hydroaryl radical. Addition of the hydrogen atom to an arene ring is not expected to be very selective relative to hydrogen transfer by the RRD pathway. Hydrogen atom addition to the solvent will also occur in competition with hydrogen transfer to diarylmethanes. Thus hydrogen from the solvent can be consumed without the scission of C-C bonds, and in some solvent mixtures is predicted to dominate the hydrogen-transfer chemistry.

To compare the rate of product formation from the H atom pathway to the RRD pathway, we utilized a computer "label" of the products arising from each competing pathway. In this way, competitive pathways involving the same intermediates can be quantitatively predicted. For example, we "label" the alkyl-arene bond-scission precursor, ipso addition of a hydrogen atom by to the alkyl position of Ar-x, arising from the RRD pathway as ArXH (equation 14), whereas ipso addition of a hydrogen atom by to the alkyl position of Ar-x arising from the HA pathway, gives ArxH (equation 4). Both "ipso adducts", ArXH and ArxH, are "chemically" the same intermediate; they cleave at the same rate to yield the scission product, labelled RRD(H) (equation 18) and HA(H) (equation 17) respectively. In this manner, we can account for the yield of scission by each competing pathway even when the same intermediate is involved. To calculate the relative rates of solvent-induced scission of Ar-x by each pathway, we compared the predicted yield of the scission product as a function of thermolysis time. Thus, the percent C-C bond scission by H atom pathway = [HAH] /{[HAH] + [RRDH]}.

Scheme I. Example of kinetic hydrogen-transfer pathways in An/AnH_2

intiation/termination									
1	AnH_2	+	An	->	AnH	+	AnH,		
2,	AnH	+	AnH	->	AnH_2	+	An,		
H atom pathways									
4,	Anx	+	H	->	AnxH				ipso
5,	Anx	+	H	->	AnHx				nonipso
6,	AnHx			->	Anx	+	H		solvent
7,	AnH			->	An	+	H		
8,	An	+	H	->	AnH				
9,	AnH_2	+	H	->	AnH	+	H_2		
10,	AnH_2	+	An	->	HAn	+	AnH		1-4,5-8 position
11,	HAn	+	AnH_2	->	H_2An	+	AnH		
12,	H_2An	+	AnH_2	->	H_3An	+	AnH		
13,	H_3An	+	AnH_2	->	H_4An	+	AnH		
RRD									
14,	AnH_2	+	Anx	->	AnH	+	AnXH		
15,	AnH_2	+	Anx	->	AnH	+	AnHx		abstraction
16,	AnH_2	+	AnHx	->	AnH_2x	+	AnH		
scission									
17,	AnxH			->	AnH	+	HA(H)		HA
18,	AnXH			->	AnH	+	RRD(H)		RRD
19,	AnH_2x			->	AnH	+	RED'C(H)		nonipso

Examination of Table I clearly shows the importance of free hydrogen atoms in the scission of diarylmethane coal linkages. The only clear case of C-C bond scission by the RRD pathway is in An/AnH_2 solvent mixtures. This can be explained by the stability of the 9-hydroaryl radical. Table II lists the predicted relative total rate of diarylmethane bond scission (the sum total of both RRD and H atom contributions) in the series of solvent mixtures for each substrate, giving

an indication of the "best" solvent for a given diarylmethane structure. A comparison of bond-induced scission of Nap-CH_2Ph in An/AnH_2 verses Phen/$PhenH_2$ illustrates the selectivity differences between the HA and RRD pathways. The model predicts nearly equal rates of solvent-induced scission; however, the selectivity of bond scission is expected to be greater in An/AnH_2 because of the contribution bond scission by the more selective RRD pathway. McMillen and Malhotra[3a] have observed that although there is very little difference in the rate of bond scission of 1,2-dinaphthylmethane in Phen/$PhenH_2$ and An/AnH_2 solvents, there is a substantial difference in the observed selectivity. They suggest that the difference in selectivity is due to the operation of the RHT pathway in An/AnH_2 solvents; however, our current analysis suggests that the increase in selectivity is due to the operation of the RRD pathway in An/AnH_2 solvents.

EXPERIMENTAL STUDIES.

To test both the rate and selectivity predictions of our mechanistic model of hydrogen transfer pathways from dihydroarenes to diarylmethanes, we have utilized experimental thermolysis studies of 1,2-dinaphthylmethane (DNM) in AnH_6 and An/AnH_2 solvent mixtures. Our model suggests that cyclic olefins, e.g. AnH_6, will be faster and less selective than An/AnH_2 solvent mixtures with less selectivity in the solvent-induced scission of DNM.

Cyclic Olefins. 1,4,5,8,9,10-Hexahydroanthracene **AnH_6**.

The predicted rate of bond scission in Ph/PhH_2 solvent mixtures as shown in Table II suggests that cyclic olefins are a special class of dihydroarenes donor solvents. Bedell and Curtis[10] have demonstrated that cyclic olefins provide enhanced liquefaction yields relative to their dihydroarene isomers. However, we note a chain-decomposition pathway of the cyclic olefins can limit the efficiency of C-C bond scission by this family of donors as shown in Scheme II.

Scheme II Chain Decomposition Pathways of Cyclic Olefin Donor Solvents.

Abstraction						
AnH_6	+	H	->	AnH_5	+	H_2
AnH_5			->	AnH_4	+	H
AnH_4	+	H	->	AnH_3	+	H_2
AnH_3			->	AnH_2	+	H
AnH_2	+	H	->	AnH	+	H_2
Addition						
AnH_6	+	H	->	H_7An		
H_7An	+	AnH_6	->	H_8An	+	AnH_5
H_8An	+	H	->	H_9An		
H_9An	+	AnH_6	->	H_{10}An	+	AnH_5

Thermolysis of neat AnH_6 at 380°C results in a variety of hydroanthracene isomers with total consumption of the cyclic olefin in less than 20 minutes. The conversion of 1,2'-dinaphthylmethane (DNM) in hexahydroanthracene at 380°C is dependant on the starting concentration of DNM; at lower DNM concentrations, hydrogen atoms add competitively to the solvent AnH_6. Thermolysis of DNM in AnH_6 results in a 20-30% consumption of DNM in the first 20 minutes followed by a much slower conversion.[11] The observed selectivity of bond scission as measured by the yield of 2-Methylnaphthalene/1-Methylnaphthalene (1.6) is what is expected for a free-hydrogen-atom scission pathway.[3a]

Dihydroarene. Anthracene/9,10-Dihydroanthracene **An/AnH_2**

Thermolysis of mixtures of An/AnH_2 at temperatures above 380°C result in a dynamic exchange of hydrogen atoms between the anthracene structures with very little hydrogen formation of hydrogen gas. The process results in a shift of hydrogen from 9,10-dihydroanthracene (AnH_2) to anthracene to yield 1,2,3,4-tetrahydroanthracene (AnH_4). Formation of the AnH_4 has been suggested to occur by a series of RHT steps from AnH∘ to the outer ring of anthracene.[12] However, we have found that the time-dependant formation of AnH_4 can be fit to a series of RRD steps without the need to invoke the RHT pathway.

Thermolysis of DNM in mixtures of An/AnH_2 yields <1% consumption in the first 20 minutes (as compared to >30% in AnH_6). The selectivity of bond scission as measured by 2-Methylnaphthalene/1-Methylnaphthalene is higher, between 4-6. As predicted by our MKM results, the selectivity does not change substantially as the ratio of An/AnH_2 is increased as has been previously suggested[3a]. However, the selectivity is predicted to be very sensitive to the addition of a diluent, such as biphenyl (BP). Adding BP lowers the rate of bond scission by the RRD pathway, but has little effect on the rate of scission by the HA pathway. The net result of the dilution studies is thus a predicted decrease in rate as well as selectivity. The results of

the thermolysis study and the predictions of our mechanistic model are shown in Figure I. A set of control experiments was performed to investigate the occurrence of secondary thermolysis events. When a small amount of tetralin, 10% by weight, was added to the starting reaction mixtures of DNM in An/AnH_2, we found that the tetralin was consumed under the reaction conditions at high An/AnH_2 solvent ratios. This is most likely due to the low concentration of AnH_2 donor available for capping the radicals formed by the solvent induced scission. Formation of tetralin products can arise from adding of hydrogen to nonipso positions of DNM.[3c] If these reduced products are consumed in secondary events under the reaction conditions, e.g. low donor concentration and long reaction times, one could be led into believing that a change in hydrogen-transfer pathways was leading to a more efficient utilization of hydrogen from the donor solvent when in fact, the same hydrogen-transfer process could be in operation but the hydrogen is recycled.

Conclusions. MKM and thermochemical kinetic estimates predict that hydrogen atoms dominate the chemistry of strong bond scission. Cyclic olefins are predicted by MKM and have been found experimentally to be extremely rapid with little selectivity and only limited by competition with self reactions consumpting the solvent.

All model compound studies that we have examined[13] can be explained by conventional hydrogen transfer pathways when consideration is given for the uncertainty in estimating the arrhenius-rate parameters. We are gratified that the results from our simple mechanistic model, utilizing only free hydrogen atoms and reverse radical disproportionation pathways, reproduced our own experimental observations regarding relative rates and selectivities of diarylmethane alkyl-arene bond scission in hydroarene donor solvents as well as other published observations.

While the uncertainty in the thermochemical data of free radical pathways does not rule out the possibility of some contributing RHT type pathway, it does require faith to propose a novel hydrogen pathway such as RHT based solely on MKM results. Until either rigorous theoretical approaches or direct, unambiguous experimental evidence is obtained, we suggest caution in invoking the RHT pathway between arenes. On a note of RHT optimism, we suggest that further studies of the RHT pathway should be investigated when polarized transition states are possible.[14]

Experimental. All solvents and reagents were purchased from Aldrich. Anthracene was sublimed, and dihydroanthracene was recrystallized three times from 95% ethanol. Thermolysis experiments of mixtures containing anthracene and dihydroanthracene were prepared in sealed pyrex tubes. Stock mixtures 1/1, 1/5, 5/1 wt/wt were prepared in bulk by grinding the pure compounds together with a roller-ball mixer. Mechanistic Modeling. Acuchem[15] utilizes a variable step integrator to solve stiff integration problems. Temperature dependent molar density of anthracene was obtain from the API reference guide available through Chemical Abstracts online service in file DIPPR.

ACKNOWLEDGEMENT
This work was supported by the U.S. Department of Energy, Office of Basic Energy Research. The Pacific Northwest Laboratory is operated for the U.S. Department of Energy by Battelle Memorial Institute under Contract DE–AC06–76RLO 1830.

REFERENCES AND NOTES

1. Derbyshire, F. J., Varghese, P., and Whitehurst, D. D. *Fuel*, **1982**, *61*, 859.
2. McMillen, D. F., and Malhotra, R. *Fuel Preprints*, **1984**, *30*(4), 297.
3. (a) Malhotra, R., and McMillen, *Energy Fuels* **1990**, *4*, 184. (b) Malhotra, R. and McMillen, D. F., *Energy Fuels* **1993**, *7*, 227. (c) McMillen, D. F., and Malhotra, R *Energy Fuels* **1991**, *5*, 179.
4. Stein, S. E., *Acc. Chem. Res.* 1991, *24*, 350.
5. Diarylmethanes $Ar\text{-}CH_2Ar$, are one of the most thermally stable carbon-carbon bonds in coal related structures. Homolytic bond scission of diarlmethane is BDE >90 kcal/mol.
6. Franz, J. A., Ferris, K. F., Camaioni, D. M., and Autrey, S. T., submitted to *Energy Fuels*
7. a) Stein, S. E., and Brown, R. L, *J. Am. Chem. Soc.* **1991**, *113*, 787. (b) Freund, H., Matturro, W. N., Olmstead, W. N., Reynolds, R. P. Upton, T. H. *Energy Fuels* **1991**, *5*, 840. (c) Tsang, W. *J., Phys. Chem.*, **1986**, *90*, 1152. (d) Nicovich, J. M., and Ravishankara, A. R. *J. Phys. Chem.*, **1984**, *88*, 2534. (e) Burkey, T. J., Majewski, M., and Griller, D., *J. Am. Chem. Soc.*, **1986**, *108*, 2218. (f). Lias, S. G., Bartmass, J. E., Liebman, J. F., Holmes, J. L., Levin, R. D., and Mallard, W. G. *J. Phys. Chem. Ref. Data*, **1988**, *17*, 1. (g) reference 3a.
8. Manka, M. J., and Stein, S. E., *J. Phys. Chem.* **1984**, *88*, 5914.
9. Billmers, R., Griffith, L. L., Stein, S. E., *J. Phys. Chem.* **1986**, *90*, 517.
10. Bedell, M. W., and Curtis, C. W. *Energy Fuels* **1991**, *5*, 469.
11. The slower reaction is from RRD from the AnH_2 formed under the reaction conditions.

12. Arends, I. W. C. E., in *Thermolysis of Arene Derivatives with Coal-Type Hydrogen Donors*, Ph.D. Thesis, 1993, Leiden University, The Netherlands.
13. (a) Camaioni, D. M., Autrey, S. T., and Franz, J. A., *J. Phys. Chem.*, **1993**, *97*, 5791 (b) Autrey, S. T., Camaioni, D. M., Ferris, K. F., and Franz. J. A., *Coal Science Proceedings, International Conference on Coal Science*, **1993**, 336.
14. (a) Metzger, J. O., and *Angew. Chem.* **1986**, *25*, 80. (b) Wagner, P. J., Zhang, Y. and Puchalski, A. E., *J. Phys. Chem.* **1993**, *97*, 13368. (c) Naguib, Y. M. A., Steel, C, and Cohen, S. G. *J., Phys. Chem.* **1988**, *92*, 6574. (d) reference 12.
15. Braun, W., Herron, J. T., and Kahaner, D. K. *Int. J. Chem. Kinet.*, **1988**, *20*, 51.

Table I. Predicted contribution of scission by H-atom pathway, balance RRD. 400°C (Ar/ArH_2 3/1) 10% by weight substrate Ar-R.

	Ph/Ph$_2$	Nap/NapH$_2$	Phen/PhenH$_2$	An/AnH$_2$
Ph-R	100	100	100	98
Nap-R	100	99	99	29
Phen-R	100	69	82	13
An-R	76	58	56	0

Table II. Relative Rate of scission by RRD and H atom pathways. 400°C (Ar/ArH_2 3/1) 10% by weight substrate Ar-R.

	Ph/Ph$_2$	Nap/NapH$_2$	Phen/PhenH$_2$	An/AnH$_2$
Ph-R	3100	40	6	1
Nap-R	1900	80	10	6
Phen-R	1560	100	13	17
An-R	100000	2300	650	12600

Figure I. Mechanistic kinetic model predicted and experimental observed selectivity of Bond Scission. Thermolysis of DNM in Anthracene/Dihydroanthracene (An/AnH$_2$) with (w) and without (w/o) biphenyl and a cyclic olefin 1,4,5,8,9,10-Hexahydroanthracene (AnH$_6$).

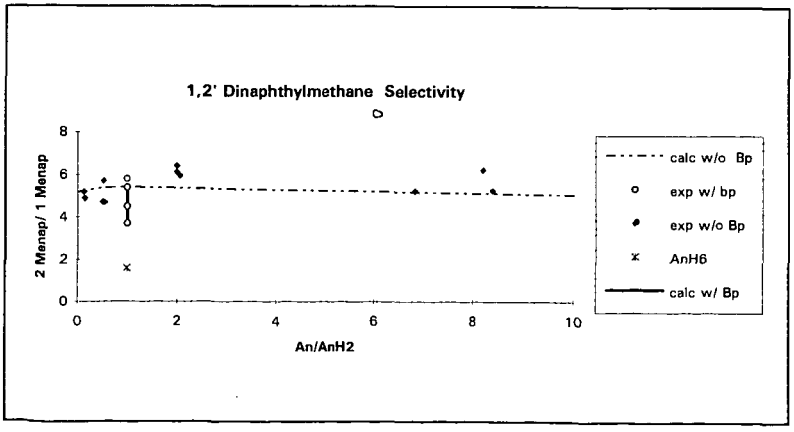

IS RHT ALIVE AND LIVING IN VENEZUELA?

Donald F. McMillen and Ripudaman Malhotra
SRI International, Menlo Park, California 94025

Key Words: Hydrogen transfer, bond cleavage, coal liquefaction.

INTRODUCTION

Under coal liquefaction conditions, hydrogen transfer reactions of various types are so facile, and coal structures so varied and unknown, that were it not for model compounds, the concept of "hydrogen transfer" in coal liquefaction would be little more than a mantra which we recite. Several years ago, studies of hydrogen-transfer reactions in model compounds led to the suggestion, if not the rigorous proof, that a "missing link" in the system of known H-atom transfer reactions was not only kinetically accessible under liquefaction conditions, but also played a key role in bond cleavage during liquefaction.(1-4) More recently, however, specific model-compound and computational studies (5-7) have led researchers to question the general accessibility of "radical hydrogen-transfer" (RHT) compared to other H-transfer pathways. In light of this recent work, it is important to articulate more clearly the limited "window of opportunity" originally posited (2) for RHT, and to reconsider some other model compound systems in each of which one or more of the various alternative transfer pathways are themselves insufficient to account for the observed reaction. The particular difficulty embodied in the following discussion is that no single system has yet been identified in which RHT can be claimed to be free of competition with *all* other H-transfer routes. The ultimate goal of this reconsideration of model compound studies is to obtain an improved view of the probable importance of RHT in coal liquefaction and in catalytic hydrotreatment of heavy oils.

There are two aspects of hydrogen transfer as related to fossil fuel conversion: what hydrogen transfer accomplishes, and how the transfer takes place. In recent years there has been an evolution of thinking related to both aspects. H-transfer was once considered to come only after weak-bond homolysis, serving merely to prevent retrogressive reactions of fragment radicals. In recent years, however, many model compound studies (1,2,4,8-10) have shown beyond a doubt that H-atom transfer, both abstractive and additive, and not involving free H-atoms, induces the cleavage of strong bonds in coal-related structures under the conditions of coal liquefaction. However, the precise modes by which the additive H-transfer occur under any specific conditions have been very difficult to determine with any certainty. It is this latter aspect that we primarily address in this paper.

EXPERIMENTAL SECTION

This paper relys primarily on thermochemical data from the literature and on published model compound kinetic studies, including those of the authors. In most cases, the experimental techniques have involved batch reaction at 350-400°C in borosilicate or fused-silica ampoules housed in a pressure vessel, or in small stainless steel micro-reactors.(2-4) Analyses were generally performed by GC-FID and GC-MS.

RESULTS AND DISCUSSION

Trends in RHT competitiveness with Shifts in Thermochemistry. As reiterated recently (7), it has been asked repeatedly over the last 50 years (2,3,6,11,12) whether direct bimolecular transfer of a hydrogen atom from a hydrocarbon radical to an unsaturated system (RHT) might occur directly. That is, might a direct bimolecular reaction, occurring without the intervention of a free H-atom, be competitive under some conditions with the well-established sequence of H-atom elimination, followed by a separate step in which the H-atom adds to the unsaturated reactant? The answer to that limited question is probably yes. However, because RHT has to compete not only with sequential elimination and addition of H-atoms, but also with H-transfer from closed-shell H-atom sources (e.g., reverse radical-disproportionation, or RRD from hydroaromatic donor molecules themselves), there is likely a substantial range of structures and conditions for which RHT cannot easily be competitive. Notwithstanding difficulty of experimentally determining the precise contribution of RHT when the competitive reactions produce an identical set of products, the thermochemical requirements for a competitive RHT process can be easily delineated.

We will discuss these criteria starting with the anthracene-dihydroanthracene system, since it was the principal solvent used by us in the presentation of the case for RHT, and because Stein and coworkers (13) have used it as both the solvent system and the reaction substrate in studying the kinetics of the net process shown in Reaction 1 (An* in Reaction 1 below is simply anthracene, labeled with an ethyl group at the relatively unreactive 2-position).

$$AnH_2 + An^* \rightleftharpoons An + An^*H_2 \qquad 1)$$

In this case, the reverse radical-disproportionation we have posited as a common initiation step for RHT (often rapid enough to be a pre-equilibrium) simply becomes the stoichiometric transfer step.

$$AnH_2 + An^* \rightleftharpoons 2\ An^*H\bullet \qquad 2)$$

The overall process is completed by H-abstraction (Reaction 3).

$$An^*H\bullet + AnH_2 \rightleftharpoons An^*H_2 + H + AnH\bullet \qquad 3)$$

First, it should be stressed that the system in Reaction 1 is not really a good case for RHT, as becomes clear when the component steps are examined. As we have already noted, in the system studied by Stein (13), RRD is the stoichiometric transfer step; by the time that RHT potentially appears on the scene, the net H-transfer has already been accomplished. Obviously, the only possibility for RHT to play a substantial role in the production of An^*H_2 would be in the limit where the labeled acceptor was in a substantial minority, with respect to an unlabeled acceptor or solvent.

Even in the case where the dominant acceptor is not the substrate to be cleaved, one may ask the intuitively appropriate question, "Why would it be favorable , if the original source of hydrogen in any case is to be AnH_2, to shuttle the hydrogen through the carrier radical AnH•, when this does not in any way change the overall $\Delta H°$?" This question is posed schematically in Figure 1. The answer to the question is (a) in coal liquefaction, an entire assembly of acceptor species, polycyclic Ar, are likely to be present in the solvent at high concentration, and may be statistically (and perhaps thermochemically) favored as the first acceptor of hydroaromatic donor hydrogen, and (b) the stoichiometry of AnH• production by RRD means that two molecules of the carrier radical AnH• are produced in each RRD step, so that the steady state concentration of ArH• varies exponentially with $1/2\ \Delta H°_{RRD}$ (i.e., the thermodynamic "cost" of producing ArH• is only one-half that of producing two ArH•). This is illustrated in Figure 1 by the hypothetical potential energy diagram where anthracene, dihydroanthracene, and dinaphthylmethane are representatives of the generalized system of aromatic /hydroaromatic solvent system (Ar/ArH_2) and cleavable acceptor Ar'-X.

$$ArH_2 + Ar \quad 2ArH\bullet \qquad 4)$$

$$ArH_2 + Ar'\text{-}X \rightarrow ArH\bullet\ Ar'\text{-}XH\bullet \qquad 5)$$

$$ArH\bullet\ Ar'\text{-}X \rightarrow Ar + Ar'\text{-}XH\bullet \qquad 6)$$

$$Ar'\text{-}XH\bullet \xrightarrow{fast} Ar' + X \qquad 7)$$

$$\frac{Rate_{RRD}}{Rate_{RHT}} = \frac{k_{RRD}\,[ArH_2]\,[Ar'\text{-}X]}{k_{RHT}\,[ArH\bullet]\,[Ar'\text{-}X]} = \frac{k_{RRD}\,[ArH_2]}{k_{RHT}\,(K_4\,[ArH_2]\,[Ar])^{1/2}}$$

$$\frac{A_{RRD}\,(e^{-E°_{RRD}/RT})\,[ArH_2]}{A_{RHT}\,e^{-E_{RHT}/RT}\,([e^{\Delta S°/R}\,e^{-\Delta H°_{RRD}/RT}]\,[ArH_2]\,[Ar])^{1/2}}$$

For $[Ar] = [ArH_2]$, $\Delta S°_{RRD} = 0$, $E_{RRD} = \Delta H°_{RRD}$, $A_{RRD} = A_{RHT}$, and where Ar and Ar'-X are equally good H-acceptors, at equal concentrations, this becomes:

$$\frac{Rate_{RRD}}{Rate_{RHT}} = \frac{e^{-\Delta H°\ RRD/RT}}{e^{-(E_{RHT} + \frac{1}{2}\Delta H°_{RRD})/RT}}$$

Thus, when Ar and Ar'-X are equally good acceptors, reaction via RHT ArH• (Reaction 6) will tend to be preferred to the extent that the activation energy for the thermoneutral RHT is $< 1/2\ \Delta H°_{RRD}$. One-half of $\Delta H°_{RRD}$ is 17 kcal/mol in the anthracene system; all other kinetic factors being equivalent, an activation energy for RHT of less than 17 kcal/mol or a concentration of Ar greater than that of ArH_2 will favor transfer via RHT, rather than directly from ArH_2 to Ar'-X.

As it happens, our original fitting of data for dinaphthylmethane cleavage in anthracene/dihydroanthracene (14) resulted in an activation energy for thermoneutral RHT of

16.5 kcal/mol, that is, putting RHT in the $An/AnH_2/An'$-X system only at the threshold of RHT feasibility. However, as the H-accepting thermochemistry of the substrate Ar'-X moves away from being thermoneutral, the RHT process can become more accessible, depending on whether its major competition is from RRD or free H-atom addition.

If, as will commonly be the case with an anthracene/dihydroanthracene solvent system, RRD is the major competitor to an (actual or potential) RHT, then a shift in the substrate (or solvent) thermochemistry so as to make the substrate to be a relatively *poorer* acceptor, raising the $\Delta H°$ for both RRD and RHT, will make RHT relatively more favorable. While this may seem counter-intuitive, it results because on the one hand, the increase in $\Delta H°_{RRD}$ leads to an exactly equal increase in E_{RRD} (as a reaction with zero intrinsic activation energy, i.e., essentially no activation energy in the reverse direction, there can be no further lowering of the intrinsic activation energy). On the other hand, the activation energy for RHT will increase, in the terms of the Evans-Polanyi formalism, by only a fraction of the increase in $\Delta H°_{RHT}$ (the fraction being given by $1-\alpha$, where α is the Evans-Polyani factor describing the fraction of a change in the thermodynamics ($\Delta\Delta G°$) of an exothermic reaction that is applied to the kinetics (E_a) of the reaction). Thus an increase in $\Delta H°_{RHT}$ from 0 to roughly +13 kcal/mol as the substrate Ar'-X in an anthracene/dihydroanthracene solvent system goes from an H• acceptor that is equally as good as anthracene to one that is 13 kcal/mol poorer (e.g., naphthalene) (14), will result in an increase of 13 kcal/mol in E_{RRD}, but in an expected increase of only roughly 50 to 70% of this value, or 6 to 9 kcal/mol, in E_{RHT}. At 400°C, this will result in a shift toward RHT, relative to RRD, by a factor of 20 to 200. Thus the thermochemistry predicts that RHT will be relatively more favored, in anthracene, by an Ar'-X that is a *poorer* acceptor than anthracene.

In contrast to the case for competition with RRD, if the major competition for an RHT process is sequential elimination and addition of a free H atom, then change in the substrate (or solvent) so as to make RHT more *exothermic* will be a relative benefit to RHT. This is a more easily intuited result than that discussed above: if the solvent system is one in which the carrier radical ArH• eliminates an H atom fairly readily (e.g., phenanthrene/dihydrophenanthrene), then making the substrate Ar'-X a better acceptor, so that the RHT is exothermic, will obviously not influence the unimolecular H-elimination, but will facilitate the RHT step by $\alpha(\Delta\Delta H°_{RHT})$, or 30 to 50% of the $\Delta\Delta H°_{RHT}$. In the case of moving from a phenanthrene-like to an anthracene-like acceptor, this will result, At 400°C, in a shift toward RHT *relative* to free H-atom transfer, by a factor of 10 to 40.

The above considerations reiterate that we expect the contribution of RHT to be sandwiched in a limited region between dominance by RRD on the one hand, and dominance by free H-atoms on the other. More specifically, they indicate that the thermoneutral-RHT system, anthracene/dihydroanthracene/anthracene-X, investigated by Stein (13) is, as he indicated, not the best system for observing RHT, whereas the anthracene/dihydroanthracene/naphthalene-X in which we claimed to have observed RHT (2,14), is relatively much better for this purpose. The exothermic-RHT system, phenanthrene/dihydrophenanthrene/anthracene-X, where Stein did claim (3) to observe substantial RHT, is a relatively good system for that purpose, much better than the near-thermoneutral-RHT system, phenanthrene/dihydrophenanthrene/naphthalene-X, where our data fitting (14) suggested transfer by free H-atoms was twice as important as RHT, even at an aromatic/hydroaromatic ratio of 2/1.

H-Transfer Efficiency and Selectivity. In those of the above cases where the cleavage of dinaphthylmethane was involved, the task of determining the dominant pathway was often made more difficult by competition from indirect cleavage pathways involving initial H-transfer to a non-ipso position on Ar'-X, followed by additional H-transfers to generate reduced, uncleaved products. These uncleaved products can then undergo cleavage either by homolysis of bonds that have been made doubly benzylic by the partial reduction, or by H-abstraction to produce the initially desired, easily fragmentable ipso-radical. In the case of our studies on the anthracene/dihydroanthracene/dinaphthylmethane system, we attempted to limit this additional difficulty by focusing on reaction conditions that minimized multiple H-transfers , i.e., high ratios of anthracene/dihydroanthracene. The high aromatic/hydroaromatic ratio increases H-transfer efficiency by limiting the chances that an initial hydrogen transfer to a non-ipso position (by whatever transfer mechanism) would be followed by additional transfers so as to result in a reduced-uncleaved product. This observed increase in efficiency under conditions of high PAH content, which has been previously discussed 10,14), is strikingly parallel to observed shifts in efficiency in both liquefaction (16) and gasification. (17)

The additional route to cleavage through multiple-H-atom reduction that is discussed in the previous paragraph has made it somewhat difficult to unambiguously apply the otherwise very definitive selectivity diagnostic for the active H-transfer agent. Nevertheless, we believe that positional selectivity in H-atom transfer is a least arguably a useful indicator. Free H-atoms are highly reactive and are expected, and found (14), to show relatively little positional preference for attack at the electronically favored 1-position of naphthalene, as compared to the slightly less favored 2-position. Thus, dominant free H-atom-induced cleavage of 1,2-dinaphthylmethane approaches a 2-methylnaphthalene/1-methylnaphthalene ratio of about 1.6. (14) Any increase from this this ratio necessarily represents a contribution from some other, more selective, H-transfer agent. Cleavage in the anthracene/dihydroanthracene system is found (14) to be highly selective, with the above ratio reaching a value of about 6. However, both RHT

and RRD are expected to be very selective, and so this high value, by itself, does not constitute evidence for RHT. In dihydrophenanthrene, however, where RRD is ruled out as a stoichiometric H-transfer step (and where free H-atoms are the main RHT competitor), the observed ratios are 3.0 to 3.5, still substantially higher than 1.6. The higher selectivity ratio would be unequivocal evidence for RHT contribution, were it not for the fact that, even at fairly high phenanthrene/dihydrophenanthrene ratios, there is still a substantial amount of product derived from reduction followed by cleavage.

In the pyrene/dihydropyrene system, the observed selectivity appears still more suggestive, even if not fully unambiguous. Since cleavage rates are about two times higher than in the anthracene solvent system under comparable conditions, and the C-H bond strength in dihydropyrene is 5 kcal/mol *higher* than in dihydroanthracene (14), transfer by RRD is completely ruled out as the cleavage-inducing step. On the other hand, the 2-methylnaphthalene/1-methylnaphthalene selectivity ratio is about 4, well above the 1.6 expected for free H-atoms.(2) The obvious conclusion is that H transfer by RHT is substantial in the case of pyrene; however, here too, the result remains somewhat tainted by the contribution of pathways that involve reduction followed by cleavage.

1,2-Dihydronaphthalene Disproportionation. As is well appreciated by those who have attempted to use either simple product identification or kinetic modeling of total rates, determination by these means of the precise portion of reaction that is accounted for by RHT tends to be very difficult. The best chance for distinction usually lies with an internal comparison and its shift as concentrations change, such as in simple dilution. One of the earliest cases of this approach was that of 1,2-dihydronaphthalene (DHN) disproportionation.(1) The radical-chain disproportionation of 1,2-dihydronaphthalene gives equal amounts of tetralin and naphthalene. The propagation steps, as shown in Scheme 1, are abstraction of a hydrogen from the 3-position of DHN by tetralyl radical (T•), followed by either an RHT to transfer a hydrogen from the 1-hydronaphthyl (NH•) radical to DHN, or sequential H-atom elimination from NH• and addition to DHN, to accomplish the same net change.

The sole difference between these disproportionation pathways involving either free H-atoms or RHT stems from the fact that free H atoms can not only add to DHN, but also abstract from DHN to form H_2. RHT cannot produce H_2. In the case of H-abstraction by H•, the net products of DHN self-reaction become naphthalene and H_2, rather than naphthalene and tetralin. Since the H-transfer by RHT with which the elimination-addition sequence may be competing is a bimolecular reaction, its rate will be decreased by dilution, whereas that for the unimolecular elimination will be unaffected. The subsequent addition of, and abstraction by, H atoms are bimolecular reactions that will be slowed by dilution, but since they both involve reactions with the same molecule, namely DHN (Reactions 7a and 7b in Scheme X), their ratio will not shift with dilution. Thus, the only change with dilution will be the competition between RHT (Reaction 4) and H-atom elimination (Reaction 6). Increasing dilution will increase the relative chance of H-atom elimination, and, to the extent that abstraction by H• competes with addition of H•, the parasitic production of H_2 and naphthalene production without tetralin production will increase.

The quantitative expectations from a steady-state analysis of this system are shown in Figure 2 (reprinted from reference 1), as a series of calculated lines, each of which is based on a particular values of the fraction of free H• that add to (rather than abstract from) DHN. If the reactions in Scheme 1 correctly describe the disproportionation, then the data should be fittable to one of the curves in Figure 2 simply by adjustment of the k_4/k_6 ratio.

Although the naphthalene-tetralin ratios did not vary widely for a substantial range of dilutions, the data are not scattered, and they fit the function form very well, so as to leave little room for adjustment. The very existence of a curved data plot in Figure 2 is significant: if there is no H-transfer by RHT, there will be no competition for the chain propagation by free H-atoms, and there can be no shift in the naphthalene/tetralin ratios with dilution. In fact, these measurements were prompted by related data of Allen and Gavalas (18), and of Franz and coworkers (19), which indicated shifting H_2 yields with changes in dilution. Thus, the observation of *any* shift in the naphthalene/tetralin ratio is evidence for a competing RHT reaction. This conclusion is uniquivocal, *if* (a) the chain length is long and the reverse of the intiation step (a bimolecular reaction) is not a significant product generator, and (b) other side reactions do not distort the product ratio. Both of these qualifications were considered in our original publication and judged to be unimportant.(1) Nevertheless, given the apparently unequivocal nature of the evidence for RHT from this earlier dilution study, and current questions about the accessibility and generality of RHT, we believe the case of 1,2-dihydronaphthalene disproportionation should be re-examined.

SUMMARY

Re-examination of the trends in competition between RHT, RRD, and free H-atom elimination/addition that one expects from thermochemical consideration, reiterates that the supposed case of RHT that has been most called into question by recent studies (7), is in fact expected to be among the poorest of all specific examples of RHT yet claimed. Specific cases of either exothermic or endothermic RHT (e.g., phenanthrene/dihydrophenanthrene, anthracene, or

anthracene/dihydroanthracene/dinaphthylmethane, or pyrene/dihydropyrene/dinaphthylmethane are all more expected and more credible. Reexamination of the original 1,2-dihydronaphthalene disproportionation data continues to make this case appear a very credible example of RHT. Nevertheless, the framework of thermochemical considerations discussed here again makes it clear that there is a limited window of opportunity for RHT, in between RRD on the one hand and free H-atom elimination/addition on the other. Current attention would be most usefully directed to this window.

In any event, the case of shifting hydrogen-utilization efficiencies illustrates the important point that competing and shifting competition between various transfer pathways does not render consideration of them irrelevant. On the contrary, the shifting competition makes for situations in which liquefaction effectiveness can vary substantially with shifts in solvent composition or temperature. The situation is indeed complex, and model compounds, judiciously chosen and interpreted in light of data with actual coals or heavy oils, represent the only feasible route for us mortals into the labyrinth of fossil fuel chemistry.

ACKNOWLEDGMENT

The results reviewed in this paper were made possible, in substantial part, by support through several different DOE research contracts.

REFERENCES

1. McMillen, D. F.; Chang, S.-J., Nigenda, S. E.; Malhotra, R. *Am. Chem. Soc. Div. Fuel Chem. Preprints* **1985**, *30*(4), 297.
2. McMillen, D. F.; Malhotra, R.; Chang, S.-J., Ogier, W. C.; Nigenda, S. E.; Fleming R. H. *Fuel* **1987**, *66*, 1611.
3. Bilmers, R.; Brown, R. L.; Stein, S. E. *Int. J. Chem. Kinetics*, **1989**, *21*, 375.
4. Smith, C. M.; Savage, P. E., *Chem. Eng. Sci.* **1993**, *49*, 259.
5. Camaioni, D. M.; Autrey, S. T.; Franz, J. A. *J. Phys. Chem.* **1993**, *97*, 5791.
6. Ruchardt, C.; Gerst, M.; Nolke, M. *Angew. Chem. Int. Ed. Engl.* **1992**, *31*, 1523.
7. Franz., J. A.; Ferris, K. F.; Camaioni, D. M.; Autrey, S. T. *Energy Fuels* **1994**, *8*, XXX.
8. McMillen, D. F.; Malhotra, Hum, G. P.; R. Chang, S.-J. *Energy Fuels* **1987**, *1* , 193.
9. Malhotra, R.; McMillen, D. F., Tse, D. S.; St.John, G. A. *Energy Fuels* **1989**, *3* , 465.
10. McMillen, D. F.; Malhotra, R.; Nigenda, S. E.; *Fuel* **1968**, *68*, 380.
11. Jackson, R. A.; Waters, W. A. *J. Chem. Soc.* **1958**, 4632.
12. Metzger, J. O. *Angew. Chem.* **1986**, *25*, 80.
13. Billmers, R.; Griffith, L. L; Stein, S. E.*J. Phys. Chem.* **1986**, *90*, 517.
14. Malhotra, R.; McMillen, D. F.*Energy Fuels* **1990**, *4* , 184.
15. McMillen, D. F. ; Malhotra, R.; Tse, D. S. *Energy Fuels* **1991**, *5* , 179.
16. Mochida, I.; Yufu, A.; Sakanishi, K. Korai, Y. *Fuel* **1988**, *67* , 114.
17. Gorbaty, M. L.; Maa, P. S. *Am. Chem. Soc. Div. Fuel Chem. Preprints* **1986**, *31*(4), 5.
18. Allen, D. T.; Gavalas, G. R. *Int. J. Chem. Kinetics*, **1983**, *15*, 219.
19. Franz, J. A.; Barrows, B. O.; Camaioni, D. M. *J. Am. Chem. Soc.* **1984**, *106*, 3964.
20. Franz, J. A.; Camaioni, D. M.; Beishline, R. R.; Dalling, D. K. *J. Org. Chem.* **1984**, *49*, 3563.

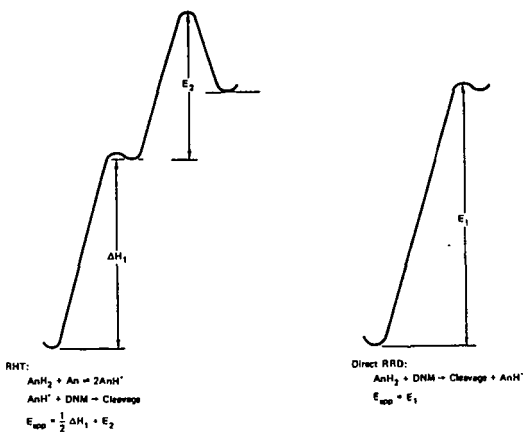

Figure 1. Illustrative potential energy diagram for direct- (RRD) and carrier-radical-mediated hydrogen-transfer (RHT) in the anthracene/9,10-dihydroanthracene/1,2-dinaphthylmethane system.

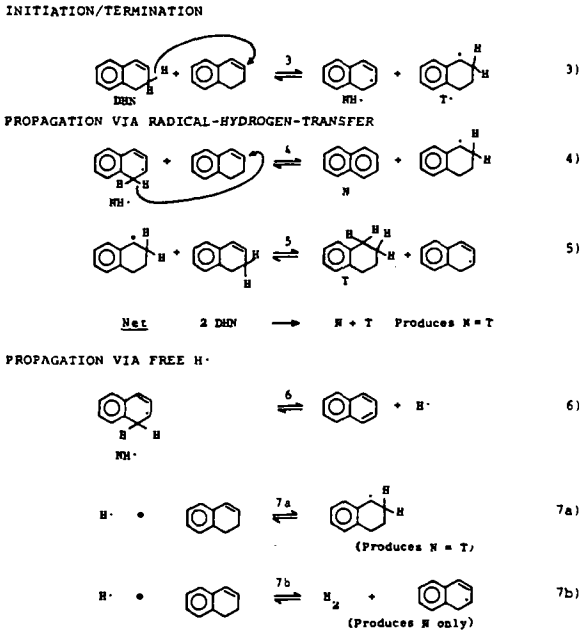

Scheme 1. Radical-chain reaction sequence for 1,2-dihydronaphthalene disproportionation.

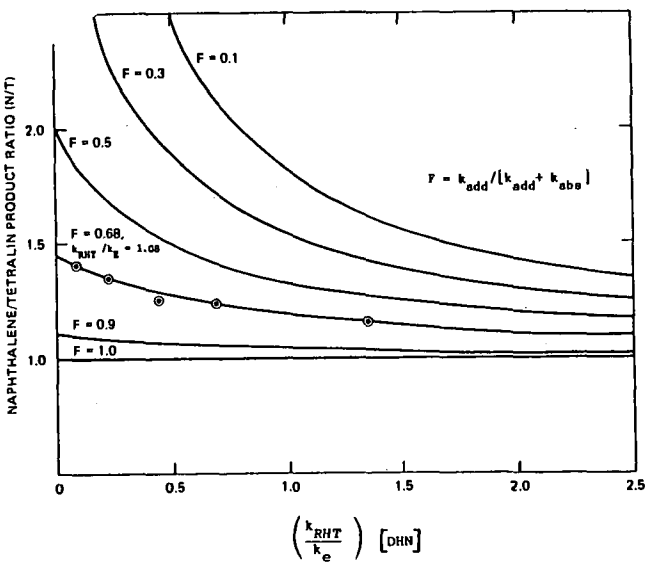

Figure 2. Observed and calculated effect of dilution with biphenyl on the naphthalene/tetralin product ratio in the disproportionation of 1,2-dihydronaphthalene at 385°C.

INTRINSIC BARRIERS FOR H–ATOM TRANSFER REACTIONS

Donald M. Camaioni, S. Tom Autrey, and James A. Franz
Pacific Northwest Laboratory, PO Box 999, Richland, WA 99352

Keywords. H-abstraction, Radical hydrogen transfer, intrinsic barrier

Hydrogen transfer reactions play a well recognized role in coal liquefaction. While H–abstraction reactions between radicals and H–donors have been well studied, understanding of structure-reactivity relationships remains surprisingly incomplete. The Bell-Evans-Polanyi relationship[1] expressed by Equation 1 is used routinely to correlate and predict rates of H–abstraction from a homologous series of donors.

$$E_a = \alpha \Delta H_r + C \qquad 1)$$

The constant, C, is interpreted as the activation barrier if the reactions were to occur with zero enthalpy change. For hydrocarbon radicals, the value of C is usually assigned the barrier for the identity reaction of methyl plus methane with justification being that the few identity reactions that have been measured are all within a few kcal/mol of this value. However, uncertainties of this amount when combined with uncertainties in the reaction enthalpy can lead to orders of magnitude errors in rate estimates.

Another form of hydrogen transfer known as radical hydrogen transfer (RHT)[2,3,4,5,6] is currently the subject of much speculation with respect to its role in coal liquefaction. RHT is unusual in that the radical donates a β–hydrogen to an acceptor molecule rather than abstracting hydrogen from a donor molecule. RHT is known to take place readily between ketones and ketyl radicals.[6] But in hydrocarbon systems, it remains controversial due to a lack of information about its activation barrier. The reaction is thought to be important in high temperature liquid-phase reactions of hydrocarbons[3,4c] and in coal liquefaction[4c,5] where it provides a simple route for migration of hydrogen from hydroaryl to aryl structures and for cleavage of aryl-alkyl bonds. However, multi-step reaction pathways to the same products are usually possible. For RHT to be important, its activation barrier must be sufficiently low to compete with these alternative pathways. In particular, RHT must compete with unimolecular scission of H–atom from the radical and subsequent rapid reactions of free H atoms. Thus, RHT remains controversial due to the lack of information about activation barriers for RHT reactions.

Marcus Theory[7] has been shown to be applicable to atom transfer reactions in the form of Equation 2 but it has received little attention until recently.[8,9,10]

$$E_a = \Delta E^{\ddagger}_i \left(1 + \frac{\Delta E_r}{4\Delta E^{\ddagger}_i}\right)^2 \qquad 2)$$

Marcus theory[7] defines the intrinsic barriers as above and equates it with one-fourth of the bond reorganization energy for forming the transition state (TS) structure. Marcus theory also recognizes that the intrinsic barrier may depend on both the attacking radical and the H donor, and defines the intrinsic barriers for unsymmetrical reactions as the average of the barriers for contributing symmetrical identity reactions. Finally, the Marcus equation simplifies to the Bell-Evans-Polanyi equation when Equation 2 is expanded and the quadratic term is negligible (*i.e.*, reactions that exhibit small exothermicities and large intrinsic barriers). Nonetheless, the possibility that intrinsic barriers are unique for each set of radical and donor should not be neglected.

Recent theoretical[8,11,12] studies of H–abstraction reactions of simple hydrocarbons and functionalized methanes have shown significant variation in intrinsic barrier heights and essentially have validated the assumption of Marcus theory that the intrinsic barrier for cross reactions are approximately the average of that for the two contributing identity reactions. However, a complete understanding of structural effects is still incomplete: for although these studies have shown how the effects of alkyl and heteroatom functional groups attached to the reaction site effect the intrinsic barrier, the effects of delocalizing groups such as vinyl and aryl groups on intrinsic barriers for H–abstraction remain to be examined. Since no kinetic data are available for hydrocarbon RHT reactions, theory-based insights to rate-controlling factors are needed to aid experimental verification and elucidation of this pathway.

COMPUTATIONAL METHODOLOGY. MNDO-PM3[13] calculations of TS geometries and energies (ΔH°_f) were performed using MOPAC (Quantum Chemistry Program Exchange, Department of Chemistry, Indiana University, Bloomington, IN; QCPE No. 455 ver. 6.0). Geometries of transition states for H-atom transfer reactions were optimized using the Hartree-Fock (RHF) half–electron Hamiltonian. TSs for identity reactions were located using the default optimizer by forcing the breaking/forming C-H bonds to have equal lengths. TS geometries for nonidentity reactions were optimized using one or more of the following methods available in MOPAC ver. 6: Bartel's nonlinear least squares minimization routine, McIver-Komornicki gradient minimization routine, and the eigenvector follower optimizers. Force calculations were performed to

establish that optimized geometries actually were saddle points for H transfer (only one negative vibrational frequency). The TS energies for twenty H-abstraction reactions were correlated with experimental energies (obtained by summing experimental ΔH°_f of the abstracting radicals and hydrogen donors, and experimental activation enthalpies). The least squares fit yielded the following equation and statistical parameters: $\Delta H^{\circ\ddagger}_f$(expt)=1.14$\Delta H^{\circ\ddagger}_f$(calc)–8.1 kcal/mol; r^2=0.9984; standard error ΔH°_f(calc.)=1.9 kcal/mol. ΔH°_f for radicals and donors were obtained from the literature[14] or derived from standard estimation methods[14] when experimental data were unavailable. Rate data for H–abstraction reactions are from the literature.[15,16] For reactions in which temperature-dependent rate data are lacking, Arrhenius activation energies ($E_{a,x}$) were estimated using Equation 3, which equates the difference in activation energies between the reaction of interest and a basis reaction of known activation energy with the log of the relative rate constant at a known temperature and statistically corrected for the number of donatable-hydrogens.

$$E_{a,2} - E_{a,1} = n_1/n_2 \cdot \ln(k_2/k_1) \qquad 3)$$

RESULTS. Analysis of Errors in the MNDO-PM3 Method. PM3 yields ΔH°_f that differ systematically from experimental values with different errors for different structural classes.[17] For example, experimental ΔH°_f for polycyclic aromatic hydrocarbons show a linear correlation with PM3 heats. The fit to benzene, naphthalene, phenanthrene and anthracene is excellent (r^2=0.99993). Inclusion of higher aromatic hydrocarbons gives a very good fit as well, except for benz[a]phenanthrene, triphenylene, pyrene and tetracene data which are sufficiently far from the line to warrant skepticism about their accuracy. An important feature of the fit is that its has non-unit slope and non-zero intercept. Thus, agreement between theory and experiment differs according to the magnitude of a compound's ΔH°_f. In the case of radicals, the errors are systematic for families of structurally-related radicals. For example, primary, secondary and tertiary radicals each exhibit an excellent correlation, deviating -12, -16, and -18 kcal/mol from experiment. We find that experimentally-determined H-abstraction TS energies correlate with PM3 calculated energies, too. The linear correlation between experimental[18] and calculated TS enthalpies is surprisingly good, especially considering that the data base includes reactions of methyl, ethyl, benzyl, and diphenylmethyl radicals with alkane, alkene and aromatic donors and reaction enthalpies range from thermoneutral to -20 kcal/mol. Unlike the correlation for alkyl radicals, a simple offset correction will not suffice to reproduce experimental data. The least squares fit (see Methodology section) to the data yields a non-unit slope of 1.15 and a negative intercept. Therefore, calculated TS energies may be lower than experiment, approximately equal to experiment, or higher than experiment depending on the magnitude of the TS energy.

Barriers for H-Transfer Identity Reactions. The above findings indicate that energy minima and maxima on PM3 potential energy surfaces for H-transfer correlate with experiment. With this insight, reliable structure-barrier trends can be obtained for H-transfer identity reactions provided that the necessary corrections are applied to the reactant energies when the barrier is obtained by taking the difference between TS and reactant energies. We have opted to use experimental data for reactants in our calculations because it reduces the number of structures to be calculated and eliminates the need to determine reactant errors. Barriers so obtained reproduce experimental trends qualitatively.

Barriers for H-Abstraction Identity Reactions. Figure 1 shows results for alkyl radical systems. Intrinsic barriers for H–abstractions decrease in the order: methyl > ethyl ≈ *t*–butyl > *i*–propyl.[19] The barriers for methyl, ethyl and *i*–propyl correlate well with the decrease in bond dissociation energies (BDE) of the R–H bond as expected from ab initio calculations and valence-bond curve-crossing models.[11] We think that the *t*–butyl system is anomalous because PM3 over compensates for methyl group repulsions that develop in the pyramidal TS. Support for this explanation is found in comparisons of the calculated and experimental energies for the isomeric alicyclic butanes and pentanes.[14] PM3 ΔH°_f errors parallel the degree of branching. The calculated ΔH°_f for *n*-butane is 1.3 kcal/mol larger than the experimental value whereas isobutane is larger by 2.9 kcal/mol. For the pentanes, the calculated ΔH°_f are larger by 0.6 kcal/mol for *n*-pentane, 2.4 kcal/mol for isopentane, and 4.5 kcal/mol for neopentane. Allowing for this error, the overall trend in alkyl radical H-abstraction identity barriers is in keeping with experiment[20] and higher level theory.[11] *The downward trend in intrinsic barriers with methyl group substitution shows that the effect of branching at the reaction site stabilizes the TS more than the reactants.*

The effect of conjugation with the reaction site operates in the opposite direction. Results for systems involving π–delocalizing aryl and vinyl groups also appear in Figure 1. Intrinsic barriers for phenyl substitutions increase in the order: ethyl < benzyl < diphenylmethyl. This effect was first noted by Stein[21] who compared the reactivity of methyl, benzyl and diphenylmethyl radicals. A similar effect is calculated for alicyclic polyenyl and arylmethyl systems with intrinsic barriers for increase the order: allyl < pentadienyl < heptatrienyl and benzyl < 1–naphthylmethyl < 9–anthrylmethyl. Good linear correlation with R–H BDEs are obtained for these homologous series, especially when uncertainties associated with radical ΔH°_f and BDEs are taken into consideration. *These consistent trends indicate that the TS is stabilized less than the reactants by π–delocalization.*

Interestingly, cyclic donors have lower intrinsic barriers than acyclic polyenyl and arylmethyl systems. Barriers for cyclohexadienyl-plus-cyclohexadiene and hydroanthryl-plus-dihydroanthracene systems are substantially lower than barriers for 1,4-pentadien-3-yl plus 1,4-pentadiene and diphenylmethyl plus diphenylmethane. This trend is attributed to the release of strain in the TS that is present in the cyclic donors but not in the acyclic donors. Cyclic hydroaromatic donors are better than arylalkyl donors for coal liquefaction. Having lower intrinsic barriers for donating H is probably an important but unrecognized contributing factor.

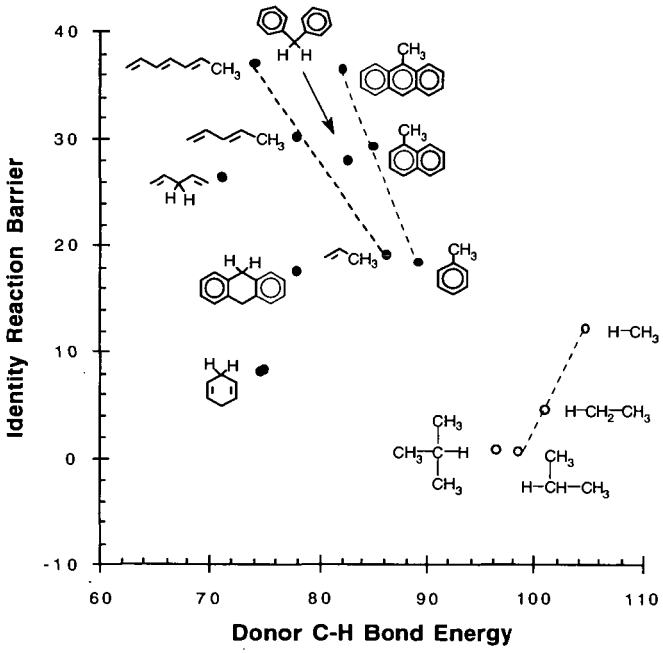

Figure 1. The effects of radical-site branching and conjugation on calculated barriers for H-abstraction identity reactions of hydrocarbon systems: barriers for alkyl systems (o) decrease with donor C-H bond dissociation energy; barriers for conjugated systems (•) show the opposite trend.

Barriers for RHT Identity Reactions. Due to the complete lack of rate data for RHT reactions, a correlation for TS energies cannot be demostrated. However, a rigorous ab initio calculation has been carried out on the prototypical reaction, ethyl plus ethylene. The barrier (26.9 kcal/mol) we calculate using PM3 agrees well with the ab initio barrier (27.2 kcal/mol),[22] provided that the PM3 barrier is obtained from the calculated TS energy and the experimentally-derived ΔH°_{f} for ethyl and ethylene. PM3 also reproduces the salient features of the ab initio transition structure (linear C–"inflight H"–C bond angle, planar carbons β to inflight H, pyramidal carbons α to "inflight H").[23]

Calculations of TS energies for higher homologs were performed to elucidate structure-reactivity trends for the RHT reaction. In all cases, RHT barriers were obtained from the difference between PM3 TS energies and experimental reactant energies. Barriers for RHT identity reactions were calculated for a series of hydroaryl-plus-arene systems as well as 1-methylallyl plus butadiene. Figure 2 shows trends for conjugated systems plotted against donor radical (HA•) C–H bond energies (estimated from thermochemical data[14] as follows: cyclohexadienyl, 25; 1–hydronaphthyl, 31; ethyl, 36; 9–hydroanthryl, 43; 1–methylallyl, 46). The barriers for hydroaryl radicals *increase* in the series: cyclohexadienyl < 2–hydronaphthyl < 1-hydronaphthyl < 9-hydrophenanthryl < 9-hydroanthryl. The barriers correlate well with the C–H bond strengths for the AH• donor radicals indicating that the BDE is an indicator of the relative RHT barrier heights for aromatic systems. A similar trend is apparent for ethyl and methylallyl radical donors. BDEs for AH• increase because the radicals derive more resonance energy than the olefins or arenes from π–delocalizing benzo and vinyl groups. Similarly, RHT barriers increase because the reactants (mainly the radicals) are being stabilized more than the TS by conjugation effects.

DISCUSSION. It is most noteworthy and surprising that RHT barriers are a substantial fraction (~80% for ethyl-plus-ethylene) of the β-C-H bond energy. In contrast, H-abstraction reactions occur with barriers that are a small fraction (~15% for ethyl-plus-ethane) of the donor C-H bond energy. Our calculations indicate clearly that RHT is intrinsically more difficult than H abstraction. Furthermore, they show that barriers vary significantly with structure such that a single or average intrinsic barrier cannot be used to estimate H-transfer reaction rates accurately. Inspection of the TS geometries calculated for H–abstraction and RHT reactions provides fundamental insight to both the noted effects of π-delocalizing groups and the substantial difference between H-abstraction and RHT barriers. TS structures for H abstraction resemble an H atom in transit between two alkyl groups, not alkyl radicals. A radical sp^2 carbon exhibits a relatively low barrier to pyramidal distortion compared to that for planar distortion of alkyl sp^3 carbon.[24] Consequently, most of the structural reorganization occurs at the radical carbon. Overlap with adjacent π–delocalizing groups is diminished in the TS with the net result being that the reactants are most effected by π-stabilization. For the RHT reaction, the radical site remains planar because it is remote to the carbons that are transferring the H atom. Carbons with greater reorganization energies, sp^3 alkyl and sp^2 alkene/arene, are at the reaction site and must deform to achieve the TS geometry. The sp^3 carbon that is donating the H–atom deforms substantially towards sp^2 character to achieve the TS. Thus, the RHT TS resembles an H atom interacting with the termini of two olefinic or aromatic moieties. With these insights, the greater barriers for RHT compared to H-abstraction are not surprising. The increase in barrier with benzannelation of the cyclohexadienyl–plus–benzene and vinylogous homologation of the ethyl–plus–ethylene systems is also consistent with these insights. Radicals derive relatively more stabilization from conjugation than olefins and arenes. Otherwise, the HA• BDEs would not increase with conjugation. The loss of radical character and development of olefin/arene character on forming the RHT TS causes the reactants to be stabilized more by conjugation; which explains why RHT barriers correlate so well with the AH• BDEs.

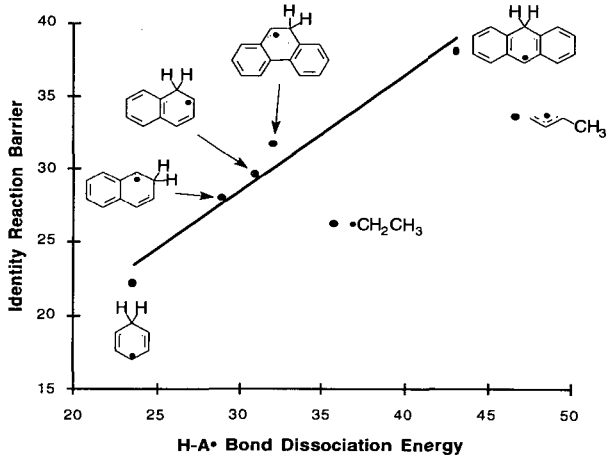

Figure 2. Barriers for radical hydrogen transfer identity reactions of conjugated systems increase with degree of conjugation. The effect correlates well with the bond dissociation energies of homologous radicals.

ACKNOWLEDGEMENT. This work was supported by the U.S. Department of Energy, Office of Basic Energy Research, Division of Chemical Sciences, Processes and Techniques Branch. The authors thank Dr. Kim F. Ferris (PNL) for discussions and Terrance E. Salinas (undergraduate summer research fellow, Northwest Association of Colleges and Universities for Science) for assistance.

REFERENCES

1. Bell, R. P.; Proc. R. Soc. (*London*)**1936**, *A154*, 414. Evans, M. G.; Polanyi, M. *Trans. Faraday Soc.* **1936**, *32*, 1333.

2. Jackson, R. A.; Waters, W. A. *J. Chem. Soc.* **1958**, 4632.

3. Metzger, J. O.; *Angew. Chem. Int. Ed. Engl.*. **1986**, *25*, 80.

4. a) Billmers, R.; Griffith, L. L.; Stein, S. E. *J. Phys. Chem.* **1986**, *90*, 517. b) Billmers, R.;

Brown, R. L.; Stein, S. E. *Int. J. Chem. Soc.* **1989**, 21, 375. c) Stein, S. E. *Acc.. Chem. Res.* **1991**, *24*, 350.

5. (a) Malhotra, R.; McMillen, D. F. *Energy and Fuels* **1993**, *7*, (b) McMillen, D. F., Malhotra, R., Tse, D. S. *Energy and Fuels* **1991**, *5*, 179. (c) Malhotra, R. and McMillen, D. F. *Energy and Fuels* **1990**, *4*, 184. (d) McMillen, D. F.; Malhotra, R.; Hum, G. H.; Chang, S. -J. *Energy and Fuels* **1987**, *1*, 193. (e) McMillen, D. F.; Malhotra, R.; Chang, S. -J.; Ogier, W. C.; Nigenda, S. E. *Fuel* **1987**, *66*, 1611.

6. (a) Wagner, P. J.; Zhang, Y.; Puchalski, A. E. *J. Phys. Chem.* **1993**, *97*, 13368. (b) Neckers, D. C.; Schaap, A. P.; Harry, J. *J. Am. Chem. Soc.* **1966**, *88*, 1265.

7. Marcus, R. A. *J. Phys. Chem.* **1968**, *72*, 891.

8. Lluch, J. M.; Bertran, J.; Dannenberg, J. J. *Tetrahedron* **1988**, *44*, 7621-7625. Dannenberg, J. J. *Adv. Molec. Modelling* **1990**, *2*, 1.

9. Fox, G. L.; Schlegel, H. B. *J. Phys. Chem. Soc.* **1992**, *96*, 298-302

10. Denisov, E. T.*Mendeleev Commun.* **1992**, 1-2; *Kinet. Katal.*, **1991**,*32*, 461-5.

11. Yamataka, H.; Nagase, S. *J. Org. Chem.* **1988**, *53*, 3232.

12. Pross, A.; Yamataka, H.; Nagase, S. *J. Phys. Org. Chem.* **1991**, *4*, 135.

13. Steward, J. J. P. *J. Comput. Chem.* **1989**, *10*, 209, 221.

14. Lias, S. G.; Bartmess, J. E.; Liebman, J. F.; Holmes, J. L.; Levin, R. D.; Mallard, W. G. *J. Phys. Chem. Ref. Data* **1988**, *17*, Sup. 1. Cox, J. D.; Pilcher, G. *Thermochemistry of Organic and Organometallic Compounds*; Academic Press: New York, 1970, pp 516. Griller, D.; Martinho Simoes, J. A.; Sim, B. A.; Wayner, D. D. M. *J. Am. Chem. Soc.* **1989**, *111*, 7872. Nagaoka, T.; Berinstain, A. B.; Griller, D.; Wayner, D. D. M. *J .Org. Chem.* **1990**, *55*, 3707. Seakins, P. W.; Pilling, M. J.; Niiranen, J. T.; Gutman, D.; Krasnoperov, L. N. *J. Phys. Chem.* **1992**, *96*, 9847.

15. Kerr, J. A. *Free Radicals;* Kochi, J. K., Ed.; Wiley, New York: 1973; Vol. 1; p. 15; Ingold, K. U. *ibid.*, pp. 74, 75.

16. Bockrath, B.; Bittner, E.; McGrew, J. *J. Am. Chem. Soc.* **1984**, *106*, 135; Franz, J. A.; Alnajjar, M. S.; Barrows, R. D.; Kaisaki, D. L.; Camaioni, D. M.; Suleman, N. K. *J. Org. Chem.* **1986**, *51*, 1446; Manka, M. J.; Brown, R. L.; Stein, S. E. *Int. J. Chem. Kinet.* **1987**,*19*, 943.

17. The AM1 Hamiltonian yields similar results. Camaioni, D. M. *J. Am. Chem. Soc.* **1991**, *112*, 9475.

18. TS energies are obtained by summing values for the experimental activation enthalpy, and ΔH_f of reactants, $\Delta H_f(\mathrm{TS}) = E_a - \mathrm{RT} + \Delta H_f(\mathrm{R\text{-}H}) + \Delta H_f(\mathrm{R}\bullet)$

19. If the barriers are obtained using PM3 energies for the reactants, then an opposite and erroneous trend is obtained: methyl, 11.7; ethyl, 13.5; isopropyl, 14.7; *t*-butyl, 18.6.

20. Identity barriers for *t*-butyl and isopropyl radicals are estimated to be 9 and 11 kcal/mol respectively from experimental data[15] for the cross reactions of isobutane and propane with methyl and ethyl radicals.

21. Manka, M. J.; Brown, R. L.; Stein, S. E. *Int. J. Chem. Kinet.* **1987**, *19*, 943-957

22. The cited value is for a PMP2/6-31G** calculation that includes corrections for spin annihilation, thermal and zero point energy differences, and basis set superposition errors. Franz, J. A.; Autrey, T. A.; Camaioni, D. M.; Ferris, K. F., To be published.

23. Reaction site parameter, ab initio value, PM3 value: C_α-"inflight H", 1.36 Å, 1.42 Å; C_β–C_α–"inflight H", 113°, 106°; C_β-C_α-H-H reaction site torsional angle, 143°, 152°.

24. Yamada, C. Hirota, E.; Kawaguchi, K. *J. Chem. Phys.* **1981**, *75*, 5256.

MECHANISTIC MODELLING OF 9,10-DIMETHYLANTHRACENE THERMOLYSIS

P.S. Virk and V.J. Vlastnik
Department of Chemical Engineering
M. I. T., Cambridge, MA 02139

KEYWORDS: Thermolysis, Mechanism, Kinetics, Numerical Simulation, Modelling.

INTRODUCTION

Motivation. The present work on modelling thermolysis of a methylated aromatic acene continues our studies [1,2] of simple substrates that mimic the chemical moieties found in complex fossil materials of engineering interest. The 9,10-dimethylanthracene, abbr. 910DMA, substrate was chosen because its acene ring is prototypical of the aromatic ring systems found in fossil materials, while its methyl groups typify the electron-donating substituents commonly pendant thereon.

Previous Work. Thermolysis of 910DMA has not previously been studied by other authors.

Outline. Our modelling of 910DMA thermolysis is based upon a 10-step mechanism, valid at low conversions, that was recently formulated to describe experimental observations [1,2]. Thermochemical parameters for all stable and radical species occurring in the mechanism were estimated from first principles. Next, enthalpies of reaction were calculated for each elementary step and used to infer Arrhenius parameters in both forward and reverse directions. Rate constants were then calculated for each reaction at a selected temperature, and these were used in conjunction with the differential conservation relations for each species to effect a full numerical solution of the model system, starting from an initial condition of pure substrate. The numerical simulation of 910DMA thermolysis kinetics and product selectivities was directly compared with experimental observations at the same conditions. A sensitivity analysis was performed to discern how errors in the estimated Arrhenius parameters affected the model results. Finally, the Arrhenius parameters of certain elementary steps were adjusted, within their error limits, to provide an optimized model that best-fit the experimental observations.

REACTION PATHWAYS & MECHANISM

Pathways. Earlier experiments have identified three primary parallel pathways for thermolysis of 910DMA, namely: (P1) hydrogenation to *cis-* and *trans*-9,10-dihydro-9,10-dimethylanthracene, abbr. DHDMA, (P2) demethylation to 9-methylanthracene, abbr. 9MA, and (P3) methylation to 1,9,10- and other trimethylanthracene isomers, abbr. TMA. The primary demethylation product 9MA is associated with methane gas formation, and considerable amounts of heavy products are formed, including both pure- and cross-termination types of dimeric species related to 910DMA and DHDMA.

Mechanism. A possible mechanism for 910DMA thermolysis is presented in Fig. 1. This elementary step "graph" is constructed with substrate and all stable molecular products arrayed in the bottom row and unstable radical intermediates arrayed in the top row. Reaction "nodes", arrayed in the middle row, connect the individual species in the bottom and top rows with arrows indicating the initial direction of reaction (all reactions are, of course, reversible). Initiation reactions are denoted by solid interconnecting lines, propagation reactions by various kinds of dashed lines and termination reactions by dotted lines. Arrow weights depict the relative elementary reaction traffic, to be discussed in the next section.

The free-radical cycle is initiated by the bimolecular disproportionation of substrate (R1), an intermolecular hydrogen transfer reaction, to form the respectively dehydrogenated and hydrogenated radical species 910DMA* and HDMA*. Of these, the latter can either abstract hydrogen from 910DMA by (R2), to form DHDMA products, or undergo a β-scission type of radical decomposition by (R3), forming 9MA product and a methyl radical CH_3*. The CH_3* can either abstract H from 910DMA by (R4), to form methane product, or add to 910DMA by (R5), to form the trimethyl radical HTMA1*. The latter can then abstract H from 910DMA via (R6) to form the observed TMA product. The radical cycle is terminated by the species 910DMA* and HDMA* engaging in both pure- and cross-combinations, (R7-R9), to form various dimeric products. HDMA* radical can also terminate by disproportionation, (R10), to form 910DMA and DHDMA.

The proposed mechanism accounts for the major products, 9MA, TMA, DHDMA, CH_4 and heavies, observed during the initial stages of 910DMA thermolysis. Each of the observed triad of primary pathways arise naturally as limiting cases of the graph, with P1, hydrogenation, comprising the set [R1, R2, R7]; P2, demethylation, the set [R1, R3, R4, R7]; and P3, methylation, the set [R1, R3, R5, R6, R8]. The stoichiometry of these sets restricts the maximum selectivity of each major product to 1/3, which is of the magnitude of the highest selectivities observed. The mechanism also suggests that the relative kinetics of the observed hydrogenation and demethylation pathways, (P1)/(P2), are controlled by the HDMA* radical, through the ratio of its H-abstraction to β-scission reactions (R2)/(R3). Further, the observed methylation to demethylation pathway ratio, (P3)/(P2), is governed by competition between methyl radical reactions (R4) and (R5), in which CH_3* either abstracts H from or adds to the 910DMA substrate.

MODELLING

Thermochemistry. Enthalpies of formation, ΔH^0_f, for all chemical species participating in our 910DMA thermolysis model were estimated by a "macro" group-additivity technique, using a basis set of bond strengths, D^0 kcal/mol, steric corrections, C^0 kcal/mol, and stable species enthalpies of formation, ΔH^0_f, assembled from a variety of literature sources [3-10]. Fig. 2 illustrates the estimation procedures. For the stable species 9MA in (a), we started with the largest, most structurally similar basis species available, namely ANT; other basis species and steric corrections, in this case 1MN, NAP and an alkene gauche interaction, were then either added or subtracted to bridge the structural differences between the starting and the desired species. The method provided both ΔH^0_f, kcal/mol, and its rms error, kcal/mol. Calculations for a radical species, HDMA*, are shown in Fig. 2(b).

Arrhenius Parameters. Arrhenius expressions of the form $\log_{10} k = \log_{10} A - E^*/\Theta$, with rate constant k (l, mol, s units), pre-exponential factor A (same units as k), activation energy E^* (kcal/mol), and scaled temperature $\Theta = 0.004573*(T\ C + 273.2)$, were generated for each elementary step of the 910DMA thermolysis mechanism, as summarized in Table 1. An elementary reaction was first classified (column 2), using standard free-radical reaction notation. Next, kinetic data [5, 11-14] for that type of reaction was analyzed to ascertain its activation parameters. Of these, $\log_{10}A = \log_{10}A_{int} + \log_{10}(rpd)$ was decomposed into an intrinsic portion, $\log_{10} A_{int}$ (column 3) and a reaction path degeneracy, rpd (column 4). Activation energy E^* was determined by an Evans-Polanyi expression (column 5), of form $E^* = E_0 + \alpha.\Delta H^0_r$ with α = 0 (combinations), 0.5 (H-abstraction and transfer) or 1 (homolysis, beta-scission). Values of the enthalpy of reaction ΔH^0_r (column 6), derived from thermochemical estimates of the previous section, then led to E^* (column 7) and the final Arrhenius expression (column 8).

Numerical Solution. The model 910DMA thermolysis reaction system was solved by a computer code called ACUCHEM [15]. This program numerically solves a system of differential equations that describe the temporal behavior of a spatially homogeneous, isothermal, multicomponent chemical reaction system. Integrations are performed by the method of Gear [16], appropriate for the stiff differential equations encountered in the present case. Two types of tests were performed to ensure reliable results. First, in regard to stability, it was verified that the program generated the same concentration profiles, regardless of the time step size. Second, in regard to fidelity, the concentrations of all species, both radical and stable, calculated by the numerical solution at low conversions X < 0.1 were found to agree with the corresponding concentrations obtained from pseudo-steady-state algebraic solutions at similar conditions.

RESULTS & DISCUSSION

Original Model. Numerical solutions of the 910DMA thermolysis model were obtained at selected conditions covering the entire experimental grid, 315 < T C < 409 and 0.082 < $[910DMA]_0$ mol/l < 2.47. The complete concentration histories of all radical and stable species obtained from each simulation were then used to prepare the illustrations in Figs. 1, 3 and 4.

Reaction Traffic. The arrows in Fig. 1 graphically depict the elementary reaction traffic as calculated at T = 355 C, $[910DMA]_0$ = 0.82 mol/l, and conversion X = 0.31, the thicker arrows denoting reactions with the greater net (forward - reverse) rates. The 910DMA substrate decomposes mainly, but not exclusively, by (R1). The rates of hydrogenation (R2) and of demethylation (R3) are of comparable magnitudes, with (R3) > (R2). Methyl radical quenching by H-abstraction from substrate (R4) greatly exceeds its addition to the substrate (R5). Among termination reactions, (R7 - R10), 910DMA* combination (R7) is dominant.

Kinetics. Fig. 3 compares substrate decay half-lives t* calculated from the model (hollow points and dashed lines) with those observed experimentally, (solid points and lines). Fig. 3(a), a semi-logarithmic Arrhenius-type plot of t^* vs. $1/\Theta$, shows that, at constant $[910DMA]_0$ = 0.82 mol/l, the calculated t* are about 3-fold higher than experimental at all temperatures. Decomposition kinetics predicted by the model are thus slower than experimental, but exhibit roughly the same apparent activation energy. Fig. 3(b), a log-log plot of t^* vs. $[910DMA]_0$ at constant T = 355 C, shows that the calculated t* are 2- to 10-fold higher than experimental, the more so at the lowest $[910DMA]_0$, with the model predicting an apparent decomposition reaction order ~2, somewhat greater than the experimentally observed order ~1.5.

Product Selectivities. Fig. 4 compares (a) the selectivity to 9MA product and (b) the ratio of TMA/9MA products, as calculated from the model, with those observed experimentally, using semi-logarithmic Arrhenius-type coordinates of either S(9MA) or R(TMA/9MA) vs. $1/\Theta$ at constant $[910DMA]_0$ = 0.82 mol/l. In Fig. 4(a) the model is seen to predict a 9MA selectivity S(9MA) from 0.1 to 0.7 orders of magnitude below experimental, while in Fig. 4(b) model predictions of the major product ratio R[TMA/9MA] lie within ±0.2 orders of magnitude of the experimental observations.

Sensitivity Analyses. The significance of the differences between model predictions and experimental observations was sought from sensitivity analyses at T = 355 C and $[910DMA]_0$ = 0.82 mol/l, the central point of the experimental grid, by separately perturbing the kinetics of selected elementary steps. The effects of these perturbations on the predicted decay half-life t^*, 9MA selectivity S(9MA), and the primary product ratio R[TMA/9MA], are shown by the vertical dashed lines in Figs. 3 and 4. In Figs. 3(a) and (b), for example, the uncertainty in t* was estimated by perturbing the activation energy E^*_1 by ± 4.4 kcal/mol (the inherent error in ΔH^0_{r1}), since the elementary reaction R1 contributes most heavily to the destruction of 910DMA substrate in our model. The upper and lower ends of the vertical dashed lines in each portion of Fig. 3 represent values of t^* obtained by negative and positive perturbations, respectively, of E^*_1. This sensitivity analysis shows that the inherent uncertainties of ± 1.5 orders of magnitude in values of t^* calculated by the model considerably exceed the 0.5 to 1.0 order of magnitude differences between the model results and experimental observations. That is, within its (large) error limits, the model yields half-lives in agreement with experiments. Similar sensitivity analyses provided the vertical dashed lines in each of Figs. 4(a) and (b), showing that, within its error limits, the model also yielded 9MA selectivities and TMA/9MA ratios in accord with experiment.

Optimized Model. The preceding comparisons between model and experimental results are mildly noteworthy because all the kinetic parameters employed in the original model were derived from first principles and used without adjustments. However, these comparisons also revealed the empirical alterations that might permit a best-fit of experimental results for engineering purposes, termed the "optimized" model. Specifically, the best-fit of all experimental data for 910DMA thermolysis at T = 355 C with $[910DMA]_0$ = 0.82 mol/l arose by altering the original activation energies E^*_1, E^*_2, E^*_{-2} and E^*_3 by respective amounts of -1.2, +1.2, -1.2 and -1.2 kcal/mol, all of these changes being well within the inherent uncertainties of these parameters, respectively, ±4.4, ±2.4, ±2.4 and ±3.7 kcal/mol. Figs. 5 (a) and (b) compare substrate and product histories obtained from the optimized model (lines) to the experimental data (points) for 910DMA, 9MA, TMA, CH4, and DHDMA. Fig. 5(a) shows the optimized model to well predict the observed 910DMA decay, with decay half-lives t^* = 25000 s from the model versus 22000 s experimental. The absolute amounts of 9MA and of TMA formed by the model are both about 1.5-fold lower than experimental in Fig. 5(a), but the model well predicts the relatively small amounts of DHDMA,

and its delicate variation with time, in Fig. 5(b). Finally, Figs. 6(a) and (b) show that the optimized model provides the correct magnitudes of the major product ratios R[DHDMA/9MA] and R[TMA/9MA], as well as a qualitative indication of their respective variations with conversion. For example, at all conversions $0.0 < X < 0.54$ the ratio R[TMA/9MA] ~ 0.25 from the model lies astride the experimental data.

Modelling Perspective. In regard to both thermolysis kinetics and the selectivities of major products, the predictions of the optimized model are appreciably closer to the experimental observations than those of the original model. However, the differences between the activation parameters of the optimized and original models, of order 1.2 kcal/mol, are small relative to the inherent uncertainties in these parameters, of order 3.5 kcal/mol. Thus, although the optimized model effects an appealing cosmetic improvement over the original model, of possible value in engineering applications, the two models remain statistically similar. Substantive scientific improvements in modelling thermolyses such as the present must await better methods, and more reliable data, for deriving the kinetics of the underlying elementary reactions.

ACKNOWLEDGEMENT: This work was supported in part by Cabot Corporation, Boston, MA.

REFERENCES

[1] Virk, P.S.; Vlastnik, V.J.: PREPRINTS, Div. of Petrol. Chem., ACS, 38(2), 422 (1993).
[2] Virk, P.S.; Vlastnik, V.J.: PREPRINTS, Div. of Fuel Chem., ACS, 39(2), 546 (1994).
[3] Stull, D.R.; Westrum, Jr., E.F.; Sinke, G.C.: The Chemical Thermodynamics of Organic Compounds, Wiley, New York (1969).
[4] Benson, S.W.; Cruickshank, F.R.; Golden, D.M.; Haugen, G.R.; O'Neal, H.E.; Rodgers, A.S; Shaw, R.; Walsh, R.: Chem. Rev., 69, 279 (1969).
[5] Benson, S.W.: Thermochemical Kinetics, 2nd Ed., Wiley, New York (1976).
[6] Stein, S.E.; Golden D.M.; Benson, S.W.: J. Phys. Chem., 81, 314 (1977).
[7] Shaw, R.; Golden, D.M.; Benson, S.W.: J. Phys. Chem., 81, 1716 (1977).
[8] Pedley, J.B.; Naylor, R.D.; Kirby, S.P.: Thermochemical Data of Organic Compounds, Chapman & Hall, London (1986).
[9] Bordwell, F.G.; Cheng, J.P.; Harrelson, Jr., J.A.: J. Am. Chem. Soc., 110, 1229 (1988).
[10] Stein, S.E.; Rukkers, J.M.; Brown, R.L.: Structures and Properties Database and Estimation Program, Ver. 1.1, NIST, (1991).
[11] Ingold, K.U.; pp 37-66 in Kochi, J.K.: Free Radicals Vol. I, Wiley, New York, (1969).
[12] Kerr, J.A.; pp 1-36 in Kochi, J.K.: Free Radicals Vol. I, Wiley, New York, (1969).
[13] Holt, P.M.; Kerr, J.A.: Int. J. Chem. Kinet., 9, 185 (1977).
[14] Billmers, R.; Griffith, L.L.; Stein, S.E.: J. Phys. Chem., 90, 517 (1986).
[15] Braun, W.; Herron, J.T. and Kahaner, D.K.: Int. J. Chem. Kinet., 20, 51 (1988).
[16] Gear, C.W.: Numerical Initial Value Problems in Ordinary Differential Equations, Prentice-Hall, N.J., 1971.

Table 1. Evans-Polanyi Relations and Arrhenius Parameters for Model Elementary Reactions.

	Type of Reaction	$\log_{10} A_{m}$ $l\ mol^{-1}\ s^{-1}$	rpd	Evans-Polanyi Relation: E^{*} =	ΔH_r° kcal/mol	E^{*} kcal/mol	Arrhenius Expression: $\log_{10} k$ =
R1	molecular disproportionation	8.5	24	ΔH_r°	43.4	43.4	9.9 - 43.4/θ
R-1	radical disproportionation	8.5	1	0	-43.4	0	8.5
R2	H-abstraction	8.1	6	17.5 + $\Delta H_r^{\circ}/2$	1.2	18.1	8.9 - 18.1/θ
R-2	H-abstraction	8.1	2	17.5 + $\Delta H_r^{\circ}/2$	-1.2	16.9	8.4 - 16.9/θ
R3	methyl scission	13.5	1	2.1 + ΔH_r°	29.5	31.6	13.5 - 31.6/θ
R-3	CH3* addition	8.3	1	2.1	-29.5	2.1	8.3 - 2.1/θ
R4	H-abstraction	8.1	6	17.5 + $\Delta H_r^{\circ}/2$	-22.7	6.2	8.9 - 6.2/θ
R-4	H-abstraction	8.1	4	17.5 + $\Delta H_r^{\circ}/2$	22.7	28.9	8.7 - 28.9/θ
R5	CH3* addition	8.3	4	5.1	-18.6	5.1	8.9 - 5.1/θ
R-5	methyl scission	13.5	1	5.1 + ΔH_r°	18.6	23.7	13.5 - 23.7/θ
R6	radical H transfer	8.1	2	17.5 + $\Delta H_r^{\circ}/2$	-13.2	10.9	8.4 - 10.9/θ
R-6	radical H transfer	8.1	1	17.5 + $\Delta H_r^{\circ}/2$	13.2	24.1	8.1 - 24.1/θ
R7	radical combination	9.3	1	0	-54.2	0	9.3
R-7	homolytic dissociation	15.5	1	ΔH_r°	54.2	54.2	15.5 - 54.2/θ
R8	radical combination	9.3	1	0	-52.4	0	9.3
R-8	homolytic dissociation	15.5	1	ΔH_r°	52.4	52.4	15.5 - 52.4/θ
R9	radical combination	9.3	1	0	-50.7	0	9.3
R-9	homolytic dissociation	15.5	1	ΔH_r°	50.7	50.7	15.5 - 50.7/θ
R10	radical disproportionation	8.5	1	0	-42.2	0	8.5
R-10	molecular disproportionation	8.5	4	ΔH_r°	42.2	42.2	9.1 - 42.2/θ

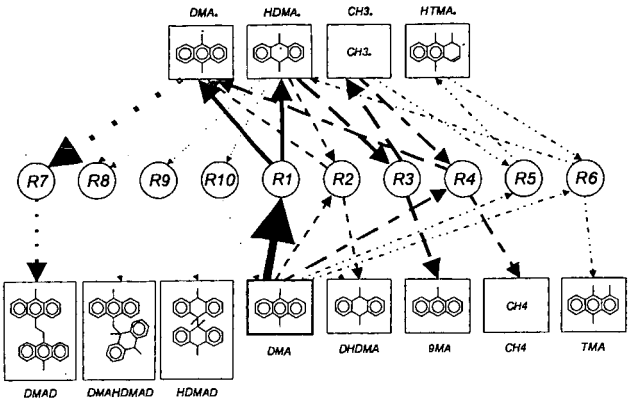

Figure 1. Elementary Step Graph of 910DMA Thermolysis Mechanism. Arrow weights depict relative reaction traffic at T = 355 C, [910DMA]o = 0.82 mol/l, and conversion X = 0.31, as calculated from the original model (see text).

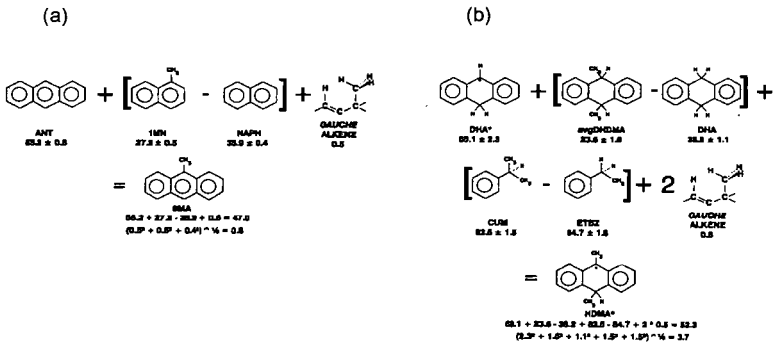

Figure 2. Illustration of Macro-Group Additivity Scheme for Estimation of Thermochemical Properties of (a) Stable and (b) Radical Species.

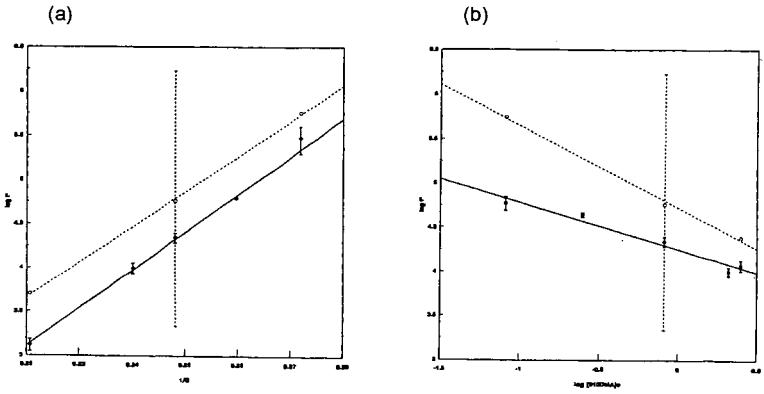

Figure 3. Decay Half-Lives t* Experimental (solid circles and lines) Versus Calculated From Original Model (hollow circles, dashed lines) at (a) constant [910DMA]o = 0.82 mol/l and (b) constant T= 355 C.

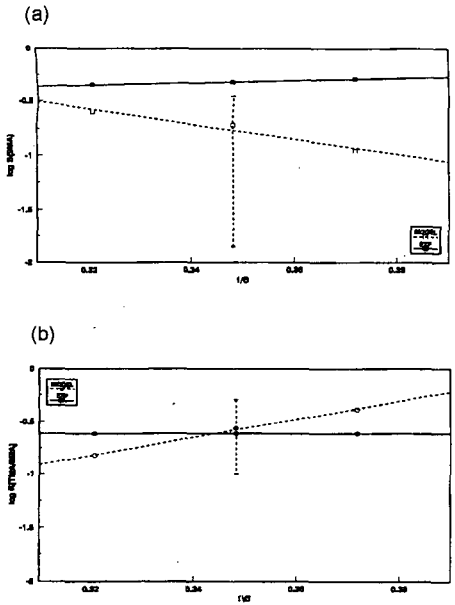

Figure 4. Original Model Results
(hollow points, dashed lines) vs.
Experiments (solid points, solid lines).
(a) Selectivity to 9MA, (b) Ratio [TMA/9MA].

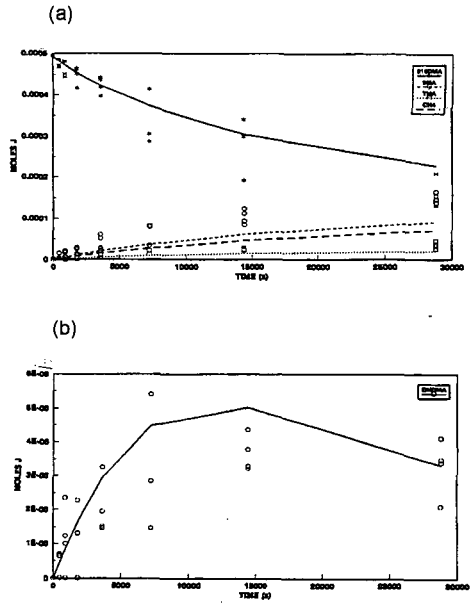

Figure 5. Optimized Model Results
(lines) vs. Experiments (points) at
T = 355 C with [910DMA]o = 1.82 mol/l.
(a) 910DMA, 9MA, CH4, TMA, (b) DHDMA.

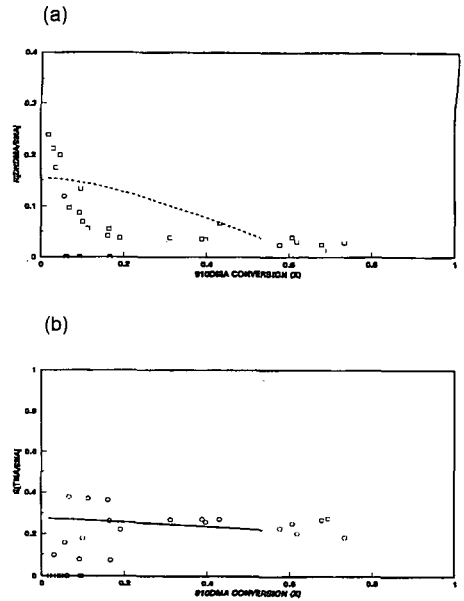

Figure 6. Optimized Model Results
(lines) vs. Experiments (points) at
T = 355 C with [910DMA]o = 1.82 mol/l.
(a) Ratio DHDMA/9MA, (b) Ratio TMA/9MA.

HEAT TREATMENT OF COALS IN HYDROGEN-DONATING SOLVENTS AT TEMPERATURES AS LOW AS 175-300℃

Masashi Iino and Jianli Shen
Institute for Chemical Reaction Science, Tohoku University,
Katahira 2-1-1, Aoba-ku, Sendai 980, Japan

Keywords;Heat treatment,Bituminous coal,Hydrogen-donating solvent

INTRODUCTION

CS_2-N-methyl-2-pyrrolidinone(NMP) mixed solvent(1:1 by volume) gave high extraction yields(40-65%, daf) at room temperature for many bituminous coals(1). We also found that the extracts obtained include a considerable amount of the very heavy extract component which is not soluble in THF or pyridine, but soluble in the mixed solvent(2). This mixed solvent was used as an extraction solvent for the heat treatment products of the bituminous coals at 300-450℃ in tetralin(TET) or naphthalene (NAP)(3). The results showed that retrogressive reactions occur more readily for the heaviest fraction, i.e., THF-insoluble, CS_2-NMP mixed solvent soluble fraction(TIMS) than other lighter fractions such as benzene-insoluble , THF-soluble(preasphaltene). The heat treatment of TIMS itself, which was obtained from the extraction of Zao Zhuang coal with the CS_2-NMP mixed solvent at room temperature, in several solvents at 100-350℃ showed that retrogressive reaction, i.e., the conversion of TIMS to the mixed solvent insoluble fraction (MI), was suppressed by adding a strong hydrogen-donating solvent such as 9,10-dihydroanthracene(DHA) or 1,4,5,8,9,10-hexahydroanthracene(HHA)(4). It was also found that as more hydrogen was transferred from the solvent to TIMS, the extent of the retrogressive reaction decreased.

In this study, heat treatments of raw Zao Zhuang and Upper Freeport coals were carried out at 175-300℃ in various solvents. The coal was found to undergo either retrogressive or dissolution reaction even at temperatures as low as 175℃ , depending on the hydrogen donatability of the solvnet used. The mechanisms for these reactions are discussed.

EXPERIMENTAL

Zao Zhuang(China) and Upper Freeport(Argonne Premium Coal, USA) coals were used. The ultimate and proximate analyses are given in Table 1. Heat treatment solvents used are TET, NAP, 1-methylnaphthalene(MNA), DHA, HHA and liquefaction recycle solvent(LRS). LRS(88.5%C, 9.7%H) was obtained from the 1t/day liquefaction plant of Wyoming coal operated by NEDO(New Energy Development Organization, Japan).

Heat treatment of the coal was performed in 50mL magnetically stirred autoclave at 175, 250, and 300℃ , respectively. 1g of the coal and 5g of the solvent were charged to the autoclave, which was pressurized with nitrogen to 5.0 MPa at room temperature. After the heat treatment, the coal components were fractionated into the CS_2-NMP mixed solvent-insoluble fraction (MI) and -soluble fraction(MS), and then MS further into TIMS and TS(and the solvent), with the mixed solvent and THF at room temperature under ultrasonic irradiation, as shown in Figure 1. The quantity of MI and TIMS was determined after drying overnight in cacuum oven at 80℃ and that of TS was calculated by difference, i.e., 100-MI-TIMS. The dissolution yield was defined here as the sum of TIMS and TS.

The quantity of hydrogen transferred from DHA and HHA to the coal was determined from GC analysis. GC showed that the main solvent-derived products are anthracene for the heat treatment in DHA, and tetrahydroanthracene and octahydroanthracene for

that in HHA, respectively. Hydrogen transferred in both treatments was determined from the quantity of anthracene, and from the difference of tetrahydroanthracene and octahydroanthracene, respectively.

RESULTS

Figure 2 shows the fraction distribution after the heat treatment of Zao Zhuang coal in 5 solvents at 175℃, 250℃ and 300℃, together with that for the raw coal, which was obtained from the fractionation of the extract of the raw coal with the CS_2-NMP mixed solvent at room temperature. At 175℃ and 250℃ in NAP and TET, MI increased and TIMS decreased, compared with those for the raw coal. While, in a strong hydrogen-donating solvent such as DHA and HHA, MI decreased and TS increased by the treatment. Contrary to the results at 175℃ and 250℃, MI decreased and TS increased in TET at 300℃. The same tendency was observed, to a lesser extent in NAP, than TET. In DHA, HHA and LRS the decrease of MI and the increase of TS was further enhanced at 300℃. Especially, in HHA, TS increased to 42.1% from 13.8% of the raw coal and the dissolution yield, i.e., TIMS + TS increased to 83.4% from 63.0% of the raw coal. The dissolution yield and TS are the order of HHA > DHA > LRS. Figure 3 shows that Upper Freeport coal gave similar results as those for Zao Zhuang coal, except that MI did not decrease at 300℃ with MNA or TET, and the dissolution yields are 86.8% and 90.6% at 300℃ in DHA and HHA, respectively, which are higher than that for Zao Zhuang coal.

Figure 4 shows the dependence of the fraction distribution on the heat treatment time for Zao Zhuang coal in HHA at 250℃. The Figure shows that for the reaction times up to 1 h MI decreases and TS increases with increasing reaction time, but little change occurs over 1 h. Figure 5 and 6 show the dependence of hydrogen transferred from the solvent to the coal and the dissolution yield on the heat treatment temperature. The Figures indicate that the increase of the dissolution yield is closely related to the hydrogen transferred, and hydrogen transferred are always higher for HHA than those for DHA, indicating that HHA is a stronger hydrogen donating solvent than DHA. Figure 7 also shows that hydrogen transferred is well correlated with the dissolution yield when the heat treatment time was varied. Table 2 shows that spin concentration of acetone-insoluble fraction(AI) after the heat treatment of ZZ coal in HHA is much smaller than that of the raw ZZ coal. The yields(raw coal base) were more than 90% and acetone-soluble fraction has much smaller spin density than AI.

DISCUSSION

The result that MI increased and TIMS decrease at 175℃ and 250℃ in TET indicates the occurrence of retrogressive reactions. Although TET is often used as a hydrogen-donating solvent in the study of coal liquefaction above 350℃, this result indicates that TET was little hydrogen-donating like NAP or MNA at the low temperatures. While, in a much stronger hydrogen-donating solvent than TET, i.e., DHA or HHA, the hydrogen donation from the solvent to the coal occurs even at 175℃ and 250℃, resulting in the dissolution reactions, i.e., the decrease of MI and the increase of TS. These dissolution reactions occur more easily at 300℃.

When temperature rises to 300℃, the hydrogen donatability of TET and the reactivity of the coal radicals may increase. So, the retrogressive reaction in TET was suppressed. NAP, which has no donatable hydrogens, gave no suppression of the retrogressive reaction even at 300℃. MNA also gave a similar result as NAP. It should be noticed that LRS is a better solvent than TET in this treatment. It is probably due to the fact that LRS

contains a lot of hydrogenated condensed aromatic compounds which can easily donate hydrogens.

The close relationship between the dissolution yield and the quantity of hydrogen transferred from the solvent to the coal and the decrease of radical concentration after the heat treatment indicated that coal radicals may be responsible for the results observed here. When the radicals are stabilized by the hydrogen donation, the dissolution occurs. While, in a poor hydrogen donating solvent which hardly donate hydrogen to the radicals, retrogressive reactions such as the addition to aromatic rings of coal network and coupling reactions between them may occur. It is not clear that the radicals, which are responsible for the dissolution and retrogressive reaction, are formed by the scission of weak covalent bonds and/or indigenous radicals activated by heat at 175-300℃. The fact that the extent of the dissolution reaction increased with the heat treatment time up to 1 h suggests that the dissolution reactions are rather slow. So, the radicals may be formed by slow bond scissions, not indigenous ones, since the thermal activation of the latter radicals seems to be a rapid process. There are several kinds of weak covalent bonds which break at these low temperatures. For example, it is well known that as the number of phenyl groups replacing hydrogen atoms in ethane increases, its central C-C bond strength markedly decreases, and pentaphenylethane readily dissociates into the triphenylmethyl and diphenylmethyl radicals below 100℃. Stronger bonds than described above are possibly broken by solvent-mediated hydrogenolysis proposed by Malhotra and McMillen(5).

Finally, it should be noted that the results above described were obtained by the use of the CS_2-NMP mixed solvent as an extraction solvent for the reaction mixture. If THF is used as an extraction solvent instead of the mixed solvent, we can only see small change of TS by the heat treatments carried out here.

CONCLUSIONS

Heat treatments of Zao Zhuang and Upper Freeport coals were carried out in several hydrogen-donating solvents at 175-300℃ under N_2 atmosphere. Retrogressive reaction of the coal was observed in TET at temperatures as low as 175-250℃. While, in DHA or HHA, which are much stronger hydrogen donors than TET, the coal underwent dissolution reactions at 175-300℃. The quantity of hydrogen transferred from the solvents to coals was found to be well correlated with the degree of the dissolution reactions, and spin concentration in coal components decreased after the dissolution reactions, suggesting hydrogen donation to coal radicals in this heat treatment.

ACKNOWLEDGEMENT

The authors thank NEDO(New Energy and Development Organization, Japan) for providing LRS sample used in this research. This work was supported by a Grant-in Aid for Energy Research from Ministry of Education, Science and Culture, Japan.

REFERENCES

(1) Iino,M.; Takanohashi,T.; Ohsuga,H.; Toda, K. *Fuel* 1988, *67*, 1639-1647.
(2) Iino,M.; Takanohashi,T.; Obara,S.; Tsueta,H.; Sanokawa,Y. *Fuel* 1989, *68*, 1588-1593.
(3) Wei,X.; Shen,J.; Takanohashi,T.; Iino,M. *Energy Fuels* 1989, *3*, 575-579.
(4) Shen, J.; Takanohashi,T.; Iino, M. *Energy Fuels* 1992, *6*, 854-858.
(5) Malhotra, R.; McMillen, D.F. *Energy Fuels* 1993, *7*, 227-233.

Table 1 Ultimate and Proximate analyses of the coals

	Ultimate analysis (wt%, daf)					Proximate analysis (wt%, db)		
	C	H	N	S	O[a]	VM	Ash	FC
Zao Zhuang	86.9	5.1	1.5	1.6	4.9	28.6	7.4	64.0
Upper Freeport	86.2	5.1	1.9	2.2	4.6	28.2	13.1	58.7

[a]By difference

Table 2 Spin Concentration of Zao Zhuang coal and acetone-insoluble fraction(AI) of coal components after the heat treatment in HHA

	heat treatment (HHA, 1 h)	yield[a] (wt %, db)	spin concentration (10^{19} spin / g, daf)
raw coal	-	-	2.34
AI	175 °C	96.3	2.04
AI	250 °C	94.4	1.68
AI	300 °C	89.8	0.91

[a] Based on the raw coal

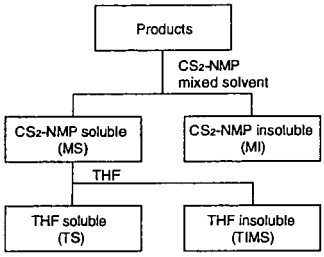

Figure 1 Extraction and fractionation procedures for the heat treatment mixture.

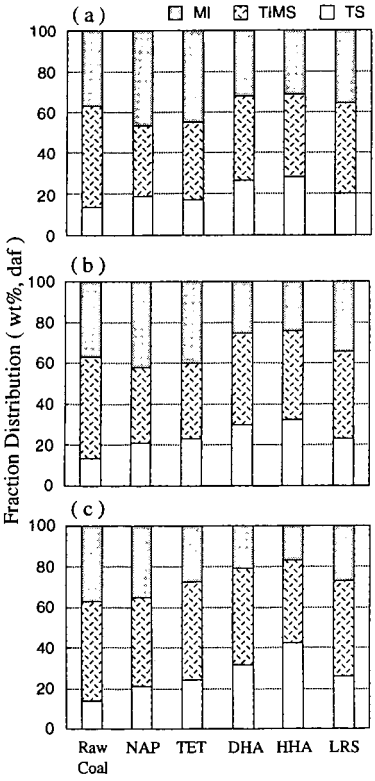

Figure 2 Fraction distribution after the heat treatment of Zao Zhuang coal in NAP, TET, DHA, HHA and LRS at 175℃(a), 250℃(b) and 300℃(c) for 1h, together with that for the raw coal.

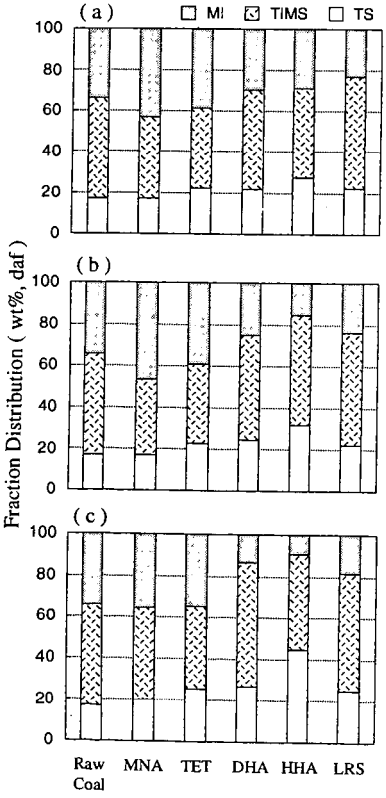

Figure 3 Fraction distribution after the heat treatment of Upper Freeport coal in MNA, TET, DHA, HHA and LRS at 175℃(a), 250℃(b) and 300℃(c) for 1h, together with that for raw coal.

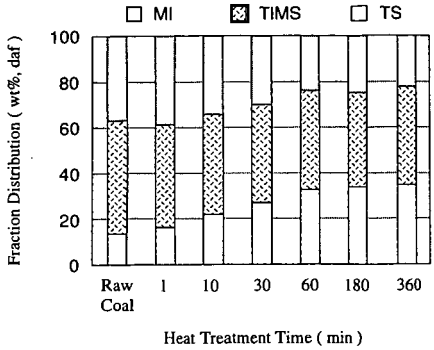

Figure 4 Fraction distribution after the heat treatment of Zao Zhuang coal in HHA at 250℃ for 1-360 min, together with that for the raw coal.

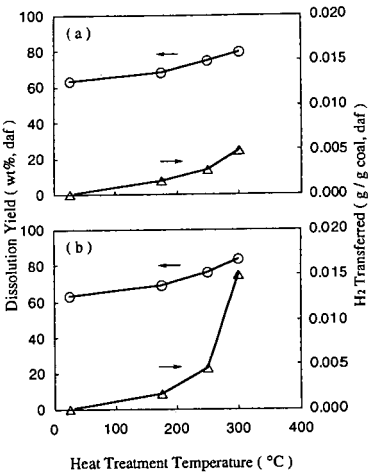

Figure 5 Plots of dissolution yield(○) and H_2 transferred(△) with heat treatment temperature for Zao Zhuang coal in DHA(a) and HHA(b) for 1h.

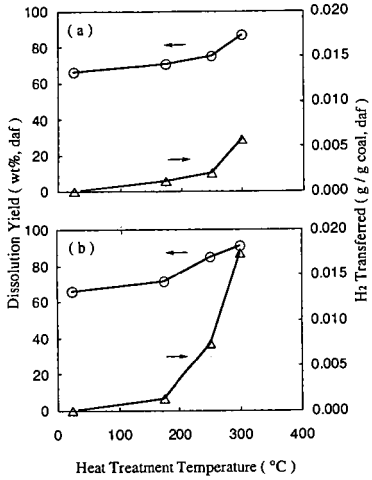

Figure 6 Plots of dissolution yield(○) and H_2 transferred(△) with heat treatment temperature for Upper Freeport coal in DHA(a) and HHA(b) for 1h.

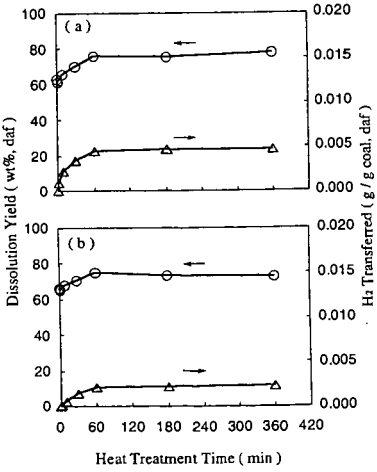

Figure 7 Plots of dissolution yield(○) and H_2 transferred(△) with heat treatment time for Zao Zhuang coal in HHA(a) and Upper Freeport coal in DHA(b) at 250℃.

SUBSTITUENT EFFECTS ON C-H BOND STRENGTHS OF THE BENZYLIC POSITIONS IN COAL-MODEL COMPOUNDS: EFFECTS OF SULFUR, OXYGEN, NITROGEN AND AROMATIC MOIETIES ON THE STABILITIES OF RADICALS.

Mikhail Alnajjar,*,[1] Gerald Gleicher,[2] James Franz,[1] Scott Truksa,[2] Xian-Man Zhang,[3] and Frederick Bordwell,[3]. [1]Pacific Northwest Laboratory, P. O. Box 999, Richland, Wa USA 99352-0999 [2]Department of Chemistry, Oregon State University, Corvallis, OR USA 97331-4003 and the [3]Department of Chemistry, Northwestern University, Evanston, IL USA 60201

Key Words: Coal-Model Compounds, BDEs, Thermochemical Cycle

Abstract: Incorporation of equilibrium acidities of week acids (A-H) and the oxidation potentials of their conjugate bases (A^-) in a thermochemical cycle enable accurate determination of the effects of substituents on bond dissociation energies (BDEs) of the adjacent C-H bonds. Substraction of these (BDEs) from the BDE of methane provided a measure of the radical stabilization energies (RSEs) for the corresponding radicals relative to that of methyl radical. In this study, we have examined the effects of sulfur, oxygen, nitrogen, aromatic and coal-model structures on RSEs in RX(CH·)**A**, where the acceptor function (**A**) is phenyl, fluorenyl and PhC(O). For the heteroatom substituents with **A** equal to PhC(O), RSEs follow the trend: N > S = O). Substitution of phenyl group stabilizes the adjacent carbon radical by 10.5 kcal/mole (referred to hereafter as kcal). Naphthyl, phenanthrenyl, and 9-anthracenyl substituents provided less stabilization to the radical center than a phenyl group. Explanations are given for the difference in stabilities of these radicals and of other types of radicals studied.

Introduction: The effects of electron donors and electron acceptors on the stability of an attached carbon radical center have been well recognized. The electron donor and acceptor groups often stabilize the radical to an extent greater than would be expected on the basis of the individual contributions of both substituents.[4-8] The terms push-pull resonance,[5] merostabilization,[6] and captodative[7] have been used to describe the extra stabilization that results from the presence of both donor and acceptor groups. Kinetic data and theoretical calculations have been used to support as well as deny the existence of substituent effects on radical stabilities.[9,10] Viehe and his co-workers[7] have concluded on the basis of electron spin resonance data and qualitative theoretical interpretation that the effects are always synergistic. However, the recent results of theoretical calculations by Pasto[10] cast doubt on the existence of the captodative phenomenon and suggest that the effects will vary depending on the nature of the donors and acceptors.

The discrepancies outlined above demonstrate the difficulties in obtaining BDEs and in establishing the existence of synergistic stabilization that results from the interactions between the unpaired electron of the radical and the adjacent substituents. The measurement of homolytic bond dissociation energies have been proven to be difficult[11,12] even in the simplest of molecules.[13-15] The values of the C-H bond strengths of labile systems are even more scarce. For example, the homolytic bond dissociation energies and the thermochemistry associated with labile high molecular weight hydrocarbons and sulfur-containing organic structures important to coal are lacking because these systems are inappropriate for the most common gas-phase techniques.

Recently, we have used an electrochemical method[16-20] to estimate BDEs of the acidic H-A bonds in weak acids (eq. 1).

$$BDE = 1.37pK_{HA} + 23.1E_{ox}(A^-) + 73.3 \qquad (1)$$

The method requires that the acids be strong enough to allow acidity measurements to be made in DMSO solution. Equation (1) is based on a thermochemical cycle[17,18] in which the factors **1.37** and **23.1** are used to convert pK_{H-A} units and oxidation potential (eV) units to kcal/mol. The constant

73.3, relates the free energies in solution to gas-phase $\Delta H°$ values, and is made up of the free energies of formation (ΔG°_{f}) and solvation (ΔG°_{s}) of the hydrogen atom, the free energy of proton transfer (ΔG°_{t}) from water to DMSO, and $T\Delta S°$ for the reaction of RH ---> R· + H·. The oxidation potential values of the conjugate bases (A^-) are obtained from cyclic voltammetric measurements in dilute DMSO relative to ferrocene/ferrocenium ion. This electrochemical method is very powerful as it provides BDEs for large numbers of compounds that otherwise would be difficult or impossible to obtain. Also, the effects of electron donor (**D**) and acceptor (**A**) groups attached to a radical center can now be accurately determined. The experimental conditions used are very mild[16], so that the BDEs of acidic C-H bonds of thermally labile molecules can be easily estimated.

In this paper we have obtained quantitative experimental estimates of the size of radical stabilization energies (RSEs) of radicals of the type **D-(CH·)-A** and **D_2-(C·)-A** from the homolytic bond dissociation energies of the C-H bonds in α-substituted acetophenones by using eq. 1. These BDEs provide good estimates of the RSEs, relative to the stability of the methyl radical (BDE of C-H in CH_4 is 105 kcal).[11] For example, the BDEs of the acidic C-H bond in $PhCOCH_2Me$ and $PhCOCH_2OMe$ are 88 and 81 kcal respectively, and that of the acidic C-H bond in acetophenone is 93 kcal. Therefore, the RSE of the $PhCOCH_2(\cdot)$ radical is estimated to be 12 kcal, and the RSEs estimated for PhCOCH(·)Me and PhCOCH(·)OMe radicals are 17 and 24 kcal respectively. This means that the presence of the methyl and methoxy groups has increased the stability of the $PhCOCH_2(\cdot)$ radical by 5 and 12 kcal respectively. We have also examined the effects of aromatics, sulfur and other heteroatoms on the donor-CH-acceptor type radicals and have found that, for sulfur functions, the RSEs increased progressively as the acceptors changed along the series: Ph, fluorene and PhCO. Most of the polyaromatic substituents were studied with the acceptor being PhCO. The RSE reached the minimum when the α-substituent was 9-anthracenyl system, presumably due to the large steric inhibition.

Results and Discussion: The radical stabilization energies (RSEs)[21] of carbon-centered radicals attached to sulfur, oxygen and nitrogen groups are presented in Table I. Our study of the effects of heteroatom substitution on homolytic bond dissociation energies provides new bond strengths and new insights into structural features controlling stabilization energies.

RSEs for PhCH(·)-SPh. Examination of the data in Table I (entry 2) shows that the BDE of the acidic C-H in $PhCH_2$-SPh is 84 kcal. This value was estimated by the combination of the pK_{HA} of $PhCH_2$-SPh and the E_{ox} of the conjugate base using eq. 1. Comparison with the known BDE value for toluene (88), leads to 4 kcal extra stabilization relative to the $PhCH_2(\cdot)$, or 21 kcal compared to the $CH_3(\cdot)$ radical.[22] The sum of the RSEs for the $PhSCH_2(\cdot)$ radical (12 kcal, 105 -93) and $PhCH_2(\cdot)$ radical (17 kcal, 105 - 88) is 8 kcal larger than the RSE of PhCH(·)-SPh (29 vs. 21 respectively).

RSE for 9-PhS-Fl(·). Entry 5 of table I shows that the PhS group has a larger radical-stabilizing effect (2 extra kcal) on the fluorenyl radical (Fl·) than on the benzyl radical (compare entries 2 and 5). It is surprising to observe such behavior since Fl· is supposed to be stabilized more than benzyl radical by delocalization. Because of this inherent stabilization of Fl· radical, one would expect that the stabilizing power of the sulfur atom be less in the fluorenyl system than in the benzyl system.[23] The extra stabilization of the PhS-substituted Fl· may be explained by virtue of contributor **I**.

9-PhS-Fl(·) <--------> 9-PhS$^{+\cdot}$-Fl($^-$)
(**I**)

RSEs for PhS-CH(·)COPh: The BDE of the C-H bond in PhS-CH_2COPh is 81.5 kcal. The RSE for the corresponding

radical is 23.5 kcal relative to $CH_3(\cdot)$ radical. The value of 23.5 kcal is 0.5 kcal lower than the combined RSEs for $PhSCH_2(\cdot)$ and $(\cdot)CH_2COPh$ radicals (24 kcal, 12 + 12). Table I shows clearly that RSEs for sulfur containing radicals increase progressively as the acceptors change along the series: Ph, fluorene (Fl), and COPh with the latter being the most stabilizing acceptor (12 kcal relative to acetophenone). The special electronic effects of the carbonyl in combination with the sulfur substituents is probably due to the conjugative and electrostatic interactions between the negatively charged oxygen and the positively charged sulfur (**II**). However, the RSEs of PhSCH(·)-**A** radicals are always smaller than the sum of the RSEs estimated from the individual radicals {$PhSCH_2(\cdot)$ and $(\cdot)CH_2$-**A**}.

$$PhSCH(-)\text{-}COPh \xrightarrow{-e^-} PhSCH(\cdot)COPh \longleftrightarrow \underset{\textbf{(II)}}{PhS^{+\cdot}CH = CO(^-)Ph}$$

The effect of a second PhS substitution into already doubly substituted methane (entries 3, and 9) is negligible. The small decrease in BDE compares well with the third phenyl substitution into methane (ΔBDE = 1 kcal) and is probably due to a large steric effect.[11,16]

Also from Table I, it is evident that the alkyl or aryl groups attached to the sulfur are not exerting any appreciable effects on the radical center connected to the sulfur atom (compare entries 5 & 6, and 8 & 10). The sulfur atom appears to act as an insulator thereby preventing the conjugation between the radical center and the group attached to the sulfur donor.

RSEs for MeO-CH(·)COPh and c-C_5H_{10}NCH(·)COPh: The acidic C-H bonds in $MeOCH_2COPh$ and c-$C_5H_{10}NCH_2COPh$ are 81 and 72 kcal respectively, giving RSEs of 24 and 33 kcal (Table I, entry 11 and 12). The RSEs for the corresponding radicals are equal to the sum of the RSEs of the individual radicals, indicating the apparent absence of synergism in the systems studied.

α-Substituent effects on BDEs of the α-C-H bond in acetophenone: In table I we saw that the introduction of phenylthio group into the α-position of acetophenone causes a 11.5 kcal increase in RSE of $PhCOCH_2(\cdot)$ radical. However, in table II (entries 2-6) we see that the introduction of a phenyl, naphthyl, phenanthrenyl, or anthracenyl substituent causes a smaller increase in RSE. The 9-anthracenyl substituent (entry 7) gave the smallest increase probably because of the greater steric and stereoelectronic demands of the 9-anthracenyl than the PhS and the other aryl groups. Furthermore, the role of a polar contributor must be larger for the PhS to show greater ability than the aryl groups in stabilizing the phenylacetyl radical. For example, contributor (**III**) dominates over contributor (**IV**) due to the electrostatic interaction between the sulfur and the oxygen atoms. The Ph group is less effective in this delocalization because contributor (**IV**) is higher in energy due to the loss of aromaticity of the phenyl ring. Substitution of an α-hydrogen in acetophenone by a pyrenyl group lowers the BDE of the α-C-H bond by 12.5 kcal (entry 8). This increase in RSE, compared to the other aromatic systems, is attributed to the delocalization of the unpaired electron into the larger pyrenyl moiety, an effect comparable in magnitude to that of aryl methyl radicals.[24]

$$\textbf{PhS}\text{-}CH(\cdot)\text{-}COPh \longleftrightarrow \underset{\textbf{(III)}}{\textbf{PhS}^{+\cdot}\text{-}CH = CO(^-)Ph}$$

$$\textbf{Ph}\text{-}CH(\cdot)\text{-}COPh \longleftrightarrow \underset{\textbf{(IV)}}{\textbf{Ph}^{+\cdot}\text{-}CH = CO(^-)Ph}$$

Remote substituent effects on BDEs of the α-C-H bond in ketones: The BDEs of acetone, acetophenone, p-methyl-, p-methoxy-, p-cyano-acetophenone are also presented in table II. Examination of entries 9-13 show that remote electron donating and electron accepting groups make the

ketone less or more acidic, but have no effect on BDE's of the α-C-H bonds. The changes in acidities of the ketones are offset in eq.1 by shifts of $E_{ox}(A^-)$ to less or more positive potentials. The result is no change in BDE. This observation indicates that the remote substituent is not interacting directly with the incipient radical to provide additional stabilization.

Chromium tricarbonyl effect on BDE of the α-C-H bond in phenylacetophenone: We have shown so far the effectiveness of eq.1 in estimating the BDEs of the acidic α-C-H bonds in substituted acetophenones. We now extend our studies to chromium tricarbonyl complex of α-phenylacetophenone. The π-coordination of $Cr(CO)_3$ to benzene ring attached to the α-position is conclusive based on the NMR data. Our objective here is to obtain the first quantitative information concerning the effect of transition metal complexes on the pK_{AH} values and BDEs of the acidic C-H bonds. Entry 14 of table II shows that $Cr(CO)_3$ group increases the acidity of the α-C-H bond by 4.7 pK units (6.3 kcal; compare entries 2 & 14). This large increase is probably due to the field and inductive effects of the three carbonyl groups attached to the chromium atom. Similar acidity effects were observed when $Cr(CO)_3$ was π-coordinated to benzoic and phenylacetic acids.[25] The oxidation potential of the complex anion is less negative than that of the parent compound giving once again no net change in BDE.

Conclusion: Homolytic bond dissociation energies in DMSO for α-C-H bonds in aryl, sulfur-, oxygen-, and nitrogen-containing compounds have been measured using pK_{HA} and $E_{OX}(A^-)$ data in eq 1. In every case, the radical stabilization energies (RSEs) of RXCH(·)-**A** are always equal or smaller than the sum of RSEs of the two radicals. The increase in RSEs for sulfur group along the series: Ph, Fl, and COPh, is in correspondence with the ability of the acceptor to stabilize the negative charge on carbon for contributor of the type **PhS**$^{+\cdot}$-CH = CO($^-$)Ph. Remote electron withdrawing, electron accepting and $Cr(CO)_3$ groups have little or no effects on BDEs of the acidic α-C-H bonds indicating that these groups do not interact directly with the unpaired electron situated on the carbon radical center.

References and Notes:

1. Supported by the Office of Basic Energy Sciences, U. S. Department of energy, under contract DE-AC06-76RL0 1830.
2. Same as in 1.
3. Supported by the Donors of Petroleum Research Fund administered by the American Chemical Society, and by National Science Foundation.
4. (a) Bausch, M. J.; Guadalupe-Fasano, C.; Peterson, B. M. J. Am. Chem. Soc. **1991**, 113, 6384. (b) Crans, D.; Clark, T.; Schleyer, P. V. R. Tetrahedron Lett. **1980**, 3681.
5. Negoita, N.; baican, R.; Balaban, A. T. Tetrahedron Lett. **1973**, 1877.
6. (a) Baldock, R. W.; Hudson, P.; Katritzky, A. R.; Soti, F. J. Chem. Soc., Perkin Trans. 1, **1974**, 1422. (b) Katritzky, A. R.; Soti, F. Ibid, **1974**, 1427.
7. (a) Viehe, N. C.; Mer'enyi, R.; Stella, L.; Janousek, Z. Angew. Chem., Int. ed. Engl. **1979**, 18, 917. (b) Viehe, H. G.; Janousek, Z.; Mer'enyi, R.; Stella, L. Acc. Chem. Res. **1985**, 18, 148.
8. Dewar, M. J. S. J. Am. Chem. Soc. **1952**, 74, 3353.
9. Korth, H. G.; Sustmann, R.; Merenyi, R.; Viehe, H. G. J. Chem. Soc., Perkin Trans. 2, **1983**, 67.
10. Pasto, D. J. J. Am. Chem. Soc. **1988**, 110, 8164.
11. McMillen, D. F.; Golden, D. M. Annu. Rev. Phys. Chem. **1982**,33, 493.
12. Castelhano, A. L.; Griller, D. J. Am. Chem. Soc. **1982**, 104, 3655.
13. Coa, J.-R.; Back, M. H. Int. J. Chem. Kinet. **1984**, 16, 961.
14. Islam, T. S. A.; Benson, S. W. Int. J. Chem. Kinet. **1984**, 16, 995.
15. Tsang, W. J. Am. Chem. Soc. **1985**, 107, 2872.

16. Bordwell, F. G.; Cheng, J. P.; Harrelson, J. A. J. Am. Chem. Soc. **1988**, 110, 1229.
17. Friedrich, L. E. J. O. Chem. **1983**, 48, 3851.
18. Nicholas, A. M. P; Arnold, D. R. Can. J. Chem. **1982**, 60, 2165.
19. Bordwell, F. G.; Zhang, Xian-Man.; Alnajjar, M. J Am. Chem. Soc. **1992**, 114, 7623.
20. Bordwell, F. G.; Bausch, M. J. J. Am. Chem. Soc. **1986**, 108 , 2473.
21. The radical stabilization energies are defined as RSE = ΔBDE = BDE(A-CH_2-H) - BDE(A-CH_2-D), where A and D are the acceptors and the donors respectively.
22. The BDE of CH_3-H = 105 kcal[3]. The RSE of PhCH(·)-SPh relative to methyl radical is 21 kcal (105 - 84).
23. Katritzky, A. R.; Zerner, M. C.; Karelso, M. M. J. Am. Chem. Soc. 1986, 108, 7213.
24. Herndon, W. C. J. Org. Chem. **1981**, 46, 2119.
25. Nicholls, B.; Whiting, M. C. J Chem. Soc. **1959**, 551.

Table I. Acidities and Bond Dissociation Energies (BDEs) for the α-C-H Bonds in Heteroatom-Containing Systems.

Entry	Substrates	pK_{HA}[a]	$E_{ox}(A^-)$[b]	BDE[c]	RSE[g]
1.	$PhCH_2$-H			88[d]	0.0
2.	$PhCH_2$-SPh	30.8	-1.353	84	4
3.	$PhCH(SPh)_2$	23.0	-1.000	82	6
4.	H-FL-H	22.6	-1.064	80	0.0
5.	9-PhS-FL-H	15.1	-0.860	74[e]	6
6.	9-MeS-FL-H	18.0	-1.015	74.5	5.5
7.	H-CH_2COPh	24.7	-0.607	93	0.0
8.	PhS-CH_2COPh	17.1	-0.660	81.5[f]	11.5
9.	$(PhS)_2$-CHCOPh	12.0	-0.370	81	12
10.	PrS-CH_2COPh	19.9	-0.850	81	12
11.	MeO-CH_2COPh	22.9	-1.030	81	12
12.	c-$C_5H_{10}NCH_2$COPh	23.5	-1.439	72	21

[a]Measured in DMSO against two indicators. [b]In volts; irreversible oxidation potentials (E_p) measured in DMSO by cyclic voltammetry and referenced to the ferrocene/ferrocenium couple. [c]Calculated(in kcal/mol)using eq 1. [d]Radical stabilization energy(RSE = 17 kcal/mol)relative to CH_3-H(BDE = 105 kcal/mol). [e]Relative to H-FL-H(BDE = 80 kcal). [f]Relative to $PhCOCH_2$-H(BDE = 93 kcal). [g]RSE = ΔBDE.

Table II. Acidities and Bond Dissociation Energies (BDEs) for the α-C-H Bonds in Ketones.

Entry	Substrates	pK_{HA}[a]	$E_{ox}(A^-)$[b]	BDE[c]	RSE[f]
1.	$PhCOCH_3$	24.7	-0.607	93	0.0
2.	$PhCOCH_2Ph$	17.7	-0.650	82.5	10.5
3.	$PhCOCH_2$Naph-1	17.6	-0.626	83	10.0
4.	$PhCOCH_2$Phen-3	17.2	-0.576	83.5	9.5
5.	$PhCOCH_2$Phen-9	17.5	-0.597	83.5	9.5
6.	$PhCOCH_2$Anth-1	17.2	-0.625	82.5	10.5
7.	$PhCOCH_2$Anth-9	18.9	-0.635	84.5	8.5
8.	$PhCOCH_2$Py-1	15.7	-0.618	80.5	12.5
9.	CH_3COCH_3	26.5	-0.674	94	0.0
10.	$PhCOCH_3$	24.7	-0.607	93[d]	1.0
11.	p-$MePhCOCH_3$	25.0	-0.597	94	0.0
12.	p-$MeOPhCOCH_3$	25.7	-0.657	93	1.0
13.	p-$CNPhCOCH_3$	22.0	-0.436	93	1.0
14.	$PhCOCH_2Ph$ $\pi Cr(CO)_3$	13.1	-0.377	82.5	10.5

For [a], [b], and [c]See footnotes in table I. [d]Relative to acetone (BDE = 94 kcal). [e]Relative to $PhCOCH_2$-H(BDE = 93 kcal). [f]Radical stabilization energy (RSE).[21]

SOLUTION PHASE REACTIONS OF ATOMIC HYDROGEN[1]

Dennis D. Tanner
Department of Chemistry, University of Alberta
Edmonton, Alberta, Canada T6G 2G2

Key words: Hydrogen atoms, olefins, arenes, organosulfur compounds.

INTRODUCTION

We have recently developed a method for studying the reactions of hydrogen atoms in solution. The hydrogen atoms are generated in a flow system at 3 torr by a microwave discharge (2540-MHz) to produce a plasma of H_2 and He or H_2 alone (see Fig. 1).

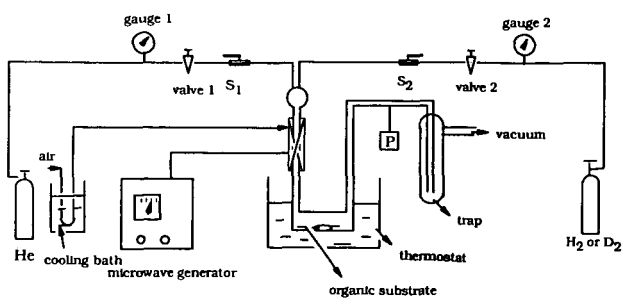

Fig. 1. Diagram of the Apparatus Used for the Generation of Atomic Hydrogen

The discharge gases are passed over a stirred solution of the substrate. Reactions take place and produce thermolyzed intermediates. The correlation of the products produced from these intermediates with the structure of the reactants yields fundamental and potentially useful information.

The reactions are efficient and surprisingly selective. Qualitatively the reaction rates follow the order:

disulfides > sulfides > olefins > aromatics > alkanes

Reactions with Olefins - Hydrogen or deuterium atoms produced from hydrogen or molecular deuterium in the cavity of a microwave generator were allowed to react with two olefins: 1-octene and 1-methylcyclohexene. A detailed mechanism for the formation of the products, both monomers and dimers, was determined. The addition reactions were regioselective, >99% addition to the terminal carbon of 1-octene and >99% to the secondary carbon of 1-methylcyclohexene. No products from allylic abstraction were detected. The product ratios for the addition of deuterium and protium were the same, see Tables 1 and 2.

[Table 1 and 2]

The disproportionation to combination ratios (k_d/k_c) of the 1-methylheptyl and 1-methylcyclohexyl radicals were determined at several temperatures. The extrapolated ratios were found to be in good agreement with the literature values reported for reactions studied at room temperature.

The 1-methyl-5-hexenyl radical formed by the addition of a hydrogen atom to the terminal position of 1,6-heptadiene led to a complex mixture of products resulting from open chain and cyclized radicals, see Table 3.

[Table 3]

The cyclized radicals were formed reversibly and the final product mixture contained only minor amounts of *cis*-1,2-dimethylcyclopentane (the product of kinetic control) while the major cyclized product was methylcyclohexane. Although an equilibrium mixture could not be obtained the dimethylcyclopentyl and 3-methylcyclohexyl radicals were shown to be formed reversibly, see Scheme 1.

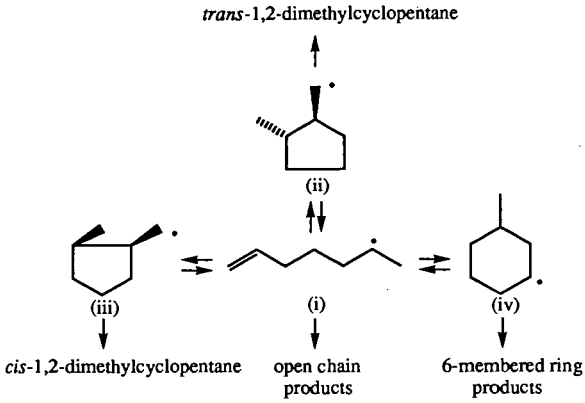

Scheme 1

Reactions with Sulfides and Disulfides - The reactions of hydrogen atoms with a series of unsymmetric disulfides were carried out. The regioselectivities and mechanisms of the reactions were investigated. The primary products of the reactions are thiol and thiyl radicals. The symmetric disulfides in the product mixtures were formed at -78°C by radical combination reactions, and not by radical displacements on the unsymmetric disulfides. The displacement, which favors attack of hydrogen on the least hindered sulfur is proposed to involve a metastable trivalent sulfur intermediate. The reactions of hydrogen atoms with a series of unsymmetric sulfides were carried out. A mechanism was proposed in which atomic hydrogen adds to the sulfur and forms an intermediate. The cleavage of the intermediate favors the most stable radical.

Reactions with Arenes[2] - When hydrogenation atom promoted sidechain fragmentation of arenes was investigated it was concluded that addition to the aromatic ring was reversible but that when ipso-attack occurs alkyl radical fragmentation may take place. Saturation of the ring is competitive with reversal or sidechain fragmentation. Polymerization of the arenes occurs even at 135°C. The model compounds studied were: toluene, bibenzyl, 9-dodecylanthracene and dodecylbenzene.

ACKNOWLEDGMENT: We wish to thank the Natural Sciences and Engineering Research Council of Canada, the University of Alberta and the Department of Energy, Mines and Resources - CANMET for their generous support of the work.

LITERATURE CITED

1. Taken in part from the Ph.D. dissertation of Liying Zhang, University of Alberta, 1994.
2. Taken in part from the CANMET Final Report on "Low Temperature Hydrogenation of Bitumen Vacuum Reside and Syncrude Products Using Microwave Generated Hydrogen Free Radicals", 1993.

Table 1. The products, yields and mechanisms for the reaction of H• with 1-octene (-78°C)[a]

Products	Yield (%)	Mechanism[c]
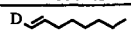	17.1	addition-disproportionation
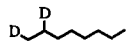	26.9	addition-addition
	30.8	addition-disproportionation
	2.8	addition-disproportionation
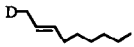	9.1	addition-disproportionation
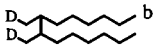	11.8	addition-dimerization
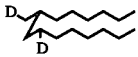	1.4	addition-radical addition

[a] Neat 1-octene.
[b] A (1:1) mixture of *meso*- and *d,l*-dimers.
[c] Monodeuterated alkane/monodeuterated alkene = 1.
[d] k_d/k_c = 2.4 at -78°C.

Table 2. The products, yields and mechanisms for the reaction of H• with 1-methylcyclohexene (-78°C)[a,b]

Products	Yield (%)	Mechanism[d]
	15.3	addition-disproportionation
	7.9	addition-disproportionation
	20.2	addition-addition
	39.4	addition-disproportionation
	15.3	addition-disproportionation
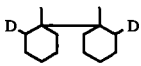	1.5	addition-dimerization
other[c]	0.5	addition-dimerization

[a] Neat 1-methylcyclohexene.
[b] Monodeuterated alkane/monodeuterated alkene = 1.
[c] Five dimeric products.
[d] k_d/k_c = 26.2.

Table 3. Reaction of D• with 1,6-Heptadiene[a,b]

	Product %	Proposed Mechanism[c]
	12.5	D atom addition - disproportionation
	26.3	D atom addition - disproportionation
	8.7	D atom addition - D atom addition
(*trans-* + *cis-*)	11.4	D atom addition - disproportionation
	6.0	D atom addition - cyclization - D atom addition
	5.3	D atom addition - cyclization - disproportionation
	3.9	D atom addition - cyclization - disproportionation
	7.0	D atom addition - cyclization - D atom addition
	5.8	D atom addition - cyclization - disproportionation
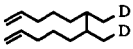 (*d,l-* and *meso-*, 1:1)	13.1	D atom addition - combination

[a] Concentration in acetone (0.16 M).
[b] Conversion = 3.1%.
[c] $P_6/P_5 = 1.46$ (six membered ring/five membered ring products); monodeuterated alkane/monodeuterated alkene; $k_d/k_c = 2.3$ (-78°C).

THERMODYNAMIC AND KINETIC EVALUATIONS OF RADICAL STABILITIES

M.J. Bausch, David Autry, Carlos Garcia, Yong Gong, Rudy Gostowski, and Weixing Li
Department of Chemistry and Biochemistry
Southern Illinois University at Carbondale, Carbondale IL 62901

Key words: free radicals, substituent effects, dimerization kinetics

Abstract When inserted into appropriate thermochemical cycles, redox data have proven invaluable in the studies of heterolytic and homolytic bond strengths. Judicious use of microelectrode-based cyclic voltammetry also enables determinations of the rates of degradation for several classes of solution phase reactive intermediates. Described in this paper are (a) new bond strength results from our group that shed light on the effects of ß-substituents on the thermodynamic stabilities of various carbon- and nitrogen- centered radicals; and (b) recent evaluations of second-order rate constants for dimerization reactions of electrochemically-generated carbon-centered radicals.

Introduction

It has been shown that insertion of selected acid-base[1] and redox data into thermochemical cycles[2] (as in eq 1[3]) results in accurate (±1-2 kcal/mol) determinations of relative and absolute

$$\Delta G^{\circ}_{hom}(R\text{–}H) = 1.36pK_a(R\text{–}H) + 23.1[E_{NHE}(R^{-}/R\bullet)] + 57.2 \text{ kcal/mol} \quad (1)$$

free energies of homolysis[3] [ΔG°_{hom}(R–H)] for several classes of reactions.[4] For example, we have shown that the C–H homolytic bond dissocation energies for phenalene (**1**) and its isomeric

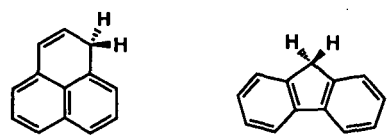

1 **2**

analogue fluorene (**2**) are 65 and 80 kcal/mol, respectively.[5] These data are of interest due to the persistence of the planar phenalenyl radical, as well as the continuing interest in polycyclic aromatic chemistry.

In other published work, evidence for the importance of charge separation as it pertains to radical stabilization was provided from studies of the effects of electron-withdrawing and electron-donating moieties on #9C–H anthrylmethyl homolytic bond strengths, for the substituted anthracenes (**3**) depicted below. Specifically, while the singular presence of G=CN, or G'=PhO,

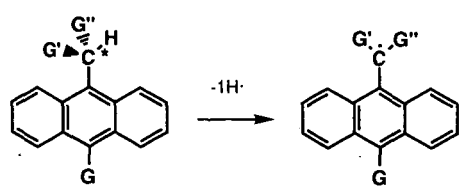

3

weakens the indicated (*) bond by ca. 1.5 and 3 kcal/mol, respectively, the simultaneous presence of these substituents weakens the same bond by ca. 9 kcal/mol.[6] These results provided support for the idea that appropriately substituted solution-phase radicals can be stabilized *via* delocalization of the unpaired electron even when that delocalization results in some charge separation.[6]

Results and Discussion

N-H Bond Strengths

In light of the importance of nitrogen in the chemistry of coal, we have therefore endeavored to collect the pK_a (R–H) and $E_{NHE}(R^-/R\bullet)$ data that enable determination of the ΔG°_{hom}(R–H) values for several variously substituted perimidines (**4**), a nitrogen analogue of

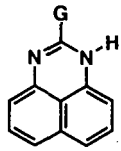

4

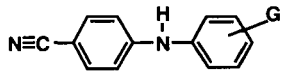

5

phenalene, as well as several diphenylamine analogues (**5**). The bond strengths for **4** shed important light on the effects of ß-substituents on N–H bond strengths, while the analogous data for **5** provide new insights into the effects of aryl substituents on N–H bond strengths. The acidity and bond strength data are listed in Tables I and II.

ß-Effects on N–H Bond Strengths Inspection of the acidity data in Table I reveals that ß-substituents have relatively large effects on N–H equilibrium acidities. For example, 2-methylperimidine (pK_a=17.2) is ca. 8 kcal/mol less acidic than 2-chloroperimidine (pK_a=11.4). The magnitude of the acidifying effects of the ß-substituents is surprising since there we are not aware of the existence of resonance contributing structures in which formal negative charge is present on the sp^2-hybridized #2-carbon atom. It is also of interest to compare the C–H pK_a for phenalene (18.2[5]) with the N–H pK_a for perimidine (16.2). The 2 pK unit greater acidity of the nitrogen analogue is not surprising in light of the pK_a's for fluorene (22.6) and carbazole (19.9),[1] and is readily explained by the greater electronegativity of nitrogen, compared to carbon.

Examination of the ΔG°_{hom}(R–H) data for the substituted perimidines reveals that the substituent effects on homolytic bond strengths are substantially smaller (by a factor of three) than the substituent-induced variation in the pK_a's for the same species. These results are consistent with a hypotheses which states that inductive (de)stabilizing effects of substituents on radical stabilities are small, compared to the resonance effects of those same substituents. The ΔG°_{hom}(R–H) value for carbazole (88 kcal/mol)[7], when compared to the ΔG°_{hom}(R–H) value for perimidine (75 kcal/mol), is reasonable in light of the ΔG°_{hom}(R–H) values for fluorene and phenalene (76 and 61 kcal/mol, respectively). Both sets of data are consistent with the notion that N–H bonds are generally stronger, in a homolytic sense, than C–H bonds found in structurally similar species.

Remote Substituent Effects on N–H Bond Strengths Inspection of the pK_a and ΔG°_{hom}(R–H) data in Table II reveals that substituents that weaken N–H bonds in **5** in an acid-base sense (i.e. electron-withdrawing substituents such as 4-nitro, 4-cyano, and 3-chloro) strengthen the same N–H bonds in a free radical (i.e. homolytic) sense. Although the pK_a results are readily understood and indicative of planarity in the diphenylamine nitranion (Hammett treatment of the data yields a linear plot with a ρ value of 2.6, r=0.99),[8] the ΔG°_{hom}(R–H) values are perhaps best rationalized by noting the electron-deficient nature of the nitrogen-centered radicals.

In an effort to comprehend the ΔG°_{hom}(R–H) values for **5**, it is instructive to compare the ΔG°_{hom}(R–H) data in Table II with ΔG°_{hom}(R–H) data for (4-nitrophenyl)phenylamine; (4-cyanophenyl)phenylamine; (3-chlorophenyl)phenylamine; diphenylamine; (4-methylphenyl)-phenylamine; and (4-methoxyphenyl)phenylamine (87,[7] 85, 84,[7] 83,[7] 83,[7] and 82[7] kcal/mol, respectively). Here too the acidifying electron-withdrawing substituents appear to strengthen the diphenylamine N–H bond in a homolytic sense. The results therefore suggest that nitranion-stabilizing substituents act to *de*stabilize nitrogen-centered radicals. For both sets of ΔG°_{hom}(R–H) data, a complex interplay of resonance and inductive effects must be considered. Therefore, we are currently investigating the N–H bond strengths for several additional diphenylamines, including ten different nitrodiphenylamines, in an attempt to gain additional understanding of these phenomena.

C-H Bond Strengths

The previous section described results which indicate that more data are needed regarding resonance and inductive effects as they pertain to homolytic bond strengths and radical stabilities. In an effort to separate resonance and inductive effects, we have synthesized and evaluated the

bond cleavage chemistry for 9-(trimethylsilylmethyl)fluorene (**6**) and 9-(cyanomethyl)fluorene (**7**).

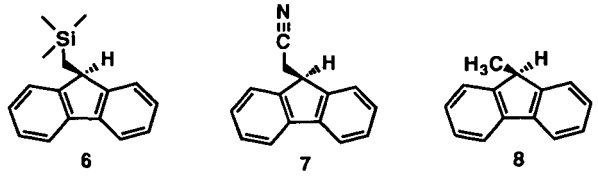

The relevant pK_a and ΔG°_{hom}(R–H) data for **6** and **7**, along with similar data for 9-methylfluorene (**8**), are listed in Table III.

Inspection of the data in Table III reveals that the ß-trimethylsilyl and ß-cyano substituents both acidify 9-methylfluorene. These results are consistent with the notion of an enhanced electron accepting ability for silicon atoms[9] and cyano moieties (relative to hydrogen). On the other hand, comparison of the ΔG°_{hom}(R–H) data for **6**, **7**, and **8** reveals that the electron-withdrawing ß-cyano substituent strengthens the #9C–H bond in fluorene by ca. 2 kcal/mol, while the ß-trimethylsilyl substituent appears to weaken the same bond by about 3 kcal/mol. In other work, we have shown that the ß-trimethylsilylmethyl and ß-cyano substituents have somewhat similar effects on fluorenium *cation* stabilities.[10a] Specifically, ß-trimethylsilylmethyl weakens the #9C–H bond, in a heterolytic cation-hydride forming sense, by 8 kcal/mol (relative to hydrogen), while ß-cyano strengthens the same bond by 3 kcal/mol.[10a] It appears, then, that the inductive and/or hyperconjugative effects of these two ß-substituents on radical stabilities is similar to their effects on carbocation stabilities, in suggesting that (1) electron-withdrawing inductive effects destabilize carbon-centered radicals; and (2) electron-donating hyperconjugative effects stabilize carbon-centered radicals. These results provide additional evidence for rationalizing much of the chemistry of carbon-centered radicals as if they were electron-deficient species. We are currently examining several other ß-substituted organic molecules in an effort to better understand these results.

Kinetics of Radical Dimerizations

A limitation of bond strength data obtained from thermochemical cycles that utilize irreversible redox potentials is that the peak potentials are not truly thermodynamic. This fact introduces some degree of uncertainty in bond strengths obtained using irreversible data. That the irreversible peak potentials (obtained at scan rates of 0.1 V/s) for various nitranion oxidations were nearly equal to the reversible $E_{1/2}$ values (obtained at scan rates of 1,000 V/s) for the same oxidations provided some evidence for the viability of irreversible potentials when used judiciously.[10b] In addition, data obtained using the FSCV technique can be used to derive rate constants for the chemical reactions that follow the initial electrochemical reaction.

For example, shown in Fig 1 are two CV traces for the oxidation of the 9-(2-methylphenyl)fluorenide anion. Examination of Fig 1 reveals that the carbanion oxidation is fully reversible at 1,000 V/s scan rates, but essentially ireversible at 0.1 V/s scan rates. Use of the equations developed by Nicholson and Shain[11] enables evaluation of the velocity of the reaction that removes the electrochemically generated radical from solution (*via* a second-order reaction) prior to its reduction on the reverse scan. With a microelectrode-equipped apparatus, second-order rates as high as 10^8 $M^{-1}s^{-1}$ are accessibile. Listed in Table IV are rates determined in this way for the second order reactions of variously substituted fluorenyl radicals that have been generated anodically at a platinum working electrode.

Steric Effects on Radical Dimerizations Examination of the rate data listed in Table IV reveals that the tertiary 9-methylfluorenyl radical dimerizes[12] at the same rate as the 9-cyanofluorenyl and 9-phenylfluorenyl radicals, since the uncertainty in the rates listed in Table IV is estimated to be ca. ±10%. Significantly, none of these species dimerizes at the diffusion-limited rate in DMSO (estimated at 2×10^9 $M^{-1}s^{-1}$). It is likely that solvation effects and solvent reorganization plays some role in the slight rate retardation.

Comparison of the k_2 values for 9-*tert*-butylfluorenyl and 9-methylfluorenyl radicals (5×10^5 and 3×10^7, respectively) provides direct evidence for the importance of steric effects on radical persistence. Evidently, the sterically demanding 9-*tert*-butyl group slows the dimerization rate by about two powers of ten (compared to 9-methyl), despite the fact that the homolytic bond strength data for these two species indicates that the 9-*tert*-butylfluorenyl radical is about 4 kcal/mol *less stable* than the 9-methylfluorenyl radical.

Furthermore, molecular models as well as bond strength data for 9-phenylfluorene, 9-(2-

methylphenyl)fluorene, and 9-mesitylfluorene [ΔG°_{hom}(R–H)=70, 71, and 72 kcal/mol, respectively] suggest that the presence of *ortho* methyl groups on the #9-phenyl moiety causes the phenyl ring in 9-phenylfluorenyl radicals to twist out of the plane of the fluorene. Kinetic evidence for this assertion is provided in Table IV, since the k_2 values for 9-phenylfluorenyl, 9-(2-methylphenyl)fluorenyl, and 9-mesitylfluorenyl radicals are 1×10^7, 8×10^3, and 1 $M^{-1}s^{-1}$, respectively). These results (i.e. solution-phase dimerization rates for delocalized fluorenyl radicals) are the first of their kind, and provide additional evidence for the notion that radical persistence is largely a kinetic phenomenon that is usually associated with steric hindrance in the immediate vicinity of the unpaired electron. We are continuing studies of the kinetics of dimerization reactions of delocalized carbon-centered radicals, and have also embarked on similar evaluations of the dimerization reactions of delocalized nitrogen-centered radicals.

Experimental Section

DMSO was purified, potassium dimsylate was synthesized, and the pK_a and redox experiments were carried out as described previously.[5,6,10] ΔG°_{hom}(R–H) values calculated as described in Reference 10a. Substrates synthesized as described in references 6, 8, and 10. The PMV device was using specifications described by Griller et al.[14] Reference 12 (submitted to *J. Org. Chem.*) contains experimental details of the FSCV device.

Acknowledgment We are grateful to the United States Department of Energy Office of Basic Energy Science for their financial support of this research. We also are grateful to Dr. Chang-ling Miaw for collecting some of the diphenylamine nitranion redox data. We also are grateful to Dr. D.D.M. Wayner (Steacie Institute for Molecular Sciences) for his advice as it pertained to the set-up and operation of the photo-modulated voltammetry apparatus

References

(1) Bordwell, F.G. *Acc. Chem. Res.* **1988**, *21*, 445-463.
(2) Wayner, D.D.M.; Parker, V.D. *Acc. Chem. Res.* **1993**, *26*, 287-294.
(3) Parker, V.D. *J. Am. Chem. Soc.* **1992**, *114*, 7458-7462.
(4) (a) Bordwell, F.G.; Bausch, M.J.; Wilson, C. *J. Am. Chem. Soc.* **1987**, *109*, 5465-5470. (b) Bordwell, F.G.; Cheng, J.-P.; Harrelson, J. *J. Am. Chem. Soc.* **1988**, *110*, 1229-1231.
(5) Bausch, M.J.; Gostowski, R.; Jirka, G.; Selmarten, D.; Winter, G. *J. Org. Chem.* **1990**, *55*, 5805-5806.
(6) Bausch, M.J.; Guadalupe-Fasano, C.; Peterson, B.M. *J. Am. Chem. Soc.* **1991**, *113*, 8384-8388.
(7) Bordwell, F.G.; Zhang, X.; Cheng, J.-P. *J. Org. Chem.* **1991**, *56*, 3216-3219.
(8) Bausch, M.J.; Li, W. *J. Org. Chem.* submitted.
(9) On theoretical grounds: Stang, P.J.; Ladika, M.; Apeloig, Y.; Stanger, A.; Schiavelli, M.D.; Hughey, M.R. *J. Am. Chem. Soc.* **1982**, *104*, 6852-6854. From gas phase experiments: Wetzel, D.M.; Brauman, J.I. *J. Am. Chem. Soc.* **1988**, *110*, 8333-8336.
(10) (a) Bausch, M.J.; Gong, Y. *J. Am. Chem. Soc.* in press. (b) Bausch, M.J.; Gostowski, R. *J. Org. Chem.* **1991**, *56*, 6260-6262.
(11) Nicholson, R. S.; Shain, I. *Anal. Chem.* **1964**, *35*, 706-723.
(12) Product analyses: chemical oxidation of the 9-methylfluorenide carbanion resulted in the production and isolation of substantial quantities of the head-to-head 9-methylfluorene dimer. NMR and mass spectral evidence was used to confirm the existence of the 9-methylfluorene dimer. Reference 11 contains detailed discussions of the protocol used to verify that the electrochemically-generated product degrades *via* a second-order process. While product analyses were *not* carried out for the balance of the reactions in Table IV, the data are clear in their indication that the electrochemically-generated fluorenyl radicals are degrading in a reaction that is second-order in fluorenyl radical.[13]
(13) Bausch, M.J.; Gostowski, R. *J. Org. Chem.* submitted.
(14) Wayner, D.D.M.; McPhee, D.J.; Griller, D. *J. Am. Chem. Soc.* **1988**, *110*, 132-137.

Table I. Dimethyl Sulfoxide (DMSO) Acidity (pK_a and ΔpK_a) and Homolytic Bond Strength [(ΔG°_{hom}(R–H) and $\Delta\Delta G^\circ_{hom}$(R–H)] Values for 2-Substituted Perimidines (**4**).

Substrate	pK_a	ΔpK_a (kcal/mol)	ΔG°_{hom}(R–H) (kcal/mol)	$\Delta\Delta G^\circ_{hom}$(R–H) (kcal/mol)
2-methylperimidine	17.2	+1.4	75	0
perimidine	16.2	(0)	75	(0)
2-phenylperimidine	14.7	-2.0	73	-2
2-thiomethylperimidine	13.3	-4.0	72	-3
2-chloroperimidine	11.4	-6.6	73	-2

Table II. Dimethyl Sulfoxide (DMSO) Acidity (pK_a and ΔpK_a) and Homolytic Bond Strength [(ΔG°_{hom}(R–H) and $\Delta\Delta G^\circ_{hom}$(R–H)] Values for Remotely Substituted Diphenylamines (**5**).

Substrate	pK_a	ΔpK_a (kcal/mol)	ΔG°_{hom}(R–H) (kcal/mol)	$\Delta\Delta G^\circ_{hom}$(R–H) (kcal/mol)
4-methoxyphenyl-4-cyanophenylamine	21.2	+1.1	84	-1
4-methylphenyl-4-cyanophenylamine	20.8	+0.5	85	0
phenyl-4-cyanophenylamine	20.4	(0)	85	(0)
3-chlorophenyl-4-cyanophenylamine	18.9	-2.1	87	+2
bis(4-cyanophenyl)amine	17.4	-4.1	88	+3
4-nitrophenyl-4-cyanophenylamine	15.5	-6.7	89	+4

Table III. Dimethyl Sulfoxide (DMSO) Acidity (pK_a and ΔpK_a) and Homolytic Bond Strength [(ΔG°_{hom}(R–H) and $\Delta\Delta G^\circ_{hom}$(R–H)] Values for Variously Substituted Fluorenes **6**, **7**, and **8**.

Substrate	pK_a	ΔpK_a (kcal/mol)	ΔG°_{hom}(R–H) (kcal/mol)	$\Delta\Delta G^\circ_{hom}$(R–H) (kcal/mol)
9-(trimethylsilylmethyl)fluorene	21.4	-1.6	69	-3
9-(cyanomethyl)fluorene	19.9	-3.7	74	+2
9-methylfluorene	22.6	(0)	72	(0)

Table IV. Dimethyl Sulfoxide (DMSO) Acidity (pK_a and ΔpK_a) and Homolytic Bond Strength [(ΔG°_{hom}(R–H) and ΔG°_{hom}(R–H)] Values for Variously Substituted Fluorenes **6**, **7**, and **8**.

Radical (R•)	ΔG°_{hom}(R–H) (kcal/mol)	$\Delta\Delta G^\circ_{hom}$(R–H) (kcal/mol)	k_2 ($M^{-1}s^{-1}$)
9-methylfluorenyl	72	(0)	3×10^7
9-cyanofluorenyl	71	-1	2×10^7
9-phenylfluorenyl	70	-2	1×10^7
9-*tert*-butylfluorenyl	76	+4	5×10^5
9-(2-methylphenyl)fluorenyl	71	-1	8×10^3
9-mesitylfluorenyl	72	0	<1

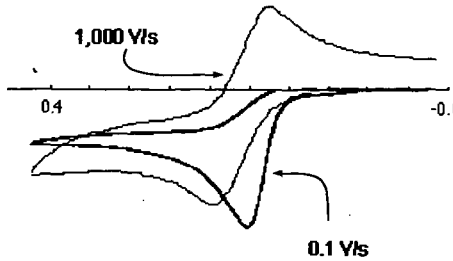

Fig 1. CV traces (at 1000 and 0.1 V/s scan rates) for the anodic oxidation of the 9-(2-methylphenyl)fluorenide anion.

THERMOLYSIS OF SILICA-IMMOBILIZED 1-(4'-HYDROXYPHENYL)-2-PHENYLETHANE UNDER D_2. A HYDROLIQUEFACTION MODEL.

Robert D. Guthrie
Sreekumar Ramakrishnan
Department of Chemistry
University of Kentucky
Lexington, KY 40506

Phillip F. Britt
A. C. Buchanan, *III*
Oak Ridge National Laboratory
P. O. Box 2008
Oak Ridge, TN, 37381

Burtron H. Davis
Kentucky Center for Applied Energy Research
3572 Iron Works Pike, Lexington, KY 40511

Keywords: hydroliquefaction, surface-attached, phenol H/D exchange

INTRODUCTION

In previous work, reactions of coal model compounds with D_2 at temperatures to 450 °C and pressures of 2000 psi in isolation from metal surfaces were studied. The distribution of deuterium in recovered starting materials and products, determined by GC/MS and by ^1H and ^2H NMR allowed identification of viable pathways for hydroliquefaction with increased certainty. Studies carried out with 1,2-diphenylethane (bibenzyl), **DPE**,[1] various deuterium-labeled diphenylethanes,[2] 1,2,3,4-tetraphenylbutane,[3] 2,2,5,5-tetramethyl-3,4-diphenylhexane,[4] and 1-[4-(2-phenylethyl)benzyl]naphthalene[5] model a mechanistic scheme for hydroliquefaction in which radicals formed by the homolysis of weak bonds, react with D_2 in competition with hydrogen-atom abstraction from benzylic sites. The reaction with D_2 produces deuterium atoms which react reversibly at unsubstituted positions in monocyclic aromatic compounds by the sequence of eqs 1 and 2.

$$R\bullet + D_2 \rightarrow R\text{-}D + D\bullet \qquad (1)$$

$$D\bullet + H\text{-}Ar \rightarrow D\text{-}Ar + H\bullet \qquad (2)$$

where H-Ar represents any aromatic compound. Eq 2 is probably a two-step process. Reaction of D or H atoms at alkyl-substituted positions produces alkyl radicals as proposed by Vernon.[6] These react relatively unselectively with available H- and D-atom donors. Kinetic chains involving D (H) atoms are short because of addition of these species to alkenes and polycyclic arenes as well as abstraction of benzylic C-H. The radicals produced in these processes undergo termination through disproportionation, reducing overall hydrocracking efficiency.

In 1986, Buchanan, Poutsma and coworkers demonstrated that the attachment of 1-(4'-hydroxyphenyl)-2-phenylethane, **DPE-OH**, to a silica surface via a carbon-oxygen-silicon linkage dramatically changes the distribution of thermolysis products when compared with unattached **DPE** in the absence of H_2.[7] Large increases in the amounts of rearrangement and cyclization products, removed from the surface subsequent to thermolysis, signaled the involvement of radicals which were not free to undergo the chain transfer and termination processes typical of solution and gas-phase chemistry. Subsequently, Buchanan, Britt and Biggs, for several different substrates, showed that H-atom transfer reactions on silica surfaces can be moderated by the presence of labile H-atoms in interspersed spacer molecules.[8]

We felt it would be interesting and instructive, concerning possible effects produced by the restricted mobility of the coal matrix, to examine the reaction of surface-immobilized substrates under hydroliquefaction conditions with D_2. Clearly, in order for the results to be easily interpretable, the substrates must not be removed from the surface through the action of D_2. Earlier temperature-programmed hydropyrolysis experiments suggested that this would not be a problem.[9]

EXPERIMENTAL

DPE-OH was attached to fumed silica (Cabosil M-5, Cabot Corp.) in the manner prescribed by

Buchanan, et. al.[7] The sample used for the experiments reported in Tables I and II had a surface loading of 0.32 or 0.51 mmoles/g. Samples of surface-attached material (500 mg) were placed in glass reactors described earlier.[1] The substrate was heated under N_2 or D_2 pressure in a fluidized sand bath. Temperatures reported are corrected by using a thermocouple-containing reactor and are measured under H_2. Times reported are actual time-in-bath measurements and should be shortened by approximately 5 min to allow for a measured 8 min heat-up period. Reaction mixtures were analyzed by vacuum transfer of volatile materials at 2 X 10^{-5} Torr and 80 - 100 °C into a liquid nitrogen-cooled trap for 2 h. The contents of the trap were treated with a measured amount of biphenyl in CH_2Cl_2 and the solution analyzed by gas chromatography on a 30 m, 0.25 mm capillary column coated with DB-1 at 0.25 μm. Samples were also subjected to GC/MS analysis. After removal of volatile materials, the residual coated silica (150 - 200 mg samples) was hydrolyzed with 30 to 35 mL of 1 N NaOH for 12 to 16 h at 25 °C then treated with a measured amount of a standard solution of 4-hydroxybiphenyl in 0.1 N NaOH. The hydrolysis mixture was acidified and extracted with CH_2Cl_2. After removal of the solvent, the residue was treated with a solution of N,O-bis(trimethylsilyl)trifluoroacetamide containing pyridine and trimethylsilyl chloride. The trimethylsilylated material was analyzed by GC and GC/MS as described above. Control experiments to document silica-promoted aromatic hydrogen exchange were carried out by sealing phenol-$\underline{d}_6$ (Aldrich Chemical Co.) with Cabosil and any other desired reactants into a $\underline{ca}$. 7" X 10 mm Pyrex tube under argon and heating for the desired time. Work up was carried out as described above for N_2 and D_2 reactions.

RESULTS AND DISCUSSION

Hydropyrolysis of **DPE-OH** attached to fumed silica at a coverage of 0.51 mmoles/g (close to maximum level) at 410 °C was carried out under both N_2 and D_2 at 2000 psi in a glass reactor as previously described for the hydropyrolysis of **DPE**.[1] The reactor design is necessarily different from that employed by Buchanan, Britt, and coworkers[7,8,9] in their studies of silica-bound **DPE-OH** which was configured so that volatile products, including small amounts of phenol driven from the surface in the early stages of the reaction were continuously removed from the reaction zone. In the present study, volatile materials remain in the hot reactor throughout the heating period. The product distribution under N_2 pressure (Table I) is, nevertheless, consistent with that previously reported in vacuum with a relatively high yield of rearrangement product, HOPhCHMePh (isolated after hydrolysis of silica as its trimethylsilylated derivative).[7] For comparison purposes, we have carried out the gas-phase thermolysis of **DPE-OH** itself in D_2 under comparable conditions and found the amount of HOPhCHMePh to be less than 0.5 mole%. Thus, D_2 does not diminish the rearrangement reaction under conditions of restricted mass transport.

The most significant effect of D_2 is the increased yields of hydrocracking products: benzene, ethylbenzene (PhEt), phenol (PhOH) and 4-ethylphenol (EtPhOH) shown in Table I. Also, the amount of 4'-hydroxystilbene (HOPhCH=CHPh), is reduced under D_2. These effects were also observed in the hydropyrolysis of free **DPE**.[1,6]

An unanticipated outcome of the surface attachment experiments was the change in deuterium distribution pattern. Table II summarizes the free **DPE-OH** data (column 3) and compares them to those for silica-attached **DPE-OH**, **DPE-OSi**, (columns 1 and 2). In comparing 10 min runs for attached and free material it is apparent that the preference for deuterium incorporation in oxygen-substituted rings has increased substantially for **DPE-OSi**. This is particularly evident in the material with lower surface coverage, column 1, where the D content of oxygen-substituted rings is two to three times greater than that of unsubstituted rings. This effect is particularly dramatic (a factor of 3 to 6) where the different rings of **DPE-OH** are compared, but is also evident when comparing PhMe with HOPhMe, etc. This selectivity is somewhat reduced for high coverage **DPE-OSi** at 410 °C but is observed for this material as well at lower temperature.[10]

In previous experiments with **DPE**, it was clear that in the presence of thermolysis-produced radicals, aromatic exchange takes place by eqs 1 and 2. It is reasonable to assume that the same sequence occurs for **DPE-OH**. Because radical reactions might be expected to be insensitive to ring substituents, particularly at the temperatures involved, it was expected, and indeed found, that when **DPE-OH** is heated with D_2 the unsubstituted and HO-substituted rings contain equal numbers of D atoms after reaction.

We suspected that the most reasonable explanation for selective deuteration of oxygen-substituted rings is that the exchange process becomes electrophilic. If, for example, the underivatized SiOH groups remaining on the surface were somehow to be converted to SiOD groups it seemed possible that, at temperatures of the order of 400 °C, these might catalyze exchange at suitably

reactive ring positions. To test this, we subjected phenol-$\underline{d}_6$ to treatment with silica (Cabosil) at 400 °C and indeed observed exchange. With excess silica, up to three of the ring D atoms in phenol-$\underline{d}_6$ could be replaced by H. Moreover, a mixture of phenol-$\underline{d}_6$ and MePhOH heated with silica produced MePhOH deuterated at ring positions. The temperature threshold for the exchange of phenol-$\underline{d}_6$ with silica could be shown to be about 140 °C and thus at 400 °C, the exchange goes rapidly to an equilibrium distribution. Thus it seemed clear that, were a mechanism available to exchange D atoms from D_2 with SiOH groups on the silica, our results could be explained. In support of this scheme, we were able to determine the presence of SiOD groups on recovered silica by infrared spectroscopy after removal of volatile products. It is important to note that the silica-catalyzed exchange reaction (using phenol-$\underline{d}_6$), in the absence of D_2, works only for phenolic compounds and not for benzene or even for anisole (methyl phenyl ether).

It seems almost certain, despite the apparently heterolytic nature of the reaction of SiOD with PhOH, the exchange of SiOH with D_2, moderated by phenolic compounds, must have radical components. D_2 thermolysis of surface-attached PhOH, **Ph-OSi**, which offers no obvious route for radical production, led to some exchange in the recovered PhOH. However, the amount of D is small relative to comparable **DPE-OSi** experiments and, moreover, radical processes must contribute even here as evidenced by the formation of trace amounts of benzene with relatively high D content.

We have noted above that small amounts of phenolic compounds driven from the surface and removed from the reaction zone in vacuum experiments[7,8,9] remain in the reaction vessel under the conditions of the present studies. The phenolic species are presumably generated by a process analogous to that for dehydroxylation of silica at elevated temperatures (≡Si-OAr + ≡Si-OH → ≡Si-O-Si≡ + HOAr). Moreover, molecules of water absorbed on the surface prior to reaction are available to hydrolyze Si-OAr bonds under D_2. Under present conditions, this typically leads to 5 to 10% of free phenolic material (based on materials obtained following vacuum transfer).

Stein,[11] Bockrath,[12] and others have noted that even though the ArO-H and $ArCH_2$-H bond energies are about the same, H abstraction by ArO• radicals is inherently faster. At 170 °C, Bockrath[12] has found that benzyl radicals abstract H atoms from ArO-H roughly 15 times faster than from benzylic structures in $PhCH_2CH_2Ph$, etc. Given that radicals produced in these thermolyses seem likely to be reacting with small amounts of phenolic compounds shown to be free of the surface (eq 3), the phenoxyl radicals produced seem certain to react with D_2 to produce D atoms by eq 4.

$$\text{ArOH} + \text{R}\bullet \rightarrow \text{ArO}\bullet \qquad (3)$$

$$\text{ArO}\bullet + D_2 \rightarrow \text{ArOD} + D\bullet \qquad (4)$$

D atoms produced in this way could be involved in the usual exchange at aromatic sites (eq 2), but could also react with phenols by eq 5.

$$D\bullet + \text{HOAr} \rightarrow \text{DH} + \text{ArO}\bullet \qquad (5)$$

The reactions of eqs 4 and 5 constitute a chain process which results in the conversion of HOAr to DOAr. This would presumably also occur in the thermolysis of **DPE-OH** under D_2 and, therefore, of itself, must not be sufficient to produce selective exchange in O-substituted rings. However, if, in the presence of silica, exchange of O-substituted rings with DOAr is catalyzed, selective D incorporation can be explained. To document the viability of eq 3, we heated **DPE** with phenol-O-$\underline{d}$ and showed deuterium to be present in the toluene produced.

Focussing on the non-oxygen-substituted rings reveals evidence that the free radical chain for H/D substitution is more efficient for gas-phase species than for surface immobilized molecules. Cleavage-produced free molecules, benzene, PhMe, PhEt as well as **DPE** (presumably formed by radical recombination) contain at least twice as mucb deuterium as the unoxygenated ring in recovered **DPE-OH** suggesting that the latter is a less active participant in the D-atom promoted exchange.[13] Particularly convincing is the lower D content of $PhCH_2$' fragments from **DPE-OH** as compared with those from PhEt. As **DPE-OH** spends most of its time on the surface, this argues that D atoms react predominantly with gas-phase substrates.

SUMMARY

The important conclusions of this study are: 1. The presence of D_2 at 2000 psi does not alter the

tendency of surface-attached radicals to rearrange. 2. Hydrocracking is observed for hydropyrolysis of surface-attached materials. 3. Radical D/H exchange is more efficient in the gas phase. 4. The reaction of benzylic radicals with phenols has been documented. 5. Phenoxyl radicals catalyze exchange between D_2 and SiOH groups on silica which in turn promotes exchange at ortho and para ring positions in phenolic compounds.

ACKNOWLEDGEMENTS

The authors gratefully acknowledge support from the Department of Energy, Office of Basic Energy Sciences, Division of Chemical Sciences, under Contract No. DE-AC05-840R21400 with Martin Marietta Energy Systems, Inc. (PFB and ACB) and from the United States Department of Energy, Pittsburgh, for a grant, DE-FG22-91-PC91291 (RDG, SR and BHD).

REFERENCES

1. (a) Guthrie, R. D.; Shi, B.; Sharipov, R.; Davis, B. ACS Div. Fuel Chem. Prepr., **1993**, 38, 526-533. (b) Guthrie, R. D.; Shi, B.; Rajagopal, V.; Ramakrishnan, S.; Davis, B. H., submitted to J. Am. Chem. Soc.

2. Rajagopal, V.; Guthrie, R. D.; Shi, B.; Davis, B. H. ACS Div. Fuel Chem. Prepr., **1993**, 38, 1114.

3. Ramakrishnan, S.; Guthrie, R. D.; Shi, B.; Davis, B. H. ACS Div. Fuel Chem. Prepr., **1993**, 38, 1122.

4. Sharipov, R.; Guthrie, R. D.; Shi, B.; Davis, B. H. ACS Div. Fuel Chem. Prepr., **1993**, 38, 1129.

5. Shi, B.; Ying, J.; Guthrie, R. D.; Davis, B. H., submitted to Energy and Fuels.

6. Vernon, L. W. FUEL **1980**, 59, 102-106.

7. Buchanan, A. C., III, Dunstan, T. D. J.; Douglas, E. C.; Poutsma, M. L. J. Am. Chem. Soc. **1986**, 108, 7703-7715.

8. (a) Buchanan, A. C., III; Britt, P. F.; Biggs, C. A. Energy and Fuels **1990**, 4, 415-417. (b) Buchanan, A. C., III.; Biggs, C. A. J. Org. Chem. **1989**, 54, 517-525. (c) Britt, P. F.; Buchanan, A. C., III J. Org. Chem. **1991**, 56, 6132-6140.

9. Mitchell, S.C.; Lafferty, C. J.; Garcia, R.; Snape, C. E.; Buchanan, A. C., III; Britt, P. F.; Klavetter, E. Energy and Fuels **1993**, 7, 331-333.

10. Data to be reported in future publications.

11. S. E. Stein in "Chemistry of Coal Conversion", Schlosberg, R., Ed.; Plenum Press, NY 1985, pp 13 - 44.

12. Bockrath, B. C.; Bittner, E. W.; McGrew, J. J. Am. Chem. Soc. **1984**, 106, 135-138.

13. It may be noticed that the D content of benzene, toluene and ethylbenzene from free **DPE-OH** is also high, but this is misleading because the **DPE-OH** reaction proceeded to higher conversion.

Table I. Product Distrihution in the Thermolysis of Surface-Attached 4'-Hydroxy-1,2-diphenylethane at 410 °C under N_2 and D_2. Coverage = 0.51 Mmoles/g.

Mole % of Total Products

Product[a]	10 min/N_2	10 min/D_2	30 min/N_2	30 min/D_2
Benzene	1.2	6.0	0.5	6.9
PhMe	28.6	25.9	31.5	22.8
PhEt	0.8	5.5	1.0	7.0
$PhCH_2CH_2Ph$	0.7	2.6	1.0	1.9
PhCH=CHPh	----	---	0.3	<0.02
TMSOPh[b]	2.8	6.8	1.3	8.7
TMSOPhMe[b]	27.4	23.3	28.6	27.5
TMSOPhEt[b]	0.8	4.8	1.2	6.2
$TMSOPhCH_2Ph$[c]	1.5	1.1	3.7	1.9
TMSOPhCHMePh[c]	11.3	11.5	9.2	11.3
$TMSOPhenH_2$[c,d]	<0.3	---	0.3	----
TMSOPhCH=CHPh[c]	23.2	10.7	18.6	2.6
TMSOPhen[c,d]	1.8	1.7	2.8	3.2

[a] Conversions were 33.5, 26.8, 53.0 and 58.1% for the 4 runs. Recoveries of listed products ranged from 75 to 85%. A few GC peaks for which tentative identification can be made are not listed. Majority appear to be siloxytriphenylpropane isomers. Some styrene may be present. A large numher of very small unidentified peaks were observed for which individual peaks represent less than 0.05 mole %. [b] Represents sum of volatile and hydrolysis-recovered products. [c] These were measured after hydrolysis of recovered silica and trimethylsilylation. [d] Phen = phenanthryl, $PhenH_2$ = dihydrophenanthryl.

Table II. Deuterium Content of Products from Thermolysis of **DPE-OSi** and **DPE-OH** for 10 Minutes at 410 °C Under D_2.

Average Number of D Atoms per Molecule

Product	**DPE-OSi** (0.32)[a]	**DPE-OSi** (0.51)[a]	**DPE-OH**[c]
Benzene	1.11	1.01	0.87
PhMe	0.66	0.95	0.80
PhEt	1.19	1.29	1.10
--> $PhCH_2^+$	0.74	0.69	0.43
PhOH	2.50 (2.55)[b]	1.55 (1.22)[b]	0.95 (0.91)[b]
MePhOH	2.20 (2.01)[b]	1.43 (1.09)[b]	0.79 (0.77)[b]
EtPhOH	2.37 (2.34)[b]	1.69 (1.23)[b]	1.23 (1.30)[b]
[d] --> $PhCH_2^+$	1.99	1.25	0.50
$PhCH_2CH_2Ph$	3.25	1.77	1.07
[d] --> $PhCH_2^+$	1.87	0.90	0.59
TMSOPhCHMePh	2.23	0.90	1.12
$TMSOPhCH_2CH_2Ph$	2.1	1.04	0.82
[d] --> $PhCH_2^+$	0.34	0.24	0.46
[d] --> $TMSOPhCH_2^+$	1.9	0.89	0.47

[a] Surface coverage in mmoles/g. [b] First value is for vacuum-transferred material. () represents trimethylsilylation products after hydrolysis of silica. The difference at high coverage appears to be real. Hydrolysis procedures do not change D content. [c] Conversion was higher for this material (60%) compared to 22% and 27% for first two columns. [d] Mass spectral fragment.

UNCATALYZED REACTION OF SELECTED UNSATURATED COMPOUNDS WITH D_2

Venkatasubramanian K. Rajagopal
Robert D. Guthrie
Department of Chemistry
University of Kentucky
Lexington, KY 40506

Buchang Shi
Burtron H. Davis
Kentucky Center for Applied Energy Research
3572 Iron Works Pike, Lexington, KY 40511

Keywords: hydroliquefaction, alkenes, polynuclear aromatic compounds

INTRODUCTION

In our previous study of the reaction of 1,2-diphenylethane (bibenzyl), **DPE**,[1] and other compounds[2] with D_2 at temperatures to 450 °C and pressures of 2000 psi in isolation from metal surfaces, we were able to provide strong evidence for a mechanistic scheme wherein radicals formed by the homolysis of weak bonds, react with D_2 to give D atoms. These participate in short radical-chain processes responsible for hydrocracking and exchange of H for D at unsubstituted aromatic positions. In contrast to the simple thermolysis of **DPE** wherein stilbene (PhCH=CHPh), **STB**, is formed as a major product, the reaction of **DPE** with D_2 produces relatively small amounts of this compound. Moreover, the mole % of **STB** among the products decreases as conversion increases, indicating that initially produced **STB** is consumed. It, therefore, seemed important to examine the reaction of **STB** with D_2. This study has subsequently been extended to other unsaturated compounds and the results are reported below.

EXPERIMENTAL

Reaction Procedure. Reactions were carried out as described earlier,[1] placing the reactants along with glass beads for agitation in a glass bulb (ca. 12 mL) with a long capillary neck. The vessel was then suspended in glass wool in the interior of a stainless steel reaction tube having a long neck to house the capillary section of the vessel. The entire apparatus was evacuated, pressured with D_2 gas, closed off and shaken at the desired temperature in a fluidized sand bath. Temperatures reported were corrected from bath calibrations using a thermocouple-containing reactor and were measured under H_2. Times reported are actual time-in-bath measurements and should be shortened by approximately 5 min to allow for a measured 8 min heat-up period. When the heating period was complete, carbon disulfide was added and products removed for analysis using a long syringe needle. In the absence of gas generation within the tube, our observation has been that at least for high concentration runs, an insignificant amount of material is lost from the interior of the bulb. Control experiments in which a hydrogenation catalyst was deliberately added showed complete saturation of aromatic compounds under the reaction conditions. Product mixtures were analyzed by gas chromatography (GC) and by gas chromatography/mass spectrometry (GC/MS). Products present in substantial quantities were separated by preparative gas chromatography and analyzed by ^1H and ^2H NMR at 400 MHz in carbon disulfide. cis-Stilbene did not separate from **DPE** by GC, but was determined from mass spectral analysis using calibrating mixtures of these compounds.

Reactants. Reactants were generally the best quality of commercially-available material. 1-methylstyrene was distilled to remove polymerization inhibitor. Several grades of trans-stilbene were tested and, as all contained small amounts of **DPE**, this compound was synthesized by a modified Wittig synthesis to produce **DPE**-free material.[3] The synthetic material was a mixture of cis- and trans-stilbene, but had no effect on reaction outcome because equilibrium between these two isomers was attained early in the reaction period.

RESULTS AND DISCUSSION

Table I presents data for reaction of several unsaturated compounds with D_2 at 2000 psi and 410 °C. It will be noted that for the four compounds studied to date, **STB**; α-methylstyrene ($Ph(CH_3)C{=}CH_2$), **MS**; anthracene, **AN**; and phenanthrene, **PN**; all except **PN** show substantial reaction with D_2 at 410 °C. The reactive compounds produce dihydro products which contain D atoms as well as incorporating deuterium themselves.

General Mechanistic Considerations. It was demonstrated in our earlier studies that D atoms add reversibly to phenyl rings in **DPE** and its hydrothermolysis products by eqs 1 and 2.

$$D\bullet + H\text{-}Ar \rightarrow H\bullet + D\text{-}Ar \quad (1)$$

$$H\bullet + D_2 \rightarrow H\text{-}D + D\bullet \quad (2)$$

As double bonds, lacking the resonance stability of benzene rings are certain to at least equally reactive toward D atoms, it seems clear that the general process of eq 3 will be important if D atoms are present.

$$D\bullet + C{=}C \rightarrow D\text{-}C\text{-}C\bullet \quad (3)$$

The radicals generated in eq 3 would then be expected to either undergo the reaction of eq 4, completing a kinetic-chain sequence, or undergo termination either by coupling or disproportionation. As coupling would be a reversible process under the conditions of this study, it is necessary only to consider disproportionation, eq 5.

$$D\text{-}C\text{-}C\bullet + D_2 \rightarrow D\text{-}C\text{-}C\text{-}D + D\bullet \quad (4)$$

$$2\ D\text{-}C\text{-}C\bullet \rightarrow D\text{-}C\text{-}C\text{-}(D \text{ or } H) + C{=}C(D \text{ or } H) \quad (5)$$

Several alternative mechanisms are possible. For the extreme case in which eqs 3 and 4 are fast and irreversible, dihydrocompounds containing exactly two D atoms would be obtained and there would be no D in recovered C=C. Clearly, this situation does not transpire for any of the reactions in Table 1. In principle it should be possible to determine the extent to which products were formed via eq 5 from the amount of D introduced into recovered C=C. However, the analysis is confounded by the fact that aromatic exchange is expected via eqs 1 and 2. Of course, it is always possible that radical processes are not involved and that the reaction of C=C with D_2 would occur by a one-step cycloaddition process. In such a process one might expect to see simple second-order kinetics and no introduction of D atoms at sites other than those directly involved in the hydrogen transfer.

Stilbene, STB. The data presented in Table 1 show that **STB** is reduced to **DPE** and a total of approximately 2 atoms of D are introduced in the combined products. While it is difficult to distinguish aromatic and vinylic D in recovered stilbene, ^2H NMR shows 0.37 atoms of aromatic D in **DPE** produced in runs comparable to those in Table 1. As aromatic sites in **STB** and **DPE** should have comparable reactivity with D atoms, most of the D in recovered stilbene seems likely to be at aromatic sites. Consistent with this, an ^2H NMR upper limit for vinyl D in stilbene at <0.05 atoms can be established. This suggests that products formed via eq 5 make a relatively minor contribution when low concentrations of **STB** are present.

A complication for **STB** is that as **DPE** is produced it undergoes thermolysis by processes detailed earlier.[1] In fact, under conditions only slightly more vigorous than those of Table 1, stilbene can be completely converted to a mixture of **DPE** and its hydrothermolysis products with very high D content (average of 8.6 atoms of D in **DPE**). It seems likely that once **DPE** is produced in the reaction mixture, radicals produced in its thermolysis constitute the major initiating species via reaction with D_2 followed by the sequence of eqs 3 and 4. The question of how the process is initiated in the absence of all radical producing species is difficult to answer. The third entry of Table 1 shows that **DPE** is produced even when synthetic **STB** (free of **DPE** to detection limits) is employed.

Despite the complexities discussed, the strong concentration dependence of the reaction suggests that chains of moderate length are operative at low concentration. At low concentrations, we suggest that the predominant pathway for the reaction of **STB** with D_2 involves the sequence of eqs 3 and 4 plus some reaction with H atoms when these are generated by eq 1. When the initial concentration is increased, the efficiency of conversion to **DPE** is reduced by higher radical concentrations which increase competition by eq 5.

α-Methylstyrene, MS. On comparable treatment with D_2, **MS** produces cumene. However the D content is less than observed for **DPE** from **STB** and decreases with increasing concentration of **MS**. For the higher concentration runs of Table 1, the D atom content of cumene plus **MS** is close to 1 atom per equivalent of cumene formed. This is different from **STB** and **AN** for which two or more atoms of D are incorporated. This lower D incorporation suggests chain transfer involving **MS** as shown in eq 6 forming monodeuterated cumene and the 2-phenylallyl radical. It will be noted that for **STB** and **AN**, the substrate is unlikely to act as

an H-atom donor.

$$Ph(CH_3)(CH_2D)C\bullet + Ph(CH_3)C{=}CH_2 \;\text{-->}\; Ph(CH_3)(CH_2D)C\text{-}H + Ph(H_2C{=})C\text{-}CH_2\bullet \quad (6)$$

It seems likely that the 2-phenylallyl radical thus formed reacts with **MS** to give higher molecular weight products as these are found in nearly equal amount to cumene and increase with increasing concentration of **MS** as might be expected. It will be noted that this substrate is the only one studied for which conversion increases with amount used.

Earlier study of the thermolysis of bicumyl ($Ph(CH_3)_2C\text{-}C(CH_3)_2Ph$) under D_2 has shown that cumyl radicals ($Ph(CH_3)_2C\bullet$) are relatively reluctant participants in the reaction of eq 4.[4] This being the case, it might be expected that eq 5 is the major route to product formation. However, such a scheme should lead to more D in recovered **MS** than observed. Perhaps because of the higher temperature and lower radical concentrations here, as contrasted with the bicumyl experiments, eq 4 becomes more competitive.

In contrast to the case of **SB**, the hydrogenation product from **MS** (cumene) would not seem to be capable of serving as an initiator, thus requiring some different type of initiation step. We suggest the reaction of eq 7 in which two molecules of **MS** undergo a "molecular disproportionation" reaction to give the 2-phenylallyl radical ($Ph(H_2C{=})C\text{-}CH_2\bullet$) and a cumyl radical.

$$2\ Ph(CH_3)C{=}CH_2 \;\text{-->}\; Ph(H_2C{=})C\text{-}CH_2\bullet + Ph(CH_3)_2C\bullet \quad (7)$$

The cumene formed <u>via</u> eq 6 would be monodeuterated but, to the extent that eq 6 was a viable path for the cumyl radical formed in eq 7, some of the cumene would be produced without deuterium. Significantly, the predominant cumene isotopomer is d_1 in the 50 mg run but d_0 in the 300 mg run.

Anthracene, AN. Under the same conditions, **AN** reacts with D_2 to give dihydroanthracene, $\mathbf{ANH_2}$ (taken to include ANHD, AND_2, etc.). This reaction has been reported earlier with H_2 at 430 °C in methylnaphthalene solvent.[5] The total amount of D incorporated in **AN** plus $\mathbf{ANH_2}$ was to 2.1 to 2.6 atoms of D per equivalent of $\mathbf{ANH_2}$ produced. This reaction shows no significant concentration dependence and, therefore seems unlikely to be a kinetic chain process. The mechanism probable for the preceding systems in which D atoms add to **AN** to form adduct radicals, **AND•**, and these disproportionate as shown in eq 8 is one possibility.

$$2\ \mathbf{AND\bullet} \;\text{-->}\; \mathbf{AN} + \mathbf{ANHD}\ (\text{or } \mathbf{AN\text{-}d_1} + \mathbf{ANH_2}) \quad (8)$$

If this mechanism is correct, it is necessary to account for the initial production of D atoms. Coupling of two **AN** molecules as reported by Stein[6] is a possibility. The reaction of eq 8 is known to be reversible[7] so that once $\mathbf{ANH_2}$ and its isotopomers are formed, exchange of H and D atoms would be rapid and, moreover, this will occur <u>via</u> a radical mechanism. The question which remains is whether the adduct radicals (**ANH•** and **AND•**) are sufficiently reactive to remove D atoms from D_2. While further experiments will be required to answer this question definitively, it is significant that ^2H NMR studies show that there is very little aromatic D in $\mathbf{ANH_2}$. Also the D atoms in recovered **AN** are located to > 80% (detection limit) in the 9,10-positions. A mechanism wherein half of the deuterium incorporated arrives as D atoms can be reconciled with these observations only if D atoms are highly selective for the 9,10-positions.

One possibility which cannot be discounted by any of the evidence presently at hand. is that the addition of D_2 to **AN** is a 2 + 4 cycloaddition. It is the only system in this study for which cycloaddition to give a stable product is symmetry allowed.

Phenanthrene, PN. **PN** does not react under these conditions. The fact that **AN** does react could be taken as evidence for 2 + 4 cycloaddition which is not symmetry allowed for **PN**. On the other hand, the 9,10-positions in **AN** are notoriously reactive[7d] and initiation processes with **AN** might be more effective than comparable reactions with **PN**. The striking difference in reactivity of these two compounds will require further study for complete analysis.

ACKNOWLEDGEMENTS

The authors gratefully acknowledge a grant from the United States Department of Energy, Pittsburgh, DE-FG22-91-PC91291, supporting this work.

SUMMARY

The reaction of D_2 with several unsaturated substrates has been documented. The reaction involved no intentionally added hydrogenation catalyst and, with the possible exception of **AN**, is believed to involve D atom addition to the unsaturated compound with the resultant adduct radical either reacting with D_2 or undergoing disproportionation. In the case of anthracene, the results are consistent with a direct 2 + 4 cycloaddition.

REFERENCES

1. (a) Guthrie, R. D.; Shi, B.; Sharipov, R.; Davis, B. ACS Div. Fuel Chem. Prepr., **1993**, 38, 526-533. (b) Guthrie, R. D.; Shi, B.; Rajagopal, V.; Ramakrishnan, S.; Davis, B. H., submitted to J. Am. Chem. Soc.

2. (a) Rajagopal, V.; Guthrie, R. D.; Shi, B.; Davis, B. H. ACS Div. Fuel Chem. Prepr., **1993**, 38, 1114. (b) Ramakrishnan, S.; Guthrie, R. D.; Shi, B.; Davis, B. H. ACS Div. Fuel Chem. Prepr., **1993**, 38, 1122. (c) Sharipov, R.; Guthrie, R. D.; Shi, B.; Davis, B. H. ACS Div. Fuel Chem. Prepr., **1993**, 38, 1129. (d) Shi, B.; Ying, J.; Guthrie, R. D.; Davis, B. H., submitted to Energy and Fuels.

3. Daniel, H.; LeCorre, M. Tetrahedron Letters **1987**, 28, 1165-1168.

4. Bicumyl undergoes thermolysis at temperatures below 400 °C to give equal amounts of cumene and **MS** with only small D uptake, unpublished study by R. D. Guthrie, S. Ramakrishnan and B. Shi.

5. Chiba, K.; Tagaya, H.; Suzuki, T. Sato, S. Bull. Chem. Soc. Jpn. **1991**, 64, 1034-1036.

6. Stein, S. E.; Griffith, L. L.; Billmers, R.; Chen, R. H. J. Org. Chem. **1987**, 52, 1582-1591.

7. (a) Camioni, D. M.; Autrey, S. T.; Franz, J. A. J. Phys. Chem. **1993**, 97, 5791-5792. (b) Billmers, R.; Griffith, L. L.; Stein, S. E. J. Phys. Chem., **1986**, 90, 517-523. (c) Billmers, R.; Brown, R. L.; Stein, S. E. Int. J. Chem. Kin. **1989**, 21, 375-386. (d) Stein, S. E. in "Chemistry of Coal Conversion", R. Schlosberg, Ed.; Plenum Press, NY 1985, pp 13-44.

Table 1. Reaction of Unsaturated Compounds with D_2 (2000 psi) at 410 °C for 20 min.[a]

Compound	Amount[b] (mg)	% H-C-C-H[d]	D atoms in H-C-C-H[e]	D atoms in C=C[e]
STB	25[c]	22[g]	1.67	0.23
STB	50[c]	13[g]	1.47	0.10
STB	25[f]	22[g]	1.73	0.22
STB	50	5.4[k]	1.5[j]	<0.03
STB	100	1.8	1.5[j]	<0.01
MS	50	14[h]	1.34	0.13
MS	150	18[h]	0.80	0.09
MS	300	27[h]	0.65	0.16
AN	50	33[i]	1.55	0.37
AN	100	35[i]	1.20	0.48
AN	300	26[i]	1.10	0.57
PHN	50	<0.2	---	<0.05
PHN	100	<0.2	---	<0.05
PHN	300	<0.2	---	<0.05

[a] The 20 min time period refers to the time after temperature equilbrium is reached inside of the cell. There is an 8 min heat-up period. [b] This is the weight of material inside of an approximately 12 mL reaction vessel. [c] Average number of D atoms per molecule as determined by GC/MS analysis. [d] Balance of material is recovered C=C, except as otherwise noted. [e] Commercial material contains 0.7% of **DPE**. [f] Synthetic material contains < 0.01% **DPE**. [g] Product mixture also contains 5 - 10% of products of **DPE** reaction (benzene, toluene, ethylbenzene, styrene, 1,1-diphenylethane, diphenylmethane, etc. [h] Similar amounts (12, 17 and 21%) of other products, most of which appeared to be dimers and dehydrodimers of expected intermediate radicals. [i] Tetrahydroanthracenes were formed in amounts of up to 3% increasing with increasing concentration. [j] Corrected for **DPE** in starting **STB**. [k] This run should be the same as the previous 50 mg run, but gave lower conversion. It is believed that this is due to temperature variations. The first three **STB** runs were carried out on a different day from the last two.

THERMOLYSIS OF PHENETHYL PHENYL ETHER. A MODEL OF ETHER LINKAGES IN LOW RANK COAL.

Phillip F. Britt, A. C. Buchanan, III and E. A. Malcolm
Chemical and Analytical Sciences Division
Oak Ridge National Laboratory, P.O. Box 2008
Oak Ridge, TN 37831-6197

INTRODUCTION

Currently, an area of interest and frustration for coal chemists has been the direct liquefaction of low rank coal. Although low rank coals are more reactive than bituminous coals, they are more difficult to liquefy and offer lower liquefaction yields under conditions optimized for bituminous coals.[1] Solomon, Serio, and co-workers have shown that in the pyrolysis and liquefaction of low rank coals, a low temperature cross-linking reaction associated with oxygen functional groups occurs before tar evolution.[2,3] A variety of pretreatments (demineralization, alkylation, and ion-exchange) have been shown to reduce these retrogressive reactions and increase tar yields,[2,3] but the actual chemical reactions responsible for these processes have not been defined. In order to gain insight into the thermochemical reactions leading to cross-linking in low rank coal, we have undertaken a study of the pyrolysis of oxygen containing coal model compounds.[4] Solid state NMR studies suggest that the alkyl aryl ether linkage may be present in modest amounts in low rank coal.[5] Therefore, in this paper, we will investigate the thermolysis of phenethyl phenyl ether (PPE) as a model of β-aryl ether linkages found in low rank coal, lignites, and lignin, an evolutionary precursor of coal. Our results have uncovered a new reaction channel that can account for 25% of the products formed. The impact of reaction conditions, including restricted mass transport, on this new reaction pathway and the role of oxygen functional groups in cross-linking reactions will be investigated.

Background The thermolysis of PPE has been previously studied under a variety of conditions. Liquid-phase studies by Klein[9] and Gilbert[10] found phenol and styrene as the primary decomposition products, but different mechanisms were proposed to rationalize the data. Klein proposed a concerted retro-ene reaction based on the first-order reaction kinetics (1.16 ± 0.12 in PPE) which was

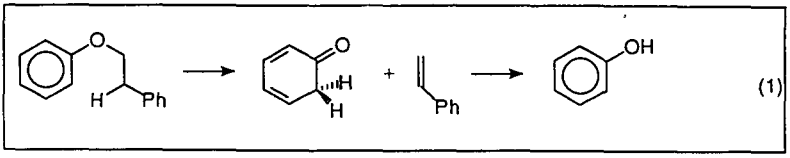

(1)

unaffected by tetralin, and the Arrhenius parameters, log A = 11.1 ± 0.9 s^{-1} and E_a = 45 ± 2.7 kcal mol^{-1}. It was proposed that secondary decomposition of styrene produced the minor amounts of toluene and ethylbenzene that were detected. Gilbert proposed a free radical chain mechanism for the decomposition of PPE based on the fractional reaction order (1.21 in PPE), the rate acceleration by added free radical initiator, and the Arrhenius parameters, log A = 12.3 s^{-1} and E_a = 50.3 kcal mol^{-1}. The chain propagation steps are shown below. PPE has also been studied under coal liquefaction

$$PhCH_2CH_2OPh + PhO\bullet \rightarrow PhCH(\bullet)CH_2OPh\ (1) + PhOH \quad (2)$$

$$PhCH(\bullet)CH_2OPh \rightarrow PhCH{=}CH_2 + PhO\bullet \quad (3)$$

conditions, i.e. in tetralin under high pressure of hydrogen,[11] and under catalytic hydropyrolysis conditions, with iron and zinc metal.[12] In both these studies, the dominant products were phenol and ethylbenzene, since under these reaction conditions, styrene would be hydrogenated to ethylbenzene.

EXPERIMENTAL

Phenethyl phenyl ether was synthesized by alkylation of phenol with phenethyl tosylate with K_2CO_3 in dimethylformamide. Vacuum fractional distillation afforded PPE in > 99.9% purity by GC. Biphenyl was purified by successive recrystallization from ethanol and benzene/hexanes while *p*-phenylphenol, 2-naphthol, and *p*-benzylphenol were recrystallized from benzene/hexanes until

purity was > 99.9% by GC. Tetralin was purified by washing with conc H_2SO_4 until the layers were no longer colored, 10% Na_2CO_3, water, dried over Na_2SO_4, filtered, and fractionally distilled under vacuum from sodium two times taking the center cut. Purity was 99.4 % by GC. The synthesis of the surface-attached phenethyl phenyl ethers, ≈$PhCH_2CH_2OPh$ (≈PPE-3) and ≈$PhOCH_2CH_2Ph$ (≈PPE-1) has been previously reported.[6] Two-component surfaces were prepared by co-attachment of the phenols in a single step,[7] and had final purities of >99.7% (by GC). Surface coverages are listed in Table 2.

Thermolyses of PPE in the fluid and gas phase were performed in a fluidized sand bath (±1 °C) in Pyrex tubes, degassed by six freeze-pump-thaw cycles, and sealed under vacuum (ca. 10^{-5} Torr). Tubes were rinsed with acetone (high purity) containing standards, analyzed by GC and GC/MS, and quantitated by the use of internal standards with measured GC detector response factors. Thermolyses of surface-immobilized PPE were performed at 375 ± 1 °C in T-shaped tubes sealed under high vacuum (ca. 10^{-6} Torr). The volatile products were collected as they formed in a cold trap (77 K), analyzed by GC and GC/MS, as above. The surface-attached products were removed from the silica surface as the corresponding phenols by a base hydrolysis procedure,[8] silylated to the trimethylsilyl ethers, and analyzed as above. All products were identified by their mass spectra and whenever possible, by comparison to an authentic sample.

RESULTS AND DISCUSSION

Phenethyl Phenyl Ether Thermolysis of PPE in the liquid phase at 345 °C (1.2% conversion) produced styrene (36 mol%) and phenol (38 mol%), as the major products, and toluene (11 mol%) and benzaldehyde (12 mol%) as the minor products (eq 4). Small amounts

$$PhCH_2CH_2OPh \rightarrow PhCH{=}CH_2 + PhOH + PhCHO + PhCH_3 \quad (4)$$

of $Ph(CH_2)_2Ph$ (0.7 mol%), $Ph(CH_2)_3Ph$ (0.7 mol%), PhH (0.6 mol%) and $PhCH_2CH_3$ (0.3 mol%) were also formed. As the conversion increased, several secondary products, $Ph(CH_2)_3Ph$, $PhCH_2CH_3$, 1,3,5-triphenylpentane, and 1-phenoxy-2,4-diphenylbutane, grew in at the expense of the styrene. The material recovery decreased steadily with increasing conversion (based on recovered products), from 99.9% at 1.2% conversion, to 85% recovery at 17.9% conversion. The addition of 0.82 mol% and 7.0 mol%, 2,3-dimethyl-2,3-diphenylbutane, as a free radical initiator, increased the rate of reaction by 25% and 200%, respectively, while not altering the product distribution.

Thermolysis of PPE was also investigated at 375 °C with biphenyl (BP), as an inert diluent, (see Table 1) and in the gas phase from 28 - 260 kPa. Although the rate of decomposition is slower than in the liquid, the product composition is much simpler with $PhCH{=}CH_2$, PhOH, PhCHO, and $PhCH_3$ as the dominant products (>95%). The product selectivity, i.e. ($PhCH{=}CH_2$ + PhOH) / (PhCHO + $PhCH_3$), is independent of PPE concentration and conversion, if secondary products are taken into account. This indicates PhCHO and $PhCH_3$ are formed by a primary reaction pathway competitive with $PhCH{=}CH_2$ and PhOH. Additionally, a kinetic order of 1.30 ± 0.03 was determined from the slope of a log-log plot of initial rates vs. concentration.

A free radical chain pathway can be written for the thermal decomposition of PPE which can rationalize the primary and secondary products, acceleration by a free radical initiator, and the fractional kinetic order. Secondary products arise from the

$$PhCH_2CH_2OPh \rightarrow PhCH_2CH_2\bullet + PhO\bullet \quad (5)$$

$$PhO\bullet + PhCH_2CH_2OPh \rightarrow PhCH(\bullet)CH_2OPh\ (\mathbf{1}) + PhOH \quad (6)$$

$$\mathbf{1} \rightarrow PhCH{=}CH_2 + PhO\bullet \quad (7)$$

$$PhCH_2CH_2OPh + PhO\bullet \rightarrow PhCH_2CH(\bullet)OPh\ (\mathbf{2}) + PhOH \quad (8)$$

$$PhCH_2CH(\bullet)OPh \rightarrow PhCH_2CH(Ph)O\bullet \quad (9)$$

$$PhCH_2CH(Ph)O\bullet \rightarrow PhCH_2\bullet + PhCHO \quad (10)$$

$$PhCH_2\bullet + PhCH_2CH_2OPh \rightarrow \mathbf{1} + \mathbf{2} + PhCH_3 \quad (11)$$

reaction of $PhCH_2\bullet$, **1**, and **2** with $PhCH{=}CH_2$. Steps 8-11 have been added to the mechanism proposed by Gilbert[10] to explain the formation of PhCHO and $PhCH_3$ as primary products of a competitive reaction path. Although **1** is estimated to be ca. 7 kcal mol^{-1} more stable than **2**,[13] the unexpected competition between eq 8 with eq 6 can be rationalized by polar effects in the hydrogen transfer reaction between the electrophilic phenoxy radical and PPE (eq 8). Polar effects have been reported in the hydrogen abstraction reaction between the *t*-butoxy radical and substituted anisoles. A Hammet plot shows a good $\sigma\rho$ correlation with ρ = -0.4 indicating the development of cationic character in the transition state which can be stabilized by the adjacent oxygen.[14] Additionally, there is precedence for the competitive formation of products from the thermodynamically less stable radical of tetralin (2-tetralyl radical)[15] and 1,4-diphenylbutane (1,4-diphenyl-2-butyl radical)[8] at these temperatures. Since radical **2** does not have a facile β-scission route, it undergoes a 1,2-phenyl shift from oxygen to carbon (eq 9). β-Scission of the rearranged radical affords benzaldehyde and the chain carrying benzyl radical (eq 10). The chain length of the reaction, i.e. the number of chain turnovers per number of free radical formed, is ca. 10. Analogous intramolecular 1,2-phenyl shifts have been reported in the thermal decomposition of phenetole ($PhOCH_2CH_3$)[16] and anisole at 400 °C.[17] Also, spectroscopic and kinetic data have been obtained for the rearrangement of 1,1-diphenylethoxy radical ($Ph2C(CH_3)O\bullet$) to 1-phenyl-1-phenoxyethyl radical (PhC(CH3)(●)OPh.[18]

The thermolysis of PPE was also studied in tetralin, a model liquefaction solvent, at various concentrations (Table 1). Dilution of PPE with tetralin or BP decreased the rate of decomposition in a similar fashion but the product selectivity increased from 3 to 9 as the tetralin concentration increased. This is a consequence of changing the chain carrying radical from phenoxy to the tetralyl radical. Hydrogen abstraction at the carbon adjacent to the oxygen to form **2** is enhanced for the electrophilic phenoxy radical as a consequence of favorable polar contributions. However, this polar effect is not present for hydrocarbon radicals such as tetralyl, and hydrogen abstraction to form **2** is less favorable resulting in an increase in product selectivity. Similar changes in the selectivity were obtained when diphenylmethane, $PhCH_2Ph$, was used as the hydrogen donating solvent.

<u>Surface-Immobilized Phenethyl Phenyl Ether</u> Thermolysis of surface-immobilized PPE, $\approx PhCH_2CH_2OPh$ (≈PPE-3), at 375 °C at low conversions produces the products shown in eq 12. The selectivity

$$\approx PhCH_2CH_2OPh \rightarrow \approx PhCH{=}CH_2 + PhOH + \approx PhCH_3 + PhCHO \qquad (12)$$

of the reaction ($\approx PhCH{=}CH_2 + \approx PhCH_2CH_3 + PhOH$) / ($\approx PhCH_3 + PhCHO$) is slightly larger than that found for PPE as a consequence of the para-silyloxy substituent on the aromatic ring. This substituent enhances the hydrogen abstraction at the benzylic carbon and favors the production of $\approx PhCH{=}CH_2$ and PhOH. A similar increase in selectivity is observed for the thermolysis of p-$(CH_3)_3SiOPhCH_2CH_2OPh$, as a model of surface attached PPE, where in the gas phase at 375 °C, the selectivity is 4.4 ± 0.5. As for PPE, a free radical chain mechanism can be written for the decomposition of surface-immobilized PPE. Restricted mass transport does not affect the new reaction pathway, i.e. hydrogen abstraction at the β-carbon, rearrangement, and β-scission, to form $\approx PhCH_3$ and PhCHO.

The influence of co-attached aromatics on the rate and selectivity of the thermolysis of ≈PPE-3 are shown in Table 2. No new products were detected for the two component surfaces. Dilution of ≈PPE-3 with biphenyl (≈BP) or naphthalene (≈Naph) results in a decrease in the rate of decomposition compared to the high coverage ≈PPE-3. However, in the presence of ≈DPM, a rate acceleration was observed compared to ≈PPE-3 diluted with ≈BP or ≈Naph, which is in contrast to that observed in the fluid phase (Table 1). These results suggest that rapid hydrogen transfer reactions involving DPM are occurring on the surface that allows radical centers to migrate to the reactive substrate, i.e. ≈PPE. Evidently, the orientation of the molecules on the surface enhances the rate of hydrogen transfer, through the A-factor, relative to hydrogen transfer reactions in a nonconstrained environment, i.e. the fluid phase. A similar rate acceleration via radical relay processes has been

reported in the thermolysis of surface-immobilized diphenylpropane and diphenylbutane in the presence of hydrogen donors.[7,8]

Interpretation of the selectivity data is more complicated. Surprisingly, the inert spacers increase the selectivity (Table 2). Since these spacers should not effect the thermodynamics of hydrogen abstraction, the packing of the molecules on the surface must be hindering the 1,2-phenyl shift such that a bimolecular hydrogen transfer reaction and β-scission (eq 13 and 14) can compete with rearrangement (eq 15). This hypothesis is currently

$$\approx PhCH_2CH_2OPh + \approx PhCH_2CH\bullet OPh \rightleftarrows \approx PhCH\bullet CH_2OPh + \approx PhCH_2CH_2OPh \quad (13)$$

$$\approx PhCH\bullet CH_2OPh \rightarrow \approx PhCH{=}CH_2 + PhO\bullet \quad (14)$$

$$\approx PhCH_2CH\bullet OPh \rightarrow \approx PhCH_2C(Ph)HO\bullet \rightarrow \approx PhCH_2\bullet + PhCHO \quad (15)$$

being investigated with the thermolysis of ≈PPE-3 and surface-attached benzene (≈PhH), which should not hinder the rearrangement but still dilute the molecules on the surface. Therefore, the change in the selectivity for ≈DPM/≈PPE-3 is likely a consequence of two factors. First, the methylene linkage in DPM allows the phenyl ring to rotate away from the adjacent ≈PPE such that the 1,2-phenyl shift should not be hindered, thus decreasing the selectivity (theoretically back to that observed for high coverage ≈PPE-3). Second, since ≈DPM can participate in a radical relay process, an increase in selectivity would be expected for this nonpolar radical, ≈PhCH•Ph, compared to the electrophilic phenoxy radical. It is interesting to note that in the fluid phase, dilution of PPE with an 8-fold excess of DPM increases the selectivity by a factor of 2.6, which is similar to the factor of 2.4 found for the surface-immobilized substrates.

The thermolysis of $\approx PhOCH_2CH_2Ph$, ≈PPE-1, at 375 °C produces the products shown in eq 16. The rate of decomposition is enhanced

$$\approx PhOCH_2CH_2Ph \rightarrow \approx PhOH + PhCH{=}CH_2 + \approx PhCHO + PhCH_3 \quad (16)$$

relative to ≈PPE-3 as a consequence of the para-silyloxy substituent. As for PPE and ≈PPE-3, a free radical chain mechanism can account for the products. Based on the selectivity, surface-immobilization does not appear to hinder the 1,2-phenyl shift to form ≈PhCHO and $PhCH_3$. However, ≈PhCHO undergoes free radical decomposition to form a surface-attached phenyl radical as shown in eq 17. The bond dissociation energy of benzaldehyde (87 kcal mol^{-1}) is similar to that of toluene ($PhCH_2$-H, 88 kcal mol^{-1}).[19].

$$\approx PhCHO + R\bullet \rightarrow \approx PhC\bullet O + RH \rightarrow \approx Ph\bullet + CO \quad (17)$$

At 13% conversion, over 41% of the ≈PhCHO has decomposed by decarbonylation to produce ≈PhH (73%) by hydrogen abstraction, ≈PhPh (14%) by aromatic substitution, and $\approx PhCH_2Ph$ (13%) by coupling with a gas phase benzyl radical. Stein has shown that the selectivity for hydrogen abstraction vs. arylation of toluene by the phenyl radical is 5.2 ± 0.5 at 400 °C in the gas phase.[20] Therefore, even in the presence of hydrogen donors, the phenyl radical could lead to arylation, which would form a more refractory linkage, i.e. a cross-link. These results show how decomposition of ether linkages may lead to cross-linking in low rank coal. Additionally, aromatic methoxy groups ($ArOCH_3$), which are present in high concentrations in low rank coals, could rearrange to aromatic aldehydes ($ArOCH_2\bullet \rightarrow ArCH_2O\bullet \rightarrow ArCHO$), under free radical reaction conditions. Subsquent decarbonylation could again lead to cross-linking.

SUMMARY

Investigations into the pyrolysis mechanisms of model β-aryl ether linkages have provided fundamental insights into the role of oxygen functional groups in retrogressive reactions. A previously undetected reaction pathway has been found for the free radical decomposition of PPE in the fluid phase and under conditions of restricted diffusion. Under conditions of restricted mass transport, the rates and product selectivities can be altered by the physical *and* chemical structure of the neighboring molecules. In the presence of a hydrogen donor, radical migration can occur on the the surface to transport radical sites to reactive molecules. Pyrolysis of the β-aryl ether linkage can lead to cross-linking reactions by the free radical decomposition of benzaldehyde to the

highly reactive phenyl radical, which can undergo aromatic substitution reactions competitively with hydrogen abstraction.

ACKNOWLEDGEMENTS
Research was sponsored by the Division of Chemical Sciences, Office of Basic Energy Sciences, U. S. Department of Energy under contract DE-AC05-840R21400 with Martin Marietta Energy Systems, Inc.

REFERENCES

1. Derbyshire, F. J.; Whitehurst, D. D. *Fuel* **1981**, *60*, 655.
2. (a) Solomon, P. R.; Fletcher, T. H.; Purmire, R. J. *Fuel* **1993**, *72*, 587. (b) Solomon, P. R.; Serio, M. A.; Despande, G. V.; Kroo, E. *Energy Fuels* **1990**, *4*, 42.
3. Serio, M. A.; Kroo, E.; Charpenay, S.; Solomon, P.R. *Prep. Pap.-Am. Chem. Soc., Div. Fuel Chem.* **1993**, *38(3)*, 1021.
4. Britt, P. F.; Buchanan, III, A. C. *Proc., 7th Int. Conf. Coal Sci.*, Banff, Alberta, Canda, **1993**, *Vol 2*, 297.
5. Solum, M. S.; Pugmire, R. J.; Grant, D. M. *Energy Fuels* **1989**, *3*, 187.
6. Britt, P. F.; Buchanan, III, A. C.; Hitsman, V. H. *Proc., 6th Int. Conf. Coal. Sci.*, Newcastle-upon-Tyne, United Kingdom, **1991**, 207.
7. Buchanan, III, A. C.; Britt, P. F.; Biggs, C. A. *Energy Fuels* **1990**, *4*, 415.
8. Britt, P. F.; Buchanan, III, A. C. *J. Org. Chem.* **1991**, *56*, 6132.
9. Klein, M. T.; Virk, P. S. *Ind. Eng. Chem. Fundam.* **1983**, *22*, 35.
10. (a) Gilbert, K. E.; Gajewski, J. J. *J. Org. Chem.* **1982**, *47*, 4899. (b) Gilbert, K. E. *J. Org. Chem.* **1984**, *49*, 6.
11. Korobkov, V. Y.; Grigorieva, E. N.; Bykov, V. I.; Senko, O. V.; Kalechitz, I. V. *Fuel* **1988**, *67*, 657.
12. Cassidy, P. J.; Jackson, W. R.; Larkins, F. P. *Fuel* **1983**, *62*, 1404.
13. Benson, S. W. *Thermochemical Kinetics*, 2nd Ed.; Wiley-Interscience: New York, 1976.
14. Sakurai, H.; Hosomi, A.; Kumada, M. *J. Org. Chem.* **1970**, *35*, 993.
15. Franz, J. A.; Camaioni, D. M. *J. Org. Chem.* **1980**, *45*, 5247.
16. Collins, C. J.; Roark, W. H.; Raaen, V. F.; Benjamin, B. M. *J. Am. Chem. Soc.* **1979**, *101*, 1877.
17. Afifi, A. I.; Hindermann, J. P.; Chornet, E.; Overend, R. P. *Fuel* **1989**, *68*, 498.
18. Falvey, D. E.; Khambatta, B. S.; Schuster, G. B. *J. Phys. Chem* **1990**, *94*, 1056.
19. McMillen, D. F.; Golden, D. M. *Ann. Rev. Phys. Chem.* **1982**, *33*, 493.
20. Chen, R. H.; Kafafi, S. A.; Stein, S. E. *J. Am. Chem. Soc.* **1989**, *111*, 1414.

Table 1. Effect of Diluents on the Thermolysis of PPE at 375 °C

Diluent	Diluent[a]/PPE	Rate $*10^5$ Ms^{-1}	Selectivity[b]
None	--	32.8	2.8
BP	1.03	25.7	2.7
Tetralin	0.96	14	6.0
BP	4.54	5.1	2.9
Tetralin	3.87	6.5	9.3
BP	8.42	2.1	3.1
Tetralin	8.05	2.4	9.5
DPM	8.76	2.6	8.1
BP	19.1	0.67	3.7

[a]BP = biphenyl; DPM = diphenylmethane
[b]$PhCH{=}CH_2$+PhOH/$PhCH_3$+PhCHO

Table 2. Product Selectivity in the Thermolysis of Surface Attached PPE at 375 °C

Surface Comp.	Coverage (mmol g^{-1})	Rate (% h^{-1})	Selectivity[a]
≈PPE-3	0.54	8.3	5±1
≈PPE-3/≈BP	0.050/0.536	3.6	21±2
≈PPE-3/≈Naph	0.072/0.45	3.4	20±5
≈PPE-3/≈DPM	0.059/0.48	8.5	12±2
≈PPE-1	0.50	81	3.1±0.3[b]

[a] (≈$PhCH{=}CH_2$ +≈$PhCH_2CH_3$+PhOH) / (≈$PhCH_3$+PhCHO)
[b]$PhCH{=}CH_2$/$PhCH_3$

RESTRICTED MASS TRANSPORT EFFECTS ON FREE RADICAL REACTIONS

A. C. Buchanan, III, Phillip F. Britt, and Kimberly B. Thomas
Chemical and Analytical Sciences Division
Oak Ridge National Laboratory
P. O. Box 2008
Oak Ridge, Tennessee 37831-6197

Key words: Model compounds, free radicals, hydrogen transfer, mass transport

INTRODUCTION

Research aimed at the development of improved coal utilization technologies such as coal liquefaction and hydropyrolysis continue to benefit from the insights provided by well-designed model compound studies[1]. The importance of controlling hydrogen utilization in the development of economically competitive processes is well-recognized. The donation of hydrogen atoms to a reactive site in coal, such as a free radical, can occur from molecules native to the coal structure, hydrogen gas, or a liquefaction donor solvent. The hydrogen transfer can also be mediated by the presence of a catalyst. Model compound studies continue to probe the mechanisms of hydrogen transfer and utilization potentially involved in coal liquefaction.[1]

Coal possesses a complex chemical and physical structure. The cross-linked, network structure can lead to alterations in normal thermally-induced, free-radical decay pathways as a consequence of restrictions on mass transport. Moreover, in coal liquefaction, access of an external hydrogen donor to a reactive radical site can be hindered by the substantial domains of microporosity present in coals.[2,3] Larsen et al. have recently investigated the short contact time liquefaction of Illinois No. 6 coal in the presence of either tetralin or 2-*tert*-butyltetralin as the hydrogen donor solvent.[2] Remarkably, both the yields of pyridine extractables and the amount of hydrogen transferred from the donor solvent are the same despite the presence of the bulky *tert*-butyl group. Diffusion effects do not appear to be playing an important role in this coal conversion chemistry. Several possible explanations for this phenomenon were advanced including the potential involvement of a hydrogen hopping/radical relay mechanism recently discovered in model systems in our laboratories.[4,5]

We have employed silica-anchored compounds to explore the effects of restricted mass transport on the pyrolysis mechanisms of coal model compounds.[4-7] In studies of two-component systems, cases have been discovered where radical centers can be rapidly relocated in the diffusionally constrained environment as a consequence of rapid serial hydrogen atom transfers. This chemistry can have substantial effects on thermal decomposition rates[4] and on product selectivities.[5] In this study, we examine additional surfaces to systematically investigate the impact of molecular structure on the hydrogen atom transfer promoted radical relay mechanism. Silica-attached 1,3-diphenylpropane ($\approx Ph(CH_2)_3Ph$, or $\approx$DPP) was chosen as the thermally reactive component, since it can be considered prototypical of linkages in coal that do not contain weak bonds easily cleaved at coal liquefaction temperatures (ca. 400°C), but which crack at reasonable rates if benzylic radicals can be generated by hydrogen abstraction. The rate of such hydrogen transfers under restricted diffusion will be highly dependent on the structure and proximity of neighboring molecules.[4,7]

EXPERIMENTAL

The two-component surfaces shown below were synthesized from the corresponding phenols by co-reaction with the surface hydroxyls of a nonporous, fumed silica (surface area of 200 ± 25 m^2/g) as previously described.[4-7] The compounds are covalently anchored to the silica surface by a thermally robust Si-O-C_{aryl} linkage. The resulting two-component surfaces had purities of ≥ 99.3%.

Pyrolyses were performed in sealed, evacuated (2×10^{-6} torr), T-shaped tubes at 375°C. During the reaction, any volatile materials formed migrated out of the heated zone and were collected in the sidearm cold trap (77K). After the reaction, the volatile products in the trap were dissolved in acetone and analyzed by GC and GC-MS with the use of internal calibration standards. Base hydrolysis (1N NaOH) of the silica residue liberated the surface-attached

products and unreacted starting materials, which were isolated as the corresponding phenols following neutralization and extraction with CH_2Cl_2. These products were silylated with *N,O*-bis(trimethylsilyl)trifluoroacetamide in pyridine (2.5M), and the corresponding trimethylsilyl ethers were analyzed in the presence of internal standards by GC and GC-MS.

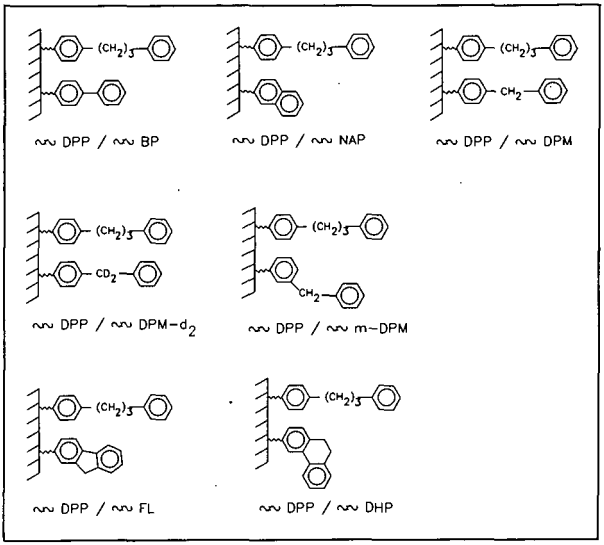

RESULTS AND DISCUSSION

If the rate of decomposition of 1,3-diphenylpropane were governed solely by homolysis of its weakest bond (about 74 kcal/mol) to form $PhCH_2\bullet$ and $\bullet CH_2CH_2Ph$, then DPP would be stable at 400°C with a half life on the order of 19 years.[8] The fact that DPP is thermally reactive even at 375°C derives from the incursion of a free-radical chain decomposition pathway that produces benzylic radicals capable of cracking by β-scission. For silica-immobilized DPP (≈DPP), this reaction produces the cracking products shown in Eq. 1 with the radical chain propagation steps shown in Eqs. 2-4.[7] As shown in Table 1, the rate of ≈DPP decomposition decreases substantially with decreasing surface coverage as the rate for the hydrogen atom transfer step 4 decreases. This should be particularly important

$$\approx Ph(CH_2)_3Ph \rightarrow PhCH_3 + \approx PhCH{=}CH_2 + \approx PhCH_3 + PhCH{=}CH_2 \quad (1)$$

$$\approx PhCH\bullet CH_2CH_2Ph\ (\mathbf{1}) \rightarrow \approx PhCH{=}CH_2 + PhCH_2\bullet \quad (2)$$

$$\approx PhCH_2CH_2CH\bullet Ph\ (\mathbf{2}) \rightarrow \approx PhCH_2\bullet + PhCH{=}CH_2 \quad (3)$$

$$\approx PhCH_2\bullet\ (\text{and } PhCH_2\bullet) + \approx Ph(CH_2)_3Ph \rightarrow \approx PhCH_3\ (\text{and } PhCH_3) + \mathbf{1} + \mathbf{2} \quad (4)$$

for hydrogen abstraction by the surface-attached benzyl radical, $\approx PhCH_2\bullet$, as the spatial separation between reactants increases with decreasing surface coverage. Similar rate decreases are observed in pyrolysis of liquid-phase DPP when the concentration is decreased by dilution with an inert solvent.

Discovery of the radical relay mechanism originated from studies of the pyrolysis of the surfaces, ≈DPP/≈BP, ≈DPP/≈NAP, and ≈DPP/≈DPM, where the biphenyl and naphthalene spacers were innocuous, but the diphenylmethane spacer molecules resulted in greatly enhanced decomposition rates (ca. 10-fold) for ≈DPP when compared at similar surface coverages of ≈DPP (see Table 1).[4] This is in contrast to liquid phase DPP pyrolyses where DPM behaves as other inert diluents.[4] In the surface-immobilized cases, no new products were formed, and the involvement of diphenylmethane moieties in the relay pathway was confirmed from the study of ≈DPP/≈DPM-d_2. In addition to an apparent deuterium isotope effect on the reaction rate, incorporation of substantial amounts of deuterium in the vapor-phase and surface-attached toluene products was detected. A pictorial representation of the radical relay process is shown below. The facility of this process, which leads to rates

comparable to saturated coverages of ≈DPP without spacer molecules, is likely a consequence of enhanced A-factors for the bimolecular hydrogen transfer steps on the surface for these "pre-organized" reactants. Similar effects have been proposed to explain the enhanced rates often observed for organic reactions on clay surfaces, which are attributed to a "reduction in the dimensionality of the reaction space".[9]

Table 1. Effect of Spacer Structure on Pyrolysis of ≈DPP at 375°C

Surface Composition	*Coverage (mmol g^{-1})*	*Rate x 10^4 (% s^{-1})*
≈DPP	0.59	24.0
	0.14	1.1
	0.10	0.72
≈DPP / ≈BP	0.13 / 0.51	2.2
≈DPP / ≈NAP	0.12 / 0.44	1.9
≈DPP / ≈DPM	0.17 / 0.42	21.0
	0.13 / 0.37	17.0
≈DPP / ≈DPM-d_2	0.16 / 0.36	12.0
≈DPP / ≈*m*-DPM	0.17 / 0.31	27.0
≈DPP / ≈FL	0.17 / 0.42	86.0
≈DPP / ≈DHP	0.21 / 0.36	8.6
	0.065 / 0.47	13.0

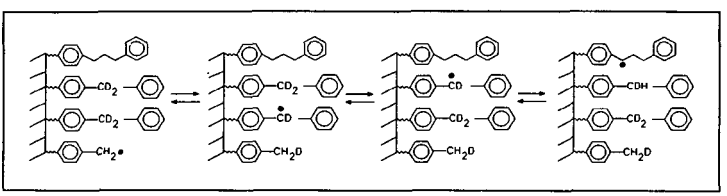

As shown in Table 1, the use of the isomeric *meta*-diphenylmethane spacer similarly produces enhanced rates, and appears even more effective than the *para*-analog at participating in the radical relay process. The fluorene spacer (≈FL) is a cyclic analog to ≈*m*-DPM, which is known to have faster kinetics for hydrogen donation to benzyl radicals because it does not require phenyl rotations to be frozen in the transition state.[8] However, in the surface-attached analog, the fact that the benzylic hydrogens are attached to a carbon locked in a ring could potentially lead to geometrical constraints in the hydrogen transfer steps on the surface. As shown in Table 1, the ≈DPP pyrolysis rate is substantially enhanced in the presence of ≈FL compared even with the DPM cases. However, for ≈DPP/≈FL, we have found that the majority of the ≈PhCH=CH_2 product has undergone reaction with fluorenyl radical in a chain transfer step (Eq. 5). The resulting radical does not terminate the chain, but abstracts hydrogen to provide an additional pathway for relaying radical centers on the surface (Eq. 6 and 7). This additional pathway apparently also contributes to the facile decomposition of ≈DPP.

≈FL• + ≈PhCH=CH_2 → ≈PhCH•CH_2-FL≈ (5)

≈PhCH•CH_2-FL≈ + ≈Ph$(CH_2)_3$Ph → ≈PhCH_2CH_2-FL≈ + **1** + **2** (6)

or, ≈PhCH•CH_2-FL≈ + ≈FL-H → ≈PhCH_2CH_2-FL≈ + ≈FL• (7)

The hydroaromatic, 9,10-dihydrophenanthrene (DHP), is often employed as a model hydrogen donor liquefaction solvent. It can be seen from Table 1 that ≈DPP reacts faster in the presence of co-attached DHP (≈DHP) than in the presence of the inert aromatics, biphenyl (≈BP) and naphthalene (≈NAP), although not as fast as in the presence of ≈DPM. The radical relay chemistry is more

complicated with ≈DHP, however, because chain propagation can also occur via hydrogen atoms donated by the intermediate hydrophenanthryl radicals, ≈DHP•, which would not experience diffusional constraints (Eqs. 8 and 9). Consistent with this premise, we observe formation of modest amounts of surface-attached phenanthrene (≈PHEN), as well as new products resulting from hydrocracking of ≈DPP (accounting for ca. 2% of the reacted ≈DPP) to form ≈PhH + PhC_3H_7 and PhH + ≈PhC_3H_7. However, it is interesting that the ≈DPP decomposition rate is substantially greater for the diphenylmethane spacers which serve only as radical relay catalysts.

$$\approx DHP\bullet \rightarrow \approx PHEN + H\bullet \quad (8)$$

$$H\bullet + \approx Ph(CH_2)_3Ph \rightarrow H_2 + \mathbf{1} + \mathbf{2} \quad (9)$$

CONCLUSIONS

This study shows that the rate at which surface-immobilized 1,3-diphenylpropane thermally decays at 375°C can span a substantial range that is dependent on the structure of neighboring molecules on the surface. It seems clear that it is possible for radical centers to relocate in diffusionally constrained environments at relevant coal liquefaction temperatures, without the need for physical movement, by means of rapid serial hydrogen atom transfers. There may exist an optimum set of chemical structures that possess the appropriate thermochemical and structural properties to promote the radical relay phenomenon under conditions of restricted diffusion, and we continue to explore additional spacer molecules.

The significance of these results for coal liquefaction encompasses two points. If the cleavage of a linkage embedded in a microporous domain in coal requires formation of a radical precursor (as typified by DPP in the current study), then a radical relay mechanism could transfer that needed "reactivity" to the linkage in question. Alternatively, if a radical is formed in an inaccessible region of the coal network and needs to be capped by a hydrogen source to prevent a retrogressive reaction, then a radical relay pathway could relocate the radical center to a region in the coal that is accessible to a hydrogen donor in the liquefaction medium. It remains to be determined whether such a phenomenon contributes to the coal liquefaction behavior recently reported by Larsen (*vide supra*).[2]

ACKNOWLEDGEMENT

This research was sponsored by the Division of Chemical Sciences, Office of Basic Energy Sciences, U.S. Department of Energy, under Contract No. DE-AC05-840R21400 with Martin Marietta Energy Systems, Inc.

REFERENCES

1. Buchanan, III, A. C.; Britt, P. F. *Prepr. Pap.-Am. Chem. Soc., Div. Fuel Chem.* **1994**, *39(1)*, 22.
2. Larsen, J. W.; Amui, J. *Energy Fuels* **1994**, *8*, 513.
3. Walker, Jr., P. L.; Mahajan, O. P. *Energy Fuels* **1993**, *7*, 559.
4. Buchanan, III, A. C.; Britt, P. F.; Biggs, C. A. *Energy Fuels* **1990**, *4*, 415.
5. Britt, P. F.; Buchanan, III, A. C. *J. Org. Chem.*, **1991**, *56*, 6132.
6. Buchanan, III, A. C.; Dunstan, T. D. J.; Douglas, E. C.; Poutsma, M. L. *J. Am. Chem. Soc.* **1986**, *108*, 7703.
7. Buchanan, III, A. C.; Biggs, C. A. *J. Org. Chem.* **1989**, *54*, 517.
8. Poutsma, M. L. *Energy Fuels* **1990**, *4*, 113.
9. Laszlo, P. *Acc. Chem. Res.* **1986**, *19*, 121.

THE EFFECT OF COAL ADDITION ON SOLVENT HYDROGENATION AND COAL CONVERSION IN A MODEL ALKYLNAPHTHALENE SOLVENT

Kurt S. Rothenberger, Anthony V. Cugini,
Karl T. Schroeder, Garret A. Veloski, and Michael V. Ciocco
U.S. Department of Energy, Pittsburgh Energy Technology Center,
P.O. Box 10940, Pittsburgh, PA 15236

INTRODUCTION

Model compounds are useful because they offer insight into the processes of more complex systems. They allow one to study a controlled system of known structure and relatively well mapped reaction pathways, in the hope that the information obtained therein is transferable to real systems. The problem with the study of model systems is that those very constraints which make the system easy to understand may in turn hinder the application of that understanding to real systems. This is particularly true in the study of coal liquefaction, where the complexity of the coal system often gives rise to unanticipated results.

The current paper discusses how the addition of even small amounts of coal (1:1 coal:catalyst) can dramatically affect the catalytic hydrogenation of model two-ring aromatic solvents. The catalyst, a novel, unsupported molybdenum catalyst preformed during a separate solvent hydrogenation step, appears to be selectively deactivated toward solvent hydrogenation, but not coal conversion. The effect is observed in two model solvent systems, 1-methylnaphthalene and Panasol. Adding coal-derived preasphaltene and asphaltene materials seems to have the same effect.

EXPERIMENTAL SECTION

Materials. Panasol®, a mixture containing mostly alkyl naphthalenes, was obtained from Crowley Chemical Company and used without further purification. Purified grade 1-methylnaphthalene from Fisher Scientific Company, found to be 99% pure by gas chromatography, was used without further purification. Blind Canyon coal, DECS-6, from the U.S. Dept. of Energy's Coal Sample Program, was used in these studies. A unique, high surface area, preformed molybdenum catalyst was prepared at the U.S. Dept. of Energy's Pittsburgh Energy Technology Center (PETC). The catalyst consisted of the recovered solid from a semi-batch 1-L stirred autoclave reaction of ammonium heptamolybdate, hydrogen sulfide, and Panasol under 17 MPa (2500 psi) hydrogen at 425°C [1]. The catalyst contained 50% C, 30% Mo, and 20% S, and possessed a BET surface area of approximately 250 m^2/g. The supported iron catalyst was prepared by precipitation of FeOOH from a solution of ferric nitrate onto Raven® carbon black. The supported molybdenum catalyst was prepared in a similar fashion from ammonium heptamolybdate.

Reactions. Reactions were completed in a stainless steel batch microautoclave reactor system constructed at PETC. The cylindrical reactor portion has a volume of 43 mL, and the total internal volume, including all tubing and connections, is 60 mL. The reactor was equipped with an internal thermocouple and a pressure transducer for continuous monitoring of pressure and temperature throughout the run. The reactor was mounted on a rocker arm, which extends into an electrically heated sand bath. In typical experiments, the reactor was charged with various combinations of solvent, coal, catalyst, a sulfur source, and then was pressurized with hydrogen. Unless otherwise stated, a full charge consisted of 6.6 g solvent, 3.3 g coal, 0.1 g catalyst, 0.1 g sulfur, and 7 MPa (1000 psi) ambient temperature hydrogen gas. The reactor was then attached to the rocker arm (180 cycles / minute) and plunged into a preheated sand bath, where it was heated up to 425°C in 2 to 4 minutes. It was held at temperature in the sand bath for 30 minutes, and then removed and allowed to air cool, typically in less than 5 minutes, to room temperature. The reactor was vented and the gas collected for analysis.

Sample Workup Procedure and Coal Conversion Calculation. During workup, the reactor (including tubing) was cleaned and rinsed with tetrahydrofuran (THF). The material collected was combined and filtered through a 0.45 micron filter under 40 psi nitrogen gas pressure, yielding the "THF solubles" and "THF insolubles." Coal conversion was calculated based on the mass of MAF coal from the measured mass of THF insolubles adjusted for catalyst and coal mineral matter. After the THF insolubles were

weighed, the soluble material was stripped of solvent on a rotary evaporator until mass balance was obtained. Although this generally removed most of the THF solvent, some was occasionally observed by H-1 nuclear magnetic resonance (NMR) in the resulting THF soluble fraction. In runs where coal was used in the reactor, the THF solubles were extracted by heptane, and the procedure was repeated to obtain a heptane-soluble fraction. In each case, the soluble portion was derived essentially from the original Panasol or 1-methylnaphthalene solvent and its reaction products, and (when coal was present) a small amount of coal-derived material.

Gas and Pressure Analyses. At the completion of each run, product gases were collected and analyzed at PETC by a previously published method [2]. Total hydrogen consumption for the run was calculated based on the difference between initial and final (cold) gas pressure as adjusted for product gas slate. In some runs, gas composition data were not available, or had to be estimated from a similar experiment. Hydrogen consumption as a function of time was calculated from the total (hot) gas pressure, recorded at 10 s intervals during the run, total hydrogen consumption, and the assumption that product gases were produced in a linear fashion throughout the run. Assumptions were also made concerning the liquid-vapor equilibrium of the solvent, the solubility of hydrogen in the liquid phase, and the fact that part of the reactor tubing does not extend down into the hot sand bath. A more complete description of the hydrogen consumption measurements is found in reference 3.

Gas Chromatography. Gas chromatography was performed either with a Hewlett Packard HP5880A gas chromatograph (GC) equipped with flame ionization detector (FID) or a Hewlett Packard HP5890A GC equipped with an HP5970 mass selective detector (GC/MS).

Low-Voltage, High-Resolution Mass Spectrometry (LVHRMS). LVHRMS data were obtained on a Kratos MS-50 high-resolution mass spectrometer interfaced to a personal-computer-based data system developed at PETC. The sample was introduced into the ion source through the batch inlet system at a temperature of 200°C. The magnet was operated with a static resolving power exceeding one part in 30,000 with an average dynamic resolving power (while scanning) of one part in 26,000. Quantitative calibration of tetralins relative to naphthalenes was accomplished with known mixtures of tetralin and 1-methylnaphthalene. Further details on the LVHRMS technique and data reduction routines are provided in references 4 and 5.

Nuclear Magnetic Resonance. Both H-1 and C-13 NMR of the samples were recorded on CD_2Cl_2 solutions of the samples on a Varian VXR-300 NMR spectrometer equipped with a 5-mm broadband probe. C-13 NMR spectra were the result of 700 time-averaged scans recorded with 90° pulse widths and a recovery time of 60 s, requiring approximately 12 hours of spectrometer time per spectrum. Decoupling was applied only during acquisition.

RESULTS AND DISCUSSION

Verification of Analytical Results: 1-Methylnaphthalene and Panasol Solvents. In order to verify the accuracy and reproducibility of the analytical methods, microautoclave hydrogenations were made using 1-methylnaphthalene solvent, 7 MPa initial (cold) hydrogen pressure, and (if used) catalyst. The series consisted of a thermal (no catalyst) run, the preformed dispersed molybdenum catalyst (Mo), an iron (Fe/C) and a molybdenum (Mo/C) catalyst, the latter two supported on carbon black. 1-Methylnaphthalene, 5- and 1- methyltetralin, naphthalene, and tetralin constitute 97% of the products (by GC) from this simple solvent system. Independent determinations of 1-methylnaphthalene hydrogenation to tetralins were made by each of the analytical methods: gas analysis, GC, LVHRMS, and NMR. The results, their averages and standard deviations are listed in Table 1.

Panasol is a fairly complex hydrocarbon mixture, with some 130 GC peaks above the 0.01% threshold level. It contains about 80% alkylated naphthalenes (2-methylnaphthalene is the largest single constituent at 22%), and 5-10% each of alkylated benzenes, tetralins, and biphenyls. It has a proton aromaticity of 0.48, and a carbon aromaticity of 0.84, corresponding to an "average" structure of dimethylnaphthalene. Since the alkylnaphthalenes in Panasol were expected to hydrogenate similarly to 1-methylnaphthalene, a series of microautoclave reactions with Panasol was completed under the same conditions as those for the samples of Table 1.

The results are given in Table 2. For GC and LVHRMS, the hydrogenation determination was made from direct measurement of naphthalenes and tetralins in the products as compared to the starting Panasol. Hydrogenation was estimated from gas analysis by fitting the hydrogen consumption with that necessary to convert a given amount of dimethylnaphthalene to the corresponding tetralins. Hydrogenation was estimated from NMR data by fitting the aromaticity change to a given conversion of dimethylnaphthalene to the corresponding tetralins. Although the hydrogenation estimates for Panasol do not agree with each other as well as they do in Table 1, the average results are still within the standard deviation of the 1-methylnaphthalene hydrogenations.

Effect of Coal Addition on Solvent Hydrogenation Using Preformed, High Surface Area Mo Catalyst. A series of microautoclave experiments was completed using 6.6 g of either 1-methylnaphthalene or Panasol solvent, 7 MPa initial (cold) hydrogen pressure, and 0.1 g preformed high surface area molybdenum catalyst. The runs contained 0.0, 0.1, 0.2, and 3.3 g of coal, respectively. Figure 1 shows the hydrogen consumption plotted as a function of time over the course of each run. A substantial amount of hydrogen is consumed during the heat-up period (i.e., before time zero in Figure 1); in fact, the "liquefaction" of the 0.1 and 0.2 g coal samples is probably completed by the time the plot starts. The residual, or observed hydrogen consumption is most likely due to hydrogenation of the solvent. In the Figure, it can be seen that the rate of hydrogen consumption consistently follows the order 0.0 g > 0.1 g > 0.2 g. The rate for the 3.3 g coal sample is still trending downward at the end of the run, with hydrogen consumption probably attributable to coal conversion rather than solvent hydrogenation.

Total hydrogen consumption for these runs, including the heat-up periods, is listed in Table 3. Not surprisingly, the greatest hydrogen consumption, 55 mmol, was found with the highest loading of coal, 3.3 g. This can be attributed to the fact that two acceptors were available for the gaseous hydrogen - both the solvent and the coal. Consistent with Figure 1, the addition of small amounts of coal to the solvent does not produce an intermediate result. Rather, the total hydrogen consumption with both 0.1 g (26 mmol H_2) and 0.2 g (22 mmol H_2) of added coal is <u>less</u> than that for either no added coal (29 mmol H_2) or 3.3 g added coal. For comparison, the thermal hydrogenation of 1-methylnaphthalene and Panasol, listed in Tables 1 and 2, consumed only 2 and 3 mmoles hydrogen, respectively. The results are more striking when one examines hydrogenation of naphthalenes in the solvent as analyzed by LVHRMS. The percentage of naphthalenes converted to tetralins is highest in the no coal case, and decreases rapidly with increasing amounts of added coal, from 31% to 12%. Unfortunately, heptane contamination from the workup procedure makes it impossible to obtain a quantitative estimate of solvent hydrogenation from NMR aromaticity measurements. However, the results are qualitatively supported by examination of the NMR spectra.

These results demonstrate that the rate of hydrogenation of these solvents is diminished by the presence of small amounts of coal in the reactor. However, the total hydrogen consumption was still greatest for the maximum loading of coal. That is, hydrogen was still going to the coal though not to the solvent. One explanation for this phenomenon might be that the type of structures present in the coal and initial coal derived products hydrogenate more readily than the solvent. In a popular model of liquefaction, the first products of coal dissolution are the asphaltenes and preasphaltenes. These are generally thought of as large, aromatic systems consisting of three or more condensed rings. This argument is supported by work which has shown that three ring systems hydrogenate faster than two ring systems [6]. However, the argument is difficult to accept in circumstances where only a small amount of coal is present. The results of Figure 2 would seem to indicate that coal dissolution happens very quickly in these cases. Even if the coal-derived products hydrogenate more quickly, there would still be adequate time and hydrogen to hydrogenate the solvent.

Effect of Recycled Catalyst on Subsequent Reactions. The next sequence of experiments helps illustrate what happened to the catalyst on exposure to coal. These experiments begin with the THF insolubles from the reaction which had employed 0.2 g of coal with fresh catalyst, cited in the previous series ("A" in Figure 2). This material, presumably consisting of the recovered catalyst and a very small amount of unreacted coal, was used as the catalyst for a new experiment, hydrogenating 1-methylnaphthalene solvent with no fresh coal ("B" in Figure 2). The THF insolubles from the second run were used as the catalyst in a third run, this time containing 1-methylnaphthalene solvent and 3.3 g coal ("C" in Figure 2). The total hydrogen consumption, solvent hydrogenation as measured by LVHRMS, and coal conversion (in the cases where 3.3 g of coal was

reacted) are summarized in Figure 2. The same data for experiments with 3.3 g coal with fresh catalyst ("D"), and 0.0 g of coal with fresh catalyst ("E"), are included for comparison.

Solvent hydrogenation, as seen in Figure 2, is highest for the case of fresh catalyst, and no added coal. Solvent hydrogenation drops by a factor of over two upon exposure of the catalyst to 0.2 g coal, and does not recover, maintaining its value when the recycled catalyst is used in a subsequent run. Solvent hydrogenation drops further when the catalyst is exposed to more coal. Coal conversion, on the other hand, is uninhibited by the use of recycled catalyst. Hydrogen consumption is highest for the experiments which employed a full charge (3.3 g) of coal, intermediate for the case of fresh catalyst and no coal, and lowest for cases in which the catalyst had been exposed to coal but there was not enough coal present to take up hydrogen itself.

In an effort to pinpoint the origin of the catalyst inhibitor, 0.4 g of the THF-solubles, heptane-insolubles fraction (i.e., asphaltenes and preasphaltenes) was taken from a reaction which had employed 3.3 g coal and fresh catalyst and added to a hydrogenation reaction containing 1-methylnaphthalene and fresh catalyst, but no coal. The result ("E") is displayed with the others in Figure 2. Solvent hydrogenation (at 4%) was almost completely suppressed to levels below those obtained with 3.3 g coal present. Hydrogen consumption was much the same as when fresh catalyst was used with small amounts of coal or recycled catalyst was employed.

Discussion and Conclusion. The results of Figure 2 are not consistent with a simple competition for catalyst sites. The fact that solvent hydrogenation with coal present did not recover to previous levels with the "recycled" catalyst indicates some persistent change in the catalyst, i.e., poisoning. The fact that there was no impairment of coal conversion when coal was added, together with a hydrogen consumption value similar to what it would have been for fresh catalyst, indicates that any deactivation of the catalyst did not affect coal conversion.

Plainly, some deactivation of the catalyst has taken place. Otherwise the diminution in solvent hydrogenation would not have occurred. However, a substantial amount of catalytic activity remains. There is no other explanation for the coal conversion or total hydrogen consumption data with 3.3 g coal.

Supported and unsupported catalysts have been used for first stage coal liquefaction. Exposure to coal has been known to affect the long-term activity of supported catalysts. Unsupported catalysts are normally once-through catalysts and are not exposed to coal for long times. Long term deactivation of unsupported catalysts would not be a problem. Rapid and selective deactivation of specific catalyst sites upon exposure to coal would be a greater concern.

Deactivation of supported catalysts has been the subject of a number of studies [7]. The poisoning effect of nitrogen bases on catalysts, especially for those catalysts which have acidic active sites, has been extensively studied in the areas of petroleum cracking [8], coal liquefaction [9], and coprocessing [10]. The formation of carbonaceous deposits on the catalyst surface has also been implicated in the loss of hydrogenation activity in coal liquefaction catalysts [11]. Studies have shown that carbon supports confer higher resistance to fouling by carbonaceous deposits than do alumina supports [12]. The preformed, high surface area molybdenum catalyst used in the coal addition studies reported here is an unsupported catalyst in the sense that it is being developed for once-through use. However, the catalyst still contains 50% carbon, and probably shares much in common with molybdenum catalysts on carbon supports. The observation of catalyst poisoning is therefore significant.

The fact that solvent hydrogenation (at least that of double-ring aromatic compounds) is inhibited while coal conversion, a process which also requires hydrogen, is not, would support the existence of different types of catalytically active sites. Suppose the catalyst contains different types of active sites, and some of these sites bind substrates more strongly than others. In this representation, the best, i.e., most strongly interacting sites are required for hydrogenation of Panasol. However, other weaker sites exist in greater numbers, and are adequate for providing hydrogen to the decomposing coal matrix. Most catalyst poisons act by adhering to an active site and preventing interaction with any other substrates. If the poisoning agent, whatever its identity, is not a particularly strong catalyst poison, it would only adsorb and adhere to the most strongly interacting

sites. In this manner, the sites needed for solvent hydrogenation would no longer be available. On the other hand, the byproducts of coal conversion can use the less active sites, so conversion remains relatively unchanged. Such a system would exhibit the observed characteristics of both catalyst poisoning and competition for catalyst sites.

At this point, it is not known whether the hydrogen going to the coal is involved with hydrogenating aromatic rings, or simply capping fragments formed from bond scission. However, these preliminary results would appear to serve as a warning that the best catalysts for coal liquefaction may not necessarily be found by hydrogenating model compounds.

Further work is in progress to identify the poisoning agent or agents, and to determine if its effect on the catalyst is reversible.

ACKNOWLEDGEMENTS

The authors gratefully acknowledge Dr. Bradley D. Bockrath for suggestions and helpful conversations regarding this project.

DISCLAIMER

Reference in this report to any specific commercial product, process, or service is to facilitate understanding and does not necessarily imply its endorsement or favoring by the United States Department of Energy.

REFERENCES

1. Cugini, A.V.; Krastman, D.; Lett R.G.; Balsone, V.D. Catalysis Today, **1994**, 19(3) 395-408.

2. Hackett, J.P.; Gibbon, G.A. In Automated Stream Analysis for Process Control, Manka, D.P., Ed., Academic Press, 1982; pp 95-117.

3. Ciocco, M.V.; Cugini, A.V.; Rothenberger, K.S.; Veloski, G.A.; Schroeder, K.T. To be published in Proc. 11th Ann. Int. Pittsburgh Coal Conf.; September 12-16, 1994; Pittsburgh, PA.

4. Schmidt, C.E.; Sprecher, R.F.; Batts, B.D. Anal Chem., **1987**, 59, 2027-2033.

5. Schmidt, C.E.; Sprecher, R.F. In Novel Techniques in Fossil Fuel Mass Spectrometry, ASTM STP 1019, Ashe, T.R.; Wood, K.V., Eds., American Society for Testing and Materials: Philadelphia, 1989; pp 116-132.

6. Weisser, O.; Landa, S. In Sulphide Catalysts, Their Properties and Applications, Pergammon: London, 1973; pp 126-127.

7. Derbyshire, F.J. In Catalysis in Coal Liquefaction, IEA Coal Research: London, 1988; Chapter 8.

8. Mills, G.A.; Boedekker, E.R.; Oblad, A.G. J. Am. Chem. Soc., **1950**, 72, 1554-1560.

9. Adkins, B.D.; Milburn, D.R.; Davis, B.H. Prepr. Pap. - Am. Chem. Soc., Div. Fuel Chem., **1988**, 221-228.

10. Ting, P.S.; Curtis, C.W.; Cronauer, D.C. Energy and Fuels, **1992**, 6, 511-518.

11. (a) Kovach, S.M.; Bennett, J. Am. Chem. Soc. Div. Fuel Chem. Prepr., **1975**, 20(1), 143-160. (b) Ocampo, A.; Schrodt, J.T.; Kovach, S.M. Ind. Eng. Chem. Prod. Res. Dev., **1978**, 17, 56-61.

12. Scaroni, A.W.; Jenkins, R.G.; Walker, Jr., P.L. Appl. Catal., **1985**, 14, 173-183.

TABLE 1: Comparison of Analytical Results for 1-Methylnaphthalene Hydrogenation

Technique	Thermal	Mo	Mo/C	Fe/C
Gas Analysis	2%	37%	58%	33%*
GC	2%	31%	50%	25%
LVHRMS	0%	29%	50%	20%
C-13 NMR	2%	29%	45%	20%
AVERAGE±SD	2±1%	32±4%	51±5%	**25±6%**

* gas pressure data estimated due to leak

TABLE 2: Comparison of Analytical Results for Panasol Hydrogenation

Technique	Thermal	Mo	Mo/C	Fe/C
Gas Analysis	4%	34%	55%	27%
GC/MS	NA	NA	46%	17%
LVHRMS	1%	31%	56%	31%
C-13 NMR	5%	25%	36%	27%
AVERAGE	3%	**30%**	**48%**	**26%**

TABLE 3: Effect of Added Coal on Naphthalene Hydrogenation by Preformed Dispersed Molybdenum Catalyst

Solvent	Coal (g)	mmol H_2 Consumed	% Naph to Tet (LVHRMS)
Panasol	0.0	29	31
1-MeNp	0.1	26	22
Panasol	0.2	22	14
Panasol	3.3	55	12

Figure 1: Effect of Added Coal on the Rate of H2 Consumption.

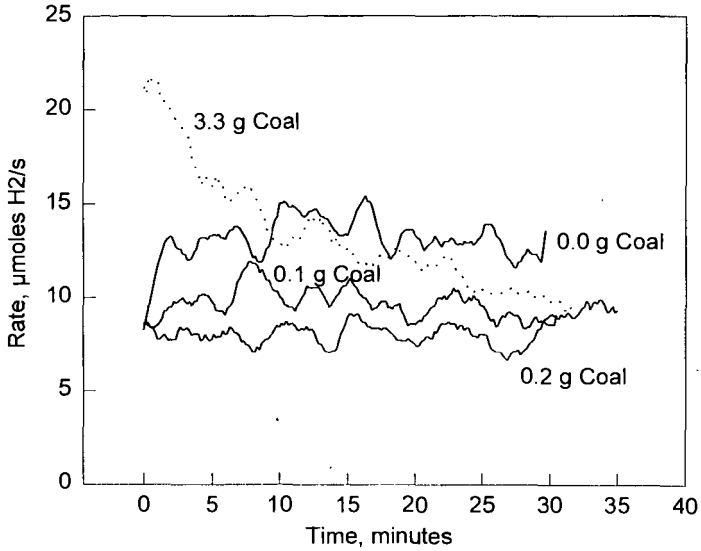

Figure 2: Summary of Coal Conversion, Solvent Hydrogenation and Hydrogen Consumption for Fresh and Recycled Catalyst

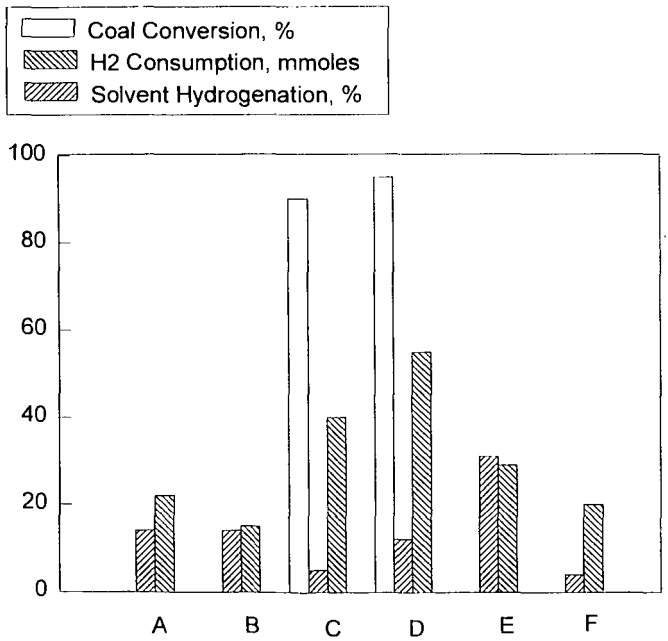

A: 0.2 g Coal, Fresh Catalyst
B: No Coal, Recycled Catalyst from "A"
C: 3.3 g Coal, Recycled Catalyst from "B"
D: 3.3 g Coal, Fresh Catalyst
E: No Coal, Fresh Catalyst
F: No Coal, 0.4 g THF Solubles, Fresh Catalyst

THE EFFECT OF PRESSURE AND SOLVENT QUALITY ON FIRST STAGE COAL LIQUEFACTION WITH DISPERSED CATALYSTS

A.V. Cugini, K.S. Rothenberger, M.V. Ciocco,
G.A. Veloski, and D.V. Martello,
U.S. Department of Energy, Pittsburgh Energy Technology Center,
P.O. Box 10940, Pittsburgh, PA 15236-0940.

Introduction

Dispersed catalysts, both molybdenum and iron based, have been shown to be effective for coal liquefaction.[1] Most studies have tested the effectiveness of these catalysts at moderate to high hydrogen pressures, on the order of 1500 to 2500 psig (10.3 to 17.2 MPa). Coal liquefaction at lower pressures is well known. Hydrogen donor solvents, such as tetralin and dihydrophenanthrene, are capable of transferring hydrogen to the coal at low pressures, less than 400 psig (2.8 MPa).[2]

This study is aimed at exploiting a combination of dispersed catalyst activity with donor solvent quality to reduce the overall pressure of first stage coal liquefaction. Two questions are being addressed in this study. The first is how effective are dispersed catalysts for hydrogenation at lower pressures and the second is to what extent are dispersed catalysts capable of catalyzing the transfer of hydrogen to the coal. This paper presents preliminary studies aimed at addressing these two questions with model coal liquefaction solvents PANASOL (non-hydrogen donor) and tetralin (hydrogen donor).

Experimental

Feed Coal. Experiments were conducted with Blind Canyon bituminous coal (DECS-6, from the DOE/Penn State Coal Sample Bank). This coal was selected because of its low pyritic sulfur content. An analysis of the coal was presented earlier.[1]

Catalyst. A high surface area MoS_2 catalyst was used. The catalyst preparation was discussed previously.[1] The MoS_2 was prepared by reduction of ammonium heptamolybdate under H_2/H_2S in the 1-L semi-batch autoclave at 2,500 psig (17.2 MPa), 4 SCFH (0.11 Nm^3/h) of $H_2/3\%H_2S$, 425°C, and 0.5 h.. The catalyst has a BET surface area of 261 m^2/g, and elemental composition of 30% Mo, 20 % S, and 50% C.

Liquefaction Studies. Experiments were conducted by adding 3.3 g coal to a 40-mL tubular microautoclave reactor with 6.6 g of a mixture of PANASOL (obtained from Crowley Chemical) and tetralin. In experiments in which catalysts were used, 1000 ppm of Mo was added as high surface area MoS_2. The reactor was charged with the desired pressure of hydrogen and sealed. The pressurized reactor was then rapidly (1-2 minutes) heated to the liquefaction temperature (425°C) in a fluidized sandbath. Following the liquefaction period (0.5 h), the reactor was cooled and depressurized. Coal conversion was calculated from the solubility of the coal-derived products in tetrahydrofuran (THF) and in heptane as determined by a pressure filtration technique.[3] One experiment was conducted in a 1-L flow-through reactor to hydrogenate PANASOL. The conditions used in this reactor were 400 g PANASOL, 1000 ppm Mo as MoS_2, 2,500 psig (17.2 MPa), 4 SCFH (0.11 Nm^3/h) of $H_2/3\%H_2S$, 425°C, and 0.5 h.

Solvent Hydrogenation Studies. Experiments were conducted by adding 6.6 g of PANASOL or tetralin to a 40-mL tubular microautoclave reactor. In experiments in which catalysts were used, 1000 ppm of Mo was added as high surface area MoS_2. The reactor was charged with the desired pressure of hydrogen and sealed. The pressurized reactor was then rapidly (1-2 minutes) heated to the liquefaction temperature (425°C) in a fluidized sandbath. Following the liquefaction period (0.5 h), the reactor was cooled and depressurized. The liquid products were recovered from a THF rinse of the reactor.

Analytical characterization of the products is discussed in a separate paper submitted to this symposium.[4]

Discussion of Results

Solvent-Only System

A series of tests was made to investigate the effect of pressure on solvent hydrogenation. Hydrogenation of PANASOL in the presence of a high surface area MoS_2 catalyst was studied in the microautoclave. The extent of hydrogenation was determined by hydrogen consumption from the gas phase, elemental analysis, combined gas chromatography-mass spectrometry (GC-MS), low voltage high resolution mass spectrometry (LVHRMS), and nuclear magnetic resonance (NMR). The % hydrogenation of the solvent is defined as the mol% naphthalenes converted to their corresponding tetralins. Figure 1 shows the levels of hydrogenation determined from the various techniques as a function of pressure. Also on Figure 1 are the equilibrium conversions calculated for the naphthalene/tetralin system at 425°C from the data reported by Frye and Weitkamp[5]. The hydrogenation of PANASOL at 1000 psig (6.9 MPa) with no catalyst and the hydrogenation of PANASOL in the 1-L semi-batch reactor are also shown. As shown in Figure 1, the levels of hydrogenation observed in the microautoclave are significantly lower than the equilibrium for the naphthalene/tetralin system. However, hydrogenation was observed at pressures as low as 400 psig cold (2.8 MPa), 780 psig (5.4 MPa) at temperature. The results in Figure 1 illustrate the range of values of % hydrogenation obtained by the different analytical techniques. Finally, Figure 1 indicates that higher levels of hydrogenation are obtainable in the stirred 1-L autoclave (with gas flow) than in the batch microautoclave.

The reverse of this reaction, dehydrogenation of tetralin, was also studied in the microautoclaves. The dehydrogenation was done at different hydrogen pressures, 400 psig (2.8 MPa) and 1000 psig(6.9 MPa), with and without a high surface area MoS_2 catalyst for 0.5 h at 425°C. The yields of dehydrogenated compounds (naphthalenes) determined by gas chromatography with flame ionization detection (GC-FID) were < 1.0% for 1000 psig (6.9 MPa) and no catalyst, 8.0% for 1000 psig (6.9 MPa) with MoS_2, and < 1.0% for 400 psig (2.8 MPa) and no catalyst. The equilibrium distribution of naphthalene and tetralin at the higher pressure condition is (from Frye and Weitkamp) between 7.5 and 8.0 mol% naphthalene. The results indicate that significant levels of dehydrogenation were only observed with the catalyst present. The MoS_2 is quite effective for tetralin dehydrogenation and, in this case, equilibrium was reached from the tetralin side within the 0.5 h reaction time.

Effect of Coal on Solvent Hydrogenation

The effect of coal addition on the hydrogenation of PANASOL was studied in another series of microautoclave tests. The effect of adding 0 g, 0.1 g, 0.2 g, and 3.3 g of DECS-6 Blind Canyon coal on the amount of hydrogen taken up by the solvent in the presence of MoS_2 was investigated. The total amount of hydrogen consumed in these tests were 0.029, 0.026, 0.022, and 0.055 (0.052 and 0.055 in replicate tests) for 0, 0.1, 0.2, and 3.3 g coal respectively. Note that with no catalyst and no coal present, 0.006 moles of hydrogen was consumed and when 3.3 g coal and no catalyst were present, 0.025 mol was consumed. Hydrogen consumption with 0.1 g (0.026) and 0.2 g (0.022) coal was lower than when no coal was added or with 3.3 g coal. The relative rates of hydrogen consumption are also informative. In the absence of coal, total pressure fell gradually over the entire span of reaction time. In the presence of 3.3 g coal, the pressure dropped rapidly, then approached a limiting value, asymptotically less than when no coal was added. The rate of hydrogen consumption is presented in a figure in a separate paper at this symposium.[4] Product inspection in the latter case indicated that 8 mol% of methyltetralins was formed, but 30 mol% was formed in the former case.

The effect of added coal (3.3 g) on the hydrogenation of PANASOL to tetralins at different pressures was determined by LVHRMS. The results are summarized in Figure 2. Also shown on Figure 2 is the effect of pressure on the hydrogenation of PANASOL with no added coal. Considerably less hydrogenation of PANASOL was observed when coal was added.

To distinguish whether the added coal was competing with the PANASOL for catalytic sites or if coal was suppressing catalytically active sites, THF washed catalyst (plus any residual insoluble coal) from the test using 0.2 g coal was added to a separate test with just PANASOL. The rate of hydrogen consumption was very similar to the original case in which 0.2 g coal was

added. Since solvent hydrogenation was diminished in the absence of added coal, it appears suppression rather than competition for active sites takes place. In a third test the catalyst was washed with THF and again added with PANASOL and 3.3 g DECS-6 coal. The overall coal conversions and rate of hydrogen consumption was the same as with fresh catalyst. This indicates that even though the activity of the catalyst for solvent hydrogenation was suppressed by the presence of coal, the catalyst remained effective for coal liquefaction and conversion. A separate paper that discusses this effect in more detail has been submitted to this session.[4]

The effect of coal on MoS_2 catalyzed dehydrogenation of tetralin was also studied. The amount of hydrogen produced was determined by gas analysis. When no coal was present during the dehydrogenation of tetralin, under 1000 psig N_2 (6.9 MPa), 0.005 mol of hydrogen was evolved with no catalyst present and 0.050 mol of hydrogen was evolved with added MoS_2. Exposing the MoS_2 to 0.2 g of coal resulted in the evolution of 0.010 mol of hydrogen. It appears that the presence of coal also suppresses the dehydrogenation activity of the MoS_2 catalyst (though more hydrogen was evolved than with no catalyst added). Tetralin dehydrogenation was studied in the presence of 3.3 g of coal under 1000 psig (6.9 MPa) N_2. With coal and no catalyst present, 0.003 mol of hydrogen was produced. With added MoS_2 in the presence of coal, 0.013 mol of hydrogen was produced (about 4.3 times the amount produced with no catalyst). However, coal conversion to THF and heptane soluble products was similar for the two cases.

Effect of Pressure and Solvent Quality on Coal Conversion

The effect of varying the cold pressure from 200 to 1000 psig (1.4 to 6.9 MPa) on coal conversion with added MoS_2 catalyst was investigated. The conversion of coal to THF and heptane soluble product is shown in Figure 3. The results show that coal conversion is affected by pressure; however, higher conversions are observed at 400 psig cold (2.8 MPa) with catalyst than at 1000 psig cold (6.9 MPa) without catalyst. This indicates that the catalyst is effective even at pressures as low as 400 psig cold (2.8 MPa). Figure 4 presents the effect of pressure on C_1-C_4 gas produced. As shown in Figure 4, higher amounts of gas were produced with increasing pressure (also increasing conversion).

The effect of solvent quality on coal conversion with no added catalyst was investigated by varying the ratio of tetralin to PANASOL. These results are shown on Figure 5. Also shown in this Figure are the earlier results using added catalyst with 100% PANASOL at different pressures. In order to compare the magnitude of the catalytic (100% PANASOL) with the hydrogen donor (varying tetralin to PANASOL ratios) effect, a common basis was selected in the following way. The positioning of the catalytic data (obtained at different pressures with 100% PANASOL) with respect to the x-axis was determined based on the observed amounts of tetralins produced from PANASOL as a function of pressure in tests with no coal added (from Figure 1). Thus, these estimates represent the maximum expected concentration of tetralins in the PANASOL/coal/catalyst system that could be achieved by the end of the 0.5 h span of reaction. Using this as a basis, higher conversions of coal to soluble products are observed with added catalyst than with tetralin/PANASOL mixtures. The differences become smaller as maximum THF conversion is approached in both systems.

Effect of Catalyst Addition on Mixed Donor/Non-Donor Systems

In non-catalytic experiments at 400 psig H_2 (2.8 MPa), hydrogen was transferred to the coal from the dehydrogenation of tetralin. With a mixture of 25% tetralin with 75% PANASOL as the solvent for DECS-6 coal, the hydrogen transferred to the coal was calculated based on the amount of tetralin converted to naphthalene (by LVHRMS) and the detected hydrogen in the gas phase. The calculated amount of hydrogen transferred to the coal was 0.011 mol (the total hydrogen produced from the tetralin was 0.015 mol). This level of hydrogen transferred was equivalent to the hydrogen transferred from the gas phase in catalytic cases with a non-donor at 300-400 psig H_2 cold (2 to 2.8 MPa).

MoS_2 was added to a system containing a mixture of 20% tetralin and 80% PANASOL as the solvent for DECS-6 coal at 400 psig H_2 cold (2.8 MPa). Dehydrogenation of the tetralin produced 0.038 mol of hydrogen, and 0.024 mol of hydrogen were transferred to coal. Approximately 2.5 times the amount of hydrogen was produced from the tetralin than in the non-catalytic case, and 2.0 times the amount of hydrogen was transferred to the coal than in the non-

catalytic case. It is not clear whether the additional hydrogen was transferred to the coal by direct catalytic hydrogen transfer or catalytic dehydrogenation to the gas phase followed by catalytic hydrogenation of the coal. Note that the addition of catalyst to the mixed hydrogen donor/non-donor system resulted in higher coal conversion to THF soluble product than in the non-catalytic system (80% with a catalyst compared to 68% without a catalyst).

Conclusions and Future Efforts

The major results from this effort can be summarized as:

1) Catalyst activity for coal conversion is observed at pressures as low as 400 psig (2.8 MPa).

2) MoS_2 catalysts can act as effective dehydrogenation catalysts even under hydrogen pressures, therefore these catalysts may be effective for transferring hydrogen from solvents to coal.

3) Production of C_1-C_4 gases increases with increasing hydrogen pressure.

4) While coal can inhibit the activity of MoS_2 catalysts for solvent hydrogenation, the activity of these catalysts for coal conversion remains high after several passes in a coal liquefaction environment.

Future tests are planned to investigate the interrelationship of solvent quality, pressure, and catalyst activity in an effort to reduce the overall pressure used in coal liquefaction. Based on the results obtained thus far, an appropriate combination of solvent quality and catalyst activity may allow significant reductions in the overall pressure of first stage coal liquefaction.

Disclaimer

Reference in this report to any specific commercial product, process, or service is to facilitate understanding and does not necessarily imply its endorsement or favoring by the United States Department of Energy.

References

1) Cugini, A.V., Krastman, D., Martello, D.V., Frommell, E.F., Wells, A.W., and Holder, G.D., Energy & Fuels, **8**(1), 83-87(1994).

2) Schindler, H., "Coal Liquefaction: A Research Needs Assessment," DOE/ER-0400, UC-108 (available from NTIS, Springfield, VA), 1989.

3) Utz, B.R., Narain, N.K., Appell, H.R., and Blaustein, B.D., "Coal and Coal Products: Analytical Characterization Techniques" (Ed. E.L. Fuller, Jr.), ACS Symposium Series No. 205, 1982, 225-237.

4) Rothenberger, K.S., Cugini, A.V., Schroeder, K.T., Veloski. G.A., and Ciocco, M.V., Am. Chem. Soc., Div. of Fuel Chem., Preprints, submitted.

5) Frye, C.G. and Weitkamp, A.W., Journal of Chemical and Engineering Data, **14**(3), 372-375(1969).

Figure 1. Effect of Reactor Pressure on PANASOL Hydrogenation in a Microautoclave at 425 °C with 1000 ppm Mo

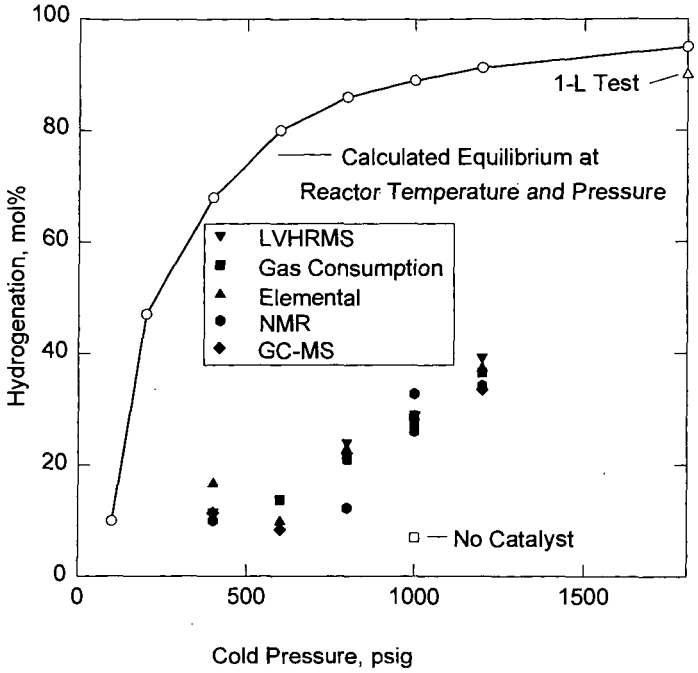

Figure 2. Effect of Pressure on %Tetralins in Total Product from a Microautoclave at 425 °C with 1000 ppm Mo

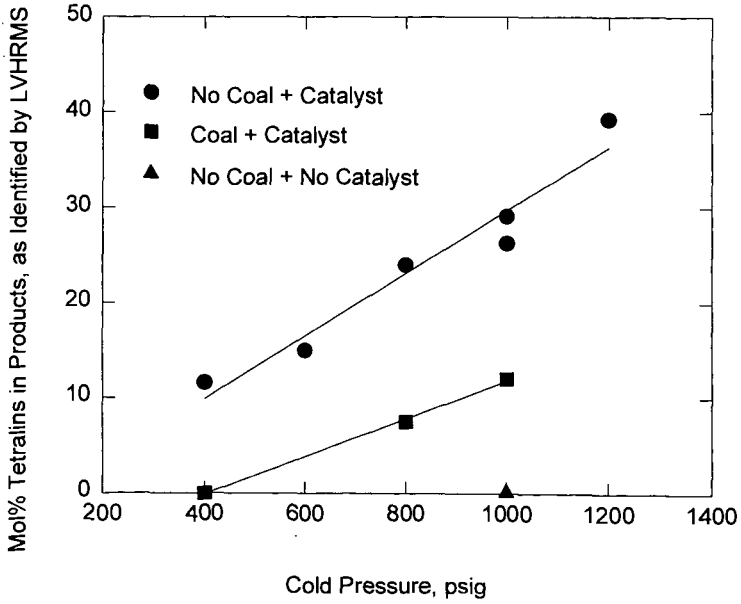

Figure 3. Effect of Pressure on DECS-6 Coal Conversion with PANASOL in a Microautoclave at 425 °C with 1000 ppm Mo

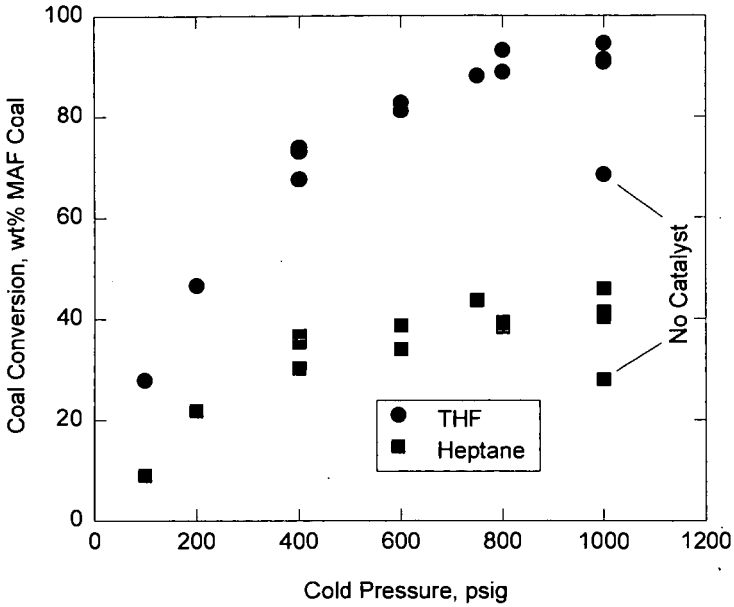

Figure 4. Effect of Pressure on C_1-C_4 Produced in Microautoclave at 425 °C with 1000 ppm Mo using DECS-6 and PANASOL

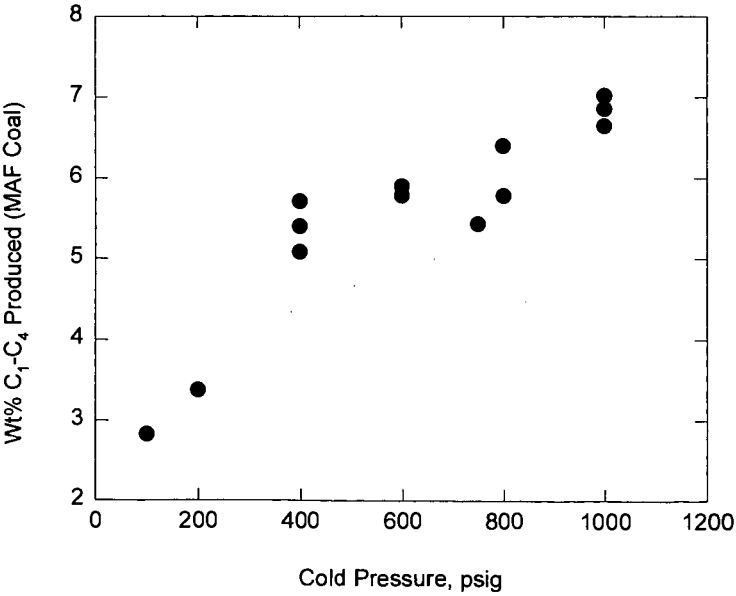

Figure 5. Comparison of coal conversions in mixtures of tetralin/PANASOL with no catalyst to 100% PANASOL (at different pressures) with a catalyst.

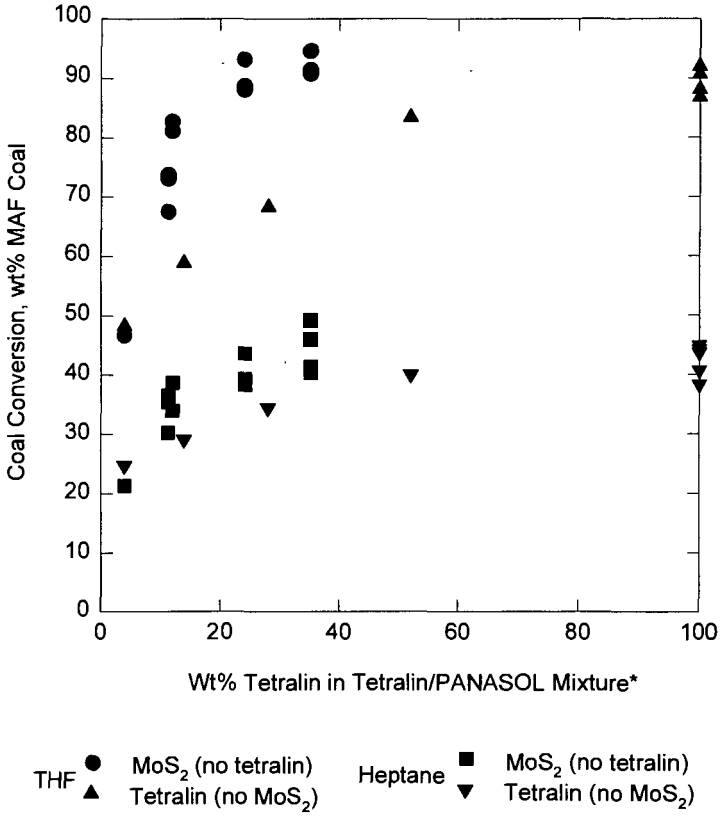

* Calculated for Catalytic System

PILLARED MONTMORILLONITE CATALYSTS FOR COAL LIQUEFACTION

R.K. Sharma and E.S. Olson
University of North Dakota
Energy & Environmental Research Center
Grand Forks, ND 58202

Keywords: coal liquefaction, catalysts, clays

ABSTRACT

Pillared clays contain large micropores and have considerable potential for catalytic hydrogenation and cleavage of coal macromolecules. Pillared montmorillonite-supported catalysts were prepared by the intercalation of polynuclear hydroxychromium cations and subsequent impregnation of nickel and molybdenum. Infrared and thermogravimetric studies of pyridine-adsorbed catalysts indicated the presence of both Lewis and Brönsted acid sites. Thus, the catalysts have both acidic properties that can aid in hydrocracking and cleavage of carbon–heteroatom bonds as well as hydrogen-activating bimetallic sites. These catalysts were applied to the hydrodesulfurization and liquefaction of coal-derived intermediates. The reactions of model organosulfur compounds and coal liquids were carried out at 300°-400°C for 3 hours in the presence of 1000 psi of molecular hydrogen. Reaction products were analyzed by GC/FT-IR/MS/AED. The catalysts have been found to be very effective in removing sulfur from model compounds as well as liquefaction products.

INTRODUCTION

Catalytic functions required for coal liquefaction are hydrogenation of aromatics and hydrocracking of C–C bonds as well as C–S, C–O, and C–N bonds. Thus, metal or metal sulfide sites activate hydrogen for addition to aromatic rings or for hydrogen transfer reactions, and acidic sites are important for bond cleavage activity in coal liquefaction catalysts. High surface areas for the metal sulfide sites are desired for high activity; this can be achieved by dispersion of the metals on a supporting material with some acidic properties.

Because of their acidic properties, smectite clays have been used as catalysts in petroleum cracking and various other reactions. Unfortunately, they dehydrate and collapse at temperatures above 200°C. New coal liquefaction catalysts being investigated at EERC utilize pillared clays as supports for the metal sulfide sites (1–3). Artok and others used a copper-pillared clay for coal liquefaction (4). In pillared clays, large polyoxymetal cluster cations are exchanged (intercalated) between the negatively charged clay layers in place of the hydrated metal ions. When calcined to drive off the water, the polyoxymetal cations form pillars that maintain the clay layer structure, thus creating large spacings between the layers. These structures are stable to 450° and 500°C. Hypothetically, the micropore volumes will be large enough to accommodate macromolecules of the feedstock to be hydrocracked. Chromia-pillared clays, which have interlayer spacings somewhat larger than those present in alumina-pillared clays used in petroleum refining, have considerable potential for coal liquefaction.

RESULTS AND DISCUSSION

A survey of the catalytic hydrocracking activities of various derivatives of natural montmorillonite clay was conducted. These derivatives included both pillared and unpillared forms of the clay as well as the catalysts obtained by impregnating nickel–molybdenum sulfide on the pillared clay as a support. These tests were carried out in a rocking microreactor (tubing bomb) under 1000 psi of hydrogen at temperatures of 300° to 400°C. Bibenzyl (1,2-diphenylethane), diphenyl sulfide, diphenyl ether, and other hydrocarbon compounds were utilized as substrates to model the structural moieties of the coal, especially the bridging groups believed to link the aromatic clusters. Some of the catalysts were then tested with first-stage coal liquids (low-severity Wyodak liquefaction product), and conversions to distillate materials were determined.

To study the effects of acidic sites present on a clay, the concentration of acidic sites on montmorillonite was maximized by converting the clay to an acid-exchanged form. This form of montmorillonite was prepared by washing the cleaned sodium form of the clay with hydrochloric acid. The reaction of the acid-washed clay (AM) with bibenzyl at 350°C gave a 75% conversion of bibenzyl, whereas a blank hydrogenation reaction of bibenzyl with no clay or catalyst gave only 1% conversion to toluene. The yield of benzene resulting from the clay-catalyzed hydrocracking test was only 34 wt%. The yields of ethylbenzene and toluene were very small (1.9% for each). A two-step reaction of the bibenzyl is believed to occur, producing benzene and ethylbenzene in the first step, and ethylbenzene is further cleaved to benzene and ethane in the second step. Yields of the gas products such as ethane were not measured. Toluene is produced in a different type of reaction. The higher yield of benzene compared to toluene in the montmorillonite reaction indicates that Brönsted acid catalysis (ipso protonation mechanism) is more important in the reaction than Lewis acid catalysis (5, 6). Much of the bibenzyl was

converted to condensation products such as phenylethylbibenzyl. These products are formed from addition reactions (Friedel-Crafts reactions) of the carbonium ion intermediates with bibenzyl or products. The large amounts of condensation products observed in the reaction of bibenzyl with the clay indicate that the selectivity of the acid-washed clay for condensation versus cracking is poor.

Chromia-pillared montmorillonite was prepared with two different concentrations of chromia pillars. The low-concentration chromia-pillared clay (LCPC) gave an 80% conversion of bibenzyl, but as with the acid-washed clay, low yields of benzene (27 wt%), toluene (1 wt%), and ethylbenzene (3 wt%) were obtained from hydrocracking. Condensation products were abundant in the reaction products, indicating poor selectivity for hydrocracking. Results with the clay having a high concentration of chromia pillars (HCPC) gave somewhat higher conversion (93%) and more benzene (47 wt%). Formation of cyclohexanes by single-ring hydrogenation reactions was not observed with either of the chromia-pillared clays or with the unpillared acid-washed clay.

Nickel and molybdenum were impregnated in the high chromia-pillared clay and sulfided to give the active clay-supported catalyst (NMHCPC), and the hydrotreatment reaction with bibenzyl was conducted to determine its effectiveness. A conversion of 91% was achieved at 350°C. This conversion is significantly better than the 64% conversion obtained with the high-chromia-pillared clay support, which did not contain the nickel and molybdenum catalyst. The conversion increased to 99% when the reaction was carried out at 400°C.

The products from the reactions of bibenzyl catalyzed by the NMHCPC were found to be a mixture of aromatics and cycloalkanes. The major products were benzene and ethylbenzene, and the minor products were cyclohexane, methylcyclohexane, and alkylbenzenes. These products resulted from hydrocracking as well as from hydrogenation of the aromatic compounds. In contrast to the reactions carried out with HCPC, the amounts of oligomeric condensation products formed during the reaction with NMHCPC were negligible. From these data, we conclude that the introduction of nickel and molybdenum has moderated the activity of the support so that selectivity for hydrocracking relative to condensation is obtained. The high conversion may be attributed to bimetallic sulfide activation of hydrogen to effect at least partial hydrogenation of the aromatic rings. Activation energies for bond cleavage reactions may be lower in the reduced intermediates. Carbonium ion intermediates are more easily reduced by hydride transfer reactions from the hydrogenated intermediates or dissociated hydrogen on the metal sulfide. Thus, the carbonium ions are rapidly reduced and do not survive long enough to undergo addition reactions to aromatic rings that result in condensation and coking.

Reactions of the LCPC with other alkylbenzenes were investigated to determine if the reactions were consistent with the proposed carbonium ion mechanism. Isopropylbenzene (cumene) reacted very rapidly, giving 100% conversion. Benzene was the major product. The more rapid reaction is expected for a reaction involving cleavage of the aryl–alkyl bond of the *ipso*-protonated ring intermediate to give the secondary isopropyl carbonium ion plus benzene. The reaction with phenyldecane occurred with 81% conversion to give benzene as the major product. A large number of various alkylbenzene and indan products were formed in the reaction as a result of carbonium ion rearrangements and cleavage reactions. Cyclohexanes were not observed in the reaction products.

Although single aromatic rings were not hydrogenated by the clay supports, it was interesting to find out whether multiring aromatic systems could be hydrogenated as they are with other acid catalysts such as zinc chloride. Thus, pyrene was reacted with the chromia-pillared montmorillonite to determine if acid-catalyzed hydrogenation of the multiring systems could be effected. The conversion of pyrene to a hydrogenated pyrene mixture was found to be 15%, which is considerably less than that observed for zinc chloride catalysts. For catalysts containing molybdenum and other transition metals, hydrogenation of multiring systems occurs readily. The reaction with pyrene at 350°C did not result in hydrocracking or rearrangements of the pyrene or hydropyrene rings to phenanthrene or other ring systems.

Reactions of diphenyl sulfide were extensively investigated in order to determine the effects of pillaring and nickel molybdenum sulfide loading on hydrodesulfurization activities. The acid-exchanged form of montmorillonite gave a 99+% conversion at 300°C. The products were benzene and thiophenol in a molar ratio of 9.3:1. The relatively high benzene-to-thiophenol ratio shows that the catalyst is effective in cleaving both carbon–sulfur bonds of the diphenyl sulfide; that is, the thiophenol intermediate is further converted to benzene and hydrogen sulfide. The blank hydrogenation reactions of diphenyl sulfide carried out with no clay or catalyst present resulted in conversions of 1 % at 300°C and 10% at 400°C. The excellent conversion obtained with the acid-exchanged clay may be attributed to the high acidity of the catalyst. The anionic aluminosilicate

layers of the clay may also have some ability to stabilize cationic intermediates prior to a reduction step in the hydrodesulfurization mechanism.

The catalytic activity of sodium-exchanged montmorillonite was also tested at 300°C with diphenyl sulfide, and a conversion of only 11 % was obtained. Both benzene and thiophenol were formed (molar ratio of 6.9:1). The sodium-exchanged clay has some residual Brönsted acidity from the polarization of the water of hydration of the sodium cations and the hydroxyl groups of the clay layers.

Our hydrodesulfurization studies were then extended to the chromia-pillared montmorillonites. Hydrogenation of diphenyl sulfide with the LCPC resulted in a conversion of 95% to benzene and thiophenol in equimolar amounts. The high conversion can again be attributed to the high Brönsted acidity of the pillared clay. Catalytic acidic sites may be present on the polyoxychromium cation pillars, since they retain some hydroxyl functionality (7).

Formation of equal moles of benzene and thiophenol in the pillared clay-catalyzed reaction suggests that cleavage of only one carbon–sulfur bond of the diphenyl sulfide occurred. In order to determine if the second carbon–sulfur bond can actually be cleaved in this catalytic system, a reaction of thiophenol was carried out with LCPC under the same conditions used for diphenyl sulfide. Analysis of the reaction products showed 95% conversion of the thiophenol to benzene. These results suggest that during the hydrogenation of diphenyl sulfide, the acidic sites in the clay may be poisoned by the hydrogen sulfide product. Further studies at higher temperatures are in progress to determine whether the deactivation can be reversed.

The HCPC was also tested in the reaction with diphenyl sulfide. This catalyst gave a conversion similar to that obtained with the LCPC, but a much higher molar ratio of benzene to thiophenol (12:1) was found in this test. Thus, the final step of the reaction, which involves hydrogenolysis of the thiophenol, proceeded much more completely with the HCPC catalyst.

Hydrotreating diphenyl sulfide with the NMHCPC catalyst resulted in a 98% conversion. A nearly quantitative amount of benzene was formed with only a trace of thiophenol and a small amount of cylcohexane from reduction of the benzene.

Coal liquefaction tests were carried out with the low-severity product from Wyodak subbituminous coal (LSW) and 1000 psi hydrogen at 400°C in rocking microreactors without added solvent, and the product was distilled to determine the conversion of the nonvolatile portion of the LSW to distillate. Acid-washed clay, pillared clay supports, and NMHCPC catalyst, as well as a commercial silica–alumina-supported Ni-Mo catalyst, gave results paralleling the reactions with the test substrates described above. With a commercial nickel–molybdenum (HDN) catalyst, the conversion to distillate was only 20% under the conditions used. The LSW in the presence of acid-washed montmorillonite gave a conversion of 10%. The LCPC and HCPC with LSW gave very poor conversions (2% and 8% respectively) to distillate. Thus, the supports by themselves are evidently too acidic or too nonselective to be useful for coal liquefaction. But addition of metal sulfides to the support modifies this behavior substantially. A conversion of 29% to distillate was obtained for the NMHCPC catalyst. This is a significant improvement over the conversion obtained with the commercial catalyst. Further testing is required to determine whether the catalysis is actually occurring in the interlayer micropores or simply on the outer surface of the clay. Higher conversions of the LSW to distillate were reported earlier for montmorillonite-supported zinc chloride catalyst (1). Zinc chloride complex catalysts are exceptionally active and efficient in cracking coal, but suffer some disadvantages such as deactivation and emission of hydrogen chloride in the presence of sulfur.

CONCLUSION

Hydrotreatment of first-stage coal liquids and model compounds with a selection of acidic and pillared clays with and without incorporated bimetallic hydrogenation catalysts showed that the combination of support acidity and hydrogen activation catalysis was effective in cleaving C–S and aryl–alkyl bonds and hydrocracking coal materials. Some differences in the activities of the support were noted that depended on the nature and concentration of oxymetal ion used in pillaring the clay. Further efforts are needed to clearly understand these differences.

REFERENCES

1. Olson, E.S.; Diehl, J.W.; Sharma, R.K. *Prepr. Pap. Am. Chem. Soc., Div. Fuel Chem.* **1990**, *35*, 563.
2. Olson, E.S.; Yagelowich, M.L.; Sharma, R.K. *Prepr. Pap. Am. Chem. Soc., Div. Fuel Chem.* **1992**, *37*, 262.
3. Sharma, R.K.; Olson, E.S. *Prepr. Pap. Am. Chem. Soc., Div. Fuel Chem.* **1993**, *38*, 1008.

4. Artok, L.; Malla, P.B.; Komarneni, S.; Schobert, H.H. *Energy & Fuels* **1993**, *7*, 430–431.
5. Sharma, R.K.; Olson, E.S.; Diehl, J.W. *ACS Div. of Fuel Chem. Preprints* **1990**, *35*, (2), 463.
6. Olson, E.S.; Diehl, J.W.; Sharma, R.K. *ACS Div. Fuel Chem. Preprints* **1991**, *36*, (2), 578.
7. Pinnavaia, T.J.; Tzou, M.S.; Landau, S.D. *J. Amer. Chem. Soc.* **1985**, *107*, 4783–4785.

ACKNOWLEDGMENT
The support of the U.S. Department of Energy (Contract No. DOE-FC21-86MC10637) is gratefully acknowledged.

TABLE 1

Catalytic Hydrocracking of Bibenzyl
(1000 psig hydrogen pressure, 350°C, 3 hr, catalyst wt/substrate wt = 0.5)

Catalyst	Conv. %	Yield of Products, wt%
None	1	Toluene (trace)
AM	75	Benzene (34.1) Toluene (1.9) Ethylbenzene (1.9)
LCPC	80	Benzene (27.3) Toluene (1.0) Ethylbenzene (3.4)
HCPC	93	Benzene (47.1) Ethylbenzene (3.6)
NMHCPC	91	1-ring (49.1) 2- and 3-ring (46.8)
NMHCPC*	99	1-ring (76.2) 2- and 3-ring (23.1)

* At 400°C.

TABLE 2

Catalytic Hydrotreating of LSW

	Product (%)			
Catalyst	THF-I	THF-S	Distillate	Actual Distillate
AM	20.0	46.0	28.0	10.0
HDN*	14.3	49.6	35.0	20.0
HCPC	29.4	27.6	26.3	8.0
NMHCPC	6.0	46.0	43.0	28.8

THF-I = Tetrohydrofuran - insoluble
THF-S = Tetrohydrofuran - soluble
HDN* = Commercial Nickel-Molybdenum catalyst

SYNTHETIC CLAY-SUPPORTED CATALYSTS FOR COAL LIQUEFACTION

E.S. Olson and R.K. Sharma
University of North Dakota
Energy & Environmental Research Center
Grand Forks, ND 58202

Keywords: coal liquefaction, catalysts, clays

ABSTRACT

Synthetic clays with nickel substitution in the lattice structure are highly active catalysts for hydrogenation and hydroisomerization and, consequently, have considerable promise for the catalytic upgrading of coal liquids. Nickel-substituted synthetic mica montmorillonite (NiSMM) was prepared and subsequently impregnated with molybdenum and sulfided. The reaction of model compounds with these catalysts in the presence of hydrogen has been investigated to provide mechanistic models for coal liquefaction. The results indicate that NiSMM has active Brönsted acid sites for hydrocracking and hydroisomerization. The hydrogen-activating ability of the molybdenum and nickel sulfide sites proximate to the acid sites results in effective depolymerization catalysis.

INTRODUCTION

Acid smectite clays have been used as catalysts in petroleum-cracking and various other reactions. Unfortunately, they dehydrate and collapse at temperatures above 200°C. In pillared clays, intercalation of hydroxylated or complexed metal cations maintains the clay layer structure after loss of water and generates large micropore volumes. These structures are stable to 450° and 500°C. The alumina cluster-pillared clays are effective supports for use in hydrogenation and hydrocracking catalysis as well as in coal liquefaction (1–3). Chromia-pillared clays with even larger pore spacings have considerable potential for upgrading large coal macromolecules (4). Schobert and others reported copper-impregnated montmorillonite was effective for catalysis of coal liquefaction (5).

Synthetic clays were reported to be more active catalysts than natural clays (6–8). Synthetic mica montmorillonite (SMM) containing cobalt or nickel or another hydrogen-activating component dramatically improves the hydrocracking and hydroisomerization activity (9-12). Exactly how the activity is enhanced is not known (13). In the EERC catalyst program, a selection of synthetic clays with and without incorporated hydrogen-activating components were tested for coal liquefaction as well as with model compounds. The catalysis of C-S and alkyl-aryl bond breakage as well as arene hydrogenation and hydroisomerization of n-alkanes was investigated.

EXPERIMENTAL

Catalyst Preparation. NiSMM was prepared by the procedure of Heinerman and others (14). SMM was prepared by the procedure from the French patent (15).

Preparation of Clay-Supported Molybdenum Catalysts. The synthetic clays were loaded with 5 wt% molybdenum using the incipient wetness method. Ammonium molybdate tetrahydrate (0.046 g) was dissolved in 50 mL of deionized water. To this solution 0.5 g of desired clay was added and stirred overnight. The solvent was removed by evaporation, and the resulting product was calcined in air at 350°C for 6 hours.

Sulfidation. The catalyst was placed in a 12-mL microreactor. The reactor was evacuated and pressurized with 200 psi of hydrogen sulfide. The reactor was placed in a rocking heater preheated to 350°C. The heating was continued for 3 hours. The reactor was cooled to room temperature, degassed, and opened. The catalyst was recovered and stored in airtight bottles.

Reduction. Nickel-substituted synthetic mica montmorillonite was reduced in hydrogen (1000 psi) at 450°C for 16 hours. The reduction was carried out in a microreactor heated in a rocking heater as described above.

Catalytic Reactions. In a typical run, 0.5 g of model compound and 0.25 g of the catalyst were placed in a tubing bomb (12-mL microreactor). The microreactor was evacuated, pressurized with 1000 psig of hydrogen, and placed in a rocking autoclave heated to desired temperature. The heating was continued for 3 hours. At the end of the reaction period, the microreactor was cooled in a dry ice–acetone slurry, degassed, and opened. The desired amount of the internal standard was added to the product slurry, and the product slurry was transferred into a centrifugation tube by washing with methylene chloride and the solid catalyst removed by centrifugation. The liquid sample was analyzed by gas chromatography(GC)/flame ionization detection(FID) and GC/Fourier transformation infrared (FT-IR)/mass spectroscopy (MS). The solid was dried in vacuum at 110°C for 3 hours.

RESULTS AND DISCUSSION

Synthetic mica montmorillonite (SMM) and nickel-substituted synthetic mica montmorillonite (NiSMM) were prepared and used as supports for molybdenum sulfide. Both the synthetic clays and the molybdenum-loaded catalysts were tested for hydrocracking, hydrodesulfurization, hydroisomerization, and hydrogenation activities using bibenzyl, pyrene, dibenzothiophene, and *p*-cresol as test substrates.

Bibenzyl Cracking. The synthetic clay support materials were tested to determine their reactivities prior to molybdenum incorporation. The reaction of bibenzyl with synthetic mica montmorillonite (SMM) gave a very small conversion of bibenzyl into products. However, in the nickel-substituted SMM, where octahedrally coordinated aluminum ions were replaced by nickel ions, the hydrocracking activity increased considerably. The reaction of bibenzyl with NiSMM catalyst converted 67% of bibenzyl into lighter products. Major products were benzene and ethylbenzene. Formation of these products is indicative of a carbonium ion mechanism catalyzed by Brönsted acid sites (16). This mechanism proceeds via ipso protonation followed by cleavage of the aryl–alkyl bond to form the phenylethyl carbonium ion intermediate. The carbonium ion is then reduced to the alkyl group. Ethylbenzene is further cracked to benzene via the same steps, the extent depending on the activity of the catalyst. The formation of toluene may have been Lewis-acid catalyzed. In addition to these products, a very large number of other products in much smaller concentrations were also observed. Detailed characterization of these products is under investigation. These products may have been formed from the hydrogenation, hydroisomerization, or ring-opening reactions. No oligomeric material was observed.

NiSMM was reported to have activity comparable to that of zeolites. It was suggested that nickel-substituted clays crystallize in smaller platelets, resulting in more exposed edges and, consequently, higher surface area and increased activity (13). Based on the FT-IR measurements of adsorbed ammonia on NiSMM, it has been shown that the number of Brönsted acid sites increases following Ni reduction (14, 17). These newly created acidic sites are responsible for the increased activity of NiSMM compared with SMM in which no nickel is substituted for Al^{3+} in the octahedral sites. Robschlager and others (17) reported that for this catalyst to be active for the isomerization of pentane, lattice Ni^{2+} has to be reduced to zero-valent nickel, and the activity of the catalyst decreased when metallic nickel was removed by treatment with carbon monoxide. In contrast, the bibenzyl hydrocracking data for the reduced NiSMM indicates that the activity of the catalyst did not change significantly with reduction of Ni^{2+} to metallic nickel. In fact, a slight decrease in the catalytic activity was seen for the reduced catalyst. However, reduction of the Ni^{2+} during hydrotreating cannot be ruled out.

Sulfidation of the NiSMM gave a substantial increase in catalytic activity for hydrocracking. The reaction of bibenzyl with presulfided NiSMM gave significantly higher conversion (82%) than NiSMM. The product distribution was similar to that of NiSMM reaction. Small amounts of benzene and alkylbenzenes were converted into cyclohexane and cycloalkanes probably by NiS-catalyzed hydrogenation of the single aromatic rings. The increase in hydrocracking activity on sulfidation might be attributed to a facilitation of the addition of hydrogen to some intermediate involved in hydrogen (hydride) transfer, but further work is required to fully understand the nature of the catalytic activity in the NiSMM catalysts.

The reaction of bibenzyl with SMM- and NiSMM-supported MoS_2 gave significantly higher conversions (34% and 92%, respectively) of bibenzyl into products. Major products were found to be benzene, toluene, and ethylbenzene. Small amounts of cyclohexane, methyl cyclohexane, and ethyl cyclohexane were also formed. A significant portion of the bibenzyl was reduced to benzylcyclohexane and other hydrogenated products, but no oligomeric products were formed. Extensive conversion to isomeric aliphatic compounds also occurred. The conclusion from the hydrocracking experiments is that the NiSMM is a very active support for the molybdenum sulfide and the combination has high activity as a hydrogenation, hydrocracking, and hydroisomerization catalyst.

Almost quantitative amounts of catalyst were recovered at the end of each reaction. Unlike highly acidic zeolite catalysts, these catalysts do not catalyze retrogressive reactions or coke formation (18).

Hydrogenation of Pyrene. Pyrene was used as a test compound to investigate hydrogenation activity of NiSMM catalysts. The reactions were carried out by heating pyrene and the desired catalyst at 350°C for 3 hours in the presence of 1000 psi of molecular hydrogen. The effects of sulfiding the NiSMM and supporting the (MoS_2) hydrogenation catalyst on NiSMM were also investigated.

The reaction of pyrene with NiSMM gave a high conversion (90%) of pyrene into hydrogenated products. The majority of the products were di-, hexa-, and decahydropyrenes. Small amounts of hexadecahydro- and tetrahydropyrenes were also

formed. Numerous other components were formed by hydrocracking and rearrangement reactions.

The synthetic clay-supported MoS_2 catalyst gave similar high conversions of pyrene, and the product distribution was changed. Much more of the decahydropyrene (three isomers) and hexadecahydropyrene (three isomers) were formed, owing to the increased activity for hydrogenation of the di- and monoaromatic intermediates. The products also included those formed by rearrangement and hydrocracking reactions.

The commercial nickel-molybdenum catalyst (HDN-30) gave a lower conversion of pyrene (69%). Yields of the hexadecahydropyrene and decahydropyrene products were considerably lower than those obtained with either the NiSMM or MoS_2-NiSMM catalysts, but the dihydropyrene component was greater.

A reaction of pyrene with NiSMM was also carried out at 400°C. As expected, the conversion was lower because of the lower equilibrium constant at the higher temperature. The yields of the hexadecahydropyrene and decahydropyrene were low, but somewhat more cracking occurred.

Heteroatom Removal from Model Compounds. The hydrodeoxygenation, hydrodesulfurization, and hydrodenitrification activities of NiSMM were investigated by using *p*-cresol, dibenzothiophene, and quinoline as test substrates. The reactions were carried out at 400°C for 3 hours in the presence of 1000 psi of molecular hydrogen. Relevant analytical data are given in Table 1.

The reaction of *p*-cresol with NiSMM gave a high conversion (83%) of the substrate into many hundreds of products. Some of the major components are reported in Table 1. The reaction of *p*-cresol gave considerable amounts of o- and *m*-cresols, which could have been formed by acid-catalyzed rearrangement reactions. Toluene and methylcyclohexane were also major products. The reaction of dibenzothiophene also gave hundreds of products, including methylcyclopentane, benzene, toluene, ethylbenzene, and biphenyl as the major products. Quinoline gave tetrahydroquinoline, alkylbenzenes, aniline, and methylpyridine as the major products.

REFERENCES

1. Olson, E.S.; Diehl, J.W.; Sharma, R.K. *Prepr. Pap.—Am. Chem. Soc., Div. Fuel Chem.* **1990**, *35*, 563.
2. Olson, E.S.; Yagelowich, M.L.; Sharma, R.K. *Prepr. Pap.—Am. Chem. Soc., Div. Fuel Chem.* **1992**, *37*, 262.
3. Sharma, R.K.; Olson, E.S. *Prepr. Pap.—Am. Chem. Soc., Div. Fuel Chem.* **1993**, *38*, 1008.
4. Sharma, RK.; Olson, E.S. *Prepr. Pap.—Am. Chem. Soc., Div. Fuel Chem.* **1994**, *39*.
5. Artok, L.; Malla, P.B.; Komarneni, S.; Schobert, H.H. *Energy & Fuels* **1993**, *7*, 430–431.
6. Granquist, W.T. U.S. Patent 3 252 757, 1966.
7. Capell, R.G.; Granquist, W.T. U.S. Patent 3 252 889, 1966.
8. Granquist, W.T. *BRD Offenlegungsschrift* 1973, *231*, 2743.
9. Jaffe, J.; Kittrell, J.R. U.S. Patent 3 535 229, 1970.
10. Kittrell, J.R. U.S. Patent 3 632 501, 1970.
11. Swift, H.E.; Black, E.R. *Ind. Eng. Chem. Prod. Res. Dev.* **1974**, *13*, 106.
12. Swift, H.E.; Black, E.R. *ACS Div. of Petr. Chem. Preprints* **1974**, *19* (1), 7.
13. Bercek, P.G.; Metzger, K.J.; Swift, H.E. *Ind. Eng. Chem. Prod. Res. Dev.* **1978**, *17*, 214.
14. Heinerman, J.J.L.; Freriks, I.L.C.; Gaaf, J.; Pott, G.T.; Coqlegem, J.G.F. *Journal of Catalysis* **1983**, 80, 145.
15. Plee, D.; Schutz, A.; Borg, F.; Poncelet, G.; Jacobs, P.; Gatineau; Fripiat, J. French patent 2, 563, 446, 1984.
16. Olson, E.S.; Diehl, J.W.; Sharma, R.K. *Prepr. Pap.—Am. Chem. Soc., Div. Fuel Chem.* **1991**, *36* (2), 578.
17. Robschlager, K.H.W.; Emms, C.A.; Van Santen, R.A. *Journal of Catalysis* **1984**, *86*, 1.
18. Sharma, R.K.; Olson, E.S.; Diehl, J.W. *Prepr. Pap.—Am. Chem. Soc., Div. Fuel Chem.* **1990**, *35* (2), 463.

ACKNOWLEDGEMENT

The support of the U.S. Department of Energy (Contract No. DOE-FC21-86MC10637) is gratefully acknowledged.

TABLE I

Hydrocracking and Hydrogenation Activity of Synthetic Clays
Reaction Time = 3 h, H_2 = 1000 psi
Catalyst wt/Substrate wt = 0.5

Catalyst	Temperature, °C	Substrate, mmol	Conv., %	*Major Products*, mmol
SMM	350	BB (2.71)	2	Benzene (0.03) Toluene (0.03) Ethylbenzene (0.01)
NiSMM	350	BB (2.72)	67	Benzene (1.46) Toluene (0.11) Ethylbenzene (0.41)
Reduced NiSMM	350	BB (2.79)	65	Benzene (1.29) Toluene (0.13) Ethylbenzene (0.45)
Sulfided-NiSMM	350	BB (2.75)	82	Benzene (1.84) Toluene (0.02) Ethylbenzene (0.65)
Sulfided-MoSMM	350	BB (2.89)	34	Benzene (0.05) Toluene (0.05) Ethylbenzene (0.05) Cyclohexane (0.08)
Sulfided-MoNiSMM	350	BB (2.80)	92	Benzene (1.18) Toluene (0.10) Ethylbenzene (0.40) 4,5-Dihydropyrene (0.21) Methylcyclohexane (0.14) Ethylcyclohexane (0.10) Tetralin (0.15)
Sulfided-NiSMM	350	Pyrene (2.43)	90	Hexadecahydropyrene (0.07) (3 isomers) Decahydropyrene (0.36) (3 isomers) 1,2,3,3_a,4,5-Hexahydropyrene (0.26) 1,2,3,6,7,8-Hexahydropyrene (0.38) 4,5,9,10-Tetrahydropyrene (0.06)
Sulfided-HDN-30 Ni-Moly	350	Pyrene (2.47)	69	Hexadecahydropyrene (0.03) (3 isomers) Decahydropyrene (0.12) (3 isomers) 1,2,3,3_a,4,5-Hexahydropyrene (0.21) 1,2,3,6,7,8-Hexahydropyrene (0.45) 4,5,9,10-Tetrahydropyrene (0.24) 4,5-Dihydropyrene (0.64)
Sulfided-NiSMM	400	Pyrene (2.66)	65	Hexadecahydropyrene (trace) Decahydropyrene (0.05) (3 isomers) 1,2,3,3_a,4,5-Hexahydropyrene (0.13) 1,2,3,6,7,8-Hexahydropyrene (0.17) 4,5,9,10-Tetrahydropyrene (0.06) 4,5-Dihydropyrene (0.41)
Sulfided-NiSMM	350	Naph. (3.98)	62	Tetralin (2.18) Benzene (0.04) Toluene (0.02) Indan (0.02)
Sulfided-NiSMM	400	*p*-Cresol (4.66)	83	Toluene (0.17) Methylcyclohexane (0.16) *m*-Cresol (0.74) *o*-Cresol (1.90)
Sulfided-NiSMM	400	DBT (2.78)	84	Methylcyclopentane (0.26) Benzene (0.28) Toluene (0.10) Ethylbenzene (0.14) Biphenyl (0.13)
Sulfided-NiSMM	400	Quinoline(4.11)	87	C_3-benzene (0.25) Tetrahydroquinoline (0.10) Aniline (0.20) Methylpyridine (0.10)

DBT = Dibenzothiophene.
BB = Bibenzyl.

MODEL REACTIONS AS A MEASURE OF MoS_2 ACTIVITY

Karl T. Schroeder, Bradley C. Bockrath, Ronald D. Miller
U.S. Department of Energy, Pittsburgh Energy Technology Center, P.O. Box 10940, Pittsburgh, PA 15236

ABSTRACT The activity of dispersed molybdenum sulfide liquefaction catalysts was studied using a high-temperature (≤400°C), low-pressure (≤400 kPa) micro-flow reactor. Model compounds were introduced by one of three methods: injection, continuous flow, or injection into a continuous flow. The dehydrogenation of tetralin, the hydrodesulfurization of benzothiophene, and the hydrodeoxygenation of benzofuran were used as examples of reaction types thought to be important for coal conversion. Transient effects, such as the adsorption of the model compound, could be seen in the injection mode of operation. Under steady-state flow conditions, the catalytic conversion of the reactant could be measured. Injection into the continuous flow demonstrated transient and longer lasting effects of quinoline on the catalytic activity. Two dispersed MoS_2 catalysts were compared in terms of their activity, selectivity, and sensitivity to temperature change.

INTRODUCTION This work employed the known catalytic reactions of model compounds to compare the effectiveness of two dispersed MoS_2 liquefaction catalysts. The HDS of benzothiophene, the dehydrogenation of tetralin, the reaction of benzofuran, and the effect of quinoline on activity were used as the basis of the comparison. The reaction mechanisms of these and other model compounds under hydroprocessing conditions have been critically reviewed recently.[1] One of the catalysts studied was a MoS_2 sample recovered as part of the residue from a liquefaction experiment; the other was a MoS_2 formed under dispersing conditions in the absence of coal. This work used a packed column heated in the oven of a GC as a reactor. Although only low hydrogen pressures could be employed, the GC was used to differentiate transient from steady-state behavior and allowed for the rapid adjustment of reaction temperature. This provided an experimental technique which allowed kinetic data to be obtained within a reasonable time period.

EXPERIMENTAL A Hewlett-Packard 5890 gas chromatograph was used as the basis for a high-temperature, low-pressure reactor. A packed column injection port was used to provide a large volume for the expansion of the vaporizing model compound solution. The catalyst was packed into a stainless steel tube and connected to the injector. The amount of catalyst or catalyst-containing residue was adjusted to give 90 mg of molybdenum in the reactor. Reactor pressures up to about 400 kPa of hydrogen were obtained by adding lengths of metal-clad capillary tubing to the end of the reactor. The total effluent flow was monitored using the Hewlett-Packard TCD detector. Model compound solutions were injected into the hydrogen carrier gas in the usual manner except that a slow injection speed was used. Reactants and products were recovered by condensation upon exiting the reactor. The eluant was analyzed by GC-FID and/or GC-MS to determine the identity and quantity of the products. An alternative method of introducing the model compound solution used a Hewlett-Packard Series 1050 pump to provide a continuous stream of solution. In a third type of experiment, a pulse of material was injected into the continuous stream. Regardless of the technique used to introduce the sample, all of the material was vaporized in the injection port of the GC before entering the reactor. Three types of catalytic materials have been studied. The first was a coal liquefaction residue recovered from a batch reaction which had been prepared using a Blind Canyon coal (DECS-17). The residue (IK87-5) contained 50% by weight MoS_2. The remaining 50% was coal ash and organic matter insoluble in THF. Recycling IK87-5 in a second liquefaction experiment with fresh coal showed it was still active for coal conversion and hydrogen up-take. Only a preliminary report has appeared on this material,[2] but its preparation and recycle activity are similar to those found for an Illinois No. 6 coal.[3] IK87-5 was used as an example of a used dispersed catalyst. The second material was an MoS_2 formed by heating ammonium molybdate and tetralin under liquefaction conditions but in the absence of coal or other added solid support (BCP-287). It was used as an example of a fresh, dispersed catalyst. Third, a commercial (Harshaw 0402T) alumina-supported CoMo catalyst was sulfided *in situ* using injections of dimethyldisulfide into the flowing hydrogen. To date, the majority of the work has been done using the first catalyst.

RESULTS AND DISCUSSION The three methods of sample introduction provide different types of information. The injection technique provides a limited amount of material which passes through the reactor as a nearly Gaussian-shaped peak. Strong adsorption on the catalyst and/or support may appear as a peak tail if desorption is fast

relative to the time the material is in contact with the catalyst, or as a loss of peak intensity due to material losses if the desorption is relatively slow. Although significant peak tailing was not seen in our experiments, the preferential loss of material from some samples was seen. Material balances were determined by quantitative GC analysis of the condensed eluant. The preferential adsorption of diphenylether from injections of a 10% solution in n-undecane is shown in Figure 1. The recovered material contained n-undecane, diphenylether and a small amount of benzene amounting to about 3% of the diphenylether injected. No phenol was detected. The recovery of undecane in these experiments averaged 90% and was fairly constant from injection to injection. In contrast, the diphenylether recovery ranged from 65% to 80% and appeared to increase with injection number. A similar though less severe loss of a different oxygenate was seen when aliquots of a 10% solution of benzofuran were injected under the same conditions. In this case, the undecane recovery was 97% while the benzofuran recovery was only 91%. Although the loss of oxygenate in the presence of catalysts dispersed in coal solids has been fairly small, the extent of adsorption can become large in some cases. This can be seen in Figure 2 where the loss of benzofuran is shown for a commercial supported catalyst. In these experiments, benzofuran was introduced as 10 μL injections of a 10% solution, 5 μL injections of the neat material, or 10 μL injections of the neat material. The three sets of data form a single curve showing increased recovery as a function of the total amount of benzofuran injected. Thus, the catalyst appears to adsorb only a certain amount of model compound. Once its capacity has been reached, no further adsorption occurs. Such phenomenon may be important for the proper interpretation of batch data, especially when the amount of model compound is comparable to the amount the catalyst can adsorb. However, they would be expected to disappear in flow experiments where steady-state can be attained. This is the second type of experiment conducted with this reactor.

Steady-state flow conditions were attained by continuously introducing the model compound solution into the injection port of the GC using an HPLC pump. Flows of less than 20 μL/min were necessary to prevent overloading the packed-column injection port. Injector overload caused a decrease in recovery. A similar effect is seen when too much material is injected into an analytical gas chromatograph.[4] In addition to alleviating the problems associated with model compound adsorption, steady-state operation allows for kinetic measurements. For example, the conversion of tetralin to naphthalene at 400°C in the presence of residue IK87-5 is shown in Figure 3. At the lowest flow rate of 2 μL/min, a naphthalene yield of nearly 15% was obtained, well above the amount attributable to a thermal reaction. Increasing the flow rate produced less conversion and the rate appears to be first order in tetralin. Similar measurements at 375°C and 350°C were used to determine the temperature coefficient for the reaction. A value of 300 kj/mol was obtained. Thermolysis reactions typically have values of this magnitude.

Benzothiophene was also used as a model compound to investigate the effectiveness of the residue for HDS reactions. A solution containing 1% benzothiophene yielded recovered starting material along with ethylbenzene as its only product. No styrene was detected in any of the product solutions. When the initial concentration of benzothiophene was raised to 10%, an additional product was also found. The material produced a mass spectrum consistent with dihydrobenzothiophene, C_8H_8S. The recoveries of the benzothiophene and its two products are shown in Figure 4. The amount of C_8H_8S obtained in these experiments decreased with increasing residence time. The presence of dihydrobenzothiophene has been observed in some[5,6], but not all[7] reports on the MoS_2 catalyzed HDS of benzothiophene. Benzothiophene desulfurization by a molybdenum naphthenate derived material has been proposed to follow a pathway dominated by the initial hydrogenation to form dihydrobenzothiophene.[5]

In the third type of experiment, an injection of a second material is made into a steady flow of model compound in solution. An example of this type of experiment is shown in Figure 5 where the TCD trace resulting from injections into a flowing solution is simulated. The recovery data from experiments in which a 10% solution of quinoline was injected into a continuous flow of 1% benzothiophene in tetralin are displayed in Figure 6. The first three determinations in Figure 6 correspond to samples taken on the plateau prior to the first injection of quinoline, roughly between 50 and 100 time units in Figure 5. These determinations consistently gave the conversion of benzothiophene to ethylbenzene to be 50% and the overall material balance to be 91%. The fourth determination results from the collection of the material that elutes with the quinoline pulse from about 110 to 130 time units. The quinoline recovered from the pulse amounted to 80% of that injected. No tetrahydroquinoline or further reduction products were detected. The major effect of the

pulse was to inhibit the production of ethylbenzene. The total recovery of benzothiophene remained constant but the proportion of HDS product decreased to less than 43%. Determination 5 represents a sample taken on the plateau after the quinoline pulse had passed, roughly in the area of 150 to 175 time units. This sample contained neither quinoline nor its reduction products. Figure 6 shows that the conversion of benzothiophene to ethylbenzene had regained about half of the activity lost during the pulse but had not yet fully recovered. Sample 6 contained the material eluting with the second pulse of quinoline and sample 7 contained the material eluting on the plateau after the quinoline pulse. The same results as were obtained with the first pulse are repeated in the second pulse. This indicates that at least two mechanisms of nitrogen base inhibition are operative in this residue. Competitive inhibition in which the quinoline competes with the benzothiophene for adsorption at catalyst active sites may account for a portion of the lost activity seen during the pulse. However, the loss in activity that persists after the quinoline pulse has passed more likely arises from a poisoning of catalyst HDS sites by the base. This poisoning is thought to result from an adsorption mechanism similar to that seen for the diphenylether.

In summary, the liquefaction residue IK87-5 has shown only moderate catalytic activity in the model compound studies. Dehydrogenation and HDS reactions occurred but were significant only when the reaction temperature approached 400°C. Adsorption of heteroatom species occurred and, in the case of quinoline, appeared to be associated with a loss in catalytic activity. The temperature coefficient for the dehydrogenation was quite large and may reflect a thermal rate limiting step.

Work using the fresh, dispersed catalyst BCP-287 is just beginning. Preliminary results indicate much higher rates of tetralin dehydrogenation and benzothiophene HDS than were seen with the liquefaction residue.

CONCLUSIONS Model compound reactions have been used to investigate the catalytic activity of a coal liquefaction residue. The poor dehydrogenation effectiveness of the residue makes it a poor candidate for a hydrogenation catalyst at higher hydrogen pressures. However, in liquefaction experiments at 375°C, this material has been shown to be effective at inducing the uptake of hydrogen gas by coal and the conversion of coal.[2] On the basis of the above results, this ability must be related to some activity other than aromatic hydrogenation.

ACKNOWLEDGEMENT The authors gratefully acknowledge Anthony Cugini for the donation of a sample of the BCP-287 catalyst.

DISCLAIMER Reference to a brand or company name is made to facilitate understanding and does not imply endorsement by the U.S. Department of Energy.

REFERENCES

[1] Girgis, M.J.; Gates, B.C. *Ind. Eng. Chem. Res.* **1991**, *30*, 2021-2058.
[2] Bockrath, B.; Illig, E,; Keller, III, M.; Schroeder, K.; Bittner, E.; Solar, J. *Proceedings, Coal Liquefaction and Gas Conversion Contractors' Review Meeting, September 27-29, 1993* **1993**, 71-83.
[3] Bockrath, B.C.; Illig, E,G.; Keller, III, M.J. *Prepr. Pap.-Am. Chem. Soc., Div. Fuel Chem.* **1992**, *37*(1), 133-140.
[4] Schomburg, G.; Behlau, H.; Dielmann, R.; Weeke, F.; Husmann, H. *J. Chromatogr.* **1977**, *142*, 87-102. Wylie, P.L.; Philips, R.J.; Klein, K.J.; Thompson, M.Q.; Hermann, B.W. *J. High Res. Chromatog.* **1991**, *14*, 649-655.
[5] Ng, F.T.T.; Walker, G.R. *Can. J. Chem. Eng.* **1991**, *69*, 844-851.
[6] Van Parijs, I.A.; Hosten, L.H., Froment, G.F. *Ind. Eng. Chem. Prod. Res. Dev.* **1986**, *25*, 437-443.
[7] Kilanowski, D.R.; Gates, B.C. *J. Catal.* **1980**, *62*, 70-78.

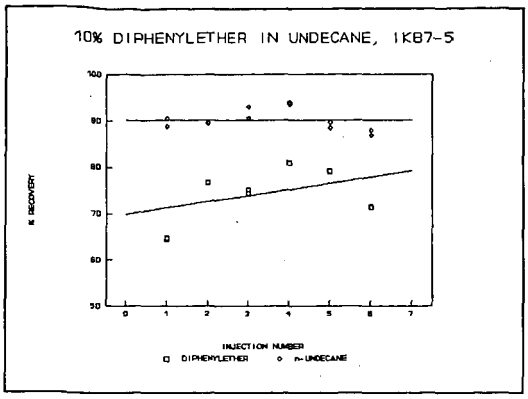

Figure 1. Coal Residue Containing MoS_2 Exhibiting Preferential Adsorption of Diphenylether at 300°C, 100 kPa Hydrogen.

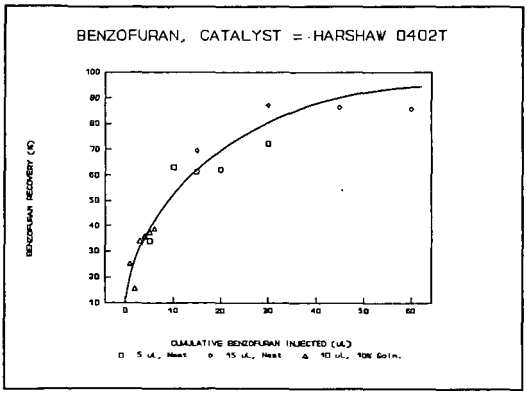

Figure 2. Data Illustrating the Adsorption of Oxygenate by a Supported Catalyst at 300°C, 100 kPa Hydrogen.

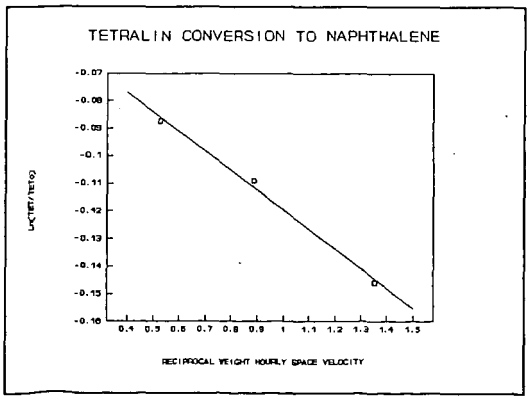

Figure 3. First Order Rate Constant Determination, 400°C, 340 kPa Hydrogen.

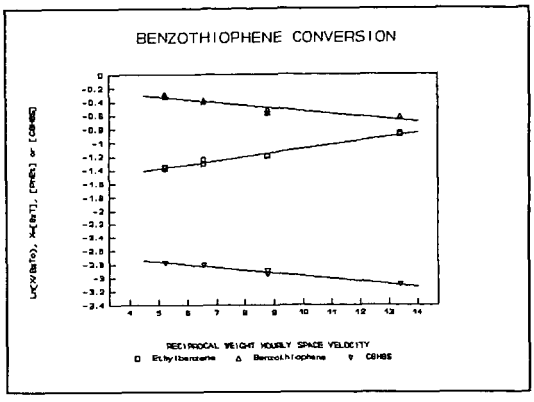

Figure 4. First Order Rate Constant Determination Showing Dihydrobenzothiophene Intermediate Formed at 400°C, 340 kPa Hydrogen.

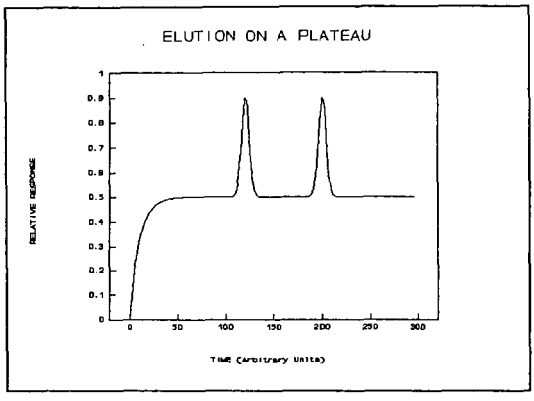

Figure 5. Typical TCD Signal from an Elution on a Plateau Type of Experiment. Units Are Arbitrary.

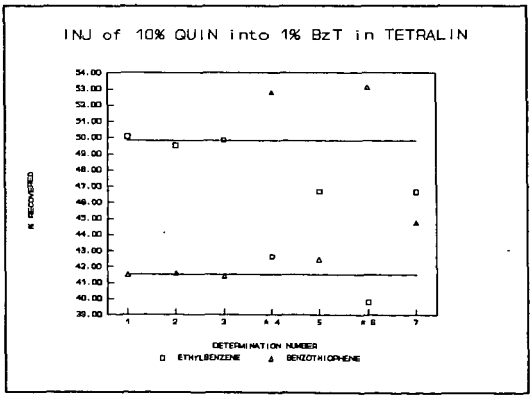

Figure 6. Quinoline Inhibition of the HDS of Benzothiophene, 400°C, 340 kPa. Injection on a Plateau Type Experiment.

ROLES OF MOLECULAR HYDROGEN AND A HYDROGEN DONOR SOLVENT IN THE CRACKING OF COAL MODEL COMPOUNDS WITH DISPERSED CATALYST

Toshimitsu SUZUKI, Na-oki IKENAGA, Takahiro SAKOTA, Takao MATSUI

Department of Chemical Engineering, Faculty of Engineering, Kansai University Suita, Osaka, JAPAN 564

Keywords: benzyl phenyl ether, dibenzyl ether, metal carbonyl catalyst

Introduction

Roles of a catalyst and a hydrogen-donor solvent in the direct coal liquefaction involves still controversial arguments, because complex reactions such as thermal decomposition or hydrocracking of C-O and C-C bonds and hydrogenation of polycyclic aromatic compounds are involved in coal liquefaction reaction. Therefore, it is of great importance to evaluate quantitative hydrogen transfer process by using coal model compounds with a hydrogen-donor solvent.

Cronauer *et al.* showed that in the cracking of benzyl phenyl ether the hydrogen required to stabilize free radicals comes from a donor solvent or intramolecular rearrangement and not from gaseous hydrogen in the absence of a catalyst.[1] Korobkov *et al.*[2] and Schlosberg *et al.*[3,4] showed that the thermolysis of benzyl phenyl ether and dibenzyl ether were accomplished by intramolecular rearragements. Yokokawa *et al.* reported that tetralin retarded the catalyzed hydrocracking of coal model compounds containing C-C and C-O bonds.[5] However, few studies dealt with quantitative discussion in the hydrogen transfer process from a hydrogen-donor solvent or molecular hydrogen to free radicals derived from a model compound except a series of studies by Nicole and co-workers.[6,7]

On the other hand, it is well known that the amount of naphthalene produced from tetralin decreases after the liquefaction of coal in tetralin with catalyst as compared to the liquefaction in the absence of catalyst.[8-10] To account for this, two mechanisms are proposed. One is that the catalyst hydrogenates naphthalene produced from tetralin,[8] and the other is that the catalyst promotes the direct hydrogen transfer from molecular hydrogen to free radicals.[10,11]

The purpose of this work is to elucidate the role of catalyst and tetralin by means of the quantitative treatment of the hydrogen transfer reaction stabilizing thermally decomposed free radicals. Cracking of benzyl phenyl ether (BPE), dibenzyl ether (DBE), 1,2-diphenylethane, and 1,3-diphenylpropane was studied in tetralin in the presence of highly dispersed catalyst.

Experimental

Cracking of coal model compounds was carried out in a batch 50 mL autoclave made of Hastelloy C. Prescribed amounts of a model compound (3.6 - 3.9 g, 19.5 mmol), a catalyst (0.01 - 0.08 g, 0.025 - 0.4 mmol), tetralin (4.0 g, 30.0 mmol) or tetralin/naphthalene (4.0 g / 0.5 g, 30.0 mmol / 4.0 mmol), and an activated carbon (0.5 g) as a dispersing agent for the catalyst were put into the autoclave. Activated carbon was added in uncatalyzed runs, in order to elucidate catalytic effect of activated carbon. In catalyzed runs with $Fe(CO)_5$ and $Mo(CO)_6$, a molecular sulfur was added.

The reactor was pressurized with a hydrogen to 5.0 MPa at a room temperature. The autoclave was heated to the desired temperature (648 or 698 K) with a preheated stainless-steel heat block equipped with a shaker. After a given reaction time (20 - 240 min.), the autoclave was cooled to room temperature by air blowing. The gas was collected into a gas buret. The liquid products were recovered from the autoclave by filtering off the activated carbon with a sintered glass filter, followed by repeated washing with tetrahydrofuran.

The amount of hydrogen transferred from gas phase was determined with the difference between the amount of hydrogen charged and recovered.

Results and Discussion

Cracking of Benzyl Phenyl Ether. Table I summarizes results of the reactions carried out under different reaction conditions by using several catalysts. Conversion of BPE was 100 % in all cases at 648 K for the reaction time of 30 min.

As shown in Scheme I, the identified products from cracking of BPE were benzene (PhH), toluene (PhMe), phenol (PhOH), diphenylmethane (DPM), 1,2-diphenylethane (DPE), isomeric (hydroxyphenyl)phenylmethanes (HPPM), benzyltetralins[7] (BT, m/z=222 in GC-MS), and benzylnaphthalenes[7] (BN, m/z=218 in GC-MS). The major products were PhMe and PhOH, and the other products such as DPM and DPE were minor. BPE was thermally decomposed at a relatively low temperature and seemed to produce quantitatively benzyl radical and phenoxy radical, and these radicals abstract hydrogen from tetralin or benzyl radical may combine with tetralyl radical. The material balances between charged BPE and recovered products in these reactions were good to very good and in the range of 87 mol% to 98 mol%. The products formed from tetralin were naphthalene, decalin and 1-methylindan.

H_2-R in Table I indicates the amounts of hydrogen required for stabilizing thermally produced organic free radicals from BPE. They were calculated from the amounts of cracked products assuming the following over all stoichiometric reactions (not showing exact chemical path).

$$\text{Ph-CH}_2\text{O-Ph} \rightarrow \text{Ph-CH}_2 + \text{Ph-O}\cdot \quad (1)$$

$$\text{Ph-CH}_2\cdot + 3\text{H} \rightarrow \text{Ph-H} + \text{CH}_4 \quad (2)$$

$$\text{Ph-CH}_2\cdot + \text{H} \rightarrow \text{Ph-CH}_3 \quad (3)$$

$$\text{Ph-O}\cdot + \text{H} \rightarrow \text{Ph-OH} \quad (4)$$

$$\text{Ph-CH}_2\text{-(C}_6\text{H}_4\text{)-OH} + 2\text{H} \rightarrow \text{Ph-CH}_2\text{-Ph} + \text{H}_2\text{O} \quad (5)$$

The rest of the products such as DPE and HPPM can be produced by the recombination of radicals or rearrangements of BPE, and no hydrogen were required.[7] H_2-TL in Table I exhibits the amount of hydrogen transferred from tetralin. It was calculated from the amount of naphthalene and decalin formed by the dehydrogenation and the hydrogenation of tetralin, assuming that all four hydrogens in tetralin are utilized. H_2-G shows the amount of hydrogen transferred from gas phase. Considering the experimental error, fair agreement between the amount of hydrogen required (H_2-R) and that of hydrogen transferred (H_2-G plus H_2-TL) was obtained.

In the reaction without catalyst (Run 1) the amounts of PhMe and PhOH were 11.3 mmol and 13.7 mmol respectively, these amounts were smaller than those in the reactions with $Mo(CO)_6$-S and $Ru(acac)_3$. The reaction in a smaller amount of tetralin (Run 2 BPE/TL= 2), the amounts of PhMe and PhOH further decreased and those of DPM and DPE slightly increased.

The amount of hydrogen required for stabilizing free radicals (H_2-R) were 13.9 mmol (Run 1) and 12.4 mmol (Run 3) in the reactions under a hydrogen or a nitrogen atmosphere. They were predominantly supplied from tetralin (12.0 mmol and 10.4 mmol respectively). These results clearly show that all four hydrogen atoms in tetralin are utilized to transfer to fragment radicals. With a decrease in the tetralin concentration contribution of hydrogen in gas phase increased even in the absence of catalyst (Run 2 probably catalyzed by wall).

$$R\cdot + TL \rightarrow RH + TL\cdot \quad (6)$$

$$2TL\cdot \rightarrow TL + DHN\ (\text{dihydronaphthalene}) \quad (7)$$

$$R\cdot + DHN \rightarrow RH + DHN\cdot \quad (8)$$

$$DHN\cdot + TL\cdot (\text{or } DHN\cdot) \rightarrow Naph + TL\ (\text{or } DHN) \quad (9)$$

$$R\cdot + TL\cdot \rightarrow R\text{-}TL \quad (10)$$

$$R\cdot \xrightarrow{H_2/\text{catalyst}} RH \quad (11)$$

$$TL\cdot \xrightarrow{H_2/\text{catalyst}} TL \quad (12)$$

The amount of hydrogen absorbed slightly increased with $Fe(CO)_5$-S, although ten times larger amount of Fe was used in these runs as compared to Mo and Ru. The ability of $Fe(CO)_5$-S catalyst to activate molecular hydrogen seems not to be high.

In the reactions with $Mo(CO)_6$-S (Runs 6 - 8), or $Ru(acac)_3$ (Runs 9-11) the amounts of toluene and phenol increased, and the amount of HPPM decreased correspondingly. These results indicate that the hydrogen transfer from gas phase to benzyl radical and phenoxy radical proceeded more smoothly than in the uncatalyzed reactions. Decreases in H_2-TL and increases in H_2-G in the catalyzed runs with $Mo(CO)_6$-S and $Ru(acac)_3$ suggest the possibility of direct hydrogen transfer from gaseous hydrogen to benzyl and phenoxy radicals more efficiently (equation 11).

Cracking of Dibenzyl Ether. Cracking of DBE was carried out under the same condition as the cracking of BPE except that the reaction time was shortened to 20 min. The results are summarized in Table II. The identified products from cracking of DBE were benzene, toluene, benzaldehyde (PhCHO), benzyl alcohol (BA), 1,2-diphenylethane, benzyltetralins, and benzylnaphthalenes. H_2-R was calculated according to the following over all stoichiometric equations (not showing exact chemical paths).

$$Ph\text{-}CH_2OCH_2\text{-}Ph \rightarrow Ph\text{-}CH_2\cdot + Ph\text{-}CH_2O\cdot \quad (13)$$

$$Ph\text{-}CH_2\cdot + 3H \rightarrow Ph\text{-}H + CH_4 \quad (14)$$

$$Ph\text{-}CH_2\cdot + H \rightarrow Ph\text{-}CH_3 \quad (15)$$

$$Ph\text{-}CH_2\cdot + Ph\text{-}CH_2O\cdot \rightarrow Ph\text{-}CH_3 + Ph\text{-}CHO \quad (16)$$

$$Ph\text{-}CH_2O\cdot + H \rightarrow Ph\text{-}CH_2OH \quad (17)$$

$$Ph\text{-}CH_2O\cdot + 3H \rightarrow Ph\text{-}CH_3 + H_2O \quad (18)$$

It is noteworthy in these reactions that PhMe was produced more than the amount that was evaluated from equations 15 and 16. An excess amount of PhMe could be originated from the hydrogenation of oxygen containing compound as shown in equation 18. Amount of H_2O was about 14.2 mmol, corresponding to the occurrence of reaction 18. Estimated H_2-R was smaller than H_2-G plus H_2-TL due to unidentified minor products in most catalyzed runs.

As shown in Table II, in the uncatalyzed reactions at 648 K (Runs 12 in H_2 and Run 13 in N_2) the amounts of PhMe were 23.2 and 23.1 mmol and those of PhCHO were 6.1 and 7.5 mmol respectively indicating the lowest yields of PhMe and the highest yields of PhCHO. In addition under a nitrogen atmosphere DPE increased to 3.2 mmol, suggesting that the recombination of benzyl radicals most likely proceeded. On the other hand, H_2-R (15.1 mmol) is in fair agreement with H_2-TL (14.7 mmol), indicating that most of hydrogen required to stabilize fragment radicals transferred from tetralin.

When $Fe(CO)_5$-S was employed for the cracking of DBE (Runs 14 and 15), the amounts of H_2-TL and H_2-G (15.4 mmol and 1.9 mmol in Run 14) were approximately same as those in the uncatalyzed run (14.7 mmol and 0.5 mmol in Run 12). However, H_2-TL decreased to 9.0 mmol and H_2-G increased to 9.8 mmol when smaller amount of tetralin was used (8.0 mmol, Run 15). The amount of PhCHO (2.1 mmol in Run 14) was less than that in Run 12 (6.1 mmol). These results suggest that the possibility of direct hydrogen transfer from gaseous hydrogen to benzyl and Ph-$CH_2O\cdot$ radicals to form toluene is enhanced.

In the catalyzed runs with $Mo(CO)_6$-S and $Ru(acac)_3$ (Runs 16 and 19), PhCHO and BA were scarcely detected and PhMe was increased to 27.5 mmol and 29.6 mmol suggesting considerable possibility of reaction 18. Although H_2-R was estimated to be smaller than H_2-G plus H_2-TL due to unidentified minor products, correspondingly increases in H_2-R could be expected. Furthermore,

with these catalysts, decreases in H_2-TL to 1/3 of the H_2-R (11.7 and 9.2 mmol) and increases in H_2-G to about 80 % of H_2-R (22.5 and 22.7 mmol) were observed similar to the reaction with BPE. However, in the reaction with $Mo(CO)_6$-S the amount of H_2-TL was larger than that in the cracking of BPE with the same catalyst. The contribution of tetralin for the hydrogen transfer process to stabilize the thermally decomposed free radicals increased in the cracking of DBE. Whereas, if we decreased the amount of tetralin to 8 mmol (Run 17 and 20), H_2-TL decreased to 5.5 and 4.6 mmol and H_2-G increased to 25.7 and 27.3 mmol as seen in the reaction with $Fe(CO)_5$-S, suggesting that the possibility of direct hydrogen transfer from gaseous hydrogen to radicals increased.

Cracking of benzyl phenyl ether and dibenzyl ether in tetralin-naphthalene mixed solvent. In the cracking of BPE and DBE in tetralin using finely dispersed catalyst, two possibilities were proposed for the decrease in the amount of naphthalene after the reactions. One is the direct hydrogen transfer process from molecular hydrogen activated on the catalyst to free radicals, consequently contribution of the hydrogen transfer from tetralin to free radicals decreased. The other is the hydrogenation of naphthalene formed after hydrogen transfer to radicals with catalyst. In order to confirm the possibility of hydrogenation of naphthalene, the cracking of BPE or DBE was carried out in tetralin/naphthalene mixed solvents, and the results are summarized in Runs 8, 11, 18 and 21 in Tables I and II.

In the reactions in tetralin with the catalyst (Runs 4, 6 and 9), 3.3 - 4.9 mmol of decreases in naphthalene were observed as compared to the uncatalyzed run (Run 1 in Table I). If these decreases are ascribed to the hydrogenation of naphthalene, a certain amount of added naphthalene would be hydrogenated to give tetralin in the reaction with mixed solvents. As seen in Runs 8 and 11, 4.1 and 5.7 mmol of naphthalene was recovered respectively. If we assume that the same amount of naphthalene was formed from tetralin (Runs 6 and 9) in the presence of tetralin-naphthalene mixed solvents and no hydrogenation of added naphthalene did occur, hypothetical amount of naphthalene after the reaction would be estimated to be 4.7 (0.7 + 4.0) and 4.2 (0.2 + 4.0) mmol for Runs 8 and 11, respectively. In Run 8, 4.1 mmol of naphthalene was observed, indicating that only 0.6 mmol of naphthalene was hydrogenated in the course of the reaction. In Run 11, 5.7 mmol of naphthalene was detected. This is rather increase in 1.5 mmol of naphthalene, as compared to the hypothetical amount of naphthalene. These results suggest that hydrogenation of naphthalene did not or slightly occurred during the cracking of BPE. As shown in Runs 18 and 21 in Table II, hydrogenation of naphthalene during the reaction was also examined in the cracking of DBE. It was found that 0 - 1.3 mmol of naphthalene was hydrogenated in the course of cracking of DBE.

In separate experiments, hydrogenation of naphthalene or naphthalene in tetralin did proceed considerable extent with all the catalysts employed here. Thus in the presence of polar substances or free radicals, the activity toward the hydrogenation of aromatic nuclei would be reduced considerably due to the stronger interaction of the catalyst with them.

On the other hand, 0.3 mmol to 2.1 mmol of BT were produced in the cracking of BPE and DBE even with the active catalyst such as $Mo(CO)_6$-S and $Ru(acac)_3$, and BT increased in the cracking of DBE at 698 K. This seems to provide possibility of formation of tetralyl radical which in turn combined with benzyl radical or were hydrogenated to tetralin on the catalyst surface as proposed in the previous study.[12] Cochran *et al.* have suggested that the direct hydrogen transfer is the predominant route in tin-catalyzed coal liquefaction.[10] Importance of molecular hydrogen in the catalyzed coal liquefaction with highly dispersed catalysts has been pointed out by Charcosset et al.[13] The direct hydrogen transfer from gas phase hydrogen activated on the catalyst not only to free radicals derived from BPE or DBE but also tetralyl radical.

Cracking of 1,2-diphenyl ethane and 1,3-diphenylpropane Cleavage of C-C bonds in coal is much more important reactions in the hydroliquefaction of subbituminous or bituminous coal. In order to examine catalytic effects of dispersed catalyst on the dissociation of C-C bond, 1,2-DPE and 1,3-diphenylpropane (1,3-DPP) in tetralin was carried out without or with dispersed catalysts. Results are summarized in Table III. Cracked products are benzene, toluene, and ethylbenzen, in addition to small amounts of BT and BN.

Much lower conversions were obtained in both model compounds even at higher reaction temperature of 425 °C and longer reaction period of 60 min. In the absence of catalyst, the amount of hydrogen required to stabilize thermally cracked free radical is in good agreement with the amount of hydrogen produced from tetralin calculated from the amount of naphthalene formed (see Runs 22 and 23).

With the addition of dispersed catalysts not significant differences in the amounts of cracked products were observed, indicating poor capability of metal sulfides or metal species on the hydrocracking of C-C bond. Due to the lower conversion of model compounds, the amounts of hydrogen absorbed from gas phase could not be measured accurately. However, the amount of naphthalene formed after the reaction decreased as compared to the run without catalyst, when a smaller amount of tetralin was employed. Such phenomena were pronouncedly observed, when $Mo(CO)_6$-S and $Ru(acac)_3$ catalysts were used. In these cases (Runs 27 and 30), the amount of hydrogen required to stabilize free radicals from DPE exeeded the amount of hydrogen dehydrogenated from tetralin. This indicates that hydrogen transfer from molecular hydrogen to organic radicals on the catalyst occurred. However, in the abundant hydrogen donor solvent, hydrogen transfer from tetralin to benzy radical did proceed more effectively to give toluene.

Such tendencies are seen in the cracking of DPP. Only Ru based catalyst effectively promoted hydrogen transfer from gas phase hydrogen to organic free radicals.

These results indicate that C-C bonds in the coal model structure were thermally dissociate to give free radicals and they abstract hydrogen to give stable organic compounds either from a hydrogen donor solvent or molecular hydrogen activated on the catalsyst. However, even in the

presence of an active catalsyst, hydrogen was pronouncedly supplied to such hydrocarbon radicals from a hydrogen donor solvent like tetralin.

Two reasons for this can be proposed. One is that due to a higher bond dissociation energy of C-C bonds in the model compounds, the rate of benzyl radical formation is small, and consequently abundant hydrogen donor solvent could provide hydrogen to organic free radicals. The other is that benzyl radical could be less strongly adsorbed on the active catalyst as compared to the oxygen containing free radicals derived from BPE and DBE. Therefore, hydrogen transfer from gas phase to benzyl radical only slightly occurred.

Conclusion

Quantitative hydrogen transfer process from tetralin to organic free radicals was clarified. Direct hydrogen transfer from molecular hydrogen on the dispersed catalyst was proposed for the cracking of oxygen containing coal model compounds, in the presence of hydrogen donor such as tetralin.

References

1) Cronauer, D.C.; Jewell, D.M.; Shah, Y.T.; Modi, R.J. *Ind. Eng. Chem. Fundam.* **1979**, *18*, 153-162.
2) Korobkov, V.Y.; Grigorieva, E.N.; Bykov, V.I.; Senko, O.V.; Kalechitz, I.V. *Fuel* **1987**, *67*, 657-662.
3) Schlosberg, R.H.; Ashe, T.A.; Pancirov, R.J.; Donaldson, M. *Fuel* **1981**, *60*, 155-157.
4) Schlosberg, R.H.; Davis, W.H.; Ashe, T.A. *Fuel* **1981**, *60*, 201-204.
5) Yokokawa, C.; Ikenaga, N.; Fukumi, J.; Oda, H. *Proceedings of International Conference on Coal Science* ; pp. 911-914, 1989, Tokyo.
6) Meyer, D.; Nicole, D.; Delpuech, J.J. *Fuel Process. Technol.* **1986**, *12*, 255-268.
7) Meyer, D.; Oviawe, P.; Nicole, D.; Lauer, C.; Clement, J. *Fuel* **1990**, *69*, 1309-1316.
8) Guin, J.A.; Tarrer, A.R., Lee, J.M.; Lo, L.; Curtis, C.W. *Ind. Eng. Chem. Process Des. Dev.* **1979**, *18*, 371-376.
9) Moritomi, H.; Nagaishi, H.; Naruse, M.; Sanada, Y.; Chiba, T. *J. Fuel Soc. Jpn.* **1983**, *62*, 254-262.
10) Cochran, S.J.; Hatswell, M.; Jackson, W.R.; Larkins, F.P. *Fuel* **1982**, *61*, 831-833.
11) Suzuki, T.; Yamada, O.; Takahashi, Y.; Watanabe, Y. *Fuel Process. Technol.* **1985**, *10*, 33-43.
12) Suzuki, T.; Yamada, H.; Sears, P.L.; Watanabe, Y. *Energy Fuels* **1989**, *3*, 707-713
13) Charcosset, H.; Bacaud, R.; Besson, M.; Jeunet, A.; Nickel, B; Oberson, M. *Fuel Process. Technol.* **1986**, *12*, 189-201.

Table 1 Cracking of Benzyl Phenyl Ether and the Amount of Hydrogen Transferred to Radicals[a]

Run	Catalyst	Solv. mmol	PhMe	PhOH	DPM	DPE	HM	BT[b]	BN[b]	Naph	TL	H_2-R[c]	H_2-T[d]	H_2-G[e]
			mmol											
1	none	28.9	11.2	13.7	1.5	0.7	4.0	0.7	0.5	5.1	19.9	13.9	12.0.	0.6
2	none	8.8	8.7	11.8	1.8	1.0	3.9	0.3	0.6	2.9	3.1	12.0	7.5	4.4
3	none(N_2)	30.6	10.9	12.3	1.4	0.2	3.7	0.7	0.5	4.5	23.0	12.4	10.4	—
4	$Fe(CO)_5$-S[f]	29.1	6.0	12.8	0.3	0.9	5.3	2.5	0.6	1.8	24.6	9.6	6.3	2.6
5	$Fe(CO)_5$-S[f]	8.1	8.8	12.2	0.4	1.2	4.3	0.4	0.5	2.4	4.4	9.8	4.2	6.6
6	$Mo(CO)_6$-S[g]	29.5	14.2	15.7	0.4	0.4	2.3	0.9	0.3	0.7	28.0	15.4	2.6	17.0
7	$Mo(CO)_6$-S[g]	8.3	12.4	14.5	0.8	0.5	2.5	0.6	0.4	0.9	6.2	14.3	3.0	15.5
8	$Mo(CO)_6$-S[g]	T/N[h]	14.6	15.6	0.3	0.2	2.0	0.4	0.4	4.1	29.2	16.0	1.5	15.4
9	$Ru(acac)_3$	30.3	14.2	15.5	0.7	0.2	1.8	0.5	0.2	2.0	26.2	15.6	5.7	9.1
10	$Ru(acac)_3$	8.2	13.3	16.1	0.7	0.7	2.0	0.6	0.4	0.9	6.1	15.4	3.0	19.3
11	$Ru(acac)_3$	T/N[h]	13.5	14.9	0.8	0.1	2.3	0.5	0.6	5.7	26.8	15.5	4.9	11.3

a) BPE 19.5mmol, active carbon 0.5g, $P(H_2) = 5.0$MPa, reaction time 30min, conversion = 100%.

b) m/z=222 (BT, benzyltetralins) and 218 (BN, benzylnaphthalenes).

c) Calculated amount of hydrogen to stabilize radicals.

d) Amount of hydrogen transferred from tetralin. e) Amount of hydrogen transferred from gas.

f) Sulfur 0.8mmol. g) Sulfur 0.22mmol. h) Solvent : TL, 30.0mmol; Naph, 4.0mmol.

Abbreviations : DPM, diphenylmethane; DPE, 1,2-diphenylethane;

HM, (hydroxyphenyl)phenylmethanes; Naph, naphthalene; TL, tetralin.

Table II Cracking of Dibenzyl Ether and the Amount of Hydrogen Transferred to Radicals [a]

Run	Catalyst	Solv.	PhMe	PhCHO	BA	DPE	BT[b]	BN[b]	Naph	TL	H_2-R[c]	H_2-T[d]	H_2-G[e]
				mmol							mmol		
12	none	29.8	23.2	6.1	trace	1.2	0.6	1.0	6.4	21.1	15.1	14.7	0.5
13	none(N_2)	30.1	23.1	7.5	1.6	3.2	0.4	0.8	5.6	21.7	19.8	13.6	—
14	$Fe(CO)_5$-S [g]	29.3	24.3	2.1	—	1.0	1.6	2.4	4.4	16.3	21.9	15.4	1.9
15	$Fe(CO)_5$-S [g]	8.3	22.8	3.8	—	1.7	0.3	1.3	2.8	3.1	18.1	9.0	9.8
16	$Mo(CO)_6$-S [i]	30.0	27.5	—	trace	1.4	1.8	1.7	3.3	21.4	27.9	11.7	22.5
17	$Mo(CO)_6$-S [i]	8.1	25.7	—	—	2.0	0.9	1.1	2.0	4.0	29.8	5.5	25.7
18	$Mo(CO)_6$-S [i]	T/N [h]	25.2	trace	—	1.2	1.7	1.9	6.0	23.3	24.8	8.7	21.0
19	$Ru(acac)_3$	30.2	29.6	0.7	trace	0.8	1.2	0.7	3.4	22.8	27.9	9.2	22.7
20	$Ru(acac)_3$	8.0	29.0	trace	—	1.4	0.8	0.7	1.3	5.0	28.9	4.6	27.3
21	$Ru(acac)_3$	T/N [h]	29.6	trace	—	0.7	1.1	0.8	6.7	25.2	29.4	7.5	25.0

a) DBE 19.5mmol, active carbon 0.5g, $P(H_2)$ = 5.0 MPa, reaction time 20min,
b) m/z=222 (BT, benzyltetralins) and 218 (BN, benzylnaphthalenes).
c) Amount of hydrogen transferred to radicals.
d) Amount of hydrogen from tetralin. e) Amount of hydrogen from gas.
f) Mol percent against DBE charged. g) Sulfur 0.8mmol.
h) Solvent : TL, 30.0mmol; Naph, 4.0mmol. i) Sulfur 0.22mmol.
Abbreviations : BA, benzyl alcohol; DPE, 1,2-diphenylethane; Naph, naphthalene; TL : tetralin.

Table III Cracking of 1,2-diphenylethane and 1,3-diphenylpropane in tetralin[a]

Run	Catalyst	metal	Time	Solv	PhH	PhMe	PhEt	Naph	TL	H_2-R	H_2-TL
		mmol	min				mmol				
			Diphenylethane								
22	None		60	8.3	0.86	5.20	0.83	1.4	5.7	3.3	2.9
23	None		60	30.1	0.53	5.30	0.46	2.1	25.4	3.1	4.2
24	None		240	29.9	1.47	15.74	1.67	5.3	17.6	9.4	10.6
25	$Fe(CO)_5$-S	0.40	60	8.3	0.92	5.81	1.06	1.2	5.5	3.9	2.3
26	$Fe(CO)_5$-S	0.40	60	29.5	0.52	5.31	0.55	2.8	24.2	3.2	5.5
27	$Mo(CO)_6$-S	0.05	60	8.2	0.93	4.96	0.97	0.8	6.5	3.2	1.6
28	$Mo(CO)_6$-S	0.05	60	28.8	0.69	6.03	0.99	5.6	19.1	4.0	11.1
29	$Mo(CO)_6$-S	0.05	240	30.9	1.43	17.20	2.03	5.9	16.8	10.6	11.9
30	$Ru(acac)_3$	0.025	60	8.1	0.88	4.92	0.86	0.9	5.8	3.3	1.8
31	$Ru(acac)_3$	0.025	60	30.0	0.49	5.72	0.53	2.3	24.8	3.4	4.6
			Diphenylpropane								
32	None		60	4.1	0.13	1.36	1.14	0.54	2.1	1.3	1.1
33	$Fe(CO)_5$-S	0.06	60	4.12	0.11	1.99	2.07	0.82	2.6	2.1	1.6
34	$Mo(CO)_6$-S	0.08	60	4.11	0.22	1.99	1.95	1.05	2.3	2.1	2.1
35	$Ru(acac)_3$	0.04	60	4.11	0.18	2.01	2.12	0.42	3.27	2.16	0.9

a) Diphenylethane: 19.5 mmol, Diphenyl propane: 2.5 mmol active carbon 0.50 g, 425 °C, PH_2= 5.0 MPa,
Other abbreviations are the same as Table I.

MECHANISMS OF IRON-BASED CATALYSIS INVESTIGATED USING MODEL COMPOUNDS

John C. Linehan, Dean W. Matson, John G. Darab, S. Thomas Autrey, James A.. Franz, and Don M. Camaioni.
Pacific Northwest Laboratory[1]
P.O. Box 999, Richland, WA

Key words: Model compounds, catalysis, iron oxides.

Abstract. The catalytic mechanism of highly active, nanophase iron-based coal liquefaction catalysts was investigated using a series of model compounds. The iron-oxide phases ferric oxyhydroxysulfate (OHS), 6-line ferrihydrite, hematite, and goethite, were evaluated as catalyst precursors with systematically substituted diphenylmethanes in the presence of a hydrogen donating solvent. The activity of the catalysts was observed to be dependent upon the functionality on the model compounds. The results of these model compound studies and their relationship to possible reaction mechanisms are presented.

Introduction. There has been recent interest in the development of inexpensive, new, and potentially disposable, catalysts for the first stage direct liquefaction of coal.[2] A major emphasis has been placed on developing highly active iron-based liquefaction catalysts as substitutes for the current molybdenum-based catalysts which are more expensive. The new iron-containing catalysts for this purpose have been screened using either model compounds or select coals. While numerous studies have been undertaken to synthesize and test iron-based catalysts with enhanced catalytic activity for hydrogenolysis,[2] few studies have systematically focused on the bond cleavage or hydrogenation mechanism(s) involved when these catalysts are employed.[3]

In previous papers we have focused on either developing techniques for the production of nanoscale iron-oxides or the identification of active iron oxide catalyst precursor phases.[4-6] In this paper we concentrate on the organic structures which are attacked by the iron-based catalysts. We describe our preliminary results using systematically altered model compounds with a variety of iron oxide catalyst precursors to elucidate carbon-carbon bond scission pathways supported by iron-based catalysts.

Experimental. The model compounds diphenylmethane (DPM) (Aldrich) and 4,4'-dimethyl diphenylmethane (4,4'DPM) (TCI) were used as received. The model compounds methyl diphenylmethane (MeDPM), 2,5 -dimethyl diphenylmethane (Me2DPM), and 2,4,6-trimethyl diphenylmethane (Me3DPM) were synthesized from neat mixtures of the appropriate methylated aromatic (toluene, p-xylene, and mesitylene respectively) and benzyl alcohol with the addition of concentrated sulfuric acid. The reaction products were distilled under reduced pressure and the products were shown to be 99% pure by GC and proton NMR. The only exception was MeDPM which was found to be an inseparable 50:50 isomeric mixture of 2-methyldiphenylmethane and 4-methyl diphenylmethane by NMR.

The catalyst precursors were made according to literature procedures and milled to -325 mesh, except for the 6-line ferrihydrite[4] which was produced by the RTDS method[5,7] at low reaction temperatures and was also sieved to -325 mesh. The catalyst testing procedure, which has been detailed previously, consisted of loading 15 µl of the model compound with 3 mg of the catalyst precursor, 3 mg of elemental sulfur and 100 mg of pure (>99%) 9,10-dihydro-phenanthrene into a Pyrex tube. The tube was sealed under vacuum and heated at 400±3 °C for 1 hour in a fluidized sand bath. The products were identified by GC and the residual model compounds were quantified with an internal standard.

Results and Discussion. Table I shows the percent consumption of the five model compounds using four iron oxide catalyst precursors. As can be seen from the Table, the relative order of model compound consumption increases with increasing methyl substitution. Figure 1 shows these results as a function of the number of methyl groups on substituted diphenylmethanes. Both Table I and Figure 1 show the dramatic increase in consumption of the model compound in going from Me2DPM to Me3DPM. The yields more than double for most of the catalysts. All of the iron oxide precursors used promoted over 75% consumption of Me3DPM. These results support the findings that many different forms of iron-containing powders have been found to be active bond scission catalysts under the appropriate reaction conditions.

The increase in the percent consumption of model compound correlates with the decrease in the oxidation potential of benzene upon increasing methyl substitution. The oxidation potential drops approximately 0.6 V in going from toluene to 1,2,3,5-trimethylbenzene.[8,9] We estimate that the oxidation potentials of the model compounds used here would decrease in a corresponding manner with increasing methyl substitution. The observed relationship between oxidation potential and bond scission enhancement does not necessarily prove a REDOX mechanism. The cyclohexyldienyl radical intermediate generated by a free radical pathway would also be stabilized with an increase in methyl substitution and would increase the rate of bond cleavage.

The products of the model compound consumption reactions were mixtures of products resulting from cleavage of bonds A , B, and C (see Figure 2). For DPM and 4,4'DPM, the products of bond A and bond B cleavage were indistinguishable, the products from bond A being toluene and the methylated aromatic. For MeDPM, Me2DPM, and Me3DPM, the bond A methylated aromatic products were toluene, p-xylene, and mesitylene respectively. Bond B cleavage yielded benzene and the methylated aromatic with one additional methyl group. For MeDPM, Me2DPM, and Me3DPM, bond B cleavage yielded xylene, 1,2,5-trimethyl benzene, and 1,2,3,5-tetramethyl benzene respectively. Bond C cleavage involved the loss of a methyl group from the model compound and yielded the parent compound minus one methyl group.

For the uncatalyzed reactions, products from bonds B and C cleavage predominated. The bond B:C cleavage product ratios were less than one and the bond B:A cleavage ratios were greater than one. The small thermal conversions with some of the uncatalyzed model compound reactions precluded accurate or statistically significant reporting of product distributions.

The products of the catalyzed reactions of the methylated diphenylmethane compounds were almost exclusively derived from bond A cleavage. The major products were toluene and the methylated aromatic (toluene, p-xylene, mesitylene) derived from the substituted ring. Very little benzene, from bond B cleavage, was detected. There was little evidence for methyl cleavage from the methylated diphenylmethanes in the iron catalyzed reactions. This has also been seen for other methylated systems when using other iron and molybdenum-based catalysts.[10] The B:A bond cleavage ratio for the ferric oxyhydroxysulfate catalyzed reaction was over 50 and the B:C ratio over 100 for Me3DPM model compound. The ratios of B:A products and B:C products increased with increasing number of methyl substitution for a given catalyst. There was little difference in these ratios between the products of reactions involving different catalyst precursors when similar conversions were obtained.

The total amount of the model compound hydrogenation was less than 2% of the total products for any of the model compounds or catalyst precursors. This is consistent with other results with iron-based catalysts in the presence of sulfur for both diphenylmethane and naphthyl bibenzylmethane, even under high hydrogen pressures.[3,4] Other iron-based catalysts have previously been shown to be active for hydrogenation of polycyclic aromatics in the absence of good leaving groups.[10]

Summary Iron-based materials catalyze the consumption of more substituted diphenylmethanes faster than less substituted diphenylmethanes. The catalyzed reactions were very selective for cleavage between the aromatic carbon of the most substituted ring and the methylene carbon. Little evidence for catalyzed cleavage of methyl groups was detected. The relative reactivity of the iron oxide precursors was similar to that previously found for NBBM.

Acknowledgements We gratefully thank Dr. Glen Fryxell (PNL) for developing the methodology for the model compound synthesis. The model compound work was supported by the Director, Office of Energy Research, Office of Basic Energy Sciences, Chemical Sciences Division of the Department of Energy and the catalyst development work was supported by the U. S. Department of Energy, Office of Fossil Energy under contract DE-AC06-76RLO 1830.

REFERENCES

1. Pacific Northwest Laboratory is operated for the U.S. Department of Energy by Battelle Memorial Institute under contract DE-AC06-76RLO 1830.
2. See the first 21 papers in *Energy & Fuels*, **1994**, 1, and references therein.
3. Wei, X. Y.; and Zong, Z-M. *Energy & Fuels*, **1992**, 6, 236. Wei, X. Y.; Ogata, E.; Zong, Z.-M.; and Niki, E. *Energy & Fuels*, **1992**, 6, 868.
4. Linehan, J. C.; Matson, D. W.; and Darab, J. G. *Energy & Fuels* **1994**, 8, 56.
5. Matson, D. W.; Linehan, J. C.; Darab, J. G.; and Buehler, M. F. *Energy & Fuels* **1994**, 8, 10.
6. Darab, J. G.; Linehan, J. C.; Matson, D. W.; and Campbell, J. A. In Proceedings of the 7th International Conference on Coal Science Vol I, pg 24, 1993.
7. Matson, D. W.; Linehan, J. C.; and Bean, R. M. *Materials Lett.*, **1992**, 14, 222.
8. Gould, I.R; Ege, D.; Moser, J.E.; and Farid, S. *J. Am. Chem. Soc.* **1990**, 112, 4290.
9. Howell, J.O.; Goncalves, J.M.; Amatore, C.; Klasine, L.; Wightman, R.M.; and Kochi, J.K. *J. Am. Chem. Soc.*, **1984**, 106, 3968.
10. Tang, Y. and Curtis, C.W. *Energy & Fuels*, **1994**, 8, 63.

Table I
Percent Consumption of Model Compounds with
Iron-Based Catalysts at 400°C in the Presence of 9,10-Dihydrophenanthrene

Model Compound	Catalyst Precursor: Hematite	Goethite	6-Line Ferrihydrite	Ferric Oxyhydroxy-Sulfate	None
DPM[a]	nm	4 ± 3	6 ± 3	9 ± 3	0
MeDPM	13 ± 2	3 ± 2	8 ± 3	29 ± 2	1 ± 1
Me2DPM	36 ± 3	9 ± 3	19 ± 2	58 ± 2	6 ± 3
Me3DPM	86 ± 5	95 ± 5	75 ± 5	98 ± 2	5 ± 3
4,4'DPM	43 ± 4	7 ± 3	6 ± 2	60 ± 5	3 ± 2

a) See reference 6.

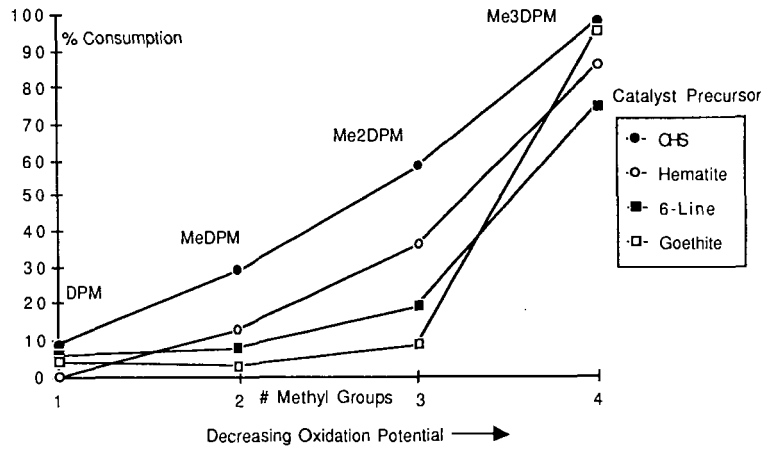

Figure 1. A plot of model compound consumed (at 400°C, 60 minutes, with catalyst and dihydrophenanthrene) vs methyl substitution for diphenylmethane.

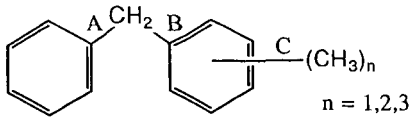

Figure 2. Schematic of the substituted diphenylmethanes and the bond designation.

HETEROGENOUS CATALYSIS:
Mechanisms of Selective Cleavage of Strong Carbon-Carbon Bonds.

Malvina Farcasiu and Steven C. Petrosius
U.S. Department of Energy
Pittsburgh Energy Technology Center
P.O. Box 10940, Pittsburgh, PA 15236

Key Words: heterogenous catalysis, carbon-carbon bond cleavage, mechanism

INTRODUCTION

This paper discusses the catalytic cleavage of strong carbon-carbon bonds in compounds which also contain relatively weaker carbon-carbon bonds which can be cleaved thermally by a homolytic, free radical process. The majority of the reactions described here are performed under condition where the thermal background is very small or nonexistent.

We will discuss the reactivity of two model compounds (Figure 1) relevant to fossil fuels (oil and coal) in the presence of several heterogenous catalysts: carbon black, graphite and solid acids. Previously, we have reported a very selective carbon black C-C cleavage of bonds between a polycondensed aromatic moiety and an adjacent aliphatic carbon[1-4] and on carbon black catalyzed dehydroxylation and dehalogenation of polycondensed aromatic phenols and halogenated polycondensed compounds[5]. We attributed the observed catalytic activity and selectivity in hydrocracking reactions to the formation of radical cations on the surface of carbon-based catalysts at temperatures over 320 °C[2] and the dehydroxylation and dehalogenation reactions to a free radical mechanism identical with that of the thermal reaction[5]. We concluded that two types of catalytic active centers are present on carbon black. In this presentation we will elaborate on the nature of carbon black catalytic activity and contrast it to that of graphite.

The ion radical mechanism for the C-C cleavage mechanism which we observe in the case of carbon black catalysts is disputed by Penn and Wang based on an extensive presentation of literature data and on their own experimental results for radical-cation generated in solution in the presence of polar solvents[6]. Under their reported conditions, no cleavage of any C-C bond is observed unless a tetraaryl-substituted ethane was used as a substrate. They conclude that the ion-radical mechanism we proposed for the carbon black catalyzed reactions is incorrect and that the solvent-assisted ipso addition of a hydrogen atom[7] is the most likely explanation for both thermal and catalytic carbon-carbon cleavage of the type we observed. The role of the catalyst is considered to be to accelerate either the formation of the hydrogen atom or the addition of the hydrogen atom to the substrate, or both. The source of the H-atom is the solvent.

We will discuss in this paper the data that rise doubts about extending the free radicals (including ipso addition of hydrogen atoms from solvents) as the initial step in the cleavage of specific strong C-C bonds under the conditions of heterogenous catalysis on carbon catalysts.

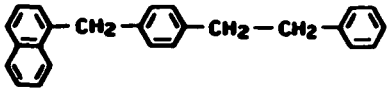

4-(1-naphtylmethyl) bibenzyl (I)

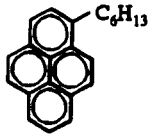

n-hexyl-pyrene (II)

Fig. 1 Model compounds used in this study

EXPERIMENTAL

The experimental conditions for testing the model compounds described in Fig.1 and the methods used for products identification and conversion calculations have been already published[2,3]. In this study, the catalytic reactions of I and II have been studied both in tetralin and perdeuterated tetralin, both from Aldrich Co.

RESULTS AND DISCUSSION

Carbon-catalyzed C-C cleavage reactions were performed for I and II, compounds having the general formula Aryl-CH^2-R, where aryl is naphthalene (I) or pyrene (II). The selective cleavage is catalyzed by carbon black at temperatures of 320 to 420°C. The graphite does not catalyze the cleavage. Unlike the dehydroxylation and dehalogenation reactions which require the presence of a H-donor, the carbon black catalyzes the C-C cleavage both in the presence and absence of the H-donor. Another reaction observed in the presence of deuterotetralin is H-D exchange. This reaction is catalyzed both by carbon black and graphite. At 350°C and reaction time of one hour the degree of H-D exchange is 58% in the presence of BP2000 and 12% in the presence of graphite. At 400°C and one hour reaction time the H-D exchange is 93% in the presence of BP2000 and 74.6% in the presence of graphite. However, the yield of selective cracking of the bond adjacent to the naphthalene ring is 20.4% in the case of BP2000 and zero for graphite. In the presence of graphite, the cracking is less than 1% and the selectivity is typical of the thermal reaction[2]. We conclude that it is no connection between the mechanism of H-D exchange and the selective cleavage of C-C bond described above. We believe that this result, together with the calculations of Ades et.al.[8,9] and the results of Charge Distribution Analysis reported previously[2] make the ipso addition unlikely as the mechanism of the carbon black catalyzed C-C cleavage.

The mechanism we propose can be described as follows: the condensed polyaromatic moiety of the compounds studied is adsorbed preferentially on the surface of the carbon black concurrent with the carbon surface becoming positively charged (at temperatures over 320 °C). Subsequently an electron is transferred from the condensed aromatic ring to the carbon catalyst. In the ion radical formed, the weakest bond becomes the C_{ar} - C_{aliph} adjacent to the polyaromatic system[8,9]. If the temperature is high enough for cleavage of this bond, the reaction will take place and the free radical formed from the substituent group will abstract a hydrogen atom from another molecule (for example the hydrogen donor present in excess). The naphthalene fragment resulting from cleavage has a higher oxidation potential than I (1.54 eV for naphthalene[10] vs 1.257 eV for I[11] and will not transfer an electron to the carbon black. Consequently, a free naphthalene radical will desorb and abstract a hydrogen from another molecule. This initial cleavage of the ion radical could explain why cleavage reactions are obtained only at temperatures where the surface becomes positively charged and why the cleavage is observed at temperatures much below the thermal background.

The high energy, very likely more delocalized radical ions typically formed in mass spectrometers could also exhibit very different reactivity from the radical ions formed on a surface. The extrapolation, therefore, of gas-phase ion-radical reactivity to surface reactions is tenuous at best and can be misleading when interpreting results from heterogeneous catalytic reactions.

The data presented above may be useful for understanding some of the observed differences in the chemistry of radical ions in the gas phase or solution as compared with reactions on a surface. They could also be helpful for understanding why many of the heterogeneously catalyzed reactions require higher temperature than those under homogenous catalysis conditions.

CONCLUSIONS

Our data indicate that the mechanism of selective C-C cleavage in the presence of carbon black involves in the first step an electron transfer from a condensed aromatic ring to the carbon black surface when this surface become positively charged (i.e. at temperatures higher than 320° C). The result is a very different reactivity and selectivity of the ion-radicals toward C-C bond cleavage than that taking place in solution or in a mass spectrometer.

ACKNOWLEDGEMENTS

The contribution of Dr. R.R. Anderson, Dr. P.B. Kaufman and of E.P. Ladner, to the study of the deuterium isotopic effect is gratefully acknowledged. A full manuscript with their participation is in preparation. Helpful discussions and exchange of experimental information with Dr. J.H. Penn are acknowledged. This research was supported in part by an appointment (SCP) to the U.S. Department of Energy Fossil Energy Postgraduate Research Training Program administered by Oak Ridge Institute for Science and Education.

Present address for S.C. Petrosius: Mines Safety Appliances Co. P.O. Box 439, Pittsburgh, PA 15230.

REFERENCES

1. Farcasiu, M.; Smith, C.M. *Prepr. Pap.- Am. Chem. Soc. Div. Fuel Chem.* **1990**, *35*, 404.
2. Farcasiu, M.; Smith, C.M. *Energy & Fuels*, **1991**, *5*, 83.
3. Farcasiu, M.; Smith, C.M.; Hunter, E.A. 1991 Conference on Coal Science Proceedings, ed. IEA Coal Research Ltd., Butterworth, Heinemann Ltd., **1991**, p.166.
4. Farcasiu, M.; Smith, C.M.; Ladner, E.P.; Sylwester A.P. *Prepr. Pap.- Am. Chem. Soc. Div. Fuel Chem.* **1991**, *36*, 1869.
5. Farcasiu,M.; Petrosius, S.C.: Ladner, E.P. *J. Catal.* **1994**,*146*, 313.
6. Penn, J.H.; Wang, J *Energy & Fuels*, **1994**, *8*, 421 and the references therein.
7. (a) Mc.Millen, D.F.; Malhotra, R.; Chang, S.J.; Ogler, S.; Nigenda, S.E.;Fleming, R.H. *Fuel* **1987**,*66*, 1611. (b) Malhotra, R.; McMillen D.F. 1991 Conference on Coal Science Proceedings, ed. IEA Coal Research Butterworth, Heinemann Ltd., **1991**, p.174.
8. Ades, H.F., Companion A.L., Subbaswamy K.R. *J. Phys. Chem. Soc.*, **1991**, *95*, 2226.
9. Ades, H.F., Companion A.L., Subbaswamy K.R. *J. Phys. Chem. Soc.*, **1991**, *95*, 6502.
10. Pysh, E.S.; Yang, E.C. *J.Am. Chem. Soc.*, **1963**, *85*, 2124.
11. Alnajjar, M., Franz, J., personal communication.

These pages intentionally left blank.

The Effect of Promoter Metals on the Catalytic Activity of Sulfated Hematite for Model Compound Reactions

G. T. Hager, R. Ochoa, E. N. Givens, P. C. Eklund, F. J. Derbyshire
Center for Applied Energy Research
University of Kentucky
3572 Iron Works Pike
Lexington, KY 40511-8433

Abstract

Iron based catalysts have long been known to enhance the conversion in a direct coal liquefaction process. Attempts to increase the moderate activity of these catalysts have focussed on reducing particle size, enhancing and maintaining dispersion, and modifying the structure by addition of promoters. The use of sulfated hematite has been shown to yield enhanced conversion for the liquefaction of a subbituminous coal as compared to hematite. Further, the use of promoter metals such as molybdenum and tungsten on the sulfated hematite was shown to further improve the activity of these particles. More recently it has been shown that the addition of combinations of promoters, such as nickel and molybdenum, may increase the activity of the particles at lower promoter loading. The role of the promoter metals on sulfated hematite will be compared to other unsupported catalysts using model compound reactions.

Introduction

The utility of iron based dispersed catalysts in direct coal liquefaction has been well established since the early 1900's, particularly for the liquefaction of low rank coals. Since that time considerable effort has been directed at improving the activity of these catalysts. This effort has focussed on reducing the particle size, enhancing and maintaining the dispersion, and modifying the structure by addition of promoters. Reducing the particle size will increase the surface area to volume ratio and result in higher activity at similar weight loadings. Further, sufficiently small particles may have properties different from those of the bulk, particularly with regard to surface energetics.

The use of oil soluble organometallic precursors offer the highest possible initial dispersion. However, one study found that these precursors tend to agglomerate and form larger particles at a faster rate than a particulate precursor.[1] This agglomeration quickly reduces the high dispersion and associated surface area for the oil soluble precursors. This would seem to indicate that particulate catalysts can maintain high dispersion for longer times and may therefore have higher activities than the organometallic precursors.

Efforts to improve the activity of iron oxide particulate catalysts by reducing the particle size may have reached a limit in the form of Nanocat produced by Mach I. These particles are reported to have an average diameter of 30 Å. The small size of the particles makes identification of the phase difficult by traditional techniques. The Nanocat particles have been identified as α-Fe_2O_3, γ-Fe_2O_3, and FeOOH by the manufacturer and various researchers, respectively.[2,3] These particles have shown improved activity for the liquefaction of a low rank coal.[4]

Several studies have shown the high activity of sulfated hematite for both liquefaction and coprocessing of coal with a petroleum resid.[5,6,7] The use of molybdenum or tungsten as a promoter metal further improved the activity of these particles.[8,9] The use of nickel, cobalt, tungsten, and molybdenum have been examined as promoter metals, both individually and in combination.[10] Molybdenum showed the largest increase in activity when used as a promoter on the sulfated hematite. While the activity of tungsten and cobalt, when used in combination with molybdenum, appeared nearly additive, the combination of nickel and molybdenum exhibited a synergistic

effect, resulting in higher conversions and lower promoter loading.

Unsupported molybdenum carbides and nitrides have been prepared and tested for their activity using model compound reactions.[11 12] The results indicate the significant activity of these particles for hydrodesulfurization (HDS) and hydrodenitrogenation (HDN). The molybdenum carbide was found to be resistant to bulk sulfidation during the reaction, although it was reported that a surface layer of MoS_2 may have been formed. The sulfided Mo_2N was reported to have higher activity for HDS than either MoS_2 or molybdate indicating that the surface was not MoS_2, although the exact surface composition was not determined.

The role of catalysts in coal liquefaction is obscured by the complexity of the coal molecule itself. The exact nature of the structure of coal has been the object of considerable study. While the structure is not known, it is generally accepted that coal is composed of highly aromatic clusters connected by crosslinking bonds. These crosslinks may consist of aliphatic (methyl or ethyl) bridges or heteroatom (O,S,N) bridges. The role of catalyst in selective cleavage of these bonds may be elucidated by the use of model compound reactions. The activity for cleavage of the sulfur bridges may be studied by the HDS of benzothiophene. Similarly, the activity for cleavage of the etheric bond may be inferred from the HDO of diphenyl ether and the activity for nitrogen removal by the HDN of quinoline.

Experimental

The reactions were carried out using 25 ml stainless steel microautoclave reactors. The reactors were loaded with a 5 wt% solution of reactant in hexadecane. The catalysts were loaded at 5 wt% on reactant basis and 0.017 g dimethyldisulfide (DMDS) was added in most runs. Experiments were carried out using DMDS alone in order to determine its influence on activity and selectivity. The reactors were purged and pressurized to 800 psig (cold) with hydrogen. The loaded reactors were placed in a heated fluidized sand bath at 385°C and agitated vertically at 400 cycles/minute to minimized any mass transfer constraints. The reactions were carried out for times of 15 to 60 minutes after which the reactor was quenched in a cool sand bath.

The reaction products were removed from the reactor by washing with THF. A gas chromatograph (Hewlett Packard 5890 Series 2) using both a 30 m DB-5 and a 30m carbowax column was utilized to analyze the products of the reaction. The activity was determined by the rate of model compound disappearance.

The spent catalyst was collected and stored with the product to reduce oxidation from exposure to air. The major phase of the particles was determined by XRD and the average particle diameter was estimated from the peak broadening using the Debye-Scherrer relationship. This allowed the comparison of catalyst conversion to reaction conversion.

Catalyst Synthesis and Characterization

The iron based catalysts used in this study were prepared using an aqueous precipitation technique. This method involves the coprecipitation of iron and a promoter metal in the presence of sulfate ions. In this study, urea was used to effect the precipitation of ferric ammonium sulfate (iron alum), following the method of Kotanigawa et al.[5] The promoter metal molybdenum was incorporated by addition of ammonium molybdate to the iron alum solution, as described previously.[10] Ammonium nickel sulfate hydrate and cobalt sulfate hydrate were used to add nickel and cobalt, respectively. The precipitated catalysts were filtered and dried in an air flow oven overnight and then calcined in air at 475 °C for 30 minutes.

The promoted sulfated hematite catalysts were analyzed by XRD, XPS, TEM, SEM, and nitrogen BET adsorption. The results of the electron microscopy have shown that the catalysts consist of a loose agglomeration of particles with an acicular shape with average dimensions of ~10x50 nm, shown in Figure 1. Surface areas were

measured by the nitrogen BET adsorption and were found to be in the range of 100-200 m^2/g. The addition of up to 10 wt% of molybdenum had little effect on the particle size and no apparent effect on the major phase identified by XRD, shown in Figure 2. The XRD spectra of the as-formed catalyst indicate the major phase is α-FeOOH in addition to a trace of α-Fe also present. After calcination the major phase was α-Fe_2O_3 with α-Fe still present. The relative amount of α-Fe does not appear to be affected by the calcination.

Elemental analysis of the sulfated hematites indicated sulfur contents of 2-6 wt%. It has been reported that the sulfur is present on the surface of the hematite as chemisorbed SO_3. XPS confirmed this showing that the surface sulfur concentration was significantly higher than the bulk concentration. It was found that the sulfur content decreased with increasing molybdenum concentration. This may indicate that molybdenum is chemisorbed as MoO_3 displacing the sulfur on the surface. The XPS studies confirm this, showing that the surface concentrations of molybdenum, sulfur, and tungsten are substantially higher than the bulk concentrations. Nickel and cobalt, on the other hand, have similar bulk and surface concentrations indicating that they are substituted into the iron oxide matrix. It follows from Goldschmidt's rules of substitution that the hexavalent ions, Mo, W, and S cannot substitute for iron while the nickel and cobalt can substitute.[13]

The molybdenum nitride (Mo_2N), molybdenum carbide (Mo_2C), and molybdenum sulfide (MoS_2) catalysts were produced by a laser pyrolysis technique. This method utilizes the intersection of a tunable CO_2 laser with a gas stream to create a small (~1mm^3) pyrolysis zone. The flow rate of the gases determines the residence time in the reaction zone and, consequently, the particle size and phase. This method has been shown to produce monophasic particles with a narrow size distribution. The particles have an average diameter of ~5 nm and a surface area of 65 m^2/g.

Results

The use of the unsulfided molybdenum promoted sulfated hematite showed little impact on the hydrogenation of naphthalene varying only slightly from the thermal conversion of 7% at 60 minutes. The addition of sulfur alone impacted more favorably on the reaction increasing the conversion at 60 minutes to 19%. The synergism between the sulfur and the promoted sulfated hematites is clear in the experiments using added sulfur with the catalyst. In these runs the conversion increased to 82% at 60 minutes. This corresponds well with other work which has shown that the activity of iron based catalysts is dependent on the partial pressure of H_2S present.[14]

The unsulfided molybdenum nitride, with a conversion of 59% at 60 minutes, showed higher activity for naphthalene hydrogenation than the unsulfided molybdenum promoted sulfated hematite. The addition of sulfur to the molybdenum nitride had only a minor effect on conversion. However, the use of a molybdenum sulfide resulted in a significant increase in conversion to 46% at 30 minutes compared to 29% for the sulfided molybdenum nitride. This indicates that the nitride is stable at these conditions and resists surface sulfidation, agreeing well with previous findings.[12]

The activity of the promoted sulfated hematite for the HDO of diphenyl ether followed a similar trend. The unsulfided molybdenum promoted sulfated hematite showed a slight increase in conversion to 26% at 60 minutes, compared to 21% for the thermal run. The addition of sulfur alone caused a significant decrease in conversion at 60 minutes to 12%. The combination of sulfur and molybdenum promoted sulfated hematite resulted in an increase in conversion to 39% at 60 minutes again due to the attainment of the active phase.

The molybdenum nitride showed a higher activity for HDO than molybdenum promoted sulfated hematite both with and without sulfur. The conversion at 60 minutes was 53%, significantly higher than the 39% achieved with the promoted hematite with sulfur. The addition of sulfur to the molybdenum nitride resulted in a substantial loss of activity yielding a conversion of only 20% at 60 minutes. This indicates that the

addition of sulfur severely inhibits the catalytic activity of the molybdenum nitride.

Conclusions

The activity of promoted sulfated hematite has been compared to the activity of other unsupported catalysts using model compound reactions. Preliminary results indicate that the molybdenum promoted sulfated hematite shows significantly higher activity for the hydrogenation of naphthalene to tetralin when sufficient sulfur is added to the reaction. In the absence of added sulfur the activity of the promoted sulfated hematite was negligible.

The molybdenum nitride exhibits the highest activity for HDO of diphenyl ether. The addition of sulfur increased the activity of the promoted sulfated hematite but severely inhibited the activity of the molybdenum nitride.

In both reactions the catalyst loading was 1 wt% on reactant solution. Since the cost of the promoted sulfated hematite is substantially lower that the molybdenum nitride, due to a lower molybdenum content, the results of this study indicate that significant improvements in process economics may be achieved through the use of these catalysts.

Acknowledgements

The authors would like to gratefully acknowledge support for this project recieved from the United States Department of Energy under contracts DE-AC22-91PC91040 and DE-FC22-93PC93053.

References

1. Djega-Mariadassou, G., *et al. Fuel Processing Technology* **12**, 143-153 (1986).
2. Srinivasan, R., Keogh, R.A. & Davis, B.H. *ASC-Division of Fuel Chemistry Preprints* **38**, 203-210 (1993).
3. Zhou, J., Feng, Z., Huggins, F.E., Shah, N. & Huffman, G.P. *ACS-Division of Fuel Chemistry Preprints* **38**, 196-202 (1993).
4. Anderson, R., Givens, E.N. & Derbyshire, F. *ACS-Division of Fuel Chemistry Preprints* **38**, 495-502 (1993).
5. Kotanigawa, T., Yokoyama, S., Yamamoto, M. & Maekawa, Y. *Fuel* **68**, 618-621 (1989).
6. Pradhan, V.R., Tierney, J.W., Wender, I. & Huffman, G.P. *Energy & Fuels* **5**, 497-507 (1991).
7. Pradhan, V., Tiemey, J.W. & Wender, I. *ACS Preprint - Fuel* **36**, 597-604 (1991).
8. Pradhan, V.R., Herrick, D.E., Tiemey, J.W. & Wender, I. *Energy & Fuels* **5**, 712-720 (1991).
9. Pradhan, V.R., Hu, J., Tierney, J.W. & Wender, I. *Energy & Fuels* **7**, 446-454 (1993).
10. Hager, G.T., Givens, E.N. & Derbyshire, F.J. *ACS-Division of Fuel Chemistry Preprints* **38**, 1087-1092 (1993).
11. Schlatter, J.C., Oyama, S.T., Metcalfe, J.E., III & Lambert, J.M., Jr. *Ind. Eng. Chem. Res.* **27**, 1648-1653 (1988).
12. Markel, E.J. & Zee, J.W.V. *Joumal of Catalysis* **126**, 643-657 (1990).
13. Faure, G. *Principles and Applications of Inorganic Geochemistry* 1-626 (Macmillan Publishing Company, New York, 1991).
14. Sweeny, P.G., Stenberg, V.I., Hei, R.D. & Montano, P.A. *Fuel* **66**, 532-541 (1987).

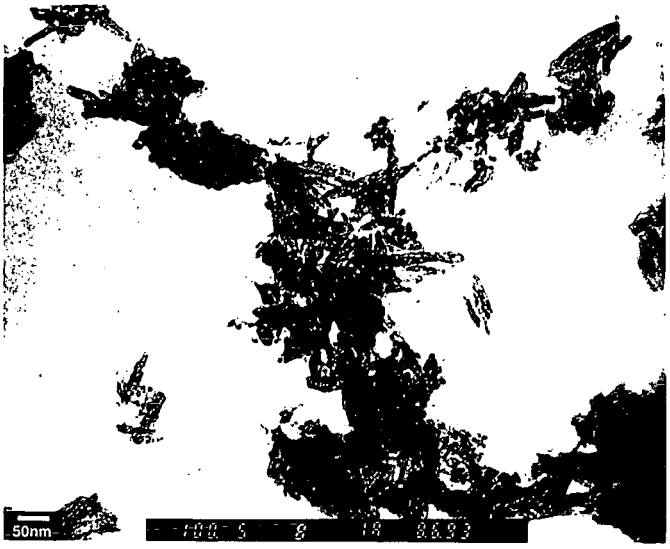

Figure 1. TEM micrograph of molybdenum promoted sulfated hematite

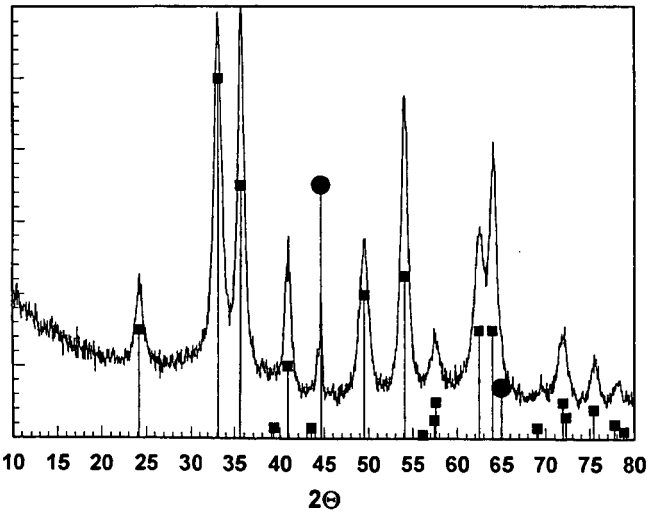

Figure2. XRD spectrum of molybdenum promoted sulfated hematite indicating peaks identified as hematite and α–Fe

MODEL HYDROCRACKING REACTIONS OVER MONOMETALLIC AND BIMETALLIC DISPERSED CATALYSTS.

Eckhardt Schmidt and Chunshan Song*

Fuel Science Program, Department of Materials Science and Engineering, 209 Academic Projects Building, The Pennsylvania State University, University Park, PA 16802

Coal liquefaction involves cleavage of methylene and dimethylene bridges connecting polycyclic aromatic units. The selected compound for model coal liquefaction reactions is 4-(1-naphthylmethyl)bibenzyl (NMBB). This work describes the synthesis and screening of several hetero- and homometallic complexes as precursors of dispersed catalysts for hydrocracking of NMBB. Experiments were carried out at 400 °C for 30 min under 6.9 MPa H_2 pressure. $(NH_4)_2MoS_4$ and $MoCl_3$ converted NMBB predominately into naphthalene and 4-methylbibenzyl. Small amounts of secondary products were formed by hydrogenation and fragmentation of the primary products. Lewis acid-type $MoCl_3$ catalyst gave lower selectivity to the primary products, with relatively larger amounts of methyltetrahydronaphthalene- and methylnaphthalene-derivatives. In contrast, the organometallic catalyst precursors $Cp_2Co_2Mo_2(CO)_2S_4$, $Cp_4Fe_4S_4$ and $(Ph_4P)_2(Ni(MoS_4))$ inflict less fragmentation and less hydrogenation of primary cleavage products. $Cp_2Co_2Mo_2(CO)_2S_4$ converted a substantial amount of starting material even at 350 °C; whereas, a noncatalytic run under the same conditions showed only small conversion. Greater product selectivity can be achieved by means of organometallic precursur and low severity reaction conditions. Inorganic and bimetallic catalyst precursors gave similar conversions. The synergistic effect of heterometallic over homometallic catalyst precursors was demonstrated by Co-Mo and Ni-Mo, which gave far higher conversion than the thiocubane-type catalyst containing four iron atoms. The addition of sulfur to $Mo(CO)_6$ and $Co_2(CO)_8/Mo(CO)_6$ gave higher conversion but reduced the yield of hydrogenation products.

Keywords: Model reactions, hydrocracking, dispersed catalysts, monometallic and bimetallic catalysts.

Introduction

First attempts to liquefy coal were carried out in the beginning of the 20th century by Bergius (1). The process is intricit and involves hundreds of different coal components with various functional groups in interconnected aromatic systems. The complexity of coal liquefaction reactions makes it very difficult to study the reaction mechanisms. Therefore, it is extremely difficult to find optimum reaction conditions for selective bond cleavage. Furthermore, coals from different sources may react differently with different catalysts. We selected therefore the model compound 4-(1-naphthylmethyl)bibenzyl (NMBB), which consists of functionalities that are related to coal structures (2-6). Among these are alkyl groups which interconnect aromatic moieties and different ring systems. Of particular interest to our group was the fact that its reaction can give us information about the features of different catalysts. In a typical hydroliquefaction reaction, coal reacts at temperatures above 400 °C with 7 MPa H_2 pressure for a period of ca. 30 min to primary liquefaction products. Efficient conversion can only be achieved by transition metal containing catalysts and metal concentrations of 1 wt % or lower. Suitable catalytic systems contain Co, Ni, Mo or its combinations, either as inorganic complexes, or organometallic species. Good solubility of catalyst precursors generally leads to better catalyst dispersion and greater effectiveness for liquefaction reactions (7,8). One way to achieve better dispersion is the use of soluble organometallic precursors which produce in situ finely dispersed active catalyst particles at elevated tempertures. Greater catalyst surface area increases the yield of products dramatically, due to greater hydrogen acitivation by augmented reactive catalyst sites. Hirschon and Wilson (9,10) demonstrated that highly dispersed catalysts from organometallic precursors can be effective for hydrogenating the coal with molecular hydrogen without relying upon a donor solvent .

This paper reports our work on hydrocracking experiments of NMBB over different transition metal catalyst precursors. The effects of inorganic and organometallic (monometallic and bimetallic) catalyst precursors on conversion and product selectivity will be discussed. Also, the influence of the reaction temperature on the product distribution will be investigated.

Experimental Section

Preparation of Catalyst Precursors. The complexes $(Ph_4P)_2(Ni(MoS_4))$ (11) (Ni-Mo) and $Cp_4Fe_4S_4$ (12) (Fe4) were prepared according to the methods described in the literature, based on the procedures of Brunner and Wachter (11) and Schunn, Fritchie and Prewitt (12). The thiocubane cluster $Cp_2Co_2Mo_2(CO)_2S_4$ (CoMo-TC2) was synthesized earlier (13) in our laboratory. Samples were stored at - 25 °C prior to use. All recrystallizations of the homo- and heterometallic cluster compounds were carried out quickly. The crystalline products are stable on exposure to air but decompose slowely in solution. Sulfur and $(NH_4)_2MoS_4$ (ATTM) were purchased from Aldrich, $Mo(CO)_6$, $Co_2(CO)_8$ from Alfa and the model compound MNBB from TCI America. GC-MS confirmed sufficient purity of NMBB (> 99 %) and it was used without further purification.

Model compound reactions. A stainless steel reactor (tubing bomb) with a capacity of 33 ml was loaded with ca. 0.25 g NMBB, 2.11 wt % catalyst precursor and 0.125 g solvent (tridecane). The reactor was purged three times with H_2 and then pressurized with 6.9 MPa H_2 at room temperature for all experiments. A preheated fluidized sand bath was used as heating source and the reactor agitated via an oscillator by vertical shaking of the horizontal micro reactor (about 240 strokes/min.) After the reaction the hot tubing bomb was quenched in cold water and the gaseous products collected in a gas bag for further analysis. The liquid contents were washed with 15 ml CH_2Cl_2 through a low speed filter paper and stored in small glass bottles for qualitative and quantitative GC analysis. All runs were carried out at least twice to confirm reproducibility.

The compounds were identified by capillary gas chromatography-mass spectrometry (GC-MS) using a Hewlett-Packard 5890 II GC coupled with a HP 5971A mass-selective detector operating at electron impact mode (EI, 70 eV). The column used for GC-MS was a J&W DB-17 column; 30-m X 0.25-mm, coated with 100 % phenylmethylpolysiloxane with a coating film thickness of 0.25 µm. For quantification a HP 5890 II capillary GC with a flame ionization detector and the same type of column (DB-17) was used. Both Hewlett-Packard GC and GC-MS were programmed from 40 to 280 °C at a heating rate of 4 °C/min and a final time of 30 min. The response factors of 10 pure compounds were determined. More experimental and analytical details may be found elsewhere (14-17).

Results and Discussion

Hydrocracking of NMBB. Tables 1 and 2 show the results of hydrocracking of the model compound NMBB over different catalyst precursors. In the absence of a catalyst, the conversion at 300 °C is only 1 % and increases to about 4 % at 400 °C. The inorganic catalyst precursor ATTM increased the conversion at 350 °C relative to the thermal run by 54 %. A

run at 400 °C shows the effect of elevating reaction temperatures. The conversion increased by additional 30 %. Molybdenum trichloride proved to be less effective and gave about 70 % conversion.

Of the catalysts tested, $(Ph_4P)_2(Ni(MoS_4))$ and $Co_2(CO)_8$+S showed the highest conversion (95 %). Ni-Mo consists of a chain like structure with tetrahedral enviroment around nickel and molybdenum (Scheme 1).

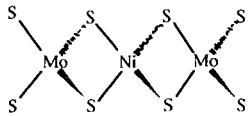

Scheme1: Structure of the bimetallic sulfide $[Ph_4P]_2[Ni(MoS_4)_2]$

From the data in Tables 1 and 2 Ni-Mo is apparentely the best precursor and $Cp_4Fe_4S_4$ is the worst among the catalyst precursors tested. A general observation is that the activity of the in situ generated catalysts is smaller at lower temperatures and increases at elevated temperatures. In an attempt to examine the role of bonding between transition metals, we tested the bi-metallic thiocubane-type catalyst $Cp_2Co_2Mo_2(CO)_2S_4$ (Scheme 2), the homometallic cluster $Cp_4Fe_4S_4$ (Scheme 2), and different metal carbonyl combinations which may give (after thermal decomposition) similar catalyst composition as Co-Mo-TC2.

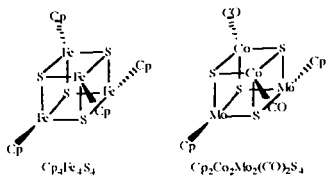

Scheme 2: Structure of the thiocubane-type catalyst precursors $Cp_4Fe_4S_4$, and $Cp_2Co_2Mo_2(CO)_2S_4$.

There are direct metal-metal bonds between Co-Mo, Co-Co and Mo-Mo, besides the sulfur bridges in CoMo-TC2. The question is, do in situ generated catalysts from catalyst precursors which have metal-metal bonds, show different catalytic behaviour. Table 1 shows the superior performance of catalysts containing either Mo, or Co+Mo. Using $Mo(CO)_6$ alone gave similar results as runs with the mixture of two corresponding metal compounds that can also be found in $Cp_2Co_2Mo_2(CO)_2S_4$. Among the testet metal carbonyls, $Co_2(CO)_8$ is less active compared to the thiocubane type catalyst Co-Mo-TC2 and mixed metal carbonyls. A beneficial effect could be observed, when sulfur was added to $Co_2(CO)_8$. NMBB conversion increased dramatically. Addition of sulfur to $Mo(CO)_6$ did not improve the convertibility of NMBB, but added sulfur to $Mo(CO)_6/Co_2(CO)_8$ gave 10 % higher conversion. Work on the advantage of using different metals in a single catalyst reports the synergistic effect of heterogeneous catalysis. The addition of Co or Ni to MoS_2-containing precursors increased their catalytic activity considerably. However, little work has been done on comparison of catalytic effects between mixed metal carbonyls, inorganic- and organometallic heteroatomic precursors. Previous work (18-22) reports mainly the mixture of different transition metal salts.It is known (24-27) that catalyst precursors like metal carbonyls require the addition of sulfur for sufficient activity. The beneficial effect of sulfur addition to hydrogenation reactions was studied on the system molybdenum sulfide and oxide (21). There seems (23) to be consensus that the sulfides of the transition metals are more active in catalytic hydroliquefaction than their oxides. The reason for this remains unclear. Montano and co-workers (28,29) have emphasized the importance of correct stoichiometry between molybdenum oxides and sulfur in high temperature conversion reactions in order to generate catalytically active MoS_2 particles. Temperatures as high as 350 °C are required for this activation process. The analogue transformation of $Fe(CO)_5$ into pyrrhotite ($Fe_{1-x}S$, where $0 \leq x \leq 0.125$) is difficult to perform and iron carbonyls tend to form less reactive iron carbides and oxides (25) during the activation process. This might explain the low activity of our catalyst precursor $Cp_4Fe_4S_4$. The iron catalyst from $Cp_4Fe_4S_4$ would not be active due to the difficulty of forming pyrrhotite. Another reason for the low effectiveness of the iron-cluster in hydrocracking reactions may be that iron appears to function by removing oxygen functionalities whereas Mo catalysts are good hydrogenation catalysts (9). In our previous work, it has been demonstrated that the thiocubane CoMo-TC2 is superior to the mixtures of $Mo(CO)_6$, $Co_2(CO)_8$, and sulfur for liquefaction of a subbituminous coal (13). Comparison of the results in tables 1 and 2 indicates that the thiocubane bimetallic catalysts are not superior to the corresponding mixtures of Co, Mo and sulfur. The rather expensive preparation of the bimetallic catalyst precursors leads to the conclusion that cheaper metal combinations can achieve comparable results. We focused therefore our attention to product selectivity under low severity reaction conditions to study product distribution of NMBB hydrocracking reactions under the influence of homo- and bimetallic catalyst precursors.

Product Distribution

Hydrocracking of NMBB yields three product categories that can be explained by the cleavage of the bonds between the aromatic moieties. The identified products can be classified into hydrocracking, hydrogenation and isomerization products. Those coming from hydrocracking reactions form the major pool of reaction products, followed by hydrogenation and isomerization products. Figure 1 shows the product distribution from catalyst-free reactions. The thermal reaction of NMBB at 300 °C yields only two products, 4-methylbibenzyl (4-MBB) and napththalene (N). Higher temperature (400 °C) gave enhanced conversion and twice as much products. Besides 4-MBB and N, 1-(naphthyl)-4-tolyl methane (NTM) and tetralin can be found as high temperature products. Generally, increased temperature results in lower selectivity. The ratio of major products in our model reactions over thiocubane catalysts (Figure 2) remains similar over a wide temperature range. We can see in Figure 2 more 4-MBB than BB and more naphthalene (N) than tetralin. Several studies, including the present work have shown that NMBB tends to undergo cleavage of bond a connecting the naphthyl group to the remainder of the molecule when subjected to a variety of catalysts under a variety of conditions. Farcasiu et al. suggested a reaction mechanism in which the first stage consists of the formation of a radical cation. The loss of electron density leads to a weakened a-bond which can then be broken relatively easily. This is in contrast to model studies in which phenyl-containing compounds undergo preferably b-cleavage (6).

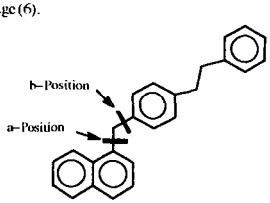

Scheme 3: Potential Cleavage sites in 4-(1-naphthylmethyl)bibenzyl.

In the work of Penn and Wang (6) radical cations were generated in the mass spectrometer under a variety of conditions which had little impact on the bond cleavage pathway. Preference for b-cleavage was observed. It was explained by resonance stablization of the intermediates formed via bond b cleavage. Both intermediates are resonance stabilized. Thermochemical calculations (30) show that reaction pathway b is 30 kcal/mol lower for both neutral and radical cationic species than pathway a. In contrast, neither of the intermediates resulting from bond a cleavage is stabilized. However, in the presence of a catalyst, the major reaction pathway mainly involves the cleavage of bond a (Scheme 3). These studies indicate that a new decomposition pathway mechanism must be

developed to explain the results of bond cleavage involving model reactions on NMBB. The product distribution is different over metal carbonyls (Figure 3). The main reaction product is 4-MBB, but the ratio of tetralin/naphthalene depends on the addition of sulfur. Sulfur-free metal carbonyl precursors are relatively better hydrogenating catalysts than sulfur containing metal carbonyls and their combinations. This becomes more apparent in the case of Co+Mo and Co+Mo+S. Sulfur enhances the formation of naphthalene and surpresses the generation of tetralin. In order to get more information about the influence of sulfur on hydrogenation reaction, we carried out experiments with tetralin in tridecane as solvent, with and without added sulfur. A sulfur-free run showed only a negligible amount of naphthalene (naphthalene/tetralin ration ≈ 0), but the addition of sulfur lead to a substantially higher naphthalene-to-tetralin ratio (0.08).

Products found in hydrocracking of NMBB over the inorganic catalyst precursor (Figure 4) at 400 °C are similar to those found in runs with organometallic precursors. Unlike all other catalysts, the lewis-acid-type complex $MoCl_3$ gave a different product distribution. $MoCl_3$ is the only catalyst that cleaved both bond a and b in NMBB with about equal probability. The aggressiveness of $MoCl_3$ as catalyst precursor is also demonstrated by a relatively larger percentage of isomerization products. The general observation is that low serverity reaction conditions benefit higher selectivity. At 350 °C ATTM gives a considerable amount of hydrogenation and isomerization products, whereas the organometallic complex CoMo-TC2 yields only products, coming from hydrocracking and hydrogenation reactions. The latter category of compounds can not be found in a reaction involving $Cp_2Co_2Mo_2(CO)_2S_4$ at 300 °C. Higher product selectivity can also be found in experiments with Fe4. This relatively inreactive precursor yields at 400 °C mainly hydrocracking products.

Acknowledgment. This project was supported by the U.S. Department of Energy, Pittsburgh Energy Technology Center under contract DE-AC22-92PC92122. We are grateful to Professor Harold Schobert for his encouragement and to Dr. Udaya Rao of PETC for his support. We also thank Mr. R. Copenhaver for the fabrication of micro-tubing bomb reactors.

References cited

1. Stranges, A. N. *Fuel Proc. Technol.*, **1987**, **16**, 205-225 .
2. Farcasiu, M.; Smith, C. *Prepr. Pap. - Am. Chem. Soc., Div. Fuel Chem.* , **1990**, **35**, 404-13.
3. Farcasiu, M.; Smith, C. *Fuel Processing Technology* , **1991**, **29**, 199-208.
4. Farcjasiu, M.; Smith, C. and Ladner, E. P. *Prepr. Pap. - Am. Chem. Soc., Div. Fuel Chem.*, **1991**, **36**, 1869-77 .
5. Tang, Y.; Curtis, C. W. *Energy Fuels*, **1994**, **8**, 63-70.
6. Penn, J. H.; Wang, J.-H. *Energy Fuels*, **1994**, **8**, 421-425 .
7. Weller, S.; Pelipetz, M. G. *Ind. Eng. Chem.*, **1951**,**43**, 1243.
8. Weller, S. W. *Coal Liquefaction with Molybdenum Catalysts. In Chemistry and Uses of Molybdenum; Climax Molybdenum Co.*, **1982**, 179-186.
9. Hirschon, A. S.; Wilson Jr, R. B. *Coal Science II , ACS Sym. Ser.*, **1991**, 273-83.
10. Hirschon, A. S.; Wilson Jr, R. B. *Fuel*, **1992**, **71**, 1025-31.
11. Mueller, A.; Ahlborn, E.; Heinsen, H.-H. *Z. anorg. allg. Chem.*, **1991**, **386**, 102-106.
12. Schunn, R. A.; Fritchie, C. J.; Prewitt, C. T. *Inorganic Chemistry*, **1966**, 892-899.
13. Song, C.; Parfitt, D. S.; Schobert, H. H. *Energy Fuels*, **1994**, **4**, 313-219.
14. Song, C.; Hanaoka, K.; Nomura, M. *Energy Fuels*, **1988**, **2**, 639.
15. Song, C.; Schobert, H. H. *Prep. Pap.- Am. Chem. Soc., Div. Fuel Chem.*, **1992**, **37**, 976.
16. Song, C.; Lai, W.-C.; Schobert, H. H. *Ind. Eng. Chem. Res.*, **1994**, **33**, 534-547.
17. Song, C.; Saini, A. K.; Schobert, H. H. *Proc. 1993 Int. Conf. Coal Sci., Banff, Canada, Sept. 12-17, 1993*, **1993**, **1**, 291.
18. Nomura, M.; Miyake, M.; Sakashita, H.; Kikkawa, S. *Fuel* , **1982**, **61**, 18-20.
19. Garg, D.; Givens, E. N. *Fuel Process. Technol.*, **1984**, **8**, 123-143.
20. Song, C.; Nomura, M.; Miyake, M. *Fuel*, **1986**, **65**, 922-926.
21. Song, C.; Nomura, M.; Ono, T. *Prepr. Pap. - Am. Chem. Soc., Div. Fuel Chem.*,**1991**, **36**, 586-596.
22. Sommerfeld, D. A.; Jaturapitpornsakul, J.; Anderson, L.; Eyring, E. M. *Prepr. Pap. - Am. Chem. Soc., Div. Fuel Chem.*, **1992**, **37**, 749-755.
23. Weller, S. *Energy Fuels*, **1994**, **8**, 415-420.
24. Yamada, O.; Suzuki, T.; Then, J.; Ando, T.; Watanabe, Y. *Fuel Process. Technol.*, **1985**, **11**, 297-311.
25. Herrick, D.; Tierney, J.; Wender, I.; Huffamn, G. P.; Huggins, F. E. *Energy and Fuels* , **1990**, **4**, 231.
26. Suzuki, T.; Ando, T. ; Watanabe, Y. *Energy Fuels* , **1987**, **1**, 299-300.
27. Artok, L.; Davis, A.; Mitchell, G. D.; Schobert, H. H. and Schobert, H. H. *Energy Fuels* , **1993**, **7**, 67-77.
28. Montano, P.; Bommannavar, A. J. *J. Mol. Catal.*, **1983**, **20**, 393.
29. Montano, P. *ACS Fuel Prepr.*, **1986**, **31**, 226.
30. Ades, H. F.; Companion, A. L.; Subbaswamy, K. R. *Prepr. Pap. - Am. Chem. Soc., Div. Fuel Chem.*,**1991**, **36**, 420-4.

Table 1. Hydrocracking of NMBB over dispersed metal carbonyls and mixed metal carbonyl with and without added sulfur at 400 °C

Reaction temperature (°C)	300	400	400	400	400	400	400	400
Catalyst Precursor	None	None	$Mo(CO)_6$	$Mo(CO)_6$+ S	$Mo(CO)_6$+ $Co_2(CO)_8$	$Mo(CO)_6$+ $Co_2(CO)_8$ +S	$Co_2(CO)_8$	$Co_2(CO)_8$ +S
Products [wt %]								
Cyclohexane							1.1	2.1
Bezene		0.6	0.2	0.7	0.7	0.7		
Toluene		0.3	1.4	0.5	0.4	0.1	0.7	0.8
p-Xylene			0.7	0.2	0.1		0.3	
Tetralin		0.2	17.3	15.1	21.0	11.7	6.8	5.3
Naphthalene	0.4	0.6	13.8	15.3	5.1	19.2	5.4	28.0
2-MTHN			0.8	0.9	0.6	0.8		0.2
1-MTHN			1.8	1.2	2.4	0.9	1.0	0.5
2-MN			0.5	0.4	0.4	0.5		1.2
1-MN			1.7	1.6	0.5	2.0	0.4	3.0
Bibenzyl			7.7	10.5	6.3	10.3	1.0	9.9
2-MBB			0.4					
4-MBB	0.6	1.3	39.8	38.6	38.3	40.7	14.0	44.8
1-NB							0.4	
NTM		0.9						
THNMBB							6.6	
Other-THNMBB							7.9	
Conversion [wt %]	1.0	3.9	86.1	85	75.8	86.9	45.6	95.8

[a] Reactor residence time in preheated sand bath 30 min. [b] wt % based on the initial weight of NMBB feed.

Table 2: Effect of inorganic and thiocubane-type precursors on hydrocracking reactions[a] of NMBB at 300-400 °C

Reaction temperature (°C)	350[a]	400[a]	400[a]	400[a]	400[a]	300[a]	350[a]	400[a]	400[b]
Catalyst Precursor	ATTM	ATTM	$MoCl_3$	Ni-Mo	Fe4	Co-Mo	Co-Mo	Co-Mo	Co-Mo
Products [wt %]									
Benzene		0.7	0.6	4.9	0.6			0.5	0.6
Toluene		0.1	1.3	1.0				0.6	0.9
p-Xylene			0.3	0.5			0.3		0.4
Tetralin	6.5	14.2	4.5	8.5		0.5	1.6	6.7	9.4
Naphthalene	14.3	16.9	20.9	23.6	4.3	4.0	11.0	24.4	23.2
2-MTHN	0.2			0.4					
1-MTHN	0.8	1.2	0.4	0.8			0.1	0.5	0.6
2-MN	0.1			0.7					
1-MN	1.5	1.7	2.7	2.7			0.6	2.0	2.2
Bibenzyl	3.4	6.3	19.2	6.9	0.3	0.5	1.7	4.7	6.0
2-MBB			3.7	0.2					
4-MBB	28.9	45.1	16.4	44.5	6.5	6.8	18.2	40.9	44.5
Conversion [wt %]	55.7	86.2	70.0	94.7	11.7	11.8	33.5	80.3	87.8

[a] Reactor residence time in preheated sand bath: 30 min. [b] 60 min.

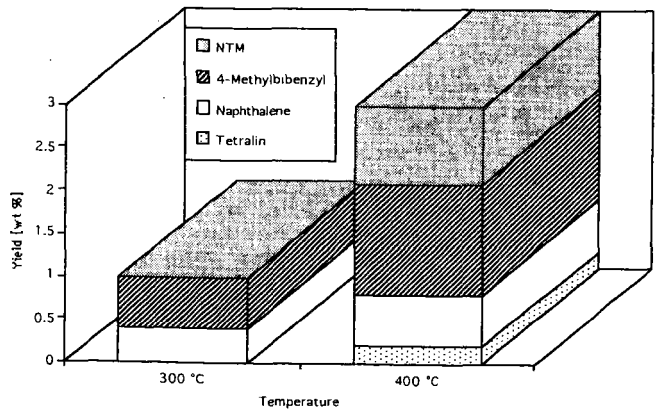

Figure 1: Yields of products excluding gases for non-catalytic thermal hydrocracking of NMBB at 300-400 °C.

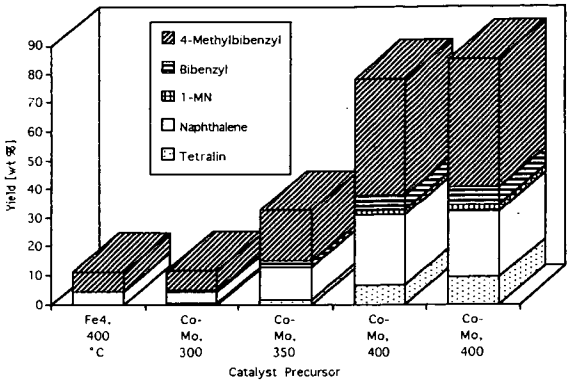

Figure 2: Catalytic activity of thiocubane-type catalysts in the temperature range of 300-400 °C for 30-60 min.

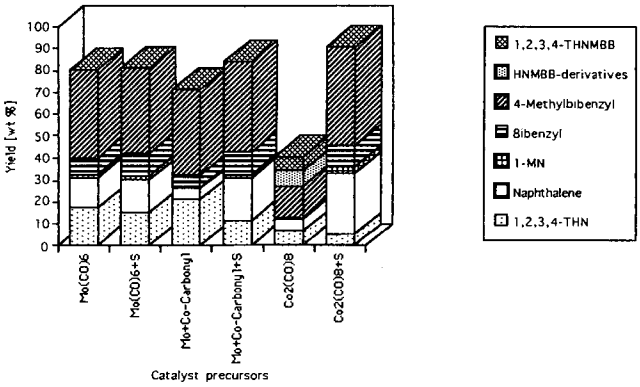

Figure 3. Catalytic activity of mixed metal carbonyls and the mixture plus added sulfur on hydrocracking of NMBB.

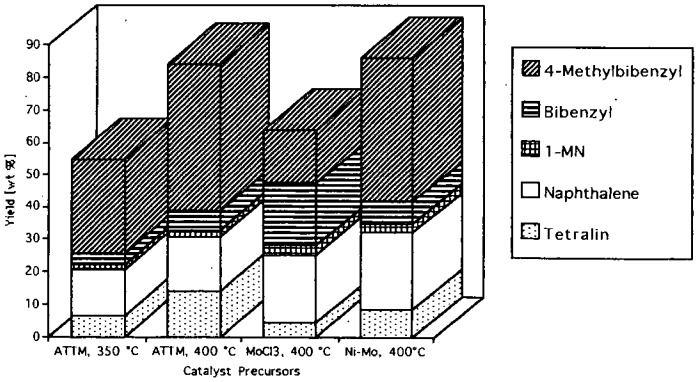

Figure 4: Effect of temperature on hydrocracking of NMBB using inorganic catalyst precursors at 350-400 °C for 30 min.

MICROBIAL DESULFURIZATION MECHANISMS

Edwin S. Olson, Daniel C. Stanley, Ramesh K. Sharma, and John R. Gallagher
Energy & Environmental Research Center
University of North Dakota
Grand Forks, ND 58202

Key Words: Bacterial desulfurization, sulfur-specific degradation

ABSTRACT

Sulfur-specific desulfurization with *Rhodococcus rhodochrous* IGTS8 and related microorganisms may be a useful technology for upgrading high-sulfur carbonaceous materials to more environmentally acceptable fuels. Model compound studies with the organism showed that dibenzothiophene was converted to 2-hydroxybiphenyl or 2,2-dihydroxybiphenyl, depending on whether growth or nongrowth conditions were used in the desulfurization experiments. The pathways that lead to the two key intermediates in the degradation (2'-hydroxybiphenyl-2-sulfinic acid and 2'-hydroxybiphenyl-2-sulfonic acid) and the subsequent conversion of these intermediates to the phenol products required further understanding. The synthesis of an ^{18}O-enriched sulfone substrate has been accomplished, and experiments were performed to elucidate the mechanism of the conversion to the sultine intermediate.

INTRODUCTION

Microbial systems that desulfurize organosulfur compounds have potential use in removing sulfur from fossil fuels. Some organisms utilize a catabolic pathway that results in excision of the sulfur without converting organic carbon to carbon dioxide. Dibenzothiophene (DBT) has been useful as a model compound to investigate the sulfur-specific behavior in bacterial systems. Intermediates corresponding to this thiophenic-ring scission (4S) pathway have been isolated and characterized (1).

The desulfurization of DBT by *Rhodococcus rhodochrous* IGTS8 was recently demonstrated to proceed via two pathways that result in formation of either 2-hydroxybiphenyl or of 2,2'-dihydroxybiphenyl, depending on whether growth or nongrowth conditions are used in the desulfurization experiments (2). Under nongrowth conditions, the DBT was converted to 2'-hydroxybiphenyl via the 2'-hydroxybiphenyl-2-sulfinate (analyzed as the cyclic sultine ester form). Under growth conditions, very little of the 2'-hydroxybiphenyl-2-sulfinate was converted to 2-hydroxybiphenyl; instead, most was oxidized to 2'-hydroxybiphenyl-2-sulfonate (analyzed as the sultone form), and 2,2'-dihydroxybiphenyl was the major product. The oxidation of the sulfinate to the sulfonate occurs spontaneously (nonenzymatically) in aqueous buffer exposed to air, but the sulfinate may also be oxidized in an enzyme-catalyzed reaction. These pathways are summarized in Figure 1. Further understanding of the details of the pathways and mechanisms of the various steps in the pathways is needed.

The initial reaction in the 4S pathway is the oxidation of DBT to the sulfoxide (DBT-5-oxide) (Reaction A). Further oxidation to the sulfone (DBT-5,5-dioxide) also occurs. What is not known is whether the sulfoxide (Reaction B) or the sulfone (Reaction G) is the immediate precursor for the 2'-hydroxybiphenyl-2-sulfinate under nongrowth conditions and whether the sulfone can be converted directly to 2'-hydroxybiphenyl-2-sulfonate (Reaction E) under growth conditions. Is the sulfone an intermediate in the 4S pathway or a by-product?

When sulfone was fed to the bacterium under nongrowth conditions, 2'-hydroxybiphenyl-2-sulfinate and 2'-hydroxybiphenyl were produced (2). Since the sulfone is reduced back to the sulfoxide, whether the sulfoxide or the sulfone is the precursor of 2'-hydroxybiphenyl-2-sulfinate could not be distinguished in the earlier experiments.

This paper describes the use of ^{18}O-enriched sulfone (DBT-5,5-dioxide-$^{18}O_2$) to elucidate the pathway involving the sulfone. If prior reduction of the sulfone to sulfoxide occurred in the pathway (reverse of Reaction D), then loss of one labeled oxygen would be observed in the sultine and sultone intermediates.

RESULTS AND DISCUSSION

The ^{18}O-labeled DBT sulfone substrate (98% isotopic purity) was utilized in the desulfurization experiment with the bacterium *Rhodococcus rhodochrous* (ATCC #53968) under nongrowth conditions. The supernatant from centrifugation of the culture medium was extracted with ethyl acetate, and gas chromatography (GC) analysis showed only starting sulfone and final product, 2-hydroxybiphenyl, and no sultine (cyclic form of the sulfinate) was present. From experiments with unlabelled sulfone, we know that all the sulfinic acid intermediate present in the culture medium is present in the open sulfinate form, but cyclizes to the sultine when the pH is lowered. The sultine can then be easily extracted with ethyl acetate and analyzed by GC. Therefore, the aqueous layer obtained

after the initial extraction (from the experiment with ^{18}O-enriched substrate) was acidified and again extracted. GC/mass spectrometry (MS) was performed to obtain the isotopic abundances for the peaks corresponding to the sultine and sultone.

It must be pointed out that the cyclization to the sultine or sultone form displaces one oxygen from the sulfur, thus half of the label will be eliminated from each molecule of sultine. Hence, the sultine molecules will contain a single labeled oxygen if Reaction G is followed. If the pathway involving Reaction B is followed, half of the sultine molecules will be single labeled and half unlabeled, as a result of the oxygen displacement. These projections assume no occurrence of exchange or disproportionation, which would decrease or increase the numbers of labeled oxygens on sulfur.

The mass spectrum of the sultine product showed molecular ions at m/e 218 and 216 (corresponding to single-labeled and unlabeled species, respectively) in the ratio 2.7. Since this greatly exceeds the ratio of 1 predicted for Pathway B, the ratio is consistent with Reaction G, and the much smaller number of unlabeled molecules must have been formed by exchange with water or disproportionation. The sultine mass spectrum shows a large fragment ion at m/e 190, resulting from loss of $C^{16}O$, and no peak at m/e 188, corresponding to loss of $C^{18}O$. Therefore, all the ^{18}O must be attached to the sulfur, and none is on the phenolic carbon.

Thus, the pathway must proceed directly from the sulfone to the sulfinate (**Reaction G**) rather than reducing sulfone back to the sulfoxide intermediate. The reaction that forms the sulfinate from the sulfone is actually a reduction with respect to the sulfur. When the carbon–sulfur bond is cleaved, the electrons flow to the sulfur to form the sulfinate anion.

The cleavage reaction that involves formation of the sulfinate is similar to that in the electrochemical (3) and metal reduction of sulfones (4), except that hydroxyl is introduced at one aryl site in bacterial reaction, whereas hydrogen is added in the electrochemical and metal reduction reactions. The reactions of DBTs with basic reagents, such as KOH, have been investigated. Attack of nucleophilic oxygen was reported to occur at the ring carbon at high temperatures in the presence of crown ether, resulting in the formation of 2'-hydroxybiphenyl-2-sulfinate (5). In the absence of crown ether, very small amounts of the sulfinate were formed, and attack at the sulfur occurred (5, 6).

In the bacterial system, the initial stage of the mechanism is more likely to involve addition of oxygen to the benzene ring via a hydroperoxyflavin cofactor. This type of mechanism has been described for oxygenase reactions, such as the salicylic acid and *p*-hydroxybenzoic acid oxygenase reactions that occur in other bacteria.

Formation of the sulfonate anion by simple addition of oxygen to the sulfinate anion would not be expected to change the number of labeled oxygens on the sulfur, and the sulfonate would be expected to be double-labeled. Cyclization of the sulfonate to the sultone involves loss of one of the oxygens on the sulfur. Thus one-third of the sultone would be double-labeled and two-thirds would be single-labeled. But the sulfinate oxidation reaction might be more complex, and the labeling will provide some information on this oxidation.

The mass spectrum of the sultone exhibited the molecular ion peaks at 236, 234, and 232 in the ratio 5.6:3.2:1. Thus the sulfonic acid corresponding to the sultone must have been primarily triple-labeled. The obvious explanation for this fact is that the sulfinate undergoes a dimerization reaction and subsequently transfers labeled oxygen between sulfur atoms as the sulfonic acid is formed (7). The sulfur that lost oxygen in the reaction of the dimer may end up, after subsequent oxidation, as part of the unlabeled sultine that was observed.

The results not only prove that the sulfone is directly converted to the sulfinate, but also that the oxidation of the sulfinate to sulfonate follows accepted chemical mechanisms. A pathway involving Reaction E is therefore very unlikely to occur, since it would not produce triple-labeled sultone product.

The results would be more straightforward if the sulfinate were analyzed by conversion to a derivative that preserves both labeled oxygens attached to sulfur. The methylsulfone derivative was prepared by treating the sulfinate with methyliodide, and analysis of this derivative will be used to confirm the findings from the sultine derivative.

REFERENCES

1. Olson, E.S.; Stanley, D.C.; Gallagher, J.R. *Energy Fuels* **1993**, *7*, 159–164.
2. Gallagher, J.R.; Olson, E.S.; Stanley, D.C. *FEMS Microbiol. Lett.* **1993**, *107*, 31–36.
3. Simonet, J. In *The Chemistry of Sulfones and Sulphoxides*; Patai, S.; Rappoport, Z.; Stirling, C.J.M., Eds; John Wiley and Sons: New York, 1988; Chapter 22.
4. Rossi, R.A.; Bunnett, J.F. *J. Amer. Chem. Soc.* **1974**, *96*, 112.

5. Squires, T.G.; Venier, C.G.; Hodgson, B.A.; Chang, L.W. *J. Org. Chem.* 1981, *46*, 2373–2376.
6. LaCount, R.B.; Friedman, S. *J. Org. Chem.* 1977, *42*, 2751.
7. Kice, J.L.; Pawlowski, N.E. *J. Amer. Chem. Soc.* 1963, *28*, 1162.

ACKNOWLEDGMENTS
This work was supported in part by the U.S. Department of Energy (Contract No. DE-FC21-93MC30097). The assistance of David J. Miller is gratefully acknowledged.

FIGURE 1

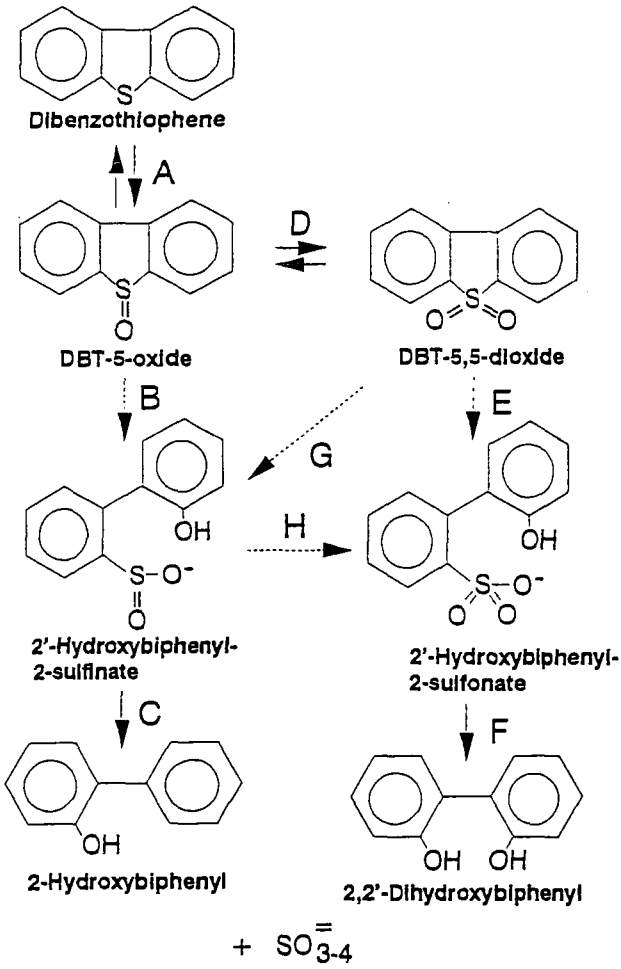

THE USE OF THERMOGRAVIMETRIC ANALYSIS TO FOLLOW CHANGES DURING SHORT-CONTACT-TIME COAL LIQUEFACTION

He Huang, Keyu Wang, William H. Calkins* and Michael T. Klein
Dept of Chemical Engineering, University of Delaware, Newark, DE 19716

Key words: thermogravimetric analysis, coal liquefaction, short-contact-time

INTRODUCTION

The study of the chemical reactions involved in coal liquefaction is aided by elucidation of the processes occurring in the very early stages (low conversions), before secondary reactions of the products become significant. To this end, as reported in previous papers[1,2], we have developed a reactor system capable of carrying out liquefaction reactions at accurately known reaction times from as short as a few seconds (low conversions) to as long as 60 min or more. The analytical methods to monitor these reactions must provide sensitive measures of the coal conversion and product yield information. We have found thermogravimetric analysis (TGA) useful since it provides sensitive, rapid and reproducible results concerning the various weight loss changes that can be connected to the physical and chemical changes occurring during coal liquefaction.

Thermogravimetric analysis has other desirable features as well. First, only very small samples (about 30 mg) are required for each TG run. Second, by suitable adjustments in the work-up procedures and the TG running parameters, such as heating rate and atmosphere, thermogravimetric analyses yield important information concerning the reaction pathways.

It is to illustrate the usefulness of thermogravimetric analysis of coal liquefaction products that this paper is presented.

EXPERIMENTAL

Apparatus. The design and operation of the SCTBR reactor system have been described in detail previously[1]. In brief, both the empty preheater and reactor are immersed in a Techne IFB-52 fluidized sand bath. They are brought up to the predetermined reaction temperature prior to the start of the reaction. High pressure nitrogen gas provides the driving force to deliver the reaction mixture of a coal-tetralin slurry from a small blow case into the empty reactor through the preheater tubing. Nitrogen gas is then bubbled through the reactor from the bottom to provide the agitation needed in the heterogeneous reaction system. The degree of agitation is controlled by the exit gas flow rate from the top of the reactor. The temperature of the reactant mixture (ca. 30 g) approaches the desired reaction temperature to within 5-8 °C of preset temperature during the transport process (approximately 0.3 seconds). This temperature is maintained within ±2 °C during the experiment. At a preselected reaction time, high pressure nitrogen gas is again used to drive the reactor contents from the reactor into a cold receiver through the precooler. Both receiver and precooler are immersed in a water bath. Cooling of the product mixture to about 25 °C is achieved within 0.3 seconds.

Coal Liquefaction Runs. All reactions were run as mixtures of tetralin (T, the H-donor solvent) and coal (C) at ratio of T/C = 8. About 4 grams of coal were used for each reactor run together with added tetralin to make up the reactant slurry. The reactor runs are summarized in Table I. Hold up of material on the surfaces of the reactor, preheater, and precooler prevented complete recovery of the reaction products. However, the recoveries were high, and varied from about 80-90 wt%. The measure of conversion and subsequent analytical results were therefore based on representative aliquots.

Thermogravimetric Analysis. The thermogravimetric analyzer (TGA) was a Model 51 TGA (TA Instruments, New Castle, Delaware). A representative TG scan on the Illinois #6 coal from the Argonne Premium Coal Sample program is shown in Figure 1. The weight loss resulting from heating in nitrogen at 100 cm^3(STP)/min with a heating rate of 10°C/min to 950°C and hold for 7 min at 950 °C defines the amount of volatile matter (VM). For this illustrative sample VM was 36.64 wt%. Further weight loss occurred at 950°C after the introduction of oxygen. This was due to the oxidation of the remaining combustible material, the so called "fixed carbon (FC)", in the char, which amounted to 48.42 wt% for the illustrative sample of Figure 1. The residue represents the ash content (14.94 wt%). Thus the two phases, i.e., 1) the heating rate to 950°C in nitrogen and hold for 7 min; and 2) the oxidation at 950°C, provided measures of VM, FC, and Ash, respectively. The experimental error for determination of these TGA characteristic variables (VM, FC, and Ash) is less than ±2% of the measured values.

Thermogravimetric analysis can also be run in a hydrogen atmosphere. This provides additional information regarding the structure of coal and liquefaction residue. However, it is required that nitrogen be introduced to replace hydrogen in the TGA system for about 10 min before the introduction of oxygen.

RESULTS AND DISCUSSION

Effect of Heating Rate and Atmosphere in TG Runs. The effect of heating rate on the DTG analysis of the Illinois #6 coal is illustrated in Figure 2. The two small peaks in the VM portion of the DTG curves gradually disappear as heating rate increases. This is due to the lower resolution of DTG profile at the higher heating rate. The DTG curves of the Illinois #6 coal in nitrogen and in hydrogen demonstrated in Figure 3 show the similar pyrolysis rate patterns. However, all three peak temperatures in the VM portion of TG pyrolysis in hydrogen are shifted to lower temperatures than those of TG pyrolysis in nitrogen.

Figures 4(a), 4(b) and 4(c) show plots of VM for Illinois #6, Utah Blind Canyon bituminous coals and Wyodak Black Thunder subbituminous coal, respectively. They were determined by TG pyrolysis in nitrogen and in hydrogen at heating rates varying from 10°C/min to 200°C/min. The heating rate had a strong effect on the volatile matter in nitrogen and in hydrogen. The VM yields in nitrogen (VM_{N2}) increased with increasing heating rate until it leveled off at about 50 °C/min. This can be tentatively attributed to an unstable component in the coal when the volatile product is only slowly removed from the coal in nitrogen which results in free radical retrograde reactions and low volatile yields. The VM yields in hydrogen (VM_{H2}) are always higher than those in nitrogen. This is because the presence of hydrogen in the TG pyrolysis apparently stabilizes or quenches these radicals to give the higher VM yields. VM_{H2} decreased with increasing heating rate. This may be due to the longer pyrolysis times at the low heating rates. The different behavior in VM determined by TGA shown by the various coals in nitrogen and in hydrogen (see Figure 4) may represent an indication of the potential relative instabilities of the various coals. While the Illinois and Utah bituminous coals showed similar behavior with heating rate in hydrogen or nitrogen atmosphere, the Wyodak subbituminous coal showed only a small effect of heating rate on VM in the presence of nitrogen and quite a strong and reverse effect in the presence of hydrogen. Further research is being directed toward a better understanding of these phenomena.

Conversion Determination and Work-up Procedures for Coal liquefaction Runs. During coal liquefaction, the mineral matter of the coal primarily remains with the unconverted coal, and is essentially insoluble in the tetralin. The coal liquids, however, are largely extracted into the tetralin solvent, although some remain with the coal residue. This provides a means of measuring the conversion of the coal by determining the ash content of the residue when it has been washed free of the coal liquids. All the tetralin and tetralin-derived products must also be removed or an error in the conversion calculation will result. The conversion can be calculated using Eq. 1:

$$Conversion = (1 - \frac{X_o}{X}) \times 100 \ (wt\%) \qquad (1)$$

where X_o and X are the ash contents of the control sample and the coal liquefaction residue, respectively. The control sample is the original coal which is processed exactly as a liquefaction residue except running at room temperature.

After a liquefaction run, the product mixture is filtered and the residue washed with tetralin thoroughly and dried in a vacuum oven at about 105°C for 48 hours. A DTG curve for one of these samples is shown in Figure 5. Comparison of this curve with that of unreacted coal shows that there is an incomplete peak on the low temperature side of the principal VM peak in the coal residue. That this is due to the presence of residual tetralin is shown by a control sample treated by processing a tetralin-coal slurry through the reactor at room temperature. To measure the coal conversion accurately, the tetralin and the tetralin-derived materials as well as the coal liquefaction liquid products must be removed from the residue. The most satisfactory solvent we have found for this purpose is methylene chloride (see Figure 5). The tetralin peak disappears after methylene chloride washing. For this reason, we have adopted the work-up procedure including the methylene chloride treatment.

The conversion of Illinois #6 in tetralin vs. time at 390° C under 1000 psig nitrogen gas determined by Eq. 1 is illustrated in Figure 6. Within 30-60 seconds, the coal conversion has reached about 18 wt%. This rapid liquefaction may be resulted from the extraction of a soluble portion of coal into the tetralin. From the contact time of 1 min to 30 min, the coal conversion only increase about 19 wt% (reaching 37 wt%), probably due to the coal matrix itself being attacked. Finally, the coal conversion reached 47 wt% at 60 min.

Change of DTG Profiles with Conversion during Coal Liquefaction in Tetralin. Figure 7 shows DTG vs temperature curves for the residues of the Illinois #6 coal after liquefaction in tetralin at 390 °C under 1000 psig nitrogen at selected times. The two small peaks in the VM portion gradually disappear. Such chemical changes have been supported by previously observed changes in the total oxygen content and hydroxyl content[3-5] of the

coal during the early stages in coal liquefaction.

Change of Volatile Matter in N_2 and in H_2 with Conversion during Coal Liquefaction in Tetralin. Interesting insights into the coal structure and the coal liquefaction process can be obtained by running thermogravimetric analyses in nitrogen and in hydrogen at various heating rates on the samples taken at various reaction times. The coal liquefaction process, even at low conversion, greatly changes the TG behavior of the partially reacted coal residue. Figure 8 shows an example of the VM determined by TG pyrolysis in nitrogen and in hydrogen at various heating rates for the liquefaction residue of the Illinois #6 coal reacted in tetralin under 1000 psig nitrogen gas at 390°C for 30 seconds. The VM_{N2} no longer shows the strong sensitivity to heating rate. Furthermore, it decreased with increasing heating rates. This suggests that the unstable component of the coal may have been stabilized in the very early stage of the liquefaction process.

SUMMARY AND CONCLUSIONS

Thermogravimetric analysis provides various weight changes in coal residua arising from coal liquefaction and these reveal significant information concerning the underlying chemical and physical processes.

A workup protocol including the methylene chloride washing to eliminate the error due to the presence of tetralin and/or coal liquids has been devised which is being used along with TGA to determine liquefaction conversion.

Interesting differences have been observed in the three Argonne Premium Coal Samples (Illinois #6 bituminous coal, Utah Blind Canyon bituminous coal, and Wyodak Black Thunder subbituminous coal) studied by running TGA at different heating rates and in nitrogen or hydrogen atmosphere. These experiments suggest the presence of an unstable component in the coal or coal-derived liquid which is rapidly removed or stabilized by very short contact time under liquefaction conditions.

Acknowledgements. The support of this work by the Department of Energy under DE-FG22-93PC93205 is gratefully acknowledged. The use of the Argonne Premium Coal Samples provided by Dr. Karl Vorres is also gratefully acknowledged. Additional funds for purchase of thermal analysis equipment was provided by the University of Delaware.

References

1. Huang, H; Calkins, W.H.; Klein, M.T. A Novel Short Time Reactor System for Studying the Initial Stages of High Temperature and High Pressure Reactions. *ACS Fuel Chem Div. Preprints* **1993**, **38** (3), 1080.
2. Huang, H.; Calkins, W.H.; Klein, M.T.; A Novel Laboratory Scale Short Contact Time Batch Reactor System for Studying Fuel Processes. 1. Apparatus and Preliminary Experiments, submitted in *Energy & Fuels*.
3. Huang, H.; Provine, W.D.; Jung, B.; Jacintha, M.A.; Rethwisch, D.G.; Calkins, W.H.; Klein, M.T.; Dybowski, C.R.; Scouten, C.G. Short Time Reactor System for Studying the Initial Stages of Coal Liquefaction. *Proceedings of the International Conference on Coal Science*, **1993**, Ed. K.H. Michaelian, Vol. **I**, 266.
4. Jung, B.; Provine, W.D.; Calkins, W.H.; Klein, M.T.; Scouten, C.G. Changes in Organic Oxygen Contents of Illinois #6 Coal during Coal Liquefaction. *ACS Fuel Chem Div. Preprints* **1992**, **37** (2), 670.
5. Provine, W.D.; Jung, B.; Jacintha, M.A.; Rethwisch, D.G.; Huang, He; Calkins, W.H.; Klein, M.T.; Scouten, C.G.; Dybowski, C.R. A Kinetic Investigation of Coal Liquefaction at Short Reaction Times. *Catalysis Today*, **1994**, Ed. D.B. Dadyburjor and J.W. Zondlo, Vol. **19**, No. *3*, 409.

Table I Illinois #6 Coal Liquefaction Runs

Sample	Contact time min	T/C (wt)	Temperature °C	Recovery wt%
DOE001	15.00	8	15	78%
DOE012	0.17	8	390	86%
DOE015	0.50	8	384	92%
DOE016	0.75	8	385	89%
DOE017	1.00	8	386	88%
DOE021	5.00	8	387	87%
DOE013	10.00	8	390	82%
DOE009	30.00	8	390	85%
DOE010	60.00	8	390	81%

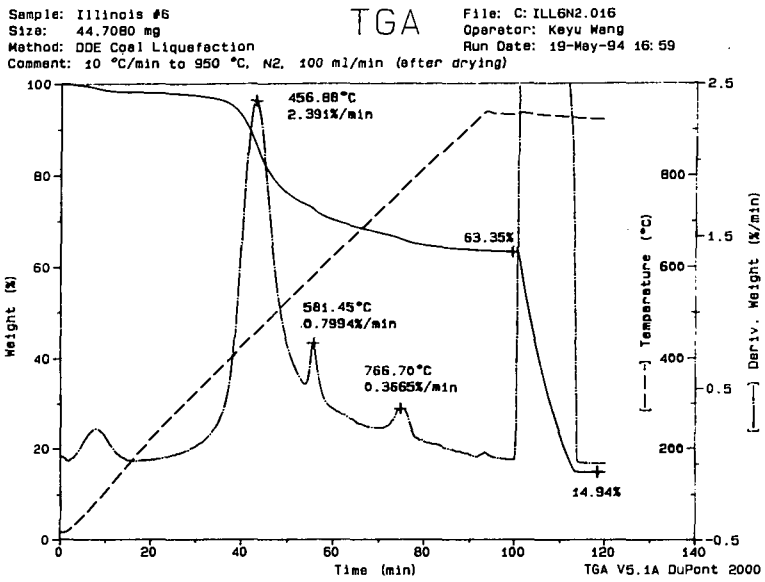

Figure 1. A TG scan on the Illinois #6 coal

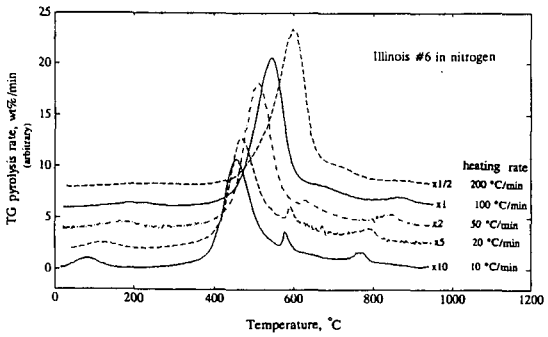

Figure 2. Effect of heating rate on DTG of the Illinois #6 coal pyrolysis in N_2

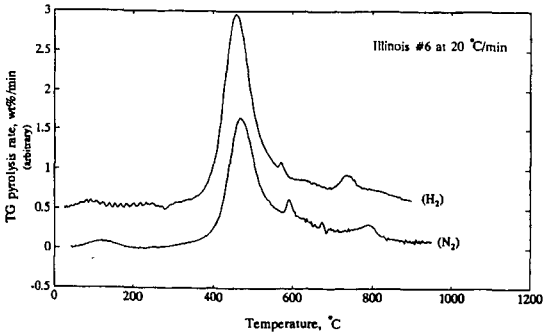

Figure 3. Effect of gas atmosphere on DTG of the Illinois #6 coal pyrolysis at heating rate of 20 °C/min

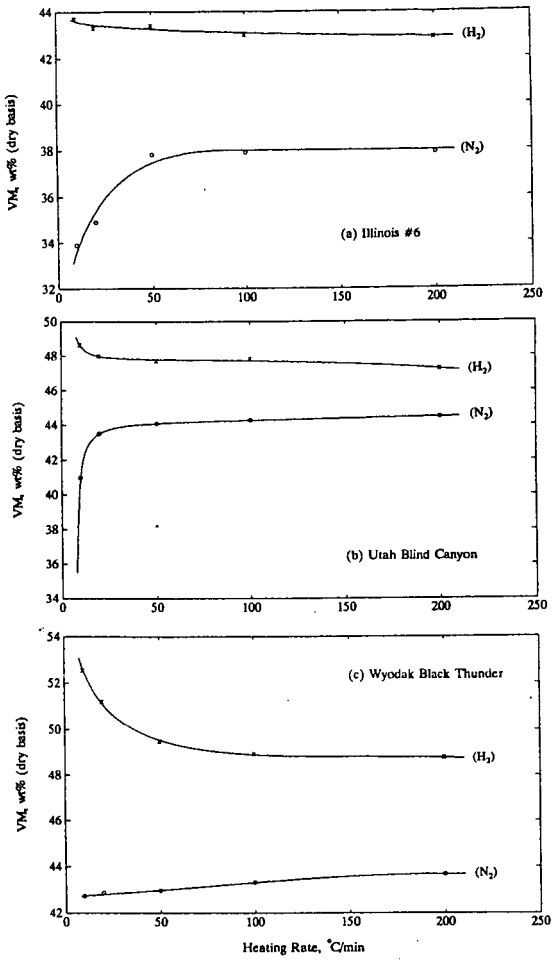

Figure 4. Effect of heating rate on the VM yields determined by TG pyrolysis in N_2 and in H_2

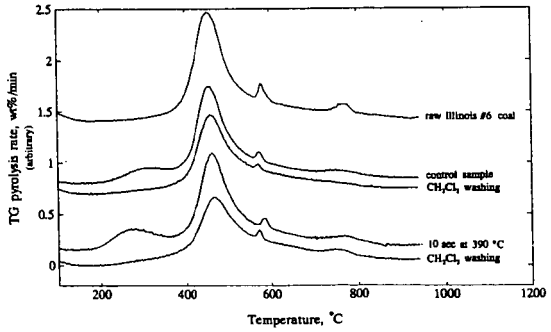

Figure 5. Disappearance of the incomplete peak on the low temperature side of the principal VM peak due to the presence of residual tertalin in the control sample and the reacted solid residue by methylene chloride washing

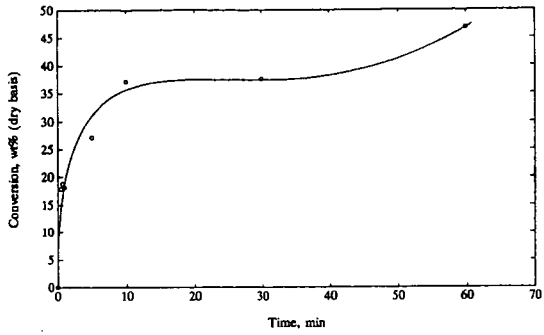

Figure 6. Kinetics of the Illinois #6 coal liquefaction in tetralin (1000 psig N_2 gas; 390 °C; T:C = 8:1)

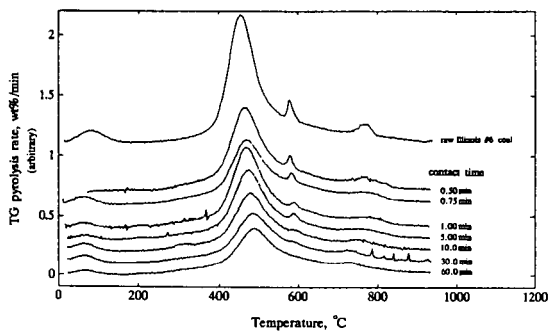

Figure 7. DTG profiles for residues of the Illinois #6 coal after liquefaction in tetralin at the selected contact times (TG scan at 10 °C/min in N_2; liquefaction run at 390 °C under 1000 psig N_2 with T:C = 8:1)

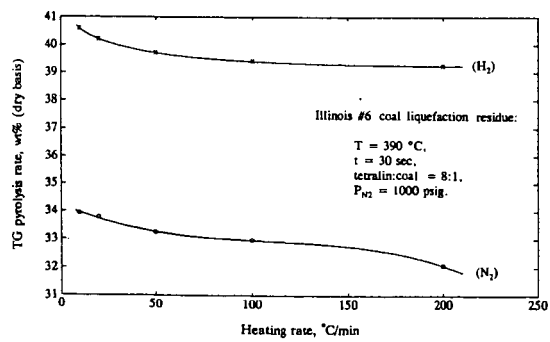

Figure 8. Effect of heating rate on VM yields of Illinois #6 coal liquefaction residue determined by TG pyrolysis in N_2 and in H_2

THE RELEASE OF NITROGEN IN THE COMBUSTION AND PYROLYSIS OF COALS AND MACERALS

C.J. Hindmarsh, J.E. Varey and K.M. Thomas
Northern Carbon Research Laboratories, Dept. of Chemistry,
Bedson Building, University of Newcastle, Newcastle upon Tyne,
NE1 7RU, U.K.

Keywords: Coal, char, combustion, pyrolysis, macerals, NO_x

Introduction

The release of nitrogen and sulphur oxides during coal combustion is a major environmental problem. NO_x and SO_x are contributors to acid rain whereas N_2O is a 'greenhouse' gas. In coal combustion the following stages occur: 1) rapid devolatilization followed by 2) ignition of volatiles and 3) the slower char gasification [1]. The nitrogen and sulphur species are partitioned into the volatiles and the char. The minimization of the environmental impact of coal combustion by improved burner technology and flue gas desulphurization is currently underway. In the case of NO_x emissions, the retrofitting of 'low NO_x' burners in power stations has been undertaken. In these combustion systems, the char nitrogen is the major contributor to NO_x emissions [2]. The volatiles are released in a zone where the oxygen concentration is low and the formation of molecular nitrogen is favoured. Therefore the release of nitrogen and sulphur oxides during coal combustion has major implications for the environment.

The release of nitrogen oxides is controlled to an extent by the combustion conditions but there are also variations due to coal properties [3-5]. In low NO_x burners and fluidized bed combustion, fuel nitrogen is the major contributor to NO_x formation. Therefore an understanding of the nitrogen in coal and its release during combustion is an important consideration. Coals are a complex heterogeneous material with a cross-linked macromolecular structure. This gives rise to problems when characterising the coal for combustion purposes. This structural heterogeneity can be described at a variety of levels. At the macroscopic level coals may have a banded structure. At the microscopic level the structure may be described as microscopic components, macerals or associations of macerals which are termed microlithotypes. Macerals can be separated and have distinct physical and chemical properties, for example, volatile matter, nitrogen content, reactivity etc. When considering coal the heterogeneity must be considered since the small particles used in pulverised fuel (pf) combustion, depending on the coal, may be regarded as pure macerals or associations of macerals [6-9]. When considering the nitrogen in coal at the molecular level the nitrogen functionality must be considered. The nitrogen may be described as pyrrolic, pyridinic or quaternary nitrogen.

The objective of this paper was to study the release of coal nitrogen as NO_x during temperature programmed combustion of coals and macerals, with the emphasis being on the identification of reactive intermediate species and a comparison of the differences between macerals.

Experimental

Materials used

The characterisation data for the coals and maceral concentrates used in this study are given in Table 1. Maceral concentrates were obtained by the density gradient centrifugation (DGC) technique [10-12].

Temperature Programmed Combustion

The temperature programmed combustion studies were carried out using a Thermal Sciences thermogravimetric analysis - mass spectrometer system (TG-MS). This system consisted of a thermogravimetric analysis (TGA) instrument coupled with a VG Quadrupoles 300 amu mass spectrometer. Gas sampling was carried out at two positions: 1) approximately 1 cm directly above the sample and 2) at the exit of the thermogravimetric analyser. The former sampling point allows reactive intermediate species to be detected while the latter essentially samples the gases at equilibrium. The evolved gas profiles were measured at both sampling positions. Approximately 5 mg of the coal was used in each run. The sample was heated at 15 K min^{-1} in 20% oxygen/helium and the evolved gas profiles recorded. The following mass/charge (m/z) ratios were monitored throughout the course of the reaction: 2, 14-65.

Temperature Programmed Pyrolysis

The temperature programmed pyrolysis was carried out in argon at a flow rate of 50 cc min^{-1} at a heating rate of 15 K min^{-1} in a similar manner to the combustion experiments. In this case gas sampling was carried out at the exit of the thermogravimetric analyser.

Results

A comparison of the temperature programmed combustion required evolved gas profiles for Illinois No. 6, in 20% oxygen/helium with sampling directly above the sample and at the exit of the thermogravimetric analyser. These are shown in Figures 1(a) and 1(b) respectively. It is apparent that whilst there are similarities between the two sets of evolved gas profiles there are also marked differences. The profiles have a complex series of emissions. The integrated gas concentration ratios for some of the species evolved during the temperature programmed combustion of the Illinois No. 6 coal are given in Table 2. The CO and CO_2 profiles show a shoulder on the low temperature side. This corresponds to the evolution of small hydrocarbons and tars. In addition, the CO/CO_2 ratios for gas sampling directly above the sample and at the exit of the thermogravimetric analyser were 0.535 and 0.096 respectively. This clearly indicates that CO is being formed and released into the gas phase where it is converted to CO_2 by homogeneous gas phase reactions. Another noticeable difference in intensities is the increase in m/z 30 concentration and decrease in m/z 27 concentration when comparing sampling directly above the sample and at the exit of the TGA. This can be explained by the conversion of HCN released in the gas combustion process and converted to NO by gas phase oxidation reactions. The fraction of coal nitrogen converted to NO is 0.362 when measured by sampling directly above the sample and this increases to 0.961 when the gas sampling is carried out at the exit of the TGA. Not all of the m/z 27 and m/z 30 are HCN and NO respectively. Undoubtedly there are small contributions from hydrocarbons, and/or fragmentation in the mass spectrometer which make a contribution for some m/z ratios. When gas sampling is carried out directly above the sample, a high CO concentration is observed. Since NO is in relatively low concentration, there may be a significant contribution to the NO peak from $^{12}C^{18}O$. This

contribution can be corrected for by subtracting 0.002*CO peak. The peak which occurs at the lowest temperature ~300°C is consistent with the release of hydrocarbons. This precedes the release of tars when the coal starts to pyrolyse. Figure 1(a) shows that intermediate species such as COS and HCN are released during the temperature programmed combustion. Evolved gas profiles have been monitored for all m/z values in the range 14-65. It is apparent that when gas sampling is carried out directly above the sample many of the masses have weak profiles. It is difficult to assign the peaks unequivocally to various species due to the complex nature of the mixture of gases evolved and fragmentation effects in the mass spectrometer. However, it is apparent that in some coals, a peak was observed for m/z 52 at the beginning of the char gasification region whereas no corresponding peaks were observed at m/z 51 and 53. This peak was observed at the same temperatures as peaks at m/z 26 and 27 corresponding to HCN and its fragments. Therefore it is reasonable to assign the peak at m/z 52 to $(CN)_2$. The evolved gas profiles for m/z 41, 42 and 43 were all bimodal. The lowest temperature peak for m/z 43 occurs at a position coincident with m/z values which can be assigned to the evolution of small hydrocarbon species. The higher temperature peak for m/z 43 which occurs at a similar temperature to m/z 52 and 27 is possibly due , in part, to HOCN. The evolved gas profiles at 41, 42, 43, 52, 60 etc are either not observed or are very weak when gas sampling is carried out at the exit of thermogravimetric analyser thereby confirming that reactive intermediate species can be detected by gas sampling close to the sample during temperature programmed combustion. A suite of coals with a range of rank have been studied in detail, in addition, to the coal described above. These include Blind Canyon and Pocohontas from the Argonne Premium Coal Sample Bank and Illinois No. 6 from SBN. These reveal significant differences in the release of species such as COS, $(CN)_2$ etc. during temperature programmed combustion.

The corresponding temperature programmed pyrolysis profiles are shown in Figure 1(c). In this case the gas sampling was carried out at the exit of the TGA. The results show that a range of small gaseous molecules CO_2, CO, NO, N_2, HCN, SO_2 and CH_4 are evolved over a range of temperatures. At the lowest temperatures low molar mass hydrocarbons were detected. Tars were condensed out and not detected. It is apparent that the temperature programmed pyrolysis technique is capable of distinguishing the release of gaseous species. Some of the peaks, for example, m/z 27 (HCN) occurs at the same temperature for both the pyrolysis and combustion.

The temperature programmed combustion evolved gas profiles for the entrained flow reactor chars prepared from Illinois No. 6 are shown in Figure 2. The results show similarities to the temperature programmed combustion of the raw coal. The CO concentration measured by sampling directly above the sample is high but this is reduced when evolved gas sampling is carried out at the exit. The CO/CO_2 ratio decreases from 0.355 measured directly above the sample to 0.076 measured at the exit of the TGA. It is apparent that the primary product CO is again converted to CO_2 by gas phase homogeneous reactions as in the coal studies. In addition the m/z 27 peak (mainly HCN) virtually disappears and the m/z 30 (NO) increases slightly when gas sampling is carried out at the exit. The fraction of char nitrogen converted to NO measured directly above the sample was 0.225 and this increased to 0.399 when measured at the exit of the TGA. This is similar to the results for the corresponding coals but the effect is much smaller. This is consistent with the HCN released being converted to NO in the gas phase. Reactive species released during temperature programmed coal combustion, for example, COS, are not observed when gas sampling is carried out at the exit of the TGA.

The temperature programmed combustion evolved gas profiles for vitrinite (density 1.2 - 1.27 g cm^{-3}) and fusinite (density 1.5 - 1.60 g cm^{-3}) with gas sampling directly above the sample and at the exit of the TGA are given in Figure 3. As expected the vitrinite profiles are very similar to those obtained for raw coals with a pronounced shoulder on the low temperature side of the evolved gas profile. The corresponding CO and CO_2 profiles for the fusinite are more complex consisting of several peaks and reach a maximum at a higher temperature than the vitrinite fraction as expected from the lower reactivity of the inertinite fraction. This is observed when gas sampling is carried out at both directly above the sample and at the exit of the TGA. The observation that the CO and CO_2 evolved gas profiles of the fusinite are more complex than the profiles of the vitrinite fraction may be due to a number of factors. The samples were prepared by the DGC and it may be that different types of inertinite fraction are being resolved in the temperature programmed combustion. Also, higher concentrations of mineral matter were observed in the fusinite fraction and this may give rise to catalytic gasification effects. The NO evolved gas profile for the fusinite showed a peak at ~300°C followed by profile in the char gasification region which could be resolved into three peaks with similar temperatures to the CO and CO_2 profiles. The m/z 27 (mainly HCN) evolved gas profiles for gas sampling directly above the sample for the vitrinite and fusinite are both bimodal but these peaks virtually disappear when sampling is carried out at the exit of the TGA. It is surprising that the m/z 27 peaks occur at a higher temperature in the vitrinite concentrate than the fusinite. This may indicate structural differences. The m/z 14 peak is also bimodal when gas sampling is carried out directly above the sample. The high temperature peak in the profile is also observed when gas sampling is carried out at the exit of the TGA. This suggests that this peak is due to nitrogen.

The integrated gas concentration ratios for some of the species evolved in the temperature programmed combustion of the macerals are given in Table 2. A comparison of gas concentration ratios obtained when sampling directly above the sample and at the exit of the TGA shows similar trends to those observed for the raw coals. It is evident from the CO/CO_2 ratio that substantial amounts of CO formed in the combustion are converted in the gas phase to CO_2. Similarly a comparison of the two sampling positions indicates that the NO/N ratio is higher while the (m/z 27)/N *i.e.* mainly HCN/N, was virtually absent when gas sampling is carried out at the exit of the TGA. This is most probably due to the conversion of HCN and other nitrogen containing species to NO in the gas phase and is similar to the results obtained for the coals.

Discussion

Temperature programmed combustion is a useful technique for studying the release of nitrogen and sulphur species during the combustion of coals and chars. The evolved gas profiles have the following general characteristics [7, 8, 13-16].

1. For coals, there is a shoulder on the low temperature side of the CO and CO_2 evolved gas profiles for the coals. This shoulder corresponds to the release of low molecular mass species and tars and it is absent in the corresponding evolved gas profiles of the chars.

2. The release of NO and HCN during temperature programmed combustion is complex with several peaks. For low rank coals the NO peak is observed for the release of volatiles and the gasification of the char. The latter is sometimes asymmetric consisting of a number of peaks.

3. The NO profiles for the chars are delayed relative to the CO and CO_2 profile. The NO profiles always reach a maximum at a higher temperature than the corresponding CO_2 profiles. As a result the NO/CO_2 and NO/CO profiles usually increase with increasing burn-off. The NO/CO and NO/CO_2 ratios tend to decrease in the region where volatiles are released from the coals.

In this study, two gas sampling positions have been used: 1) ~1 cm above the sample and 2) at the exit of the thermogravimetric analyser. The results of this study show that reactive intermediate species can be detected by sampling close to the sample undergoing combustion. Some of the reactive species which have been identified are COS, $(CN)_2$, HCN and CO as well as hydrocarbon species. These species are either not detected or are observed in very much lower concentrations for sampling at the exit of the TGA. These studies have shown that under temperature programmed conditions there are a number of well defined stages which can be assigned to the release of low molecular mass gases, tars and combustion products and char gasification. Therefore the thermogravimetric analyser - mass spectrometer allows the extent of gas phase reactions to be assessed. In comparison, pyrolysis studies can also be carried out under temperature programmed conditions.

Previous temperature programmed combustion studies [6-9, 13-16] of a suite of coals and chars covering a wide range of rank have shown that the fraction of coal/char nitrogen converted to NO decreases with increasing reactivity. These studies were carried out with the gas sampling directly above the sample. In the case of the coals, substantial amounts of HCN were detected and if this were assumed to be converted to NO this would modify the trend for conversion of the coal nitrogen to NO for gas sampling at that position. In these studies the suite of coals studied covered a range of reactivities. Therefore the nitrogen species are released over the different temperature ranges. The release of the NO may vary with temperature and this may be a factor which influences the observed trend. Isothermal reactivity studies have also shown that a similar correlation exists [16] between char reactivity and the fraction of char nitrogen converted to NO. Hence it is apparent from the trends that gas sampling of the temperature programmed combustion of the coals allows reactive nitrogen species to be detected and that the NO release is similar to that for the char. The results of a more detailed investigation show that a range of reactive species can be detected.

Conclusions

The use of temperature programmed combustion for studying the release of reactive intermediate species from coal has been investigated. It is apparent that a comparison of gas sampling carried out directly above the sample and at the exit of the TGA shows that reactive species can be detected. Species detected include CO, COS, HCN, $(CN)_2$. The conversion of the nitrogen intermediate species to NO has been followed by the technique. It is apparent that temperature programmed combustion is a useful technique for following the release of nitrogen and sulphur during coal and char combustion.

Acknowledgements

The authors would like to thank SERC for support under Grant No.GR/J 12161

References

1. Laurendeau N.M.,
   Prog. in Energy and Combustion Science, **4**, 221-270, 1978.
2. Phong-Anant D., Wibberley L.J. and Wall T.F.,
   Combustion and Flame, **62**, 21, 1985.
3. Shimizu T., Sazawa Y., Adschin T. and Furusawa T.,
   Fuel **71**, 361, 1992.
4. Pels J.R., Wojtowicz M.A. and Moulijn J.A.,
   Fuel **72**, 373, 1993.
5. Gavin D.G. and Dorrington M.D.,
   Fuel **72**, 381, 1993.
6. Crelling J.C., Thomas K.M. and Marsh H.,
   Fuel **72**, 359, 1993.
7. Crelling J.C., Thomas K.M. and Marsh H.,
   Ironmaking Proceedings-Iron and Steel Society of AIME, **51**, 407-413, 1992.
8. Hindmarsh C.J., Wang W.X., Thomas K.M. and Crelling J.C.,
   Fuel (in press).
9. Crelling J.C. and Thomas K.M.,
   Abstracts of Papers of the American Chemical Society, 207, p. 3, 1994.
10. Dyrkacz G., Blomquist C. and Ruscic L.,
    Fuel **63**, 1367, 1984.
11. Dyrkacz G., Blomquist C. and Horwitz P.,
    Sep. Sci. Technol. 16, 1571, 1981.
12. Dyrkacz G. and Horwitz P.,
    Fuel **61**, 3, 1982.
13. Brown S.D. and Thomas K.M.,
    Fuel **72**, 359, 1993.
14. Wang W.X., Brown S.D., Thomas K.M. and Crelling J.C.,
    Fuel **73**, 341, 1994.
15. Wang W.X., Brown S.D., C.J. Hindmarsh, A.I. Gonzalez de Andres
    and Thomas K.M.,
    Proc Int. Conf. Coal Sci., Banff, Canada **2**, 144, 1993.
16. Gonzalez de Andres A.I. and Thomas K.M.,
    Fuel **73**, 635, 1994.
17. Brown S.D., Wang W.X. and Thomas K.M.,
    (Unpublished results).

Table 1 Characterisation data for the coal, char, and maceral concentrates.

Coal/ Maceral	Illinois No6 (APCS) Coal	Illinois No6 (APCS) Char	Coal A Vitrinite	Coal A Fusinite
Proximate Analysis				
Volatile Matter (daf)/ %	47.39	4.43	41.97	35.76
Ash (dry)/ %	15.48	29.84	1.21	31.26
Elemental Analysis				
C (daf)/ %	77.67	99.63	82.57	79.01
H (daf)/ %	5.00	0.67	5.28	4.25
N (daf)/ %	1.37	1.82	1.72	0.83
O (daf)/ %	13.51		12.16	15.68
Random Relectance/ %	0.43	0.43	0.65	0.65
Maceral Analysis				
Vitrinite/ %	85.00			
Liptinite/ %	5.00			
Inertinite/ %	10.00			
Minerals/ %	18.10			

Table 2 Temperature programmed combustion evolved gas concentration ratios

Sample	CO/ CO_2	NO/ N	HCN/ N
Illinois No6 (APCS) Coal			
-Above the Sample	0.535	0.362	0.209
-At the Exit	0.096	0.961	0.036
Illinois No6 (APCS) Char			
-Above the Sample	0.355	0.225	0.096
-At the Exit	0.076	0.399	0.016
Coal A Vitrinite Concentrate			
-Above the Sample	0.606	0.356	0.167
-At the Exit	0.067	0.546	0.025
Coal A Fusinite Concentrate			
-Above the Sample	0.314	0.797	0.325
-At the Exit	0.082	0.893	0.053

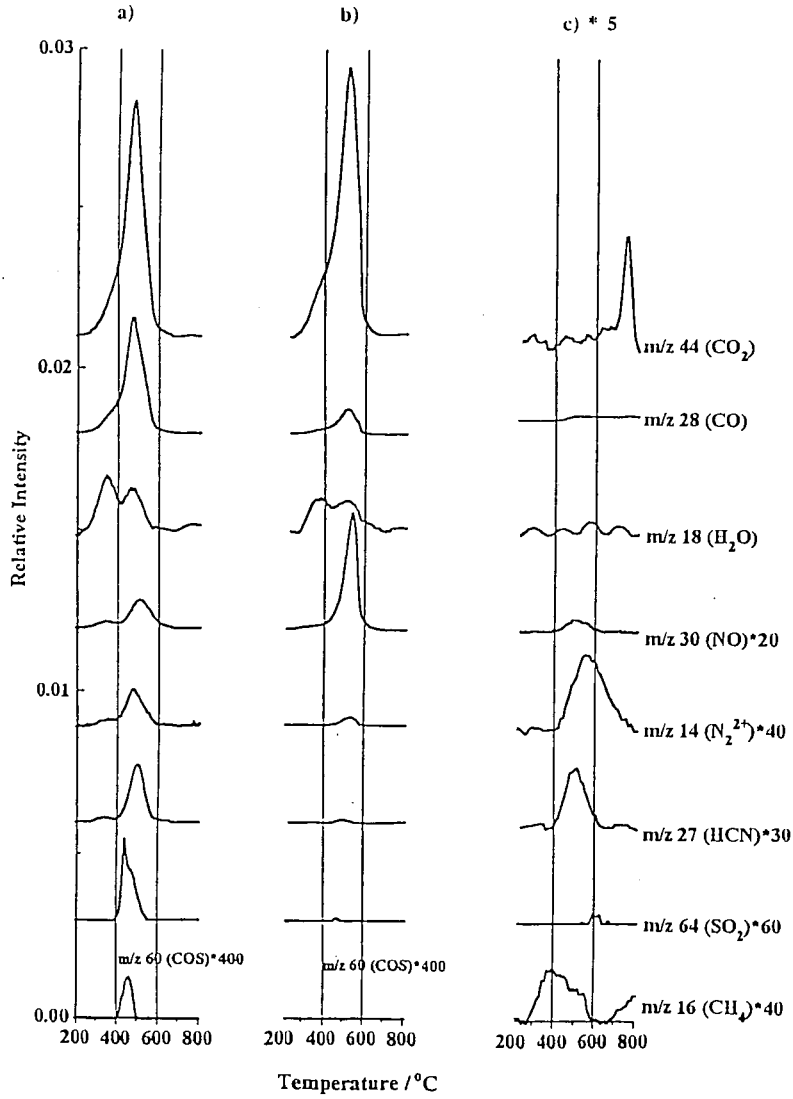

Figure 1 Temperature programmed evolved gas profiles for Illinois No6 (Argonne) coal in a) 20% oxygen/ helium with gas sampling directly above the sample, b) in 20% oxygen/ helium with gas sampling at the exit of the thermogravimetric analyser and c) in argon with gas sampling at the exit of the thermogravimetric analyser.

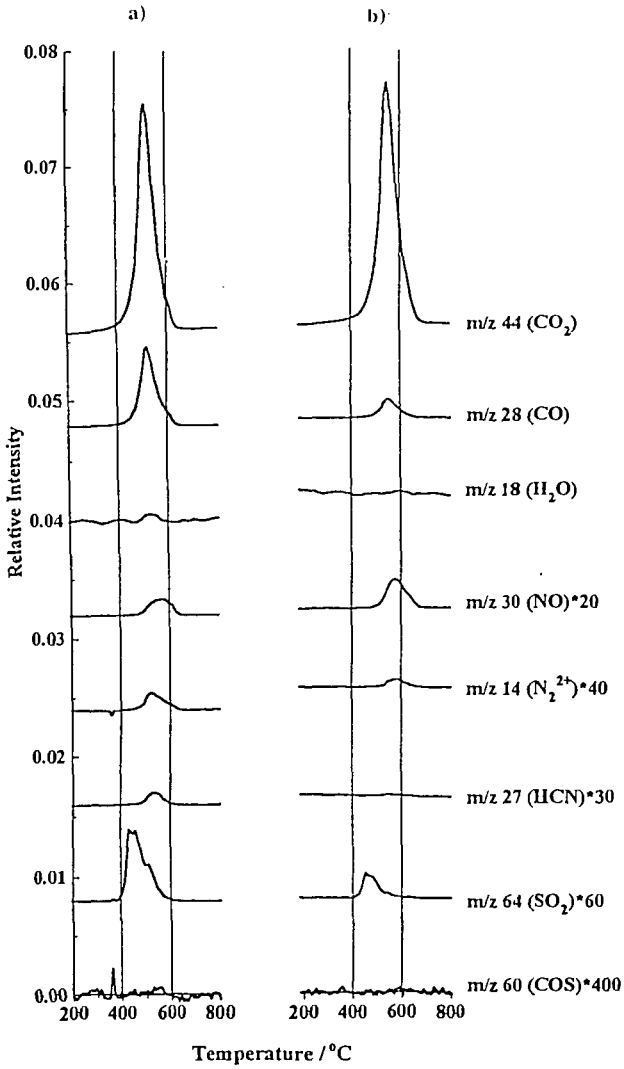

Figure 2 Temperature programmed combustion evolved gas profiles for Illinois No6 (Argonne) EFR char (HTT 1273 K) in 20 % oxygen/ helium with gas sampling a) directly above the sample and b) at the exit of the thermogravimetric analyser.

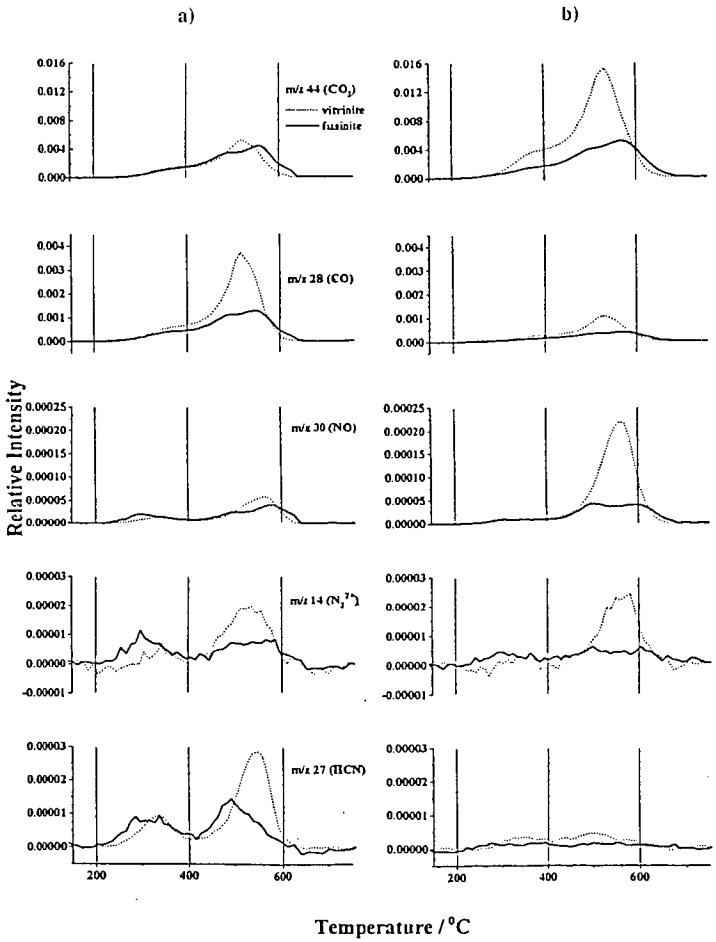

Figure 3 Temperature programmed combustion evolved gas profiles for maceral concentrates derived from coal A in 20 % oxygen/ helium with gas sampling a) directly above the sample and b) at the exit of the thermogravimetric analyser.

THE CHEMISTRY OF SULFUR DURING HYDROPYROLYSIS OF COALS

M. L. Gorbaty, S. R Kelemen, S. N. Vaughn, M. Sansone, P. J. Kwiatek

Exxon Research and Engineering Company
Annandale, NJ 08801

G. N. George

Stanford Synchrotron Radiation Laboratory
Stanford, CA 94309

Keywords: Sulfur, XANES, XPS, Hydropyrolysis

Sulfur K-edge X-Ray Absorption Near Edge Structure Spectroscopy (XANES) and sulfur 2p X-Ray Photoelectron Spectroscopy have been used to identify organically bound sulfur forms in coals (1-3), and to follow the chemistry of organic sulfur during various treatments including mild oxidation (4), pyrolysis (5-7) and chemical reductions (8). This paper focuses on the changes which take place with organically bound sulfur functionalities in coals of various ranks when they are subjected to hydropyrolysis conditions. Data from both X-Ray techniques and temperature programmed decomposition-mass spectrometry were used in tandem.

Experimental Section

Most coal samples used in this study were obtained from the Argonne Premium Coal Program (9). The sample of Rasa coal was obtained from Dr. C. M. White of PETC. The procedures for obtaining and interpreting XPS and XANES spectra of coals have been reported and discussed previously (1, 2). XPS spectra were obtained on a Vacuum Generators (VG) ESCA lab system using Mg K_α non-monochromatic radiation using a five channel detection system. XANES spectra were recorded at the National Synchrotron Light Source at Brookhaven National Laboratory on beam line X-10C. Fluorescence spectra were recorded using a Stern-Heald-Lytle detector. Hydropyrolysis char thermal reactivity data were obtained using a temperature programmed decomposition (TPD) apparatus, the design and use of which are described elsewhere (5, 6). Samples were heated under ultrahigh vacuum from room temperature to 750 °C at a rate of 0.5 °C/s, while the off gases were monitored by a mass spectrometer. Hydropyrolysis experiments were carried out in a closed reactor pressurized at room temperature to 70 atm with a 95% hydrogen - 5% helium gas mixture. Pyrolysis was done in helium, at 1 atm in a quartz lined reactor (5). For pyrolysis experiments, the samples were heated at a linear heating rate of 0.5 °C/s to 400 °C followed by holding at that temperature for 5 minutes. The reactor temperature program for hydropyrolysis was similar except that the maximum temperature was 427 °C and the samples were held for 30 minutes under isothermal conditions. Samples were analyzed after the linear heatup and isothermal stages. These kinetic conditions favored the retention of coal liquid products in the pyrolysis and hydropyrolysis residues.

Results and Discussion

The coals were subjected to hydropyrolysis conditions and the hydropyrolysis residues were collected and examined by elemental analysis to determine sulfur loss, by XPS and XANES to determine the forms of bound sulfur remaining, and by TPD to determine the thermal reactivity of the residues. Table 1 shows the sulfur to carbon atomic ratios for samples of starting Rasa and Illinois No. 6 coals, as well as those for the residues from heating to 400 °C under helium pyrolysis and hydropyrolysis after heating to 427 °C as determined from bulk elemental analysis and from XPS by integration of the areas for sulfur and carbon (1). The bulk and XPS elemental analyses are in good agreement for Rasa coal, which contains virtually no pyrite, and are not in agreement for Illinois No. 6. The discrepancy between the bulk elemental and XPS data for Illinois No. 6 coal is due to the fact that the surface concentration of pyrite and its oxidation products are different on this coal's surface relative to that in the bulk(10). However, both analyses indicate that more sulfur was lost during hydropyrolysis than pyrolysis under nitrogen. The bulk elemental analyses indicate that about 22% of the sulfur was lost from Rasa and 32% from Illinois No. 6 under these hydropyrolysis conditions. XPS sulfur 2p spectra of the 427 °C hydropyrolysis residues from Rasa and Illinois No. 6 coal are shown in Figure 1. Included in the figure are the actual spectra and the curve resolved aromatic and aliphatic sulfur components. The results of the curve resolution analysis (1, 2) of these

spectra are shown in Table 2. The table shows the XPS results for aliphatic sulfur for the initial coals, hydropyrolysis residues obtained at 200, 350 and 427 °C, and previously obtained data (5) on helium pyrolysis chars. The results indicate that the hydropyrolysis chars contain the same ratio of aliphatic to aromatic sulfur as the starting coals, and considerably more than that contained in the pyrolysis residues. XANES data on the same samples confirm these findings. In addition, the feature attributed to pyrite in the fresh Illinois No. 6 coal and its 200 °C hydropyrolysis residue largely disappears in the 350 °C residues and is replaced by a feature attributed to pyrrhotite.

The effect of temperature on the reactivity of bound sulfur on the hydropyrolysis residues was examined by TPD. Traces of the relative intensities of the m/e = 34 mass spectra of the initial Rasa and Illinois No. 6 coals and their hydropyrolysis residues prepared at 200, 350 and 427 °C are plotted as a function of temperature in Figure 2. These were normalized so that the data for a given coal appear on the same relative intensity scale. Up to 350 °C, Rasa coal continues to evolve H_2S, but at 427 °C the amount released is considerably diminished. The TPD traces for fresh Illinois No. 6 coal and its 200 °C hydropyrolysis residue show evolution of H_2S from both aliphatic sulfur and pyrite, but the total amount of H_2S released from the 350 °C residue is diminished, and that from pyrite is virtually gone. There is even less H_2S evolution from the 427 °C hydropyrolysis residue.

Taken together the data present an apparent discrepancy. It is known that on pyrolysis in an inert environment at 400 °C, aliphatic sulfur is lost from the coal as H_2S (5, 6). Aromatic sulfur does not evolve at these temperatures (11). Somewhat more sulfur is lost during hydropyrolysis than pyrolysis, but the differences are not great. TPD data indicate that most of the reactive sulfur in the hydropyrolysis residues had evolved at 427 °C. Nevertheless, XPS and XANES analyses indicate that the hydropyrolysis residues contain about as much aliphatic sulfur as the starting coals; the ratio of aliphatic to aromatic sulfur is about the same, even though significant amounts of H_2S evolved during the hydropyrolysis.

To account for these observations, we postulate that molecules containing aromatic sulfur forms are partially hydrogenated under hydropyrolysis conditions as follows:

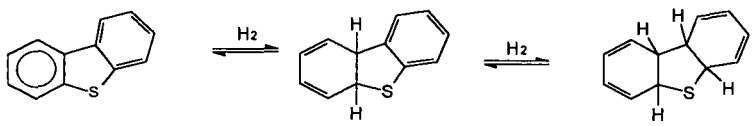

To the XPS and XANES probes, the sulfur in the hydrogenated molecules appear as aliphatic sulfurs. However, during heating, carbon sulfur bonds are not cleaved; rather the molecules lose hydrogen to regain their aromaticity.

Conclusions

Unlike pyrolysis under inert gas, pyrite in coals is converted to pyrrhotite during hydropyrolysis, and significant quantities of aliphatic sulfur are detected in the residues. It is believed that these aliphatic sulfur forms result from partial hydrogenation of aromatic sulfur species. While these sulfur species appear to be aliphatic to the X-ray probes, they are not, and do not behave thermally as aliphatic species.

References

1. Kelemen, S. R.; Gorbaty, M. L.; George, G. N. *Fuel*, **1990**, *69*, 939, 945.
2. George, G. N.; Gorbaty, M. L.; Kelemen, S. R.; Sansone, M. *Energy Fuels*, **1991**, 5, 93.
3. Huffman, G. P.; Mitra, S.; Huggins, F. E.; Shah, N.; Vaidya, S.; Lu, F. *Energy Fuels*, **1991**, *5*, 574.
4. Gorbaty, M. L.; Kelemen, S. R.; George, G. N.; Kwiatek, P. J. *Fuel*, **1992**, *71*, 1255.
5. Kelemen, S. R.; Gorbaty, M. L.; George, G. N.; Kwiatek P. J.; Sansone, M. *Fuel*, **1991**, *70*, 396.

6. Kelemen, S. R.; Vaughn, S. N.; Gorbaty, M. L.; Kwiatek, P. J. *Fuel*, **1993**, *72*, 645.
7. Taghiei, M. M.; Huggins, F. E.; Shah, N.; Huffman, G. P. *Energy Fuels*, **1992**, *6*, 293.
8. Chatterjee, K.; Stock, L. M.; Gorbaty, M. L.; George, G. N.;. Kelemen, S. R *Energy Fuels*, **1991**, *5*, 773.
9. Vorres, K. *Energy Fuels*, **1990**, *4*, 420.
10. Kelemen, S. R.; Gorbaty, M. L.; George, G. N.; Kwiatek, P. J. *Energy Fuels*, **1991**, *5*, 720
11. Calkins, W.H.; Torres-Ordonez, R. J.; Jung, B.; Gorbaty, M. L.; George, G. N.; Kelemen, S. R. *Energy Fuels*, **1992**, *6*, 411.

TABLE 1

	SULFUR/CARBON ATOM RATIO (x100)	
	XPS	BULK
RASA		
INITIAL	6.20	6.10
PYROLYSIS	4.70	5.30
HYDROPYROLYSIS	4.51	4.82
ILLINOIS #6		
INITIAL	1.25	2.32
PYROLYSIS	0.98	2.25
HYDROPYROLYSIS	0.96	1.58

TABLE 2

	XPS MOLE PERCENT SULFIDIC SULFUR	
	RASA	ILLINOIS #6
INITIAL	26	29
HYDROPYROLYSIS (200 °C)	25	30
HYDROPYROLYSIS (350 °C)	26	--
HYDROPYROLYSIS (427 °C)	25	26
PYROLYSIS (400 °C)	8	13

FIGURE 1

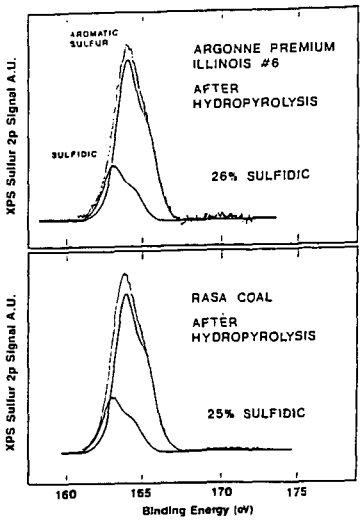

FIGURE 2

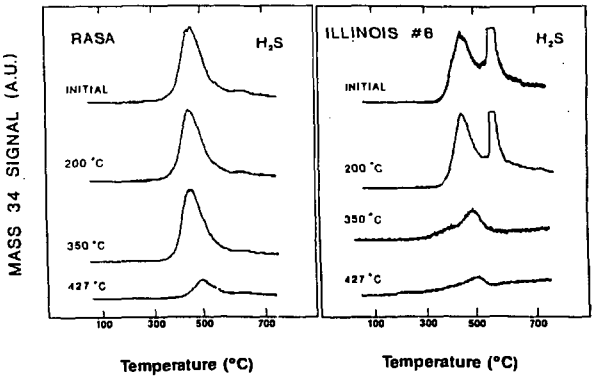

REMOVAL AND RECOVERY OF NITROGEN AND SULFUR COMPOUNDS FROM COAL TAR FRACTIONS USING SUPPORTED ALMINIUM SULFATE UNDER SUPERCRITICAL CO_2 CONDITIONS

Kinya Sakanishi, Hiroaki Obata, Isao Mochida*, and Tsuyoshi Sakaki[+)]
Institute of Advanced Material Study, Kyushu University,
Kasuga, Fukuoka 816, Japan
[+)] Kyushu National Industrial Research Institute,
Tosu, Saga 841, Japan

Keywords: Recovery of nitrogen compounds, Supported aluminium sulfate, Supercritical CO_2

ABSTRACT

Removal and recovery of nitrogen and sulfur compounds from coal tar fractions such as crude naphthalene and methylnaphthalene oils are examined using 10 wt% $Al_2(SO_4)_3/SiO_2$ as a solid acid under atmospheric or supercritical CO_2 (50℃, 80 atm) conditions. Repeated use of the solid acid is achieved by purging adsorbed nitrogen compounds with higher pressure (150 atm) CO_2 and methanol as an entrainer solvent, recovering effectively quinoline bases as well as purifying methylnaphthalenes.

Benzothiophene (BT) is dimerized over $Al_2(SO_4)_3/SiO_2$ catalyst under supercritical CO_2 conditions in order to separate BT from crude naphthalene as well as to purify naphthalene. BT was more selectively dimerized under supercritical CO_2 conditions(100℃, 100 atm) than in atmospheric n-octane solution at 100℃, allowing its selective dimerization and adsorption on the solid acid with selective extraction of naphthalene.

Effects of supercritical CO_2 conditions on the above adsorptions and reactions are discussed based on the analysis of recovered fractions and products.

INTRODUCTION

Crude methylnaphthalene oil(CMNO) is prepared as a residue of naphthalene oil (b.p. 210~260℃) of coal tar after the recovery of crude naphthalene.[1)] CMNO is further extracted with sulfuric acid and then neutralized with alkali to recover basic quinoline oil.[2,3)] However, because of the consumption of both acid and base as well as sludge formation, such a purification procedure appears no more feasible in the modern industry.[4)]

The present authors have reported that a consecutive solvent extraction with first methanol and then hexane concentrates the pyrroles and phenols in the hexane insoluble-methanol soluble fraction (HI-MS).[5)] Major basic nitrogen species staying in the methanol insoluble fraction(MI) are captured and recovered by adsorption and desorption, using nickel sulfate.[6-8)] The sulfate is known acidic and neutral, respectively, when it is dehydrated or rehydrated.[9)] High dispersion and proper heat-treatment of the sulfate increase the number and strength of acidic sites by supporting on silica gel for larger capacity against the adsorption of basic nitrogen compounds.[7,8)]

The present authors succeeded in removing nitrogen compounds from CMNO and recovering them in concentrated form using alminium sulfate on silica gel as the adsorbent.[10)] The supporting on silica gel disperses the sulfate on the surface, increasing the acidic strength and number of acidic sites. Hence, the surface which can get access to quinoline bases is essential as the support, larger pores being preferable. It was also reported that non-polar and poor solvents such as hexane and pentane appear to behave as an anti-solvent to expel the polar as well as basic compounds in methylnaphthalenes onto the adsorbent. Poorer solvents such as supercritical propane and carbon dioxide appear attractive.

In the present study, the removal and recovery of nitrogen compoumds in crude methylnaphthalene oil (CMNO) obtained from coal tar were investigated using $Al_2(SO_4)_3$, more acidic than $NiSO_4$, supported on silica gel to obtain highly denitrogenated CMNO as well as to recover

basic quinoline bases under atmospheric or supercritical CO_2 conditions.

Crude naphthalene is commercially purified by hydrotreatments to remove nitrogen and sulfur compounds, however these heterocyclic compounds such as indole and benzothiophene could be used as valuable chemicals and medicines if they could be recovered. In the present study, recovery of benzothiophene(BT) was also examined using the $Al_2(SO_4)_3$ catalyst by designing the selective dimerization of BT with extraction of purified naphthalene followed by BT de-dimerization under the supercritical CO_2 conditions.

EXPERIMENTAL

Aluminium sulfate(10 wt%) was supported by impregnation from aqueous solution on silica gel of MB-4B provided by Fuji-Davison Chemical Ltd. The surface area and mean pore diameter of the silica gel were 500 m^2/g and 64 Å, respectively. The adsorbent was calcined at 350℃ for 4 h in air.

Model methylnaphthalene oil (quinoline:Q 8wt%, isoquinoline:IQ 8wt%, 1- and 2-methyl-naphthalenes: 1- and 2-MN 42wt% each) was prepared for the supercritical extraction experiments. Figure 1 shows the supercritical CO_2 extraction apparatus used in the present study. The model feed was charged to extraction vessel, and supercritical CO_2 (50℃, 80 atm) was flowed at 6 l/min to carry the feed to the fixed bed column filled with the $Al_2(SO_4)_3$ adsorbent. After the adsorbent was saturated with nitrogen compounds, higher pressure CO_2 and then methanol was flowed to recover the adsorbed species and to regenerate the adsorbent for its repeated use. The eluted and recovered fractions were analyzed and quantified by GC-FID (50 m capillary OV- 101 column, 110℃).

Benzothiophene(BT) in crude naphthalene was extracted and dimerized using several catalysts in atmospheric hexane and octane, respectively or supercritical CO_2 solvent at 100℃ for 3 h in order to separate BT from naphthalene. The fractionated and reaction products were analyzed by the elemental analysis, LC and FD-MS.

RESULTS AND DISCUSSIONS

Removal and Recovery of Quinolines from Model Methylnaphthalene Oil

Figure 2 shows the elution profile of the model methylnaphthalene oil using 10 wt% $Al_2(SO_4)_3/SiO_2$ as an adsorbent in the fixed bed apparatus under supercritical CO_2 conditions. No nitrogen compounds were eluted until the extraction time of 120min, only denitrogenated methylnaphthalenes being recovered at the separation vessel. At the extraction time of 220 min when the adsorbed compounds were hardly extracted, CO_2 was pressurized upto 150 atm which was kept for 60 min to recover the adsorbates, and then methanol was added to CO_2 flow as an entrainer, almost all the adsorbed nitrogen compounds being desorbed and recovered from the adsorbent.

Figure 3 illustrates the elution curve of each compound in the model methlnaphthalene feed, where the elution conditions are same as Figure 2. 62% of methylnaphthalenes in the feed was recovered without nitrogen compounds, in other words, quinoline and isoquinoline were not eluted until about 60% of the feed was eluted. The activity of the adsorbent in the repeated adsorption/ desorption cycle is shown in Figure 4. The adsorption capacity of 10wt% $Al_2(SO_4)_3/SiO_2$ was restored to almost the same level of the first run in the second run by purging almost completely the remaining adsorbates which consist mainly of nitrogen compounds. The adsorption activity of the adsorbent was gradually decreased with the repetition number of the adsorption/desorption cycle, indicating that some deactivation of the adsorbent should take place during the adsorption/desorption repetition. More polar and/or dried entrainers may be very effective in achieving the complete recovery of nitrogen compounds without the deterioration of the adsorbent. Adsorbents should be designed in combination with eluting solvents for the completely reversible adsorption/ desorption performances.

Removal of Benzothiophene from Crude Naphthalene

Table 1 summarizes the adsorption treatment of crude naphthalene with various adsorbents in

atmospheric n-hexane solution followed by filtration to recover hexane-eluted fraction and washing of the adsorbent with benzene to recover adsorbed compounds. Sulfur as well as nitrogen compounds were removed from crude naphthalene, purified naphthalene and hetero-atom compounds being concentrated in haxane and benzene eluates, respectively, although the sulfur removal was not so effective as the nitrogen removal, because the basicity of sulfur compounds is not so strong as nitrogen compounds.

Recovery scheme of purified naphthalene(Np) and benzothiophene(BT) under supercritical CO_2 conditions is illustrated in Figure 5. BT is selectively dimerized and adsorbed on solid acid catalyst, naphthalene being purified and recovered by extraction with supercritical CO_2. BT dimer may be converted to BT monomer at a higher temperature, BT being recovered by supercritical CO_2 extraction. Figures 6 and 7 show the FD-MS spectra of the oligomerization products from the reaction of BT with 10wt% $Al_2(SO_4)_3/SiO_2$ catalyst at 100℃ for 3 h in atmospheric octane and supercritical CO_2 solvent, respectively. It is noted that BT is more selectively converted to its dimer in supercritical CO_2 solvent than in atmospheric octane solution, suggesting a remarkable solvent effect on the reactivity of BT and the selectivity to its dimer. Such a highly selective dimerization in supercritical CO_2 solvent was also observed in the oligomerization reaction of the mixture of BT and naphthalene under the same reaction conditions. More cross-oligomerization products between BT and naphthalene were produced in atmospheric octane solution at 100℃, suggesting that the supercritical CO_2 solvent may enhance the more preferable interaction of BT with the catalyst to that of naphthalene.

Reaction conditions including temperatures and pressures of dimerization and extraction, and catalyst should be further optimized to acieve more selective conversion to BT dimer and recovery of BT monomer after selective extraction of purified naphthalene.

REFERENCES

1 "Handbook of Aromatics and Tar Industry", Nihon Houkouzoku Kougyoukai, 1965, p.81 .

2 Japanese Patent 61-50942(1986).

3 Horita,Y., Togari,O., Komoto,T., Nakamura,M.,Tanji, H., J.Petrol.Inst.Jpn.,1987, 30, 94.

4 Horita,Y., Komoto,T., Arioka,H., Nakamura,M.,Tanji,H., J.Petrol.Inst.Jpn.,1987, 30, 149.

5 Fei,Y.Q., Sakanishi,K., Sun,Y.N., Yamashita,R., Mochida,I., Fuel, 1990, 69, 261.

6 Mochida,I., Fei,Y.Q., Sakanishi,K., Usuba,H. and Miura,K., Chem.Lett., 1990, 515.

7 Mochida,I., Sakanishi,K., Usuba,H. and Miura,K., Fuel, 1991, 70, 761.

8 Mochida,I., Fei,Y.Q., Sakanishi,K., Korai,Y., Usuba,H., Miura,K., Carbon, 1922, 30, 241.

9 Tanabe,K., Takeshita,T.,"Acid-Base Catalysis", Sangyo Tosho Pub. Co.,Ltd.(Tokyo), 1966.

10 Sakanishi,K., Sun,Y.N., Mochida,I., Usuba,H., Fuel Process. Technol., 1992, 32, 143.

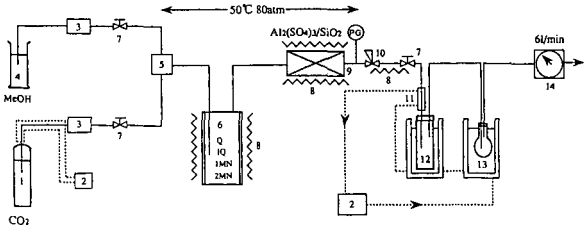

Fig 1 Supercritical CO2 extraction apparatus

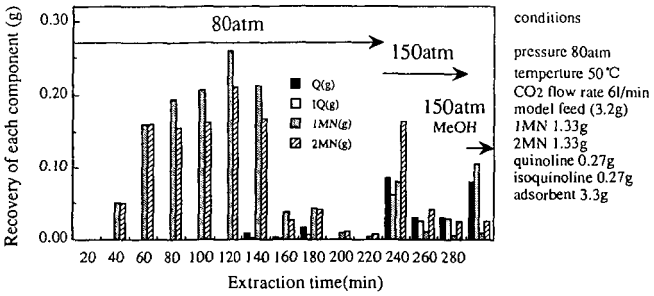

Fig2 Elution profile of model methylnaphthalene oil under supercritical CO_2 conditions

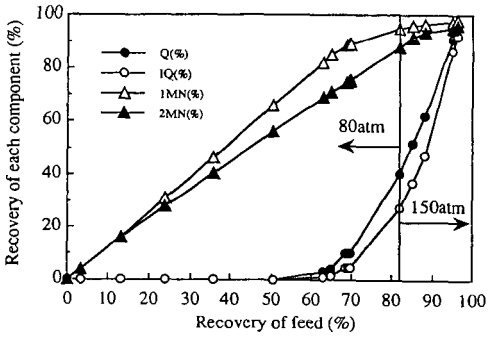

Fig3 Elution curve of each compound in the model methylnaphthalene oil under supercritical CO_2 extraction conditions (conditions;see Fig2)

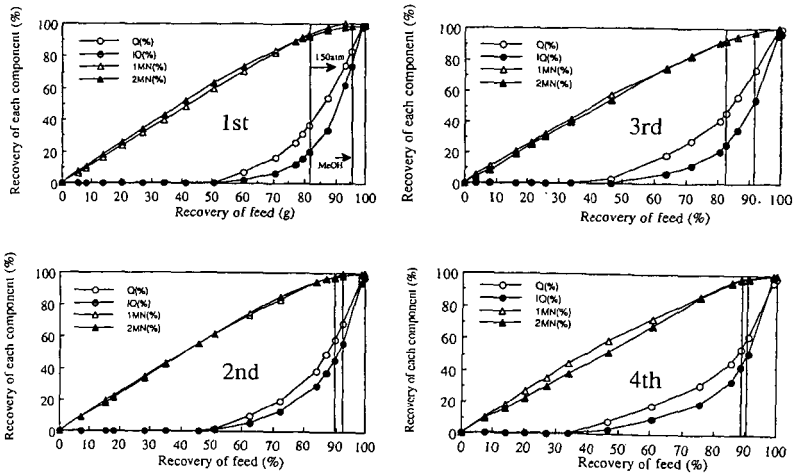

Fig 4 Repeated activity of the adsorbent for adsorption / desorption treatment of model methylnaphthalene oil under supercritical CO_2 conditions
(conditions; 50℃-80atm catalyst 2.3g)

Table 1 Adsorption treatment of crude naphthalene with various adsorbents in atmospheric hexane solution

Adsorbent	Eluting solvent	Recovery (wt%)	Elemental analysis S(%)	N(ppm)
Original crude naphthalene		—	1.6	500
$10\%Al_2(SO_4)_3/SiO_2$	hexane	91.0	1.0	50
	benzene	6.1	3.1	1700
reduced $CoMo/Al_2O_3$ [1)]	hexane	93.3	1.2	31
	benzene	4.3	5.6	—
reduced $NiMo/Al_2O_3$ [1)]	hexane	92.1	1.3	25
	benzene	6.4	4.2	—

1) Catalyst reduction pretreatment ; H_2 flow , 360℃-3h

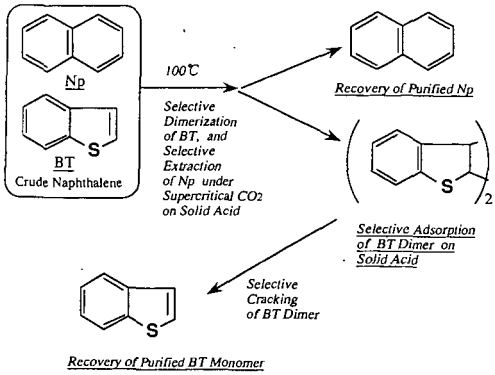

Fig 5 **Recovery Scheme of Purified Np and BT through Selective Dimerization of BT and Extraction of Np under Supercritical CO2 Conditions on Solid Acid Catalyst**

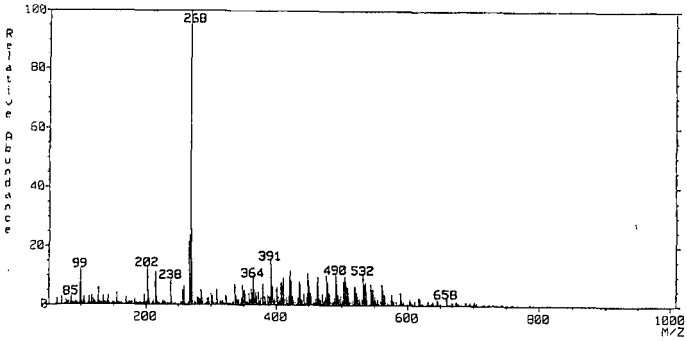

Fig6 FD-MS spectra of B.T oligomerization products conditions in atmospheric octane solution

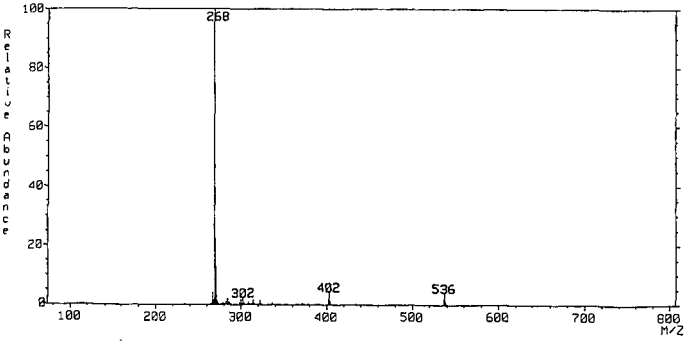

Fig 7 FD-MS spectrum of B.T oligomerization products under supercritical CO2 conditions

CHARACTERIZATION OF NITROGENOUS COMPOUNDS IN DISTILLATES DERIVED FROM TWO-STAGE COAL LIQUEFACTION

C. Bradley, R.E. Pauls, D.C. Cronauer and M.E. Bambacht
Amoco Research Center
P.O.Box 3011
Naperville, IL 60566-7011

Keywords: nitrogen compounds, coal liquids, GC/MS

INTRODUCTION

The nitrogen compounds in coal distillates have not been characterized as fully as the predominant hydrocarbon components, but are of considerable importance due to their adverse effect on fuel stability (1-3) and catalyst lifetime (4) and the potentially adverse health and environmental impact (5-7). A number of different classes of nitrogen compounds are commonly found in coal liquids (e.g. quinolines, indoles, carbazoles (7-10). These each will affect catalyst deactivation and product stability to different extents.

This report specifically addresses the nature of nitrogen compounds found in Wilsonville streams. In the current study, gas chromatography with a nitrogen-selective detector (GC/N) and gas chromatography/mass spectrometric (GC/MS) techniques were employed to identify and quantitate the major nitrogen-containing components found in concentrates prepared from coal-derived distillates from two series of Wilsonville pilot plant runs. These runs were made with Illinois No. 6 and Wyodak Coals.

While direct GC/N analysis can be done on the whole, untreated distillate, the nitrogen detector is a poor identification tool. Therefore, GC/MS was necessary for compound identification. Consequently, pretreatment of the distillates to obtain N-rich fractions was a necessary step to minimize hydrocarbon interference in GC/MS analyses and allow more detailed examination of the nitrogen components in coal distillates. However, once a typical nitrogen profile has been characterized, GC/N should allow rapid quantitation of the nitrogen compounds in an untreated distillate.

EXPERIMENTAL

Samples

The coal-derived liquids were obtained from the Advanced Coal Liquefaction R & D Facility at Wilsonville, AL. The products from five runs were characterized, three from the liquefaction of Illinois No. 6 bituminous coal (runs 250D, 250H, and 251E) and two from Wyodak subbituminous coal (runs 251-IIB and 251-IIIB). Details of these coals and their processing are given in reference 11.

Samples from the Wilsonville product streams were obtained soon after the runs and stored in a cold room to avoid degradation. Product liquid blends were prepared just before experimentation and their elemental analyses are given in Table I.

Preparation of Nitrogen Concentrates

Nitrogen-containing concentrates were prepared in the following manner. Approximately 80g of coal liquid oil was added to twice that weight of 10% NaOH aqueous solution. The resulting oil and aqueous phases were separated; phenolics were extracted into the aqueous layer. Toluene was added to the oil layer which was added to Amberlyst-15 cation ion exchange resin in a ratio of 4:2:1 of toluene:raffinate:resin, respectively. After three days of gentle mixing, the "OH, N-free" oil was recovered by filtration.

The resin was flushed with pentane and dried in a stream of N_2 at ambient temperature. It was then contacted with methanol saturated with NH_3 to recover the concentrates. About 70% of the methanol was gently stripped from these concentrates by rotary evaporation.

To confirm that essentially no organic nitrogen compounds remained on the resins after NH_3 treatment, resins from the 250D, 250H, and 251E treatments were treated with H_2SO_4. The recovered liquids were neutralized and extracted with CH_2Cl_2. These extracts contained no organic N-containing compounds. The samples of regenerated resin were checked for nitrogen content. The recovered

resins and a sample of fresh resin subjected to NH3 and H2SO4 regeneration all contained nitrogen levels of 4.1 +/- 0.1%.

Chromatographic Separations and Component Identification

Detailed analytical experimental conditions for component separations and identification are given in Table II. Dichloromethane was used as the solvent for GC/MS. Methyl t-butyl ether was the solvent used in GC/N work because of severe peak tailing and detector response problems when dichloromethane was used.

Nitrogen Compound Quantification

The thermionic nitrogen detector (TID) for GC/N quantification work was calibrated using blends of pyridines, anilines, quinolines, indoles, carbazoles, and indoline. Each of these seven types of nitrogen compounds gives a different TID response. Therefore, seven different linear calibration equations were generated. Figure 1 shows a typical GC/N calibration plot and calibration equation of an aniline.

Based on the nitrogen components identified by GC/MS, the nitrogen components in a sample were grouped by types and quantitated using the calibration equations corresponding to the nitrogen types detected. Responses relative to 4-methylpyridine were determined for available model compounds as listed in Table III. As shown, the response factors for a given nitrogen compound type are similar but vary for different types of nitrogen compounds. For the majority of alkylated nitrogen components identified by GC/MS in the samples, we have no standards. Therefore, for a given nitrogen compound class, e.g. C_0-C_{10} indoles, a single calibration equation based on the parent compound, e.g. indole, was used. There were several nitrogen components boiling above carbazole for which we had no standard whatsoever. In such cases, the peak area of these components were summed and the carbazole calibration equation used to quantitate them.

RESULTS AND DISCUSSION

Ion-Exchange

The A-15 resin adsorbed between 90 and 95% of the nitrogen compounds from the OH-free raffinate generated from the phenolics stripping step. Essentially no organic nitrogen compounds were retained in the A-15 resin after stripping with the ammonia/methanol solution.

Analytical Results

GC/MS was used to identify the nitrogen components in the nitrogen concentrates of the blends and to determine relative amounts of the various nitrogen components. Seven major types of nitrogen-containing compounds were detected in the bituminous coal liquid distillates--pyridines, anilines, quinolines, hydro-quinolines, indoles, indolines, and carbazoles. Four of these types (pyridines, anilines, hydroquinolines, and indoles) were the nitrogen classes in the subbituminous coal liquid distillates. Side-chains on the ring compounds ranged from C_1 through C_{10} chains. The parent types of nitrogen compounds detected are shown in Figure 2.

The nitrogen compounds identified by GC/MS and quantitated by GC/N are grouped by classes in Table IV. This Table also shows boiling point data for representative nitrogen-containing compounds. Boiling points range from 300°F (C_2 pyridines) up to 700°F (carbazoles). The majority of the nitrogen compounds detected boiled in the 350-700°F range. In addition, the majority of the nitrogen compounds were alkyl substituted (designated herein by the total alkyl carbon number, e.g., C_2 pyridines).

Anilines (C_0-C_6) were the major nitrogen components in all blends, with the catalytic/catalytic run (251E) bituminous product having relatively more anilines and the subbituminous products having relatively fewer anilines than that of the other runs. Run 251E product also had fewer pyridines compared with that of the other runs. The levels of anilines found in the bituminous products are consistent with the fact that the first stage catalyst would increase the extent of hydrogenation and cracking of quinolines and multiple ring species to anilines. However, it was not anticipated that the level of anilines would be so high.

In addition to nitrogen species, GC/MS detected a number of aromatic hydrocarbons, primarily biphenyls, naphthalenes, anthracenes, phenanthrenes, and pyrenes in the nitrogen concentrates of all runs. These occurred because of non-specific adsorption onto the resin. The hydrocarbons accounted for about 30% of the total peak area of the GC/MS data. There was 1-2% phenolic material in the nitrogen concentrates of 250D and 250H (none detected in the 251E nitrogen concentrate).

Table V shows comparative quantitative GC/N and GC/MS data for the bituminous 251E coal liquid distillate. The data compare very well in spite of the semi-quantitative nature of GC/MS.

CONCLUSIONS

For the characterization of coal-derived distillates for nitrogen compound distribution, it is highly beneficial to concentrate a nitrogen-component rich fraction prior to analysis. Extraction of phenolics followed by ion-exchange to concentrate nitrogen compounds appears to work well for pyridines through carbazoles boiling up to about 700°F. Analysis by GC/MS and GC/N selective detection are the preferred techniques to obtain a distribution of the nitrogen components.

Data indicate that the nitrogen concentrates derived from IL No. 6 coal contain seven types of nitrogen ring structures: pyridines, anilines, quinolines, hydroquinolines, indoles, indolines, and carbazoles. Nitrogen concentrates from Wyodak sub-bituminous coal contain mostly pyridines, anilines, hydroquinolines, and indoles. Essentially all of the nitrogen compounds in both types of cola liquids are alkyl substituted. Sidechains on the aromatic rings are C_1 to C_{10}. It was not possible to determine if there was single attachment of longer alkyl chains or multiple attachment of short chains.

High levels of anilines are present, namely about 44% of the total nitrogen components detected in the bituminous coal liquids and 29% in the subbituminous coal liquids. Other investigators have reported anilines in coal-derived liquids (9,10,12). These anilines are presumably the result of the hydrogenation and opening of aromatic nitrogen-containing rings. Anilines should donate hydrogen during coal liquefaction; however, there is a high likelihood that the resulting product forms adducts quickly, thereby resulting in measurable retrogressive reactions. Most retrogressive products have high nitrogen content.

ACKNOWLEDGEMENTS

We are grateful to P. L. Baldwin for her extraction work, D. Parisi and E. G. Lesko who analyzed the samples, and W. H. Weber, J. M. Lee, and others at the Wilsonville facility who helped obtain the samples and operating data. We also acknowledge the funding of the Wilsonville facility by the DOE, The Electrical Research Institute, and Amoco Oil Company.

REFERENCES

1. Brown, F. R. and Karn, F. W., Fuel, 59, 431 (1980).
2. Ford, C. D., Holmes, S. A., Thompson, L. F. and Latham, D. R., Anal. Chem., 53, 831 (1981).
3. Drushel, H. V. and Sommers, A. L., Anal.Chem., 38, 19 (1966).
4. Hartung, G. K.,and Jewell, D. M., Anal.Chem. Acta, 26, 514 (1962).
5. Guerin, M. R., Ho, C. H., Rao, T. K., Clark, B. R. and Epler, J. L., Environ. Res., 23, 42 (1980).
6. Lee, M. L., Novotny, M. V. and Bartle, K. D., Analytical Chemistry of Polycyclic Aromatic Compounds, Academic Press, N. Y. and London, 1981, Chp.3.
7. Schiller, J. E., Anal.Chem., 49, 2292 (1977).
8. Schweighardt, F. K., White, C. M., Friedman, S. and Schultz, J. L., Organic Chemistry of Coal, (Gould, F. R., ed.), ACS, Sec. No.71, ACS, Washington DC, 1978, Chp. 18.
9. Paudler, W. W. and Cheplen, M., Fuel, 58, 775 (1979).
10. Felice, L. J., Anal.Chem., 54, 869 (1982).
11. Pauls, R. E., Bambacht, M. E., Bradley, C., Scheppele, S. E. and Cronauer, D. C., Energy and Fuels, 4, 236 (1990).
12. Novotny, M., Komp, R., Merli, F., Todd, L. J., Anal.Chem., 52, 401 (1980).

TABLE I

Elemental Analyses of the Product Blends

Run No.	Carbon	Hydrogen	Nitrogen	Oxygen	Sulfur
250D	86.9	11.4	0.19	1.4	0.09
250H	87.2	11.6	0.13	1.4	0.17
251E	87.5	11.6	0.14	0.8	0.03
251-IIB	85.7	11.3	0.31	2.60	0.06
251-IIIB	86.3	12.7	0.15	0.84	0.06

TABLE II

Analytical Operating Conditions

CC/N

CC Unit:	Varian 3700 with a Thermionic N detector (TID); 6.90 bead current; 17 psig H_2; 4.0V bias; $1x10^{-11}$ atten
Column:	60 m fused silica capillary, 0.25 mm i.d.
Coating:	DB-1, 0.25 μm film
Temperature:	50 to 300°C at 6°/min with a 28 min hold Injector: 300°C; Detector: 350°C
Carrier:	Helium (37 psig)
Inlet Split Ratio:	60/1
Sample:	0.2μl of the sample diluted 1:2 with MTBE

CC/MS

CC Unit:	Varian 3300
Column:	60 m fused silica capillary, 0.25 mm i.d.
Coating:	DB-1, 0.25 μm film.
Temperature:	50 to 300°C at 6°/min with a 28 min hold (oven) Injector: 310°C
Carrier:	Helium (30 psig and 5 ml/min split)
Sample:	10 mg diluted with 250 μl of CH_2Cl_2
MS Unit:	VGIAB-2F
Data System:	Data General Nova 3 with Kratos software
Mass Resolution:	3000
Source Temperature:	230°C
Operational Mode:	Electron impact
Sample Rate:	0.5 sec/mass decade

TABLE III

Nitrogen Detector Response Factors

Component	TID Response relative to 4-methyl pyridine = 1.00
pyridine	1.01
2,4,6-trimethylpyridine	1.00
aniline	0.856
2,5-dimethylaniline	0.860
p-ethylaniline	0.860
quinoline	0.962
2,4-dimethylquinoline	0.956
tetrahydroquinoline	0.974
indole	1.07
carbazole	0.849
indoline	1.03

TABLE IV

Nitrogen Compounds in Coal Liquids

Component	Boiling Range, °F[a]	Wt% Component: Bituminous[b] Run 250D	Run 250E	Run 251E	Subbituminous[c] Run 251-IIB	Run 251-IIIB
Pyridine	239	0.0	0.0	0.0	0.0	0.0
C_1PY	250-300	0.4	1.0	0.0	1.8	1.1
C_2PY	303-340	1.4	2.1	0.4	4.2	1.6
C_3PY	342-375	1.7	2.0	1.0	3.7	1.6
C_4PY	370-395	1.3	1.0	0.4	1.9	4.9
C_5PY	400-420	0.0	0.0	0.0	0.6	1.6
Total Pyridines		4.8	6.1	1.8	12.2	10.8
Aniline	363	2.5	3.1	2.9	1.0	1.3
C_1An	376-390	7.4	11.0	8.0	2.5	2.7
C_2An	400-425	6.8	6.5	11.6	2.5	4.0
C_3An	435-470	4.9	4.0	7.4	3.7	4.5
C_4An	500-525	5.0	3.9	5.1	1.9	3.6
C_5An	529-550	2.0	0.6	0.6	0.6	0.8
C_6An	573-590	0.0	0.0	0.0	0.2	0.3
Total Anilines		28.6	29.1	35.6	12.4	17.2
Quinoline	462	0.0	0.0	0.0	0.0	0.0
C_1Q	478-498	1.3	1.4	0.1	0.0	0.0
C_2Q	513-560	0.5	0.2	0.4	0.0	0.0
C_3Q	576-597	0.7	0.7	0.7	0.0	0.0
C_4Q	572-595	0.4	0.8	0.1	0.0	0.0
C_5Q	607-635	0.0	0.0	0.0	0.0	0.0
C_6Q	640-671	0.0	0.0	0.0	0.0	0.0
C_7Q	675-690	1.2	0.1	0.1	0.0	0.0
C_8Q	685-700	1.2	0.0	0.0	0.0	0.0
Total Quinolines		5.3	3.2	1.4	0.0	0.0
Tetrahydroquinoline (THQ)	480	0.0	1.5	0.0	0.0	0.0
C_1THQ	483-489	3.4	3.5	1.9	0.7	1.1
C_2THQ	490-540	3.4	1.8	4.7	4.6	4.8
C_3THQ	546-585	1.3	0.5	1.6	4.3	4.8
C_4THQ	585-600	1.8	0.2	2.7	0.7	1.3
C_5THQ	590-615	0.0	0.0	0.0	0.1	0.3
Total THQs		9.9	7.5	10.9	10.4	12.2
Indole	489	0.0	0.0	0.0	0.0	0.0
C_1Indole	530-550	0.5	0.0	0.7	0.5	1.1
C_2Indole	563-570	0.5	0.6	1.1	1.4	2.1
C_3Indole	565-585	0.0	0.0	0.0	1.5	1.6
C_4Indole	570-590	0.0	0.0	0.0	0.5	0.3
C_5Indole	575-615	2.9	1.7	4.6	2.1	1.3
C_6Indole	617-636	6.4	5.9	4.9	2.1	0.8
C_7Indole	640-660	3.0	0.7	1.7	1.2	0.3
C_8Indole	670-680	0.7	0.0	0.3	0.1	0.0
C_9Indole	675-689	0.0	0.0	0.0	0.7	0.0
C_{10}Indole	680-695	0.0	0.0	0.0	0.3	0.0
Total Indoles		14.0	8.9	13.3	10.9	7.4
Indoline	466	0.0	0.0	0.0	0.0	0.0
C_1Indoline	514-540	0.0	0.5	0.0	0.0	0.0
C_2Indoline	540-565	0.0	0.0	0.2	0.0	0.0
C_3Indoline	565-580	0.0	1.3	0.0	0.0	0.0
C_4Indoline	570-590	0.0	0.1	0.0	0.0	0.0
Total Indoline		0.0	1.9	0.2	0.0	0.0
Carbazole	671	0.4	0.7	0.9	0.1	0.0
C_1C	645-670	1.5	1.5	1.0	0.9	0.0
C_2C	680-690	0.0	0.0	0.0	0.3	0.0
C_3C	675-700	0.0	0.0	0.1	0.4	0.0
Total Carbazoles		1.9	2.2	2.0	1.7	0.0
Tetrahydrocarbazoles	617-690	0.8	0.4	0.4	1.8	0.3
Phenylisoquinoline	520-535	2.0	4.0	2.9	0.0	0.0
Methylisoquinoline	480-530	0.9	0.2	0.3	0.0	0.0
C_2diphenylamine	630-650	1.3	0.1	0.3	0.0	0.0
C_3diphenylamine	650-670	0.0	0.0	0.2	0.0	0.0
Other N compounds[d]		4.0	3.2	1.6	0.0	0.0
Total Misc. N		9.0	7.9	5.7	1.8	0.3

[a] estimated boiling ranges for alkylated compounds
[b] GC/N quantitation
[c] GC/MS quantitation
[d] M.W. 193 and 209

TABLE V

Comparison of GC/N and GC/MS Quantitation

Nitrogen Component	Run 251E, % Components	
	GC/N	GC/MS
C_1-C_4 pyridines	1.8	1.9
C_0-C_5 anilines	35.6	36.5
C_1-C_7 quinolines	1.5	1.6
C_1-C_4 THQs	10.9	11.0
C_1-C_8 indoles	13.3	12.9
C_2 indolines	0.2	0.4
C_0-C_3 carbazoles	2.0	2.0

Figure 1

A GC/N Calibration Plot

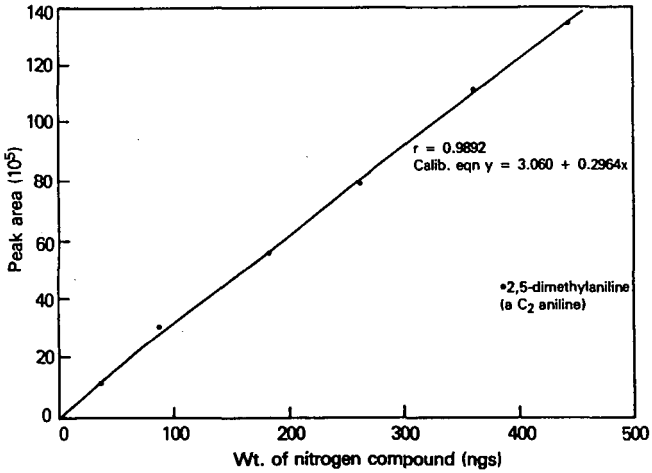

Figure 2

Types of Nitrogen Compounds Detected in Coal Liquids

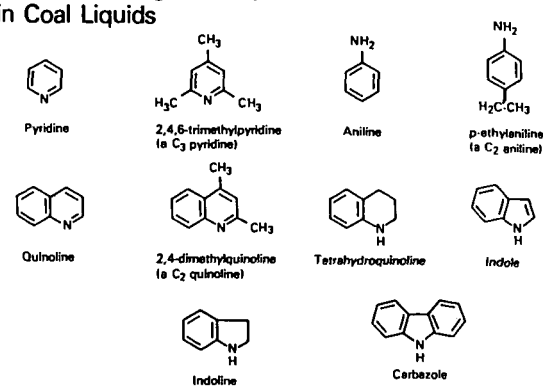

PREPARATIVE SEPARATION AND CHARACTERIZATION OF COAL LIQUID AROMATICS

James N. Story
AMOCO Corporation
Naperville, IL 60566

Keywords: liquid chromatography, coal liquids

INTRODUCTION

Information concerning the degree and nature of aromaticity in a hydrocarbon feedstock is a very important characterization parameter for refining processes designed to convert high boiling feedstocks into more valuable products. This is especially true in catalytic cracking because feeds of higher aromaticity tend to be more difficult to crack and form coke more easily. Products of the liquifaction of coals are generally highly aromatic in nature and therefore a detailed knowledge of the aromatic structures present in coal liquids is very important in predicting their processing properties.

This work describes the preparative separation and characterization of the aromatics fraction of three Wilsonville coal liquids produced by different two-stage reaction processes. The coals, the liquifaction processes, and the reaction product liquids have been described by Fatemi et. al. (1). The Black Thunder sample was produced by a two stage thermal-catalytic process, while the Illinois No. 6 and Pittsburgh No. 8 liquids were produced using a more severe catalytic-catalytic process.

An additional objective of this work was to characterize the behavior of the DNAP stationary phase in aromatic ring number separations in real samples. Several workers, including this author, have verified the accuracy of the ring number separations on analytical scale DNAP columns using model compounds. However, the limited number of model compounds available, especially of alkyl and naphtheno substituted polynuclear aromatics, and the extremely complex nature of real samples of interest require that such separations be validated more completely using real samples.

EXPERIMENTAL

The samples consisted of the 650-1000 F aromatics fractions of the three Wilsonville coal liquids. One typical petroleum gas oil (650-1000 F) was included for comparison purposes. The aromatics fractions were produced by removal of polar compounds using ion exchange resins, followed by isolation of the aromatics by silica gel chromatography. One milliliter of a 20-30 mg/mL solution of sample dissolved in cyclohexane was injected manually via HPLC sampling valve. The sample was separated by gradient elution using a hexane-MTBE gradient.

The separation on this column is produced via a charge-transfer mechanism in which structures containing larger numbers of aromatic rings (more extensive pi electron systems) are retained by the electron-withdrawing dinitroanaline stationary phase. Use of this phase has been described by Grizzle et. al. (2,3). Data obtained in our laboratory using solutions of model compounds on an analytical scale column showed that the model compounds studied in all cases eluted in the same grouping with others of the same ring number and at increasing retention time with increasing ring number. There was no case in which a compound eluted in the "wrong" group. Alkyl substitution was found to generally not affect retention time enough to move the species out of it's ring number group, although small shifts may occur.

The fractions produced were individually characterized by GC-MS and GC. GC-MS was used to identify individual components of the fractions and as an additional validation of the ring number boundary determinations. Single ion plots of ions representing common structures of different aromatic ring number were used to verify ring number regions. The fraction boundaries were also monitored spectroscopically using a Diode Array Spectrophotometer. The coal liquid fractions were collected in such a way as to attempt to obtain "heart-cuts" from each ring number group, and "boundary cuts" at the borders between groups. Solvents were removed from the fractions by evaporation using a Rotovap and fraction weights were obtained. Total recoveries of injected sample were 97% to 104%.

RESULTS

Cut points for the ring number fractions were initially estimated using model compounds. Model compounds known to lie on the boundaries of ring number regions were injected to define initial cut points between regions. These initial cut points were determined to be approximately 19.5 minutes for the 1-2 ring separation, 40 min for 2-3 ring, 60 min for 3-4 ring, and 80 min for 4-5+ ring. A 30 minute backflush step was included to completely elute the sample. Since total column capacity was limited to 20-25 milligrams to avoid overloading, and about twenty fractions were taken, fraction sizes were limited to a few milligrams at most in each fraction.

The samples used for this work were in the boiling range of petroleum gas oils, 650-1000 F. The molecular weight range was typically 200-600 Daltons with an average of about 350, as measured by mass spectroscopy. This means that for a molecule to contain only one aromatic ring, typically 70-80 percent of the atoms must be present in nonaromatic portions of the molecule. In general, increasing nonaromatic content results in increasing fraction complexity. Increasing aromaticity restricts the number of possible compound structures within a particular molecular weight range by constraining the hydrocarbons to a limited number of structures, since those structures must contain aromatic rings. Hence one of the effects were observe is that the ring number fractions become less complex as we go to higher ring numbers as a result of the decreasing variety of alkyl and naphthene substitution.

For comparison and validation purposes mass spectral data were collected by low resolution, high voltage MS using the so-called "Robinson" method (4). Table I shows a comparison of the normalized ring number distributions obtained by preparative HPLC, compared to those obtained from hydrocarbon type analysis by mass spectroscopy. Good agreement is obtained generally within the limits of the techniques used.

The liquid chromatographic separations showed the bulk of the mass isolated from the Illinois No. 6 and the Pittsburgh No. 8 liquid to consist of one and two ring material, which is consistent with the MS results. Chromatograms for these samples are very similar. These two samples represent the coals produced from a two stage, catalytic-catalytic process described in Reference (1). The fractions isolated from the Black Thunder (Wyodak) coal liquid, which were produced by a Thermal-Catalytic process, showed a much larger fraction of 3 and 4 ring material, compared to the Pittsburgh and Illinois coal liquids. The amount of one and two ring material is relatively small. Petroleum gas oil fractions showed a wide distribution of ring number structures with 1- and 2- ring structures predominating.

CHARACTERIZATION OF FRACTIONS

UV Spectra

All HPLC separations were monitored spectrophotometrically by continuous collection of spectra in the ultraviolet region. Aromatic compounds show characteristic spectra which differ significantly depending on ring number. This is a result of the extension of the aromatic ring system, which increases the probability of lower energy, longer wavelength transitions. Shifts to absorption at longer wavelengths will occur as the aromatic structures are extended to larger ring numbers. UV absorption spectra were used to help define the boundaries of the separation. Spectra from the separation of the Pittsburgh coal liquid are shown in Figure 1 to illustrate the distinct spectral changes which occur in the ring number separation. Figure 1a shows how the spectra change in the 1-2 ring transition region of the Pittsburgh coal liquid separation. All spectra are normalized to the absorbance maximum. It is clear that a distinct change occurs in the spectra of eluted sample components as we go from spectrum C in Figure 1a, taken at 19 minutes, to D, taken at 20 minutes. Spectrum C is much more typical of a one ring aromatic while spectrum D more closely resembles a two ring aromatic compound. These spectral changes are consistent with model compound data which shows the 1-2 ring transition to occur at about 19.5 minutes.

Figure 1b shows the sharp spectral transition occurring over just two minutes in the portion of the separation where 3 ring compounds begin to emerge. The much more extended absorption of spectrum B is indicative of the partial transition to 3 ring structures.

Figure 1c shows evidence of the emergence of 4 ring structures. Spectrum A is a typical 3 ring region spectrum, while spectrum B shows the emergence of

a series of bands in the region from 300 to 340 nm which is typically characteristic of 4 ring aromatics.

Figure 1d shows more clearly the difference between characteristic spectra taken from the middle region of each ring type.

Gas Chromatography and GC-MS

All of the fractions from the Pittsburgh No. 8 separation, and selected fractions from the other separations, were analyzed by high resolution capillary gas chromatography. Peak identification was performed by gas chromatography-mass spectroscopy and retention time matching with standard solutions of polynuclear aromatic mixtures. The variety of structures can be qualitatively compared by means of the number of distinct peaks observable in the chromatograms. All of the 1 ring fractions appeared to possess a large variety of structures and individual components are not well resolved into distinct peaks. Chromatographic resolution is also not complete enough to be able to identify individual components unambiguously by GC-MS. However, GC-MS data obtained from these fractions is consistent with the predominance of heavily alkyl substituted one ring aromatic structures. The two ring region was found to contain primarily alkyl diaromatics, including hexahydropyrenes, naphtheno and dinaphthenonaphthalenes, as well as alkyl acenaphthenes, but there was no evidence of 3 ring aromatics. The 2-3 ring boundary fraction contained hexahydropyrene, alkyldihydroanthracenes, and alkyl phenanthrenes. The 3 ring region showed alkylated anthracenes, phenanthrenes, and naphthenophenanthrenes as as well as alkyl benzofluorenes. The chromatograms from the four ring region showed exclusively alkylated tetraaromatics, including pyrenes, benzophenanthrenes, and benzanthracenes. A number of components, including pyrene and methyl pyrenes appear in several of the later fractions, providing evidence of significant bandspreading in this part of the liquid chromatographic separation. All gas chromatograms from this region show relatively few compounds and demonstrate a tremendous reduction in complexity which can be achieved by using LC and GC together to characterize complex hydrocarbon mixtures. Even the petroleum gas oil is vastly reduced in complexity. The backflush fraction of the Pittsburgh coal liquid shows the presence of 4, 5, and 6 ring aromatics. Model compound data from HPLC separations on DNAP indicate that ring number separations are increasingly poorly resolved above 5-6 rings, and this appears to be borne out by the wider variety of multi-ring structures appearing in this fraction.

GC-MS Verification of HPLC Ring Number Regions

GC-MS data obtained from the individual fractions were used in an additional way to verify ring number region assignments. Constraints imposed by structural and molecular weight requirements mean that some fragment masses will be much more likely to appear in the mass spectra of aromatics and substituted aromatics than others. The problem is greatly simplified by the absence of large amounts of nitrogen, oxygen, and sulfur containing compounds. Low sulfur content allows us to eliminate consideration of sulfur containing structures for the coal liquids, but not the petroleum gas oil, which contains 2.8 per cent sulfur. A consideration of the likely representative structural combinations and ions produced from those structures shows that by monitoring for a limited set of single ions representing likely fragments or molecular ions from those structures, we can characterize the ring number distribution for the sample by determining whether the observed masses are consistent with the expected ring number. For example, masses 270 and 280 are likely masses from 1 ring aromatics possessing typical alkyl or naphthenic substitution. The region of mass 270-280 was chosen because it is the minimum mass range of 6 ring aromatics. Since the average MW of these compounds is about 350, ions in this mass range will almost always represent the larger of any fragment ions produced. Unsubstituted, or minimally substituted 3 ring or 4 ring compounds such as pyrene and methyl pyrenes will not be observed within this mass range, but their elution positions in the HPLC separation are already well known from model compound studies. Masses 280 and 276 are likely products of 2 ring aromatics, and mass 276 of 3 ring aromatics. Likely masses for 4, 5 and 6 ring aromatics are derived from the same set, 270 and 276 for 4 rings, 280 for 5 rings, and 276 for 6 rings. Thus by monitoring for only three ions, 270, 280, and 276, and by reasoning that 4 ring aromatics will not likely fall into the same LC ring fraction as 1 or 2 ring aromatics, and 5 ring aromatics will not coelute with 2 ring, etc. we can obtain additional confirmation of the ring number content of each fraction by GC-MS. Of course this procedure may not work for some unusual structure types, some of which

we must expect, but it should hold true for most common structures such as those found in these fractions.

Figure 2 shows the GC-MS single ion chromatograms for 1 through 4 ring fractions of the Illinois coal liquid. Figure 2a shows the predominance of masses 270 and 280 in the 1-ring fraction. The absence of mass 276 suggests the absence of significant 2 or 3 ring material in this fraction. A heart cut of the 2 ring region taken from the Illinois coal liquid is shown in Figure 1b. No significant signal at mass 270 is found in this Figure indicating that no 1 ring material overlapped the fraction. Figure 2c shows exclusively 3 ring material in the 3 ring fraction as evidenced by the presence in significant quantity of only mass 276. Figure 2d shows a fraction from the 4 ring region containing exclusively ion mass 270, suggesting a relatively pure 4 ring fraction, without significant 3 or 5 ring "contamination". Similar ion chromatograms from later fractions showed significant overlap between 5 and 6 ring components.

CONCLUSIONS

The preparative DNAP column was found to effectively separate coal liquid aromatics fractions by ring number with only limited overlap. Distinct changes in UV spectra and GC-MS data were observed in the same boundary regions between ring numbers determined by use of model compounds. Boundary regions were less sharp for the petroleum gas oil as a result of the greater degree of alkyl substitution and the presence of significant sulfur containing components. Preparative HPLC is seen to be a very effective way of simplifying complex hydrocarbon mixtures for further study and characterization. The coal aromatics were found to consist mainly of polynuclear aromatics with limited alkyl substitution. This was especially true of the Black Thunder Coal liquid, which contained primarily 3, 4 and 5 ring material. The larger ring structures in the Black Thunder material were probably the result of the thermal-catalytic two-stage liquification process used in it's preparation. The Pittsburgh and Illinois coals were produced using a more severe catalytic-catalytic process and, as a result, contained generally smaller aromatic ring structures. The petroleum gas oil was found to contain more heavily alkyl substituted structures than the coal liquids, based on differences in UV spectra and gas chromatogram complexity. Gravimetric quantification of coal liquid ring fractions yielded results for ring number distributions similar to those obtained by low resolution, hydrocarbon type mass spectroscopy.

REFERENCES

1. S. M. Fatemi, D. C. Cronauer, and R. T. Lagman, "Separation and Characterization of Coal Liquids from Wilsonville", 1992 ACS Meeting, Div. of Fuel. Chem., Washington, D.C.
2. P. L. Grizzle and J. S. Thomson, Anal. Chem., 54, 1071 (1982)
3. J. S. Thomson and J. W. Reynolds, Anal. Chem., 56, 2434 (1984)
4. C. J. Robinson and G. L. Cook, Anal. Chem., 41, 1548 (1969)

TABLE I

RING NUMBER DISTRIBUTION BY PREPARATIVE HPLC COMPARED TO MASS SPECTROSCOPY

	Aromatic Rings				
	1	2	3	4	5+
Illinois No. 6					
HPLC	22.7%	48.2%	20.2%	8.5%	0.4%
MS	23.3	37.3	21.7	11.4	0.4
Black Thunder					
HPLC	12.1	24.8	19.3	37.1	6.7
MS	14.4	23.0	23.9	29.5	2.1
Pittsburgh No. 8					
HPLC	30.2	36.9	18.9	11.9	1.7
MS	29.7	33.2	18.4	13.7	1.1

Notes:
1. All HPLC data were obtained using the same dividing points. Dividing points were identified by spectra, model compounds, and GC-MS.
2. MS data do not add up to 100% because of the presence of unidentified species in the MS results.

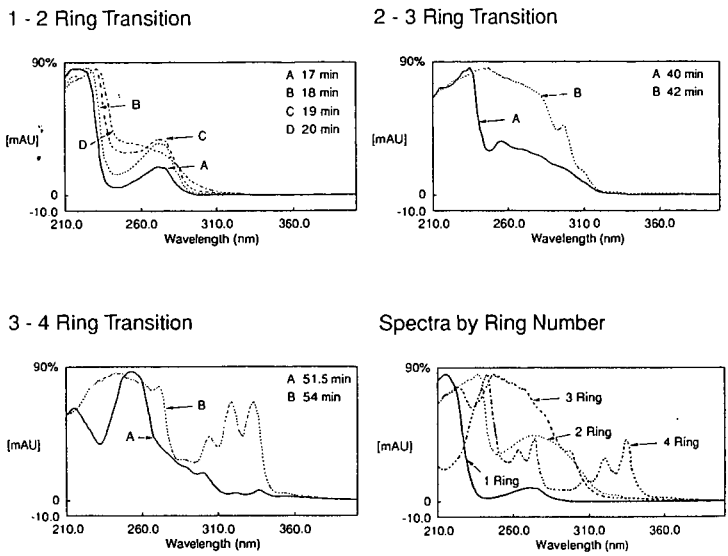

Figure 1. UV Spectra at different retention times.

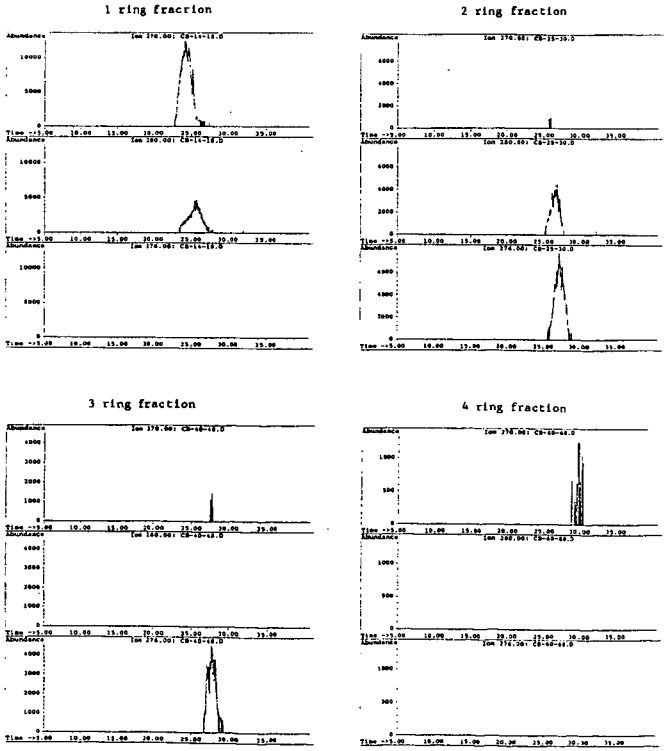

Figure 2. GC-MS ion chromatograms of ring fractions of Illinois No. 6 coal liquid.

CHARACTERISATION OF PITCH FRACTIONS BY QUANTITATIVE SOLID STATE ^{13}C NMR

J.M. Andresen [1], P.R. Dennison [1], M.M. Maroto-Valer [1], C.E. Snape [1], R. Garcia [2] and S.R. Moinelo [2]

[1] University of Strathclyde, Dept. of Pure & Applied Chemistry, Glasgow G1 1XL, UK
[2] Instituto Nacionale del Carbon, CSIC, 33080 Oviedo, Spain

Keywords: ^{13}C NMR, single pulse excitation, quaternary aromatic carbon

INTRODUCTION

Thermal and other pretreatments of pitch fractions are being widely investigated as a means to increase the extent of mesophase formation in relation to the production of high performance carbons [1-3]. The structural changes that occur can be assessed using carbon skeletal parameters but, although solid state ^{13}C NMR has been used for this purpose [4-7], the quantitative reliability of the technique has still to be established for pitch fractions. It was demonstrated previously [7] that, as for coals [8], cross-polarisation (CP) can vastly underestimate quaternary aromatic carbon concentrations. A combination of a low magnetic field strength to avoid problems with spinning sidebands and the simple Bloch decay or single pulse excitation (SPE) technique is now generally recognised as offering the most satisfactory approach for obtaining quantitative ^{13}C NMR results.for coals and related materials [8-11]. In this study, single pulse excitation (SPE) and associated relaxation measurements have been conducted at low field on coal-derived pitches and their toluene-insoluble (TI) fractions, together with a biomass-derived pitch and the results compared with those from CP.

EXPERIMENTAL

The elemental compositions of the whole coal tar pitch (CTP), the TI fraction from a CTP and the biomass pitch prepared from Eucaliptus Saligna wood are listed in Table 1.

All the ^{13}C NMR measurements were carried out at 25 MHz on a Bruker MSL100 spectrometer with MAS at 5.0 kHz as described previously [8] to give spectra in which the sideband intensities are only *ca* 7-8% of the central aromatic bands. Typically, *ca* 250 mg of sample was packed into the zirconia rotors. The ^{1}H decoupling and spin-lock field was *ca* 60 kHz and, for SPE, the 90° ^{13}C pulse width was 3.3 µs. ^{13}C thermal relaxation times (T_1s) of the pitch fractions were determined using the CP pulse sequence devised by Torchia [12] with a contact time of 5 ms in most cases. Tetrakistrimethylsilane (TKS) was added to the samples as an intensity standard. Variable contact time CP experiments were used to estimate ^{1}H rotating frame relaxation times ($T_{1\rho}$s) and the characteristic time constant for CP (T_{CH}).

Table 1 Elemental compositions of the pitch samples investigated

		Whole CTP	Toluene-insolubles	Biomass pitch
	C	94.8	92.1	72.0
%	H	5.7	4.8	6.6
	N	1.0	1.1	0.6
	S	N.D.	0.4	N.D.
	O [a]	<1	1.6	20.8
	H/C	0.57	0.62	0.91

[a] = by difference. N.D. = not determined

Depending upon the ^{13}C T_1s, relaxation delays between 50 and 80 s were used for all the normal and variable delay dipolal dephasing (DD) SPE measurements At least 5 dephasing periods in the range of 50 to 500 us were used before the first rotational modulation and this was sufficient to allow an estimate of the decay constant of the non-protonated aromatic carbon. In order to allow for variations in tuning for the variable delay DD and CP experiments, blocks of 64 scans were successively accumulated for each delay, the total number of scans being 512. No background signal was evident in the SPE spectra from the Kel-F rotor caps. All the FIDs were processed using a line broadening factor of either 20 or 50 Hz. The measurement of the small aliphatic peak areas was conducted manually as this was found to be generally more precise than using the integrals generated by the spectrometer software.

RESULTS AND DISCUSSION

Quantitative reliability Table 2 summarises the relaxation parameters determined for the whole CTP and TI fraction. The variation of the aromatic carbon peak intensity in the Torchia ^{13}C T_1 method for the CTP is presented in Figure 1. The ^{13}C T_1s for the quaternary aromatic carbons (longer component where two are listed, Table 1) are *ca* 10 and 15 s, respectively for the whole CTP and TI fraction meaning that recycle delays of 50 and 75 s are required in SPE to ensure virtual complete relaxation of the ^{13}C spins between succesive pulses. The hydrogen T_1s (T_1^H, Table 1) and rotating frame relaxation times ($T_{1\rho}^H$) are shorter for the TI fraction, mainly due to the presumed higher concentration of free radicals. The long T_1^H for the whole CTP means that, even in CP, a recycle delay of *ca* 10-15 s is appropriate to ensure complete relaxtion of the proton spins.

Table 2 Relaxation parameters for the coal tar pitch samples

Sample	T_1^H /ms	T_{CH} /µs	$T_{1\rho}$ /ms	T_{1C} /s
Whole pitch	1100 (77%)	42 (44%)	5.4	15.2 [(a)]
	3200 (23%)	780 (56%)		
Toluene-insolubles	0.2 (59%)	27 (68%)	1.5 (68%)	1.0 (32%)
	60 (41%)	310 (32%)	11 (32%)	10.0 (68%)

(a) = for quaternary aromatic carbon only.

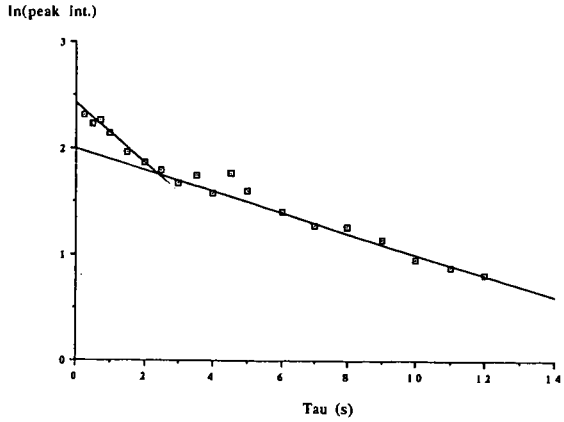

FIGURE 1 DECAY OF AROMATIC PEAK INTENSITY FOR THE TOLUENE-INSOLUBLE FRACTION IN DETERMINATION OF ^{13}C THERMAL RELAXATION TIMES

Figure 2 shows SPE spectra for the whole CTP and TI fraction. The use of TKS as an intensity standard has indicated that *ca* 90% of the carbon was observed by SPE in both fractions with a relaxation delay of 50 s (Table 3). As anticipated, the aromaticities are nearly 1 for both fractions but lower values (0.95-0.97 with a 1 ms contact) have been obtained by CP (Table 3).

Quaternary aromatic carbon Table 3 lists the aromaticities and fractions of quaternary carbon (C_q/C_A) derived from the SPE spectra for the whole CTP and TI fraction. Figure 3 compares the aromatic carbon intensity plots obtained from DD using SPE and CP with a 1 ms contact for the TI fraction. As for coals [8], CP grossly underestimates quaternary aromatic carbon concentrations. Although the value of 0.58 for C_q/C_A obtained with a contact time of 5 ms is significantly higher than that for 1 ms (0.40), it is still ,much lower than that 0.70 from SPE. The agreement between CP DD value of 0.58 for C_q/C_A and that of 0.68 for the slower relaxing carbon in the two component fit for the ^{13}C T_1 relaxation behaviour (Figure 1) is reasonably good, considering the experimental error for the latter.

As there is little aliphatic carbon and oxygen in the CTP samples (Tables 1 and 3), the errors involved in deducing the bridgehead aromatic carbon concentrations (C_{BR}/C) from the values for C_q/C_A are relatively small. The results obtained indicate that the average size of the aromatic nuclei correspond to 6/7 ring peri-condensed structures for the whole CTP and, as expected, considerably larger entities for the TI fraction

Aliphatic carbon Since the ^{13}C T_1s of the aliphatic carbons are much shorter than those of the quaternary aromatic carbons, reasonably accurate results can thus be obtained with much shorter recycle times. Figure 4 compares the aliphatic

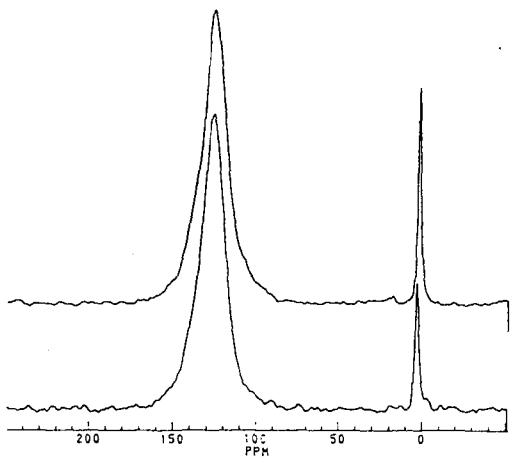

FIGURE 2 SPE ^{13}C NMR SPECTRA OF WHOLE CTP AND TOLUENE-INSOLUBLE FRACTION CONTAINING TKS

Table 3 Structural parameters for the coal tar pitch samples

Sample	Aromaticity, f_a	f_q	C_{BR}/C	% of C obs.
Whole pitch	0.98 (0.95)	0.52	0.50	93
Toluene-insolubles	>0.99 (0.97)	0.70	0.68	90

f_q = fraction of quaternary carbon of total aromatic carbon.
C_{BR}/C = mole fraction of bridgehead aromatic carbon.

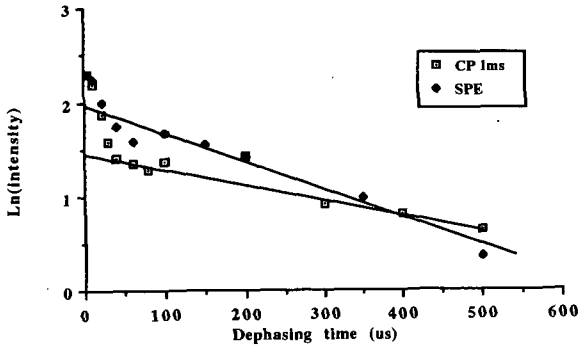

FIGURE 3 COMPARISON OF AROMATIC PEAK INTENSITIES FROM THE SPE AND CP (1 ms CONTACT) DIPOLAR DEPHASING EXPERIMENTS ON THE TOLUENE-INSOLUBLE FRACTION

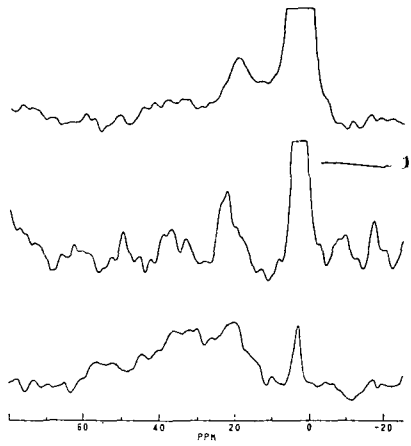

FIGURE 4 ALIPHATIC CARBON BANDS FROM SPE AND CP SPECTRA OF THE TOLUENE-INSOLUBLE FRACTION

regions from the SPE spectrum of the TI fraction obtained with a recycle delay of only 5 s with those from the CP spectra obtained with contact times of 0.5 and 2 ms. Although the signal to noise ratios are understandably low, the proportion of CH_3 (10-25 ppm) observed at the shorter contact time is only 30-40% of the aliphatic carbon due to the incomplete CP of the rotationally mobile CH_3. The proportion observed is higher at the longer contact time of 2 ms but the signal to noise ratio is less than in the SPE spectrum which indicates that CH_3 accounts for at least 60 to 70% of the aliphatic carbon.

Biomass pitch Figure 5 shows the spectra obtained by SPE with a 50 s relaxation time and by CP with a 1.5 ms contact time. Table 4 lists the relaxation parameters and the carbon aromaticity. As for the CTP, over 90% of the carbon was observed by SPE with a relaxation delay of approximately 5 times the ^{13}C T_1 for quaternary aromatic carbons (*ca* 10 s, Table 4). The biomass pitch is structurally diverse with methoxyl groups (peak at 55 ppm, Figure 5) surviving the carbonisation which clearly indicates that tar evolves at relatively low temperatures. The carbon aromaticity of 0.60 obtained by SPE compares with that of 0.58 from CP suggesting that., as for wood and other lignocellulosic materials [13], the discrimination against aromatic carbon is not as great as for low-rank coals.

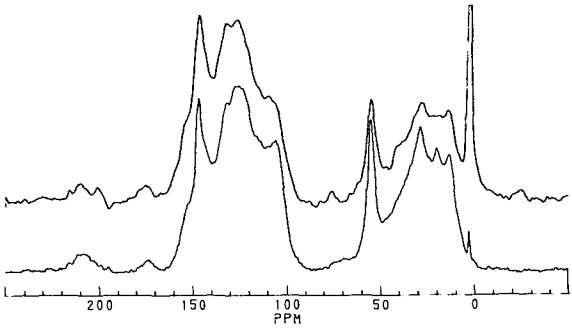

FIGURE 5 SPE AND CP (1 ms CONTACT) SPE ^{13}C NMR SPECTRA OF THE BIOMASS PITCH

Table 4 Structural and relaxation parameters for the biomass pitch.

T_1^H/ ms	T_1^C aromatic /s	% C observed	Aromaticity, f_a
46 (80%)	9.8 (44%)	96	0.60
91 (20%)	0.8 (56%)		(0.58) [(a)]

[(a)] = CP value with a contact timre of 1 ms.

CONCLUSIONS

^{13}C thermal relaxation times for quaternary aromatic carbons in coal tar and biomass pitches investigated are in the range 10-15 s and, provided that suitably long relaxation delays are used in SPE, over 90% of the carbon is observed. Further, the self-consistent quaternary aromatic carbon concentrations derived by SPE-DD are higher than those obtained from CP, even with long contact times. SPE has indicated that the aliphatic carbon present in the CTP TI fraction investigated is predominately methyl.

ACKNOWLEDGEMENTS

The authors thank the the Science and Engineering Research Council (Grant no. GR/F/87264) and the European Community (Contract No. CI 1-CT92-0028, DGXII-G) for financial support and C. Luengo of the Universidade Estadual de Campinas, Brazil for supplying the wood-derived pitch.

REFERENCES

1. H. Marsh and R. Menendez, Fuel Process. Technol., **20**, 269 (1988).
2. Z, Weishauptova, J. Medek and M. Rada, Fuel, **73**, 177 (1994).
3. M. Matsumoto, M. Higuchi, T. Tomioka and H. Sunago, Fuel, **73**, 237 (1994).
4. P. Oliver and B.C. Gerstein, Carbon, **22**, 409 (1984).
5. H. Sfihi, P. Tougne and A.P. Legrand, Fuel Process. Technol., **20**, 43 (1987).
6. A. Grint, G.P. Proud, I.J.F. Poplett, K.D. Bartle, S.Wallace and R.S. Matthews, Fuel, **68**, 1490 (1989).
7. C.E. Snape, A.M. Kenwright, J. Bermejo, J. Fernandez and S.R. Moinelo, Fuel, **68**, 1605 (1989).
8. G.D. Love, R.V. Law and C.E. Snape, Energy & Fuels, **7**, 639 (1993).
9. C.E. Snape, D.E. Axelson, R.E. Botto, J.J. Delpuech, P. Tekely, B.C. Gerstein, M.Pruski, G.E. Maciel and M.A. Wilson, Fuel, **68**, 547 (1989) and references therein.
10. J.A. Franz, R. Garcia, J.C. Linehan, G.D. Love and C.E. Snape, Energy & Fuels, 1992, **6**, 598.
11. Muntean, J.V. and Stock, L.M., Energy & Fuels, **5**, 767 (1991).
12. D.A. Torchia,, J. Magn. Reson., **30**, 613 (1978).
13. G.D. Love, C.E. Snape and M.C. Jarvis, Biopolymers, **32**, 1187 (1992).

CPMAS AND DDMAS ^{13}C NMR ANALYSIS OF COAL LIQUEFACTION RESIDUES

Chunshan SONG,* Lei HOU, Ajay K. SAINI, and Patrick G. HATCHER

Fuel Science Program, Department of Materials Science and Engineering
The Pennsylvania State University, University Park, PA 16802

Keywords: ^{13}C NMR, CPMAS, Coal Liquefaction, Residues

INTRODUCTION

We have shown in previous papers that spectroscopic analyses of liquefaction residues (by NMR, pyrolysis-GC-MS, and FT-IR) can provide important structural information which can be used for elucidating the chemical reactions of liquefaction (Song et al., 1992, 1993, 1994) as well as the effects of dispersed catalysts (Saini et al., 1992; Huang et al., 1993; Song et al., 1994). The present work involves solid-state ^{13}C NMR studies of residues of two subbituminous coals from their liquefaction at 300-425°C, using cross-polarization (CP), dipolar dephasing (DD) and magic-angle-spinning (MAS) techniques. A preliminary survey of some CPMAS ^{13}C NMR results for one of the two coals was presented previously (Song et al., 1993). In a companion paper, we report on the analysis of oils from liquefaction of these coals by two-dimensional HPLC and GC-MS (Saini and Song, 1994).

EXPERIMENTAL

Sample Preparation. Three types of samples were examined in this study. The first set of samples are THF-insoluble residues from temperature-programmed liquefaction (TPL) of a Montana subbituminous coal (DECS-9) in tetralin solvent at a final temperature ranging from 300°C to 425°C for 30 min (Song et al., 1992). The second set of samples are THF-insoluble residues from liquefaction of a Wyodak subbituminous coal (DECS-8) at 350°C with and without a solvent (Song et al., 1994). The coals were predried in vacuum at about 100°C for 2 h prior to liquefaction. The third set of samples are the fresh raw coals (DECS-8, DECS-9) and THF-extracted but unreacted coals. Our experience shows that trace amounts of THF always remain in the THF-extracted residues even after vacuum drying at 100°C for over 6 h, which interferes with spectroscopic analysis. We have solved the problem by washing the residue first with acetone, then with pentane, followed by vacuum drying at 100°C for 6 h prior to spectroscopic analysis. The residue samples were also subjected to elemental analysis.

Solid-State ^{13}C NMR. NMR spectra were acquired on a Chemagnetics M-100 spectrometer. The measurements were carried out at a carbon frequency of 25.035 MHz. The spectrometer performance was checked with a standard sample of hexamethylbenzene to assure the Hartman-Hahn match. In a typical analysis, about 0.4-0.6 g of a sample was packed in a 0.4 mL bullet-type rotor made of polychlorotrifluoroethylene (Kel-F). Kel-F does not have a CPMAS ^{13}C signal. The MAS speed of the rotor was about 3.5 kHz.

The CPMAS ^{13}C NMR spectra were obtained by using the combined high power proton decoupling, cross-polarization, and magic angle spinning techniques. The experimental conditions for all the samples are as follows: a cross-polarization contact time of 1 msec, a pulse delay time of 1 sec, 50 kHz of proton decoupling, sweep width of 14 kHz, and 20-30 Hz line broadening. Carbon aromaticity was determined by integrating the peaks between 95 and 165 ppm (ppm relative to tetramethylsilane). Spinning sideband intensity was distributed for aromatic carbons. Other details concerning CPMAS maybe found elsewhere (Hatcher, 1987).

Dipolar-dephasing ^{13}C NMR spectra (DDMAS) were acquired by using the pulse sequence described by Alemany et al. (1983) and Wilson et al. (1984). After the protons are spin-locked and cross-polarization is induced, a variable dephasing time T_{dd} is inserted, during which the high-power decoupler is turned off. During this period, which lasts from 5 to 180 μsec, carbon magnetization becomes influenced and diminished (dephased) by the strong dipolar interactions between ^{13}C and ^{1}H spins. Carbons directly bonded to hydrogens (protonated carbons) dephase much more rapidly than those without attached hydrogens (non-protonated carbons). More details about the theory and procedures of dipolar dephasing may be found elsewhere (Hatcher, 1987, 1988; Pan and Maciel, 1993). In general, protonated carbons dephase within the first 60 μsec (T_{dd}), and the signals remain after 60 μsec are due to non-protonated carbons.

RESULTS AND DISCUSSION

Structural Characteristics of THF-extracted Coals

Figure 1 shows the CPMAS and DDMAS ^{13}C NMR spectra of THF-extracted but unreacted Montana subbituminous coal (DECS-9). In the CPMAS spectrum, there are two major bands, an aromatic bands from 95 to 165 ppm and an aliphatic band from 0 to 80 ppm. Among the aliphatic bands, methyl carbons appear at 0-25 ppm, methylene carbons resonate between 25-51 ppm, methoxyl groups around 51-67 ppm and ether groups between 67-93 ppm (Yoshida et al., 1987). The aromatic region includes two shoulders which may be attributed to catechol-like oxygen-bound carbons (centered around 142-144 ppm) and phenolic carbons (centered around 152-154 ppm). There are two other bands with lower intensities, including carboxyl groups between 170-190 ppm and ketonic carbonyl groups between 190-230 ppm.

* Corresponding author.

DDMAS ^{13}C NMR was used to examine the degree of protonation of carbons. Protonated carbons decay at a rate that is dependent on T_{dd}^2 and is often referred to as the Gaussian component of signal decay; non-protonated carbons decay at a much slower rate that is exponential with respect to T_{dd} (Alemany et al., 1983). Compared to the CPMAS spectrum , signal decay in the 95-165 ppm region was due mainly to protonated aromatic carbons (95-130 ppm). The signal intensity remaining in the aromatic region in the DDMAS spectrum in Figure 1 can be attributed to bridgehead and substituted aromatic carbons (130-148 ppm) and oxygen-bound aromatic carbons (140-165). Apparently, the shoulders that we identified as catecholic (structure I) and phenolic (structure II) carbons remain in the DDMAS structure and are clearly non-protonated carbons.

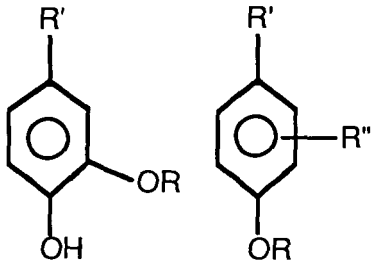

Str. I Str. II

Our assignment of the peak centred at 142-144 ppm in the DDMAS spectra is different from that of Pan and Maciel (1993). They assigned the 144 ppm peak for Beulah-Zap lignite (801) to an aniline-type aromatic carbon. We have assigned this peak to the catecholic oxygen-bound aromatic carbon (shown in structure I). This is based on the NMR spectra of lignin-related model compounds and lignin (Hatcher, 1987) and the combined CPMAS NMR and pyrolysis-GC-MS studies of low-rank coals, including DECS-9 (Song et al., 1993) and DECS-8 (Saini et al., 1992) coals used in this work, as well as a lignite (Wenzel et al., 1993).

Flash pyrolysis GC-MS of lignites (Hatcher et al., 1988; Wenzel et al, 1993), DECS-9 Montana coal (Song et al., 1993), and DECS-8 Wyodak coal (Saini et al., 1992) revealed that catechol and phenol as well as their homologs are important components in the pyrolyzates of low-rank coals. Another important evidence is that as catechol observed in the pyrolysis-GC-MS diminishes, so does the catecholic peak in the CPMAS ^{13}C NMR spectra (Hatcher et al., 1988; Song et al., 1993; Wenzel et al., 1993).

Quantitative CPMAS NMR analysis of Montana coal was performed by means of curve-fitting, as described in our recent paper (Song et al., 1993). This coal has 63-64% aromatic carbons among total carbons. Combination of DDMAS and CPMAS NMR data reveals that about 34-35% of the aromatic carbons are protonated carbons; 23-24% of aromatic carbons are chemically bound to oxygen atoms; the remaining 31-33% aromatic carbons are bound primarily to other carbon atoms and secondarily to nitrogen and sulfur. The above spectroscopic results suggest that the Montana coal contains approximately two or three protonated carbons, one or two oxygen-bound carbons, and two substituted or bridgehead carbons per aromatic ring.

Compared to the Montana coal, THF-extracted Wyodak subbituminous coal (DECS-8) has a lower aromaticity (57%). However, it also has all the characteristic peaks (aliphatic, aromatic, carboxyl, carbonyl) and shoulders (phenolic, catecholic) that DECS-9 Montana coal possess (Figure 1). The DDMAS ^{13}C NMR data are not available for this sample at the present time.

Characterization of Residues from Non-Catalytic Liquefaction

Figure 2 presents the CPMAS and DDMAS ^{13}C NMR spectra of THF-insoluble residue from non-catalytic TPL of a Montana subbituminous coal (DECS-9) in the presence of tetralin solvent at a final temperature of 350°C for 30 min. Details of TPL procedures and results may be found elsewhere (Song and Schobert, 1992). Comparative examination of DDMAS data indicates at least three trends. First, relative to the THF-extracted unreacted coal, non-protonated carbons contribute more to the aromatic band in the residue from 350°C run. Second, the catecholic peak almost disappeared after 30 min at 350°C. Third, phenolic peak does not diminish as much as the catecholic peak upon reaction at 350°C, as can be seen by comparing the two DDMAS spectra (Figures 1 and 2).

Figure 3 shows the CPMAS and DDMAS ^{13}C NMR spectra of THF-insoluble residue from non-catalytic reaction of a vacuum-dried Wyodak subbituminous coal (DECS-8) in the absence of any solvent at 350°C for 30 min under 6.9 MPa H_2. Since no donor solvent or catalyst was used, the coal conversion is very low, only about 12.5 wt%. More liquefaction results of this coal are described elsewhere (Song et al., 1994). The characteristics of both CPMAS and DDMAS spectra of this sample resemble those of the corresponding spectra for residue from Montana coal (Figure 2), although the two samples were derived from different coals under different conditions.

The reaction temperature has the most significant impact on the spectral characteristics of the liquefaction residues. We have performed both DDMAS and CPMAS ^{13}C NMR analysis of the THF-insoluble residues from TPL reactions of Montana coal (DECS-9) at 300, 350°C, 375, 400 and 425°C for 30 min. Catechol-like structures were found to be thermally sensitive and diminish gradually with increasing temperature up to 350°C. The catecholic shoulder at 142-144 ppm disappears from the residue of 375°C run. Carboxyl (165-190 ppm) and carbonyl (190-230) peaks diminish significantly after 375°C and they disappear in the spectrum of residue from 400°C run. Phenolic structures diminish with increasing temperature up to 425°C. These results clearly indicate that there are thermally reactive oxygen functional groups in coal and their reactions can take place at temperatures as low as 300-375°C.

As shown in Figure 4, the carbon aromaticity of residues increased monotonically with increasing reaction temperature after 300°C. Comparison of the curve for H/C atomic ratio and that for carbon aromaticity

indicates that THF extraction of unreacted coal and that reacted at 300°C, removed more aliphatic materials. However, the conversion level at 300°C in tetralin is below 10 wt% (dmmf). The H/C ratio of the residues decreased significantly with increasing temperature up to 425°C. The aromaticity of the residues increased with increasing coal conversion, being consistent with the observations by two other groups on residues from liquefaction (Fatemi-Badi et al., 1991; Franco et al., 1991). The increase in carbon aromaticity is driven primarily by temperature, and secondarily by the adduction of aromatic solvent molecules (Song et al., 1993, 1994). Another interesting observation is that, while the total aliphatic carbons decrease, the percentage methyl carbons relative to total aliphatic carbons increases with increasing temperature up to 425°C.

DDMAS analysis (Figure 5) shows that the degree of protonation of aromatic carbons in the residues decreased from 35% (for THF-extracted but unreacted Montana coal) to 13% for residue from the non-catalytic run at final reaction temperature of 375°C. General trends observed from DDMAS experiments for residues from DECS-9 are as follows. The degree of protonation of aromatic carbons in the residue decreases with increasing coal conversion. In other words, the higher the coal conversion into THF-soluble products, the more non-protonated aromatic carbons in the THF-insoluble residues. The higher content of non-protonated carbons among total aromatic carbons could originate from either higher degree of condensation or higher extent of substitution. Since the aromaticity increases and atomic H/C ratio decreases with increasing temperature, the decrease in the relative content of protonated aromatic carbon (or the increase of non-protonated aromatic carbons) is due mainly to the increased degree of condensation. This means that there are more bridgehead aromatic carbons or more condensed-ring aromatic structures in the residues from runs at higher temperatures.

As discussed above, there exists good correlation between carbon distribution and reaction temperature above 300°C. We have attempted mathematical correlation of the NMR data for the residue with reaction temperature (Song et al., 1993). Figure 6 shows that the changes in the aromatic, aliphatic, and oxygen-bound carbons of the residues can be related to the liquefaction temperature by a linear correlation. A general expression is given below:

$$C_i = \alpha f_i + \beta T \qquad \text{for specific carbon type } i \qquad (1)$$

where T is reaction temperature (°C), f_i and C_i represent the content of specific carbons (%) in the original coal and residue, respectively, and α and β are constants. The specific correlations for aromatic C (C_{ar}), aliphatic C (C_{ali}), and oxygen-bound carbons (C_{O-C}) are given in Figure 6. We have quantitatively analyzed the NMR spectra of 26 residues from liquefaction of DECS-9 coal under various conditions with and without solvents (Song et al., 1993). The results show that equation 1 holds for all the cases with good linear correlation.

REFERENCES

Alemany, L.B.; Grant, D.M.; Alger, T.D.; Pugmire, R.J. J. Am. Chem. Soc., 1983, 105, 6697.
Franco, D.V.; Gelan, J.M.; Martens, H.J.; Vanderzande, D.-J.-M. Fuel, 1991, 70, 811-817.
Hatcher, P.G. Org. Geochem., 1987, 11 (1), 31-39.
Hatcher, P.G. Energy & Fuels, 1988, 2 (1), 48-58.
Hatcher, P.G.; Lerch III, H.E.; Kotra, R.K.; Verheyen, T.V. Fuel, 1988, 67, 1069-1075.
Hatcher, P.G.; Wilson, M.A.; Vassallo, A.M.; Lerch III, H.E. Int. J. Coal Geol., 1989, 13, 99-126.
Huang, L.; Song, C.; Schobert, H.H. Am. Chem. Soc. Div. Fuel Chem. Prepr., 1993, 38 (3), 1093-1099.
Saini, A. K.; Song, C.; Schobert, H. H.; Hatcher, P. G. Am. Chem. Soc. Div. Fuel Chem. Prepr., 1992, 37 (3), 1235-1242.
Saini, A. K.; Song, C. Am. Chem. Soc. Div. Fuel Chem. Prepr., 1994, 37 (3-4), in press.
Pan, V.H.; Maciel, G.E. Fuel, 1993, 72 (4), 451-468.
Song, C.; Schobert, H.H.; Hatcher, P.G. Energy & Fuels, 1992, 6 (3), 326-328.
Song, C.; Schobert, H.H. Am. Chem. Soc. Div. Fuel Chem. Prepr., 1992, 37 (2), 976-983.
Song, C.; Hou, L.; Saini, A.K.; Hatcher, P.G.; Schobert, H.H. Fuel Processing Technol., 1993, 34 (3), 249-276.
Song, C.; Saini, A.K.; Schobert, H.H. Energy & Fuels, 1994, 8 (2), 301-312.
Fatemi-Badi, S.M.; Swanson, A.J.; Sethi, N.K.; Roginski, R.T. Am. Chem. Soc. Div. Fuel Chem. Prepr., 1991, 36 (2), 470-480.
Wenzel, K.; Hatcher, P. G.; Cody, G. D.; Song, C. Am. Chem. Soc. Div. Fuel Chem. Prepr., 1993, 38 (2), 571-576.
Wilson, M.A.; Pugmire, R.J.; Karas, J.; Alemany, L.B.; Woolfenden, W.R.; Grant, D.M. Anal. Chem., 1984, 56, 933-943.
Yoshida, T.; Maekawa, Y., Fuel Processing Technol. 1987, 15, 385-395.

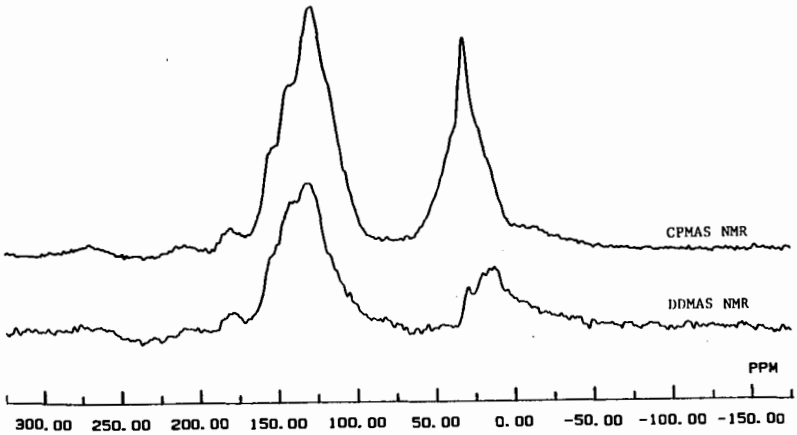

Figure 1. CPMAS and DDMAS ^{13}C NMR spectra of THF-extracted but unreacted Montana subbituminous coal (DECS-9). For DDMAS, Tdd = 60 μs.

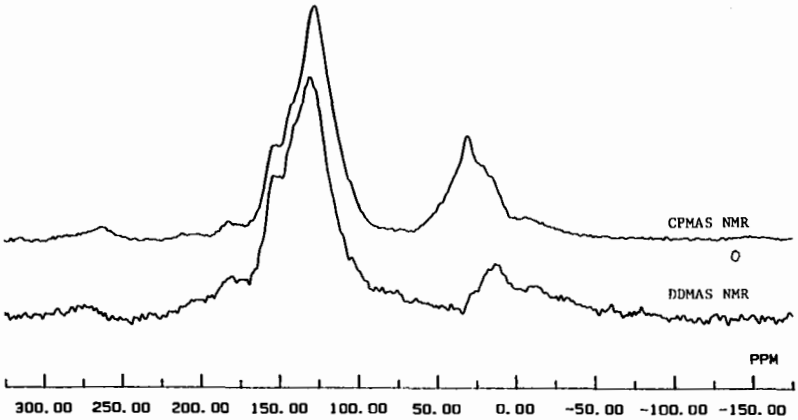

Figure 2. CPMAS and DDMAS ^{13}C NMR spectra of residue from TPL of Montana coal in the presence of tetralin at a final temperature of 350°C for 30 min. For DDMAS, Tdd = 60 μs.

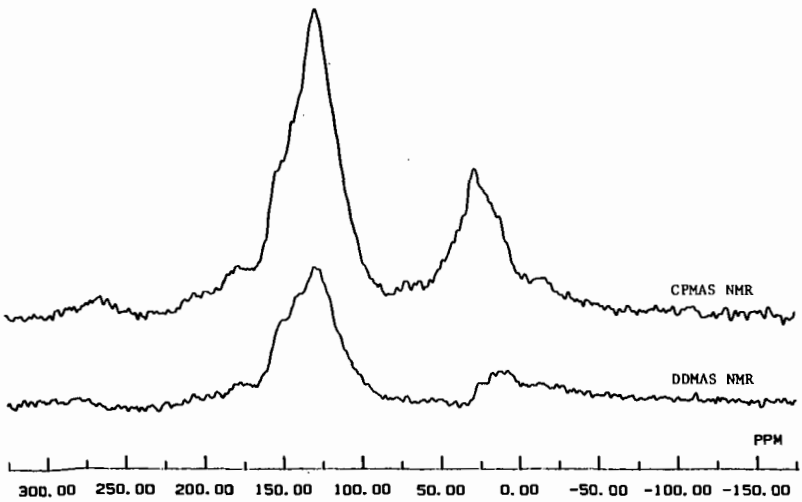

Figure 3. CPMAS and DDMAS ^{13}C NMR spectra of residue from liquefaction of Wyodak coal (DECS-8, vacuum-dried) without any solvent at 350°C for 30 min. For DDMAS, Tdd = 60 μs.

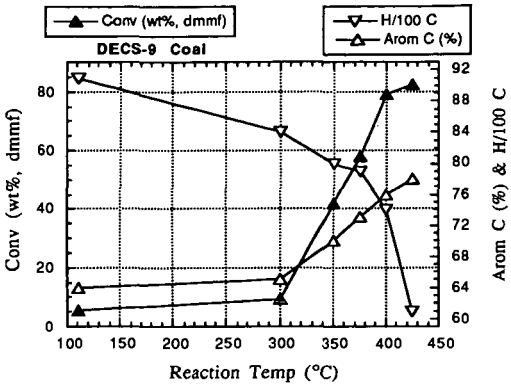

Figure 4. Conversion of Montana coal and changes in aromaticity (Arom C, %) and No. of H atoms/100 C in the residues versus final temperature of liquefaction (TPL) in tetralin.

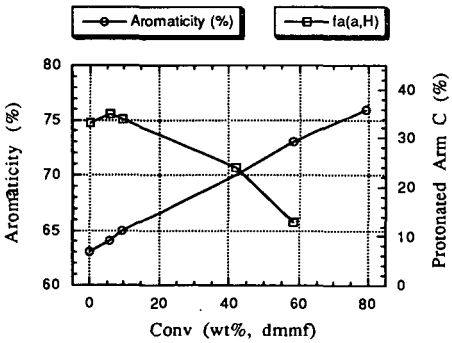

Figure 5. Change of aromaticity and percentage degree of protonation of aromatic carbons [fa(a,H)] . in the residues versus conversion of DECS-9 Montana coal in TPL with tetralin.

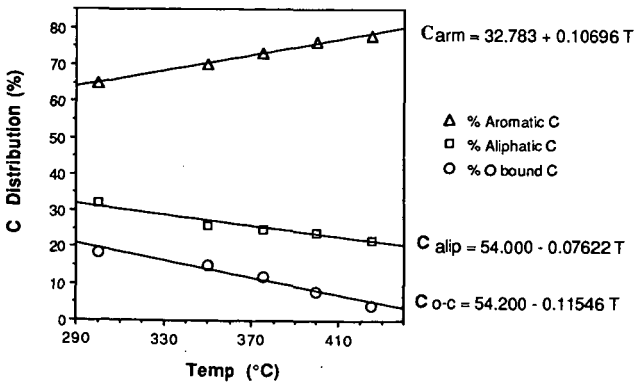

Figure 6. Linear correlation of contents of aromatic, aliphatic, and total oxygen-bound carbons in residues from DECS-9 Montana coal with final temperature of TPL in tetralin.

SCOPE AND LIMITATION OF RUTHENIUM ION CATALYZED OXIDATION OF COAL AS AN ANALYTICAL TOOL FOR AN ALIPHATIC PORTION OF COAL ORGANIC MATERIALS

Satoru Murata, Ken-ichi U-esaka, Hirohiko Ino-ue, and Masakatsu Nomura*
Department of Applied Chemistry, Faculty of Engineering, Osaka University, Suita, Osaka 565, Japan

Keywords: Ruthenium tetroxide, Oxidation of coal, Aliphatic portion of coal

Introduction

We have been investigating a chemical structure of Japanese bituminous Akabira coal by Curie-point pyrolysis GC/MS coupled with CP/MAS ^{13}C NMR and proposed a unit chemical structure of the coal on the basis of these results.[1] In that paper, we had pointed out more precise and quantitative evaluation of chemical bonds connecting aromatic rings should be clarified in order to evaluate more precise chemical structures of coal organic materials (COM). As for this, Stock *et al.*, investigated ruthenium ion catalyzed oxidation (RICO) of coal.[2] Ruthenium tetroxide is well known to have a property to attack selectively sp^2 carbons of organic substrates: for example, in this oxidation arylalkanes and diarylalkanes could be converted to aliphatic monocarboxylic and dicarboxylic acids, respectively. One of the most critical points of this reaction is believed to be the difficulty in attaining quantitative analyses of lower carboxylic acids because they are main products, showing high volatility. Stock *et al.* and Strausz *et al.* had applied the isotope dilution method[2] and esterification with phenacyl bromide[3] for the quantitative analysis, respectively. The former, however, needs preparation of deuterium-labeled carboxylic acids and the later has a slow rate of conversion of the carboxylic acids to their phenacyl esters.

In this paper, we have examined quantitative determination of carboxylic acids resulted from RICO reaction and proposed the method to accomplish this, applying this for RICO reaction of Illinois #6 (American subbituminous), Akabira (Japanese bituminous), and Zao Zhuang (Chinese bituminous) coals.

Experimental Section

Reagents, Samples, and Instruments.

As to Illinois #6 coal, Argonne premium coal sample was used. Whole coals employed in this paper were pulverized under 100 mesh and dried at 100 °C *in vacuo* (5 mmHg) for 10 h prior to use. Solvents were distilled according to conventional methods. Other reagents were commercially available and used without further purification.

Procedure for RICO Reaction of Coal.

$RuCl_3$ (40 mg) and coal (1 g) were add to a 100 ml flask containing MeCN (20 ml), CCl_4 (20 ml), and H_2O (30 ml), the mixture being stirred magnetically for 1 h. $NaIO_4$ (10 g) was added gradually and the resulting mixture was stirred at 40 °C for 24 h. After the end of the reaction, the mixture was filtered to remove an inorganic residue. The filtrate was analyzed with the following two methods; (i) For analysis of lower carboxylic acids ($\leq C_6$), aqueous NaOH solution (5 %, 100 ml) and ether (100 ml) were added to the filtrate and the aqueous phase was separated. This aqucous solution was diluted to 1000 ml by using deionized water and 5 ml portion of this solution was analyzed by a DIONEX 2000i/sp ion chromatograph (HPICE-AS-1 column). (ii) For analysis of higher carboxylic acids ($C_7\leq$), diluted hydrochloric acid (5 %, 100 ml) were added to the filtrate and the resulting solution was extracted with 100 ml of ether, twice. The ethereal solution was dried over sodium sulfate. After evaporation of ether, carboxylic acids produced were esterified with diazomethane and analyzed with a Shimadzu GC-8APF (CBP-1 capillary column, ϕ 0.50 mm x 25 m) and a Shimadzu QP-2000A GC-MS (CBP-1 capillary column, ϕ 0.25 mm x 25 m).

Results and Discussion

Problems in RICO Reaction of Coal.

At first, we have examined availability of ion chromatography to analyze a mixture of lower carboxylic acids. Figure 1 shows ion chromatograms of a model mixture containing succinic, formic, acetic, propionic, butyric, and valeric acids

and RICO products of Akabira coal, this suggesting that peak separation is relatively good and analysis of these carboxylic acids is not disturbed by the presence of I^- and IO_4^- ions contained in the reaction mixture.
We have discussed the possible factors affecting the results of RICO reaction; (i) evolution of acetic acid from hydrolysis of MeCN, (ii) oxidation rate of COM, and (iii) further decomposition of carboxylic acids produced with $RuCl_3$-$NaIO_4$. As to the first possibility, Strausz *et al.* had pointed out that EtCN should be used in place of MeCN for analysis of methyl groups attached to aromatic moieties.[3] In fact, treatment of mixture of MeCN, CCl_4, and H_2O with $RuCl_3$-$NaIO_4$ at 40 °C for 24 h was found to afford acetic acid along with small amount of formic acid. These results suggest that, in this solvent system, reliable yields of carboxylic acids having more than three carbons (propionic acid or higher) could be obtained, however, yield of acetic acid is unreliable because of contamination of the decomposition product from the solvent system. Subsequently, we decided to employ EtCN instead of MeCN, as Strausz *et al.* pointed out. Treatment of a mixture of EtCN, CCl_4, and H_2O with $RuCl_3$-$NaIO_4$ afforded formic, acetic, propionic, and butyric acids, however, yield of acetic acid from EtCN was less than that from MeCN, this suggesting that EtCN is preferable than MeCN for analysis of acetic acid.
Table 1 summarizes the results of treatment of a mixture of lower carboxylic acids with $RuCl_3$-$NaIO_4$ in the two solvent systems (MeCN or EtCN with CCl_4-H_2O). In the case of MeCN, 1.4 mmol excess of acetic acid was observed along with 0.74 mmol of formic acid. On the other hands, in the case using EtCN, excess amounts of acetic acid observed reduced to 0.77 mmol. On the basis of these results, we employed two tertiary solvent systems; one containing EtCN for analysis of acetic acid from α-methyl groups and another containing MeCN for analysis of carboxylic acids with more than three carbons (propionic acid or higher).
RICO reaction was carried out using coal model compounds in the solvent system containing EtCN. The reaction of *p*-cresol and *p*-methylanisole proceeded almost completely, while excess acetic acids (1.1 and 0.6 mmol) were produced. These results suggest that evolution of acetic acid from hydrolysis of EtCN was 0.8 ± 0.2 mmol, this value showing good agreement with the value in Table 1. These results also suggested a reactivity of oxygen containing compounds is relatively high. Since coal usually has these functional groups, it is supposed that the reactivity of coal should be high.

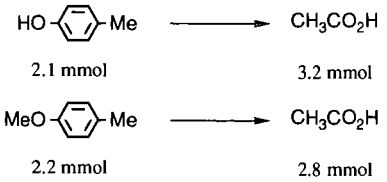

(1)

In order to get more precise information about the conversion rate of coal under above reaction conditions, we have carried out the following experiments; after the end of RICO reaction of Akabira coal, the resulting reaction mixture was filtered, the filter cake being washed thoroughly with water and CH_2Cl_2. The residue was found almost completely to be dissolved in water and CH_2Cl_2, this suggesting that the coal was converted to soluble products almost completely.

RICO Reaction of Three Coals.
Illinois #6 (C 76.6 wt%, daf), Akabira (82.3 %), and Zao Zhuang coals (86.6 %) were employed in this study. As described in the former section, the ion chromatograph was used for analysis of lower carboxylic acids ($\leq C_6$) and GC and GC-MS were used for higher carboxylic acids ($C_7\leq$) after esterification with diazomethane. In the case of the analysis of acetic acid produced, EtCN was used as a co-solvent.
Figure 2 shows gas chromatograms for RICO reaction products of Akabira coal, this indicating that Akabira coal has a wide range of alkyl side chains from C_7 to

C_{30}. Figure 3 shows the plot of yield of whole monocarboxylic acids against carbon numbers. From Figure 3, it is clear that yields of carboxylic acids decreased monotonically from acetic acid to valeric acid, this suggesting that methyl group is dominant substituents of aromatic moieties. This is parallel with the findings reported so far. As to yields of lower carboxylic acids, three coals showed very similar distribution of carboxylic acids, indicating aliphatic substitution of aromatic moieties ranging from methyl to hexyl groups are very similar to each other. These results showed a good agreement with the results reported by Stock *et al.*[2] On the other hands, yields of higher carboxylic acids are different among three coals: a lower rank coal has longer alkyl side chains attached to aromatic moieties than those of higher rank coal.
Since this RICO reaction has some limitations, a precise information about all parts of aliphatic functional groups in COM can be hardly obtained only based on this reaction. However, we have to evaluate this RICO reaction to be able to afford us very useful information about aliphatic portions of COM by the combination use of ^{13}C NMR.

Acknowledgment.
The authors greatly acknowledge the analytical assistance provided by Dr. S. Nishida and Mr. N. Shimo-irisa (KN Lab analysis).

References

(1) Nomura, M.; Matsubayashi, K.; Ida, T.; Murata, S. *Fuel Process. Technol.*, 1992, **31**, 169.
(2) Stock, L. M.; Tse, K.-T. *Fuel*, **1983**, *62*, 974; Stock, L. M.; Wang, S.-H. *Fuel*, **1985**, *64*, 1713; Stock, L. M.; Wang, S.-H. *Fuel*, **1986**, *65*, 1551; Stock, L. M.; Wang, S.-H. *Fuel*, **1987**, *66*, 921; Stock, L. M.; Wang, S.-H. *Energy Fuels*, **1989**, *3*, 535.
(3) Mojelsky, T. W.; Ignasiak, T. M.; Frakman, Z.; McIntyre, D. D.; Lown, E. M.; Montgomery, D. S.; Strausz, O. P. *Energy Fuels*, **1992**, *6*, 83.

Table 1. Treatment of Free Lower Carboxylic Acid with $RuCl_3$-$NaIO_4$ in RCN-CCl_4-H_2O Mixed Solvent[a]

	MeCN			EtCN		
	Used amount (mmol)	Observed amount (mmol)[b]	Difference (mmol)	Used amount (mmol)	Observed amount (mmol)[b]	Difference (mmol)
Formic acid	-	0.74	+0.74	-	0.083	+0.083
Acetic acid	1.74	3.11	+1.37	0.87	1.64	+0.77
Propionic acid	0.64	0.50	-0.14	0.68	0.92	+0.24
n-Butyric acid	0.49	0.48	-0.01	0.59	1.31	+0.72
n-Valeric acid	0.19	0.16	-0.03	0.50	0.47	-0.03

[a]Treatment of carboxylic acids with $RuCl_3$ (40 mg) and $NaIO_4$ (10 g) were carried out in the solvent system containing RCN (20 ml), CCl_4 (20 ml), and H_2O (30 ml) at 40 °C for 24 h. [b]Determined by an ion chromatograph.

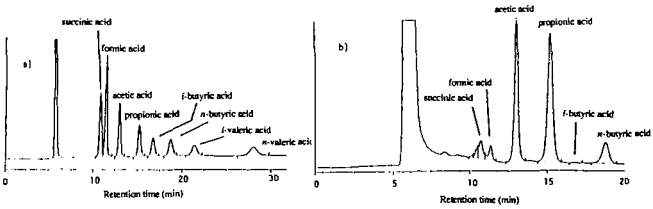

Figure 1. Ion chromatograms of model mixture of lower carboxylic acids (a) and the reaction products from the oxidation of Akabira coal (b)

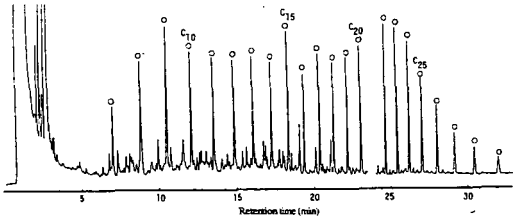

Figure 2. A gas chromatogram for carboxylic acid methyl esters from the oxidation reaction of Akabira coal

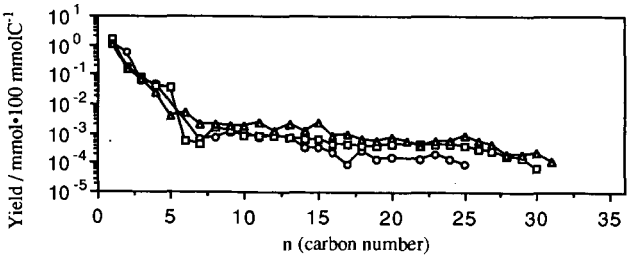

Figure 3. Yields of fatty monoacids, $C_nH_{(2n+1)}CO_2H$, from oxidation of the coals; Illinois No. 6 (△), Akabira (□), and Zao Zhuang coals (○)

Absolute Hydrogen Determination in Coal-Derived Heavy Distillate Samples*

R. J. Kottenstette, D. A. Schneider and D. A. Loy, Dept. 6212 and 1812, Sandia National Laboratories, P.O.Box 5800, Albuquerque, NM 87185.

Keywords: Hydrogen Analysis, Proton NMR, Heavy Distillate

Introduction

Coal liquefaction involves the use of recycle oils to mix slurry feed materials, and transfer hydrogen to coal as it is digested at high temperatures. Hydrogen donating abilities of recycle oils can be measured using Proton Nuclear Magnetic Resonance (^{1}H-NMR) Spectroscopy [1], liquefaction testing [2] and dehydrogenation tests [3]. This paper will describe the absolute determination of total organic elemental hydrogen by ^{1}H-NMR of small (less than one gram) heavy distillate samples produced for research purposes. A comparison will be made between a conventional combustion method and the NMR spectroscopic method.

Organic elemental hydrogen analysis is routinely performed with an automated analyzer having a high temperature combustion zone that is connected to a detector which measures the response of the product water. This technique has its historical roots in the experiments of Lavoisier [4] who in the 1770's burned alcohol and other combustible organic compounds in oxygen to gravimetrically determine the product water and carbon dioxide. Quantitative recovery and measurement of the combustion products were demonstrated by Berzelius and Liebig in the early 1800's. The work of Pregl [5] at the turn of this century advanced this technique to a high degree with the introduction and perfection of microchemical techniques (sample sizes in the milligram range). With the advent of instrumental electronics, automated microanalysis gradually replaced the gravimetric techniques mainly because of increased analysis speed. Modern automated organic elemental analysis consists of combusting the sample in the presence of a solid oxidant and sweeping the products into a thermal conductivity or infrared detector [4,5]. An alternative technique for the detection of hydrogen is to react the product water with carbonyldiimidazole to generate a quantitative amount of carbon dioxide which is measured by a coulometric titration [6].

The development of Proton Nuclear Magnetic Resonance Spectroscopy has led to the description and qualitative classification of hydrogen in organic compounds. These techniques have been especially helpful in describing hydrogen as it is classified into aliphatic, aromatic and hydroaromatic groupings [1,2,3]. In addition, low resolution proton ^{1}H-NMR has been successfully used to determine absolute amounts of hydrogen in a variety of petroleum fractions [7,8]. Our technique involves simple integration of high resolution ^{1}H-NMR spectra with careful attention given to sample preparation and spectral integration.

Experimental

Materials

Heavy distillate samples from Run 262 at the Wilsonville Advanced Coal Liquefaction Pilot Plant were supplied from CONSOL inc. The samples came from the V1074 stream and had an approximate boiling range of 650°F to 1050°F. The samples were hydrotreated in a laboratory scale trickle-bed reactor at 365°C. 1,2,3,6,7,8 hexahydropyrene (H_6Py) and deuterated chloroform (99.96%D) were purchased from Aldrich, naphthyl dibenzyl methane (NBM) was acquired from TCI America, acetanilide was obtained from Perkin Elmer and paraffin oil was purchased from LECO corporation.

Procedure

Combustion Analysis - Hydrogen amounts were determined with a Perkin Elmer model 2400 CHN analyzer. The combustion temperature was set at 925°C and the reduction tube was set at 640°C. Since the heavy distillate samples are viscous, the "standard" tin capsules could be used to contain the samples. Careful attention was paid to sample size since larger samples (>3mg) often lead to incomplete combustion or an "overload" condition which gives erratic hydrogen results. The analyzer is conditioned before sample analysis by running successive external standard samples until the hydrogen output stabilizes (usually one to two samples). The conditioning samples always show a lower than expected hydrogen value if they are preceded by a blank determination. External standards for the combustion technique include acetanilide, paraffin oil, and NBM.

Proton NMR - A Bruker AM 300 FT-NMR spectrometer was used to determine hydrogen mass percents. Heavy distillate samples were prepared in $CDCl_3$ at a concentration of 30.0 mg per 1.0 mL of solvent. External standard samples (H_6Py) were prepared at concentrations ranging from 0.5 mg to 45.0 mg per 1.0 mL of solvent to generate a calibration curve. All samples were weighed in 20 mL sample vials; $CDCl_3$ was introduced with a syringe. Solutions were immediately capped, mixed thoroughly, and transferred to 5 mm NMR tubes with Pasteur pipettes. Spectra were acquired with a total time of 2.36 seconds between 20 degree RF pulses. At low external standard concentrations (0.5 mg-30 mg), 512 scans per sample were acquired to improve signal to noise ratios. It was found that the number of scans could be reduced from 512 to 64 for distillate samples and more concentrated external samples (30 mg to 45 mg). H_6Py standard samples of 30.0, 37.7, and 45.0 mg/mL were prepared and analyzed daily for distillate analyses. $CDCl_3$ acts as a de facto internal standard having a chemical shift of 7.27 ppm; the samples are integrated between 10.5 and 0.5 ppm. Before integrating the spectra, the baseline curvature is corrected using a spline-fit algorithm incorporated in the Bruker software. Area counts due to the $CDCl_3$ of approximately 0.2 are considered negligible compared to the output for a 30 mg H_6Py standard (arbitrarily set to give 100.0 area counts). NBM was also analyzed to check the accuracy of the method.

Results and Discussion

Previous tests in our laboratory showed that heavy distillate samples acquired less than 1 wt% additional hydrogen during catalytic hydrogenation even under the most favorable of conditions. Therefore, determining hydrogen concentration changes on the order of 0.3 to 1.0 wt% has become necessary. Analyses for hydrogen in our laboratory (using the CHN analyzer) have been deemed acceptable if the precision of the analysis was ± 0.3wt%. This was not acceptable when trying to detect the small hydrogen increases in the hydrotreated distillates.

Figure 1 shows a linearity plot of area (detector response) vs. absolute hydrogen content of a wide variety of model compounds and a known heavy distillate. The data in Figure 1 shows the calibration curve constrained through the origin. This curve illustrates that a one-point calibration (such as is commonly used in automated CHN analyses) would underestimate the hydrogen in samples such as acetanilide (6.71% H) and overestimate the amount of hydrogen in paraffin oil (13.63% H). A one point calibration becomes especially inaccurate if the standard has a hydrogen content much different than the sample to be analyzed. Since the recommended sample weight for the combustion analysis should fall in the narrow range between one and three milligrams, the difficulty in establishing a linear calibration curve is compounded. One solution to this dilemma is to plot the raw data against a wide range of known hydrogen standards. This is the method illustrated in Figure 2, in which the calibration curve is not constrained through the origin. This linear regression curve-fit has a correlation coefficient of 0.994 and provides a more reliable basis for analysis of samples within the range of the calibration curve (hydrogen content between 6.71% and 13.63%).

Figure 3 shows a four point calibration curve of area vs. hydrogen content for different amounts of hexahydropyrene in deuterated chloroform as analyzed with the ^1H-NMR technique. This curve has excellent linearity over its range giving a linear regression correlation coefficient of 0.9999. The ^1H-NMR technique requires only one type of standard at different concentrations rather than multiple standards for the combustion technique. The X-axis in Figure 3 is an order of magnitude larger than the corresponding axis for the combustion technique since a typical sample weight for the ^1H-NMR analysis is ten times larger (30 mg vs. >3 mg) than for the microcombustion technique. The Y-axis presents the integrated area in arbitrary units with the 30mg /mL H_6Py standard assigned a value of 100.0.

Table 1 shows the analytical results and uncertainties for a series of heavy distillate samples and model compounds typically used in coal liquefaction research. Hydrogen concentration is presented as the average of four runs for the combustion analyses and the average of three determinations for the ^1H-NMR analyses. The theoretical hydrogen content is shown for the two model compounds, H_6Py ($C_{16}H_{16}$) and NBM ($C_{22}H_{25}$). The distillate samples were taken at different times "on-stream" with the highest hydrogen content being for the sample taken after one hour when the catalyst was the freshest. Hydrogen content decreases with time on-stream until at ten hours the reaction temperature was raised by 10°C to increase the rate of hydrogenation. Indeed this sample showed a slight increase of 0.1wt% hydrogen. In general the absolute hydrogen analyses for the two methods are remarkably close with the largest difference between the averages being no more than 0.16%. The standard deviations are larger for the ^1H-NMR determinations in general with the exception of the H_6Py sample which gave a very low (0.05%) standard deviation. Figure 4 is a parity plot comparing the results from the two

techniques. Again the correlation coefficient from a linear regression gave a good linear fit, thus the two techniques compare well, at least in the range of hydrogen concentrations studied.

Figure 5 shows an analysis of hydrogen distribution according to three broad categories. Alkyl protons are defined as alkyl α, alkyl β, and gamma having ^{1}H-NMR chemical shifts of 2.5-2.0, 1.4-1.0, and 1.0-0.5 ppm respectively. Condensed aromatic and uncondensed aromatic hydrocarbons have chemical shifts of 10.5-7.15 and 7.15-4.7 ppm, respectively. Hydroaromatic hydrogens are defined as cyclic α and cyclic β protons with proton shifts of 4.7-2.5 and 2.0-1.4 ppm respectively. Results in Figure 5 illustrate the additional benefit of the ^{1}H-NMR technique. The ^{1}H-NMR spectrum can quantitatively analyze the hydrogen species in a heavy distillate sample (not possible with combustion elemental analyses). These proton distributions can then be used to evaluate the quality of a liquid (in our case for hydrogen donation purposes).

Conclusion

Elemental hydrogen determinations giving sample repeatability of less than 0.1 wt% at the 10 wt% level have not been demonstrated with either the combustion or the ^{1}H-NMR technique. However, excellent correlation has been achieved between the combustion method and the ^{1}H-NMR method, giving results for model compounds which are quite good (see Table 1). A refinement of the combustion analysis has been shown by improving the calibration procedure from the typically used single point calibration. Small differences in hydrogen content were noted for a series of hydrotreated heavy distillate samples. In addition the absolute determination of hydrogen by ^{1}H-NMR can also yield information about the relative amounts of aromatic, alkyl and hydroaromatic protons. The ^{1}H-NMR technique can also be applied to evaluate absolute hydrogen content when a rapid combustion technique is not immediately available.

Acknowledgments

We would like to thank Ed Huffman and Sue Zeller of Huffman Laboratories for their helpful discussions about combustion and detection techniques.

References

1) J. Delpuech, D. Nicole, M. Le Roux, P. Chiche and S. Pregerman. Fuel, 1986, Vol.65, p1600.
2) R. A. Winschel, G. A. Robbins, and F. P. Burke. Fuel, 1986, Vol.65, p 526.
3) J.W. Tierney and I. Wender, Coal Liquefaction Process Streams Characterization, February,1994. DOE/PC 89883-87.
4) T.S. Ma and R.C. Rittner, Modern Organic Elemental Analysis. New York, Marcel Dekker, 1979.
5) G. Ingram, Methods of Organic Elemental Microanalysis. New York, Reinhold, 1962.
6) M. Houde, J. Champy. Michrochemical Journal, 1979, Vol. 24, p 300.
7) P. T. Ford, N.J. Friswell, and I. J. Richmond. Analytical Chemistry, 1977, Vol.49, No.4, p 594.
8) M. Bouquet. Fuel, 1985, Vol. 64, p 226.

* This work was supported by the U. S. Department of Energy at Sandia National Laboratories under contract DE-AC04-94AL85000.

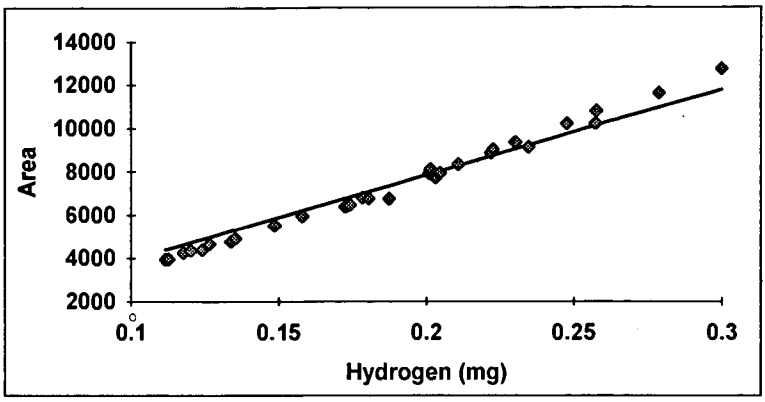

Figure 1. Calibration Curve for Combustion Elemental Hydrogen Analysis (forced through zero, r^2=.971)

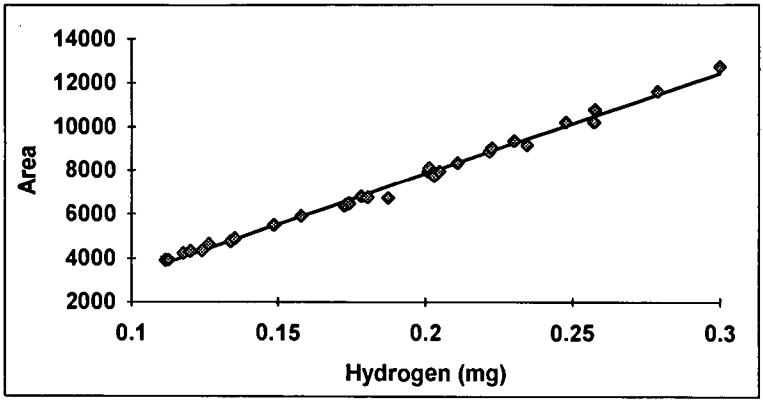

Figure 2. Calibration Curve for Combustion Elemental Hydrogen Analysis (r^2 = 0.994)

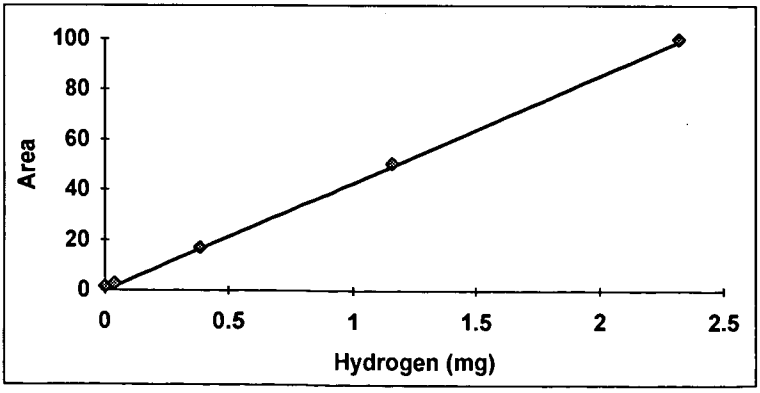

Figure 3. Calibration Curve for Proton NMR Hydrogen Analysis using Hexahydropyrene (r^2 = 0.999)

Table 1. Comparison of Combustion and NMR Hydrogen Data for Flow Reactor Product (Heavy Distillate)

Sample	%H Theory		%H Combustion	Std. Dev.		%H NMR	Std. Dev.
V1074	NA		9.66	0.23		9.68	0.12
Reactor Feed	NA		8.57	0.11		8.42	0.21
1 Hour	NA		9.33	0.06		9.34	0.37
2.5 Hour	NA		8.97	0.11		9.04	0.27
7 Hour	NA		8.81	0.06		8.94	0.30
10 Hour (+10°C)	NA		8.92	0.14		9.04	0.20
H6Py*	7.74		7.74	0.17		7.75	0.05
NBM**	6.87		6.98	0.10		6.83	NA

* 1,2,3,6,7,8 Hexahydropyrene. ** Naphthyl Dibenzyl Methane

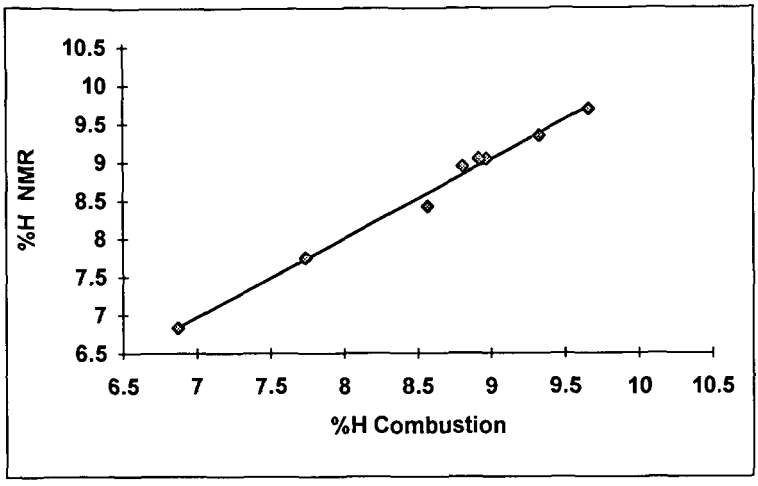

Figure 4. Comparison of Combustion Analysis with NMR Analysis ($r^2 = 0.993$)

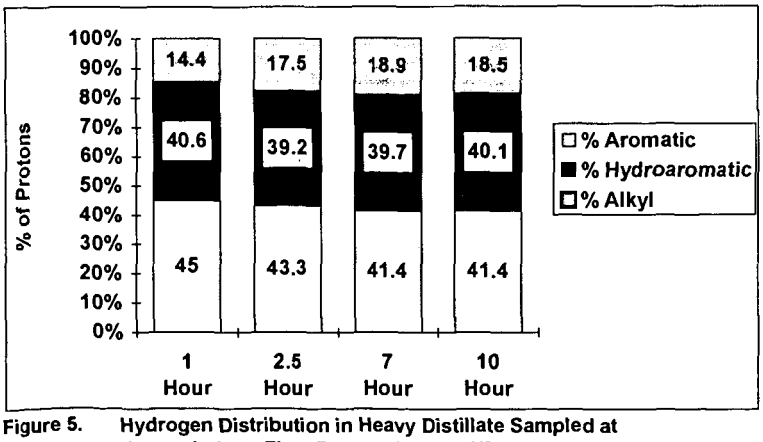

Figure 5. Hydrogen Distribution in Heavy Distillate Sampled at Intervals from Flow Reactor (Proton NMR)

TWO-DIMENSIONAL HPLC AND GC-MS OF OILS FROM CATALYTIC COAL LIQUEFACTION

Ajay K. SAINI and Chunshan SONG*

Fuel Science Program, Department of Materials Science and Engineering
The Pennsylvania State University, University Park, PA 16802

Keywords: Normal-phase, HPLC, GC-MS, Oils, Coal Liquefaction

ABSTRACT

We have employed normal-phase HPLC with photo diode array detector and GC-MS techniques to characterize the oils (hexane soluble fraction) from the catalytic and non-catalytic liquefaction of Wyodak subbituminous coal at 400 °C under 6.9 MPa H_2 pressure. The use of a dispersed Mo catalyst afforded much higher oil yield than the non-catalytic run. HPLC reveals that the oils from the catalytic runs contain more phenolic compounds and more of heavier components as compared to the oils from non-catalytic run. On the other hand, GC-MS shows that there is a significant amount of long-chain alkanes in the oils, ranging from C_{11} to C_{35}. The analytical results from the two techniques appear to be complementary to each other. The oils contain some heavier components which are detectable by HPLC but undetectable by GC-MS. GC-MS of HPLC fractions of the oils from the catalytic run confirmed the presence of significant amount of phenols and indanols.

INTRODUCTION

Catalytic coal liquefaction is a potential route to alternate liquid transportation fuels and aromatic chemicals (Song and Schobert, 1993). However, the characteristics of the liquefaction products must be clarified before effective implementation. Certain coal-derived aromatic compounds can be used to make high-value chemicals through shape-selective catalysis (Song and Kirby, 1993, 1994; Song and Moffatt, 1993, 1994; Schmidt and Song, 1994). The non-fuel use of coal liquids could improve the economics of liquefaction significantly, although the majority of the coal liquids may be used for transportation fuels (Song and Schobert, 1993; Derbyshire et al., 1994).

The present work aims at clarifying the compositional characteristics and molecular components of oils from catalytic liquefaction of Wyodak subbituminous coal using a dispersed Mo catalyst. This paper reports on the oil analysis using normal-phase high-performance liquid chromatography (HPLC) with photo diode array (PDA) detector which allows continuous two-dimensional scanning analysis of HPLC elutes over UV wavelength range.

While reversed-phase HPLC is popular for analysis of a variety of samples that are soluble in water or polar organic solvents (Poole & Poole, 1991; Wise et al., 1993), normal-phase HPLC can be used for analyzing components dissolved in non-polar organic mixtures (Snyder et al., 1988). Reversed-phase HPLC is characterized by strong interactions between the polar mobile phase and various sample molecules. However, coal-derived oils are not soluble in the common solvent systems (such as water-acetonitrile) for reversed-phase HPLC. In normal-phase HPLC, sample-adsorbent (stationary phase) or solvent-adsorbent interactions are strong but sample-solvent interactions are relatively weak. Neutral organic solvent (hexane) and weakly polar solvent (methylene chloride) can be used for normal-phase HPLC, which are also good solvents for coal-derived oils. Some bonded-phase HPLC columns for normal-phase HPLC have become commercially available recently. The conventional monochromatic UV detector has limited the amount of information that can be extracted from HPLC, since one particular wavelength may not be suitable for analyzing all the compounds in the complex mixtures (Snyder et al., 1988; Fetzer et al., 1993). PDA detector represent a recent development in the HPLC detection system, which allows sample analysis over UV range. Recently PDA has been demonstrated to be very useful in the analysis of PAHs in heavy liquids either by reversed-phase (Liu et al., 1992) or normal-phase HPLC (Clifford et al, 1994).

EXPERIMENTAL

Reagents and Materials. All the oils were derived from liquefaction of Wyodak subbituminous coal, which is one of the U.S. Department of Energy Coal Samples (DECS-8) maintained in the DOE/Penn State Sample Bank. Ammonium tetrathiomolybdate (ATTM) was dispersed as a catalyst precursor on to coal (1 wt% Mo on dmmf basis) by incipient wetness impregnation from its aqueous solution. ATTM is expected to generate molybdenum sulfide particles on coal surface upon thermal decomposition at ≥ 325 °C (Artok et al., 1993). The impregnated or the raw coal samples were dried in a vacuum oven at 100 °C for 2 h before use. The liquefaction was carried out in 25 mL tubing bomb reactors at 400°C for 30 min (plus 3 min heat up) under an initial H_2 pressure of 6.9 MPa. The oils are hexane-soluble fraction of liquefaction products. Detailed results of liquefaction may be found elsewhere (Song et al., 1993).

Various reagents were used as standards for confirmation of identification of HPLC and GC-MS peaks. The following reagents were purchased from Aldrich: phenol (99+%), 1,2,3,4-tetrahydro-1-naphthol (97%), tetralin (99%), 1-methylnaphthalene (98%), 9,10-dihydrophenanthrene (94%), and 1-naphthol (99+%). Sixteen polycyclic aromatic hydrocarbons were purchased from Supelco as a mixture defined as EPA Mixture 610. This mixture contains the following components: naphthalene,

* Corresponding author.

acenaphthylene, acenaphthene, fluorene, phenanthrene, anthracene, fluoranthrene, pyrene, benzo(a)fluoranthene, chrysene, benzo(b)fluoranthene, benzo(k)fluoranthene, benzo(a)pyrene, dibenzo(a,h)anthracene, benzo(g,h,i)perylene, and indeno(1,2,3,c,d)pyrene.

High Performance Liquid Chromatography (HPLC). The Waters HPLC system consists of U6K Universal Injector, 600E Powerline Multi-Solvent Delivery Module, and 991 Photodiode Array (PDA) Detector. The 600 Powerline Module serves as a system controller for setting up all solvent gradient conditions, injection and detection parameters and wavelength ranges. The PDA dtector is capable of continuous monitoring and acqusition of all UV/VIS wavelengths from 190 to 800 nm. Through the use of computer, the 991 PDA operates exclusively with Millenium 2010 Chromatography Manager software system, which allows fully automated data acquisition, processing, and reporting as well as 3-D graphics. The resolution of the PDA detection is 4.7 nm.

The column used for HPLC was a Hypersil PAH-2 purchased from Keystone Scientific, Inc., which is a commercially available column (150 x 4.6 mm i.d.) made by Shandon Scientific, Inc., U.K. The Hypersil PAH-2 has been developed using tetrachlorophthalimidopropyl bonded silica. This type of column can be used for analyzing the polyaromatic compounds dissolved in organic mixtures such as crude oils and coal liquids. Classical n-alkyl bonded phases are not suitable for analyzing such non-polar mixtures.

For HPLC analysis, the oils were diluted in 50%-50% hexane-methylene chloride solution (approximate concentration: 1 mg/mL) and filtered through 0.2 µm membrane filter (Supeco Iso-Disc P-32) attached to a syringe. This assures that the solution to be analyzed is free of suspeded micron-sized particles. For each HPLC analysis, about 10-20 µL of a sample solution was injected and the solvent elution was controlled by the gradient program, as shown in Table 1. Gradient elution was used: hold at 100% n-hexane for 20 min, from 100% hexane to 50% hexane-50% methylene chloride between 20 to 80 min, and to 100% methylene chloride between 80 to 100 min, followed by a 20 min hold at 100% methylene chloride. The flow rate of the mobile phase was 0.8 mL/min. The data acquisition of all the oils and standards were made in the UV wavelength range of 200 to 400 nm at the rate of 30 scans/minute. All the HPLC analyses were conducted at ambient temperature. HPLC fractions were collected for some representative samples and analyzed by GC-MS.

Gas Chromatography-Mass Spectrometry (GC-MS). The HPLC fractions of oil were analyzed on a HP 589011 GC coupled with an HP 5971A Mass Selective Detector (MSD). The column used for capillary GC was J&W DB-5 column: 30 m x 0.25 mm i.d. fused silica capillary column coated with 5% phenyl-95%methyl polysiloxane with a 0.25 mm film thickness. More analytical details may be found elsewhere (Song et al., 1994). In a typical GC-MS run, about 1 uL of the diluted methylene chloride solution of the sample was injected through the split/splitless injector in the splitless mode, with a 5 min delay of ionization to cut off the solvent. The GC oven in GC-MS was temperature-programmed as follows: 5 min isothermal holding at 40°C, subsequent heat-up to 280°C at 4°C/min, followed by isothermal holding at 280°C for 30 min.

RESULTS AND DISCUSSION

HPLC of Oils

Figures 1 and 2 show the 3-dimensional HPLC plots for oils from non-catalytic and catalytic runs, respectively, where the signal intensity (Z axis) is plotted against the UV wavelength (X, 247-390 nm) and retention time (Y). The use of a dispersed molybdenum sulfide catalyst increased oil yield from 10 to 46 wt% (based on dmmf coal). Apparently, the dispersed catalyst not only improved coal conversion, but also altered the compositional features of oils, as can be seen from the 3-D HPLC plots. The 3-D plots indicate that oils from the catalytic run contain more components that have either larger aromatic ring-size or are more polar, as compared to the non-catalytic runs.

To assist in the peak assignments, we performed HPLC analysis of two standard mixtures. Figure 3 shows 3-D plot for a standard containing 16 PAHs. The UV spectra of some peaks eluted before 20 min in the PAH mixture are in the similar wavelength range as those peaks in the real sample of oil from catalytic coal liquefaction. However, it becomes clear that the intense peaks in the 30-65 min range in the oil from catalytic runs (Figure 2) are not due to condensed PAHs (Figure 3). Figure 4 shows a maxiplot (miximum UV absorbance corresponding to each retention time unit) for the PAH standard mixture, in which the peaks were identified based on the information from the column supplier (Keystone Scientific, 1994).

As oxygen compounds are also possible products, we also analyzed the HPLC profiles of several pure polar compounds. Figure 5 gives a maxiplot for the phenolic mixture containing phenol, 1-naphthol, 1,2,3,4-tetrahydro-1-naphthol, and 1-indanol as well as aromatic hydrocarbons including tetralin, 1-methylnaphthalene, and 9,10-dihydrophenanthrene. The results with phenolic standards are very useful in understanding the differences between oils from non-catalytic and catalytic runs. Some major peaks around 60 min in the 3D-plot in Figure 2 have UV spectra similar to those of phenolic compounds.

The sample retention in normal-phase HPLC is governed by adsorption to the stationary phase. As PAHs are electron-donors, the chemically bonded electron-acceptor stationary phase (PAH-2 phase) allows the selective retention of PAHs in non-polar mobile phases. It is interesting to note that all the phenolic compounds interact so strongly with the tetrachlorophthalimidopropyl bonded-phase that their retention times (Figure 5) are longer than those of all the 16 PAHs (Figure 4). These results also indicate that, for HPLC analysis using PAH-2 column, one should be very careful in determing the ring size of aromatic compounds solely based on normal-phase HPLC. The most illustrative example is that the retention time of phenol, a single-ring compound, is even longer than that of a six-ring PAH, indeno(1,2,3,c,d)pyrene.

The HPLC results seem to imply that, as compared to the oils from non-catalytic run (Figure 1), the

oils from the catalytic runs (Figure 2) contain more phenolic compounds and more of heavier components. At first glance, these HPLC results are surprizing, as a good catalyst was used in the liquefaction. The present HPLC results, however, are in agreement with our earlier work on GPC. We have analyzed the molecular size distribution of coal-derived oils using HPLC operating in the GPC mode with polystyrene gel column (Song et al., 1988, 1989). The GPC results suggested that the oils from catalytic runs have more components with larger molecular sizes.

GC-MS of HPLC Fractions

To clarify the molecular components and to identify the HPLC peaks, we have collected eleven HPLC fractions of the oils derived from catalytic liquefaction. Figure 6 shows the maxplot together with the number and retention time ranges of individual HPLC fractions. We have analyzed all the HPLC fractions using GC-MS. The results are summarized below.

GC-MS shows that all the HPLC peaks and fractions represent a mixture rather than a single component. Fraction 1 (2-3.5 min) is a co-elute of monoaromatic compounds with long-chain alkanes, ranging from C_{11} to C_{35}. The aromatic compounds include alkylbenzenes, indanes, and tetralins. The HPLC peak intensity for this fraction does not include long-chain alkanes. Fraction 2 (3.5-6.0 min) consists of naphthalene, methylnaphthalene, and alkylbiphenyls (or acenaphthenes). Fraction 3 (6-8.0 min) corresponds to a small peak in the HPLC and contains C_2-naphthalenes and other two-ring compounds. In Fraction 4 (8-10.5 min) we detected phenanthrene and a C_4-alkyl-substituted phenanthrene. Fraction 5 (10-13.5) contains many three-ring compounds, phenanthrene and its derivatives. Fraction 6 (14-18 min) seems to give a very noisy GC-MS total ion chromatogram (TIC), but some compounds in this fraction are three-ring compounds. Fraction 7 (14-18 min) contains four-ring compounds including fluoranthene (m/z: 202) and pyrene (m/z: 202). Fraction 8 (21-30 min) contains several peaks with same molecular ion of m/z 216, and are probably methylfluoranthene and methylpyrene.

We detected significant amount of phenolic compounds in the fractions between HPLC retention time of 30 to 60 min. Begining with fraction 9 (30-38 min), phenols and indanols were observed. Fraction 10 (38-45 min) contains mainly C_1-, C_2-, C_3- and C_4-phenols. Fraction 11 (50-60 min) is the dominant phenolic fraction. It contains phenol, C_1-, C_2-, C_3-phenols and indanol, C_1- and C_2-indanols. These GC-MS results in combination with HPLC results clearly revealed that the oils from catalytic liquefaction of Wyodak subbituminous coal using a dispersed molybdenum sulfide catalyst contain more phenolic compounds (30-65 min range in HPLC) and more heavier components (70-110 min range in HPLC), as compared to oils from the non-catalytic run at 400°C for 30 min under 6.9 MPa H_2. The HPLC retention times for peaks with this sample are not exactly the same to those for the PAH and phenolic standards (due to some difference in instrumental conditions).

In addition, the fact that a catalytic run gives more phenolic compounds also provides further evidence that the initial reaction involves the cleavage of O-C bonds in coal. The stabilization of the radicals from these bond cleavages by hydrogen transfer can produce phenolic compounds, otherwise these highly reactive radicals would seek self-stabilization through retrogressive cross-linking reactions. The use of a dispersed Mo catalyst facilitates the transfer of hydrogen to radicals.

It should be mentioned that Clifford et al. (1994) analyzed several coal liquefaction process streams (oils) by normal-phase HPLC. They detected many polyaromatic compounds but did not observe oxygen compounds in their samples. The samples they analyzed represent highly 'upgraded' products, because they were derived from two-stage catalytic liquefaction of coals in Wilsonville pilot plant and HRI pilot plant. The present samples, however, were derived from primary (one-stage) liquefaction of Wyodak subbituminous coal under mild conditions (400°C, 30 min).

ACKNOWLEDGMENTS

We wish to thank Prof. Harold Schobert for his encouragement. This work was supported by the U.S. Department of Energy under contract No. DE-AC22-91PC91042.

REFERENCES

Artok, L.; Davis, A.; Mitchell, G.D.; Schobert, H.H. Energy & Fuels, 1993, 7, 67.
Clifford, D.J.; McKinney, D.E.; Hou, L.; Hatcher, P.G. Coal Liquefaction Process Strems Characterization and Evaluation. Topical Report. High Performance Liquid Chromatography (HPLC) of Coal Liquefaction Process Streams Using Normal-Phase Separation with UV Diode Array Detection. DOE/PC 89883-85, January 1994, 47 p.
Derbyshire, F.; Jagtoyen, M.; Fei, Y. Q.; Kimber, G. Am. Chem. Soc. Div. Fuel Chem. Prepr., **1994**, 39 (1), 113.
Fetzer, J.C.; Biggs, W.R. J. Chromatogr., 1993, 642, 319.
Liu, Y.; Eser, S.; Hatcher, P.G. Am. Chem. Soc. Div. Fuel Chem. Prepr., 1992, 37, 1227.
Poole, C.F.; Poole, S.K. Chromatography Today. Elsevier: Amsterdam, 1991, 1026 p.
Schmitz, A.; Song, C. Am. Chem. Soc. Div. Fuel Chem. Prepr., **1994**, 39 (3-4), in press.
Snyder, L.R.; Glajch, J.L.; Kirkland, J.J. Practical HPLC Method Development. John Wiley & Sons: New York, 1988, 260 p.
Song, C.; Hanaoka, K.; Ono, T.; Nomura, M. Bull. Chem. Soc. Japan, **1988**, 61, 3788.
Song, C.; Hanaoka, K.; Nomura, M. Fuel, **1989**, 68, 287.
Song, C.; Kirby, S. Am. Chem. Soc. Div. Petrol. Chem. Prepr., **1993**, 38 (4), 784.
Song, C.; Moffatt, K. Am. Chem. Soc. Div. Petrol. Chem. Prepr., **1993**, 38 (4), 779.
Song, C.; Schobert, H. H. Fuel Processing Technol., **1993**, 34 , 157.
Song, C.; Saini, A.K.; Schobert, H. H. Am. Chem. Soc. Div. Fuel Chem. Prepr., **1993**, 38 (3), 1031.
Song, C.; Lai, W.-C.; Schobert, H. H. Ind. Eng. Chem. Res., **1994**, 33, 534.
Song, C.; Moffatt, K. Microporous Materials, Elsevier, **1994**, in press.
Song, C.; Kirby, S. Microporous Materials, Elsevier, **1994**, in press.
Wise, S.A.; Sander, L.C.; May, W.E. J. Chromaogr., 1993, 642, 329.

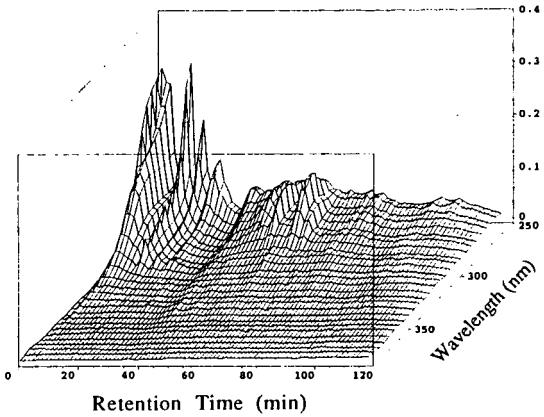

Figure 1. 3-D HPLC plot of oils from non-catalytic liquefaction of Wyodak subbituminous coal.

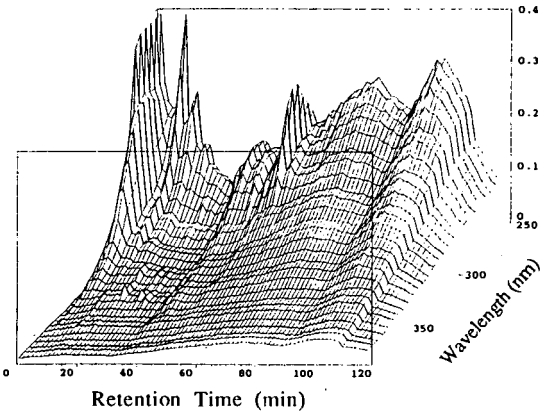

Figure 2. 3-D HPLC plot of oils from catalytic liquefaction of Wyodak subbituminous coal.

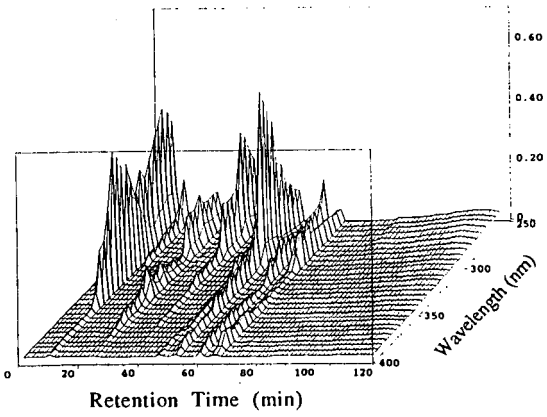

Figure 3. 3-D HPLC plot of a mixture of 16 polynuclear aromatic hydrocarbons (PAHs).

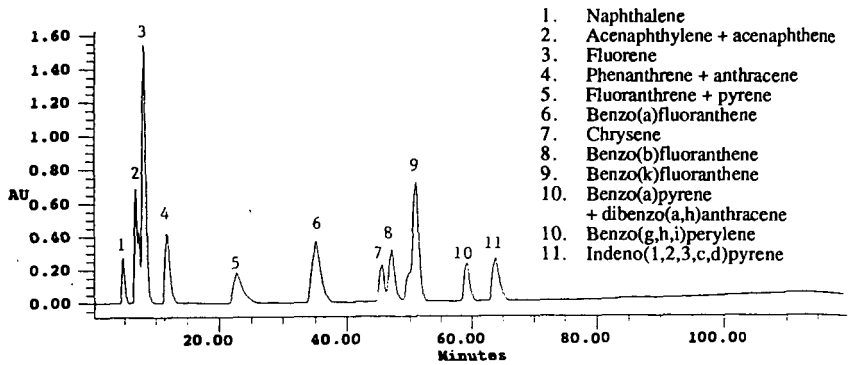

Figure 4. HPLC maxplot of PAH standard containing 16 PAHs.

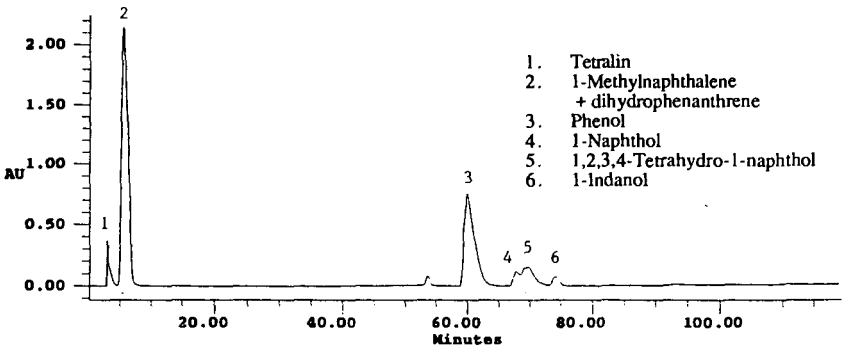

Figure 5. HPLC maxplot of phenolic standard mixture.

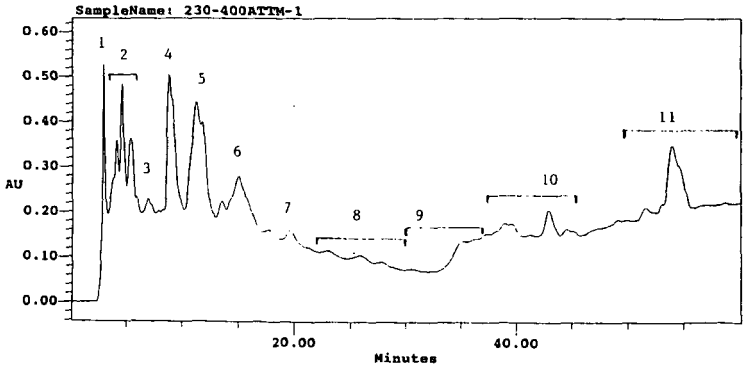

Figure 6. Expanded HPLC maxplot of oils from catalytic liquefaction at 400°C for 30 min. The number and accompanying lines indicate the retention time range of HPLC fractions collected.

USE OF HYDROPYROLYSIS-MS TO PROBE THE HYDROCRACKING OF DIPHENYLALKANE LINKAGES IN THE SOLID STATE

S.D. Brown [1], O. Sirkecioglu [1], K. Ismail [1], J. Andresen [1], C.E. Snape [1], A.C. Buchanan III [2] and P.F. Britt [2]

[1] University of Strathclyde, Department of Pure & Applied Chemistry, Glasgow G1 1XL, UK
[2] Chemistry and Analytical Sciences Division, Oak Ridge National Laboratory, Oak Ridge, Tennessee 37831, USA

Keywords: hydropyrolysis, resites, silica-immobilised substrates

INTRODUCTION

Diphenylalkanes have been extensively used as model substrates to probe the free radical mechanisms involved in C-C bond cleavage reactions during coal liquefaction [1]. However, the fact that the macromolecular structure in coals is undoubtedly subject to highly restricted motion suggests intuitively that free radical pathways are likely to be somewhat different from those encountered in the vapour phase. Indeed, this has been confirmed by the use of silica-immobilised substrates where bimolecular reaction steps are significantly perturbed for diphenylalkanes compared to the corresponding vapour phase reactions [2-5]. For pyrolysis studies, these model substrates have the inherent advantage that they do not soften and so remain in the reactor. Thus, immobilised substrates have considerable potential for modeling coal pyrolysis phenomena, particularly the effects of high hydrogen pressures (hydropyrolysis). Indeed, for immobilised benzene, the SiO-C bond linking the substrate to the surface is reasonably stable and does not cleave until above 500°C (peak maximum at 550°C) with 150 bar hydrogen pressure [6]. For immobilised diphenylmethane (DPM), it was demonstrated previously that the use of 150 bar hydrogen pressure and a sulphided Mo catalyst both reduced the peak evolution temperatures for benzene and toluene clearly demonstrating their separate contributions to promoting C-C bond cleavage [6].

An alternative class of materials to immobilised substrates that should prove equally as suitable for modeling pyrolysis phenomena are cured phenol-formaldehyde resins. These offer the option of incorporating a wide variety of hydrocarbon and heteroatomic moieties into the basic phenolic macromolecular structure. A series of co-resites were recently prepared from phenol and, as the second component, a series of sulphur-containing precursors, namely 2-hydroxy dibenzothiophene, *p*-hydroxydiphenylsulphide, 4-hydroxyphenylbenzylsulphide and 4-hydroxythioanisole [7]. These precursors have also been used previously for the preparation of silica-immobilised substrates [8] which, together with the resites have been used as calibrants in temperature programmed reduction [7-9]. To investigate the hydrocracking of diphenylalkane linkages in the solid state with the additional aim of elucidating how the nature of a particular substrate might influence the reaction pathways, hydropyrolysis experiments with on-line mass spectrometric analysis have been conducted on silica-immobilised substrates, phenolic resites and a polystyrene-divinylbenzene network using hydrogen pressures of 5 and 150 bar.

EXPERIMENTAL

Substrates and their synthesis The diphenylmethane co-resites were prepared using the procedure described by Bar and Aizenshtat [10] which was used previously for the sulphur-containing resites [7]. A total phenol to formaldehyde mole ratio of 1:2.5 was used with sodium hydroxide as catalyst for the condensation reaction, a mole ratio of 0.1 with respect to phenol being employed. The mole ratio of phenol to the monohydroxydiphenylalkanes (diphenylethane and propane) was 3:1 to ensure that a reasonably high degree of crosslinking was achieved in the initial resoles. DSC indicated that co-resoles prepared with a mole ratio of only 1:1 melted to a considerable extent in the temperature range,

250-280°C. The co-resites were cured in an oven purged with nitrogen gas at a temperature of 200°C. Solid state ^{13}C NMR was used to monitor the conversion of the ether/alcohol functional groups to methylene bridges during curing. Cross polarisation/magic-angle spinning (CP/MAS) spectra were obtained using a Bruker MSL100 instrument operating at 25 MHz for carbon.

The silica-immobilised samples were prepared from the appropriate phenol as previously described [2-5]. The loadings of the diphenylmethane (DPM) and diphenylethane (DPE) substrates investigated here are summarised below. These were determined by hydrolysing the substrates with base and conducting GC analysis of the resultant phenols which were silylated.

	Loading, mmol g^{-1}
Diphenylmethane, normal	0.45
Dideuterated diphenylmethane ($PhCD_2Ph$)	0.31
Co-attached diphenylmethane/tetralin	0.28/0.18
Diphenylethane	0.60

The polystyrene-divinylbenzene (PS-DVB) sample used, XAD-4 is commercially available.

Hydropyrolysis-MS Details on the high pressure system have been reported previously [7,8,11]. Hydrogen pressures of 5 and 150 bar were used with a heating rate of 5°C/min over the range 100-600°C. Typically, between 0.2 and 0.3 g of the resite (particle size range of *ca* 0.1-1.0 mm) was mixed with 2-3 g sand. The volatile species evolved were detected on-line using a quadrupole mass spectrometer (VG Sensorlab, 0-300 a.m.u).

RESULTS AND DISCUSSION

C_1-linkages Figure 1 shows the evolution of benzene, toluene and cresol at 150 bar pressure from a normal phenol resite not containing a second constituent. The benzene evolving at high temperature (T_{MAX} of 550°C) is considered to arise mainly from the hydrodeoxygenation of phenol, cresols and xylenols. The cresol profile and, to a lesser extent, that for m/z 91 (this probably comprises fragment ions of 108) contain peaks at *ca* 550°C which are attributed to the primary cleavage of the methylene bridges. Figure 2 compares the benzene evolution profiles at 150 bar pressure from the immobilised DPM substrates. As found previously [6], the profiles can be resolved into two broad components. The higher temperature one (530-600°C) is consistent with that anticipated for cleavage of the SiO-C bond in surface-immobilised benzene. Toluene is similarly formed following the prior hydrogenolysis of the C-C linkages in diphenylmethane according to the reaction scheme:

$$-SiOPhCH_2Ph + 2H_2 \text{ -------> } SiOPhH + PhCH_3 + -SiOPhCH_3 + PhH$$

The T_{MAX} of 480-500°C of the lower component at is very similar to that for the resite suggesting that the additional free radical chemistry that occurs in the resite does not significantly promote the cleavage of the methylene bridges at high hydrogen pressure.

The similar intensities of the m/z 78 and 79 intensities indicates that, as anticipated, extensive scrambling of the methylene deuteriums has occurred. The co-attachment of tetralin had little effect on the benzene and toluene evolution profiles both at low and high pressure (Figure 2). The greater m/z 78 intensity observed for the co-attached DPM is probably attributable to the likely contributions from tetralin breakdown products. No naphthalene was detected indicating that hydrogen transfer had not occurred to a significant extent.

C_2-linkages Figures 3 and 4 show the benzene and toluene profiles from the immobilised DPE at low and high pressure and Figure 4 compares the toluene evolution profiles for the immobilised DPE and DPE-containing resite at 150 bar. Given that the relative response factor of benzene to toluene is *ca* 3.1, the toluene concentration is much the higher at low pressure. This is consistent with

all the low pressure isothermal work on DPE (both free and immobilised) [1,2] where there is little evidence of cleaving the aryl-C bonds. At high pressure, this is cleary no longer the case with benzene concentration being considerably higher (*ca* 30% of that for toluene, Figures 3 and 4). Increasing the hydrogen pressure has also given rise to a slightly lower T_{MAX} for benzene and toluene (430 cf 450°C) and, as for DPM, resulted in much more benzene evolving above 500°C indicating the role of hydrogen pressure in circumventing char-forming reaction pathways.

By comparison with Figure 2, the contribution below 480°C in the profile for the resite can be ascribed to cleavage of the DPE linkage. Although the high temperature contributions from the remainder of the resite dominate the trace, the low temperature region matches fairly closely that for the immobilised DPE with an initial T_{MAX} occurring at *ca* 430°C.

C_3-linkages Figure 5 shows the virtually identical toluene and ethyl benzene evolution profiles from the PS-DVB at 5 and 150 bar pressure. The concentration of styrene evolving a low pressure was comparable to that of ethylbenzene. At low pressure, a sharp T_{MAX} occurs at 450°C with smaller amounts of toluene and ethylbenzene evolving at higher temperatures from secondary reactions. At high pressure, the evolution profiles are considerably broader. The volatiles begin to evolve at 320°C but the broad peak in the temperature range is the supersition of more than one distinct reaction pathway. Further, much greater quantities evolve above 470°C which again is indicative the role of hydrogen pressure in circumventing char-forming reaction pathways.

Figure 6 compares the evolution profile of toluene form the PS-DVB and DPP-containing resite. The traces are very similar indicating again that, with high hydrogen pressures, the primary scission of the C-C bonds in diphenylalkanes is fairly independent of the nature of the substrate.

CONCLUSIONS

The results have indicated increasing the hydrogen pressure reduces the extent of retrogressive chemistry for all the model substrates investigated. The primary pyrolytic event at high hydrogen pressure, as characterised by the evolution of benzene, toluene and ethylbenzene/styrene, occurs at virtually the same temperature for a given alkane linkage in the different substrates used. The C_2 and C_3 linkages investigated are cleaved at *ca* 50-100°C lower than their C_1 counterparts. The pyrolysis of immobilised diphenylmethane appears to be largely unaffected by the co-attachment of tetralin.

ACKNOWLEDGEMENTS

The research was supported at (i) the University of Strathclyde by the Science & Engineering Research Council (Grant No. GR/J/08997) and the Department of Trade & Industry and at (ii) Oak Ridge National Laboratory by the Division of Chemical Sciences, Office of Basic Energy Systems, US DoE (Contract No. DE-AC05-840R21400 with Martin Marietta Energy Systems, Inc.).

REFERENCES

1. M.L. Poutsma, Energy & Fuels, 1990, **4(2)**, 113 and references therein.
2. A.C. Buchanan III, T.D.J. Dunstan, E.C. Douglas and M.L. Poustma, J. Am. Chem. Soc., 1986, **108**, 7703.
3. A.C. Buchanan III and C.A. Biggs, J. Org. Chem., 1989, **54**, 517.
4. A.C. Buchanan III, P.F. Britt and M.L. Poustma, Prepr. Am. Chem. Soc. Div. Fuel Chem., 1990, **35(1)**, 217.
5. P.F. Britt and A.C. Buchanan III, J. Org. Chem., 1991, **56**, 6132.
6. S.C. Mitchell, C.J. Lafferty, R. Garcia, K. Ismail, C.E. Snape, A.C. Buchanan III, P.F. Britt and E. Klavetter, Energy & Fuels, 1993, **7**, 331.
7. K.Ismail, G.D. Love, S,C, Mitchell, S.D. Brown and C.E. Snape, Prepr. Amer. Chem. Soc. Div. Fuel Chem., 1994, **39(2)**, 1691.
8. S.C. Mitchell, C.J. Lafferty, R. Garcia, K. Ismail, C.E. Snape, A.C. Buchanan III, P.F. Britt and E. Klavetter, Prepr. Amer. Chem. Soc. Div. Fuel Chem., 1992, **37(4)**, 551.

9. K. Ismail, R. Garcia, S.C. Mitchell, C.E. Snape, A.C. Buchanan III, P.F. Britt, D. Franco and J. Yperman, Proc.1993 Int.Conf. on Coal Science, Banff, September 1993.
10. H. Bar and Z. Aizenshtat, J. Anal. Appl. Pyrolysis, **19**, 1991, 265.
11. C.J. Lafferty, S.C. Mitchell, R. Garcia and C.E. Snape, Fuel, 1993, **72**, 367.

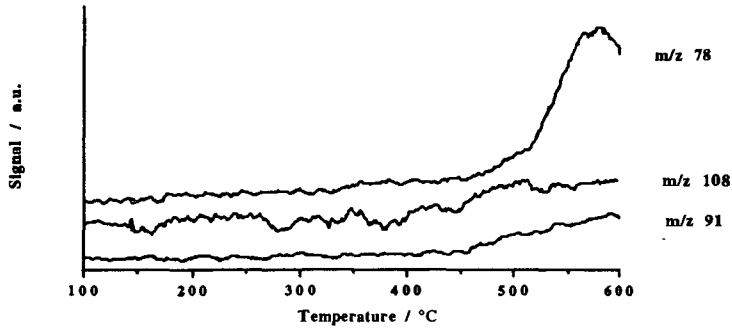

Figure 1. Hydropyrolysis evolution profiles of benzene, toluene and cresol from the normal phenolic resite under 150 bar H_2

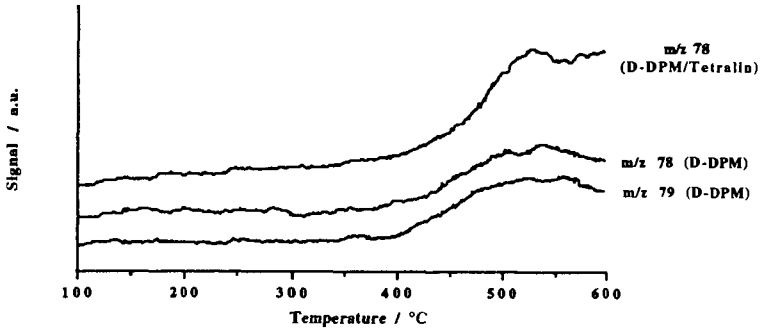

Figure 2. Evolution profiles of benzene from silica-immobilised di-deuterated diphenylmethane and silica-immobilised di-deuterated diphenylmethane with co-attached tetralin under 150 bar H_2

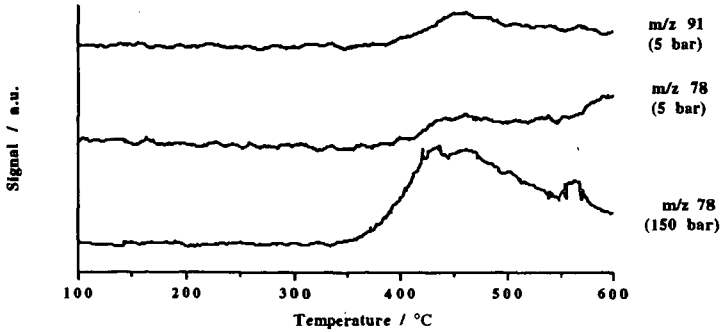

Figure 3. Hydropyrolysis-m.s. profiles of silica-immobilised diphenylethane under 5 and 150 bar H_2

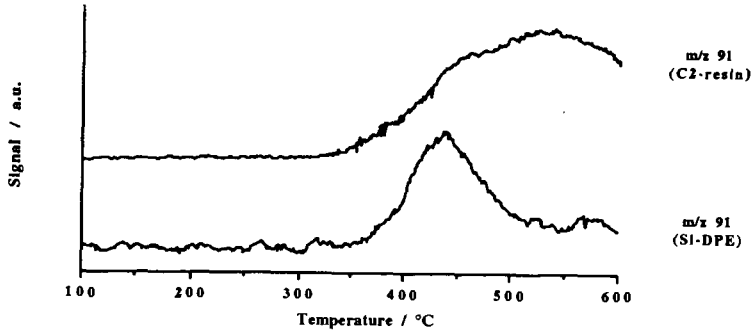

Figure 4. Toluene evolution profiles from the diphenylethane phenolic resite and the silica-immobilised diphenylethane under 150 bar H_2

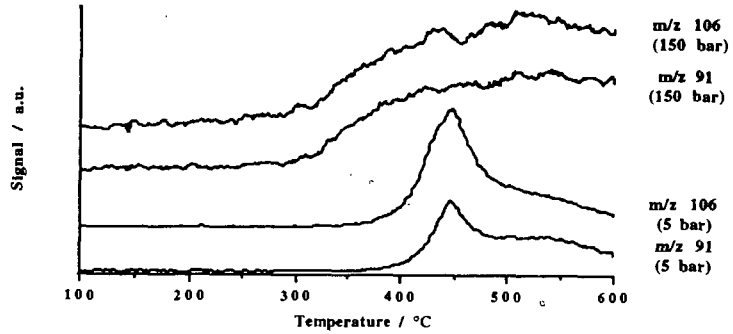

Figure 5. Evolution profiles of toluene and ethylbenzene from the PS-DVB under 5 and 150 bar H_2

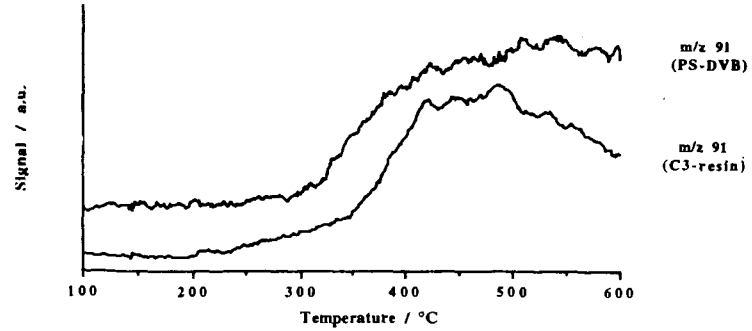

Figure 6. A comparison of the toluene evolution profiles from the PS-DVB and the diphenylpropane phenolic resite under 150 bar H_2

A CRITICAL SURVEY OF THE VALUE OF MICROWAVE HEATING FOR THE ACCELERATION OF REACTIONS OF -OH GROUPS IN COAL, AND THE RELATIONSHIP TO NEW ANALYTICAL METHODS FOR -OH DETERMINATION

Parisa Monsef-Mirzai, Harminder Manak and William R. McWhinnie
Department of Chemical Engineering & Applied Chemistry,
Aston University, Aston Triangle, Birmingham B4 7ET

Keywords: Microwave, -OH derivitisation, MASNMR.

INTRODUCTION

Research continues into coal utilisation by means which involve chemical reactions, particularly for the production of liquid products. Most of the new processes are based on hydroliquefaction, and for assessment of the suitability of particular coals for this purpose it is desirable to have detailed knowledge of their chemical constitution and reactivity. In respect of the use of coals as chemical feedstocks, as in hydroliquefaction, new classification systems might be desirable based on chemical parameters rather than on carbonisation properties as at present, and here the various functional groups attached to the coal hydrocarbon skeleton would be of great importance.

Functional groups in coals derive from the 'heteroatoms' O, N and S, and of these oxygen is by far the most important, varying regularly with coal rank between about 1 and 15% in British coals. Although -COOH and $-CH_3$ groups occur in coals of very low rank, oxygen in British coals is distributed between hydroxyl, carbonyl and ether-type groups. The hydroxyl groups, which certainly include phenolic groups, are the most important, and probably provide active reaction sites during hydroliquefaction.

Hydroxyl groups may be detected with reasonable certainty by spectroscopic methods, and can be measured by conversion into derivatives, e.g. by acetylation. Subsequent steps such as hydrolysis, distillation and titration of the recovered acetic acid afford data on -OH content. All such methods are based on heterogeneous reaction processes and there may be residual doubt as to whether the reactions have progressed to equilibrium. Indeed, a method dependent scatter of results is seen in the literature.

The ability of microwave heating to greatly accelerate chemical reactions is now well established.[1] The reaction mixture is typically contained in a microwave transparent Teflon bomb and the rate acceleration is achieved *via* an Arrhenius effect due to the superheating of the solvent. For this to be possible, it is necessary that the solvent is polar since non-polar materials will not interact with the microwave field. Following testing of a wide range of polar solvents we have found that acetonitrile is the best choice. This is because it superheats rapidly and extracts the minimum amount of the more labile components of coal under the experimental conditions employed. GC/MS analysis of the limited amount of material extracted reveals that oxygen containing materials constitute a negligible quantity of the extract. When the appropriate reagents are sufficiently soluble in acetonitrile, mixed solvents may be used as long as one is a microwave "receptor" e.g. acetonitrile/toluene. For polar reagents, e.g. transition metal salts, water is very appropriate. Of particular interest is that the method is excellent for the acceleration of a range of heterogeneous reactions.[2] In this presentation we outline the applications of microwave heating for driving coal -OH derivitisation reactions. We point out both advantages and drawbacks of the method.

Methodology

A known weight (0.5 - 1.0 g) of coal (90< 212> mm) is mixed with reagents (total liquid volume $\leq 10\ cm^3$) in a Teflon bomb. The Teflon bomb is placed in the microwave oven (even a domestic model may be used) and subjected to bursts of microwave energy until it is judged, usually on the basis of FTIR, that the reaction has reached equilibrium. The time required proves to be a function of the coal used, the reagents, and the solvent. These observations may be understood in terms of variation of porosity of the coal, differing steric demands of the reagents, and differing degrees of superheating of the polar solvents.

Acetylation

Acetylation[3] can be achieved in two ways: *(a)* With ketene, $CH_2{=}CO$, a small highly reactive gas molecule which can move easily, penetrate the porous coal structure and thus give the maximum probability of complete reaction with coal -OH groups, but the substance is very toxic and long reaction times are required due to loss of reagent *via* ketene polymers formed on the coal preventing further reaction with hydroxyl groups. Therefore after every ten hours reaction, the ketene polymers should removed by extraction with toluene then, after drying and weighing the coal, this procedure continues until a constant acetyl content is obtained. *(b)* With reagents such as acetic anhydride/pyridine, acetic anhydride/conc. H_2SO_4; acetic anhydride/$(CF_3CO)_2O$; CH_3COOH/CF_3COOH. Blom *et al.*[4] have pointed out that acetylation of coal proceeds slowly due to steric hindrance of the -OH groups, thus long reaction times are needed for reproducible data to be obtained. Likewise the hydrolysis step may need several days refluxing with barium hydroxide prior to distillation and titration of the acetic acid. It has been shown that[3] microwave heating certainly accelerates both the acetylation using the conventional reagents and hydrolysis reactions, and that greater conversions are achieved than by using the same reagents in prolonged reactions on the bench top. For example, seven days hydrolysis on the bench top produces barium silicate, which has been formed from etching the glass with weak barium hydroxide, as an undesirable side

product, but such problems are totally avoided in the microwave method. Thus not only is the microwave method more reliable in driving the reactions to equilibrium but the saving in time can also avoid unwanted reactions which are a function of the very long reaction times associated with conventional procedures.

Silylation

Even if microwave heating is used to accelerate the derivitisation and hydrolysis stages, the acetylation process is a multi-step procedure. We have developed a method based on silylation which is a "one pot" process since the silylated coal is analysed directly by quantitative ^{29}Si MASNMR methods. A range of silylation reagents is available but not all are equally effective for use in the microwave method. For studies of coals, N-(trimethylsilyl)imidazole was the preferred reagent when used in acetonitrile solution. Even with this reagent a side reaction with more tenaciously held moisture occurred to give Me_3SiOH but fortunately the presence of this material did not interfere with the analysis. A wider range of reagents could be used for the silylation of simple substituted phenols, "model compounds", although a 1:1:1 mixture of N,O-bis(trimethylsilyl)acetamide, N-(trimethylsilyl)imidazole, and trimethylchlorosilane was optimal under conditions of microwave heating.

Remarkable acceleration of reactions was achieved e.g. from 24 hours (bench) to 35 minutes (microwave) for Creswell coal, and the ultimate -OH analytical data were in excellent (Creswell) or satisfactory (e.g. Cortonwood) agreement with the definitive ketene data.[5] (Table 1a and 1b).

The analytical method for silicon requires knowledge of the spin lattice relaxation times T_1 of silylated coals (~8s) and of appropriate standard compounds (~25s). The method requires a pulse delay of $5T_1$ (maximum) seconds between pulses, thus the accumulation time for quantitative spectra with good signal to noise ratios may be considerable. However, despite this, the time taken from commencement of analysis to result may truly be described as "rapid" in comparison with other methods.

Stannylation

Tri-n-butyltin is a much more sterically demanding reagent than is Me_3Si-. It is not surprising therefore that even under microwave acceleration, stannylation of 2,6-di-t-butylphenol does not occur, whereas, by contrast, reaction with 2,6-dimethylphenol occurs readily. The less sterically demanding (smaller cone angle) Me_3Sn- group will react with more hindered phenols e.g. 2,6-diphenylphenol; the product, 2,6-$Ph_2C_6H_4OSnMe_3$, having been confirmed by single crystal X-ray crystallography.

The use of the triorganotin chlorides, R_3SnCl (R=Me, n-Bu) was not effective for coal since microwave accelerated loss of reagent *via* side reactions, and loss due to volatility, occurred. More effective was the use of the oxides $(R_3SnO)_2O$. The point illustrated is that microwave heating may accelerate both analytically desirable and undesirable reactions.

To date a range of coals and coal macerals has been successfully stannylated using TBTO (i.e. bis-tri-n-butyltin oxide) in conjunction with acetonitrile, usually mixed with toluene, in microwave driven experiments. Quantitative methods of analysis based on ^{119}Sn MASNMR are under development and it is hoped that the more sterically demanding n-Bu_3Sn- will show a lower apparent -OH content for a given coal than that determined with Me_3Si-, thus enabling the proportion of more hindered -OH groups to be established.

To date preliminary qualitative ^{119}Sn MASNMR data indicate chemical shifts similar to those observed for 2,6-di-substituted-stannylated phenols in which the 2,6-substituents are of small steric demand. Thus it does appear possible that the density of -OH sites of differing degrees of steric hindrance might be mapped out by treatment of the same coal with a range of reagents of differing steric demand.

Phosphorylation

Both ^{29}Si (4.71%) and ^{119}Sn (8.45%) are of relatively low natural abundance thus the development of quantitative MASNMR methods to include phosphorus is attractive given the 100% abundance of ^{31}P and its excellence as an NMR probe.[6] In the event the microwave acceleration of phosphorylation reactions with phosphorus(III) reagents, e.g. $P(OEt)_2Cl$, produced complex mixtures both when the substrate was coal or model compounds. In addition to direct phosphorylation of -OH, four side reactions were noted:

(i)	oxidation	P(III)	→	P(V)
(ii)	hydrolysis	P-Cl	→	P-OH
(iii)	solvolysis	P-OEt	→	P-OH
(iv)	ROH + EtO-P	→	ROP + EtOH	

This rendered quantitative study impossible. Naturally, more vigorous control of reaction conditions (exclusion of oxygen and moisture) would allow greater success but this departs from the objective of devising a simple, one pot method for coal -OH determination. Ironically, there is qualitative evidence that phosphorylation could be better than silylation for identifying subtle differences in -OH environments. Indeed when coal is the substrate there is

evidence for the occurrence of all reactions (i) — (iv) above. From the spectrum of ^{31}P chemical shifts, it may be deduced that a rich variety of phosphorus environment results from the reaction of coal with reagents of the class $P(OR)_2Cl$. In fact the oxidation reaction is very rapid and regardless of the initial reagent being P(III) or P(V), any -OH groups on the coal which are phosphorylated contain P(V). An oxidation and hydrolysis of a product reagent such as $P(OEt)_2Cl$ is $OP(OEt)_2(OH)$ and this material adheres strongly to the coal suggesting that it originates primarily from reaction with any tenaciously held coal moisture (all coal samples are dried at 105°C under N_2 over one or more hours). Thus whilst the system is not without interest chemically, the analytical usefulness is limited. It may however be noted, as mentioned above, that preliminary qualitative studies of tri-n-butylstannylated coals give chemical shifts consistent with stannylation of weakly hindered -OH groups.

Ion Exchange

It may be noted that the ability of microwave heating to accelerate the ion exchange of clay minerals[2] may also be exploited in coal science to afford transition metal exchanged -OH groups (e:g. Ni^{2+}) which are suitable for preliminary study by EXAFS to provide some information about average -OH environments.

Attempts may be made to exchange the weakly acidic sites directly, or alternatively, prior conversion to the potassium derivative may be employed. Selection of salts of copper(II) can lead to complex chemistry and ill defined products. With nickel(II) and cobalt(II) cleaner reactions could be obtained. Thus microwave derivitisation has once again proved useful in developing materials for physical study by a method (EXAFS) which may give information about the average environment of -OH groups in a given coal.

Conclusions

Microwave heating will not necessarily accelerate only a reaction of particular analytical interest, the rates of side reactions may also be accelerated. If the method is to be used to derivitise -OH groups it is desirable to select reagents with either no or with a minimum of side reactions. If that condition can be fulfilled, as it usually is if the reagent is selected from group 14, in our view microwave heating is now the preferred method for such derivitisation reactions.

References

1. Mingos, D.M.P., and Baghurst, D.R., Chem. Soc. Rev., 1991 **20**, 1.
2. Bond. S.P., Gelder, A., Homer, J., Perry, M.R., and McWhinnie, W.R., J. Mater. Chem., 1991, **1**, 327.
3. Monsef-Mirzai, P., Lawson, G.J., and Bailey, N.T., Fuel, 1990, **69**, 533.
4. Blom, L., Edelhansen, L., and Van Knevelen, D.W., Fuel, 1957, **36**, 135.
5. Monsef-Mirzai, P., Lawson, G.J., Bailey, N.T., and Ikejuani, A.O.O., Fuel, 1992, **71**, 45.
6. Wroblewski, A.E., Reinartz, K., and Verkade, J.G., Energy and Fuels, 1991, **5**, 786.

Table 1 (a)
Quantitative ^{29}Si MASNMR
determination of O_{OH}/O_{Total}

O_{OH}/O_{Total} Quantitative ^{29}Si MASNMR				
Coals	**%C**	**%O**	**O_{OH}/O_{Total} % by Silylation**	**Reaction Time**
Gedling	81.6	9.4	41	2h
Ollerton	82.6	7.5	55	2h
Linby	83.0	8.7	61	2h
Creswell	84.5	5.9	91 92	35 mins. 2h
Cortonwood	87.2	3.9	84	3h
Cwm	90.3	2.9	—	5h
Cynheidre	95.2	0.9	—	5h

Table 1(b)
Acetylation data from ketene and from conventional
reagents used in the microwave oven for comparison

O_{OH}/O_{Total} % by Acetylation					
Ketene	**Reaction Time**	**$(CH_3CO)_2O/H_2SO_4$**	**$(CH_3CO)_2O/Py$**	**$CH_{33}COOH/(CF_3CO)20$**	**$(CH_3CO)20/(CF_3CO)20$**
73	100h	53	49	47	43
59	100h	50	49	40	37
75	140h	48	50	37	33
90	125h	62 (1h) 72 (2h)	63 (1h) 65 (2h)	61 (1h) 64 (2h)	54 (1h) 54 (2h)
77	114h	83	50	78	69
55	120h	60	1.6	52	55
17	48h	117	2.5	11	23

THE APPLICATION OF PIXE/PIGE ANALYSIS TO LIQUEFACTION STUDIES

C.J. Lafferty[1], C. Eloi[2], R.K. Anderson[1] and J.D. Robertson[1,2]
[1]Center for Applied Energy Research and [2]Department of Chemistry, University of Kentucky, Lexington, KY 40511-8433.

Keywords: liquefaction, ash analysis, PIXE, PIGE.

Introduction

Proposed 'full-scale' direct coal liquefaction pilot plants all incorporate a combustion/gasification stage to recover the thermal content of the insoluble organic matter derived from the primary dissolution of the coal in process solvent. This step will result in the production of an ash which will have to be either sold as a value-added-product or most likely stored in a designated landfill, with the ongoing costs of leachate treatment added to the overall plant economics. At present, ash derived from coal burning power plants is exempt from federal regulations regarding the long-term disposal of hazardous materials. However a recent US Supreme Court ruling determined that ash produced from municipal incinerators must be treated as hazardous waste[1], increasing overall disposal costs by an estimated factor as high as 10, presenting a potentially severe economic impact upon proposed liquefaction plants. It is therefore imperative that data be obtained regarding both the composition and leaching properties of combusted liquefaction residues in order to more accurately estimate the long term processing costs of this material. Additionally, a need exists to follow the distribution and effective use of dispersed catalysts during liquefaction, as well as catalyst recovery, recycle and rejection from the system, which are especially important should more expensive catalytic systems be contemplated.

Elemental analysis with a high energy charged-particle beam is a powerful analytical tool that has moved out of the realm of the specialized 'nuclear' laboratory and found widespread use amongst researchers in many different areas. We are currently using simultaneous particle-induced X-ray and gamma-ray emission analysis (PIXE/PIGE) to investigate the fate of major, minor and trace metal species during the direct liquefaction of a sub-bituminous coal. In addition, PIXE/PIGE is being used to follow the fate of these species during the combustion of liquefaction residues.

Particle-Induced X-ray Emission Analysis (PIXE)

PIXE as an analytical procedure is a relatively recent innovation, being first reported in 1970 by workers at the Lund Institute of Technology[2]. Because the most common particle used for this purpose is the proton, the acronym has also come to mean proton-induced x-ray emission. PIXE, like other x-ray spectroscopic techniques used for elemental analysis, utilizes the x rays that are emitted from the atoms in a sample when that sample is exposed to an excitation source. The use of a proton beam as an excitation source offers several advantages over other x-ray techniques. Among these are; (1) a higher rate of data accumulation across the entire periodic table and (2) better overall sensitivities, especially for the lower atomic number elements. In the case of electron excitation, the better sensitivity is due to a lower bremsstrahlung background and, in the case of x-ray fluorescence analysis (XRF), the enhanced sensitivity is due to the lack of a background continuum across the entire spectrum. Of course, the chief disadvantage of PIXE is that it requires the use of a particle accelerator.

Particle-Induced γ-ray Emission Analysis (PIGE)

PIGE is based on the detection of prompt γ rays that are emitted following a charged-particle-induced nuclear reaction. The energy of the γ ray is indicative of the isotope present and the intensity of the γ ray is a measure of the concentration of the isotope. This technique is generally combined with PIXE to provide trace level concentration data for the light elements lithium through chlorine. Because it is based upon specific nuclear reactions, the sensitivity of PIGE varies greatly from isotope to isotope. For most light elements, the sensitivity is in the order of 1 to 100 μg per gram. A comprehensive review of the theory and analytical applications of PIGE can be found in the text by Bird and Williams[3].

2. Ashing of Samples.

In order to simulate combustion, samples of the starting coal and the liquefaction resids were ashed in a LECO MAC 400 proximate analyzer at 750°C in air.

3. PIXE/PIGE analysis.

The PIXE/PIGE measurements were performed at the University of Kentucky 7.5 MV Van de Graaf accelerator[7]. The samples were irradiated for 15 minutes with an external 2.5 MeV proton beam in 1 atm. of He. The X rays are detected with a retractable Si(Li) detector with a FWHM resolution of 165 eV at 5.90 keV (Mn Kα). A 10 μm thick critical absorber Cr foil is used to reduce the intensity of the Fe X rays, and a 350 μm thick Mylar film is used to reduce the brehmsstrahlung background. The γ rays are detected with a HpGe detector, 20% relative efficiency, with a FWHM resolution of 2.4 keV at 1274 keV. A detailed description of the IBA facility and the PIXE/PIGE analysis procedure has been previously published[8]. The system was calibrated using standard coals obtained from the US National Institute of Standards and Technology (1632a and 1632b) as well as a NIST standard coal ash (1633). Previous work has confirmed the validity of results obtained using these standards for the analysis of coals and related ashes[9].

Results

Table 1 shows the product yields determined for the liquefaction experiments, which are typical for the experimental conditions and catalysts used. Total conversions measured at 415°C for each of the iron catalyzed runs were significantly higher than the conversions measured for the non-catalyzed runs carried out at 440°C.

Table 2. lists the metal retention indices calculated for each of the liquefaction resids as well as initial composition of the feed coal. Note that a retention index of 100 implies that 100% of the metal originally present in the feed coal was retained in the resid. The retention indices obtained for molybdenum, nickel and zinc were all several orders of magnitude above those calculated from the original coal composition. This was attributed to contamination of the sample with anti-seize compound used to protect the threads of the micro-autoclave during liquefaction. This compound was found to consist of molybdenum disulfide, nickel powder and zinc oxide, which correlates with the enrichments measured. This problem has been corrected in subsequent experiments, however the data to be discussed in this paper will focus on other metals. It is of interest to note that the retention indices measured for sodium, potassium, calcium and titanium were all reduced in the catalyst impregnated resid. samples suggesting the transformation of some of these metals into an oil soluble form during liquefaction.

It is to be noted that the three catalyst-promoted resid samples all show a large increase in iron retention over the parent coal due to the iron impregnation prior to liquefaction. The most efficient form of iron impregnation appears to be the method used in run R3-208-3, super fine iron oxide addition, with 92% of the added iron being detected in the resid sample. The other two methods of iron addition, iron oxide addition and $Fe_2(SO_4)_3.5H_2O$ impregnation showed iron retentions of 75% and 50% of theoretical, suggesting that iron partitioning amongst the liquefaction products may differ as a function of catalyst precursor. Further work is currently underway to examine this hypothesis. The resid samples also showed a high degree of retention for sodium, strontium, aluminum, titanium and manganese.

Table 3. lists the metal retention indices measured for each of the combusted resid samples. Whilst the ashing temperature (750°C) was significantly lower than the temperatures that would be typically found in the combustor/gasifier systems proposed for full scale liquefaction facilities, it does, however, demonstrate the likelihood of the metallic species from the catalyst enriched resids being retained within the resulting ash.

As expected the samples resulting from the Fe catalyst promoted liquefaction runs again show a high degree of enrichment in iron over the feed coal, whilst high percentages of strontium, aluminum, titanium and manganese are also retained in the ash. The retention of these metals in the combustor ash would have important consequences on the composition of leachate generated from a storage landfill containing combustor/gasifier ash. Future work will be directed

Comparison With Other Analytical Techniques

Conventionally, analyses of minor and trace elements in coal and coal liquefaction and combustion residues have been carried out by Atomic Absorption (AA) and Inductively Coupled Plasma Atomic Emission (ICP-AE) spectroscopy, or by instrumental methods such as XRF or Neutron Activation Analysis (NAA). While the sensitivity of PIXE and PIGE for most elements is below that of AAS, ICP-AES, and NAA, it is important to keep in mind that there is no need to use a higher sensitivity than required by the analytical situation.

In comparison to PIXE/PIGE, the main disadvantage of AAS and ICP-AES is the complicated and time consuming sample preparation procedure required prior to analysis. These steps usually involve wet or dry ashing of the coal, and dissolution of the ash via acid digestion or fusion. During these procedures, great care must be taken to ensure that volatile elements such as As and Pb are not lost and that sample contamination is avoided. The other principal drawback of AAS and ICP-AES is the possibility of chemical matrix interferences.

While NAA has greater sensitivities for most metals (e.g. Hg, Cd, Sb) than PIXE in coal and coal ash, pre- or post- irradiation chemical separations are often required in order to achieve maximum sensitivities. Moreover, NAA cannot be used to determine some of the environmentally significant elements such as Pb, Tl and Sn. Finally, PIXE/PIGE can provide a rapid multielemental analysis (20 to 30 elements) in 15 to 20 minutes, whereas a complete multielemental analysis by NAA may require multiple irradiations and up to 3 months of a delayed counting period.

The principal advantage of applying PIXE/PIGE to these particular resid samples is that the technique requires only a small amount sample (≈ 100 mg) for a complete metal analysis to be performed. Other traditional techniques require several grams of sample in order that ashing and acid digestion be carried to produce sufficient solution for a complete metal analysis.

Experimental Procedure

1. Coal Liquefaction Samples.

To provide liquefaction residues for this study, experiments were performed using Wyodak coal supplied by CONSOL, Inc. from the Black Thunder mine in Wright, Wyoming. Four runs were made without added catalyst at temperatures to 440°C, and reaction times to thirty minutes using tetralin as solvent. In addition, to gauge the impact that typical catalysts may have on the composition of these residues, three runs were made at 415°C for 30 minutes with different Fe catalyst precursors.

The three precursors used included $Fe_2(SO_4)_3.5H_2O$ impregnated on the coal feed in an aqueous solution, without base precipitation (FeIII);[4] Superfine Iron Oxide (SFIO), a finely divided 30 Å iron oxide supplied by MACH I, Inc.;[5] and iron oxide (IO) used as a catalyst at the Advanced Coal Liquefaction Research and Development Facility at Wilsonville in Run 262, supplied by Kerr-McGee[6]. Additional information on these materials and methods of preparation is available in the literature cited.

In a typical liquefaction experiment, 3 g of coal, ground to -200 mesh, was added to 50 ml microautoclaves with 5.4 g tetralin. When Fe was added, dimethyl disulfide was also added in an amount sufficient to convert the Fe to pyrrhotite. The reactor was pressurized with hydrogen to 6.89 MPa (cold pressure), and agitated in a heated, air fluidized sand bath at 400 cpm. The reactor was cooled in a second sand bath, and gas products were collected and analyzed by gas chromatography. The other products were removed from the reactor with THF and extracted in a Soxhlet apparatus. The THF solubles were subsequently separated into pentane soluble (Oils) and pentane insoluble (PA+A) fractions. Total THF conversion was determined from the amount of insoluble material that remained (resid). Any added Fe was subtracted from the residue sample weight at its equivalent weight of pyrrhotite. Oils are calculated by difference, and as a result, water produced during liquefaction, as well as any experimental error, is included in this fraction. All product yields are stated on an maf coal basis.

towards obtaining larger quantities of combusted resids in order to evaluate the leaching characteristics of these materials via standard procedures.

Conclusions

The results reported in this paper have demonstrated the advantages of using PIXE/PIGE as an approach for following the distribution of metal species during liquefaction. Further employment of this technique will facilitate a greater understanding of catalyst utilization, recovery and recycle during coal liquefaction, as well as emerging solid waste disposal concerns.

Acknowledgements

Support for this work was provided by the University of Kentucky Center for Applied Energy Research and the University of Kentucky Graduate School. Preparation of the liquefaction resid samples was carried out under DOE contract DE AC22-91PC91040.

Table 3. Metal Retention Indices for Combusted Resid. Ash (% Metal retained in Ash.)

	R2-154-2	R2-154-1	R3-152-1	R3-80-1	R3-258-2	R3-208-3	R3-342-2
F	71	111	75	105	0	48	10
Na	83	88	64	86	67	56	61
Al	80	97	64	80	59	75	61
K	172	238	92	239	167	124	176
Ca	62	72	62	58	65	49	47
Ti	55	62	55	50	52	45	40
Mn	80	101	71	65	95	93	133
Fe	69	82	67	67	238	328	321
Ni	8160	17313	3397	26649	14598	3722	10866
Zn	3447	175	1698	6939	5033	107	4457
Rb	0	45	45	38	85	0	70
Sr	63	73	60	61	65	50	49
Zr	44	43	21	26	25	55	37
Mo	11421	25813	5172	28395	15408	3963	17125
Ag	44	123	143	158	46	43	0
Ba	40	64	56	40	50	43	44

References

1. American Chemical Society, *Chemical and Engineering News*, May 9, 1994, p 21.
2. T.B. Johansson, K.R. Akselsson and S. A. E. Johansson, *Nuclr. Instr. Meth. Phys. Res.* 84, 141 (1970).
3. *Ion Beams for Metal Analysis*, J.R. Bird and J.S. Williams, Eds. (Academic Press, San Diego, CA, 1989).
4. H.F. Ni, R.K. Anderson,E.N. Givens and J.M. Stencel, *Prep. Pap.- Am. Chem. Soc., Div. Fuel Chem.* 1993, *38 (3)*, 1107.
5. J. Zhao, F.E. Huggins, Z. Feng, F. Lu, N. Shah and G.P. Huffman, *Journal of Catalysis*, 1993, *143*, pp 499-509.
6. R. K. Anderson, E. N. Givens and F.J. Derbyshire, *Prepr. Pap.-Am. Chem. Soc.,Div. Fuel Chem.* 1993, *38 (2)*, 495.
7. J.M. Savage, A.S. Wong and J.D. Robertson, J. of Trace and Microprobe Tech.. 10(2-3) (1992) 151-168.
8. A.S. Wong, E.A. Lurding J.D. Robertson and H. Francis, J. of Trace and Microprobe Tech. 10(2-3) (1992) 169-182.
9. A.S. Wong and J.D. Robertson, Proc. Tenth Annual Pittsburgh Coal Conference, 1122 (1993).

Table 1. Product Yields for Liquefaction Experiments.[a]

Catalyst Added	none	none	none	none	FeIII	SFIO	IO
Rxn temperature, °C	415	415	440	440	415	415	415
Rxn time, min	15	30	15	30	30	30	30
Added Fe, wt% mf Coal	none	none	none	none	0.8	1.2	1.2
S/Added Fe, m/m	none	none	none	none	1.6	3.0	3.0
Products, wt% maf Coal							
HC Gases	0.4	0.7	0.9	1.3	0.8	1.5	1.3
$CO+CO_2$	4.2	4.4	5.0	5.8	4.9	6.0	4.4
Oils	21	28	39	45	36	37	39
PA+A	40	43	36	28	42	40	39
IOM	34	24	19	20	16	16	16
THF Conv.	66	76	81	80	84	84	84
Run numbers	R2-154-2	R2-154-1	R3-152-1	R3-80-1	R3-258-2	R3-208-3	R3-342-2

a. 3.0 g Black Thunder coal in 5.4 g tetralin, using 6.89 MPa H_2 (cold).

Table 2. Metal Retention Indices for Liquefaction Resids. (% Metal Retained in Resid.)

	A.R. Coal (ppm)	R2-154-2	R2-154-1	R3-152-1	R3-80-1	R3-258-2	R3-208-3	R3-342-2
F	58	128	143	231	116	125	121	96
Na	319	98	91	84	68	67	65	68
Al	6703	81	111	95	74	65	99	78
K	351	78	113	134	50	82	64	79
Ca	12843	67	61	56	54	39	35	36
Ti	623	80	66	58	54	38	44	39
Mn	44	109	108	71	69	76	63	124
Fe	3807	82	81	81	64	207	379	315
Ni	2	7897	14415	26323	2476	10367	3069	11079
Zn	17	2806	6295	7733	1719	3945	1003	4055
Rb	9	98	108	86	48	93	90	95
Sr	2	82	85	76	65	67	61	55
Zr	243	43	57	46	32	30	45	40
Mo	N.D.	10781	27874	31960	5457	15120	5195	19191
Ag	16	41	112	128	194	0	52	0
Ba	779	64	59	56	44	62	71	54

X-RAY CHARACTERIZATION OF THE CRYSTALLINE INORGANIC SPECIES AND THE ORGANIC MATRIX IN WILSONVILLE RECYCLE RESID FROM RUN # 259.

David L. Wertz and Charles B. Smithhart*
Department of Chemistry & Biochemistry
and
Center for Coal Product Research
University of Southern Mississippi
Hattiesburg, MS 39406-5043 USA

Key Phrases: Pyrrhotite 11-C, hard and soft x-ray fluorescence, x-ray diffraction and absorption.

INTRODUCTION.

Products recovered from the two-stage direct liquefaction of a Pittsburgh seam coal (and several other coals) produced at the Wilsonville facility have been studied extensively as part of a global project sponsored by the U.S. Department of Energy.[1]

An x-ray scattering-diffraction-fluorescence spectral study of the resids produced from processing Illinois # 6 coal at the Wilsonville facility has recently appeared. The effect(s) of the two-stage catalytic processes on the poly-cyclic aromatic character in the resids (as indirectly measured by the diffuse scattering caused by its graphitic layer stacking) and on the crystalline inorganic materials are reported.

Presented below are our preliminary finding from an x-ray study of the recycle resid produced during run # 259 at the Wilsonville facility. This study is a continuation of the group's efforts to utilize x-ray characterization methods to better understand the molecular structuring in coals and how various processes (such as liquefaction) affect that structuring.

EXPERIMENTAL.

Each sample was received (from Brandes) as a fine powder and was analyzed "as received."[1]

Diffraction Experiments. A carefully weighed amount (ca. 0.5 grams) of each sample was deposited onto the sample holder (1.0 mm depth) and mounted into our θ-2θ x-ray diffractometer. The sample was irradiated with copper x rays. Scattered x-ray intensities were accumulated by measuring the CuK_α wavelength (made monochromatic by use of a graphite crystal at $\Delta 2\theta = 0.01°$ from $2\theta = 10.00°$ to $2\theta = 90.00°$ for 2 second intervals using the conventional step-scan procedure.[3]

Absorption Experiments. A carefully weighed amount of each sample (ca. 0.1 or 0.5 grams) was deposited onto the aluminum sample holder (which served as the substrate). The intensity of the (311) peak of the aluminum was measured both in the presence of and in the absence of the resid sample.[4] For the recycle resid, an aluminum sample holder with depth of 1.0 mm was used. For its tetrahydrofuran insoluble fraction, a sample holder of 0.1 mm depth was used.

X-Ray Fluorescence Spectral Experiments. Approximately 1 gram of each resid was pressed into a pellet and then mounted into our wavelength dispersive x-ray spectrometer. Using chromium as the exciting radiation, both a soft x-ray spectrum (using a MOXTEK multi-layer as the monochromator) and a hard x-ray spectrum (using graphite as the monochromator) were obtained using the normal step-scan procedure.

RESULTS AND DISCUSSION.

X-Ray Fluorescence Experiments. The soft and hard x-ray spectra of the recycle resid and its THF-insoluble fraction are presented in Figures One and Two. After irradiation with the Cr x rays, large secondary x-ray peaks due to iron and calcium are observed, along with smaller peaks due to titanium, potassium, sulfur, and silicon are

observed in both spectra.

Mass Absorption Experiments. Shown in Figure Three are the intensities of the (311) diffraction peak from the aluminum sampleholder in the absence of and in the presence of the recycle resid sample. The mass absorption coefficient of each resid was calculated by:

$$\mu = [T \cdot \sin\theta / 2 \cdot m] \cdot \ln[A_s/A_p]. \quad (1)$$

In eq. 1, T is the irradiate surface area, $\theta = 0.5 \cdot 2\theta$ for the (311) peak, and A_s and A_p are the areas measured under the (311) peak of aluminum in the absence of and in the presence of the finely powdered resid samples. The mass absorption coefficient of each sample is presented in Table I.

X-Ray Diffractograms. The measured secondary x-ray intensity, $I(2\theta)$ was converted to the absorption corrected intensity by:

$$I^*(2\theta) = \mu \cdot m \cdot I(2\theta) / \{1 - \exp(-2 \cdot \mu \cdot m / T \cdot \sin\theta)\}. \quad (2)$$

The absorption corrected diffractograms of the recycle resid and its THF-fraction are shown in Figure Four. The absorption corrected diffractograms have been utilized throughout the remainder of this manuscript because peaks $I^*(2\theta)$ are proportional to the abundances of the various analytes in the complicated resid matrices.

The diffraction peaks due to the crystalline mineral components present in the resid (B) and its THF-insoluble component (A) are shown in Figure Six. That the mineral peak intensities are much higher in the THF-insoluble fractions is consistent with its significantly higher ash content and its significantly higher x-ray mass absorption coefficient and substantiates that extraction by tetrahydrofuran increases the relative abundances of the crystalline minerals by preferentially removing carbonaceous materials from the resid.

Huffman, Huggins, et al.[6] have recently reported that pyrrhotite ($Fe_{1-x}S$) is formed by reaction with H_2S during direct coal liquefaction processes using iron-based catalysts, with iron oxide(s) present only in the case of insufficient sulfur.[6] Our best current correlation to date of the diffraction peaks with the crystalline components present in these samples involves pyrrhotite 11-T as well as α-quartz and other minerals but not iron oxide(s).[7]

REFERENCES

* DOE EPSCoR Fellow. Funding of EPSCoR Fellowship is acknowledged.

1. Brandes, S. D., R. A. Winschel, and F. P. Burke, **Am. Chem. Soc., Div. Fuel Chem.**, 1991 (36) 1172; 1992 (37) 1243.

2. Wertz, D. L., C. B. Smithhart, M. L. Steele, and S. Caston, **J. Coal. Quality**, 1993 (12) 36.

3. Wertz, D. L., **Energy Fuel**, 1990 (4) 442.

4. Wertz, D. L., C. B. Smithhart, and S. L. Wertz, **Adv. X-Ray Anal.**, 1990 (33) 475.

5. Wertz, D. L. and M. Bissell, **Energy Fuel**, 1994 in press.

6. Huffman, G. P., F. E. Huggins, et al., **Energy Fuel**, 1993 (7) 285.

7. Joint Committee of Powder Diffraction Systems; International Centre for Diffraction Data, 1991. # 29-726.

TABLE I. MASS ABSORPTION COEFFICIENT CALCULATIONS.

SAMPLE	MASS (g)	A_s (CPS)	A_p (CPS)	μ cm_2/g
recycle resid	0.3351	26,130	2,303	13.8
THF-insoluble	0.1036	23,886	1,215	54.8

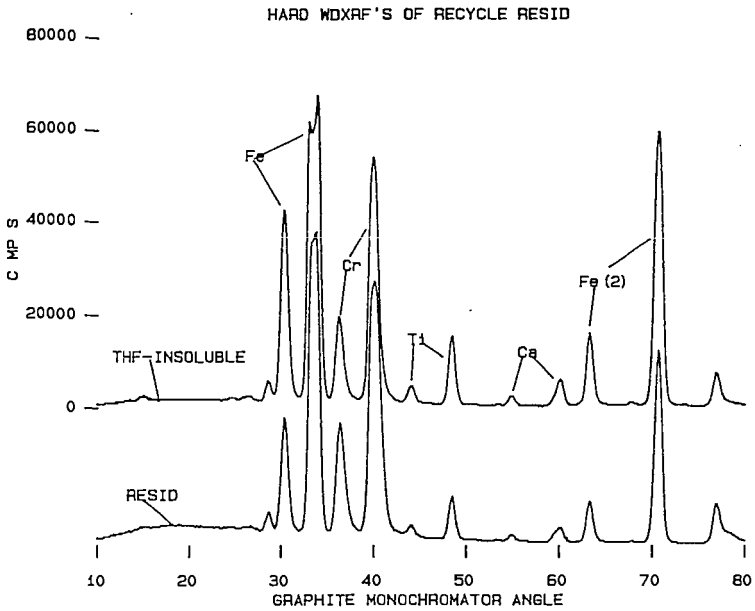

FIGURE ONE. Hard x-ray spectra of the recycle resid and its THF-insoluble fraction.

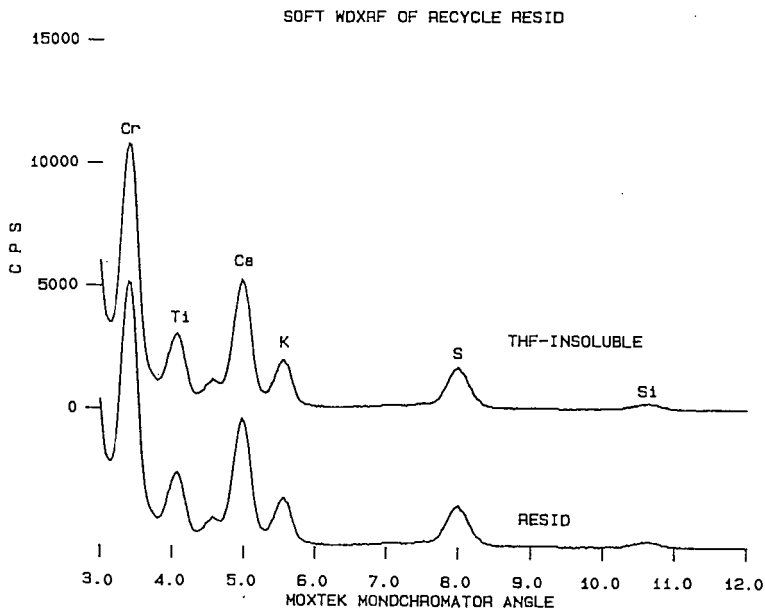

FIGURE TWO. Soft x-ray spectra of the recycle resid and its THF-insoluble fraction.

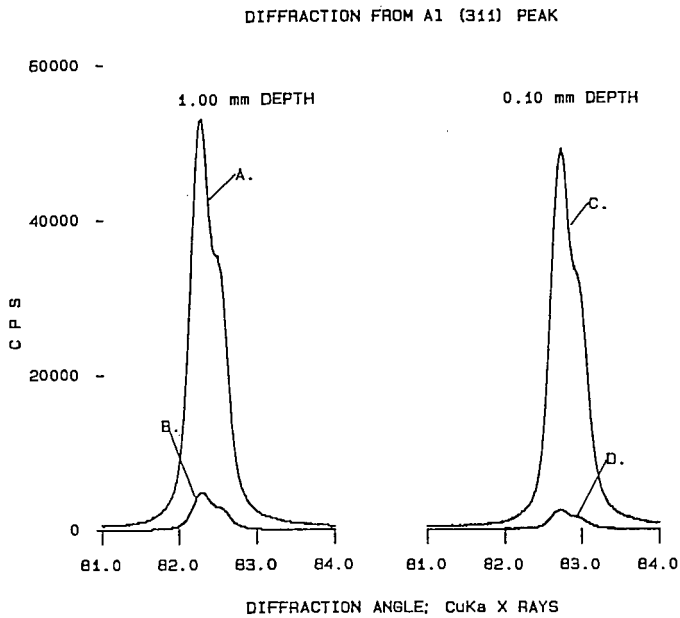

FIGURE THREE. Diffraction from the (311) of the aluminum sample holders. (A) Diffraction intensity from the sample holder with 1.00 mm depth, and (B) intensity from the sample holder with 0.3351 g of the recycle resid deposited onto it. (C) Diffraction intensity from the (311) peak of the aluminum sample holder with 0.10 mm depth, and (D) intensity from the sample holder with 0.1036 g deposited onto it.

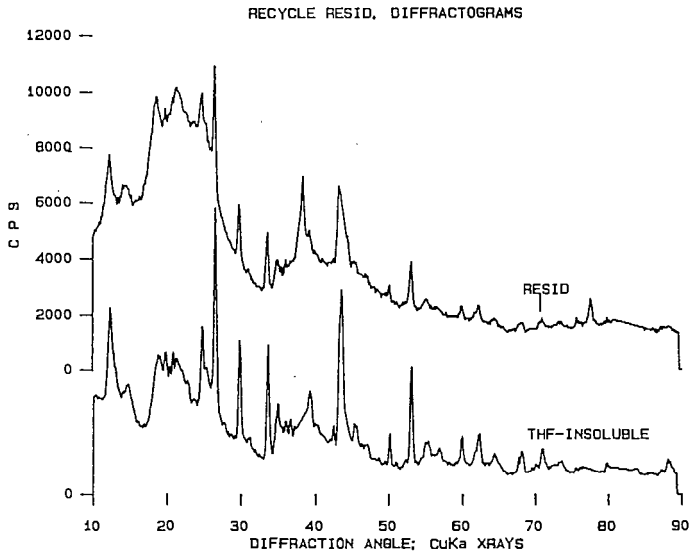

FIGURE FOUR. Absorption corrected diffractograms of the recycle resid and its THF-insoluble fraction.

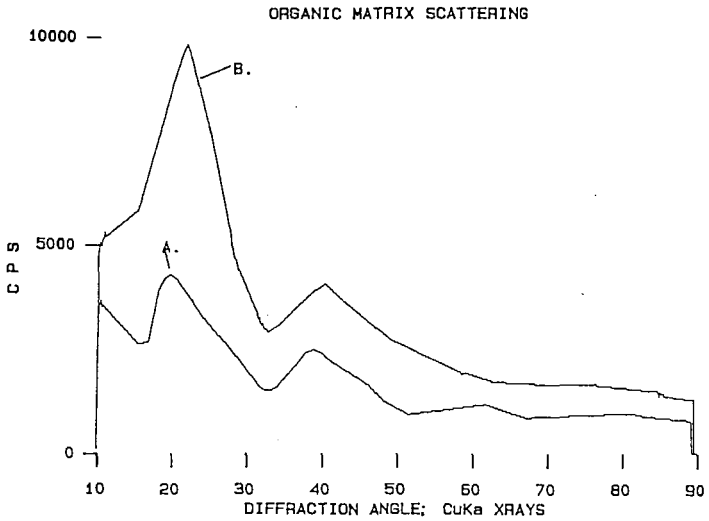

FIGURE FIVE. The diffuse scattering from the recycle resid (B) and its THF-insoluble fraction (A).

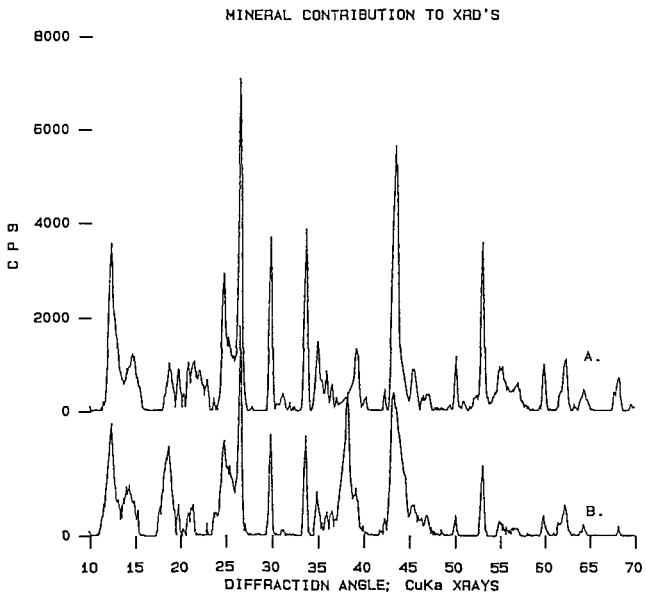

FIGURE SIX. Conventional diffraction from the crystalline materials in its THF-insoluble fraction (A) and the recycle resid.

NITROGEN XANES STUDIES OF ARGONNE COALS

S. Mitra-Kirtley[1]
O. C. Mullins[2]
J. van Elp[3]
S. P. Cramer[3,4]

[1] Dept. of Physics and Applied Optics, Rose-Hulman Institute of Technology, Terre Haute, IN 47803
[2] Schlumberger-Doll Research, Old Quarry Road, Ridgefield, CT 06877
[3] Lawrence Berkeley Lab, Berkeley, CA 94720
[4] Dept. of Applied Science, University of Califonia, Davis, , Davis, CA 95616

Keywords: XANES, nitrogen, coals

ABSTRACT

All the major forms of nitrogen in a group of Argonne coals are detected and quantified by X-ray Absorption Near-Edge Structure (XANES) studies; these forms are pyridine, pyridone, and pyrrole. In addition, there is evidence of aromatic and quarternary amines in small amounts, and virtually no saturated amines. Pyridone is found to be abundant in the low rank coals; with maturation of coals, the pyridone forms become transformed into pyridine forms. The quarternary nitrogen has been analyzed as a potential contribution to coal spectra. This compound has a distinctive peak in the nitrogen XANES spectra allowing contribution of quarternary nitrogen in the coal spectra to be determined. By this method we have found that coals generally have at most small quantities of quarternary nitrogen.

INTRODUCTION

Important natural resources such as coal often contain heteroatoms such as sulfur and nitrogen; these heteroatoms pose serious threats to the environment, as well as to effective utilization of the resources. Elucidation of the chemical structures of the heteroatom containing compounds in coals aids in the removal of the compounds, and also in understanding the complex maturation processes of these fossil fuels.

X-ray Absorption Near-Edge Structure (XANES) spectroscopy has been very versatile in direct and non-destructive studies of fossil fuel samples. Sulfur XANES studies have been performed successfully on coals(1-6), and petroleum asphaltenes(7-9). XANES studies showed that both coals and petroleum asphaltenes contain saturated and aromatic forms of sulfur; thiophenic (aromatic) is the most dominant form, followed by sulfidic (saturated) form. There are small amounts of oxidized forms in coals and asphaltenes, and unlike asphaltenes, some coals have inorganic sulfide structures present in them.

Nitrogen XANES studies have also been successfully performed on coals(10,11) petroleum asphaltenes(12), and organic parts of source rocks such as kerogens and bitumens(13). Several nitrogen model compounds have been studied to analyze the fossil fuel spectra; they are pyridine, pyridone, pyrrole, aromatic amine, porphyrin, and saturated amine. It is found that most of the nitrogen is found in aromatic forms in these fossil fuel samples, with negligible quantities of saturated forms. Pyrrolic and pyridinic are the most common forms of nitrogen in these samples. In low rank coals, considerable amounts of pyridone are also found, whereas in the high rank coals the pyridone structures are mostly replaced by pyridine structures. In addition, coals also have small quantities of aromatic amines. Some quantities of porphyrin and smaller quantities of saturated amines are present in the kerogens and bitumens in addition to the other nitrogen structures mentioned above.

Other methods which have been used in the past to elucidate the nitrogen chemical structures of fossil-fuels have been mostly destructive and indirect. Chromatographic and extraction methods have been problematic either due to high molecular weights or they are not powerful enough to study the entire sample. Several spectroscopic studies have been performed; however, they suffered mostly from resolution difficulties. X-ray Photoelectron Spectroscopy (XPS) studies on coals(14-16) and coal-related materials(17) have been informative. Earlier XPS studies on

coals(15) have shown the presence of pyridine and pyrrole; a more recent study(16) has also shown the presence of quarternary nitrogen. XPS experiments clearly could not resolve signatures arising from oxygen containing pyridone or the aromatic and saturated amine structures in coals.

In this report, preliminary XANES studies of quarternary nitrogen (pyridinium) are presented as a potential contributor to coal spectra. Several analogues of pyridinium compounds have been studied. It is found that these structures have a distinct sharp π^* resonance at 401.8 eV, and is invariant among the different analogues. The pyridinium resonance is between the pyridine and the pyridone resonances, and is distinguishable from those from other structures. The coal spectra do not show any prominent sharp feature at the pyridinium π^* energy, and at most show only small quantities of these structures. The pyridone percentage far exceeds the quarternary percentage, and the inverse connection between the pyridone and pyridine percentages is still more prominent.

EXPERIMENTAL SETUP

Nitrogen x-ray data on all the coal and model samples have been obtained at the soft x-ray beam line U4B, designed and constructed by AT&T Bell Labs(18), at the National Synchrotron Light Source at Brookhaven National Laboratory. U4B is equipped with a grating monochromator with a grating of 600 lines/mm. The sample chamber was maintained at pressures of 10^{-9} to 10^{-10} torr by means of a turbo-molecular pump and a cryopump. The samples were mounted on pieces of nitrogen-free 3M tape and positioned on a sample holder by a load-lock system. A multichannel Ge fluorescent detector(19) was used with a 2-μs shaping time. The energy resolution was about 140-400 meV.

The coal samples were provided by Dr. Karl Vorres from Argonne Premium Coal Sample Bank at Argonne National Laboratory(20). The coal sample suite consisted of eight samples; these samples belonged to varying ranks, starting from lignite to low-volatile bituminous. The samples were: a low-volatile bituminous coal from Pocahontas #3, VA (POC); a medium-volatile bituminous coal from Upper Freeport, PA (UF), four high-volatile bituminous coals from Pittsburgh #8, PA (PITT), Lewiston-Stockton, WV (WV), Blind Canyon, UT (UT), and Illinois #6, IL (IL), and a subbituminous from Wyodak-Anderson, WY (WY), and a lignite from Beulah-Zap, ND (ND).

The nitrogen model samples were obtained from Aldrich Chemical Company The pyridine samples were acridine, 4,7-diphenyl-1,10-phenanthroline, phenanthridine, di-p-tolyl pyridine, and 4-polyvinylpyridine-costyrene; the pyridinium samples were pyridinium dichromate, 1-ethyl-4-(methoxycaronyl) pyridinium iodide, and pyridinium 3-nitrobenzenesulfonate; the pyridone samples were 6-(2,2-diphenyl-2-hydroxyethyl)-2(1H)-pyridone, 2-hydroxyquinoline, 1-hydroxyisoquinoline, 1-methyl-4-pentadecyl-2(1H)-quinoline; the pyrrole samples were tetrahydrocarbazole, 2-phenylindole, 9-vinylarbazole, and carbazole; the aromatic amine samples were 2-aminofluorene, and 2,7-diaminofluorene, and the saturated samples were 1,3,5-tribenzylhexahydro-1,3,5-triazine, and diaminododecane. All the coal and the nitrogen model XANES spectra were calibrated with respect to the first π^* resonance of zinc octaethylporphyrin at 399.72 eV.

RESULTS AND DISCUSSIONS

The XANES spectra of the coals show similar features with three well-resolved resonance regions(11). The feature at 401.8 eV is relatively insignificant compared to the major resonances; it occurs at the red tail-end of the second broad resonance region between 402 and 405 eV. The major resonances are much more intense; of these, the first resonance at 399.7eV varies in intensity among the different ranked coals. The lowest rank coal has a less intense resonance at 399.7eV while the same resonance in the higher rank coals is much more intense. The second resonance region, upon close inspection, shows the presence of three resonances, at ~402eV, ~403.5eV, and at ~405 eV. The intensity of the 402 eV also varies significantly among coals of different ranks; it is more prominent in the low rank coals than in the high rank coals. The feature at 405eV is also comparatively insignificant, and is merely a valley with varying depth, with no strong trend as a function of coal rank. All the coal spectra show a prominent resonance at 408eV.

XANES studies of different nitrogen model compounds have been performed in order to analyze the coal spectra. In the present report, spectra of six groups of model compounds have been associated with the coal spectra; they are pyridine, pyridinium, pyridone, pyrrole, aromatic amine and saturated amine. In our previous work(11) we have analyzed all the above nitrogen structures except for pyridinium. The pyridinium π^* resonances are sharp, and invariant; they are well grouped together at around 401.8 eV, consistent with our earlier results(11) of the different π^* resonances of pyridine analogues (at 399.7 eV), pyridone analogues (at 402 eV), pyrrole analogues (at 403.5 eV), and aromatic amines (at 405eV). The pyridinium π^* resonances occur at a higher energy than the pyridine π^* resonances; this is consistent with the observation in the case of sulfur structures(5), where the π^* resonances are blue shifted with more positive oxidation numbers. The π^* resonances of pyridone, on the other hand, are generally at higher energies than pyridinium resonances. Perhaps with more number of analogues a small overlap may be observed between the pyridone and pyridinium resonances. The pyrroles have higher energy π^* resonances compared to pyridine; we have explained this due to the difference of the orbital location of the lone pair of electrons at the nitrogen site. The fact that each different nitrogen structure has a characteristic π^* absorption feature distinct from that of another structure helps in the analysis of coal spectra which may contain several different nitrogen structures.

The coal spectra do not show any prominent absorption resonance at the pyridinium signature (401.8 eV). The coal spectra show only a wing at this absorption energy which is at least in part due to the pyridone resonance occurring at a higher energy. This, therefore, shows that there is at most a small amount of pyridinium present in the coals. This is consistent with the XPS results(16) which show presence of small amounts of quarternary nitrogen in these coals. In contrast, XANES results show that pyridine and pyrrole are the two major nitrogen structures in coal, consistent with XPS studies(16). XANES data also show signatures arising from pyridone, aromatic amine and saturated amine. To the best of our knowledge, unlike XANES methodology, XPS technique can not resolve features arising from pyridone, aromatic and saturated amines; XANES and XPS can therefore be considered as complimentary techniques.

Previous results(11) show that the low rank coals have a significant pyridone percentage and a low pyridine percentage; on the other hand, the opposite is true with the higher rank coals. This suggests that with maturation of coal, pyridone structures lose their oxygen content, and become transformed into pyridine. The variation of the intensity of the pyridine and the pyridone peaks as a function of coal rank is much more drastic than the small pyridinium content in the different coals.

CONCLUSIONS

XANES methodology is an excellent tool for studying heteroatom structures in coals. Nitrogen occurs mostly in aromatic forms in the coals; pyridine and pyrrole are the two most common nitrogen structures; low rank coals have a high percentage of pyridone and a small percentage of pyridine, and the opposite is true with the high rank coals. This leads to the conclusion that as coals mature, oxygen is driven away, and pyridone structures are converted into pyridine structures. XANES data do not show any prominent resonance at the quarternary nitrogen π^* energy, and low rank coals have more significant amounts of pyridone than quarternary nitrogen structures.

REFERENCES

1. C. E. Spiro, J. Wong, F. W. Lytle, R. B. Greegor, D. Maylotte, and S. Lampson, Science, **226**, 48 (1984).

2. G. P. Huffman, F. E. Huggins, N. Shah, D. Bhattacharya, R. J. Pugmire, G. Davis, F. W. Lytle, and R. B. Greegor, Processing and Utilization of High Sulfur CoalsII, Y. P. Chugh et al eds. (Elsevier, amsterdam, 1987), p.3

3. M. L. Gorbaty, G. N. George, and S. R. Kelemen, Am. Chem. Soc. Div., Fuel Div. Che. Prepr., 34, 738, (1989)

4. G. P. Huffman, F. E. Huggins, S. Mitra-Kirtley, N. Shah, R. Pugmire, B. Davis, F. W. Lytle, and R. B. Greegor, Energy and Fuels, 3, 200, (1989)

5. G. P. Huffman, S. Mitra-Kirtley, F. E. Huggins, N. Shah, S. Vaidya, and F. Lu, Energy and Fuels, **5**, 574, (1991)

6. M. L. Gorbaty, G. N. George, and S. R. kelemen, Fuel, **69**, 1065, (1990)

7. G. N. George, and M. L. Gorbaty, J. Am., Chem., Soc., **111**, 3182, (1989)

8. S. R. Kelemen, G. N. George, and M. L. Gorbaty, Fuel, **69**, 939, (1989)

9. G. S. Waldo, O. C. Mullins, J. E. Penner-Hahn, and S. P. Cramer, Fuel, **71**, 53, (1992)

10. S. Mitra-Kirtley, O. C. Mullins, J. van Elp, and S. P. Cramer, Fuel, **72**, 133, (1993)

11. O. C. Mullins, S. Mitra-Kirtley, J. van Elp, and S. P. Cramer, Applied Spectroscopy, **47(8)**, 1268, (1993)

12. S. Mitra-Kirtley, O. C. Mullins, J. van Elp, S. George, J. Chen, and S. P. Cramer, J. Am. Chem. Soc., **115**, 252, (1993)

13. S. Mitra-Kirtley, O. C. Mullins, J. F. Branthaver, and S. P. Cramer, Energy and Fuels, **7(6)**, 1128, (1993)

14. P. Burchill, Proc. of the International Conf. on Coal Science, J. A. Moujlin et al eds., (Elsevier, Amsterdam, 1987)

15. P. Burchill, and L. S. Welch, Fuel, **68**, 100, (1989)

16. S. R. Kelemen, M. L. Gorbaty, S. N. Vaughn, P. J. Kwiatek, Prepr. Paper, Am. Chem., Soc., Fuel Div. Chem., **38(2)**, 384, (1993)

17. S. Wallace, K. D. Bartle, and D. L. Perry, Fuel, **68**, 1451, (1989)

18. C. T. Chen, Nucl. Instrum. Methods Phys. Res., Sect. A, **256**, 595, (1987); C. T. Chen, and F. Sette, Rev. Sci. Instrum., **60**, 1616, (1989)

19. S. P. Cramer, O. Tench, M. Yocum, H. Kraner, L. Rogers, V. Radeka, O. C. Mullins, and S. Rescia, X-ray Absorption Fine Structure, Proc. of the 6th International XAFS Conf., S. S. Hasnain ed. (Ellis Horwood, Chichester, 1991), p. 640

20. K. S. Vorres, Energy and Fuels, **4**, 420, (1990)

Comparison of Element-Specific Capillary Chromatography Detectors for the Identification of Heteroatomic Species in Coal Liquids

S.C. Mitchell, K.D. Bartle, K.M.L. Holden
School of Chemistry, University of Leeds
Leeds, LS2 9JT, UK.

C.E. Snape
Department of Pure & Applied Chemistry, Univ. of Strathclyde,
Glasgow, G1 1XL, UK.

S. Moinelo and R. Garcia
Instituto Nacional del Carbon
Apartado 73, 33080 Oviedo, Spain.

Keywords: Gas chromatography, element-selective detection, polycyclic aromatic compounds, atomic emission detection

Abstract

A series of heteroatom-rich coal and coal-derived liquids have been analysed using gas chromatography (GC) in combination with three different element-selective detectors. Selected chromatograms, including a supercritical extract (Mequinenza lignite) and aromatic fractions isolated from coal tar pitch samples are presented. In each case a series of sulphur- and/or nitrogen-containing compounds have been identified using either flame photometric detection (GC/FID/FPD) or nitrogen-phosphorous detection (GC/FID/NPD) and the information compared with that obtained from a GC coupled to an atomic emission detector (GC-AED). Preliminary results have demonstrated the relative response characteristics of each detector and their respective ability to acquire qualitative and quantitative information in interfering background matrices. Further, due to the unique capabilities of GC-AED, a number of dual heteroatomic (sulphur-oxygen and nitrogen-oxygen) compounds have been identified.

Introduction

Polycyclic aromatic compounds (PAC) predominate in coal liquids as well as in other heavy oils derived from fossil fuels. While the polycyclic aromatic hydrocarbons (PAH) are usually the most abundant PAC, nitrogen-, sulphur-, and oxygen-containing compounds are also present in significant concentrations and their impact on processing and the environment/human health are well documented[1-3]. Numerous characterisation studies have been conducted into the nature of aromatic and heterocyclic compounds present in such materials and many researchers have derived information from pyrolysis products, solvent extracts and liquefaction products[4-6]. Most of the recent work has focussed on the development of techniques for both seperation and detection of compound or element-rich fractions. The principal methods employed to date include capillary column gas chromatography[7,8], liquid chromatography[9], element-selective detection[10-16], high resolution mass spectrometry[17-20] and X-ray techniques[21].

For the identification of heteroatomic species, the most successful approach has been the use of capillary column gas chromatography in combination with gas chromatography/mass spectrometry[22-24]. However, interpretation is complicated due to the properties of aromatic heterocycles being very similar to those of aromatic hydrocarbons[2] and prior fractionation or enrichment of target compounds into compound classes is considered an essential step for their unambiguous identification[12,13].

The use of element-selective detection in gas chromatography, for simplifying the analysis of complex hydrocarbon mixtures, is now relatively commonplace[25]; but their application, particularly in the determination of trace concentrations of polycyclic

aromatic compounds, requires that due care and consideration be exercised. Flame photometric detector (FPD), has been extensively used for qualitative analysis of sulphur compounds but suffers from many inherent problems including a non-linear response (approx. quadratic) and compound dependency which makes quantitative analysis difficult and time-consuming. Moreover, quenching of the signal by coeluting hydrocarbons can considerably reduce sensitivity[26]. For nitrogen compounds, the nitrogen-phosphorous detector (NPD), with a specifity (N/C) of 10^3-10^5 and a linear response over several orders of magnitude (see Table 1) is well suited to handling trace analysis in complex hydrocarbon mixtures[27]. The relatively recent introduction of atomic emission detection (AED), as a commercially available analytical tool has received comparitively little attention[28-30]. GC-AED offers highly selective, simultaneous, multi-elemental detection and claims to suffer from none of the enigmas associated with other element-selective detectors. Based on a microwave induced plasma (MIP) and employing a moveable photodiode array (PDA) in a flat focal plane spectrometer, the AED is capable of monitoring a broad range of elements at considerably lower levels than most classical GC detectors[27]. Detector response is linear and compound independent, with the possibility of empirical and molecular formula determination.

GC analysis

HP5890 Series II Gas chromatographs were used for AED and NPD analysis. A Perkin-Elmer 8500 gas chromatograph was used for FPD analysis. The GC-AED system also comprised an HP7637A Autosampler interfaced to an HP5291A AED Chemstation.
Samples were analysed by GC-AED and GC/FID/FPD using a 25m BPX-5 or equivalent column with 0.5µm film thickness and 0.32mm i.d. For NPD analysis a 25m SE-54 column with 0.25µm film thickness and 0.25mm i.d. was used. GC and AED parameters are given below:

GC parameters

Detector	*FPD*	*NPD*	*AED*
Injection port temperature (°C)	300	300	350
Injection mode	split (1:80)	split (1:80)	splitless
Column-detector coupling	on-line	on-line	coupled to cavity
Injection volume	1µl	1µl	0.2 or 1µl
Carrier gas	Helium	Hydrogen	Helium*
Oven program	Initial temp: 50°C; Ramp rate: 4°C/min to 280°C; Hold: 20 min		

* High purity Helium (99.999999%) as recommended[28]

AED parameters

Element	Wavelength(nm)	Scavenger gas
C	193.0	H_2/O_2
S	181.4	H_2/O_2
N	174.3	H_2/O_2
O	777.3	$H_2/N_2/CH_4$

Spectrometer purge flow: Nitrogen @ 2l/min
Transfer line temperature: 350°C Cavity temperature: 350°C

Results and Discussion

The following examples illustrate the role of element-specific detectors in characterising heteroatomic species in coal liquids and demonstrate the unique capabilities of GC-AED for identifying dual or multiple heteroatom compounds in such materials. Further, from the chromatographic data accumulated to date it is anticipated that a comprehensive comparison of NPD and FPD with AED will be possible. Detailed qualitatative and quantitative information is currently being obtained by a combination of literature retention time data and model compound data. Gas

chromatography-mass spectrometry (GC-MS) and GC-AED will provide structural characterisation..

From the selected chromatograms; Figure 1a,b shows the sulphur response of GC-AED and GC/FPD chromatograms respectively from the analysis of a supercritical gas extract of Mequinenza lignite. For both detectors, the chromatograms are very similar in general appearance (i.e. no. of peaks observed) and both display a series of alkyl substituted thiophenes, benzothiophenes and dibenzothiophenes. Taking into consideration sampling variations and the higher injector temperature employed in the GC-AED system the only remarkable difference is the relative peak intensities observed by both detectors. This can be accounted for by the compound dependency of the FPD and the possibility of quenching effects due to the high hydrocarbon presence.

Figure 2a,b compares the AED and NPD traces respectively for a nitrogen-rich, heat treated, coal tar pitch aromatic fraction. As anticipated from detector response characteristics for nitrogen-containing species the chromatograms are almost identical with carbazole, substituted carbazoles, benzoacridine and benzocarbazoles being observed. The NPD has the advantage of a significantly greater selectivity over carbon (see Table 1) and consequently splitless GC injections using concentrated solutions were used for AED analysis. This results in what appears to be an instrument induced effect for the high boiling heterocyclics where peak splitting and a general distortion of peak shape occurs. Similar observations have been made for suphur and oxygen containing PACs'.

The unique capabilities of the GC-AED as a muti-element detector are demonstrated by the identification of dual heteroatom compounds present in both the supercritical gas extract and the coal tar pitch sample. Figures 3a,b show segments of the C,S,O and C, N, O, chromatograms obtained for Mequinenza lignite and heat treated pitch respectively. By correlating characteristic emission wavelength responses with retention time data, the presence of oxygen-sulphur and nitrogen-sulphur compounds have been unambiguously identified. Further conformation is obtained using a "snapshot" facility which is a selected segment of the emission spectrum showing specific elemental emission wavelengths. The exact nature of these dual heteroatom species is as yet uncertain. Figure 4 provides further evidence of the multi-element character of GC-AED where the aromatic fraction from an untreated coal tar pitch has been analysed by GC-AED for C, S, N, O (Figure 4a) and the corresponding GC/FID/NPD is shown in Figure 4b. In both cases the carbon/FID channel provides mainly evidence of nitrogen-containing species but due to the high selectivity for both sulphur and oxygen over carbon for AED (see Table 1) the presence of both sulphur and oxygen compounds (and possibly further multiple heteroatomic species) can be confirmed

References

(1) Karr, C., Jr., Ed. "Analytical Methods for Coal and Coal Products", Academic Press: New York, 1978.

(2) White, C.M., In: "Handbook of Polycyclic Aromatic Hydrocarbons", Bjorseth, A., Ed.; Marcel Dekker: New York, 1981: pp525-616.

(3) Nishioka, M., Campbell, R.M., West, W.R., Smith, P.A., Booth, G.M., Lee, M.L., *Anal. Chem.*, 1985, 57, 1868-1871 and references therein.

(4) Davidson, R.E., "Organic sulphur in coal", IEA Report No. IEACR/60, IEA Coal Research, London, UK, 1993 and references therein.

(5) Davidson, R.E.,"Nitrogen in coal", IEA Perspectives Report No. IEAPER/08, IEA Coal Research, London, UK, 1994 and references therein.

(6) Orr, W.L., White, C.M., Eds. "Geochemistry of Sulphur in Fossil Fuels", ACS Symposium Series, 0097-6156; 429, American Chemical Society, 1989.

(7) Later, D.W., In: Polycyclic aromatic hydrocarbons. Volume 2, New York, USA, Marcel Dekker Inc., pp265-350 (1985)

(8) Hardy, R.H., Davis, B.H., *Fuel Science and Technology International*, 7 (4), 399-421 (1989).

(9) White, C.M., Douglas, L.J., Perry, M.B., Schmidt, C.E., *Energy & Fuels*, 1 (2), 22-226, 1987.

(10) Kong, R.C., Lee, M.L., Iwao, M., Tominga, Y., Pratap, R., Thompson, R.D., Castle, R.N., *Fuel*, 1984, 63, 707-713.
(11) Willey, C., Iwao, Castle, R.N., Lee, M.L., *Anal. Chem.*, 1981, 53, 400-407.
(12) Nishioka, M., Campbell, R.M., Lee, M.L., Castle, R.N., *Fuel*, 1986, 65, 270.
(13) Nishioka, M. Lee, M.L., Castle, R.N., *Fuel*, 1986, 65, 390.
(14) Nishioka, M., Lee, M.L., Kudo, H., Muchiri, R.R., Baldwin, L.J., Pakray,S., Stewart, J.G., Castle, R., *Anal.Chem.*, 1985,57,1327-1330.
(15) Burchill, P., Herod, A.A., Pritchard, *Fuel*, 1983, 62, 11-19.
(16) Nelson, P.F., Kelly, M.D., Wornat, M.J., *Fuel*, 70 (3), 403-407 (1991).
(17) Winans, R.E., Neill, P.H., in "Geochemistry of Sulphur in Fossil Fuels", Symposium Series 429, American Chemical Society, 1989, pp.249-260.
(18) Sinninghe Damste, J.S., de Leeuw, J.W., *Fuel Process Technol.*, 1992, 30, 109.
(19) Cerny, J., Mitera, J., Vavrecka, P., *Fuel*, 68 (5), 596-600 (1989).
(20) White, C.M., Douglas, L.J., Anderson, A.A., Schmidt, C.E., Gray, R.J., in: "Geochemistry of Sulphur in Fossil Fuels", Symposium Series 429, American Chemical Society, 1989, pp.261-286.
(21) Bartle, K.D., Perry, D.L., Wallace, S., *Fuel Processing Technol.* ,15, 351-361, 1987.
(22) Sinninghe Damste, J.S., Eglinton, T.L., de Leeuw, J.W., Schenck, P.A., *Geochimica et Cosmochimica Acta*, 53 (4), 873-889 (1989).
(23) Sinninghe Damste, J.S.S., de las Herras, F.X.C., de Leeud, J.W., *Journal of Chromatography*, 607 (2), 361-376, 1992.
(24) Eglinton, T.I., Sinninghe Damste, J.S.S.,Kohnen, M.E.L., de leeuw, J.W., Larter, S.R., Patience, R.L., in: "Geochemistry of Sulphur in Fossil Fuels", Symposium Series 429, American Chemical Society, 1989, pp.528-565.
(25) Dreschel, M., "Selective Gas Chromatography Detectors", p.133. Elsevier Science Publishing, Amsterdam, 1986.
(26) Farwell, S.O., Baringa, C.J., *J. Chromatogr. Sci.*, 24, 483 (1988).
(27) Patterson, P.L., In: "Detectors for Capillary Chromatography", Hill, H.H., McMinn, D.G., Eds. Chap. 7, pp.139-168, Chemical Analysis Series, Volume 121, John Wiley & Son, Inc., 1992.
(28) Quimby, B.D., Sullivan, J.D., *Anal. Chem.* 62, 1027 (1991).
(29) Sullivan, J.D., Quimby, B.D., *Anal. Chem.*, 62, 1034 (1990).
(31) Wylie, P.L., Quimby, B.D., *J. High Resol. Chromatogr.*, 12, 813 (1989)
(32) Uden, P.C., *Chromatogr. Forum*, 1(4), 17 (1986).

Table 1: Detector response characteristics[1]

	Detectors		
	FPD	**NPD**	**AED**
Minimum detectable levels (pgS/sec) (pgN/sec)	2-50	0.05	(1-2) (50)
Selectivity (S/C) (N/C)	10^4-10^5	$7*10^4$	($8*10^4$) ($2*10^4$)
Linear response	No (quadratic)	Yes	Yes
Linear dynamic range	$1\text{-}5*10^2$	10^5	($1*10^4$) ($2*10^4$)

[1]Values taken from literature(26)

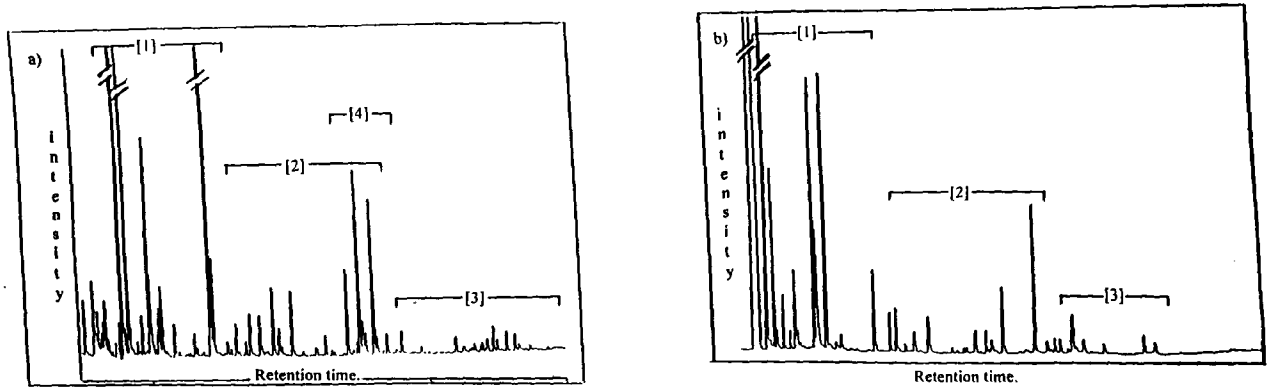

Figure 1. A supercritical gas extract of Mequinenza lignite: a) AED sulphur 181nm channel and b) FPD sulphur response. General assignments: [1] substituted thiophenes; [2] benzothiophenes and [3] dibenzothiophenes. [4] See Figure 3a) for an enlargement of this region.

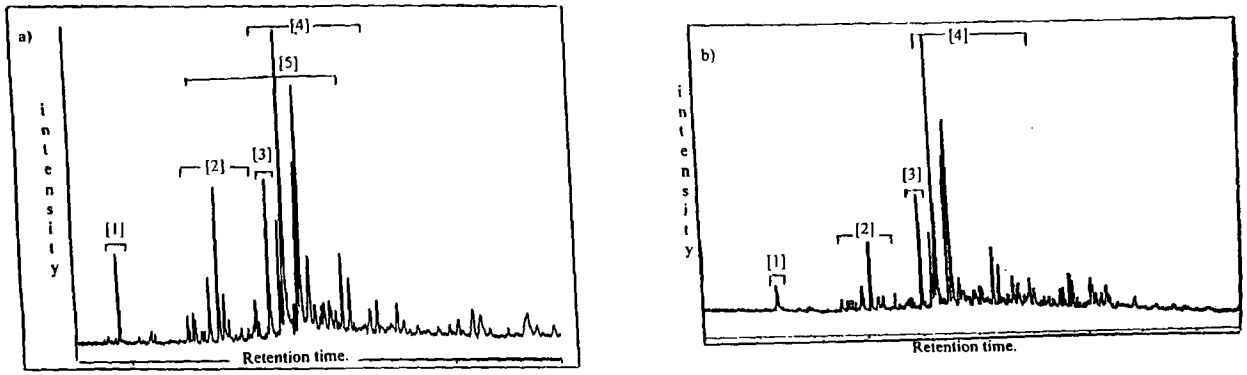

Figure 2. A coal tar pitch (S.P. 105°C), heat treated at 350°C: a) AED 175nm channel and b) NPD nitrogen response. General assignments: [1] carbazole; [2] substituted carbazoles; [3] benzoacridine and [4] benzocarbazoles. [5] See Figure 3b) for an enlargement of this region.

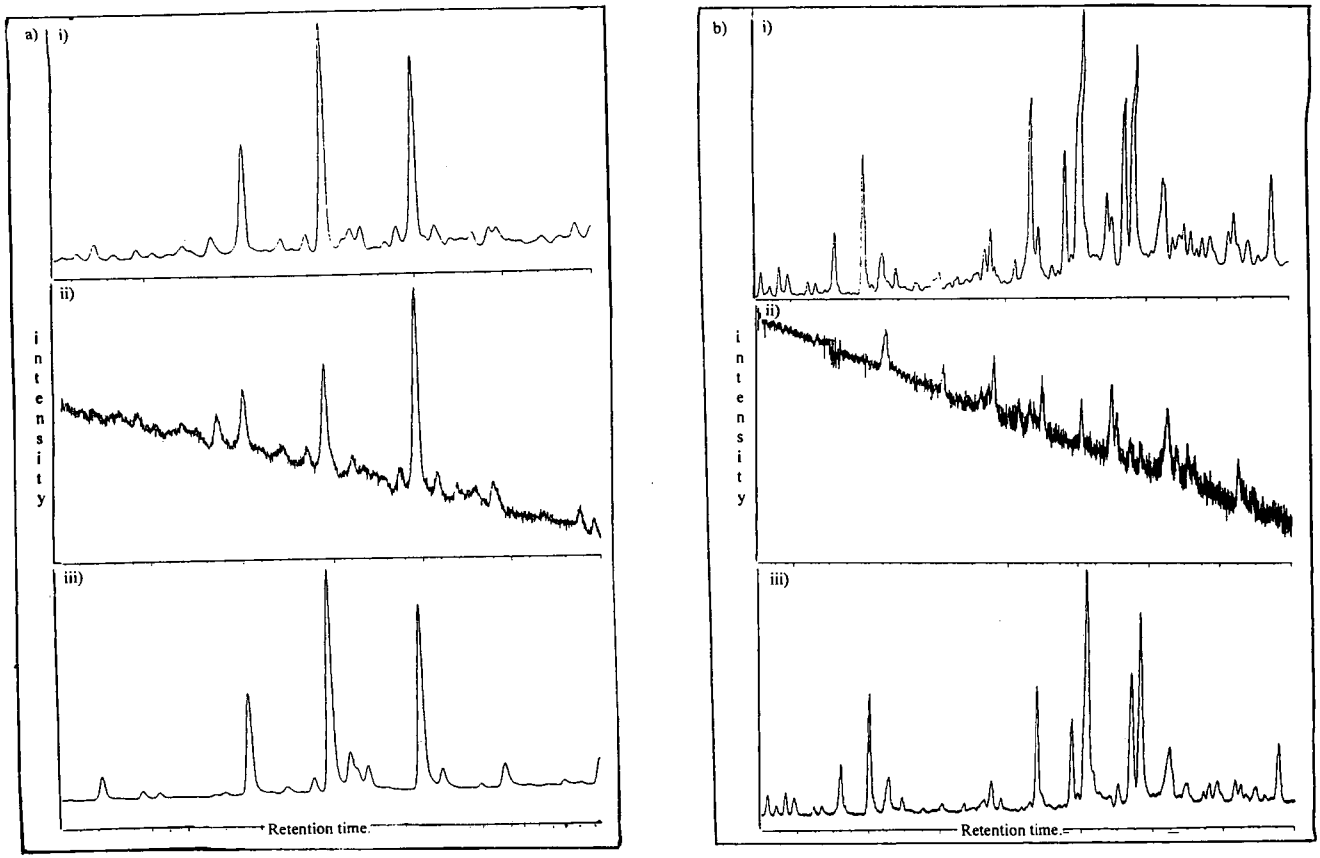

Figure 3. a) A supercritical gas extract of Mequinenza lignite: the GC-AED response on, i) the carbon 193nm channel; ii) the oxygen 777nm channel and iii) the sulphur 181nm channel.

b) A coal tar pitch (S.P. 105°C), heat treated at 350°C: the GC-AED response on, i) the carbon 193nm channel; ii) the oxygen 777nm channel and iii) the nitrogen 174nm channel.

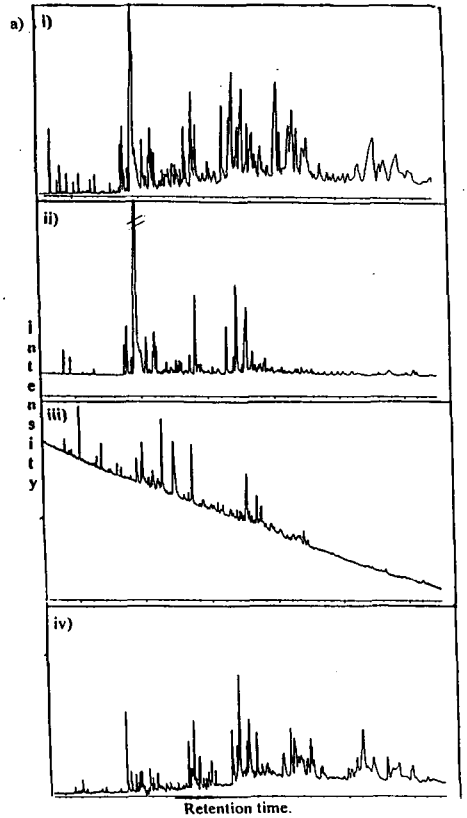

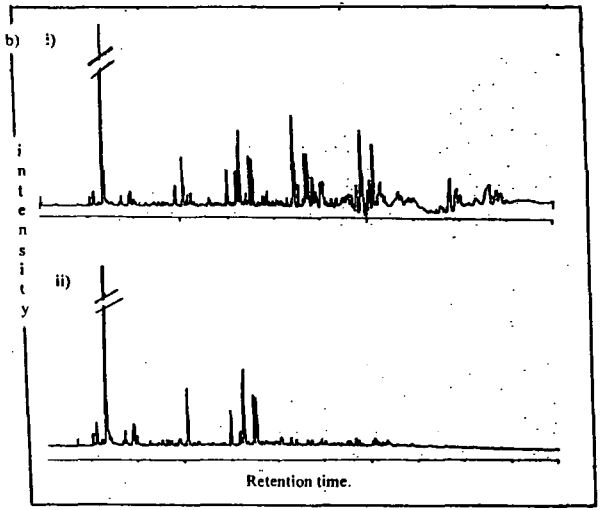

Figure 4. An untreated coal tar pitch (S.P. 35°C): a) the GC-AED response on, i) the carbon 193nm channel; ii) the nitrogen 175nm channel; iii) the oxygen 777nm channel and iv) the sulphur 181nm channel. b) i) the FID carbon response and ii) the NPD nitrogen response.

COMPARISON OF SEVERAL CONTEMPORARY IONIZATION/MASS ANALYZER TECHNIQUES FOR LARGE COMPONENTS OF COMPLEX FOSSIL-DERIVED MATERIALS

Jerry E. Hunt and Randall E. Winans
Chemistry Division
Argonne National Laboratory
Argonne, IL 60439

Keywords: Argonne Premium Coals, mass spectrometry

INTRODUCTION

Coals and coal-derived samples provide a unique mixture for development and comparison of mass spectrometric techniques for high molecular weight analyses. The Argonne Premium Coal samples (APCS), a broad array of research grade standards collected, prepared, and stored under controlled conditions, are convenient for assessing classical and novel mass spectrometric techniques. Vacuum pyrolysis mass spectrometry of APCS 4 (Pittsburgh #8) has been reported.[1] Alkyl-substituted aromatic compounds and hydroxy- and dihydroxy-substituted aromatic compounds were observed. Newer techniques such as laser desorption (LD), as well as in-beam techniques, such as desorption chemical ionization (DCI) and desorption electron ionization (DEI) are better suited to the studies of mixture characterization as presented by fossil fuels.

We have previously reported laser desorption of coal extracts that show only low molecular weight ions (<1000 amu).[2,3] The latter report compares LD with fast atom bombardment and DCI mass spectrometry. All three techniques produce similar data that differ only in minor details. Hanley reported LDMS of pyridine extracts produces a distribution of ions between 150 and 1500.[4] Field ionization mass spectrometry shows similar patterns.[5] Recently, others have interpreted their LD results in terms of high mass species (>12,000) being desorbed.[6,7] The authors present data taken from single laser shots. We believe that the data presented can best be interpreted as electronic "noise" and that the observed signals are not related to the sample. In our hands, laser desorption mass spectrometry of coals and coal-derived materials does not show any reproducible ion intensity above 2000 u. Our results have been obtained on two different time-of-flight instruments, one constructed in-house and one a commercial instrument (Kratos Kompact MALDI III).

Laser desorption mass spectrometry has recently been used to identify high molecular weight proteins of mass in excess of 100,000 amu. Thus, if there are indeed large molecular species in coals or coal extracts, LDMS is an attractive technique. However, the conditions whereby large molecular ions can be desorbed intact are very specialized. The extension of LD to heavier molecules is made possible by embedding the sample in a chemical matrix (matrix-assisted laser desorption ionization, MALDI). Without this matrix, large mass species are not observed. Recently, Herod reported results using a time-of -flight mass spectrometer designed for MALDI analysis.[8] He concluded that high mass species (up to 200,000 u) are observed in the mass spectrum. We have used our two TOF mass spectrometers for coal analysis by MALDI, have carefully analyzed our data and the instrumental conditions, and conclude that only low molecular weight ions (up to 1500 u) are observed. We interpret our results quite differently from Herod. First, results from both of our mass spectrometers are similar, i.e., ion intensities are in the mass range from about 200 to 1500. No ion peaks are observed at higher masses in either instrument. We did observe a problem with the detector in the Kratos instrument that may result in an over-interpretation of the data. The detector in the Kratos instrument is very sensitive to ion saturation, that is, high ion currents cause spurious peaks to be observed at times of flight which are uncorrelated in time and, thus, uncorrelated in mass. These may be incorrectly interpreted as "true" ion signals of high mass. If, indeed, large molecules do exist in coal, new matrices will need to be identified which are applicable to the types of compounds found in coal. We are currently investigating this area.

This study focuses on a number of complementary approaches that have been used to investigate fossil fuel-derived materials. LD, DCI, and DEIHRMS are compared as methods of volatilizing high molecular weight species present in coal samples. Also, DEIHRMS on a high resolution three-sector tandem mass spectrometer is compared to laser desorption with laser photoionization on a time-of-flight instrument for high mass mixture selectivity.

EXPERIMENTAL

The coals used in this study are the Argonne Premium Coal Samples 1 (Upper Freeport mvB) and 2 (Wyodak-Anderson subB). A complete discussion of the characteristics of the coals used in this study has been reported.[9] Vacuum pyrolysis tars were prepared by heating coal in a vacuum at 400 °C and collected at room temperature. Pyridine extracts and KOH/glycol solubilization procedures have been reported.[10] The EI and DCI mass spectra were recorded on a Kratos MS 50 triple analyzer. The reagent gas for the DCI studies was isobutane. The solids and extracts were heated in the source on a small platinum wire coil from 200 °C to 700 °C at 100 °C/min. with the source heated at 200 °C. The laser desorption and laser ionization mass spectra were recorded on a linear time-of-flight mass spectrometer constructed in-house and a Kratos Kompact MALDI III reflectron time-of-flight mass spectrometer. The fluence of the desorption laser is held constant at 10-100 mJ/cm^2 at a repetition rate of 20 Hz. For direct ion desorption the laser is operated close to the ionization threshold to minimize fragmentation of the desorbing material. The laser is operated at lower fluences for neutral ion desorption. The neutral molecules are then ionized by vacuum ultraviolet light. The 118 nm laser pulses are produced by third harmonic conversion of 355 nm light from a Nd:YAG laser in a high pressure Kr cell.

RESULTS

Figure 1 shows a comparison mass spectrum of the vacuum pyrolysis tars from APCS 1. The lower panel is the direct laser desorption mass spectrum and the upper panel the DCI mass spectrum of the same sample. In each spectrum there are only a small number of low intensity peaks below m/z=200, indicating the overall soft ionization of each technique. The two methods show similar peaks, with some variation in intensity. Overall the LD spectrum shows fewer peaks up to a mass of about 275 as compared to a more dense region for the DCI data. In LD the more volatile species sublime and are not observed. Above this mass the spectra are quite similar. The peaks in the DCI data are generally +1 species as compared to the LD data, indicating the formation of $(M+H)^+$ ions. Several homologous series are observed in the LD and DCI data. Possible structures can be assigned to each of these series based on PyHRMS results from the same coal sample. The prominent series (especially in the LD data) at m/z = 230, 244, 258, 272 is assigned to alkyl-pyrenes or fluoranthenes. Another series contains two different species, alkylphenyl–naphthalenes and alkylhydroxy-pyrenes or fluoranthenes. Thus, there is good agreement in mass, if not intensity, for these two techniques.

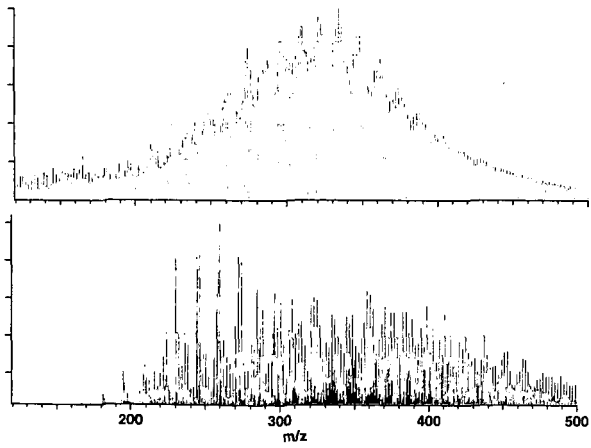

Figure 1. Comparison of LD (lower panel) and DCI (upper panel) methods for vacuum pyrolysis tars of APCS 1 (Upper Freeport mvB).

At higher masses there is also good agreement between the techniques. Several homologous series appear at these higher masses. A series at m/z = 292, 306, 320, 334, 348, 362, 376 is possibly alkylphenylpyrenes. Another series between 306 and 362, form an oxygen containing series with a suggested structure of methylbenzopyrenofuran.

The mass spectra of the demineralized pyridine extract of APCS 1 is shown in Figure 2. Spectrum A is the direct laser desorption mass spectrum of the pyridine extract and spectrum B the EI mass spectrum. Again the overall absence of ion intensity below 225 in the LD indicate soft ionization, i.e., the molecular fragmentation is minimum. Also, in laser desorption low molecular weight (volatile) molecules will be lost due to the high vacuum.

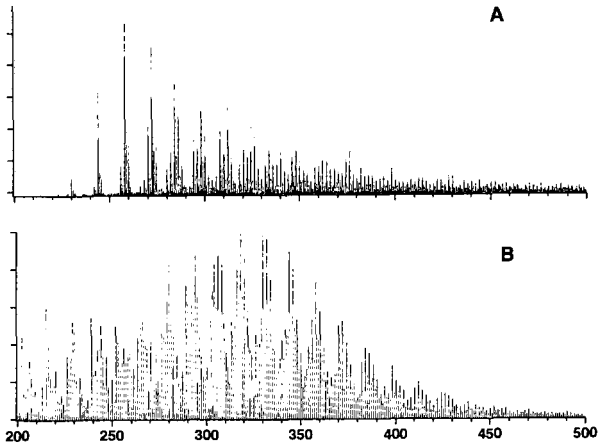

Figure 2. The pyridine extract of demineralized APCS 1. A, the LD and B, the EI mass spectrum.

Table 1. Major Ion Series in Laser Desorption of Pyridine Extract of APCS 1

Ion Series	Structural Type
230, 244, 258, 272, 286, 300, 314	alkyl pyrene or fluoranthene
242, 256, 270, 284, 298	alkyl chrysenes
252, 266, 280, 294, 308	alkyl benzopyrene or benzofluoroanthene
292, 306, 320, 334, 348, 362, 376	alkyl phenylpyrenes and pyrenobenzofuran
195, 209, 223, 237, 251	alkyl carbazoles
276, 290, 304, 318, 332	alkyl benzoperylene

In general the direct laser desorption mass spectra favor the aromatic compounds over the aliphatic, producing a simpler, cleaner mass spectrum, while the EI spectra show aliphatic as well as aromatic species.

Since direct laser desorption favors aromatic species at the expense of aliphatic species a method to enhance LD was employed. First, at low fluence, neutral molecules are desorbed, then a second laser pulse of 10.5-eV is used to ionize the neutrals. Since multiple photons can be absorbed increased ionization efficiency is expected for aliphatic species. A comparison of DEIHRMS and LD of neutral with photoionization is shown in Figure 3. The sample in this case is the hexane extract of the KOH/ glycol reaction of APCS 2 (Wyodak-Anderson). The overall similarity of the spectra is compelling. The peak from m/z = 368 to 508 are assigned as acid with the base structure $H(CH_2)_nCO_2H$, n = 23-33. An important difference in the spectra is the appearance of high mass ions in the LD/LI spectra. Coupled with time of flight mass spectrometry, the spectra exhibit parent ion abundance which conventional 70 eV electron impact lack. The peaks near m/z = 800 do not appear in the DCI MS spectra. These peaks may be assigned as very long chain fatty acids on the order of C_{50}.

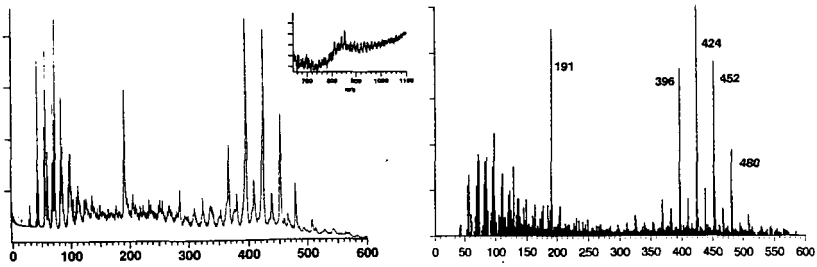

Figure 3. The laser desorption/laser ionization mass spectrum (left) and DEIHRMS (right) of the hexane extract of KOH/glycol reaction of APCS 2.

CONCLUSION

The mass spectra show different molecular weight distributions, but similar ion series. In general LD, DCI, and EI give progressively lower distributions. Furthermore, the ions present in the LD and DCI spectra are directly comparable, while LD and EI produce different ion distributions. Information on neutrals is available from LD-photoionization. The appearance of an ion series in the m/z = 700-1000 range demonstrates an advantage of 10.5-eV ionization and TOF analysis. Mass spectral data from both LDMS, DCIMS, and EIHRMS are being analyzed for all eight Argonne Premium Coal samples.

ACKNOWLEDGMENT

This work was performed under the auspices of the Office of Basic Energy Sciences, Division of Chemical Sciences, U.S. Department of Energy, under contract number W-31-109-ENG-38.

REFERENCES

1. Yun, Yongseung; Meuzelaar, Henk L.C.; Simmleit, N.; Schulten, H.-R. *Energy Fuels* **1991**, *5*, 22-29.

2. Hunt, J.E.; Lykke, K.R.; Winans, R.E. *Preprints, Am. Chem. Soc., Div. Fuel Chem.* **1991**, *36*, 1325-1328.

3. Winans, R.E.; McBeth, R.L.; Hunt, J.E.; Melnikov, P.E. *Proc., 1991 International Conference on Coal Science*; University of Newcastle upon Tyne, UK, September 16-20, 1991, pp. 44-47.

4. Burroughs, J.A.; Cadre, B.M.; Hanley, L. *Proc., 41st American Society of Mass Spectrometry;* San Francisco, CA, May 30-June 4, 1993, p. 441.

5. Herod, A.A.; Stokes, B.J.; Schulten, H.-R. *Fuel* **1993**, *72*, 31-43.

6. John, P.; Johnson, C.A.F.; Parker, J.E.; Smith, G.P.; Herod, A.A.; Gaines, A.F.; Li, C.-Z.; Kandiyoti, R. *Rap. Commun. Mass Spectrom.* **1991**, *5*, 364-367.

7. Herod, A.A.; Kandiyoti, R.; Parker, J.E.; Johnson, C.A.F.; John, P.; Smith, G.P.; Li, C.-Z. *J. Chem. Soc., Chem. Commun.* **1993**, 767-769.

8. Herod, A.A.; Parker, J.E.; Johnson, C.A.F.; John, P.; Smith, G.P.; Li, C.-Z.; Kandiyoti, R. *Proc., 7th International Conference on Coal Science*; Banff, Alberta, Canada, September 12-17, 1993; pp. 1282-1285.

9. Vorres, K.S. *Energy Fuels* **1990**, *4*, 420-425.

10. Winans, R.E.; McBeth, R.L.; Hunt, J.E. *Preprints, Am. Chem. Soc., Div. Fuel Chem.* **1993**, *38*, 561-564.

HIGH PERFORMANCE LIQUID CHROMATOGRAPHY OF COAL LIQUEFACTION PROCESS STREAMS USING NORMAL-PHASE SEPARATION WITH DIODE ARRAY DETECTION.

Daniel E. McKinney[1], David J. Clifford[1], Lei Hou[1], Michael R. Bogdan[2], and Patrick G. Hatcher[1]

1. Fuel Science Program, Department of Materials Science and Engineering, The Pennsylvania State University, University Park, PA 16802.

2. Sci-Tech, Inc., 200 Innovation Blvd., State College, PA 16803.

Keywords: HPLC, liquefaction, process streams

INTRODUCTION:

Since its introduction as an analytical method in the late 1960s and early 1970s, high performance liquid chromatography (HPLC) has become widely used in environmental studies, especially for the analysis of PAHs[1,2]. PAHs are widespread environmental contaminants and much effort has been devoted to the development of liquid chromatographic columns which are sensitive to PAH separation. Reverse-phase HPLC on chemically bonded C_{18} has become the method of choice for the separation of PAHs [3-6], and a review by Wise *et al.* [1] has described general protocols for the separation of PAHs using reverse-phase HPLC. However, direct analysis of PAHs in complex fuel mixtures using reverse-phase HPLC is complicated as sample preparations have become elaborate, due in large part to the fact that most complex organic materials contain compounds that are not usually miscible in acetonitrile, the solvent of choice for reverse-phase HPLC separations of PAHs. These materials routinely are fractionated first into general compound class categories[7] (i.e. aliphatics, polar compounds, aromatics, resins, and asphaltenes) before separation of PAHs can be performed, and usually normal-phase HPLC is relegated to general cleanup and isolation of the total PAH fraction. The development of "charge-transfer" stationary phases for separation of π-electron rich PAHs[8-10] allows for the separation of PAHs and their isomers in the normal-phase using solvents which are generally miscible with complex organic systems.

Another problem associated with HPLC analysis of complex fuel mixtures and other extracts of natural samples is that, in the past, normal-phase and reverse-phase HPLC have depended upon either fluorescence detection or monochromatic UV absorbance detection. Fetzer and Biggs[2] have pointed out, these detection methods are too selective and many compounds go unobserved due to varying optimal wavelengths for different compounds. Developments in the last fifteen years of a full spectrum UV absorbance detector (i.e. diode array detector or DAD) enable full spectrum detection of HPLC eluates. A distinct advantage of the diode array HPLC technique, which provides UV spectra of separated fractions as a function of time, is its ability to identify, by spectral comparisons, the molecular components of the eluates, including the isomers of PAHs.

In this paper, we demonstrate a sensitive method for the detection and analysis of PAHs in coal liquefaction process stream samples. This is accomplished by the normal-phase separation of PAHs and their alkylated derivatives using a TCPP-modified silica column[8] (Hypersil Green PAH-2) in combination with UV-diode array detection. This method allows for a more sensitive detection and efficient separation of multi-ring PAHs and their isomers without elaborate sample preparations or on-line coupling of a reverse-phase HPLC system.

EXPERIMENTAL:

Instrumentation: The dilute coal liquefaction process stream samples were analyzed and separated using a Waters 600E HPLC and Waters 991 photodiode array detector. The column used for HPLC separations was a Hypersil Green PAH-2 column purchased from Keystone Scientific, Inc.(Bellefonte, PA).

Mass spectral data were collected for each fraction using the solids injection probe of a Kratos MS-80 double-focusing high-resolution mass spectrometer. The ionization mode on the mass spectrometer was electron impact (EI, 70 eV). Instrument control and data collection were accomplished by using a computer-aided Data General DS90 software system.

Sample Description: A standard consisting of a mix of 16 PAH's was obtained from Supelco, Inc., Bellefonte, PA. The coal derived liquids used for two-dimensional, normal phase HPLC separation, were supplied by CONSOL, Inc. and consisted of five liquefaction process streams representing different liquefaction systems, different feed coals, and different degrees of catalytic activity (Table I).

Procedure: The standard PAH mix is subjected to HPLC analysis to derive response factors for internal standard quantitative calculations. The internal standards were benzo[b]fluoranthene and benzo[g,h,i]perylene, which were added to each diluted coal liquefaction stream sample at an appropriate concentration level. The former was used as the internal standard for samples 1, 2, and 3 because the compound elutes in a region containing few intense peaks in the sample eluates. For samples 4 and 5 we used the latter internal standard because some significant peaks were observed in the elution range of benzo[b]fluoranthene and these would co-elute with the standard.

The coal liquids are then filtered through 0.2 μm filters (Supelco brand ISO-DISC N-32 3mm diameter, nylon membrane, 0.2 μm pore size filters) in order to remove any insoluble

material. The column, equilibrated with 100% hexane, was operated in the gradient elution mode. Samples are injected onto the PAH-2 column, and following an initial 10 minute isocratic period, a linear gradient from 100% hexane to 100% dichloromethane is used up to 80 minutes followed by a final hold for 5 minutes.

RESULTS AND DISCUSSION:

Knowing that coal liquefaction process streams contain numerous amounts of polynuclear aromatic hydrocarbons and that the PAH-2 column successfully separated PAHs in a known standard, we had reason to be optimistic about its use for coal process stream liquids. The separation obtained for liquefaction process stream samples is demonstrated by 1-D maxiplots in Figure 1. Peak identifications listed in Table II were made by comparison of retention times with the PAH standard and by fraction collection combined with heated probe/mass spectrometry. The use of the latter method was deemed necessary, because many peaks did not have retention times that coincided with those of compounds in the standard, notably the alkylated PAHs.

In general, the HPLC traces are characterized by both sharp peaks identified in Table II and broad regions representing unresolved components. The broad region of unresolved peaks between 0 and 20 minutes is constituted predominantly by two and three ring aromatics as determined by mass spectrometry. Most of the compounds are alkylated PAHs having very similar UV spectra, and some compounds are alkylated hydronaphthalenes. The second broad region of absorbance extends from 20 minutes retention time through to the end of the run, containing multi-ring PAHs and alkylated PAHs having from three to nine condensed rings. The most notable peaks (7, 8 and 9) are those of pyrene and its multialkylated homologs, the internal standard, benzo(b)fluoranthene (peak 11), benzo(g, h, i)perylene (peak 12), and coronene (peak 16).

We can ascribe several important features to each chromatogram, but basically three samples (sample 1 and sample 2), the pressure filtered liquids, show very similar characteristics and differ markedly as a group from the chromatograms of the composite heavy distillates, samples 4 and 5.

Although the three pressure filtered liquid (PFL) samples from the HRI facility generally show similar features, there are subtle differences in the relative distributions of compounds reflecting process conditions. The chromatogram of sample 1, a PFL from the liquefaction of the Wyodak/Anderson coal, differs from those of sample 2 and sample 3 which were obtained from liquefaction conditions using the Illinois #6 coal as feedstock. While pyrene and alkylated pyrenes are major components of all three samples, the two process streams from the Illinois #6 coal contain relatively larger amounts of PAHs with more than four rings, compared with the sample from the Wyodak/Anderson coal. This is perhaps due to the fact that the Illinois #6 coal is of higher rank. All three samples contain significant chromatographic intensity in the two broad unresolved regions described previously. Compared with sample 3, sample 2 appears to contain more intensity in the broad unresolved region in the early eluting portion of the chromatogram ascribed to two and three-ring PAHs. This could indicate that there is a relative build up of more refractory multi-ring material as Run CC-16 progressed.

The chromatograms (maxiplot) for the two high temperature distillates shown in Figure 1 differ from the chromatograms of pressure filtered process streams in that they contain a predominance of compounds with generally fewer than five rings and virtually no compounds with more than five rings other than coronene. This data is consistent with the gc/ms data presented elsewhere[13]. The dominant peaks are those of pyrene and its alkylated homologs (peaks 7 and 8) and dihydro-benzopyrene and its alkylated homolog (peaks 9 and 10). Wyodak coal (sample 5) appears to yield a higher proportion of dihydro-benzopyrene than Illinois #6 coal (sample 4) in its high temperature distillate. This is also consistent with the gc/ms data[13]. Unresolved components dominate the early part of the chromatogram but not the later retention time range. Unlike the pressure filtered process streams, the distillates contain no significant "hump" for unresolved components between retention times of 40 and 80 min. Obviously, the samples from the Wilsonville facility, comprised of distillates boiling below 850°F, contain lower boiling PAH's, in contrast to the samples obtained from the HRI facility which were not subjected to distillation. This is also demonstrated by the solubility data (Table I), in that samples 1, 2, and 3 have lower solubilities, consistent with higher molecular weight components, compared to the higher solubilities of samples 4 and 5, consisting of lower molecular weight components.

Table II contains the quantitative data for the five samples. As mentioned above, the dominant compounds exist as 1-3 ring aromatic/hydroaromatic compounds of undetermined structure. These account for more than half of the products detected. Other multiring PAHs individually account for between 0.05% and 1.3 % of the sample weights of the samples 1-3. Summing of the concentrations of peaks 1-19 in each chromatogram for samples 1-3 reveals that 18% to 32% of the sample weights can be accounted for as detected PAHs. Samples 1 and 2, filtered process streams from two different coals at the HRI facility, appear to have similar overall concentrations of PAHs, even though the distributions are slightly different as mentioned above. The difference between samples 2 and 3, from the same coal, appear to be related to changes in process time, since they represent samples taken from different days. Samples 4 and 5, from the Wilsonville reactor, appear to have significantly lower concentrations of all detected compounds, ranging from 0.007% to a maximum of 2.3%. The significant decrease in concentrations compared to the samples from the HRI facility is indicative of the differences in liquefaction methodology. Not only are the yields of PAHs lower, but the distributions are different, as discussed previously. The low yields initially seemed puzzling, but examination of the gc/ms data presented in a previous report[13] indicates that significant amounts of unresolved complex materials having intense m/z fragment ions characteristic to structures of C_nH_{2n-3} are present. It is likely that the parent compounds of these fragment ions do not yield significant

absorptions in the UV range, thus, explaining why they remain undetected by the HPLC method. If the compounds are undetectable by UV-absorption, then they fall out of our analytical window, a pitfall for this method.

CONCLUSIONS:

The results outlined in this report from experiments performed in our laboratory have proved very encouraging. We were successful in the separation, characterization, and quantification of PAHs of a limited series of select samples which depict a broad range of liquefaction process conditions, using a newly developed normal-phase HPLC column, the Hypersil PAH-2, coupled with a UV-diode array detector. We feel this method has great potential for the characterization of liquefaction process streams along with other extracts of natural products containing high concentrations of PAHs. The success of this method was based on the fact that it enabled us to identify both qualitative and quantitative differences among the limited sample set. Perhaps the most readily observed differences are noted between samples obtained from the HRI facility and the Wilsonville facility. Thus the technique can readily distinguish between sample types from these two liquefaction facilities, regardless of the feed coal used. Those compounds detectable by HPLC from the Wilsonville samples, 850°F$^-$ distillates, appear to be of lower ring number than samples from the HRI facility, whose samples are composed of the whole process stream.

The HPLC method also allows differentiation among samples from the same facility but differing in their process conditions. For example, a different distribution of PAH's was obtained from the process stream samples in which different coal feedstocks were used. The sample liquefied from the Illinois #6 coal appears to have a higher amount of the multi-ring PAH's than the sample from the Wyodak, consistent with the fact that higher rank of coal is more likely to yield more of the higher condensed ring compounds. Another difference between samples indicative of differences in process conditions is that between samples 2 and 3. The former contains a significantly greater concentration of PAH's and, as a result, more of the sample can be quantified. The PAH distributions are similar, in a relative sense, which is indicative of the fact that the entire spectrum of PAH's is being reduced by the processing and could indicate a build-up of more refractory material as the run progressed. Subsequently, time resolved differences induce an overall decrease in PAH levels, which could be related to increased hydrogenation of the rings due to increased exposure to liquefaction conditions or to deactivation of the catalyst.

ACKNOWLEDGMENTS:

We thank Susan D. Brandes, Richard A. Winschel and Frank P. Burke (CONSOL, Inc.) for providing samples of liquefaction process streams and funding through a subcontract on U. S. Department of Energy Project DE-AC22-89PC89883.

REFERENCES:

1. Wise, S. A., Sander, L. C., May, W. E., *J. Chromatogr.*, **1993**, 642, 329.
2. Fetzer, J. C., Biggs, W. R., *J. Chromatogr.*, **1993**, 642, 319.
3. Wise, S. A., *Handbook of Polycyclic Aromatic Hydrocarbons*, vol. I, Marcel Dekker, New York, 1983, Ch. 5, p. 183.
4. Wise, S. A., *Handbook of Polycyclic Aromatic Hydrocarbons - Emission Sources and Recent Progress in Analytical Chemistry*, Vol. II, Marcel Dekker, New York, 1985, Ch. 5, p. 113.
5. Fetzer, J. C., *Chemical Analysis of Polycyclic Aromatic Compounds*, Wiley, New York, 1989, Ch. 5, p. 59.
6. Bartle, K. D., Lee, M.L., Wise, S. A., *Chem. Soc. Rev.*, **1981**, 10, 113.
7. Akhlaq, M. S., *J. Chromatogr.*, **1993**, 644, 253.
8. Holstein, W., *Chromatographia*, **1981**, 14, 468-477.
9. Grizzle, P.L. and Thomson, J.S., *Anal. Letters*, **1987**, 20(8), 1171-1192.
10. Nondek, L. and Malek, J., *J. Chromatography*, **1978**, 155, 187-190.
11. Lochmuller, C. H., in D. E. Leyden and W. Collins (Editors), *Silylated Surfaces*, Gordon and Breach, New york, **1980**, 231.
12. Herren, D., Thilgen, C., Calzaferri, G., Diederich, F., *J. Chromatogr.*, **1993**, 644, 188.
13. Clifford, D. J., McKinney, D. E., Hou, L., Hatcher, P. G., "High Performance Liquid Chromatography (HPLC) of Coal Liquefaction Process Streams Using Normal-phase Separation with UV Diode Array Detection"; Final Report, October 1993, DE-AC22-89PC89883, The Pennsylvania State University.

Table I: General information including percent solubilities for samples 1-5.

Sample #	Sample Designation[1]	Source[2]	Run Number and Period	Feed Coal	Comments	Percent Solubility (%)
1	PFL	HRI	CC-15 11	Wyodak and Anderson	filtered process stream	91.7
2	PFL	HRI	CC-16 4	Illinois No. 6	filtered process stream	92.9
3	PFL	HRI	CC-16 13	Illinois No. 6	filtered process stream	92.6
4	V-1067 Dist.	W	257 Composite	Illinois No. 6	heavy distillate	96.8
5	V-1067 Dist.	W	262 Composite	Wyodak and Anderson	heavy distillate	97.6

1) PFL = pressure filter liquid; V-1067 Dist. = 850°F- distillate of second-stage flashed bottoms
2) HRI = Hydrocarbon Research Inc.; W = Wilsonville

Table 2: Assignments and weight percents for peaks labeled in Figure 1

Peak Number	Peak Assignment	Weight % in sample #1	Weight % in sample #2	Weight % in sample #3	Weight % in sample #4	Weight % in sample #5
1	one & two ring hydro-aromatics	8.97	12.6	6.43	1.74	2.36
2	two & three ring hydro-aromatics	16.2	14.4	6.72	2.21	1.42
3	C_1-anthracene	0.463	0.397	0.656	0.0470	0.0390
4	phenylmethyl-naphthalene* C_4-phenanthrene C_5-phenanthrene	0.746	0.504	0.698	0.0590	0.0460
5	dihydro-pyrene	ND	0.115	0.0640	0.0220	0.0380
6	hexahydro-benzopyrene	ND	0.0530	0.0220	0.00700	0.0190
7	pyrene	1.29	1.10	0.887	0.111	0.0980
8	C_1-Pyrene* C_2-Pyrene C_3-Pyrene	0.650	0.598	0.498	0.0660	0.0600
9	dihydro-benzopyrene	0.407	0.563	0.379	0.0530	0.123
10	C_1-dihydro-benzopyrene* C_2-dihydro-benzopyrene hexahydro-benzo[g,h,i]perylene	0.449	0.387	0.200	0.0180	0.0390
11	benzo[b] fluoranthene	internal standard	internal standard	internal standard	ND	ND
12	benzo[g,h,i]perylene	0.326	0.384	0.349	internal standard	internal standard
13	C_1-benzo[g,h,i]perylene	0.148	0.169	0.140	ND	ND
14	C_2-benzo[g,h,i]perylene* C_3-benzo[g,h,i]perylene	0.0660	0.0960	0.0730	ND	ND
15	dihydro-dibenzoperylene* C_1-dihydro-dibenzoperylene C_2-dihydro-dibenzoperylene	0.0600	0.109	0.0770	ND	ND
16	coronene	0.246	0.276	0.265	ND	ND
17	dihydro-benzocoronene	0.105	0.151	0.133	ND	ND
18	bisanthene* C_1-bisanthene	0.0360	0.0370	ND	ND	0.00200
19	benzobisanthene* C_1-benzobisanthene	ND	0.0180	0.0160	ND	ND

ND=not detected
* = predominant contributor

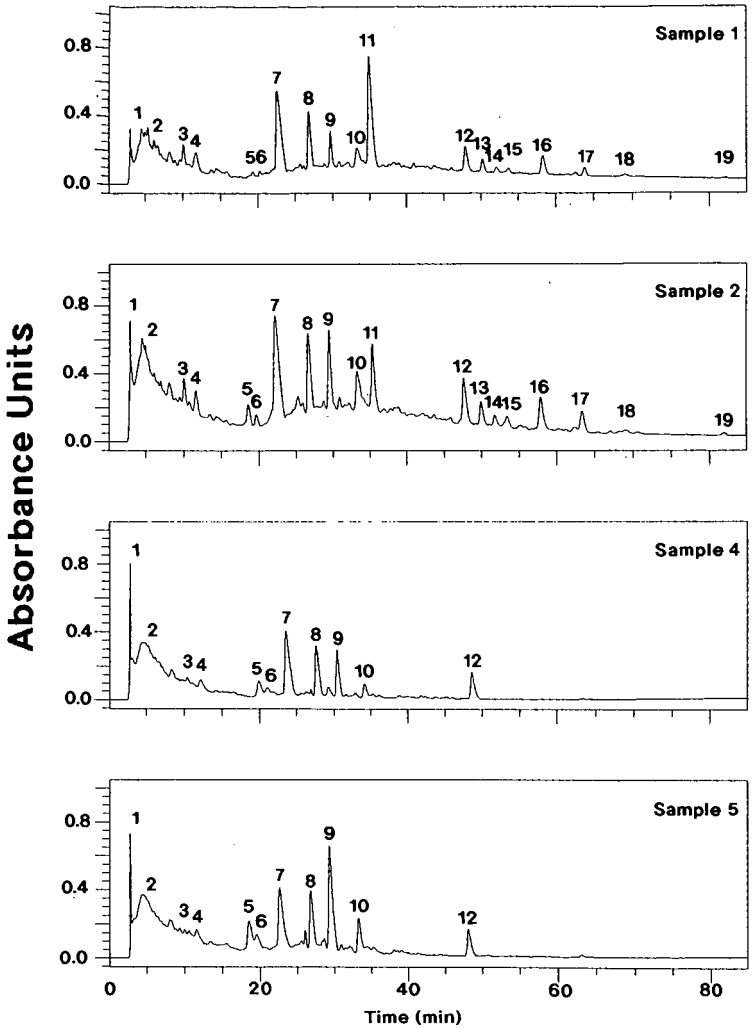

Figure 1. Maxiplots of the HPLC chromatograms for four of the five samples examined. Sample #3 is not included because its chromatogram is similar to that of Sample #2.

MOLECULAR BEAM MASS SPECTROMETRIC CHARACTERIZATION OF BIOMASS PYROLYSIS PRODUCTS FOR FUELS AND CHEMICALS[1]

F.A. Agblevor, M.F. Davis, and R.J. Evans.
National Renewable Energy Laboratory,
1617 Cole Boulevard, Golden, CO 80401

Key words: Biomass pyrolysis, multivariate analysis, molecular beam mass spectrometry.

ABSTRACTS

Converting biomass feedstocks to fuels and chemicals requires rapid characterization of the wide variety of possible feedstocks. The combination of pyrolysis molecular beam mass spectrometry (Py-MBMS) and multivariate statistical analysis offers a unique capability for characterizing these feedstocks. Herbaceous and woody biomass feedstocks that were harvested at different periods were used in this study. The pyrolysis mass spectral data were acquired in real time on the MBMS, and multivariate statistical analysis (factor analysis) was used to analyze and classify Py-MBMS data into compound classes. The effect of harvest times on the thermal conversion of these feedstocks was assessed from these data. Apart from sericea lespedeza, the influence of harvest time on the pyrolysis products of the various feedstocks was insignificant. For sericea lespedeza, samples harvested before plant defoliation were significantly different from those harvested after defoliation. The defoliated plant samples had higher carbohydrate-derived pyrolysis products than the samples obtained from the foliated plant. Additionally, char yields from the defoliated plant samples were lower than those from the foliated plant samples.

INTRODUCTION

The U.S. Department of Energy has embarked on a major program to explore alternate energy sources including biomass. Biomass is an attractive alternative energy source because if energy crops are managed sustainably, a fuel cycle results that will contribute little or no net greenhouse gases to the earth's atmosphere. Biomass feedstocks vary considerably in source and composition and some examples of biomass feedstocks are waste woods from the pulp, paper and lumber industries; demolition wood from urban areas; and agricultural residues and cultivated herbaceous and woody energy crops. It is projected that biomass energy could contribute 11 quads of the United States' energy requirement if all the biomass resources are fully developed [1].

To embark on a large scale production of biomass energy, the quality of the feedstock, that may be influenced by the time of harvest, must be assessed. Seasonal variations give rise to changes in nitrogen, minerals and carbohydrate content of the plants [2]. These changes in turn influence the pyrolysis pathways of the biomass feedstocks. Low alkali metal content of biomass species promotes cellulose decomposition pathways that favor levoglucosan formation whereas the high ash content of biomass favors hydroxyacetaldehyde and char formation reactions [3]. Similarly, a high nitrogen content of biomass favors char formation because of interaction between the amino acids and carbohydrate decomposition products [4]. Thus by judiciously selecting the harvest time of the biomass, it may be possible to influence the pyrolysis products of the feedstock.

In addition to feedstock quality, the conversion technology is equally important for a successful biomass energy program. Several technologies including pyrolysis, gasification, liquefaction and biochemical conversion are currently under development. Fast pyrolysis technologies are receiving considerable attention because they can produce a more dense and easily transportable fuel compared to the original feedstock. The pyrolysis oils can conceivably be used as a chemical feedstock for other processes.

Efficient pyrolytic conversion of biomass to fuels and chemicals requires a thorough understanding of the pyrolysis process and an efficient tool for analyzing the pyrolysis products. The molecular beam mass spectrometer (MBMS) is a unique tool that is capable of analyzing biomass pyrolysis products in real time. However, the MBMS alone offers only qualitative and semiquantitative capability, but when combined with multivariate statistical analysis, it offers a powerful tool to analyze biomass and other pyrolysis products.

---

[1] This paper will be published as a preprint of the ACS Fuels Division Meeting, August 21-26, 1994, Washington D.C.

In this paper, we discuss the application of MBMS and multivariate statistical technique in the classification and analysis of biomass feedstocks harvested at different periods. The influence of harvest time on the pyrolysis products of the feedstocks is discussed. The goal of the study is to develop a rapid method for characterizing biomass and other feedstocks pyrolysis products.

MATERIALS AND METHODS

Pyrolysis of Biomass Feedstocks

The biomass feedstocks used in this study were supplied by subcontractors of the National Renewable Energy Laboratory (NREL), Biofuels Program. The following feedstocks (harvested in various parts of the contiguous USA) were used in this study: hybrid poplar (*Populus deltoides x nigra* var. *Caudina*), sericea lespedeza (*Lespedeza cuneata* var. *Serala*), black locust (*Robina pseudoacacia* L.), and switchgrass (*Panicum virgatum* L.). Hybrid poplar samples were harvested from section #11 of Rocksburg Township, Pennington County, MN in November 1991 and March 1992; sericea lespedeza samples were harvested in October and December 1992 and black locust samples were harvested from 9-year-old plants at the Hind's Research Farm near Ames, IA in the fall of 1991 and spring 1992. Switchgrass samples were harvested from a 6-year-old stand located on the Koemel ranch 7 km south of Stephenville, TX in October 1991 and August 1992. About 1kg of each feedstock was shipped to NREL where they were prepared for pyrolysis. The feedstocks were air-dried at room temperature for 4-7 days to facilitate milling because wet samples tend to heat up during milling. The samples were milled in a Wiley mill (Model 4) until all the material passed through a 2 mm screen. The ground materials were then sieved to -20/+80 mesh size and riffled to homogenize them. We stored the sieved samples in freezers until such time the analysis were performed. The moisture content of the feedstocks prior to pyrolysis was 5-7%.

Biomass samples (20-30 mg) were weighed in quartz boats in triplicates and pyrolyzed in a quench pyrolysis reactor. The reactor consisted of a quartz tube (2.5 cm inside diameter) with helium flowing through at 5 L/min (at STP). The reactor tube was interfaced with the orifice of the molecular beam mass spectrometer (MBMS), Extrel™ Model TQMS C50, for pyrolysis vapor analysis (see detailed description of the MBMS in [5]). The reactor was electrically heated and its temperature maintained at 550±5 °C. The temperature profile of the biomass samples once introduced into the reactor, is unknown, although the pyrolysis reaction was completed in 50 s. Total pyrolysis time was 90 s (including the time the quartz boat heats up to 550°C), but the residence time of the pyrolysis vapors in the reactor pyrolysis zone was ~75 ms and this prevented secondary cracking reactions. The pyrolysis vapors were sampled through the MBMS orifice in real time. During the sampling process, the pyrolysis vapors underwent free-jet expansion during their passage through the orifice and this sufficiently cooled the pyrolysis vapors to prevent secondary reactions or condensations. The cooled pyrolysis vapors passed through a skimmer to form a molecular beam that was fed to a 22.5 eV electron impact ionization triple quadrupole mass spectrometer for real time analysis. Mass spectral data for 15-300 Da were acquired on a Teknivent Vector 2™ data acquisition system.

Multivariate Analysis of Data

Mass spectral data acquired from the pyrolysis process were analyzed by multivariate statistical techniques. The data were first normalized to the total ion current to account for the sample size variation. Data reduction and resolution were carried out on the normalized data using the Interactive Self-modeling Multivariate Analysis (ISMA) program. The correlation around the mean matrix was used to select the significant number of factors for resolution of the mass spectral data into compound classes (see details of this methodology in [6]). In this method, the data set was mean-centered by subtracting the mean from each mass variable. Each variable was weighted by its standard deviation so that all masses (both large and small) were equally important. This method was used to show the differences between the pyrolysis products of the biomass species and the influence of harvest time on the samples. On the other hand, the correlation around the origin matrix was used to extract the relative fractional concentration of compound classes in the biomass pyrolysis products. In performing factor analysis around the origin, the absolute magnitude of the relative abundance for each mass variable was also factor analyzed. However, each variable is weighted by the standard deviation so that each mass is equally important in this method as well. This is in contrast to factor analysis around the mean where only the differences between samples are used for factor analysis. The latter technique is used when only differences between samples are needed, while the former is used when fractional concentrations of components are to be determined. This can be confusing to the reader who is accustomed to factor analysis around the mean and viewing plots of factor score 1 versus factor score 2. When factor analysis around the origin is used, this same information is contained in factor scores 2 and 3, and factor score 1 contains the information about the mean of each variable. The number of factors selected for the analysis was limited to significant factors (eigenvalues >1). Factor scores from the analysis were presented in two-dimensional plots to show compositional differences between various biomass materials. Materials with similar mass spectral intensities form clusters in the factor space. The factor analyzed data were resolved into three components corresponding to lignin, hexosans and pentosans. These resolved pyrolysis products of the biomass

feedstocks were used to determine the influence of storage time on the composition of the biomass.

RESULTS AND DISCUSSION

Pyrolysis-molecular beam mass spectra (Py-MBMS) for the different biomass materials (hybrid poplar, black locust, sericea lespedeza, and switchgrass) that were harvested at two different times of the year show visual similarity for all the species except sericea lespedeza. The Py-MBMS spectra can be divided into three main classes representing pentosans with typical m/z 43, 85, 96, and 114; hexosans with typical m/z 31, 60, 73, 97, 126, 144, and 162; and lignins with typical m/z 124, 137, 150, 154, 167, 180, 194, 210, and 272. A small region, which is typical of phenolic esters and phenylpropane lignins (m/z 94, 120, and 150), is prominent in the switchgrass pyrolysis mass spectra.

The influence of harvest time cannot be readily discerned from visually inspecting most of the spectra of the feedstocks (see Figure 1a and 1b) except by multivariate statistical analysis. In the case of sericea lespedeza, the Py-MBMS from the two harvests are visually discernible (see Figure 2a and 2b). In Figure 2b, the pyrolysis products that derive from the carbohydrates are higher for the December harvest compared to the October harvest.

The Py-MBMS spectral data were further analyzed using the ISMA program to highlight the differences between the harvests. The analysis of the mass spectral data using the correlation around the mean matrix indicated that 87% of the variance in the data set could be explained using four factors. The four factors were used to perform factor analysis using a correlation around the origin matrix. The factor-score plot (Figure 3a) showed four main groups corresponding to hardwoods, switchgrass, the October sericea lespedeza harvest, and the December sericea lespedeza harvest. The repeatability of the pyrolysis runs is indicated by the triangles in the factor score plot. The variance diagram in Figure 3b also confirms the clusters in the factor score plot.

The different clusters shown in the factor space for the two sericea lespedeza harvests suggests that the pyrolysis products of these two feedstocks are different. The major difference between the pyrolysis products of the two harvests is the carbohydrate component of the feedstocks. The resolution of the pyrolysis spectra showed a relatively high concentration of carbohydrate component in the December harvest of the sericea lespedeza compared to the October sericea lespedeza harvest. This observation is similar to the seasonal carbohydrate cycles noted in deciduous trees in the temperate climate. Carbohydrate contents of stems and branches of deciduous trees are maximized near the time of leaf fall and start to decrease in late winter [2]. Although sericea lespedeza is technically not a tree, it is a woody shrub that defoliates in the fall like the deciduous trees. It is probable that the total reserve carbohydrate accumulation in this shrubby species follows a similar cycle to those observed for the trees.

In addition to the high carbohydrate content of the December sericea lespedeza harvest, the char produced during the pyrolysis was lower (16.2±1.0%) than that for the October sericea lespedeza harvest (21.4±1.0%). The difference in char yields was attributed to the significant differences between the nitrogen and ash contents of the two harvests. The October sericea lespedeza harvest had a high leaf to stem ratio (0.26) and consequently a high nitrogen content (1.14±0.10%) compared to the December sericea lespedeza harvest that was defoliated and had a nitrogen content of 0.75±0.10%. The ash contents of the October and December sericea lespedeza harvests were 2.1±0.3 and 1.3±0.4% respectively. Both the nitrogen and ash components of the biomass are known to promote char formation. Nitrogen compounds are known to react with carbohydrate decomposition products during the pyrolysis process resulting in char [4].

For switchgrass samples, although the repeatability triangles do not overlap, the differences between the pyrolysis products of the two harvests appear to be very small and statistically insignificant. The factor analysis of the data indicates that the switchgrass samples have a higher concentration of components that are rich in m/z 120 and 150 compared to the sericea lespedeza and the woody species. These masses derive from phenolic ester units known to occur in grass lignins. Nitrogen (0.59±0.08 and 0.56±0.066%) and ash (5.2±0.4 and 4.8±0.2) contents of the two harvest were similar, and hence char yields from both harvests were very similar (18.6±0.3 and 18.4±1.4 %).

Py-MBMS and factor analysis of the woody biomass species (black locust and hybrid poplar) indicated that there are no significant differences in the yield of pyrolysis products because of harvest time. The repeatability triangles overlap as shown in Figure 3a. The variance diagram also indicates that the hardwoods are richer in lignin components compared to the non-woody species (switchgrass and sericea lespedeza). The woody species have very strong peak intensities at m/z 138, 154, 167, 180, 194, and 210 which are typical lignin decomposition products. Nitrogen and ash contents of the woody species from the two harvests were very similar and hence the char yields were also very similar. Although seasonal variations in minerals, nitrogen, and reserved carbohydrates contents have been reported for hardwoods,

the influence of these changes on the pyrolysis products of the woody biomass feedstocks analyzed by our method appear to be minimal.

CONCLUSIONS

The multivariate analysis of the biomass feedstocks studied shows that the influence of harvest time on the composition of the biomass pyrolysis products is only significant for the herbaceous biomass feedstock (sericea lespedeza). The pyrolysis products of woody biomass feedstocks appear to be less affected by the time of harvest. Thus, for fuel production from sericea lespedeza this factor must be taken into account. Small changes in the biomass feedstocks can be detected by MBMS and their subsequent influence on converting the feedstocks to fuels and chemicals can be assessed. The Py-MBMS technique for analyzing biomass feedstocks has some advantages over conventional chemical analysis in that sample preparation is minimal, very small samples are required for analysis, pyrolysis time is very short, and the pyrolysis data is acquired in real time. This technique may also find application in coal and other fossil fuel analysis.

ACKNOWLEDGEMENT

The authors acknowledge H.L. Chum and R. Overend for their involvement in initiating this study; A.E. Wiselogel, the NREL Terrestrial Biomass Feedstocks Interface Program coordinator, and N. Hinman, the NREL Biofuels Program manager, for their continued support. P. Ashley prepared the biomass feedstocks for the pyrolysis studies. The work was sponsored by the U.S. Department of Energy Biofuels Systems Division through the Biofuels Program (R. Moorer, R. Costello, and J.Ferrell).

REFERENCES

1. Sunderman, D. "Using Biomass and Wastes Productively: Research Advances at the National Renewable Energy Laboratory." In *Energy from Biomass and Wastes XVI*, (D.L. Klass, ed.) Institute of Gas Technology (IGT): Chicago, 1993; pp. 1-13.

2. Kramer, P.J. and Kozlowski, T.T. *Physiology of Woody Plants;* Academic: New York, 1979; Chapters 7, 9, and 10. .

3. Evans, R.J.; Agblevor, F.A.; Chum, H.L.; Wooten, J.B.; Chadwick, D.B.; and Baldwin, S.D., "New Approaches to the Study of Cellulose Pyrolysis," *ACS Fuel Div., Preprints* (1991), 36 (2), 714-724.

4. Theander, O., and Nelson, D.A., "Aqueous High Temperature Transformation of Carbohydrates Relative to Utilization of Biomass," *Adv. Carbohydrate Chem. Biochem.*(1989), 46, 273-326 .

5. Evans, R.J., and Milne, T.A., "Molecular Characterization of the Pyrolysis of Biomass I, Fundamentals," *Energy and Fuels* (1987), 1 (2), 123-137.

6. Windig, W.; Haverkamp, J.; and Kistemaker, P.G., "Interpretation of Sets of Pyrolysis Mass Spectra by Discriminant Analysis and Graphical Rotation," *Anal. Chem.* (1983), 55, 81-88 .

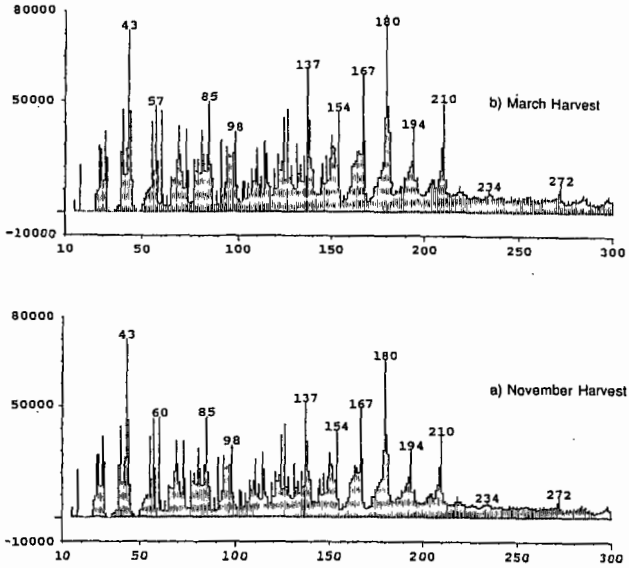

Figure 1. Pyrolysis mass spectra of hybrid poplar. Note the strong similarity in the spectra of a) the November harvest, and b) the March harvest.

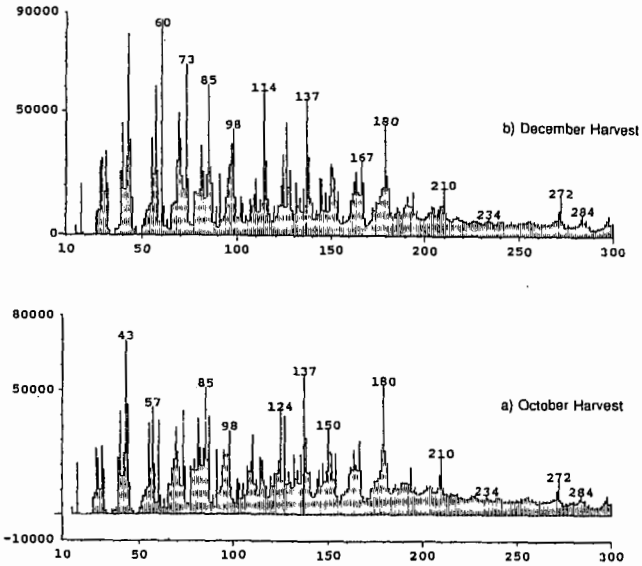

Figure 2. Pyrolysis mass spectra of sericea lespedeza. Notice the difference in the intensity of the low mass peaks (e.g.,m/z 60, 73 and 114) in a) the October harvest, and b) the December harvest.

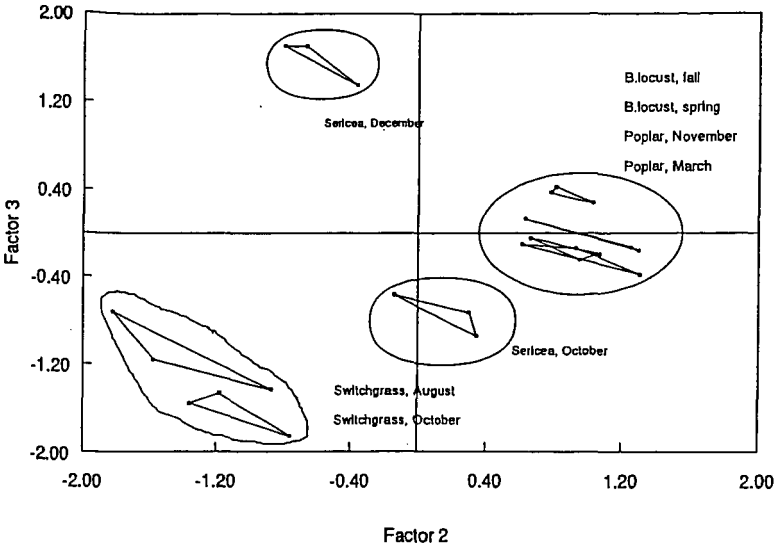

Figure 3a. Factor-score plot of Factor 2 versus Factor 3 of the different harvests of sericea, black locust, hybrid poplar, and switchgrass showing the clusters of the similar biomass samples in the factor space. The triangles show the repeatability of the pyrolysis runs.

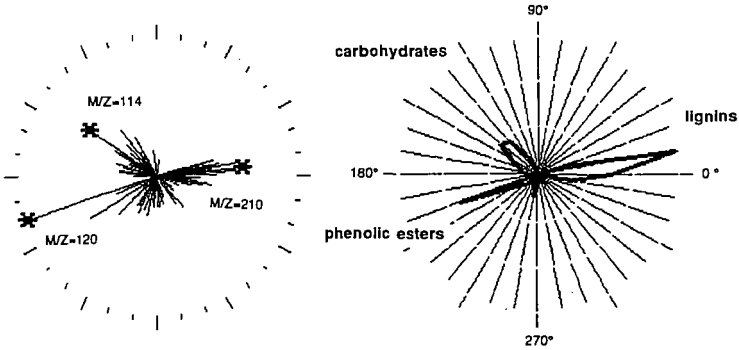

Figure 3b. Variance diagram of factor 2 versus factor 3 of the Py-MBMS of the biomass feedstocks showing compound classes in the spectra.

INFLUENCE OF THE WATER-GAS-SHIFT REACTION ON LOW TEMPERATURE PRETREATMENT OF SUBBITUMINOUS COAL

Soon Chuan Lim, J. Brian Lainhart and Edwin N. Givens
University of Kentucky, Center for Applied Energy Research,
3572 Iron Works Pike, Lexington, Kentucky 40511-8433

Kaywords: Coal, carbon monoxide, water, alkali promoters

Abstract
In previous studies, we showed that subbituminous coals treated with CO and water in the presence of a base (NaOH, Na_2CO_3) at mild temperatures (300 °C) produced an improved liquefaction feed material. In this reaction coal undergoes significant structural modification as observed by the increased THF and pyridine solubility, lower oxygen content and higher atomic H/C ratio relative to the raw coal. In this paper, we discuss the impact of the water-gas-shift (WGS) reaction on the coal reaction. Strong correlations were found over a wide range of reaction conditions between THF solubility of the pretreated coal and both CO conversion and amount of hydrogen consumed. The effect of various sodium and ammonium salts on the reaction is discussed.

Introduction
Fischer and Schrader,[1] pioneered the liquefaction of coal with CO and water. Appell and Wender[2] in the late 60's revived interest in this approach as an alternative method for directly producing hydrogen in the liquefaction reactor. This led to the CoSteam process for liquefying low rank coals. Since then, the application of CO and water for liquefying various materials and the effect of added catalysts on these reactions have been widely studied.[3] The addition of a strong base to this system significantly improves the conversion of coal to liquid products.[4] In recent years, CO and water has been used to treat coal to enhancing its conversion during liquefaction and improve the product mix.[5,6] This treatment results in chemically and structurally modifying the coal to produce an improved feed material.

The chemistry of the WGS reaction and the intermediates involved in the reaction are complex. Various mechanisms and intermediates have been proposed for coal conversion using CO and water.[7,8] Recently, Horvath et al.[9] provided evidence for the formation of formate ion at liquefaction temperature when they reacted coal with CO and water at 400 °C in a specially fitted ^{13}C NMR spectrometer. At significantly lower temperatures (200 °C and below), King et al.[10] showed that CO reacts rapidly with KOH to quantitatively form potassium formate. They showed that the production of hydrogen from the WGS reaction at these temperatures is catalyzed by the addition of a catalyst precursor such as $Mo(CO)_6$. In the absence of a suitable catalyst, the formate ion is relatively stable up to 300 °C.[11] Above 300 °C formate decomposes mainly to CO_2 and H_2 and partially undergoes dehydration to form CO. From the literature,[2-4,7] it is evident that the success of liquefaction with CO and water has been attributed to the intervention of the formate ion. In this paper we present results to show the effect of the WGS reaction on the reaction of coal with CO and water at rather mild temperatures at or below 320°C.

Experimental
Coals - Wyodak coal from the Black Thunder (BT) mine in Wright, Wyoming, was ground to -200 mesh, riffled and stored in tightly sealed containers. Ultimate analyses was as follows: carbon, 73.9%; hydrogen, 5.2%; nitrogen, 1.3%; sulfur, 0.6%; oxygen, 19.0%O (by difference). Ash content on a dry basis was 6.12 wt%. All results are expressed as weight percent, moisture and ash-free coal (maf).
Reaction Conditions - Experiments were conducted in a 25 ml micro-reactor by adding, per gram of maf coal, up to 3 g of water and 0.06 to 1.0 mmol of promoter salt (NaOH, Na_2CO_3, NaCl, NH_4NO_3). The reactor was pressurized with CO (300-800 psig) and heated to 250 to 320°C a fluidized sandbath. The reactor was agitated at a rate of 400 cycles/min for periods between 30 min to two hours, and then rapidly quenched to room temperature. Gaseous products were collected and analyzed by gas chromatography. Solid and liquid products were recovered from the reactor using distilled water, filtered, and dried. Water-insoluble materials were separated by extracting with THF in a Soxhlet thimble for 18 hours and drying overnight at 80 °C at 16 kPa. The THF solubles were concentrated by removing excess THF. A 50:1 excess volume of pentane was added and the pentane insoluble material was filtered and dried. Only a very small amount of pentane soluble material was recovered which represented only a small proportion of the overall products, particularly when high CO pressures

were used.[5] In coal reactions with a promoter and in the absence of CO or at low CO pressures (400 psig and below), soluble humic acids were recovered from the aqueous phase by precipitating the colloidal material with HCl (pH 1-2) followed by centrifugation and drying. The acidified aqueous layer was further extracted with ether. Total mass recovery, on a maf basis, was typically 90% or better at or below 300 °C and between 80-85% at 320°C. THF solubility of the solid products after pretreatment is defined as the proportion of material soluble in THF plus any humic acids, if present.

Results and Discussion

Water-Gas-Shift Reaction. Total CO_x recoveries from coal treatment runs with CO were typically greater than 98% and included unreacted CO, gaseous and dissolved CO_2, and formate ion present in the aqueous phase. For those reactions to which NaOH was added, the concentration of dissolved formate, which was based upon the equivalents of Na present, accounted for 4% of the total CO feed. No correction was made when any of the other salts were used in these reactions. Dissolved CO_2 in the aqueous phase, calculated at ambient temperature following Henry's law, accounted for only 1% of the total CO feed. CO conversions increased with temperature, with the maximum conversion of 34% being observed at 350 °C, which was equivalent to conversion of 7.5 mmol of CO per gram maf coal feed.

For a 20% conversion of CO, the theoretical amount of hydrogen produced from that portion of the CO that was converted to CO_2 via the WGS reaction was equivalent to 4.5 mmol/g maf coal. Addition of a promoter increases CO conversion significantly, but these values are low relative to the thermodynamic equilibrium value. Recovery efficiencies of H_2 were quantitative when coal was absent but decreased sharply in the presence of coal. The missing H_2 presumably was incorporated into the treated product and is reported as H_2 consumption in mg H_2/g maf coal.

Conversions of CO in aqueous solutions containing up to 2 mmol NaOH per 45 mmol CO were determined over a temperature range from 250 to 350 °C for a one hour reaction period (see Table 1). In the absence of NaOH, only 1% of the CO is converted. In the presence of NaOH, conversions increased steadily with temperature. Doubling the reaction time from one hour to 2 hours increased conversion by about 25% at 300 °C. However, under no circumstances were CO conversions equal to those that were reported previously for similar reaction conditions (~80%) attained in this study.[8]

In the presence of coal at 300 °C, 10% CO was converted in 1 hour (see Table 2). This level of conversion was significantly greater than the 1% observed in the absence of coal. When both NaOH and coal were present, 20% of the CO was converted which equalled that observed in aqueous NaOH in the absence of coal. The increase observed with coal, but in the absence of base, suggests that the cationic component in the coal may be acting as a weak promoter. This increase is still much less than observed with added NaOH, since coal added to caustic solution gave no additional CO conversion. The data indicate that reaction time is a strong dependent variable for converting CO. Conversion progressively increased over a period from 30 to 90 min from 12 to 23%, as shown in Table 3. Other salts also promote the WGS reaction. CO conversions in the presence of coal at 300 °C with added sodium carbonate, bicarbonate and chloride were 17, 21 and 16%, respectively. Since CO conversion occurs equally well in the presence of sodium chloride, obviously a basic system is not necessary for initiating CO conversion. Ammonium nitrate appears not to be a significant promoter for CO conversion, possibly because it decomposes at approximately 250 °C.

Coal Reaction. Treating Wyodak coal in CO/NaOH/water at 300 °C results in a 8 to 13 wt% decrease in the amount of solid material, as shown in Table 3. In the absence of CO or at lower CO pressures, a small amount of humic acids are also found in addition to a trace of ether soluble material. Only trace quantities of hydrocarbon gases are produced during the treatment. The major part of the decrease in weight is due to elimination of water and carbon oxides. The sizable increase in THF solubility of the treated material both in THF and pyridine indicates that significant modification has occurred to the coal structure. The solubility behavior of this THF material indicates it is almost completely pentane insoluble. Although the presence of NaOH is not necessary for achieving a reasonably high THF solubility in the water-insoluble product, there is improvement when it is present. However, the absence of CO has a much more dramatic affect on the reaction. The solubility in THF of the water-insoluble material obtained from hydrothermally treating the coal at 320°C in the absence of CO was only 11%. The water-insoluble material from the hydrothermal treatment in the presence of added NaOH at 320 °C was 9% soluble in THF. In the case of the NaOH

treatment 4 wt% humic acids and 1 wt% ether solubles were formed.

The amount of hydrogen that could not be accounted for in the material balances from these various CO treatments is presumably consumed by the water-insoluble product. The amount increased with increasing reaction time as well as temperature. For reaction periods from 30 to 90 min, the level of hydrogen incorporation in the product ranged from approximately 0.4 wt% up to 0.7 wt%, which is consistent with increases reported previously.[5]

Other salts also promote the conversion of CO, as well as produces a water-insoluble material having increased THF solubilities, as shown in Table 2. The THF solubilities of the water-insoluble materials from the sodium carbonate, bicarbonate and chloride promoted reactions were similar in magnitude to the amount of THF soluble material obtained when using NaOH. Ammonium nitrate, however, gave a material that was only 10% soluble. It is not entirely clear why NH_4NO_3 should give a lower THF solubility, even though it decomposes above 200 °C (m.p. 172°C). The hydrothermal reaction with CO should still result in a sizable improvement in the THF solubility of the water-insoluble product.

At high CO pressures, the total amount of coal derived material that is soluble in THF is equal to the THF solubility of the water-insoluble product. In the absence of CO or at low CO pressures, however, the total amount of THF soluble material derived from the coal includes humic acids and ether soluble material. A plot of total THF solubles versus the amount of converted CO from both current, as well as previously reported results, is shown in Figure 1. In these runs, Wyodak coal was treated at different temperatures, at different CO pressures, with different amount of water, and with different salts at different salt concentrations. The plot indicates a strong correlation exists between these variables.

A plot of THF solubility versus H_2 consumption also shows a strong correlation with an apparent intercept that approaches the origin (Figure 2). This parallel between THF solubility and H_2 consumption and the close approach of the H_2 intercept to the origin indicates that addition of hydrogen during treatment of the coal must be highly efficient.

Conclusions. The presence of sodium hydroxide, carbonate, bicarbonate and chloride salts promotes the conversion of CO at temperatures between 250 and 350 °C. Coal also promotes CO conversion but to a lesser extent than the sodium salts. The addition of Wyodak coal to these systems results in a water-insoluble material that is significantly more soluble in THF. Correlations were found between both the level of CO conversion and H_2 consumption and the THF solubility of the water-insoluble product. The close approach of both of these correlations to the origin is an indication of the high H_2 utilization efficiency of this treatment reaction.

Acknowledgement
The financial support of the Commonwealth of Kentucky and the Department of Energy under contract number DOE AC22-91PC91040 is gratefully acknowledged.

References

1. Fischer, F.; Schrader, H. *Brennst. Chem.* **1921**, *2*, 257. *Chem. Abs.* **1921**, *15*, 3900.
2. Appell, H.R.; Wender, I. *Preprints - Am Chem. Soc. Div Fuel Chem.* **1968**, 12, *3*, 220.
3. Oelert, H.H.; Siekmann, R. *Fuel* **1976**, *55*, 39.
4. Cassidy, P.J.; Jackson, W.R.; Larkins, F.P.; Louey, M.B.; Sakurovs, R.J. *Fuel Process. Technol.* **1986**, *14*, 231.
5. Lim, S. C.; Rathbone, R. F.; Rubel, A. M.; Givens, E. N.; Derbyshire. F. J. *Energy and Fuels*, **1994**, *8*, 294
6. Vaughn, S.N.; Siskin, M.; Katritzky, A.; Brons, G.; Reynolds, N.; Culross, C.C.; Neskora, D.R., United States Patent No. 5,151,173; Sept. 29, 1992.
7. Schuchardt, U.; Sousa, M. F. B. *Fuel*, **1986**, *65*, 669.
8. Elliott, D. C.; Sealock, Jr., L. J. *Ind. Eng. Chem. Prod. Res. Dev.* **1983**, *22*, 426.
9. Horvath, I. T.; Siskin, M. *Energy Fuels* **1991**, *5*, 933.
10. King, Jr., A. D.; King, R.B.; Yang, D. B. *J. Am. Chem. Soc.* **1981**, *103(10)* 2699.
11. Elliott, D. C.; Hallen, R. T.; Sealock, Jr., L. J. *Ind. Eng. Chem. Prod. Res. Dev.* **1983**, *22*, 431.

Table 1. Effect of Temperature on the WGS Reaction								
Temperature, °C	350	320	320	300	300	300	250	250
CO press, psig	800	800	800	800	800	800	800	800
NaOH Conc, mmols/g maf coal	1	1	Nil	1	1	Nil	1	Nil
Reaction Time, min	60	60	60	120	60	60	60	60
CO_x recovery, mole%	102	100	100	91	96	97	97	98
CO Conv, mol%	34	27	1	19	15	1	5	1

Table 2. Effect of Promoter Salt on Treatment of Wyodak Coal[a]						
Salt promoter	none	NaOH	Na_2CO_3	$NaHCO_3$	NaCl	NH_4NO_3
Salt conc, mmol/g maf coal	-	1	0.5	1	1	1
CO_x recovery, mol%	97	100	99	101	97	99
CO Conv, mol%	10	20	17	21	16	13
CO Conv, mmol/g maf coal	2.0	4.0	3.4	4.0	3.0	2.2
Missing H_2, % theoretical	84	86	82	86	51	42
H_2 Consumption, wt% maf coal	0.33	0.63	0.56	0.60	0.31	0.18
WI[b] Product, wt% maf coal	90	92	93	89	90	88
Solubility of WI in THF, wt%	22	28	32	24	24	10

a. 300 °C, 800 psig CO cold (approx. 20 mmol/g maf coal), 3 g water/g maf coal.
b. WI = water insoluble product

Table 3. Effect of Treatment Time[a]			
Reaction Time, min	30	60	90
CO_x recovery, mol%	98	100	100
CO Conv, mol%	12	20	23
CO Converted, mmol/g maf coal	2.4	4.0	4.0
Missing H_2, % theoretical	70	86	84
H_2 Consumption, wt% maf coal	0.33	0.63	0.68
WI[b] Product, wt% maf coal	91	92	87
Solubility of WI in THF, wt%	20	28	26

a. 300 °C, 800 psig CO cold (approx. 20 mmol /g maf coal), 1 mmol NaOH/g maf coal, 3 g water/g maf coal
b. WI = water insoluble product

Table 4. Legend for Figures 1 and 2[a]					
	Promoter Salt	mmol Salt/ g maf coal	CO Pressure, psig	Temp °C	Reaction Time, min
A	NaOH	0.06	300	250	60
B	NaOH	0.5	550	275	60
C	NaOH	0.06	800	250	60
D	NaOH	1.0	800	300	60
E	NaOH	1.0	800	300	30
F	NaOH	1.0	800	300	90
G	NaOH	1.0	800	320	60
H	Na_2CO_3	0.5	800	300	60
I	$NaHCO_3$	1.0	800	300	60
J	NaCl	1.0	800	300	60
K	NH_4NO_3	1.0	800	300	60
a. Water added at 3 g/g maf coal.					

Fig.1 The Effect of CO conversion on THF Solubility of Trested Coal

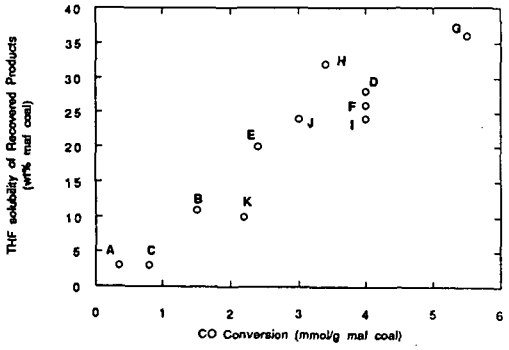

Fig.2 The Effect of Hydrogen Consumption on THF Solubility of Treated Coal

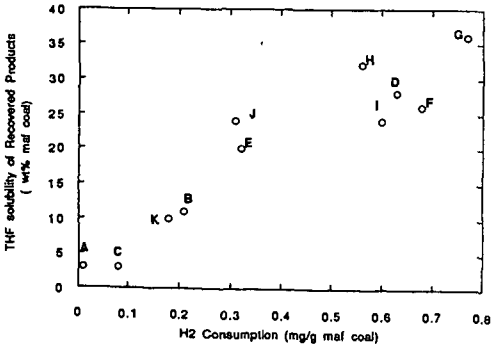

THE PERFORMANCE OF BIOMASS DERIVED ULTRACARBOFLUIDS IN STANDARD DIESEL ENGINES

M. ANWAR, R.G. Temple, C.J. Mumford.

Department of Chemical Engineering & Applied Chemistry,
Aston University, Birmingham, U.K.

Keywords: Bio-ultracarbofluids, Diesel fuel replacement.

Introduction

The impetus for the replacement of petroleum-derived diesel fuels ,whether wholly or partially,arises from the need to conserve a non-renewable energy resource and because of the significant pollutants generated by their combustion.However the use of bio-mass derived fuels may also offer strategic and economic advantages.

The majority of the world's energy resources occur in nature as solids e.g coal and various biomass and waste materials.Bio-fuels such as wood ,charcoal and agricultural residues are a major source of energy in many of the developing countries providing as much as 14% of the current world energy requirements.This is eqivalent to some 25 million barrels of oil a day,the same as OPEC's current production[1].Worldwide there is substantial land potentially available for growing energy crops.

The possibilities for diesel fuel replacement are;

i Complete replacement by a suitable vegetable oil e.g. rape seed oil [2] , soya bean oil [3], esterified sugar beet exract [4].Some research is also in progress into the use of elephant grass oil (Miscanthus)[5].

ii Partial replacement by blending diesel with vegetable oils in varying proportions up to 20% by weight[6].

iii Partial replacement by blending with an aqueous suspension of a non-renewable fossil fuel e.g.coal[7].

iv Complete replacement by a slurry of coal in vegetable oil.

or

v Complete replacement by a 100% bio-renewable ultracarbofluid. This could comprise some formulation of water, charcoal , and a vegetable derived oil.

The research summarised here is concerned with the last alternative.

Biomass-Derived Ultracarbofluids

Typically biomass derived ultracarbofluids consist of charcoal 45%-54%,oil-blend 16%-29%, water 30%-35%, surfactant 1%, plus corrosion inhibitors etc in trace amounts.

The solid constituent is of necessity finely-divided and in practice needs to be ground to < 20μm particles in order to minimise erosion in the fuel system i.e transfer lines and injectors.Clearly low ash charcoal is preferable for optimum energy efficiency but also mainly to keep residue build-up in the engine to a minimum.The higher the proportion of charcoal in the blend the greater the gross energy output.

The possible replacement of the fuel oil fraction ,typically 15% to 30%,by a bio-renewable vegetable oil is of considerable interest.Several commercially available oils have been tested as fuel components.Using ordinary vegetable oils as fuel usually results in problems with severe engine deposits,ring sticking ,accumulation of deposits on injector nozzles and lubricant contamination ..For this reason vegetable oils for use as fuel or fuel component have to be modified by trans-esterification. Rapeseed methyl ester shows great potential for use as fuel or as a fuel component for diesel engines.

The ultimate test for any fuel is to determine how well it burns over long periods of time, and the impact of its use on the combustion system and auxilliary equipment.However any blend can, of course, be characterised by conventional property measurements i.e viscosity,cetane number,grossheat combustion , cloud point, flash point, density, particle size and ash content.

Ucf Peformance

Coal-water slurries have been studied extensively as fuels.Initial results confirmed that the main problems encountered when using coal-water slurries are,with fuel injection system operability, wear and poor combustion efficiency of the coal particles .

However, improvements have been recently been reported in reduced wear of injection components,by the addition of lubricant [8].

Bio-ultracarbofluids

Initial research on bio-ultracarbofluids utilised a 4-stroke single cylinder,indirect injection diesel engine with speed range of 650-800 rpm . The optimum perfomance has been achieved using coal 40%,water 30%, fuel oil 29%, additive 1%. The operating variables were;

-coal particle mean diameter :	8 μm
-injection timing :	42 degrees BTDC
-injection pressure :	12.5 MPa
-intake air temperature :	313 K
-intake air pressure :	0.22MPa

Specimen results in comparison with Esso diesel 2000 fuel oil are given in Fig 1.

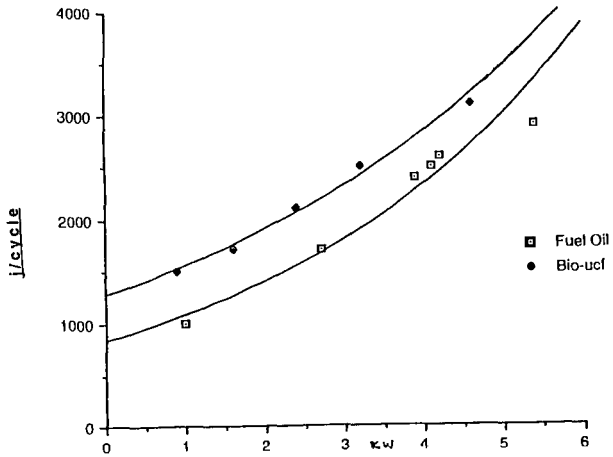

Figure 1: Energy consumption as a function of delivery power

The present research utilises a 4-stroke, 2 cylinder 600cc Lister-Petter diesel engine.A Heenan Froude hydraulic dynamometer is connected to the engine, as are auxilliary data collection apparatus as shown diagrammatically in Fig. 2.

The fuel formulation under investigation are based upon rape seed oil , peanut oil or sugar beet extract oil. Three different types of charcoal are under test. Also three different surfactants have been evaluated.In each case performance is compared with that of standard Esso diesel 2000.
The data obtained are;

engine torque	exhaust temperature
fuel consumption	oil temperature
air consumption	coolant temperature
speed	air temperature

Exhaust emissions are continuously monitored for levels of CO_2,CO and HC's levels.

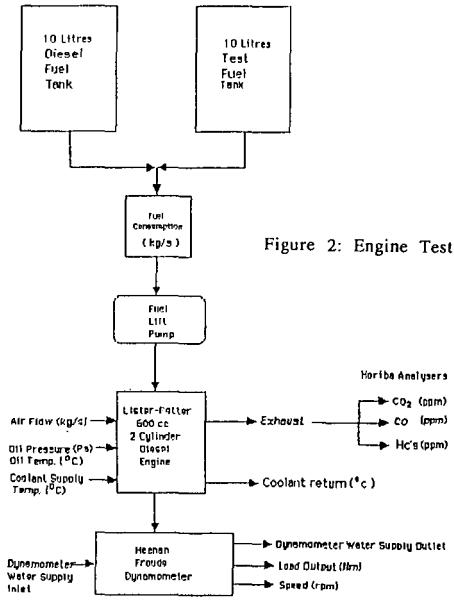

Figure 2: Engine Test Rig

Economics

The European Community's interest in bio-fuel arises in part from the Common Agriculture Policy (CAP).Farming at the present represents nearly 5% of the aggregrate Gross National Product of the EC member states and involves 9% of the workforce .Bio-mass crop production can contribute to this industrial activity and hence make a socio-economic contribution to rural development .Growing bio-mass will also avoid desertification of countryside. One tonne of crushed rapeseed produces about 320 kilograms of oil,and charcoal is readily available commercially.Additives are more expensive but are used only as 1%.It has been calculated that bio-ultracarbofluids will cost 21p per litre as compared to 12p for diesel , on the assumption that the rapeseed oil was grown on non-subsidised land .Hence preliminary estimates suggest that, with subsidies and economies of scale, the price of bio-ultra carbofluid could be comparable to diesel.

Conclusions

Results to date suggest that bio-ultrcarbofluids can be used in diesel engines without modifications. However the long term effects of corrosion, erosion and particle size on fuel handling systems require more detailed research using ASTM and EC test standards. The long term storage of the formulated fuels needs to be researched to see if this has any adverse effects such as oxidation of the oil components or settling of charcoal.

The EC is currently very keen to encourage the growing of energy crops since it will result in a reduction in the greenhouse gases, particularly CO_2 ,and reduce dependence on fuel imports. It would also encourage farmers to grow crops on set aside scheme.Hence there are good prospects for limited use of bio-ultracarbofluids.This would be greatly increased by direct or indirect state subsidies [9].

References

1. Shell "Biofuels in the European Community",May 1992.
2. Bondioli P. ,Lanzani A.,"Vegetable Oils Transesterification Reaction" , University of Milan,1989.
3. Bagby O M, "Seed Oils for Diesel Fuels" Paper number 87-1583,24 Jul 1991,Northern Regional Research Centre.
4. Edwards L S, " Science in Britain" P 39, issue 117 , January1991.
5. Speller S C," The Potential for Growing Biomass Crops for Fuel on Surplus Land in the U.K." Outlook on Agriculture Vol. 22 No1 (1993).
6. Stokes B D," Vegetable Oils in Diesel Fuels," Paper 9 p 34-39 ,1987.University of Birmingham.
7.Pavolikowski R,"The Coal Dust Engine upsets Tradition Power,"July ,1928.
8. Gislais P, Antonini G,"The Bio-UCF(Bio-ultracarbofluid):A Liquid Fuel-Oil Substitution in Boiler and Diesel Engine Applications" , July 1993.
9.The Chemical Engineer "Tax cut urged to save bio-diesel process", P 6 26 May 1994, issue 566.

THE THERMOCHEMICAL CONVERSION OF CELLULOSE TO OIL IN DIFFERENT SOLVENT-FEED RATIOS WITH DIFFERENT REDUCING GASES.

BABUL K. DATTA
DEPARTMENT OF CHEMISTRY
UNIVERSITY OF MANCHESTER INSTITUTE OF SCIENCE AND TECHNOLOGY (UMIST), MANCHESTER, UK.

** CURRENTLY*
AUDUBON SUGAR INSTITUTE
LOUISIANA STATE UNIVERSITY, BATON ROUGE, LA 70803.

Keywords: Liquefaction, Solvent, Cellulose, and Catalyst.

ABSTRACT

The conversion of cellulose (Solkaflock) with different aqueous feed ratio with 35 bar reducing gases (H_2 and CO) were studied in a batch autoclave system at 350°c in presence of 5% Pt/Al_2O_3 catalyst. Under these conditions, the conversion showed a general increase with increasing solvent/feed ratio, but more significantly when CO was used as the reducing gas. This is perhaps due to the better contact between the feed and catalyst as well as greater amount of solvent space. Decomposition of cellulose yielded mainly oil of relatively low oxygen content and high heating value. Increasing S/F ratio were produced lower amounts of oil and char but increasing the higher yields of water-soluble fractions. This is probably due to the higher liquefaction of gaseous products. Moreover, the oil were obtained from 10:1 (S/F ratio with H_2 gas) was contained 20.0% lights in comparison with 6:1 (S/F ratio with H_2 gas) contained 56.0% lights which is due to higher methanation reactions in 10:1 S/F ratio.

INTRODUCTION:

The effect of water to wood ratio has been found to be an important parameter during liquefaction with Na_2CO_3 and CO (1). In run 1, 2, 3, and 4, the effect of solvent /feed ratio, on the liquefaction of cellulose was studied using 5% Pt/Al_2O_3 catalyst in presence of CO and H_2 as reducing gases with water into fuels.

EXPERIMENTAL PROCEDURE:

These experimental works were conducted with 1-liter rocker stainless steel autoclave reactor. cellulose, catalyst and water were charged to it. Hydrogen or Carbon monoxide was added to the desired pressure (35 bar) and the autoclave was then brought to operating temperature at 350°c. and reaction time was 2 hours. After cooling the autoclave, the product gas was collected in a gas measurement system and were analyzed by GC. The aqueous phase was separated by decantation and the remaining oil and solids were removed by adding acetone, then were refluxed for 6 hours. Then filter it with filter paper by water vacuum. The residue is char and catalyst, was dried in an oven at 110°c for overnight. The filtrate was oil and acetone. The oil was recovered from acetone by rotaevaporation. These oil were further separated into lights, waxes by using solvent- heptane and then separated into asphaltene, resins,by using toluene. The feed, char, and oils were analyzed by elemental analyser.

RESULTS AND DISCUSSIONS:

The reaction inputs, operating parameters and products distribution were shown in Table 1; and depicted graphically in Figure 1.

From the Table 3, the elemental analysis, it is seen that an increase in the H/C atomic ratio and a decrease in O/C atomic ratio as S/F changed from 6:1 to 10:1 in oils of runs 1 and 2 which indicate that increasing S/F ratio did not really promote the quality of oils.

The oil obtained from run 1 contained 56.0% light volatile whereas run 2 contained 20.0 %. Also, both Asphaltenes and resins of run 2 were greater in yields than those of run 1 which is

due to higher methanation ($CO + H_2$ -----> CH_4) reactions in run 2, that is more hydrogen consumed to form CH_4 not to hydrogenation with heavier fractions like Asphaltenes and resins.

However, in runs 3 and 4; both of which involved the use of CO as reducing gas. More lights 59.0% and smaller amounts of resins 17.2% and asphaltenes (11.5%) were produced relative to those of run 3; which probably the water-gas shift reaction was greater because of the greater volume of water present.

$$CO + H_2O \text{ --------> } CO_2 + H_2$$

Therefore, the hydrogen is produced in situ which could have gained access to the sites and substrate molecules faster than the hydrogen present in the gaseous phase.

The calorific value of oil in run 1 is 7.840 Kcal/g (S/F ratio, 6:1) which is higher than that in run 2, 7.730 Kcal/g (S/F ratio, 10:1) when hydrogen is used as reducing gas. On the other hand, when CO is used as reducing gas, the calorific value of oil in run 4, (S/F ratio 10:1) is 8.530 Kcal/g is higher than that in run 3, (S/F ratio 6:1), 7.620 Kcal/g which is not likely as before. In both the cases, the increase in calorific value was probably due to higher yields of lighter materials in the oils and not to changes in S/F ratio.

The IR spectra and GC analysis of product gases in figure 3 and product gas distribution in table 5 is seen that run 3 and 4 were produced higher yields of CO_2 than run 1 & 2 because of predominance of the water-gas shift reaction in the CO atmosphere.

Run 2 produces higher yields of hydrocarbon gases which may probably the activity of the catalyst in hydrogen atmosphere.

In run 4, was produced low yield of hydrogen 3.14%, in comparison with run 3, 15.22%, may probably the reactivity of hydrogen produced in situ. If hydrogen was used up as postulated, then lower yields were expected.

The solvent water is a necessary component of the mixture undergoing the oil forming reaction. The source of water are as follows:

(a) First, most substrates contain large amounts of moisture.

(b) Second, since most organic wastes are highly oxygenated, water is formed merely by heating them to reaction temperature; so it is a reaction product.

(c) Third, added to the reaction mixture as a solvent.

Moreover, Water acts as a solvent, vehicle and reactant. Solvation can occur between the hydroxyl groups of the substrate and water. It is an excellent medium for intermediate hydrolysis of cellulose and other high molecular-weight carbohydrates to water soluble sugars. The primary reactions in the conversion to oil likely involve formation of low molecular-weight, water soluble compounds such as glucose or pyruvic acid.

Water is a mechanical vehicle for facilitating mixing of reactants and preventing condensations to char by diluting the intermediates. Water acts as a reactant. The hydrogen added to the substrate comes from water, which consumes carbon monoxide by reacting with it to form carbon-di-oxide and hydrogen (Water gas shift reaction).

CONCLUSION:

1) Lower S/F ratio resulted in greater yields of gaseous products, oil and chars. Higher S/F ratio resulted in greater yields of water solubles and water.

2) O/C atomic ratio decreased with increase in S/F ratio.

3) Changes in S/F ratio had no direct effect on the calorific values of the oils.

4) Under CO atmosphere, when the S/F ratio was 6:1, the product of gases were contained a higher percentage of H_2 (15.22%) than S/F ratio 10:1 (3.14%).

5) The high partial pressure of steam raises the operating pressure to levels where capital costs would be high.

6) The heat required to bring water to the operating temperature and pressure adds considerably to the operating costs and

7) The separation of the oil and water phases during the product recovery step is sometimes encumbered by emulsions.

8) In case of tetralin, it can participate with the reaction at low temperature as well as low partial pressure raised; although water is more cheaper than tetralin.

REFERENCES:

1) R. L. Eager, J.F. Mathews and J.M. pepper, *"Liquefaction of Aspen poplar wood", Can. J. Chem. Eng.*, 60, 289- 294, (1982).

2) J. Brendenberg, M. Huuska, J. Raty and M. Korpio, *"Hydrogenolysis and Hydrocracking of the carbon-oxygen bond", J. Cata.*, 77, 242-247, (1982).

3) P.N. Rylander, M. Kilory and V. Coven, Engelhard *Ind. Tech. Bull*, 6, 11, (1965).

4) R.B.Anderson, *"The Fischer-Tropsch Synthesis"*, Academic Press, (1984).

5) I. Monchida, *"Efficient Liquefaction of Australian Brown Coal with a Hydrogen-Donating Solvent Under Atmospheric Pressure"*, Fuel, 60, 746-747, (1981).

APPENDIX:

Table: 1 Reaction Inputs, Parameters and Product distribution

Run	1	2	3	4
Feed type (Solkaflock)	6:1	10:1	6:1	10:1
Feed (g)	40.0	40.8	40.0	40.8
Catalyst	5% Pt/Al_2O_3	5%Pt/Al_2O_3	5%Pt/Al_2O_3	5%Pt/Al_2O_3
Catalyst (g)	1.0	1.0	1.0	1.0
Suspension medium-water(g)	240.0	408.0	240.0	408.0
Reducing gas	H_2	H_2	CO	CO
Reducing gas (g)	2.09	1.8	29.34	22.40
TOTAL INPUT (g)	283.13	451.40	310.34	471.9
Temperature (°C)	350	350	350	350
Initial Pressure (atm.)	35	35	35	35
Heating up time (hr.)	2.2	2.0	2.0	2.0
Reaction time (hr.)	2.0	2.0	2.0	2.0
Max. Reaction Press. (atm.)	200.0	250.0	210.0	255.0
Final Reaction Press. (atm.)	22.0	18.0	35.0	40.0
TOTAL OUTPUT (g)	275.2	447.6	295.7	470.0
% Recovery from Autoclave	97.2	99.20	95.28	99.60
Product Distribution				
Gas recovered (g)	9.5	8.0	28.7	27.20
Water-soluble fraction (g)	3.3	12.0	4.5	14.0
Oil (g)	12.4	9.5	8.5	8.0
Char + Catalyst (g)	3.0	2.3	7.5	2.0
Water-recovered (g)	247.0	418.0	246.5	418.8
Water-Produced (g)	7.0	6.0	6.5	10.6
% Gas Produced (g)	18.42	15.68	16.50	12.5
% Water-soluble fraction	6.25	29.41	11.25	34.3
% Oil	31.0	23.28	21.25	19.60
% Char	5.0	3.18	18.25	2.40
% Water-Produced	17.5	19.60	16.25	26.47
% TOTAL RECEIVED	80.17	91.15	81.50	95.27
% CONVERSION*	92.37	95.51	75.25	96.23

Table 2. Product of gas recovery

Run	S/F* ratio	Conversion %	Initial gas (g)	Gaseous Product				
				Vol at S.T.P.	Mol. wt.	wt. (g)	Net wt.	% Prod'd
1	6:1	94.37	2.13	7.3	29.4	9.5	7.37	18.42
2	10:1	95.51	1.6	6.9	28.0	8.0	6.4	15.68
3	6:1	75.25	22.1	15.0	43.0	28.7	6.6	16.50
4	10:1	96.23	22.1	14.5	42.0	27.2	5.1	12.5

* Solvent/Feed ratio

Table no. 3. Elemental Analysis

Run	S/F ratio	Initial Press. (atm.)	Temp. (°C)	Feed Type	% Conversion	Feed stock					Char analysis					Oil analysis					H/C	O/C	Calorific value (Kcal/g)
						%	%	%	%	%	%	%	%	%	%	%	%	%	%	%			
						C	H	N	O*	Ash	C	H	N	O*	Ash	C	H	N	O*	Ash			
1	6:1	35 (H_2)	350	Cellulose	92.37	41.5	6.1	ND	52.4	ND	63.3	5.7	0.2	30.0	0.8	72.1	6.9		19.7	ND	1.14	0.20	7 840
2	10:1	35 (H_2)	350	Cellulose	95.51	41.5	6.1	ND	52.4	ND	58.4	4.8	0.8	32.0	4.0	74.0	7.8		18.0	0.2	1.28	0.18	7.730
3	6:1	35 CO	350	Cellulose	75.25	41.5	6.1	ND	52.4	ND	63.2	4.0	0.3	25.0	7.5	73.2	7.2		18.5	0.5	1.17	0.19	7.620
4	10:1	35 CO	350	Cellulose	96.23	41.5	6.1	ND	52.4	ND	63.7	6.0		30.3		71.2	7.5		19.0	2.3	1.25	0.20	8.530

S/F ratio = Solvent/Feed ratio

* Estimated by difference

Table no. 4. Product oil composition

Run	Initial Press (atm.)	Temp. (°C)	Feed Type	Product oil composition				Elemental analysis											
								Heptane Soluble (boil)				Toluene soluble				Toluene insoluble			
				Heptane Soluble (%) Light volatiles	Heptane Soluble (boil) (%) (Waxes)	Toluene Soluble (%) (Asphaltenes)	Toluene Insoluble (%) (Resins)	% C	% H	% O	% Ash	% C	% H	% O	% Ash	% C	% H	% O	% Ash
1	35 H_2	350	Cellulose	56.0	14.5	17.2	12.3	82.2	7.5	10.3	ND	80.2	6.5	2.8	10.5	76.8	6.5	1.5	15.2
2	35 H_2	350	Cellulose	20.0	3.0	45.0	32.0	75.0	5.0	20.0	–	70.0	5.5	11.0	13.5	68.5	6.2	2.0	23.3
3	35 CO	350	Cellulose	46.4	7.5	28.3	17.8	79.7	7.8	12.0	0.5	70.7	7.9	19.0	2.4	78.0	5.8	16.0	0.2
4	35 CO	350	Cellulose	59.0	12.3	11.5	17.2	72.5	4.8	20.7	2.0	69.2	5.0	22.3	3.5	66.5	5.5	2.8	25.2

Table 5. Product of gas distribution

Run	1	2	3	4
Temperature (°C)	350	350	350	350
Pressure (atm)	35	35	35 (CO)	35 (CO)
S/F ratio	6:1	10:1	6:1	10:1
Gas	H_2	H_2	CO	CO
% CO_2	28.83	17.70	58.16	71.12
%CO	48.14	25.22	24.51	22.86
%CH_4	0.082	1.58	0.91	2.14
% C_2H_6	0.039	0.53	0.25	0.60
%C_2H_4	0.044	0.05	0.28	0.0'
%C_3H_8	0.049	0.57	0.31	0.03
%C_3H_6	0.0124	0.01	0.08	0.01
% Butane	-	0.03	-	-
% Isobutylene	-	-	-	-
% 1-Butene	-	-	-	-
% Cis-2-butene	0.0233	0.07	0.12	0.03
% Trans-2-butene	0.0398	0.05	0.08	0.04
% Butadiene	0.0050	0.03	0.08	
% Total	77.27	45.84	84.78	96.86
% H_2+UP, *	22.72	54.16	15.22	3.14

* % H_2 + Unidentified Peaks were estimated by difference.

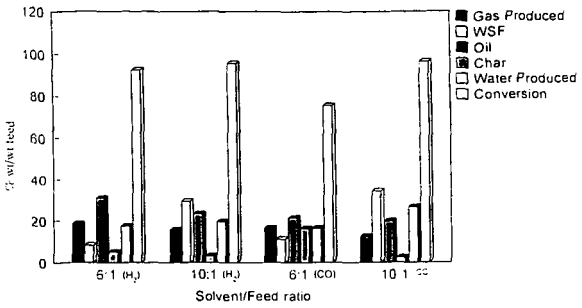

Fig. 1.The effect of S/F ratio on H_2 and CO reducing atmosphere

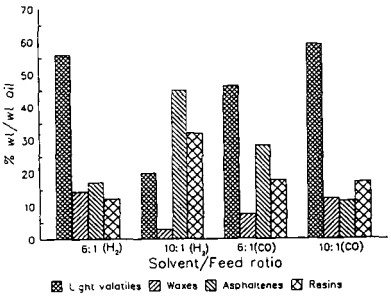

Fig. 2.The Effect of reducing gas on S/F on the Product oil Composition

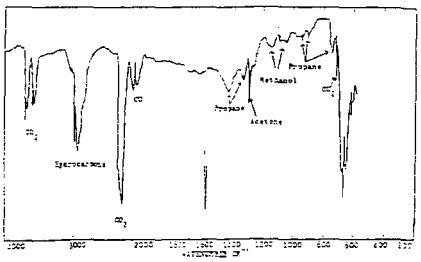

Injected Sample = 18.0cmHg

Peak No.	Gas	RT(min)
1	CO	0.98
2	CO_2	2.45
3	CH_4	1.00
4	C_2H_4	1.55
5	C_2H_6	2.15
6	C_3H_8	2.75
7	C_3H_6	6.60
8	n-Butane	7.40
9	Cis-7-butene	12.45
10	Trans-2-butene	12.30
11	Butadiene	11.75
12	Unknown	
13	Unknown	

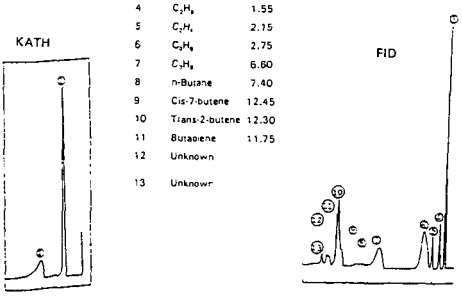

Fig. 3 : The IR spectrum and GLC chromatograms of the gaseous product from Run 1

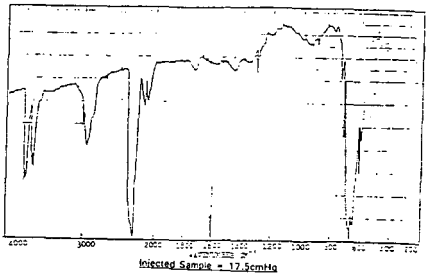

Injected Sample = 17.5cmHg

Peak No.	Gas	RT(min)
1	CO	0.98
2	CO_2	2.45
3	CH_4	1.00
4	C_2H_4	1.55
5	C_2H_6	2.15
6	C_3H_8	2.75
7	C_3H_6	6.60
8	Cis-2-butene	12.45
9	Trans-2-butene	12.30
10	Unknown	
11	Unknown	

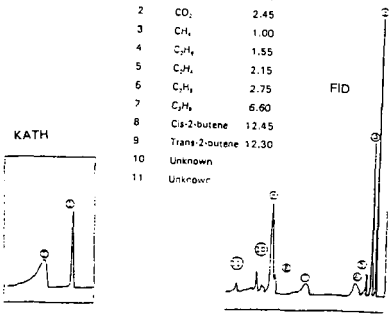

Fig. 4 : The IR spectrum and GLC chromatograms of the gaseous product from Run 4

CELLULOSE DECOMPOSITION KINETICS - GLOBAL KINETICS FOR FUELS PROCESSING AND FIRE MODELING APPLICATIONS

Ivan Milosavljevic* and Eric M. Suuberg
Division of Engineering, Brown University
Providence, RI 02912

Keywords: Pyrolysis, Cellulose, Kinetics

Introduction

There has been an ongoing debate in the literature concerning the "true" global kinetics of cellulose pyrolysis. The global kinetics are of interest in modeling cellulose decomposition in many applications in which trying to represent the full complexity of the cellulose degradation process makes no sense. Roberts noted that the activation energy data on the pyrolysis of wood and related materials tended to cluster around two values, one at about 235 kJ/mol, and the other 125 kJ/mol [1]. Various reasons were advanced, including the possible role of catalysis and sample-size related issues. Lipska and coworkers reported values for cellulose near 176 kJ/mol [2, 3], while Shafizadeh reported 113 kJ/mol [4], although they concluded elsewhere [5] that the process can be divided into an initiation step (243 kJ/mol) followed by competitive pathways to volatiles (198 kJ/mol) and char (153 kJ/mol). Broido and Weinstein obtained 230 kJ/mol and an a pre-exponential of 5.25×10^{17} s^{-1}, using a TGA technique [6]. Meanwhile Lewellen et al. obtained a much lower activation energy of 140 kJ/mol, and a pre-exponential of 6.79×10^{9} s^{-1} using a much higher heating rate [7]. Rogers and Ohlemiller obtained a similar value of activation energy, 163 kJ/mol, but at low heating rates, in a TGA [8]. Recently, Varhegyi et al. [9] obtained 234 kJ/mol and a pre-exponential of 3.9×10^{17} s^{-1}, also in a TGA system at low heating rates (10 K/min).

Thus there is not particularly good agreement as to the global kinetics of the process. The kinetics often appeared to depend upon the heating rate employed in the experiments used to deduce them. For our purposes, involving fire modeling, we were in a range of heating rates between those studied by many workers and we felt it necessary to establish more clearly what the applicable kinetics were. In addition to the question about Arrhenius parameters, there is also uncertainty concerning the order of reaction. While there is often a tendency to model the decomposition using first order decompositional kinetics, some careful studies clearly suggest fractional order kinetics are more appropriate. In this paper, we explore this subject using thermogravimetric analysis (TGA). We have also employed differential scanning calorimetry (DSC) to study the problem, and these results will be presented elsewhere.

Experimental

This work was carried out as part of a larger experimental program, concerned with the behavior of cellulosic materials under simulated fire conditions. Other results from this work have been reported previously[10]. The interest in the behavior of bulk solids under fire conditions dictated the general range of heating rates to be below 100 K/min, but we extended this to 1000 K/min for some experiments.

The pyrolysis behavior of purified cellulose in one case was studied in a standard TGA (DuPont Instruments Model 951). All TGA experiments were conducted in an inert gas environment (nitrogen). Temperature calibration of the TGA was of particular concern, since in this device the thermocouple was not in direct contact with the sample. The temperatures reported by the "standard" instrument thermocouple were observed to be significantly in error (over 20 K) depending upon how the experiments were performed (i.e., depending upon heating rate and amount of sample, gaseous environment). To obtain correct temperatures, an experimental protocol was adopted in which two identical experiments were performed, one in which a fine thermocouple was actually embedded in the sample powder. Using this procedure, we obtained much more satisfactory results, in terms of agreement with other careful work reported in the literature, as well as with our own DSC kinetics.

The cellulose used for all TGA work was a Whatman CF-11 fibrous cellulose powder that was used as-received. This cellulose is prepared from high purity cotton of 99% alpha cellulose content. The ash content is 0.009% by mass. The molecular weight of this material is in the range 36,000 to 45,000 daltons. The diameter of the fibres was 10 to 30 μm.

For some experiments, a heated wire mesh reactor was used, in order to achieve higher heating rates than are available from the TGA.This reactor consists of a thin wire gauze which is stretched between electrodes that provide current for resistively heating the gauze. The sample is held between two layers of gauze, and is uniformly heated. The apparatus is described in more detail elsewhere [11] .The samples used in this work consisted of either the same powders as used in the TGA work, or acid-washed filter paper (Munktell's OK/S2-80-200), with an ash content of 0.007%. The paper had a thickness of 168±8 μm, and was cut into rectangles approximately 1 x

* Present address: Advanced Fuel Research, Inc., East Hartford, Ct.

2cm. Since the powder and paper gave virtually identical results but had much different characteristic dimensions, this suggested that in-sample transport limitations were not important in this work, even at high heating rates. This will be further discussed below.

Results and Discussion

Figure 1 shows the results of experiments performed at high heating rates in the heated wire mesh reactor. Each datum represents the char residue yield (and thus one minus the total volatiles yield) from an isothermal experiment in which the sample is heated at the indicated rate to the abscissa temperature, and then allowed to cool at a rate of between 200 to 400 K/s. Mass loss during cooling is generally quite small compared to that during heating. The highest of the heating rates in Fig. 1 would be closer to the conditions that obtain in pulverized biomass combustion or pyrolysis, though still quite a bit lower. Nevertheless, there is good agreement with similar experiments performed at even higher heating rates [7,12]. The curves were calculated , assuming a typical moisture level of about 6%, from the parameters of [7], which were shown to apply to heating rates of 400 to 10,000 K/s.Thus the range for these global parameters is seen to now extend from about 1.7 K/s (100 K/min) to 10,000 K/s. As we have previously reported [13], there is, however, difficulty in applying these kinetic parameters at 5 K/min, as Fig. 1 also clearly shows. There is a significant underprediction of volatiles release rates observed at these heating rates.

Cellulose decomposition data from many other low heating rate studies also cannot be fit by the high heating rate parameters. Generally, activation energies of over 200 kJ/mol have been required, as noted above. Since we were interested in fire safety applications that put us in between the high and low heating rate ranges, we carried out an examination of the kinetics in this zone. This work could be carried out using TGA techniques. Two different types of experiments were performed. One type employed the ordinary constant temperature ramping techniques common in TGA work, and the other involved experiments in which the temperature was ramped at a fixed rate up to a particular temperature, and then the sample was held isothermally. Typical results of the latter ("isothermal") experiments are seen in Figure 2. The data of Fig. 2 could be analyzed to obtain kinetic parameters for a particular constant level of conversion. This is important in a case in which the kinetics change with conversion. The Arrhenius expression for a general n-th order reaction is:

$$\frac{d\left(\frac{M - M_f}{M_0 - M_f}\right)}{dt} = -\left(\frac{M - M_f}{M_0 - M_f}\right)^n A \exp\left(-\frac{E_a}{RT}\right) \qquad (1)$$

where M is the mass of cellulose or char at any time, the subscripts 0 and f denote initial and final, A is the Arrhenius pre-exponential, E_a the activation energy, R the gas constant, T temperature and t time. By taking the natural logarithm of (1), and then taking the derivative with respect to reciprocal temperature, the activation energy is calculable independently of any assumptions of order, if the calculations are performed at constant conversion. There is an issue of what to use for M_f in this case, since char yield can be a function of experimental conditions. In our TGA work, the value did not vary particularly much from 10%, and in testing our parameters for sensitivity to the assumed value, the variation proved unimportant.

Results obtained from the above calculations, using isothermal data of the type in Fig.2, are shown in Table 1. It is observed that the values obtained at these low heating rates (1 K/min) are different from those from high heating rate experiments, and that they do not depend upon conversion. The values cluster near many others reported in the literature for slow-heating experiments. The pre-exponential factors, A, may also be calculated if a reaction order of unity is assumed, and are also shown in Table 1. The values are too high to represent unimolecular decompositions, as has been noted by others as well. Clearly the decomposition process does not involve rate control by a single step, in this range of conditions. Also, for comparison, a "typical" pair of kinetic parameters derived by this approach are used to try to fit the data of Figure 1. While a fair fit may be claimed at 5 K/min and 100 K/min, a very poor fit is obtained to the 1000 K/min data. Clearly such parameters are not appropriate for high heating rate modeling.

Figure 3 shows the values of activation energy obtained from the type of experiments as shown in Fig.2, but involving heating at a rate of 60 K/min. Several features were very different from those observed at lower heating rates. First, the attempts at fitting the data with a single activation energy failed. Rather, it was found that there were two different activation energy regimes. It was decided on the basis of observed behavior to divide the results into two regimes, one above 600 K and the other below. The regime below 600 K was seen to be characterized by an activation energy (and associated pseudo-first-order pre-exponential) that was quite similar to those obtained in the slow heating experiments, and shown in Table 1. The higher temperature regime was found to be characterized by a non-constant activation energy, but the values of apparent activation energy seemed to bracket those of the high heating rate experiments. It should be recalled that since the method of fitting the data attempts to avoid questions of reaction order change, an apparent temperature dependence of mechanism is the most plausible reason for the shift.

It may be noted from Fig. 2 that the major part of the decomposition is completed below about 600 K in all cases. This lends support to the idea that there is a shift in mechanism that takes place above that temperature, since Fig. 2 gave no evidence of two distinct kinetic steps. The higher the

heating rate, the more quickly the transition temperature of 600 K is exceeded and the more the higher temperature mechanism would show itself. As heating rates become so high as to force most conversion to occur in the high temperature regime, the kinetics again begin to look more simple. Unfortunately, it has been historically the heating rate regime between 1 and 10 K/min that has been the most explored, and this has put investigators squarely between the high and low temperature regimes in many experiments. We believe that this has led to many apparently contradictory results being reported.

The more traditional heating-ramp experiments also supported the two-regime proposal. Typical data are shown in Figure 4. These data were obtained from different non-isothermal TGA results, by determining the actual mass loss rates at different heating rates for a constant value of conversion (60% in Figure 4). These mass loss rates are the tangents to the mass loss curve at any time. It is clear from Figure 4, there is a point that fits neither curve cleanly, at around 600 K. From the data obtained at low heating rate conditions (0.1 and 1 K/min), the activation energy is calculated to be between 205 and 252 kJ/mol, varying randomly with conversion. For the data obtained at high heating rates (15 and 60 K/min), the activation energy varies between 137 and 180 kJ/mol. Depending upon how the point near 600 K in Fig. 4 is "counted", considerably higher values of apparent activation energy could be obtained.

Some analyses have been performed to address the question of reaction order. Letting $\phi = [(M-M_f)/(M_0-M_f)]$, then generally speaking for any arbitrary n-th order reaction at constant temperature:

$$d\phi/dt = -[A \exp(-E_a/RT)]\phi^n = -k\,\phi^n \qquad (2)$$

Integrating yields different expressions for different values of n:

$$\phi = -k_0 t + C_0 \qquad (3)$$

$$\ln(\phi) = -k_1 t + C_1 \qquad (4)$$

$$1/\phi = k_2 t + C_2 \qquad (5)$$

where the subscripts on the constants indicate the orders assumed. The results of the isothermal experiments were examined for order, using these expressions. For convenience, a function $f(M/M_0)$ is defined such that:

$$f(M/M_0) = (F-F_{min})/(F_{max}-F_{min}) \qquad (6)$$

where F represents the values of the left hand sides of (3), (4) and (5). The order may be determined from the data by examining which assumed order gives the best approximate fit to linear, per (3), (4) or (5). Figure 5 shows a typical result, for an experiment at 584 K, following heatup at 1 K/min. Clearly first order is the best approximation to the data after an initial period of zero order. This result obtained in most low temperature (< 600 K) cases, and is consistent with earlier results in the literature [2,14]. The results of the experiments at higher temperatures did not give as clearcut results, and appeared to imply second order reaction might be involved, perhaps consistent with another report of near second order behavior [15]. Clearly this topic warrants further study.

Finally, we consider the question of transport effects as possibly responsible for the apparent shift in kinetic parameters. We believe this to be unlikely for several reasons. First, considering the analysis by Hajaligol et al. [16], it appears that despite of the endothermic nature of the pyrolysis reactions involved, the particles examined here are too small to be subject to a heat transfer limitation. Further, it is difficult to rationalize why use of a single heating rate could result in the behavior seen in Fig. 3, if a heat transfer limitation were involved. Thus it seems quite unlikely that a heat transport limitation is the cause of the observed variation in kinetic parameters.

Conclusions

It appears as though the confusing state of the literature on global kinetics of cellulose pyrolysis has as its cause a previously unrecognized shift in mechanism near 600 K. Depending upon the heating rate used to examine the kinetics, different values can easily emerge. We believe that the low temperature regime is characterized by an activation energy around 224 kJ/mol and an order that seems to go from zero, early in the process, towards first. The high temperature regime is characterized by neither constant activation energy nor order, and the apparent activation energy is centered near 140 kJ/mol. Together with an assumption of first order, a value of activation energy around 140 kJ/mol is clearly the most reasonable for applications involving pulverized combustion or pyrolysis of small cellulose particles. For fire modeling applications, both kinetic regimes may be of interest.

Acknowledgments

The support from the Center for Fire Research of NIST under grant 60NANB0D1042 is gratefully acknowledged.

References

1.Roberts, A.F., *Combustion and Flame, 14*, 261 (1970).
2. Lipska, A.E. and Parker, W.J., *J. Appl. Polymer Sci, 10*, 1439 (1966).

3. Lipska, A.E. and Wodley, F.A. *J. Appl. Polymer Sci, 13,* 851 (1969).
4. Shafizadeh, F. and Bradbury, A.G. *J. Appl. Polymer Sci, 23,* 1431 (1979).
5. Bradbury, A.G., Sakai, Y., and Shafizadeh, F.*J. Appl. Polymer Sci, 23,* 3271 (1979).
6. Broido, A. and Weinstein, M., *Comb. Sci. and Tech.* , *1,* 279 (1970).
7. Lewellen, P.C., Peters, W.A., and Howard, J.B., *16th Symp. (Int.) on Comb.*, p 1471, The Combustion Institute, Pittsburgh, 1977.
8. Rogers, F.E. and Ohlemiller, T.J. *Comb. Sci. and Tech.* , *24,* 129 (1980).
9. Varhegyi, G., Antal, M.J., Jr., Szekely, T., Szabo, P., *Energy and Fuels, 3,* 329 (1989).
10. Milosavljevic, I. and Suuberg, E.M., *ACS Div. Fuel Chem. Prepr., 37(4),* 1567 (1992).
11. Suuberg, E.M., Peters, W.A. and Howard, J.B., *I&EC Proc. Des. Dev., 17,* 37 (1978).
12. Hajaligol, M., Howard, J.B., and Peters, W.A., *I&EC Proc. Des. Dev., 21,* 457 (1982).
13. Suuberg, E.M. and Dalal, V.F., *Proc. Eastern States Sect. Comb. Inst.,* 65-1, Nov., 1987.
14. Tang, W.K. and Neill, W.K., *J. Polymer Sci, C, 6,* 65 (1964).
15. Kashiwagi, T. and Nambu, H., *Comb. and Flame, 88,* 345 (1992).
16. Hajaligol, M., Peters, W.A., and Howard, J.B., *Energy and Fuels, 2,* 439 (1988).

Table 1. Kinetic Parameters for Cellulose Decomposition from Isothermal Experiments with 1 K/min Heating

Remaining Mass (%)	E_a[kJ/mol]	A [1/s]
80	225	4.82×10^{16}
70	215	5.77×10^{15}
60	224	5.39×10^{16}
50	215	8.80×10^{15}
40	212	5.59×10^{15}
30	214	1.15×10^{16}
20	225	4.69×10^{16}

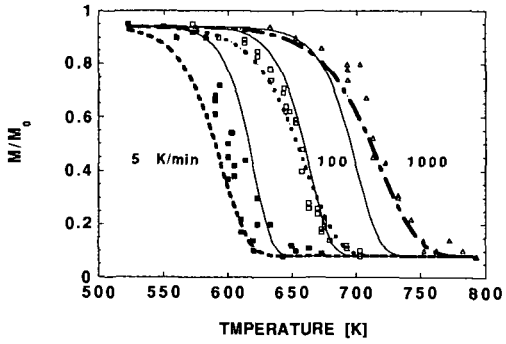

Figure 1. Comparison of char yield data obtained at indicated heating rates with model predictions. Broken lines are for kinetic parameters from [7], $A = 6.79 \times 10^9\ s^{-1}$, $E_a = 140$ kJ/mol. Solid lines are for $A = 4.12 \times 10^{16}\ s^{-1}$ and $E_a = 224$ kJ/mol.

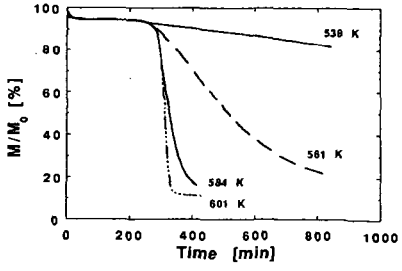

Figure 2. Typical isothermal experiment results, for 1 K/min heating to final temperature.

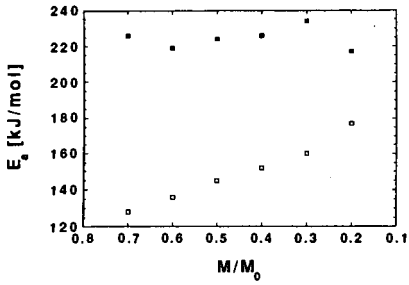

Figure 3. Activation energies obtained as a function of conversion in isothermal experiments involving heating at 60 K/min to final temperature. The open points are for results obtained for temperatures above 600 K and the solid points for temperatures below 600 K.

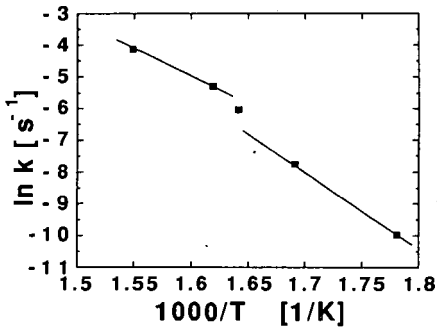

Figure 4. Arrhenius plot for $M/M_0 = 0.6$, from data obtained under nonisothermal conditions, at heating rates of 0.1, 1, 6, 15 and 60 K/min.

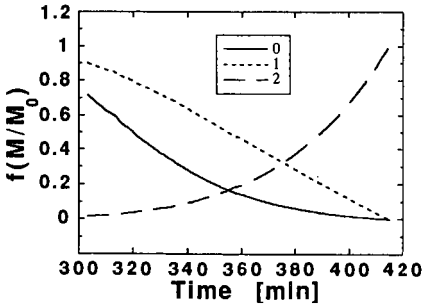

Figure 5. Test of different reaction orders on TGA data obtained in an isothermal experiment at 584 K.

Coprocessing of 4-(1-naphthylmethyl)bibenzyl with Waste Tires Using Finely Dispersed Iron and Molybdenum Catalysts

Ying Tang and Christine W. Curtis
Chemical Engineering Department
Auburn University, AL 36849

ABSTRACT

Coliquefaction of waste tires with coal is a feasible method for upgrading both materials. To evaluate the effect of waste tires on reactions that occur during liquefaction, waste tire and carbon black, a component of tires, were reacted in the presence of 4-(1-naphthylmethyl)bibenzyl (NMBB), a model coal compound known to hydrocrack at liquefaction conditions. Waste tires promoted NMBB hydrocracking compared to no additive although carbon black, introduced at the level present in waste tires increased hydrocracking more. Combining Mo naphthenate with waste tire or carbon black had a higher activity for hydrocracking than the corresponding combinations with Fe naphthenate. Selectivity for NMBB cleavage was also different with the two different catalysts. The addition of S increased the activity of Fe naphthenate with waste tire but decreased that of Mo naphthenate. Increased NMBB hydrocracking of 79.9% was obtained by combining Mo naphthenate and carbon black. Combining Fe naphthenate with carbon black or Mo naphthenate did not increase NMBB hydrocracking compared to the values obtained with the individual materials.

INTRODUCTION

Waste tires are waste disposal problems in the United States where more than 240 million tires are disposed of annually. Since waste tires are composed of either natural or synthetic rubber, aromatic oil and carbon black, waste tires are a potential energy source. Waste tires can be coliquefied with coal to produce more valuable end products. Farcasiu et al.[1,2] demonstrated that coprocessing of used rubber tires and coal produced liquids that are potential sources of transportation fuels or of aromatic oil to be used in new tires. Zondlo and coworkers[3] found that the coliquefaction of bituminous coal and rubber tires resulted in greater conversion than did either material individually. Hydrogenation catalysts used by Orr et al.[4] affected the THF soluble yields of the coliquefied material.

In order to understand more fully how waste tire and carbon black affect the thermal and catalytic reaction of coal at liquefaction conditions, the model species, 4-(1-naphthylmethyl) bibenzyl, was used as a model coal compound. In addition, coal and hydrogenation catalysts were used as additives to evaluate their effect on NMBB. The amount and selectivity of the NMBB hydrocracking were used as measures to determine the effect of the different individual additives and combination of additives.

EXPERIMENTAL

Materials. The model NMBB (99% purity) was obtained from TCI America and used as received. The catalysts tested in this study were iron naphthenate (FeNaph) (6% Fe), iron stearate (FeSTR) (9.0% Fe, 98% purity) from Strem, hydrated iron oxide (FeOOH) (63.3% Fe) from Aldrich, and molybdenum naphthenate (MoNaph) (6.0% Mo) from Shepherd Chemical. Three waste rubber samples, GF30 (30 mesh), GF40 (40 mesh) and GF80 (80 mesh), were supplied by Rouse Rubber Industries, Vicksburg, MS. The coal used in the study was Illinois No. 6 bituminous coal from Amoco and carbon black, Black Pearls 2000, was supplied by Cabot Industries. All of the additives to the NMBB reaction were used as received.

Reaction Procedures. Reactions were performed in stainless steel tubular microreactors of ~20 cm^3 at 400°C for 30 min with a H_2 pressure of 1250 psig introduced at ambient. The reactor was agitated horizontally at 450 rpm. The reaction system consisted of 0.25 g of NMBB; when additives were used, waste tire, coal or carbon black was added at an equivalent gram amount of 0.25 g. When the relative amount of the additives was changed, the amount of NMBB was held constant and the added material amount was either 5 times 0.25 g or 0.2 times 0.25 g. Catalyst precursors of MoNaph, FeNaph, FeOOH and FeSTR were added at a level of 900 to 1,100 ppm active metal on a per gram of material basis. When dual catalysts of Fe-based precursors and MoNaph were used, the total level of metal was kept constant at 900 to 1100 ppm with Fe:Mo weight ratios of 1:1. When sulfur was added to the reaction, elemental sulfur was added in a 3:1 stoichiometric ratio of sulfur to metal assuming that either Fe_7S_8 or MoS_2 was formed.

The reaction products obtained from reactions of NMBB and the various additives were analyzed by gas chromatography using a Varian Model 3700 gas chromatograph equipped with a fused silica J&W capillary DB-5 30 m column and flame ionization detection. The only products that were analyzed were those from NMBB. The products obtained from NMBB were primarily hydrocracked products; trace amounts of hydrogenated products were detected. Percent

hydrocracking (%HYC) of NMBB was defined as the moles of hydrocracked liquid products as a percentage of total moles of liquid products produced.

RESULTS AND DISCUSSION

Hydrocracking of 4-(1-naphthylmethyl) bibenzyl. The model hydrocracking compound 4-(1-Naphthylmethyl) bibenzyl (NMBB) was reacted noncatalytically and catalytically with and without sulfur in the presence of added material of waste tires, carbon black, and coal as presented in Table 1. A number of different combinations was used to test the effect of the individual additives and combinations of additives on the hydrocracking activity of NMBB. The products produced from NMBB were determined and defined as the lumped parameter, percent hydrocracking. Where NMBB was hydrocracked at the reaction conditions and in the presence of any additive or catalyst used, the primary products obtained were methylbibenzyl (MBB) and naphthalene (NAP). Secondary products, such as naphthyltolymethane (NTM), bibenzyl (BB), methylnaphthalene (MN) and toluene (TOL), were obtained in small amounts as the extent of hydrocracking increased.

The cleavage of NMBB can occur at five different sites which are shown in Figure 1 and are labeled a through e. The selectivity of the bond cleavage that occurred with the different additives is given in Table 1. The primary cleavage that occurred with all of the additives and catalysts was at bond a. In most systems, the second most prevalent cleavage occurred at bond d, with a small amount of cleavage occurring at b. No cleavage was observed at bonds c or e in any of the reactions performed. The selectivity for hydrocracking NMBB at a given bond is given in Table 1 as SA for bond a, SB for bond b and SD for bond d. These selectivities are defined as cleavage at either bond a, b, or d which is divided by the sum of the bond cleavage a, b and d. Therefore, the parameters chosen to compare the results of the different additives and catalysts on NMBB were % HYC, which described the activity for hydrocracking under the specific reaction conditions, and SA, SB, and SD, which reflected the selectivity of the additive or catalyst for NMBB bond cleavage.

Effect of Waste Rubber, Additives and Catalysts on NMBB Hydrocracking. Table 1 presents the effect of different additives and catalysts on NMBB hydrocracking. Initial reactions employed waste tires in three mesh sizes added to NMBB. With increasing mesh size from 30 to 80 and decreasing particle size, the waste tire's effect on NMBB hydrocracking increased from 11.3 to 15.3%. The decreased particle size may have allowed more contact between the reacting NMBB and the active hydrocracking component in waste tire, carbon black. All subsequent experiments were performed with GF 30 waste tire. When the weight ratio of NMBB to waste tire decreased from 1:0.2 to 1:5, the % HYC of NMBB increased from 9.3 to 13.1%, while the selectivity for bond cleavage at a decreased from 91 to 62% with a corresponding increase at d from 9 to 38%. Although the selectivity changed rather substantially with increased waste tire, the change in the total amount of hydrocracking was small.

Since carbon black composes between 20 to 30% of waste tires, the effect of carbon black on the hydrocracking of NMBB was evaluated. Introducing carbon black at a 1:1 weight ratio yielded 79.1% HYC of NMBB. Adding waste rubber or coal at the same level resulted in much less HYC, 11.3 and 7.0%, respectively. A higher ratio of NMBB to carbon black of 1:0.2 was used to approximate the lower amount of carbon black present in waste tire; the amount of HYC achieved was 17.7% which was higher than that obtained with a 1:1 ratio of NMBB to waste tire containing at a minimum 20% carbon black. Likewise, when the ratio of NMBB to waste tire was 1:5 in which carbon black was present in an equivalent amount as in the reaction with a NMBB to carbon black ratio of 1:1, the % HYC was much less yielding 13.1% compared to 79.1%. The carbon black contained in the GF 30 waste tire was not nearly as active as carbon black introduced directly. The selectivity for cleavage at bond a was greater for carbon black than for carbon black in waste tire at equivalent carbon black loadings.

In the coprocessing of waste tire with coal, hydrogenation catalysts would be used to increase the conversion of both coal and waste tire. Two slurry phase hydrogenation catalysts, FeNaph and MoNaph, were used in conjunction with NMBB individually and with additives of waste tire and carbon black. Reactions were performed with and without sulfur. When MoNaph was combined with waste tire, 38.2% HYC of NMBB occurred which was more than double the amount obtained with FeNaph. The addition of sulfur increased the amount of % HYC with FeNaph but decreased the effectiveness of MoNaph. Combining FeNaph or MoNaph with carbon black resulted in high levels of % HYC: 86.4% for FeNaph and 97.9% for MoNaph. The selectivity for cleavage at bond a was greater for Mo than for Fe even when sulfur or carbon black was added.

Ternary systems of NMBB with waste tire and carbon black were reacted without additional catalysts and with three different iron catalysts or MoNaph. The combination of waste tire and carbon black at a 1:0.2:0.2 ratio yielded 29% HYC of NMBB. Addition of MoNaph to this

ternary system increased the % HYC to 71.3% although the selectivity for cleavage at bond a remained high and constant. Increasing the amount of waste tire in the system to a ratio of 1:1:0.2 of NMBB to waste tire to carbon black increased % HYC to an even higher value of 83.5%. Utilization of three types of Fe catalysts at that same ratio resulted in % HYC of 42.6% for FeSTR, 53.7% for FeNaph and 55.2% for FeOOH. All of these hydrocracking values were lower than that obtained for MoNaph.

Reactions with NMBB and waste tires were also performed with combined catalysts containing one of the iron precursors, FeNaph, FeOOH, or FeSTR with MoNaph and sulfur. All three of the reactions yielded % HYC between 16.5 and 20.3% so that the type of iron present made little difference in the hydrocracking behavior of NMBB. The % HYC of 18.5% achieved by the combined catalyst of MoNaph with FeNaph was only slightly higher than the 17.5% HYC yielded by the reaction with FeNaph alone. The selectivity for all of the combined catalysts was very high, ranging from 94 to 98%. The presence of the combined catalysts were not synergetic for promotion of NMBB hydrocracking.

SUMMARY

The NMBB system provided a model for measuring the activity of waste tire and carbon black for hydrocracking. Since NMBB contains C-C bonds that are similar to those present in some coal molecules NMBB can be used to predict the effect of waste tire and carbon black in a liquefaction system containing coal and waste tire. Carbon black introduced directly at coprocessing conditions was highly active for hydrocracking NMBB. When carbon black was present in waste tires, carbon black's activity was much less, indicating that the processing and contact of the carbon black with other material in the waste tires was detrimental to its activity. The combination of MoNaph with either waste tire or carbon black resulted in higher hydrocracking activity and selectivity for cleavage at bond a than did FeNaph. The combination of iron catalysts with MoNaph did not promote hydrocracking of NMBB.

REFERENCES

1. Farcasiu, M., CHEMTECH, January, 22-24, 1993.

2. Farcasiu, M.; Smith, C. ACS Fuel Chemistry Division Preprints, 37, 1, 472-479, 1992.

3. Zondlo, J.W.; Liu, Z.; Dadyburjor, D.B.; Stiller, A.H., presentation in Consortium for Fossil Fuel Liquefaction Science, 7th Annual Technical Meeting, Georgia, 1993.

4. Orr, E.C.; Tuntawiroon, W.; Anderson, L.L.; Eyring, E.M., presentation in Consortium for Fossil Fuel Liquefaction Science, 7th Annual Technical Meeting, Georgia, 1993.

Figure 1. Cleavage Sites for 4-(1-Naphthylmethyl)bibenzyl.

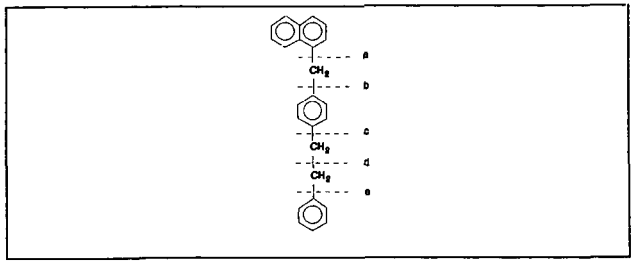

Table 1. Selectivity of the Slurry Catalysts for Hydrocracking 4-(1-Naphthylmethyl)bibenzyl

Reaction Systems	%HYC[b]	Cleavage of a+b+d[c]	Selectivity*100%		
			SA	SB	SD
NMBB (thermal)	4.9±1.3	2.5	61	0	39
NMBB+S	9.3±2.7	4.7	66	2	32
NMBB+GF30WT(1:1)	11.3±2.2	5.7	77	0	23
NMBB+GF40WT(1:1)	13.5±2.5	6.8	76	0	24
NMBB+GF80WT(1:1)	15.3±2.4	7.7	81	0	19
NMBB+WT*(1:0.2)	9.3±2.1	4.7	91	0	9
NMBB+WT(1:5)	13.1±1.7	6.6	62	0	38
NMBB+CB(1:1)	79.1±2.7	39.6	78	6	16
NMBB+CB(1:0.2)	17.7±2.7	8.9	84	4	12
NMBB+Coal(1:1)	7.0±2.1	3.5	83	0	17
NMBB+FeNaph	5.5±1.0	2.8	79	0	21
NMBB+MoNaph	6.4±0.9	3.3	76	0	24
NMBB+FeNaph+S	15.5±1.4	7.7	86	4	10
NMBB+MoNaph+S	39.4±2.3	19.7	92	5	3
NMBB+WT+FeNaph(1:1)	15.5±2.6	7.8	73	0	27
NMBB+WT+MoNaph(1:1)	38.2±2.2	19.2	95	1	4
NMBB+CB+FeNaph(1:1)	86.4±3.8	43.3	89	4	7
NMBB+CB+MoNaph(1:1)	97.9±2.2	49.0	94	4	2
NMBB+WT+FeNaph+S(1:1)	17.5±2.6	8.8	75	0	25
NMBB+WT+MoNaph+S(1:1)	30.1±2.4	15.1	96	0	4
NMBB+CB+FeNaph+S(1:1)	87.3±3.8	43.7	88	6	6
NMBB+CB+MoNaph+S(1:1)	99.7±1.6	49.8	94	5	1
NMBB+WT+MoNaph+S(1:0.2)	29.4±3.0	14.8	98	0	2
NMBB+WT+MoNaph(1:0.2)	13.8±3.0	6.9	97	0	3
NMBB+CB+MoNaph+S(1:0.2)	79.9±3.6	40.0	95	4	1

Table 1. (Continued)

NMBB+WT+MoNaph(1:5)	23.2±2.4	11.7	69	0	31
NMBB+WT+MoNaph+S(1:5)	18.0±2.1	9.1	67	0	33
NMBB+WT+CB(1:0.2:0.2)	29.0±1.7	14.6	92	3	5
NMBB+WT+CB+MoNaph (1:0.2:0.2, 1000 ppm)	71.3±2.5	35.7	95	4	1
NMBB+WT+CB+MoNaph (1:1:0.2, 1000 ppm)	83.5±2.4	41.8	93	5	2
NMBB+WT+CB+FeNaph (1:1:0.2, 1000 ppm)	53.7±2.5	26.9	89	5	6
NMBB+WT+CB+FeOOH (1:1:0.2, 1000 ppm)	55.2±3.0	27.7	95	2	3
NMBB+WT+CB+FeSTR (1:1:0.2, 1000 ppm)	42.6±2.8	21.4	97	0	3
NMBB+WT+FeNaph+MoNaph+S (1:1, 500 ppm each)	18.5±2.1	9.3	98	0	2
NMBB+WT+FeOOH+MoNaph+S (1:1, 500 ppm each)	20.3±2.2	10.2	96	0	4
NMBB+WT+FeSTR+MoNaph+S (1:1, 500 ppm each)	16.5±3.0	8.3	94	0	6

[a]WT=waste tire rubber GF30 unless specified; CB=carbon black; MoNaph=Mo Naphthenate; FeNaph=Fe Naphthenate; FeSTR=FeStearate.

[b]%HYC is defined as the moles of hydrocracked liquid products as a percentage of the total moles of liquid products produced.

[c]Cleavage of Bonds a, b, and d is defined as bond cleavage of bond a, b, and d in NMBB.

[d]Selectivity is defined as bond cleavage at a (SA) or b (SB) or d (SD) divided by the combined bond cleavage of a, b, and d.

NATURE OF THE CHEMICAL REACTION FOR FURFURAL MODIFIED ASPHALT

G. Mohammed Memon, FHWA/EBA Engineering Inc.
Brian H. Chollar, FHWA
6300 Georgetown Pike
McLean, VA 22101

Key words: Asphalt/chemically modified, Nature of reaction, Furfural.

INTRODUCTION

Three of the most serious problems of asphalt pavements today are rutting, cracking, and susceptibility to moisture damage (stripping). Asphalt manufacturers have been mixing asphalts with polymers to produce polymer-modified asphalts with improved rheological properties. However, the costs for these improved polymer-modified asphalts are almost double that of regular asphalts. FHWA researchers have found that asphalt modified by the chemical, furfural (which is prepared by simple elimination reaction of aldopentoses obtained from oat hulls), exhibited better stripping properties and was less temperature susceptible than the virgin asphalt[1,2] while costing less than polymer-modified asphalts. This paper discusses the possible structure of the furfural-modified asphalt, data for the virgin and furfural-modified asphalts and their Corbett fractions, data from a model reaction between phenol and furfural, and a possible explanation of this structure based on these data.

MATERIALS USED

An Alaskan North Slope asphalt (asphalt A5), obtained from the Strategic Highway Research Program (SHRP), was used. It is an AC-5 asphalt, SHRP number AAV. All of the reagents used were analytical grade from Baxter Scientific Products, McGraw Park, IL, unless otherwise specified.

EXPERIMENTAL METHOD

Furfural Reaction: The furfural-modified asphalt (asphalt A5F) was prepared from asphalt A5 according to the method described by Chollar, et al.[2] The model phenol-furfural product was prepared by continuously stirring phenol (10 g), furfural (10 g), and concentrated hydrochloric acid (0.19 ml) at 93.3°C for 90 min. The resulting product was analyzed by Thin Layer Chromatography (TLC), Fourier Transform Infrared (FTIR), and High Performance-Gel Permeation Chromatography (HP-GPC).

TEST METHODS

I. <u>ASTM D-4124 (Corbett Analysis):</u> ASTM D-4124 was used to fractionate asphalts A5 and A5F.

II. <u>Thin Layer Chromatography (TLC)</u>: The residual furfural starting material in asphalts was detected by TLC using the Benzidine[3] and 2,4-Dinitrophenyl hydrazine[4] spot tests. Visual observation of the resulting colors both with and without ultraviolet (UV) radiation at 254 and 366 nm wavelength was used to detect/differentiate different compounds.

III.a. <u>Reverse-Phase High Performance Liquid Chromatography (RP-HPLC)</u>: A Waters HPLC system was used for this study with a 600E brand work station. Methanol or tetrahydrofuran (THF) was used as a solvent at a flow rate of 1 ml\min. A 0.4 ml sample was always injected. Elution of the material was carried out by two methods in an isocratic mode: 1) eluting the sample with methanol for a 10 min period for detecting the furfural starting material, and 2) eluting the sample with methanol from 0 to 15 min, then with THF from 15 to 45 min, and then with methanol from 45 to 61 min to observe the changes which occurred in asphalt A5 and A5F Corbett fractions.

The following procedure was used to determine the starting material (furfural) in Corbett fractions of asphalt A5F by an HPLC technique using reverse-phase chromatography.

1. Asphalt (A5 or A5F, 10mg) was dissolved in 4 ml of 1:1 THF/methanol. The resulting solution was passed through a wet (methanol) Sep-pak C_{18} cartridge (a reverse phase HPLC technique to rapidly clean the asphalt sample and preserve the life of the RP-HPLC column) and collected. The solution from the Sep-pak was used to obtain the sample for RP-HPLC.
2. THF (2 ml) was passed through the Sep-pak. The solution was

collected in a separate vial. This fraction was used for further investigation.

3. Methanol (2 ml) was passed through the Sep-pak. The solution was collected and used for further investigation.
4. Methanol (2 ml) was again passed through the Sep-pak. The solution was collected in a fourth vial for further investigation.

A calibration curve was made by using different concentrations of furfural in methanol (1, 0.5, 0.25 and 0.125 percent). The solution (0.4 ml) was injected into the HPLC, using method #1 for 10 min in a isocratic mode, eluting in methanol. The peak area for the furfural signal was found at a retention time of 4.85 min and at a wavelength of 252 nm.

III.b. High Performance Gel Permeation Chromatography (HP-GPC): The sample preparation for HP-GPC and the method used was made according to the method reported by Memon, et al.[5]

EXPERIMENTAL PROCEDURE

Nuclear Magnetic Resonance (NMR) Spectroscopy: Asphalt samples were dissolved in deuterated chloroform in a concentration of 10 percent (W/V). These were transferred to NMR tubes and were run for ^{1}H- and ^{13}C analysis. A standard coaxial tube containing tetramethylsilane (TMS) was used as a standard.

Three different techniques were used to detect the aromatic/aliphatic carbon and proton ratio and non-protonated carbon atoms present in asphalts A5 and A5F and their polar aromatic and naphthene aromatic fractions: conventional ^{1}H-, ^{13}C distortless enhancement polarization transfer (DEPT), and gated decoupling without nuclear overhauser effect (NOE) ^{13}C-NMR.

Fourier Transform Infrared (FTIR) Spectroscopy: The asphalts A5 and A5F were run on a FTIR using neat thin films on a sodium chloride (NaCl) plate. The Stokes analysis[6] was used to calculate and compare peak areas and ratios to each other in a spectrum. Ratios used for this comparison are shown in figure 10. It has been shown that the 1378-1578 cm-1 region (aliphatic region) does not change significantly for most asphalts including A5 and A5F. Thus, ratios of this aliphatic region to other infrared peak regions for asphalt (A5) will show the increase or decrease in that regional area as compared to the same ratio for asphalt (A5F).

RESULTS

There are several ways in which furfural can react with the phenolic type compounds in asphalt. One of the most probable ways that furfural can react with phenol is by a condensation type of reaction. The model for this is:[7]

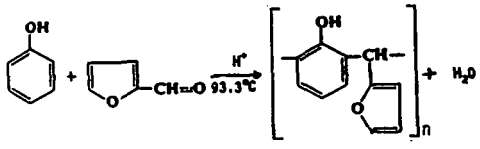

We think that this is the type of reaction that is occurring in the furfural-asphalt modification and that this is the type of product that is observed in asphalt A5F. The following data is obtained in support of this product:

1. Increase of polarity. Table I gives the Corbett analyses of asphalts A5 and A5F. There is a significant increase in asphaltene (highly polar) and a slight decrease in the polar and naphthene aromatic fractions of the furfural-modified asphalt.

Table II gives the results of the TLC analyses of asphalts A5 and A5F. There are changes occurring in the polar and naphthene aromatic fractions using 90 percent methanol - 10 percent toluene. There were no other changes in the other fractions. Therefore, a reaction occurs with a change in the polar and naphthene aromatic fractions of the asphalt. These results show the higher polarity of asphalt A5F.

2. Furfural consumption. a. The detection of furfural in the furfural-asphalt reaction was attempted by mixing different amounts of furfural (0.5, 0.38, 0.13, 0.06 and 0.03 ml) in hot asphalt A5 (50 gms) at 57°C on a hot plate for 30 s and observing the separation of the mixtures by RP-HPLC. No signal was observed at 252 nm wavelength (wavelength of the pyrrole ring with the 2-CHO

functional group in furfural) at a retention time of 4.85 min (figure 1, furfural in asphalt at 57°C). Therefore, no free furfural is found in any of the mixtures. **b.** The detection of furfural was also attempted by mixing different amounts of furfural (0.5, 0.38, 0.13, 0.06 and 0.03 ml) in 50 grams of warm asphalt A5 (26.7°C). The furfural-asphalt mixture (100-150 mg) was analyzed by the above procedure using RP-HPLC. Unreacted furfural was observed in all mixtures at 252 nm wavelength after 4.85 min retention time (figure 1, furfural in asphalt at 26.7°C). **c.** Asphalt A5 (50 g) was mixed with furfural (0.5 ml) at room temperature. Reverse- phase HPLC was used to analyze this mixture using the above procedure. Figure 1 (furfural in methanol) shows that at 4.85 min, the free furfural signal appeared. The mixture was then heated at 57°C for 30 s and analyzed. There was no furfural signal detected at that time. Thus, the reaction uses furfural and proceeds at temperatures above 27°C. **d.** The detection of furfural was attempted with asphalts A5 and A5F and their Corbett fractions using the sample preparation method above. These solutions were analyzed by the above reverse-phase method (method #2) and the results are reported in table III. There is no absorption observed at 252 nm in the three fractions of asphalt A5 and A5F at any retention time. These data indicate that furfural has been used in the furfural-asphalt A5 reaction and is not found in any of the Corbett fractions of asphalt A5F.

3. <u>The reaction converts phenolic compounds into substituted phenolic compounds.</u> Rao[8] has reported that substitution of an -OH group on benzene will give a signal at 270 nm wavelength. A disubstituted benzene shows a signal at 276 nm. O-catechol[9] is an example of this shift, showing a transition at 276 nm. A trisubstituted benzene molecule shows a transition at 287 nm wavelength[8]. The RP-HPLC data for the naphthene aromatic fraction of asphalt A5 shows a small broad signal at 272 nm (table III and figure 2) with 4.7 min retention time in THF followed by methanol (solvent system). This signal may be due to phenol. When the corresponding asphalt A5F fraction was examined, no such signal was detected. This is an indication that a reaction is occurring with phenolic compounds. When the polar aromatic fraction of asphalt A5F was analyzed, a signal at 278 nm was observed in this polar aromatic fraction of asphalt A5F having a retention time of 4.7 minutes in methanol. This signal is possibly the monosubstituted phenolic material (table III).

4. <u>The formation of more polymeric compound of higher molecular size.</u> The GPC data were calculated according to published procedures by P. W. Jennings[10] and reported as percent large molecular size (LMS), medium molecular size (MMS), and small molecular size (SMS), for each asphalt fraction. From the GPC data (table IV), it is clear that there is no significant change in the LMS, MMS, and SMS of asphalt A5F as compared to that of the asphalt A5. Thus, it is not apparent from the analysis if a reaction occurs. Furthermore, table IV demonstrates that the asphaltene fraction of asphalt A5F shows a decrease in LMS and an increase in MMS and SMS as compared to that of the asphaltene fraction of asphalt A5. The data also shows that there is a significant increase in LMS of polar aromatic fraction of asphalt A5F (4%). There is an increase in MMS of naphthene aromatic fraction (0.5%) of asphalt A5F. Thus, significant increases occurred only in the LMS of the polar aromatic fraction of the modified product. Figure 3 shows the changes observed in retention times obtained by RP-HPLC analysis of the naphthene aromatic and polar aromatic fractions of asphalts A5 and A5F . (The TLC analysis confirmed that changes occurred in only the naphthene and polar aromatic fractions). The asphaltene fractions of asphalts A5 and A5F have retention times of 16.5 and 16.8 minutes respectively. This means that there is no significant change in the LMS of the modified asphaltene fraction. The polar aromatic fraction of asphalt A5 begins around 19.5 min, whereas the corresponding asphalt A5F fraction begins around 15.5 min as shown in figure 3. This is an indication that the polar aromatic fraction of asphalt A5F has LMS materials appearing earlier than the corresponding fraction of asphalt A5. The spectrum of the naphthene aromatic fraction of asphalt A5 begins at around 20 min retention time, whereas the spectrum of the same fraction of asphalt A5F begins around 17 min retention time. Again, LMS compounds of the furfural-modified product appear earlier.

The ultraviolet spectra of the SMS of the polar aromatic fractions of asphalts A5 and A5F are in figure 4 and those of the LMS of the polar aromatic fraction of asphalts A5 and A5F are in

figure 5. The spectrum for the asphalt A5 (Figure 4) only shows a signal for phenols at 270 nm. The spectrum for the asphalt A5F fraction only shows a signal at 277 nm (figure 4). This shows the formation of a monomeric monosubstituted phenolic material in the furfural- modified asphalt. Figure 5 shows the presence of tri- or polysubstituted phenolic material of large molecular size (LMS region) in the polar aromatic fraction of asphalt A5F at 288 nm, whereas, there is no such signal in virgin polar aromatic fraction. Thus, it is possible that the furfural-asphalt reaction involves a substitution on the phenol ring in the form of a monomer in the SMS region as well as a polymer in the LMS region appearing in the polar aromatic fraction of asphalt A5F. Substituted phenolic types of compounds showing signals at 277 nm were also observed in SMS of asphaltene as well as naphthene aromatic fractions of furfural-modified asphalt.

The direct reaction between phenol and furfural was conducted under the same conditions as mentioned above. The GPC data shows that this reaction is a polymerization reaction, but it is a mixture of a monomer and a polymer, as is shown in figure 6. The GPC data shows that the model polymer product starts appearing around 22 min retention time, with peaks at 24.1, 28.3 and 30.6 min. A standard pyrene (molecular weight 202, about the weight of the monomer of phenol and furfural), appears around 29 min retention time. The molecular weight of the dimer of the furfural-phenol reaction is 346 and would be expected to be eluted around 27 to 28 min. Thus, the model reaction affords a polymer larger than that of this monomer, a material the same size as the dimer, and a material similar in size to the monomer.

These data showed that there are more large molecular size materials in the polar and napthene aromatic fractions of asphalt A5F than there are in asphalt A5. These LMS materials in the polar aromatic fraction contain tri- or polysubstituted polymeric phenols. The SMS materials of the napthene aromatic, polar aromatic, and asphaltene fractions contain monosubstituted monomeric phenols. The model reaction affords a polymer larger than that of the dimer, and a monomer of the size similar to that of the dimer of phenol and furfural. Since the model polymer was prepared under the same conditions as the furfural asphalt reaction, we can assume that furfural is reacting in the same way as the model polymer to give the same type of products.

5. Increase of aromaticity. Using the ^{13}C-NMR gated decoupling technique without NOE, NMR shows a 12 percent increase of aromatic carbon content in the polar aromatic fraction of asphalt A5F versus that of asphalt A5 (figure 7). The proton NMR spectrum of the polar aromatic fraction of asphalt A5F shows a 2 percent higher ratio of aromatic to aliphatic versus that of the polar aromatic fraction of asphalt A5 (figure 9). The infrared data (figure 10) show that the ratio of total aromatic to aliphatic content of asphalt A5F (10/5) is more than that of asphalt A5; the aromatic content of the furfural-reaction product has increased. The infrared data show that the ratio of monomeric to polymeric aromatic content of asphalt A5F (3/1) is less than that of asphalt A5, thus the polymeric substitution of the aromatic ring of the asphalt A5F has increased. These data show that the aromaticity of the asphalt A5F is higher than that of asphalt A5. Therefore, the phenolic groups in asphalt A5 are combining with furfural to produce a higher aromatic material (asphalt A5F) as suggested by the model structure.

6. Increase of non-protonated carbon atoms. Using the effect of the DEPT technique, ^{13}C-NMR showed an increase in the non-protonated carbon atom content of the polar aromatic fraction of the furfural-modified asphalt versus that of asphalt A5 (figure 8). The model structure of the modified product has more non-protonated carbon atom content than that of phenol or phenolic material reactants.

7. Increase of unsaturation. Infrared data (figure 10) show that the ratio of unsaturated to aliphatic content of asphalt A5F (4/5) is higher than that of asphalt A5. As a result, the unsaturated content of asphalt A5F has increased. With the addition of furfural, the model structure of the modified product contains more unsaturated carbon content than that of phenol or phenolic material reactants.

CONCLUSIONS

We have shown that our data for asphalt A5F using the above seven experimental results are consistent with the proposed structure of

the phenol-furfural polymeric product, and that it is possible that the furfural-asphalt reaction for phenolic materials in asphalt A5 is occurring in the same way as is proposed in the model reaction.

FHWA researchers will now pursue other reactions of this type to further improve the properties of asphalts.

REFERENCES

1. D. Kumari, B. H. Chollar, J. G. Boone, and J. A. Zenewitz, Chemical Modification of Asphalt, FHWA Report No. FHWA-RD-91-193, August 1992.
2. B. H. Chollar, G. M. Memon, N. Shashidhar, J. G. Boone, and J. A. Zenewitz, Characteristics of Furfural Modified Asphalt, 73rd TRB Meeting, January 1992.
3. F. Feigl, Quantitative Analysis by Spot Tests, Elsevier, Inc., New York, p.235, 1946.
4. R. L. Shriner, R. C. Fuson, and D. Y. Curtin, The Systematic Identification of Organic Compounds, John Wiley and Sons,Inc., New York, p.235, 1960.
5. G. Memon, J. G. Boone and B. H. Chollar, Furfural Substitutes for Chemical Modification of asphalt, ASTM STP 1241, Philadelphia, 1994.
6. B. H. Chollar, K. T. Tran, D. Kumari, J. G. Boone, and J. A. Zenewitz, Changes occurring in Asphalt in Drum Dryer and Batch (Pug Mill) Mixing Operation, FHWA Publication No. FHWA-RD-88-195, 1989.
7. D. J. Cram and G. S. Hammond, Organic Chemistry, McGraw-Hill Inc., New York, p.385, 1959.
8. C. N. R. Rao, , Calculation of Primary Band Transition($\pi \rightarrow \pi^*$), J. Sci. Res. (India), vol. 17B, 56, 1958.
9. R. M. Silverstein, G. C. Bassler, and T. C. Morril, Spectrometric Identi-fication of Organic Compounds, John Wiley and Sons, Inc., New York, p.325, 1980.
10. P. W. Jennings and J. A. S. Pribanic, The Expanded Montana Asphalt Quality Study Using High Pressure Liquid Chromatography, FHWA Report No. FHWA-MT-85-001, 1985.

TABLE I: CORBETT ANALYSIS

Sample name	Asphaltene ± SD %	Polar Aromatics ± SD %	Naphthene Aromatics ± SD %	Saturates ± SD %
Asphalt A5	12.0 ± 1.6	28.3 ± 1.5	41.9 ± 0.1	12.7 ± 1.8
Asphalt A5F	18.3 ± 1.5	27.0 ± 1.9	38.8 ± 0.9	12.2 ± 0.4

Asphalt A5 = Virgin asphalt A5
Asphalt A5F = Furfural modified asphalt A5

TABLE II: THIN LAYER CHROMATOGRAPHIC COMPARISONS OF THE CORBETT FRACTIONS OF ASPHALT A5 AND A5F.

Functions	Asphaltene Fractions	Polar Aromatic Fractions	Naphthene Aromatic Fractions	Saturate Fractions
Observation	same	different	different	same
R_f of A5	same	....	.....	.....
R_f of A5F	same	0.05 0.55	0.21	

A5 = Virgin asphalt A5 A5F = Furfural modified asphalt A5
R_f = Retardation factor ..... = Not observed

TABLE III: RP-HPLC DATA FOR FURFURAL IN ASPHALT A5 AND A5F AND IN THEIR FRACTIONS

Reten. Time	A5-A-MT	A5F-A-MT	A5-A-M	A5F-A-M	A5-A-TM	A5F-A-TM	A5-A-T	A5F-A-T
4.7MIN	---	225 nm	-- -- 244 nm	205 nm 235 nm --	-- no signal --		210 nm 215-227 nm 248 nm 262 nm	210 nm -- -- --
6.5MIN	202 nm -- 230 nm 260 nm	-- 218 nm -- 260 nm	--no signal --		-- no signal --		200 nm 233 nm 242 nm -- 265 nm	-- -- -- 245 nm --
	A5-PA-MT	A5F-PA-MT	A5-PA-M	A5F-PA-M	A5-PA-TM	A5F-PA-TM	A5-PA-T	A5F-PA-T
4.7MIN	202 nm	202 nm	210 nm --	-- 278 nm	--	205 nm	--	202 nm
6.5MIN	202 nm	202 nm	-- no signal --		--	203 nm	240 nm	--
	A5-NA-MT	A5F-NA-MT	A5-NA-M	A5F-NA-M	A5-NA-TM	A5F-NA-TM	A5-NA-T	A5F-NA-T
4.7MIN	-- 209 nm -- --	201 nm -- 222 nm 264 nm	209 nm	209 nm	220 nm 240 nm 272 nm	-- -- --	-- 220 nm 240 nm 260 nm	212 nm -- -- --
6.5MIN	203 nm 240 nm	-- --	204 nm 240 nm	-- --	-- no signal --		-- no signal --	

MT = Methanol in tetrahydrofuran
M = Methanol
A = Asphaltene fraction
NA = Naphthene aromatic fraction
TM = Tetrahydrofuran in methanol
T = Tetrahydrofuran
PA = Polar aromatic fraction
-- = Not observed

TABLE IV: GPC DATA FOR ASPHALTS A5 AND A5F AND THEIR CORBETT FRACTIONS

Sample	LMS ± SD %	MMS ± SD %	SMS ± SD %
Asphalt A5	20.9 ± 1.2	47.2 ± 0.5	31.9 ± 1.6
Asphalt A5F	20.1 ± 0.8	47.7 ± 0.3	32.2 ± 1.0
A5-AS	42.1 ± 0.5	39.2 ± 0.4	18.7 ± 0.3
A5F-AS	27.8 ± 0.03	44.4 ± 0.08	27.9 ± 0.06
A5-PA	49.3 ± 0.1	36.7 ± 0.4	9.2 ± 0.2
A5F-PA	53.0 ± 0.5	36.8 ± 0.3	10.2 ± 0.2
A5-NA	12.8 ± 0.5	48.5 ± 0.4	38.7 ± 0.04
A5F-NA	12.6 ± 0.03	50.1 ± 0.1	37.3 ± 0.2

LMS = Large molecular size
MMS = Medium molecular size
SMS = Small molecular size
AS = Asphaltene fraction
PA = Polar aromatic fraction
NA = Naphthene aromatic fraction
A5 = Virgin asphalt A5
A5F = Furfural-modified asphalt A5

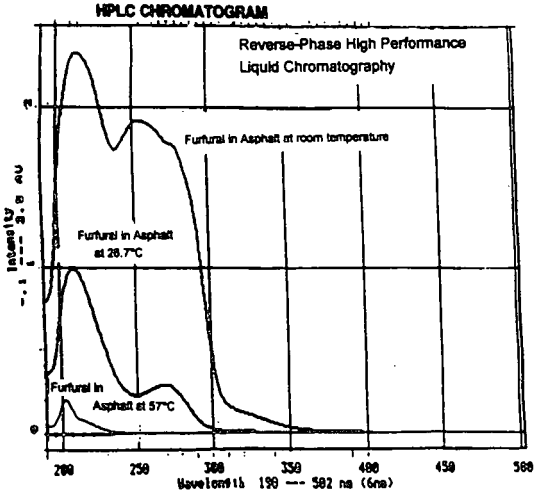

Figure 1: Wavelength spectra of furfural and asphalt for reverse-phase high performance liquid chromatography at a retention time of 4.85 min.

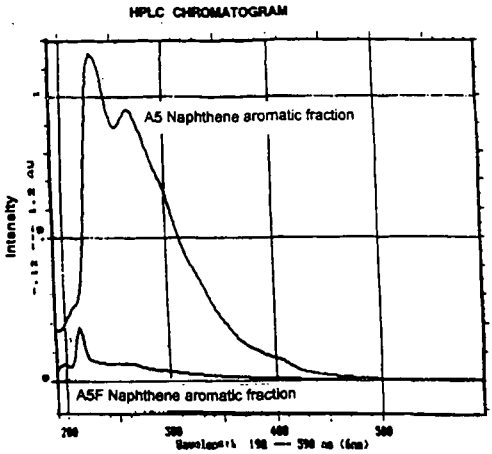

Figure 2: Ultraviolet spectra of the naphthene aromatic fraction of asphalts A5 and A5F from reverse-phase high performance liquid chromatography at a retention time of 4.7 min.

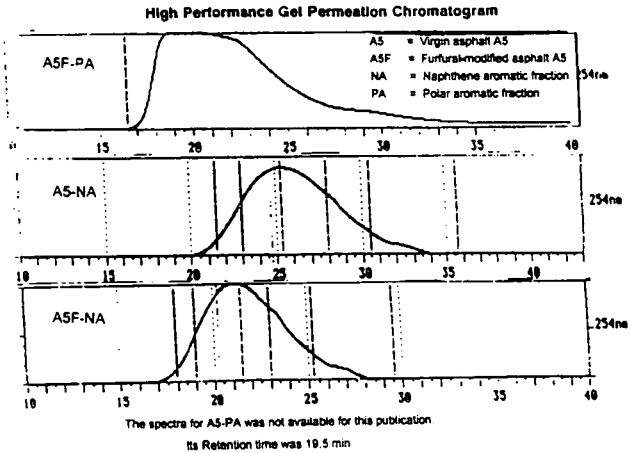

Figure 3: Chromatogram of the naphthene aromatic and polar aromatic fractions of asphalts A5 and A5F.

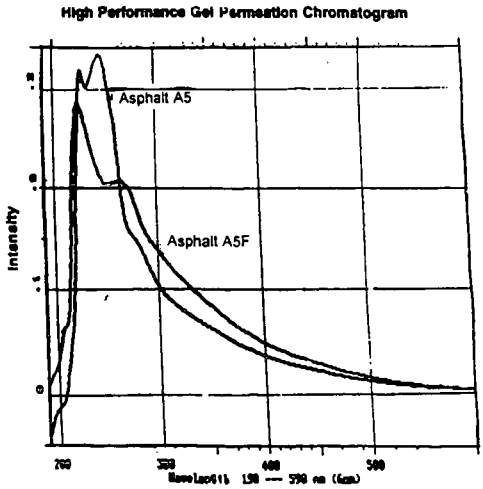

Figure 4: Ultraviolet spectra of the small molecular size polar aromatic fraction of asphalts A5 and A5F.

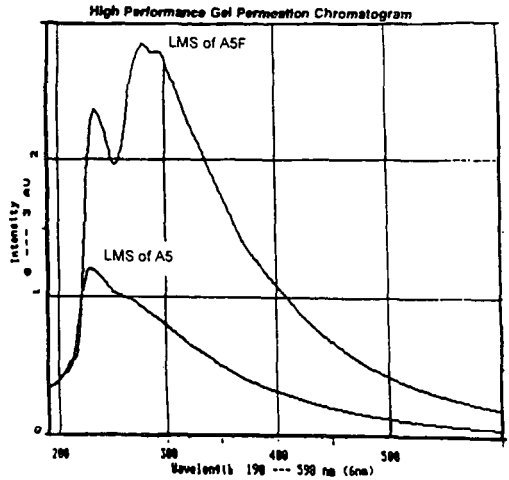

Figure 5: Ultraviolet spectra of the large molecular size polar aromatic fraction of asphalts A5 and A5F.

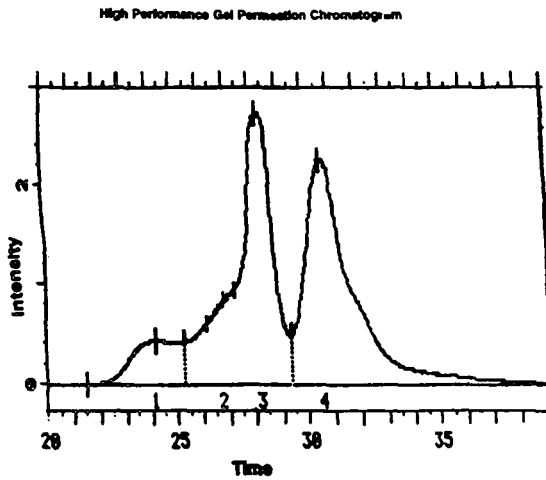

Figure 6: Chromatogram of a model polymer obtained from the reaction between phenol and furfural.

^{13}C-Nuclear Magnetic Resonance Analysis

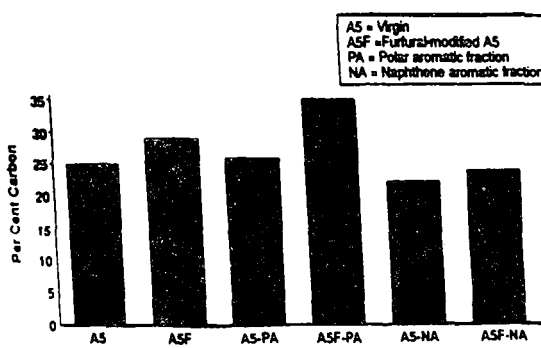

Figure 7: Nuclear Magnetic Resonance data for the percent aromatic carbon content (obtained without the Overhauser effect) present in asphalts A5 and A5F and their Corbett fractions.

^{13}C-Nuclear Magnetic Resonance Analysis

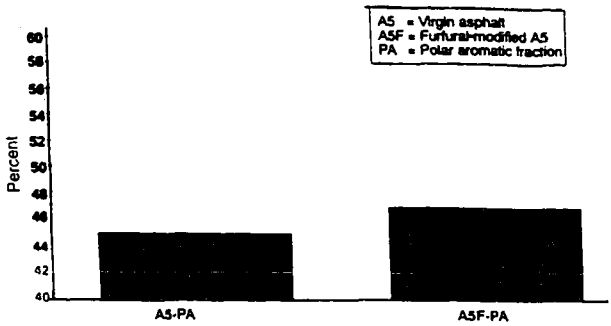

Figure 8: Nuclear Magnetic Resonance data for the percent non-protonated carbon content in polar aromatic fractions of asphalts A5 and A5F.

^{1}H-Nuclear Magnetic Resonance Analysis

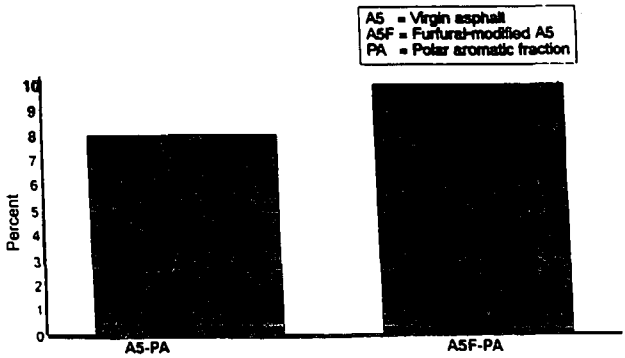

Figure 9: Nuclear Magnetic Resonance data for the aromatic to aliphatic proton ration of the polar aromatic fractions of asphalts A5 and A5F.

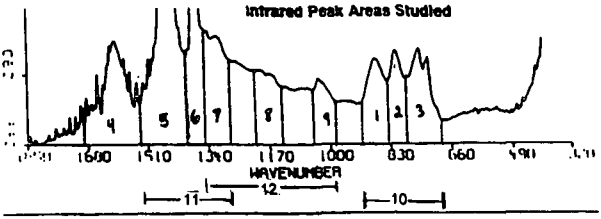

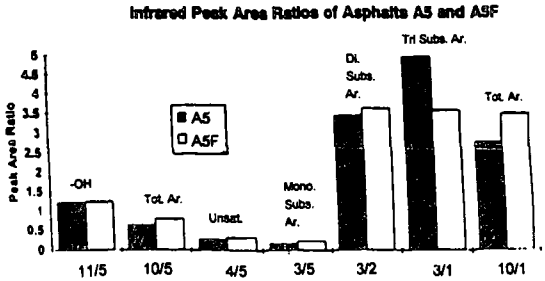

Figure 10: Infrared peak area ratios for asphalts A5 and A5F.

SELECTIVE CATALYTIC SORBENTS FOR NO_x FROM COMBUSTION FLUE GAS FOR PREPRINTS OF THE FUEL CHEMISTRY DIVISION, ACS

A. Rubel, M. Stewart, J. Stencel
University of Kentucky
Center for Applied Energy Research
3572 Iron Works Pike
Lexington, KY 40511-8433

Keywords: coal-based sorbents, selective NO_x capture, combustion flue gas

INTRODUCTION

A process which uses coal-based activated carbons as selective catalytic sorbents for the removal of NO_x from combustion flue gas is under investigation at the University of Kentucky, Center for Applied Energy Research (CAER) (1-3). Flue gas cleanup would be achieved through the selective capture of NO_x at stack temperatures of 70-120°C followed by desorption of a concentrated stream of NO_2 at elevated temperatures (140-150°C). Processing would involve repeated NO_x adsorption/desorption cycles using the same adsorbent carbon.

Numerous investigation have been conducted on the decomposition of NO_x over carboneous materials with respect to the heterogeneous reduction of NO_x (4-9). Under the reaction conditions used, the amount of NO adsorbed was less than 2 wt% of the carbon and, due to the high reaction temperatures, 40-50 wt% of the carbon was gasified (2,6). Our work has concentrated on the use of activated carbons as selective sorbents for NO_x at flue gas stack conditions without added chemicals. Our data suggests that an environmentally benign process is possible which eliminates problems associated with ammonia slippage, and provides possibilities for by-product generation such as nitrates for agricultural purposes, nitric acid, or other nitrated compounds.

This paper will discuss NO_x adsorption on coal-based sorbents, catalytic reactions involved in the adsorption process, identification of the desorbed oxide, and the possibility of making HNO_3 from adsorbed NO_x.

EXPERIMENTAL

Instrumentation. NO_x adsorption/desorption profiles were obtained using a Seiko TG/DTA 320 coupled to a VG Micromass quadrapole MS. The two instruments were coupled by a heated (170°C) fused silica capillary transfer line leading from above the sample pan in the TG to an inert metrasil molecular leak which interfaced the capillary with the enclosed ion source of the MS. The TG was connected to a disk station which provided for programmable control of the furnace, continuous weight measurements, sweep gas valve switching, data analysis, and export of data to other computers. The MS has a Nier type enclosed ion source, a triple mass filter, and two detectors (a Faraday cup and a secondary emissions multiplier). The MS was controlled by a dedicated personal computer which was also used to acquire and review scans before export to a spreadsheet for data manipulation.

TG-MS procedures. The TG heating regime used to produce NO_x adsorption/desorption profiles incorporated segments for outgassing, cooling, adsorption, desorption, and temperature-induced desorption. The details of this heating program have been discussed previously (1). Other TG conditions used have also been published (1,2).

The MS was scanned over a 0-100 amu range with a total measurement interval of approximately 30 s per 100 amu; NO (mass 30) or NO_2 (mass 30 and 46) were identified by comparing amu 30/46 ion ratios.

NO_x scrubbing test procedures. NO_x breakthrough profiles were acquired using a 7.2 ml cylindrical reactor loaded with approximately 1 g of sorbent. A small fraction of the effluent gas leaving the reactor was routed to a mass spectrometer for continuous monitoring of gas composition. The sample was outgassed at 300°C for 1 hour with a He purge at a flow rate of 150 ml/min metered at room temperature and pressure. The coal-based carbon was then cooled to an adsorption temperature of 80°C. Once this temperature was achieved, the purge gas was switched to a simulated combustion flue gas containing 2% NO, 5% O_2, and a balance of He. Subsequent to testing, the reactor was cooled and the sorbent retrieved for analysis.

Nitric acid production tests. Activated carbon which had been completely saturated with NO_x was subjected to two different wash solutions, distilled/deionized water and 3% H_2O_2 in distilled/deionized water. The washes were saved for analysis. A control, non-treated sample of sorbent was also washed with both solutions for comparison.

Analytical procedures. The sorbents were subjected to surface area determinations performed on a Quantachrome Autosorb-6 using a N_2 static volumetric flow procedure. Surface areas were calculated using the standard BET equation between relative pressures of 0.05-0.25 (10). Wash solutions from the nitric acid production testing were analyzed by ion chromatography on a Dionex 2020i instrument according to standard procedures. The pH of the wash solutions was determined by ASTM D3838-80.

Materials and simulated flue gas composition. Two coal based activated carbons, produced commercially by steam activation, were tested during this study. For the purposes of this paper, the two carbons will be identified as **a** and **b**. They had N_2 BET surface areas of 460 and 850 m^2/g, respectively.

The NO_x adsorption capacity of the activated carbons was determined using the following concentrations of gases during adsorption: 2% NO, 5% O_2, 15% CO_2, 0.4% H_2O and He as the balance. Helium was used by itself during degassing, physidesorption, and temperature programmed desorption.

The range of concentrations of flue gases studied during this work are as follows: 0.3 to 2.0% NO or NO_2; 5 to 20% O_2, 0 to 15% CO_2; 0.4 to 6% H_2O and He as the balance. During some tests, the sorbent was pre-saturated with O_2 or CO_2 to determine their contribution to the adsorption mechanism.

RESULTS AND DISCUSSION

Adsorption Capacities and sorbent gasification. Adsorption/desorption profiles, as shown in Figure 1 for sorbent **a** were used to determine adsorption capacities and recycle potential for the two carbons. On exposure to NO and in the presence of O_2 and CO_2, the weight gained in 30 minutes by sorbent **a** was 13.6%. Desorption of NO_2 from the carbon through both physidesorption and temperature programmed desorption was confirmed by mass spectra showing a major peak at amu 30 (the primary mass ion for both NO and NO_2) which coincided with the TG monitored weight loss. A peak was also observed at amu 46, a secondary mass ion for NO_2. The temperature at which maximum desorption occurred was 140°C.

Repeated cycling of the sorbent indicated that gasification and adsorption capacity losses were very small. Carbon **a**, subjected to three NO_x adsorption/desorption cycles, lost approximately 1.5% of its total adsorptive capacity (Figure 1). This loss was partially related to a small amount of carbon gasification (0.5-1.0 wt%). Since the temperature at which maximum desorption occurred, 140°C, is significantly lower than the 400°C to which the samples were heated during temperature-induced desorption, these losses can be reduced by lowering the maximum temperature to which the carbons are exposed. Results for carbon **b** were similar to those for carbon **a** except the adsorption capacity for NO_x was slightly less at 10.7 g NO_2 / 100 g carbon.

NO_x scrubbing test. The response of the mass spectrometer (amu 30) during NO_x scrubbing using sorbent **a** showed removal of NO to near the lowest detection limits of the MS over a 16 minute period (Figure 2). This implies that the NO_2 loading on the carbon was 9.1 g NO_2 / 100 g carbon.

Requirements of adsorption. To better understand adsorption mechanisms and requirements, the adsorption capacity of sorbent **a** was determined for various combinations of NO or NO_2 combined with CO_2 and/or O_2, and for NO or NO_2 on carbon pre-saturated with CO_2 or O_2 (Figure 3). The relative capacity for the combination of gases was defined as the amount of adsorption measured for each case with respect to the base case for both NO and NO_2 adsorption. The base case was the adsorption of NO or NO_2 in CO_2 and O_2. The weight gained by the carbon was the same for both base cases.

It was found that O_2 was required for significant NO adsorption and that CO_2 did not interfere with adsorption. Adsorption of NO in CO_2/O_2 was the same as for NO in O_2 alone. Almost no adsorption of NO occurred in the presence of He or CO_2. These data are consistent with other literature which show low levels of NO_x adsorption at temperatures above 200°C and in the absence of O_2 (4-9). Pre-saturating carbon with O_2 followed by NO adsorption in He improved NO adsorption over the comparable He case, but whether this was due to binding of O_2 to the carbon or slightly higher gaseous O_2 levels as a result of the inability to completely purge O_2 from the TG-MS system could not be determined. There was a slight increase in the weight (approximately 0.5 wt%) of the carbon during O_2 pre-treatment. In contrast to NO adsorption, the relative adsorption of NO_2 was found to be nearly independent of the presence or absence of CO_2 and/or O_2. The amount of NO_2 adsorbed in He was only slightly less than

in O_2.

Control experiments for the above series of experiments indicated that O_2, CO_2 and H_2O were not significantly adsorbed on the sorbent (Figure 4). For comparison, results from a base case with carbon exposed to the simulated flue gas containing NO_x, O_2, CO_2, and H_2O is also shown in Figure 4.

Adsorbed Oxide. Since identical weight was gained by the carbon when it was exposed to identical concentrations of either NO or NO_2 in the presence of O_2, the adsorbed oxide must be the same for both cases. During the adsorption of NO in O_2, a significant exotherm was observed which did not occur when NO_2 was used (Figure 5). The heat of adsorption determined from these dta curves was -1.6 kcal/g NO_2 which is consistent with the conversion of NO + O to NO_2. Detection of this heat of adsorption by the instrumentation requires that the reaction occurred at the surface or within the pores of the sorbent, suggesting the carbon's catalytic role in the conversion of NO to NO_2.

Desorbed Oxide. During all our experimentation, MS mass ion ratios were determined by monitoring amu 30/46. This ratio has been determined for all our experimental conditions and for all combination of the gases. As previously stated, mass 30 is the primary ion for both NO and NO_2 while NO_2 also exhibits a secondary mass ion at 46. The 30/46 mass ion ratio during temperature induced desorption, clearly suggests that the desorbed oxide is primarily NO_2 (Figure 6).

Nitric acid production. The catalytic conversion of NO to NO_2 by the carbon and the desorption of NO_2 as the major product suggests that nitric acid production would be a possible by-product of a process using coal-based sorbents for combustion flue gas clean-up. When carbon a, exposed to simulated combustion flue-gas, was washed with either distilled/deionized water or 3% H_2O_2, the pH of the wash solutions decreased dramatically (Table I). This decreased was caused by an increase in the nitrate ion concentrations of the solutions (Table II). More work needs to be done in this area but these results suggest the possibility that nitric acid could be produced directly from the captured NO_x without additional reactions or chemicals.

SUMMARY AND CONCLUSION

NO_x in the presence of O_2 and CO_2 was selectively captured by coal based activated carbons. The measured heat of adsorption indicated that NO present in the flue gas was catalytically converted to NO_2 at the surface of or within the carbon. The desorbed oxide species was identified as NO_2 by mass ion ratios (30/46). The presence of adsorbed NO_2, which can be simply washed from the carbon as nitrate ion, suggests that the production of nitric acid as a by-product is possible. Our research has shown that coal based sorbents have the potential to be used in an environmentally benign process to selectively remove NO_x from combustion flue gas.

REFERENCES

1. Rubel, A.M.; Stencel, J.M.; Ahmed, S.N. *Preprints Symposium on Flue Gas Cleanup Processes;* ACS, Division of Fuel Chem.: Denver, CO, 1993; 38(2), 726-733.
2. Rubel, A.M.; Stencel, J.M.; Ahmed, S.N. *Proceeding of the 1993 AIChE Summer National Meeting*; AIChE: Seattle, WA, 1993; Paper no. 77b.
3. Rubel, A.M.; Stewart, M.L.; and Stencel, J.M. *Preprints Symposium on NO_x reduction,* ACS, Division of Petroleum Chem.: San Diego, CA, 1994; 39(1), 137-140.
4. Smith, R.N., J. Swinehart, and D. Lesnini. *J. Physical Chem.* 63(1959)544.
5. DeGroot, W.F., T.H. Osterheld, G.N. Richards. *Carbon* 29(1991)185.
6. Teng, H., E.M. Suuberg, J.M. Calo, and P.J. Hall. *Proc. 19th Conf. on Carbon,* (1989)574.
7. Suuberg, E.M., H. Teng, and J.M. Calo. *23rd Symposium (International) on Combustion,* The Combustion Institute (1990)1199.
8. Teng, H., E.M. Suuberg, and J.M. Calo. *Preprints of the 200th ACS National Meeting,* Washington, DC, 35,3(1990)592.
9. Gray, P.G., N.J. Desai, and D.D. Do. *Recent Trends in Chem. Rxn Engr.*, B.O. Kkulkarni, R.A. Mashelkar, and M.M. Sharma, eds., Wiley Eastern Ltd., 1(1987)383.
10. Brunauer, S.; Emmett, P.H.; Teller, E. *J.A.M. Chem. Soc.* 1938, *60*, 309.

Table I. pH of wash solutions from nitric acid production tests

Wash solution	pH	Wash solution	pH
H_2O Control	6.0	3% H_2O_2/H_2O Control	4.8
H_2O, Unused C	6.7	3% H_2O_2, Unused C	6.4
H_2O, NO_x exposed C	2.1	3% H_2O_2, NO_x exposed C	1.9

Table II. Nitrate ion concentration in wash solutions determined by IC

Wash solution	$\%NO_3^-$	Wash solution	$\%NO_x^-$
H_2O, Unused C	< 1 ppm	3% H_2O_2, Unused C	< 1 ppm
H_2O, NO_x exposed C	0.18	3% H_2O_2, NO_x exposed C	0.23

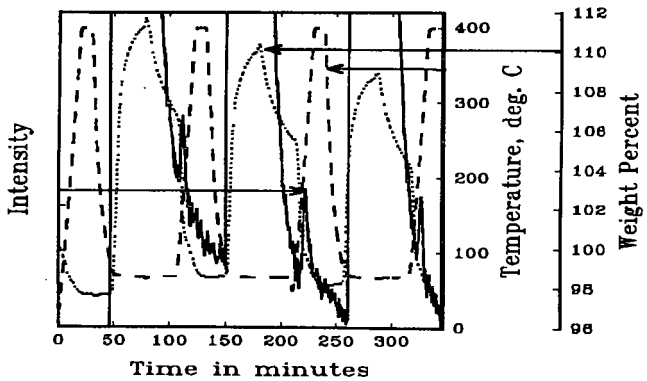

Figure 1. Three cycle ads/des profile for NO_x ads on carbon, a; gases: 2%NO, 5%O_2, 15%CO_2, 0.4%H_2O, balance He

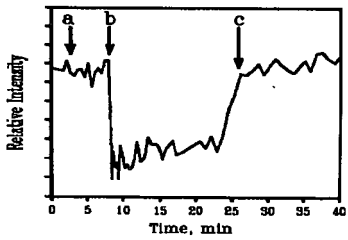

Figure 2. NO_x scrubbing test; mass 30 breakthrough curve; a = baseline NO level, b = gas pass through carbon initiated, c = NO breakthrough

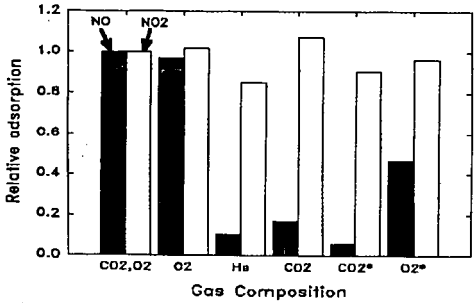

Figure 3. Relative ads of NO_x on carbon, a, in different atmospheres; * = carbon presaturated with O_2 or CO_2; ads in He

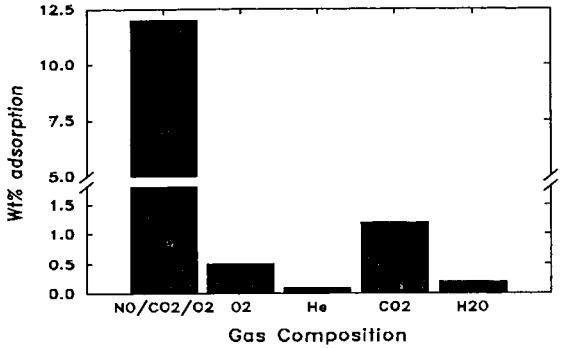

Figure 4. Adsorption of O_2, CO_2 and He on carbon. Gases: 0.6% NO; 5% O_2; 15% CO_2; 6%H2O; balanced with He

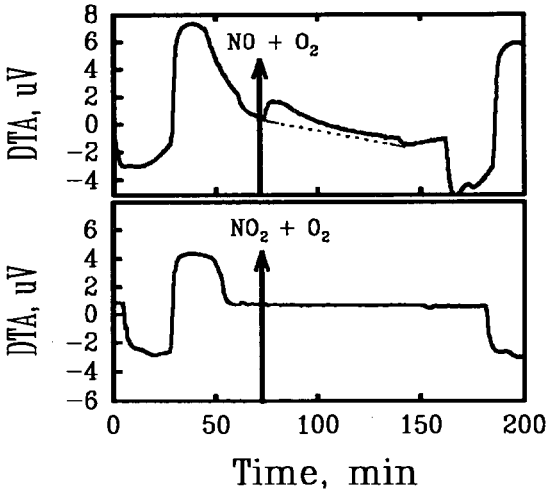

Figure 5. DTA curves for NO vs. NO_2 adsorption in the presence of O_2

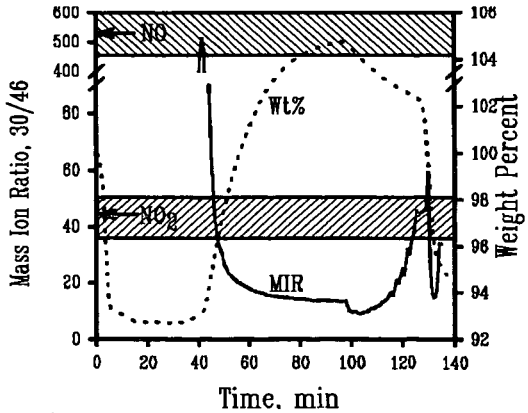

Figure 6. Mass ion ratio (30/46) during desorption

NOVEL APPROACH TO THE PRODUCTION OF GRAPHITE FROM ANTHRACITE

Joseph V. Atria, ShuMing Zeng, Frank Rusinko, Jr., Harold H. Schobert
Fuel Science Program, 209 Academic Projects Building
Pennsylvania State University
University Park, PA 16802

Keywords: Anthracite, Graphite, Optical Microscopy

INTRODUCTION

Currently the carbon/graphite industry uses petroleum coke as the main filler constituent in the manufacture of graphite. Anthracite has been successfully used as fillers for amorphous carbon electrodes, but has not been used in the production of graphite electrodes because of its non-graphitizable structure. Creating a cost-effective graphitizable anthracite, which would have characteristics to be a viable substitute for petroleum coke, would help find an alternative use for Pennsylvania's anthracite and reduce the industry's dependence on petroleum. In the present project, a unique approach to make graphite from anthracite, focused on modifying anthracite's precursor structure by adding a hydrogen-donating substance, has been conducted. This approach is based on two major hypotheses. First, a supply of donatable or transferable hydrogen is needed for the hydrogen-deficient anthracite structure to disrupt crosslink formation between aromatic structures within the coal. Secondly, an aromatic liquid medium is needed to help prevent electronic interactions between aromatic structures and provide the fluidity necessary for aromatic realignment into the graphite structure.

Several hydrogen donors were investigated. 9,10-Dihydroanthracene showed the best ability to donate hydrogen to anthracite and also formed a highly anisotropic anthracene coke in the process. Phenanthrene was selected as the aromatic liquid medium. Both anthracene and phenanthrene have been found to be highly graphitizable [1]. Although hydrogen was successfully donated to the anthracite, the hydrogen donation is believed to have only occurred at the surface and did not affect the internal structure of the coal. Previously treated samples showed good anisotropic character and approached the interlayer spacing of the graphite structure upon heating to graphitization temperatures, but the graphitized anthracites did not show any layering characteristics or crystalline height, Lc [2]. Rouzand and others have found the structure and shape of the initial porosity and flow microstructures of the raw anthracite to be a major factor in the extent of graphitization of anthracite [3]. Because of the dependence of graphitizability on pore structure and the resistance of the internal coal structure to hydrogen donation, six anthracites were studied to determine their pore characteristics. Three of the anthracites, representing a variety of pore characteristics, were then selected to investigate the hydrogenation and subsequent graphitization of the anthracites treated with dihydroanthracene.

EXPERIMENTAL

Six anthracites from various mines in the eastern Appalachian coal region were obtained from the Penn State Coal Sample Bank and Data Base. All of the pore characterization was carried out on 60–100 mesh samples. Helium pycnometry, using a Quantachrome Multipycnometer MVP-1, at room temperature was used to find true densities, weight per unit volume of the pore-free solid. Mercury porosimetry (Quantachrome Autoscan Mercury Porosimeter) was used to obtain the particle density, the weight of a unit volume of solid including pores. Values at 60 psi were taken since interparticle voids are more or less completely filled with mercury at this pressure. The volume percent of open porosity was then calculated from these two density measurements. Macro- and mesopore size distributions were also determined from mercury porosimetry. Both nitrogen and carbon dioxide surface areas were determined, at –196 °C and 0 °C respectively, using a Quantachrome Autosorb-1 automated gas adsorption system. Nitrogen surface areas were calculated using the BET equation. However, the adsorption of N_2 in microporous coals is severely limited and gives appreciably lower values. Carbon dioxide can reach much more of the coals' internal porosity [5]. The Carbon dioxide surface area was calculated using the DR method. Both BET and DR plots showed a greater then 99.5% correlation to a straight line fit. Nitrogen pore volumes were also obtained. Three anthracites were selected for subsequent experimentation: DECS-21, PSOC-1468, and PSOC-1461.

Anthracite samples, –60 mesh, were charged in 20mL capacity stainless steel microautoclave reactors with a mixture of 75% 9,10-dihydroanthracene and 25% phenanthrene, in a 1:2 coal-to-donor ratio. Ratios of higher amounts of dihydroanthracene mixture were also run. Reactions were carried out under 1000 psi nitrogen pressure in a fluidized sand bath. Reactors were continuously agitated to keep the reactants well mixed. A temperature- controlled heat treatment was used: 3h initial hold at 200 °C, temperature increased to 550 °C at the rate of 5 °C/h, and a final hold at 550 °C for 2 h. The products were extracted with tetrahydrofuran (THF) for 24h. Optical microscopy samples were then made of the THF-insoluble material and analyzed under a polarized light microscope (Nikon microphot-FXA) with 35mm camera and video ports. Optical micrographs of typical areas were taken. Samples were further heat treated at 1500 °C for 4h and observed optically then graphitized. Graphitization was conducted at the Carbide /Graphite Group Inc. in St. Marys, PA using an industrial induction furnace. Samples were heated to 2700 °C and 2900 °C for 5 hours in purified graphite crucibles. Graphitized anthracite samples were analyzed using optical microscopy again and x-ray diffraction, SCINTAG/USA PAD-V diffractometer with CuK_a radiation. Calculations of the quality and the amount of the sample in the graphite structure were made using X-ray data.

RESULTS and DISCUSSION

The open porosity of the six raw anthracites was calculated from helium and mercury densities and are recorded in Table 1. The mercury densities were calculated using the Washburn equation and all of the densities ranged from 1.53 to 1.63 g/cm^3. These values are about 0.2 g/cm^3 higher than Mahajan and Walker's results for anthracites. This difference can be explained by the fact Mahajan used de mineralized samples and a smaller particle size fraction, 40–70 mesh [6]. Helium densities ranged from 1.56 to 1.65 g/cm^3, except for PSOC-1461 which had a considerably higher density of 1.79 g/cm^3. Anthracites have shown the presence of some porosity closed to helium [7]. Curtz and Hirsh also used X-ray studies of anthracites to show interlayer spacings corresponding to true densities of 2.0 g/cm^3, as compared to helium densities of 1.5 g/cm^3 [8]. PSOC-1461 possibly had a much smaller amount of this porosity closed to helium and therefore gave a much higher density value. Volume percent open porosity values were very small, less than 5.5% with exception of PSOC-1461. PSOC-1468 showed the smallest volume percent of 1.3%.

Surface areas for nitrogen and carbon dioxide are also recorded in Table 1. Considerable care was taken to outgas the coals for over 24 hours due to the difficulties in removing moisture from the microporosity. The microporosity of these anthracite samples is clearly seen by the very low nitrogen surface areas and high carbon dioxide surface areas. Nitrogen surface areas ranged from 0.62 to 4.56 m^2/g and were expected to correspond to the amount of open porosity calculations, but PSOC-1467, 1461 and 867 did not show such relationship. Carbon dioxide surface areas were much higher since CO_2 can reach more of the coal's porosity and ranged from 320 and 460 m^2/g. DECS-21 showed the largest CO_2 surface area while PSOC-1461 had the smallest surface area.

The very small pore volumes recorded for nitrogen adsorption, Table 2, also point to a very microporous structure. Total pore volumes ranged from 0.9 to 4.6 x10^{-3} cm^3/g. Mercury porosimetry which was taken to 60,000 psi showed only an order of magnitude higher total pore volumes. The mercury intrusion results are also summarized in Table 2. The mercury pore volumes corresponded to the nitrogen volumes except for PSOC-1467. Mercury pore size distributions showed only a very small fraction of macroporosity. Mercury porosimetry can not measure the microporosity. The meso and macroporosity are of interest because this is the porosity which would be intruded by the hydrogen donor. The extensive amount of microporosity and lack of open porosity help point to the difficulties of gaining hydrogen transfer throughout the anthracite structure. There could be many reasons for some of the discrepancies seen in the pore characterization data. Smith and others listed some of the major reasons for the complications in pore characterization, of which the complex pore shapes and connectivities, along with chemical and physical heterogeneties, could easily be reasons for the difficulties in coal characterization [9].

Using the above data, three anthracites were selected for their varying pore characteristics to be further treated with the dihydroanthracene. The proximate and ultimate analyses for these three anthracites is shown in Table 3. DECS-21 was selected for its high CO_2 and N_2 surface area and mid-ranged open porosity. PSOC-1468 was selected for its low open porosity, small N_2 surface area, mid-ranged CO_2 surface area, and low total pore volume with the highest fraction of macroporosity. PSOC-1461 was selected for its high open porosity, and small CO_2 surface area. Table 3 also shows these three samples have very different ash, carbon, hydrogen and oxygen contents.

After samples were reacted, optical micrographs were taken. All three anthracites showed similar optical behavior at this stage; therefore, only the micrographs for DESC-21 (Figure 1) will be discussed. Micrograph (a) shows the anthracite heated to 550 °C without hydrogen donor. The anthracite retains its ridged shape and shows a small amount of inherent anisotropy. Micrographs (b and c) are of the coal reacted with dihydro-anthracene at different magnifications. Micrograph (b) shows how the dihydro-anthracene has been converted to an anisotropic coke which surrounds and binds the anthracite particles together. However, no structural change in the anthracite particles can be seen at this stage. Micrograph (c) shows better the flow domains produced by the mesophase development of the anthracene. This micrograph also shows a very good binding of the anthracene coke to the anthracite. In future work, optical micrographs will be taken of samples heated to 1500 °C and after graphitization to observe if any of the anthracene is imbibed into the anthracite particle and if any structural change of the anthracite has occurred. In addition, X-ray diffraction will be used to classify the quality of the graphite using interlayer spacing and Lc, and to determine the amount of graphitic material present using intensity data.

ACKNOWLEDGMENTS

The authors would like to acknowledge the Carbide/ Graphite Group Inc. for their help in the graphitization of samples and for the financial support for this work provided by the Pennsylvania Energy Development Authority.

REFERENCES

1. T. Sasaski, R. Jenkins, S. Eser, and H. Schobert, Energy & Fuels 7, 1039 (1993).
2. J. Atria, S. Zeng, F. Rusinko, Jr., and H. Schobert, Final Report, Pennsylvania Energy Development Authority(PEDA), December 1993.
3. S. Duber, J. Rouzaud, C. Beny, and D. Dumas, Extended Abstracts, 21st Biennial Conference on Carbon, 316 (June 1993).
4. H. Gan, S. Nandi, and P. Walker, Jr., Fuel 51, 272 (1972).
5. P. Walker, Jr., and I. Geller, Nature (London) 178, 1001 (1956).
6. O. Mahajan, and P. Walker, Jr., Pennsylvania State University, unpublished results (1979).
7. W. Kotlensky and P. Walker, Jr., Proceedings Carbon Conference 4th, 423 (1959).
8. L. Cartz, and P. Hirsh, Philos. Trans. R. Soc. London Ser. A252, 557 (1960).
9. D. Smith, D. Hua, and W. Earl, MRS Bulletin 19, 44 (April 1994).

Table 1. Physical properties of untreated anthracite samples.

Sample	He Density (g/cm^3)	Hg Density (g/cm^3)	Open Porosity volume %	Surface Area (m^2/g) N_2	CO_2
DESC-21	1.615	1.530	5.3	4.13	460.4
PSOC-1468	1.653	1.631	1.3	0.92	392.8
PSOC-1467	1.563	1.528	2.2	4.56	379.7
PSOC-1461	1.794	1.549	13.6	2.56	319.7
PSOC-1456	1.562	1.537	1.6	1.31	425.8
PSOC-867	1.635	1.562	4.5	0.62	320.4

Table 2. Nitrogen adsorption pore volume and mercury porosimetry.

Sample	Carbon wt% (daf)	Total Pore Volume $x10^{-3}$ (cm^3/g)	Hg Porosimetry Total Pore Volume $x10^{-3}$ (cm^3/g)	Mesopore Volume $x10^{-3}$ (cm^3/g)	Macropore Volume $x10^{-3}$ (cm^3/g)
DESC-21	90.33	3.7	40.1	39.2	0.9
PSOC-1468	95.36	1.0	28.9	27.7	1.2
PSOC-1467	93.29	4.6	86.0	82.2	2.7
PSOC-1461	93.47	4.2	48.2	48.0	0.2
PSOC-1456	94.56	1.5	31.9	31.6	0.3
PSOC-867	95.07	0.9	27.9	27.9	1.1

Table 3. Analysis of anthracite samples selected.

Sample Seam	DECS-21 Lykens Valley	PSOC-1468 Buck Mountain	PSOC-1461 Mammoth
Proximate Analysis (as rec.)			
% Moisture	3.99	4.51	3.06
% Ash	10.71	6.52	23.44
% Volatile	4.33	3.49	3.89
% Fixed Carbon	80.97	85.48	69.61
Ultimate Analysis (dry)			
% Ash	11.15	6.83	24.14
% Carbon	80.26	88.85	70.87
% Hydrogen	3.56	1.29	1.45
% Nitrogen	0.71	0.78	0.87
% Total Sulfur	0.50	0.49	0.74
% Oxygen (diff)	3.82	1.76	0.89
Atomic H/C (dmmf)	0.5328	0.1744	0.2457
PARR Atomic O/C (dmmf)	0.0295	0.0121	0.0031

a.

b.

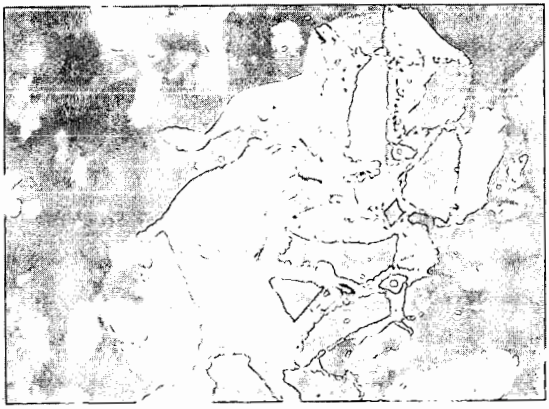

c.

Figure 1. Polarized optical micrographs of anthracite, DESC-21, heated to 550 °C; (a) untreated,, 100 X; (b) coal and 9,10-dihydroanthracene, 100X; (c) coal and 9,10-dihydroanthracene, 400X.

KINETICS MODELING OF THE ATMOSPHERIC-PRESSURE CHEMICAL VAPOR DEPOSITION OF SILICON DIOXIDE FROM SILANE AND OXYGEN

Carmen J. Giunta
Department of Chemistry
Le Moyne College
Syracuse, NY 13214-1399

Keywords: kinetics model, oxidation, silane

Abstract

The oxidation of SiH_4 by O_2 is a reaction of interest to chemists in the areas of both combustion and chemical vapor deposition. A detailed kinetics model of this reaction, developed to explain combustion data,[1] is applied with slight modification to kinetic data from atmospheric-pressure thermal chemical vapor deposition (CVD) of SiO_2 films[2]. The model is also compared to a CH_4 oxidation model under the same CVD conditions, to elucidate differences in the oxidation of SiH_4 and CH_4 under mild conditions. A key difference stems from the rates and major products of the reaction of O_2 with SiH_3 vs. CH_3 radicals.

Introduction

The first serious attempt to model the kinetics of the oxidation of silane by oxygen came from the combustion chemistry community,[3] as well as the most comprehensive effort to date (hereafter called BTW after its authors' initials)[1]. Meanwhile, materials scientists, electronics engineers, and others have been interested for over 25 years in a controlled version of silane oxidation under mild conditions, an example of the now widely used technique of chemical vapor deposition (CVD).[4] The interest of this latter group stems from the fact that this reaction can produce thin films of SiO_2, useful for a variety of purposes in the semiconductor industry and elsewhere.

This paper focuses on a report of the film growth kinetics of such a CVD process, a report rich in kinetic information (deposition rates as a function of distance along the gas flow in the reactor under a variety of concentrations and temperatures) obtained under relatively simple conditions of fluid flow (laminar flow between parallel plates).[2] The report (hereafter called EH after its authors' initials) is a source of data amenable to modeling, and I attempted to model that data using the BTW mechanism with only slight modification. The conditions employed by EH (atmospheric pressure, low SiH_4/O_2 ratios, mild reaction) are sufficiently different from those for which the BTW mechanism was developed (ignition data over a range of pressures) as to test the robustness of the BTW mechanism.

The questions I addressed are: Can the BTW mechanism adequately model the EH data? How should the mechanism be modified? What are the principal pathways of the mechanism under the conditions employed by EH? How do these pathways differ from those of methane oxidation?

Computational Method

Model growth profiles were obtained by numerically integrating the applicable differential equations for reaction and diffusion in two dimensions. The equations describing reaction in the SiH_4/O_2 system were the mass-action rate equations defined by the 70 reversible elementary reactions among 23 species listed by BTW in their Table I. (I use their numbering in referring to reactions below.) For comparison, the CH_4/O_2 system was represented by 73 reactions total among 19 species. This reaction list is the CH_4/O_2 subset of a mechanism developed to model the CVD of SnO_2 from $(CH_3)_4Sn$ and O_2.[5] The y dimension is normal to both the flow and the substrate in the horizontal, laminar-flow reactor; the x direction is along the flow, and it represents the temporal evolution of the reaction. Inclusion of the y dimension permitted explicit consideration of the large temperature gradients present in the reactor along that dimension, by allowing for spatially varying rate coefficients. It also facilitated treatment of diffusion normal to the substrate, and direct evaluation of the deposition rate from the diffusive flux onto the growth surface of species which stick to the surface. Details on the computational methods are reported elsewhere.[6]

Results and Discussion

Can the BTW mechanism adequately model the EH data?

The maximum deposition rate in the profiles reported by EH is rather weakly dependent on the temperature of the hot substrate, as shown in Fig. 1; the activation energy is about 27 kJ mol^{-1} over the range 742-845 K. The maximum film growth rate is weakly but inversely dependent on initial oxygen mixing ratio (always in large excess), as illustrated in Fig. 2. And the maximum growth rate is strongly dependent on initial silane mixing ratio, as shown in Fig. 3. If the data (only three data points) define a power-law dependence, the order with respect to silane is around 1.34. Increasing the flow rate pushes the position of the maximum deposition rate downstream and spreads it out, without greatly altering the shape of the profile. Increasing the temperature of the cool wall of the reactor increases the maximum deposition rate only slightly, and does not otherwise alter the shape of the deposition profile.[2]

The BTW mechanism led to model deposition profiles which reproduce all of the above trends, albeit with higher deposition rates and earlier deposition maxima (discussed below). The activation energy of the maximum deposition rate in the model was about 29 kJ mol^{-1} over the range 742-845 K, as shown in Fig. 1. The peak deposition rate declined slightly but noticeably upon increasing the oxygen mixing ratio from 1.7% to 25%, as illustrated in Fig. 2, although this

inverse relationship seemed to bottom out thereafter. The peak deposition rate followed a power law of order 1.46 with respect to initial silane mixing ratio, as illustrated in Fig. 3. Doubling the flow rate doubled the downstream position of the growth maximum and practically doubled the width of the deposition profile. Increasing the temperature of the cold wall had virtually no effect on the model profile.

Despite the success of the BTW model in capturing the qualitative trends described above, the deposition profiles produced by my model simulations did not greatly resemble the profiles published by EH. (See Fig. 2, which illustrates one of the better resemblances between model and experiment!) In particular, the model profiles peaked too early and too high. To understand this discrepancy, it is necessary to note that in all the model simulations presented here, the temperature was taken to be constant along the x (flow) direction. That is, the short space needed for the gases to warm up to the reactor temperature was neglected. This simplifying assumption facilitated a substantial savings in computational effort and time, and significantly enhanced the numerical tractability of the model's differential equations. However, it also altered the position and magnitude of the maximum deposition rate from what the model would predict if the development of the temperature field bad been treated explicitly. The model deposition profiles presented here put the maximum deposition rate very close to the reactor inlet, certainly within the warm-up zone. My experience with modeling another rapid oxidation of silanes[6b] suggests that treating the transient temperature field explicitly would delay the deposition maximum until the end of the warm-up zone, and spread out the deposition profile somewhat, concomitantly lowering the maximum deposition rate by some 30%. Therefore, the profiles presented here can be expected to have their deposition maxima pushed about 1 cm downstream, spread out, and lowered. These changes would bring the model profiles into much better agreement with the experimental data reported by EH. But a rigorous and quantitative comparison must await simulations in which the development of the temperature field along the flow direction is explicitly treated.

How should the mechanism be modified?

From the viewpoint of reproducing the experimental data, the model profiles should be modified to reduce the deposition peak and move it downstream. That, I expect, will occur with careful treatment of the early temperature field. Still, I considered the BTW mechanism flawed in its treatment of the reaction of the SiH_3 radical with O_2. The BTW mechanism includes several product channels for this reaction, all proceeding through an excited adduct "$xSiH_3O_2$", which is included explicitly in the mechanism. First, the rate constant assigned to formation of the adduct (R16 reverse) is two orders of magnitude greater than gas kinetic. Second, the temperature dependence of the effective BTW rate constant for the overall reaction

(1) $SiH_3 + O_2 \rightarrow$ products

appears to contradict the only published data on the subject.[7]

The first objection was easily remedied. Running the model with the rate constants for R16 and its reverse reaction decreased by a factor of 100 had no effect on the model deposition profiles. In fact, decreasing the rate constants by a further factor of 50 had a negligible effect. Thus, the BTW model results described above were not limited by the value of the rate constant for formation of the excited adduct $xSiH_3O_2$.

The second objection, however, was not so easily resolved. Slagle et al. report a small negative activation energy for reaction (1) over 296-500 K, whereas the effective activation energy in the BTW mechanism is positive over the same range. I tried replacing all the BTW reactions involving excited $xSiH_3O_2$ with a single direct reaction

$$SiH_3 + O_2 \rightarrow SiH_2O + OH\ ,$$

and I assigned to this reaction the rate constant reported by Slagle et al. The resulting model profiles differed negligibly from those discussed above. Thus, not surprisingly, the excited $xSiH_3O_2$ (when it was left in the mechanism) functioned as a flow-through species, at least under the modeled conditions. But making SiH_2O + OH the dominant products of reaction (1) is at odds with reports by Koshi et al. that HSiOOH + H are the major products (at least at room temperature and 5 Torr).[8] The BTW mechanism is actually consistent with the product branching ratio reported by Koshi et al., because it assigns a different temperature dependence to the product channels HSiOOH + H (R59) and SiH_2O + OH (R60). Thus, the BTW mechanism says that HSiOOH + H is the main channel at room temperature but SiH_2O + OH at elevated temperatures; but that temperature dependence conflicts with Slagle et al. The problem is that the model only reproduced the EH data well if SiH_2O + OH was the dominant channel. Yet it did not appear possible to construct rate constant expressions consistent with both Slagle et al. and Koshi et al. that also make SiH_2O + OH the dominant channel at the temperatures employed by EH.

What are the principal pathways of the mechanism?

Model output included concentration profiles for every species. Thus, it was possible to analyze the output to determine which reaction or reactions were primarily responsible for producing and consuming each species. Piecing together these primary pathways allowed me to construct a simplified route from SiH_4 via several intermediates to the deposited film. This scheme for the BTW model under EH conditions is shown in Fig. 4.

The scheme amounts to a branching chain reaction propagated by OH and SiH_3. SiH_4 was primarily destroyed by OH in a hydrogen abstraction reaction (reaction R13). The resulting SiH_3 radical reacted with O_2 via the flow-through intermediate $xSiH_3O_2$ to regenerate OH and produce SiH_2O (R16 reverse). SiH_2O in turn reacted with H_2O produced from reaction R13 above, yielding HSiOOH and H_2 (R62). Successive removal from HSiOOH of the remaining H atoms by reactions with O_2 (R65 and R67) produced SiO_2, the main film depositing species.* The overall reaction stoichiometry implied by this sequence (assuming that the HO_2 radicals formed in reactions R65 and R67 combine to form H_2O_2 and O_2) is:

$$SiH_4 + 2\ O_2 \rightarrow SiO_2 + H_2 + H_2O_2\ .$$

But in the model, the HO_2 radicals also provide some branching, for some of them can go back to abstract hydrogen from SiH_4 (R15).

This reduced reaction set (including HO_2 self-reaction, and supplemented by

(R23) $SiH_4 \rightarrow SiH_2 + H_2$

to initiate production of reactive intermediates and by

(R11 reverse) $OH + H_2 \rightarrow H_2O + H$

to include all the important reactions controlling OH concentration) was sufficient to capture the main features of the modeled growth profiles presented above. The dependence of the maximum growth rate on both the substrate temperature and the cool wall temperature is small. Its dependence on initial oxygen concentration is small (although, unlike the full model and experiment, positive). And its dependence on initial silane concentration is close to 1.5 order.

How do these pathways differ from those of methane oxidation?

In one sense, comparing principal pathways of methane oxidation and silane oxidation is a bit like comparing apples and oranges, for the two oxidations occur under different conditions. For example, under the concentration and temperature conditions employed by EH, methane oxidation essentially does not occur. To simulate methane depletion comparable to the modeled silane depletion under conditions of identical reactant concentrations, flow velocity, and temperature gradient, a substrate temperature nearly 300 degrees greater was necessary. Under such conditions the main pathway for carbon-containing species was the familiar sequence:

$$CH_4 \rightarrow CH_3 \rightarrow CH_3O \rightarrow CH_2O \rightarrow CHO \rightarrow CO\,[\rightarrow CO_2]\,.$$

(The final product was a mixture of CO and CO_2.) At these temperatures, CH_3 association with O_2 to reversibly form CH_3O_2 was important to the CH_3 budget, but it was essentially a detour from the oxidation path. That is, CH_3O was produced mainly by

$$CH_3 + O_2 \rightarrow CH_3O + O,$$

rather than in a pathway leading through CH_3O_2, such as decomposition of CH_3OOH.

Perhaps a more interesting comparison is to examine the oxidation of *methyl* under CVD conditions. Modeling CH_3 oxidation at these lower temperatures showed a different oxidative pathway for CH_3. Here CH_3 rapidly and reversibly associated with O_2, and the path to further oxidation passed through CH_3O_2, via

$$CH_3 + CH_3O_2 \rightarrow CH_3O + CH_3O\,.$$

Of course generating initial CH_3 concentrations equal to the initial SiH_4 concentrations employed by EH under such mild conditions is unrealistic. Still, the importance of CH_3O_2 to methyl oxidation illustrated in this hypothetical case was also seen in the simulations of ref. 5a, in which much smaller CH_3 concentrations arose from decomposition of $(CH_3)_4Sn$ under CVD conditions. In ref. 5a, the sequence that led to CH_3O was:

$$CH_3 \overset{O_2}{\leftrightarrows} CH_3O_2 \rightarrow CH_3OOH \rightarrow CH_3O\,.$$

Both here and in ref. 5a, the relatively low temperature and substantial pressure favored the associative channel in the reaction between CH_3 and O_2 so much that the chain-branching, oxygen-splitting channel to CH_3O was only a minor, even negligible, producer of CH_3O.

In contrast, neither SiH_3O nor a stabilized SiH_3O_2 played an important role in the fate of SiH_3 in the BTW mechanism under EH conditions or in direct studies of reaction (1). Several groups have reported that reaction (1) exhibits no pressure dependence, at least at the low pressures (less than 27 Torr) studied; they interpret this pressure independence as evidence that formation of a stabilized SiH_3O_2 product is negligible.[7,9] While it is quite conceivable that formation of SiH_3O_2 is negligible at 27 Torr and significant at atmospheric pressure, modeling evidence suggests that this is not the case. I varied the rate constant for SiH_3O_2 formation, and found that when it was a significant channel of the reaction (1), the activation energy of the peak deposition rate was much higher than observed by EH. If SiH_3O_2 played an important role, its decomposition (R36) with a substantial activation energy would contribute to the formation of SiH_2O and subsequent steps on the path to film deposition. Reaction (1) is clearly an important step in silane oxidation, and further study of it is needed, particularly at atmospheric pressure and elevated temperatures.

Conclusion

The BTW mechanism qualitatively reproduced trends observed by EH in the CVD of SiO_2 from SiH_4 and O_2 with respect to temperature, reactant concentration, and flow velocity. A rigorous quantitative comparison of modeled growth profiles to experimental ones must await explicit treatment of the transient temperature field near the reactor inlet. The ability of the BTW mechanism to model CVD data was not lost by changing its rate of SiH_3 association with O_2 to form a flow-through $xSiH_3O_2$, provided that $SiH_2O + OH$ is the ultimate product of the encounter. The reaction of SiH_3 with O_2 is an important step in silane oxidation, and one which differentiates silane oxidation from methane oxidation. The BTW model was consistent witb much but not all the available data on the $SiH_3 + O_2$ reaction.

References

[1]Britten, J. A.; Tong, J.; Westbrook, C. K. *Symp. (Int.) Combust., [Proc.], 23rd* **1990**, 195.

[2]Ellis, F. B., Jr.; Houghton, J. *J. Mater. Res.* **1989**, *4*, 863.

[3]Jachimowski, C. J.; McLain, A. G. NASA Technical Paper 2129: "A chemical kinetic mechanism for the ignition of silane/hydrogen mixtures", 1983.

[4]Goldsmith, N.; Kern, W. *RCA Rev.* **1967**, *28*, 153.

[5a)]Zawadzki, A. G.; Giunta, C. J.; Gordon, R. G. *J. Phys. Chem.* **1992**, *96*, 5369; [b)]Giunta, C. J.; Strickler, D. A.; Gordon, R. G. *J. Phys. Chem.* **1993**, *97*, 2275. The reactions are listed explicitly under the headings "Hydrogen Oxidation Reactions" and "Hydrocarbon Oxidation Reactions" in Table I of ref. 5b.

[6a)]Giunta, C. J.; Chapple-Sokol, J. D.; Gordon, R. G. *J. Electrochem. Soc.* **1990**, *137*, 3237; [b)]Giunta, C. J. Ph.D. Thesis, Harvard University, 1989.

[7]Slagle, I. R.; Bernhardt, J. R.; Gutman, D. *Chem. Phys. Lett.* **1988**, *149*, 180.

[8a]Koshi, M; Miyoshi, A; Matsui, H. *J. Phys. Chem.* **1991**, *95*, 9869; [b]Koshi, M; Nishida, N.; Murakami, Y.; Matsui, H. *J. Phys. Chem.* **1993**, *97*, 4473.
*My implementation of the model allowed SiO_2 as well as every silicon-containing reactive intermediate to deposit if it diffused to the surface. Any partially oxidized silicon intermediates that deposited were assumed to undergo rapid subsequent reaction on the surface to yield SiO_2 film. Unoxidized intermediates like SiH_2 and SiH_3 that deposited were assumed to yield silicon film. Thus, it is not tautologous to state that SiO_2 was the principal depositing species. SiOOH also contributed substantially to the modeled deposit.
[9a]Chasovnikov, S. A.; Krasnoperov, L. N. *Khim. Fiz.* **1987**, *6*, 956; [b]Sugawara, K; Nakanaga, T.; Takeo, H.; Matsumura, C. *Chem. Phys. Lett.* **1989**, *157*, 309.

Figures

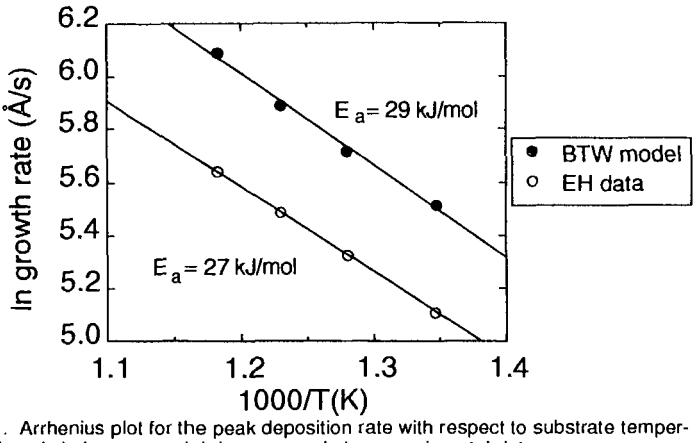

Fig. 1. Arrhenius plot for the peak deposition rate with respect to substrate temperature. Closed circles are model data; open circles experimental data.

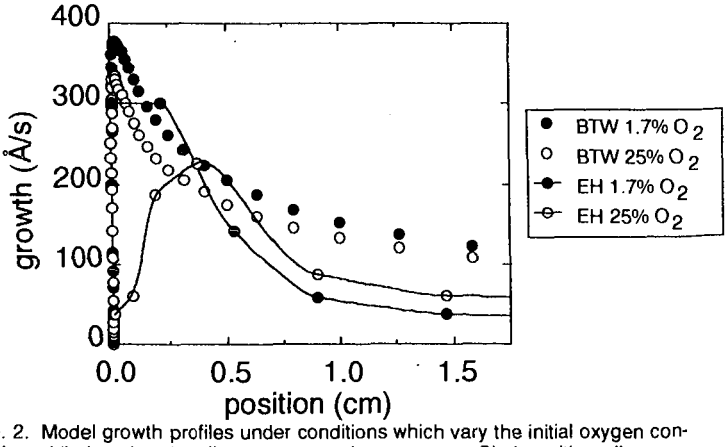

Fig. 2. Model growth profiles under conditions which vary the initial oxygen concentration while keeping the silane concentration constant. Circles without lines are model data; circles with lines are experimental data.

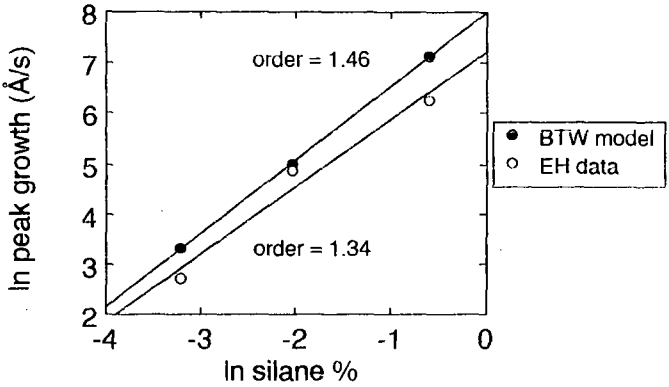

Fig. 3. Plot to determine the order of a possible power law relationship between maximum deposition rate and initial silane mixing ratio. Closed circles are model data; open circles experimental data.

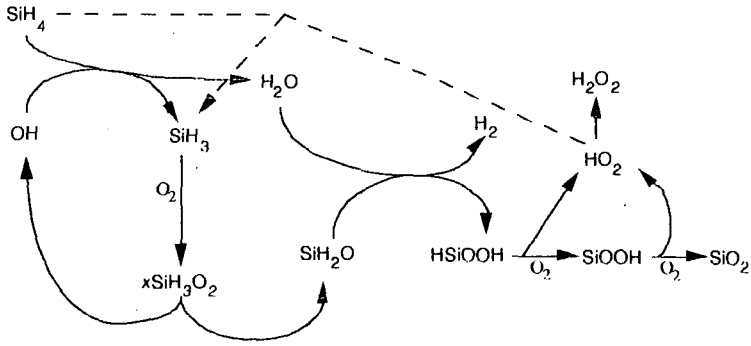

Fig. 4. Major pathways in the BTW mechanism under EH conditions. The solid lines represent primary pathways, and the dashed line branching.

Slagging Behavior of Coal Ash Under Gasifier Environment

Hyung-Taek Kim, Seok-Woo Chung
Department of Energy, Ajou University
5 Wonchen-Dong, Suwon, 441-749, Korea

Shi-Hoon Lee
Korea Institute of Energy Research
P.O.Box 103, Yousung, Daejon, 305-343, Korea

Keywords : Coal Gasification, Slagging, Fusion Temperature

Abstract

For the six different bituminous coals, the fusion temperature and chemical composition of coal ashes are determined. The slagging behavior of each coal ash is estimated by calculating two different slagging parameters. Accurate prediction of slagging behavior with calculated slagging parameters is difficult because of complex ash melting pehavior in the high temperature gasifier environment. It will be suggested that the optimum slagging condition for gasifier operation should be determined by measuring strength and deposition rate of slag in the specially-designed DTF(drop tube furnace) which is simulating 3 T/D BSU entrained-bed gasifier condition.

INTRODUCTION

Recently, thermal power plants in Korea are utilized large amounts of imported bituminous coal for their energy source. Because of different characteristics of imported coal, standard ASTM ash composition measurements are used to predict slagging behavior of coal ash in the power plant. However, the estimation of ASTM method doesn't show actual slagging/fouling behavior of coal ash because of complex ash melting behavior in the high temperature [1].

The objective of this study is to predict slagging behavior of coal ash from its physical and chemical properties and to construct a fundamental database by investigating the relationship of chemical composition, fusion characteractics and deposition strength of coal ash. The experimental results are obtained by utilizing ASTM method as well as DTF(drop tube furnace) which simulating an entrained-bed gasifier's temperature and residence time. The results will be used in determining optimum operating condition of slagging gasifier which is the major part of Integrated Gasification Combined Cycle(IGCC). Another objective of the study is intended to prevent clogging phenomena of gasifier slag at gasfier outlet which occurs due to solidification of melted slag. The result of this study can also contribute to the selection of candidate coal in the 3 T/D BSU(Bench Scale Unit) gasifier which is in the construction stage in Korea.

EXPERIMENTAL METHOD

In the systematic investigation, proximate and ultimate analysis of six different coals are conducted and the results are shown in Table 1. All the coal samples are presently used as fuel in Korean thermal power plant. Rank of the coal samples show wide range between sub-bituminous to bituminous.

Analysis of coal ash characteractics, such as chemical composition and fusion temperature, is performed in order to predict slagging behavior of coal ash. Initially, coal ash samples were made using ASTM standard ashing method [2]. Coals are heated from room temperature to 500℃ during 1 hour, then to 750℃ during 2 hour and leave for no more mass change at 750℃. Chemical composition data of each coal ash is shown in Table 2. The acidic oxide constituents, such as SiO_2, Al_2O_3 and TiO_2 are generaly considered to produce high melting temperatures. Whereas, ash melting temperatures will be lowered proportionally with relative amounts of basic oxides of Fe_2O_3, CaO, MgO, Na_2O and K_2O. Coal ash samples are shown wide range of oxides composition as in Table 2. Counting the fact that coal with low fusion temperature of coal ash has a higher propensity of slagging, it can be

predicted that Alaska coal with low contents of acidic oxide consistents and ROTO coal with high contents of Fe_2O_3 will have a higher slagging behavior than others.

The fusion temperature of each coal ash was also measured by using ash fusion determinator (LECO-600). The cones were manufactured to pyramidal shape, height 19mm, base 6.5mm. The experiment was done with reducing and oxidizing conditions, with preheating temperature of 390℃, start temperature of 538℃, final temperature of 1600℃ and heating rate of 8 ℃/min. The surrouding gases were used of H_2 and CO_2 mixture (50/50) in reducing condition and air is used in oxidizing condition. The result of ash fusion temperature measurement is shown in Table 3. The result of fusion temperature experiments represents same ash fusion behavior as determined by chemical composition data.

RESULTS AND DISCUSSION

Prediction of slagging behavior of coal ash was determined two different methods. Base/acid ratio is to be used as one of the indicators to predict slagging propensity of coal ash, which is defined as follows [3].

$$B/A = \frac{Fe_2O_3 + CaO + MgO + Na_2O + K_2O}{SiO_2 + Al_2O_3 + TiO_2} \quad \text{.....} \quad (1)$$

The calculation of slagging indicators (R_s) using B/A ratio is as follows.

$$R_s = B/A \times \text{Total sulfur} \quad \text{.....} \quad (2)$$

If the R_s value is less than 0.5, the possibility of slagging is low, more than 0.7, the slagging possibility is high and above one, the slagging propensity is severe. The R_s values of the coal ashes used in the experiment are shown in Fig. 1.

The slagging index(F_s) suggested by Gray & Moore is calculated as follows [4].

$$F_s = \frac{4(IDT) + HT}{5} \quad \text{.....} \quad (3)$$

Comparing F_s value with slagging behavior, if F_s value is from 1505℃ to 1615℃, slagging possibility is low, from 1325℃ to 1505℃, slagging possibility is high and less than 1325℃, the slagging possibility is severe level. The F_s values of the sampled coal ashes are shown in Fig. 2. The slagging behavior of Alaska coal and ROTO coal is quite high from the result of F_s value calculation of the candidate coal. For case of NOVA coal, an accurate fusion temperature can't be measured due to fusion temperature exceeds maximum temperature range of ash fusion determinator. But from the result of F_s value calculation, it is thought that NOVA ash sample deosn't show slagging characteristic in gasifier. Furthermore, result of R_s value calculation of the six coals doesn't represent any slagging behavior. But compared with the measurement of fusion temperature, Fs value and chemical composion data show slagging behavior in several coal samples. As a result, Rs values determined by Eqn. (2) and Fs values by Eqn. (3) illustrated somewhat different results of slagging behavior of coal ash.

Up to the present, coal ashes are manufactured by ASTM method and the slagging behavior of the coal ash is predicted by measuring its chemical composion and fusion temperature. But it is expected that the slag produced in actual gasifier is quite different from that by ASTM method. Because of complex processes in gasifier such as, higher heating rate and the volatilization of low melting ash component, precise prediction of slagging should be determined by measuring chemical composition, particle size, deposition rate of the slag produced by DTF, which represents simulated condition of an actual gasifier's temperature, gas compositioin and heating rate. With this finding in mind, a specially designed DTF is constructed to

determine actual slagging behavior of coal ash. It can get a heating rate of 10^4K/sec and maximum temperature of 1900K close to real furnace. The schematic diagram of the DTF system is shown in Fig. 3. Steam generator was added to simulate gasifier condition. Deposit probe is also installed to get slag from main reactor tube. In the DTF, the ash transformation process of original coal is determined by analyzing ash produced with different residence time in DTF experiment. Distribution of inorganic materials in coal and thermal, chemical, physical characteractics of ash is also considered by analyizing molten ash produced by DTF. With deposition probe at the low part of DTF, deposition rate of molten slag is measured and composition, structure and strength of deposited ash on the probe is analyzed. All of the experimental data will be used to establish the ash slagging mechanism in coal gaifier condition.

CONCLUSION

Chemical compositions and ash fusion temperatures were determined for different coals which is presently used in Korean power plant. Relationship between measured value and slagging behavior was evaluated by calculating two different slagging parameters, Rs and Fs. Slagging indicator (Rs) and Fs (slagging index) evaluation result show somewhat contraditory behavior of ash slagging behavior due to standard ASTM ashing method doesn't represent actual gasifier slagging conditon. As a result, precise slagging prediction of coal ash should be done with simulating gasifier condition such as one in DTF.

REFERENCE

1. *The Research of Combustion Characteristics in Domestic Thermal Power Plant*, Korea Institute of Energy Researce, Report, 1993.
2. Clarence Karr, *Analytical Method for Coal and Coal Products*, Academic Press, 1978.
3. J. G. Singer, *Combustion Fossil Power Systems*, Combustion Engineering Inc., 1981.
4. Gray, R.J. and Moore, G.F, *Burning the sub-bituminous coals of Montana and Wyoming in lange uitility boilers*, ASME paper 74-WA/FV-1, 1974.

Table 1. Proximate & Ultimate Analysis of coal Ash samples

Coal	Proximate Analysis				Ultimate Analysis				
	M.	V.M.	F.C	Ash	C	H	O	N	S
ULAN	2.4	30.6	51.3	15.8	81.1	5.0	10.8	1.78	0.86
Palmco	2.6	18.7	63.8	15.4	86.3	4.3	8.2	0.47	0.32
NOVA	2.4	26.6	55.9	15.1	82.8	3.9	9.7	1.88	0.71
C&A	2.4	31.7	51.7	14.0	80.0	5.0	12.6	1.74	0.62
Alaska	16.67	35.1	35.1	8.7	60.5	5.9	30.8	2.19	0.24
ROTO	5.61	46.71	51.76	1.5	69.3	4.7	24.4	1.32	0.27

Table 2. Chemical Composition of coal Ash samples

#	Caol	SiO_2	Al_2O_3	TiO_2	P_2O_5	Fe_2O_3	CaO	MgO	Na_2O	K_2O
1	ULAN	74.2	15.78	0.8	0.13	3.45	1.69	0.5	0.28	0.66
2	Palmco	66.9	20.52	0.92	0.26	4.56	1.49	0.51	0.25	0.72
3	Alaska	49.23	18.13	0.82	0.35	6.08	12.17	2.28	0.47	1.32
4	NOVA	62.53	28.64	1.21	0.29	1.19	0.25	0.26	0.07	1.88
5	C&A	57.75	23.00	1.02	0.44	4.1	2.23	0.94	0.41	1.52
6	ROTO	32.58	27.49	0.25	0.24	21.23	4.11	1.85	0.24	0.87

Table 3. Ash Fusion Temperature of coal Ash samples

	ULAN		Palmco		Alaska		NOVA		C&A		ROTO	
	Ox	Re	Ox	Re	Ox	Re	Ox	Re	Ox	Re	Ox	Re
IDT	1423	1423	1446	1414	1199	1154	>1600	>1600	1452	1373	1395	1204
ST	1478	1457	1494	1478	1222	1197	>1600	>1600	1489	1474	1424	1236
HT	1517	1476	1520	1499	1249	1217	>1600	>1600	1520	1498	1430	1257
FT	1566	1502	1538	1516	1283	1243	>1600	>1600	1541	1523	1437	1271

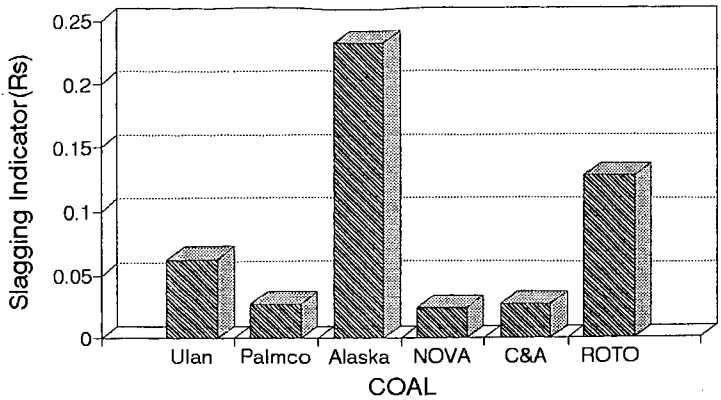

Fig. 1. Slagging Indicator (Rs) values of Six Different Coal Samples

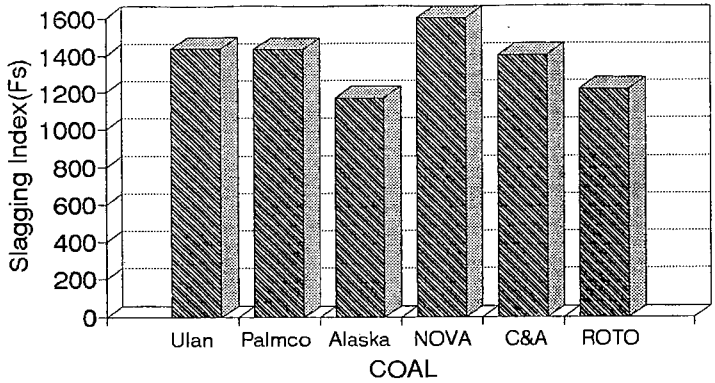

Fig. 2. Slagging Index (Fs) values of Six Different Coal Samples

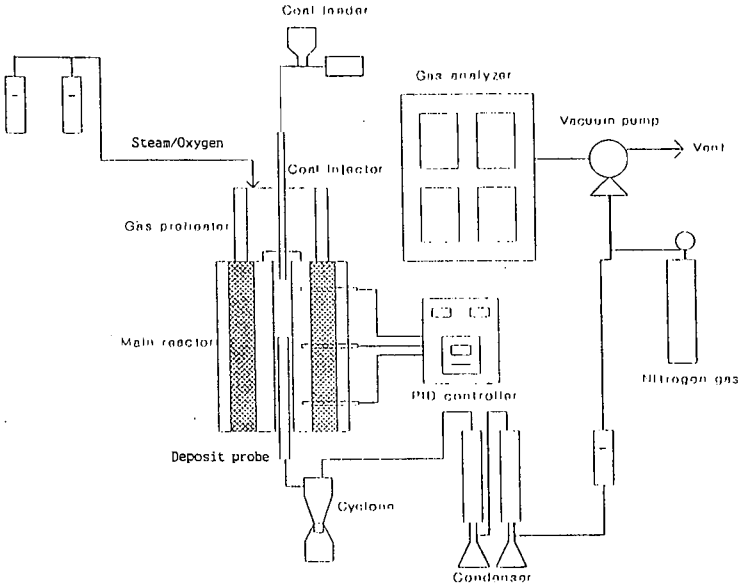

Fig. 3. Schematic Diagram of DTF

ION EXCHANGE AND ABSORPTION TECHNIQUES TO APPLY CATALYSTS FOR LIQUEFACTION OF LOWER RANK COALS

by Karl S. Vorres*, Donald C. Cronauer**, Christine W. Curtis***, and Charles J. Brannan***
* CHM/211, Argonne National Laboratory, Argonne, IL 60439
** Amoco Research Center, P O Box 3011, Naperville, IL 60566
*** Department of Chemical Engineering, Auburn University, AL 36849-5127

ABSTRACT

Samples of Beulah-zap lignite, Black Thunder and Wyodak subbituminous, and Illinois #6 high volatile bituminous coals have been prepared by acid treatment to remove exchangeable cations. Subsequent treatments were made with solutions of catalytic metals including iron or cobalt or nickel to exchange with the acid sites, or with molybdate to adsorb on the surface. Samples were then subjected to liquefaction conditions in microautoclave tubular microreactors and solvent extraction was used to establish total conversion or yields of oils, asphaltenes and preasphaltenes. Results of the liquefaction experiments are compared with the catalyst loadings.

INTRODUCTION

The use of catalysts to improve the liquefaction of lower rank coals has a number of advantages. The disadvantages of cost and recovery of these metals has led to a study of methods of application which can place small amounts of metal on the coal to minimize the cost and need for recovery. A variety of techniques have been used for catalyst application, including blending, "incipient wetness", ion exchange and surface adsorption. This paper provides details of some recent work with the ion exchange and surface adsorption techniques and subsequent liquefaction experiments.

An earlier paper (1) has indicated the value of these techniques, and some structural aspects of ion exchange studies as part of the preparation for catalyst loading.

The coal structure of low rank coals is known to contain reactive functional group types including carboxylate and phenolic. The proportion of these groups decreases with increasing rank. The carboxylates are known to be able to act as ion-exchange materials. The functional groups are frequently linked to a variety of alkali and alkaline earth cations. The inorganic cations can be detrimental due to fouling of boilers during operation or reducing yields for liquefaction.

The latter deleterious effects of calcium in the coal (and any other exchangeable cations) can be overcome by removal of these species. A number of studies have indicated that low rank coals can be treated with acids to exchange the cation species with hydrogen ions (2-4). The cations can then be washed away from the coal to minimize their effect. A sulfurous acid treatment will also remove cations and prepare the the samples for ion exchange (5).

EXPERIMENTAL

Ion Exchange - Acid Washing

The samples were a Black Thunder mine (Wyoming) subbituminous coal and the Argonne Premium Beulah-Zap lignite, Wyodak subbituminous, Illinois #6 high volatile bituminous coals (6).

The acid washing treatments involved the three Argonne coal samples. The -20 mesh samples were dry screened to -20+200 mesh. Weighed amounts (about 30 grams) of the screened samples were slurried with deionized water. Fines (still -200 mesh) were decanted away from the slurry using about 200-600 ml of water. The slurry, containing about 15-20 grams of coal, was washed into a special 50 ml burette. The burette had been fitted with a coarse fritted glass disk at the 50 ml mark to retain the coal

but allow solutions to pass. Fine coal particles had to be removed to avoid pluggage of the frit. A siphon flow provided a uniform flow of 0.1 N HNO_3 (or H_2SO_4 for some of the Wyodak coal) to the sample. Acid flow rates were typically about 1-3 ml/minute and were set according to the ability of the solution to pass through the coal bed. Following the treatment with the acid, the samples were washed with distilled water fed by the siphon, and the record of pH and ion concentration was obtained in a manner similar to that for the acid treatment. The burette tip was fitted with tubing to connect a flow-through pH electrode from Cole-Parmer, or from Microelectrodes, Inc (Londonderry, NH) and with ion-selective electrodes for Ca^{+2}, Na^{+} and K^{+}. The electrodes were used with an Orion EA940 pH meter. The pH meter in turn was connected to an IBM model AT computer for data acquisition. A program was written which allowed data points to be acquired at specific intervals in the range of 10-18 seconds. The data files were then manipulated with a word processor and Lotus 123 macros to permit plots to be drawn of the data.

For the Beulah-Zap and Illinois #6 coals, the calcite reacted with the acid to produce bubbles of carbon dioxide in the column. These bubbles tended to block the flow of acid. Therefore, an initial acid treatment was given before the burette studies for further samples. The acid wash was followed by a water rinse. Three cycles of acid wash and water rinse were used before the catalysts were added to the coals.

The Black Thunder sample was prepared by blending a large sample and screening to obtain a -8+20 fraction. This material was allowed to contact sulfurous acid for 4 hours. The acid and dissolved mineral matter were filtered and flushed with water. Samples of this treated coal were used for the catalyst loading.

Catalyst Loading

Catalyst materials were added by ion exchange or adsorption techniques. For the addition of Fe, Co or Ni, solutions containing 1000 ppm of metal were made up and added to acid washed coal samples. The solution of ferrous sulfate was acidified slightly to avoid precipitation of hydroxide species. The amount of solution used was twice the desired amount to be added for any of Fe, Co or Ni. This amount was added to the coal slurry, stirred well and allowed to exchange for up to about 42 hours. For the addition of Mo, the procedure developed by Schroeder was used (8). The Mo concentration used was 1500 ppm at a pH of 2. The adsorption is relatively rapid and provided the loadings indicated in Schroeder's procedure. Following reaction with the coal the catalyst solution was washed from the coal with several volumes of distilled or deionized water. The weighed solution was then analyzed for concentrations of the catalyst materials. Catalyst loadings were determined from the difference in the amount of material in the initial and final solutions.

Liquefaction Studies

Initial coal samples (comparing raw, water washed and acid washed) were liquefied in tubular microreactors to establish yields based on THF solubility (total conversion) and heptane solubility (oil yield). Conditions were: solvent 1-Methyl Napthalene (non-donor) , 2:1 solvent:coal; 425 C, 30 minute reaction, cold charge at 1000 psi H2, (1700-1800 hot), reactor volume of about 20 cm^3. The reactor charge was 2g of 1-methylnaphthalene as the reaction solvent and 1.33 g maf coal. Later tests with catalyst-loaded samples included 0.67 g pyrene as a test hydrogenation compound.

For the Wyodak samples, some runs were made with a process-derived solvent, designated V1074, obtained from the Wilsonville, Alabama liquefaction pilot plant. A hydrogen donor solvent, dihydroanthracene (DHA), was also used for comparison.

The products from the liquefaction reactions were removed from the reactor with THF. Conversion of coal to THF solubles was determined. In the initial test the residue solubility in heptane was also determined. For the catalyst-loaded samples The amount of pyrene hydrogenation to hydrogenated products that occurred in the reactions was obtained by gas chromatographic

analyses using a Varian Model 3400 equipped with a J&W DB-5 fused silica 30-m column and flame ionization detection.

RESULTS AND DISCUSSION

Ion Exchange

The readings from the electrodes indicated that the coals were washed free of exchangeable cations with the exception of calcium after the first cycle. The calcium came out during the water rinse over a pH range of 1.5-2.5. The possibility of calcium in the clay of the samples is assumed from this data. Additional calcium was removed during the later cycles using either the acid or the rinse water. The final concentrations were micromolar.

Liquefaction Studies

Initial runs were made to compare fresh material from ampules and acid treated Wyodak samples. Samples of the raw coal were compared with both water-washed and acid-washed Wyodak samples. Ash values were also obtained. The water-washed and acid washed samples were dried before the ash determination. The results are summarized below.

Values in %

Coal Sample	moisture	ash	dry ash	reduction
Raw	27.39	6.31	8.69	0
Water washed	6.4	7.81	8.34	4.0
Acid washed	6.96	3.46	3.72	57.2

These microreactor liquefaction results are summarized below.

Raw Sample	THF soluble (total conv.)	Heptane soluble (oil yield)
Raw	55.2,56.1	34
Water Washed	44	27
Acid washed	37	24

The total conversion and oil yields of the three initial samples decreased with the extent of treatment. This effect may be due to the amount of handling, which increases oxidation. The samples were kept under a layer of water to avoid oxidation.

Samples of acid washed Beulah-Zap, Wyodak and Illinois #6 were compared in several solvents.

The results for total conversion are indicated below:

Coal	1 MeNap.	V1074	DHA
Beulah-Zap	73.5	74.1	86.7
Wyodak	71.4	85.9	86.9
Illinois #6	86.4	86.5	86.4

The reaction conditions were: 410°C, 30 min., no catalyst and 1250 psig H_2 introduced at ambient temperature.

The Illinois #6 sample gave consistent relatively high total conversions. This sample had the highest total sulfur content in these coals. For the Wyodak coal the process derived solvent and the hydrogen donor solvent gave very similar total conversions, while the non-hydrogen donor solvent gave lower conversions. For the Beulah-Zap coal, the non-donor solvent and process-derived solvent gave very similar conversions which were less than that obtained with the hydrogen donor solvent, dihydroanthracene (DHA). The DHA gave very similar total conversions with each of the coals. The maf organic sulfur % values for the Illinois #6, Wyodak and Beulah-Zap are: 2.38, 0.47 and 0.70. The pyritic sulfur values are: 2.81, 0.17 and 0.14.

Subsequent catalyst loading produced a series of samples in several batches to give a variety of loadings in the 100-1000 ppm range. These were also run in microautoclave tubing reactors to establish liquefaction yields based on THF solubility (total conversion) and pyrene conversion (catalyst reactivity).

The samples prepared with Ni and Co were run about one month after preparation, and the others about two months after.

The results of duplicate runs are given below:

Sample	1st Cat. Ldg.	2nd Cat. Ldg.	Ave. Coal Conv.	Ave. Pyrene Conv.
Black Thunder				
One catalyst metal				
BT-1-Mo	829		65.5	5.3
BT-1-Fe	548		60.1	3.4
BT-1-Co	212		63.3	2.9
BT-1-Ni	257		64.0	2.6
BT-2-Mo	418		63.3	3.1
BT-2-Fe	483		65.9	3.0
BT-2-Co	83		65.1	2.9
BT-2-Ni	464		66.0	2.9
Two catalyst metals				
Fe-Mo-1	456	210	69.1	5.3
Fe-Mo-2	484	70	66.5	4.8
Fe-Ni-1	408	224	67.5	3.9
Fe-Ni-2	472	106	66.4	4.0
Wyodak Samples				
Wyodak, raw (no washing)	none		71.4	2.0
Wyodak, (nitric acid washed)	none		41.6	3.1
(Sulfuric acid washed)				
WY-Mo	847		74.2	4.5
WY-Fe	552		74.7	3.3
WY-Co	668		53.3	2.5
WY-Ni	822		75.5	3.1

Cobalt was much more difficult to get on the coal than the Fe or Ni. The analyses of metal loadings are good to 10%. Individual determination values ranged up to 4% different from the averages.

For the Black Thunder coal, regardless of the metal type, metal loading or batch, the coal conversion was very similar and ranged for individual determinations from a low of 59% for Fe batch 1 to a high of 70% for Ni batch 2. The coal conversions for the combined metals were slightly higher and less variable than the individual metals. Pyrene conversions tended to be higher for the combined metals than for individual ones.

Wyodak coal which had been acid washed with H_2SO_4, with the exception of the Co treated sample, gave higher coal conversions than the Black Thunder samples. The primary hydrogenation product produced in each reaction was dihydropyrene. The overall conversions do not appear to be as high as reported for a number of other catalyst preparations. The comparison sample of Wyodak which had been acid washed, but with nitric acid, gave substantially lower total conversion. This may reflect the state of oxidation of the coal.

The pyrene conversion, an indicator of hydrogenation activity, was highest for the Mo catalyst preparations.

CONCLUSIONS:

1. Catalytic metals including Fe, Ni and Co as well as Mo can be placed on lower rank coals following an acid wash in a wide range of concentrations.
2. Comparisons of raw, water washed and acid washed subbituminous samples show reduced yields for more significant treatment.

3. The preparations with different catalysts tended to give similar total conversions.
4. Somewhat higher conversions for the Wyodak coal were obtained from samples which had been treated with sulfuric acid to remove exchangeable cations.
5. Conversions were uniformly high with all solvents for the highest rank samples. Lower rank conversions were lower for the non-donor solvent and also, for the lignite, for the process derived solvent.

ACKNOWLEDGMENTS

KSV acknowledges with thanks the support from the U S Department of Energy, Office of Fossil Energy, and data as well as discussions with Anthony Cugini of the US DOE Pittsburgh Energy and Technology Center.

REFERENCES

1. K. S. Vorres, Prepr. Fuel Chem. Div., ACS, 1993, 38 (3) 1045-1051

2. C. Lafferty and M. Hobday, Fuel, 69, 78-83 (1990)

3. C. Lafferty and M. Hobday, Fuel, 69, 84-87 (1990)

4. J. T. Joseph and T. R. Forrai, Fuel, 71, 75-80 (1992)

5. C. J. Brannan and C. W. Curtis, Prepr. Fuel Chem. Div., ACS, 1993, 38 (3) 1001-1007

6. K. S. Vorres, Energy Fuels, 4, 420-426 (1990).

7. K. S. Vorres, Users Handbook for the Argonne Premium Coal Sample Program, 1993, 27, taken from R. D. Harvey, Ill. State Geol. Survey, 1988.

8. K. Schroeder, Prepr. Fuel Chem. Div., ACS 1993, (2) 512

SEDIMENT PRECURSORS IN MIDDLE DISTILLATE FUEL INSTABILITY REACTIONS

George W. Mushrush and Dennis R. Hardy,
Fuels Section, Code 6181, Naval Research Laboratory,
Washington, DC 20375-5342.

Keywords: Fuel Instability, Oxidation, Hydroperoxide, Oxygenates

ABSTRACT

The specific molecules that initiate the reactions that lead to fuel sediments are difficult to isolate chemically. Several diverse mechanisms could be invoked to explain experimental findings: electron transfer initiated oxidation mechanisms, free radical hydroperoxide initiated oxidation mechanisms and soluble macro-molecular oxidation mechanisms. In actual practice, these specific reactions, in addition to many other mechanisms are simultaneously occurring. Results from our experiments demonstrate that acid catalyzed condensation reactions followed by a rapid increase in polarity caused by hydroperoxide induced oxidation steps can mimic the sedimentation processes observed in many middle distillate fuels.

INTRODUCTION

Instability can be thought of as an interactive process involving the four main functional groups listed in Figure 1. The difficulty arises in isolating the chemical importance of each functional group and specific mechanisms to the overall process. It is amazing that less than 1 ppm of the fuel itself is involved in the process that has the potential to be detrimental to a whole storage tank.

Figure 1. Functional Groups Involved in Incompatibility Reactions.

R-C=C-	+ R-N-	+ R-S-	+ R-O-O-
Hydrocarbon	Organo-Nitrogen	Organo-Sulfur	Organo-Oxygen
Alkenes	Indoles	Sulfonic Acid	Hydroperoxides
Indenes	Carbazoles	Thiols	Dissolved Oxygen
Monocyclics	Pyrroles	Disulfides	Carboxylic Acids
Bicyclics	Qinolines	Sulfoxides	Peroxides
Polycyclics	Pyridines	Sulfides	Aldehydes
	Piperdines	Thiophenes	Alcohols

RESULTS AND DISCUSSION

Based on sediment analysis, it is a reasonable contention that the incompatibility of fuels can be explained by the functional groups listed in Figure 1. A myriad of chemical reaction pathways could be derived from these various functional groups in the following mechanisms; the hydroperoxide initiated polymerization oxidation reactions with olefins to produce gums[1]; an electron-transfer-initiated-oxygenation (ETIO)[2], followed by reactions that result in degradation; the hydroperoxide oxidization of organo-sulfur compounds to sulfonic acids which then subsequently catalyze condensation reactions between the other functional groups present leading both to incorporation of heteroatoms and a simultaneous increase in polarity and molecular weight and thus precipitation from the fuel[3]; and finally, the same reaction sequence could be used to describe the soluble macromolecular oxidatively reactive species (SMORS)[4]. The exact chemical composition of the sediment will depend on the chemical composition of the particular fuel. Individual fuels display unique sediments. These functional groups are involved in both chemical and physical processes that leads to deleterious solids. However, certain compound classes are observed to be common to all sediments. Thus, the presence of these hetero-atomic compound classes can be used as incompatibility predictors[5]. All of these processes depend on dissolved oxygen and/or hydroper-oxides to initiate the processes leading to degradation. Remove molecular oxygen and/or hydroperoxides, usually by clay filtration,

and fuel compatibility will improve dramatically[5].

In the sedimentation process, a major unknown is the identity of the soluble precursor to these sediments. Figure 2 illustrates both the chemical and physical processes that lead to sediment formation. These precursors are in the early stages of research. These precursors, SMORS, could be the result of the catalytic cracking process of the petroleum crude. A classical chemistry description of SMORS is that they are derived from monomers in the fuel itself. However, this description fails because of the inability to link any SMORS precursors in the fuel to the insolubles formed in the fuel. If this intermediate could be chemically elucidated, the sedimentation process observed in practically all middle distillate fuels, incompatibility would be better understood[4].

Figure 2. Chemical and Physical Processes that Lead to Insoluble Products

CHEMICAL PROCESSES	PHYSICAL PROCESSES
Fuel Middle Distillate Fuel	**Coalescence** insoluble products 1000 - 5000 °A
↓	↓
Soluble Macromolecular Intermediate fuel oxidation intermediates fuel soluble increasing polarity N, O, and S incorporation	**Surface Effects** Collect on walls and fuel lines
↓	↓
Insoluble Products fuel sediments high heteroatom content Molecular weight >>500	**Temperature Effects** extensive oxidation at high temperatures leads to coking

It is thus easy to imagine the situation in which a blended fuel could pass the required accelerated test method, ASTM D2274, at the refinery, but then form large amounts of insolubles when it reaches the consumer[6]. Because of the increasing use of blended stocks, there is no "one" middle distillate fuel consequently, there is also no "one" mechanism of degradation. However, the mechanism and the functional groups involved will give a general but not specific mode of incompatibility. The key reaction in all incompatibility processes is the generation of the hydroperoxide species from dissolved oxygen. Once the molecular oxygen and/or hydroperoxide concentration starts to increase, macromolecular incompatibility precursors can form in the fuel. Acid/base catalyzed condensation reactions then rapidly increase the polarity, chemical incorporation of heteroatoms, and the molecular weight.

Three related, but separate reaction regimes can be used to explain the chemical incompatibility that is occurring during the different stages that a fuel goes through in its lifetime. At the refinery or in the early life of a fuel, SMORS, incompatibility can best be explained by acid/base catalyzed condensation reactions of the various organo-nitrogen compounds in the individual blending stock themselves. These acid/base catalyzed processes are usually very rapid reactions with practically no observed induction time period. When the fuel is transferred to a storage tank or other holding tank incompatibility can be explained by a second slow mechanism; the free-radical hydroperoxide induced polymerization of active olefins (gums). This is a relatively slow reaction, because the increase in hydroperoxide concentration is dependent on the dissolved oxygen content. These gums can be quite deleterious to combustion machinery. The third incompatibility mechanism involves; the degradation reactions observed when the fuel is stored for one or more years. Extended storage is a common practice for the military. The incompatibility process can be explained by a complicated set of reactions. It involves first the buildup of hydroperoxide moieties after the gum reactions; then a free-radical reaction with the various organo-sulfur compounds present that can be oxidized to sulfonic acids; then reactions such as condensations between organo-sulfur and nitrogen compounds and esterification reactions. This is the slowest of the reactions because of the hydroperoxide induction period and the subsequent oxidation of the

organo-sulfur compounds.

A matrix involving time, temperature, heteroatoms, hydroperoxides, and other reactive species present in fuels in the context of accelerated storage is complicated. Accelerated fuel stability tests are important to both producers and users of fuels so an understanding of these interactions is important. Model dopant studies provide a method for isolating some of these variables. Model studies to define chemical incompatibility work well with gasoline and jet fuels. With chemically more complicated diesel fuels, they are somewhat less reliable. With relatively simple fuel, model studies set the parameters for incompatibility. Thus tests performed to mimic long-term storage give results that are definitive as long as the temperature employed is low enough not to initiate homolytic hydroperoxide reactions (<100°C). Higher temperatures enable storage tests to be completed in the minimum time, a producer advantage. The significance of the accompanying uncertainty of the observed sediment-producing processes in relation to the real ambient storage conditions may be dominant, a user disadvantage. Much of the early work has concentrated on the use of organo-nitrogen and sulfur compounds, both basic and non-basic, as dopants. It was demonstrated that the solid formed from these dopants were similar to the solids obtained from shale liquids themselves. The promotion of sediment formation by these dopants has been reported to be a facile process.

In a series of papers starting in 1987, results were reported that explained some of the inconsistencies observed with deposit formation and sulfur compound interactions[7,8]. The authors show that the stability of an unstable middle distillate fuel was improved by treatment with sodium hydroxide. The subsequent addition of a sulfonic acid, 10 ppm of naphthalene sulfonic acid, restored the instability of the base washed fuel. A linear relationship between deposit formation and sulfonic acid concentration confirms that the formation of a strong acid is a limiting factor in storage instability. Further, the deposits generated by the sulfonic acid treatment were found to be identical from those formed from the fuel itself on storage. It was further reported that the chemical structures observed in the sediment precursors consisted of indoles linked to a phenalene ring system[8]. In the particular diesel fuel studied, phenalene was detected. Oxidation products, i.e., various phenalenones, were observed to increase in concentration as the fuels were aged under ambient storage conditions. This appears to be a major step forward in the chemistry of sediment formation. However, much more study is needed to extend this observation to other middle distillates.

ETIO results are primarily from model systems. No results or sediments based on fuel system ETIO are available. For ETIO to be a viable concept in fuel degradation, two significant phenomena must be operative: a rate law based on oxygen order; lack of chemical response to both amine and phenolic free-radical inhibitors. Other model systems employing 3-methyl indole and the anthraquinone molecular ion have results that show ETIO operating in model systems.

The data in Table 1 show the results for a model system employing 3-methylindole and various acids present as co-dopants. A comparison of the sediment from the undoped to the carboxylic acid doped systems show a remarkable similarly in formula. Infra red and mass spectral results show that the carboxylic acid groups are not incorporated in the sediment[10]. In the case of the strong acid dodecylbenzene sulfonic acid (DBSA) however, the results are quite different. The sediment generated by this acid incorporated the DBSA moiety into the sediment, this was confirmed by ^{13}C nmr and field ionization mass spectrometry.

Table 1. Elemental Analysis Data for Sediments Derived from 3-Methylindole in a Middle Distillate Fuel with Added Co-Dopants

	Percent by Weight					
Co-Dopant*	N	C	H	O	S	Empirical Formula
None	5.36	72.63	5.88	16.13	-	$C_{15.8}H_{15.2}NO_{2.8}$
Acetic aid	5.57	72.72	5.92	15.77	-	$C_{15.2}H_{14.8}NO_{2.5}$
Hexanoic acid	5.65	72.16	5.78	16.41	-	$C_{14.9}H_{14.2}NO_{2.4}$
Decanoic acid	5.81	72.55	5.76	15.88	-	$C_{14.6}H_{13.8}NO_{2.4}$
Dodecylbenzene sulfonic acid	5.10	73.33	8.20	5.65	8.45	$C_{18.4}H_{30.3}N_{1.3}SO_{1.3}$

* Concentration dopants = 3.21×10^{-2} M
3-MI = 450 ppm N

The organo-sulfur moieties that have proved to be the most damaging are the thiols, disulfides and sulfonic acids. These results and those from other studies have indicated that some sulfur compounds might be inhibitors for controlling hydroperoxide formation in middle distillate fuels[9]. However, they control the peroxides by undergoing oxidation to sulfonic acids as depicted in Reaction Scheme 1. Partially oxidized sulfur species such as sulfoxides and sulfones are not generally deleterious[11]. Thiophene related compounds are very resistant to oxidation and are thus harmless in the stability process. Sulfonic acids are the most deleterious dopant that we have studied[11,12]. Thiols are excellent radical scavengers in both fuels and in model fuel systems[12]. The most probable mechanism for the reaction sequence for a thiol involved a hydrogen abstraction step by a t-butoxy radical that was generated from a peroxide species, such as t-butyl hydroperoxide, $t\text{-}C_4H_9OOH$. Once a disulfide is generated, steps [a and b], one or both pathways, [c and e], exists for sulfonic acid formation.

Reaction Scheme 1. Reaction Pathways of Hydroperoxides and Disulfides to Produce Sulfonic Acid

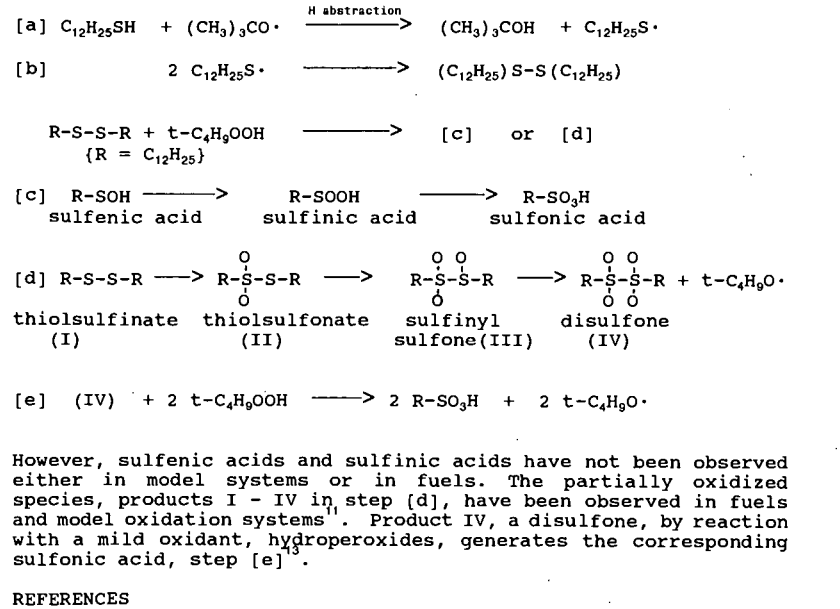

However, sulfenic acids and sulfinic acids have not been observed either in model systems or in fuels. The partially oxidized species, products I - IV in step [d], have been observed in fuels and model oxidation systems[11]. Product IV, a disulfone, by reaction with a mild oxidant, hydroperoxides, generates the corresponding sulfonic acid, step [e][13].

REFERENCES

1. Mayo, F.R., Lan, B.Y., Ind. Eng. Chem. Prod. Res. 26, 215 (1987).
2. Beaver, B.D., Treaster, E., Kehlbeck, J.D., Martin, G.S., Energy & Fuels, 8, 455 (1994).
3. Mushrush, G.W., Hazlett, R.N., Hardy, D.R., Watkins, J.M., Ind. Eng. Chem Res., 26, 662(1987).
4. Hardy, D.R., Wechter, M.A., Energy and Fuels, 4, 270 (1990).
5. Watkins, J.M., Mushrush, G.W., Hazlett, R.N., Beal, E.J., Energy & Fuels, 3, 231 (1989).
6. ASTM, in Annual Book of ASTM Standards; ASTM: Philadelphia, 1993; Part 05.01, ASTM D2274-88.
7. Pedley, J.F., Hiley, R.W., Hancock, R.A., Fuel, 66, 1645 (1987).
8. Pedley, J.F., Hiley, R.W., Hancock, R.A., Fuel, 67, 1124 (1988).
9. Dennison, G.H., Ind. Eng. Chem. 36, 477 (1944)
10. Cooney, J.V., Beal, E.J., Hazlett, R.N., Prepr. Am. Chem.Soc., Div. Pet. Chem., 29, 247 (1984).
11. Mushrush, G.W., Pellenbarg, R.E. Hazlett R.N. and Hardy, D.R., Fuel Science and Technology Int'l., 1991, 9(5), 549.
12. Hazlett, R.N., Schreifels, J.A., Stalick, W.M., Morris R.E., Mushrush, G.W. Energy & Fuels, 5, 269 (1991).
13. Field L. "Organic Chemistry of Sulfur Compounds"; S. Oae, ed., IFI/Plenum: New York, Chapter 7, 1977.

FIELD IONIZATION MASS SPECTROMETRIC ANALYSIS OF THE PHENALENONE-INDOLE COUPLING PRODUCT: THE NATURE OF INSOLUBLES FORMED IN DIESEL OILS

Ripudaman Malhotra,[1] Doris S. Tse,[1] Dennis R. Hardy,[2] George W. Mushrush,[2]
Wayne J. Stallick,[2] and Robert N. Hazlett,[2]
[1]SRI International Menlo Park, CA 94025, and
[2]Naval Research Laboratory, Washington, DC 20036

KEYWORDS: Diesel Storage Stability, FIMS, Indoles, Phenalenones.

ABSTRACT

There is a growing acceptance of the theory that insolubles formed during storage of diesel oils result from the acid-catalyzed coupling of phenalenone and alkyl indoles. Field ionization mass spectrometric analysis of the sediments show prominent peaks due to alkyl indoles as well as those due to coupling products of phenalenone with one, two, three or four alkylindole moieties. However, conspicuous by their absence are peaks due to alkylphenalenes and phenalenones. FIMS analysis of a coupling product of phenalenone with indole, shows a prominent peak at 182 Da, that can be assigned to dihydrophenalenone. Most peaks in the spectrum, including minor ones, lend themselves to straightforward interpretation in terms of the known chemistry of coupling. Peaks corresponding to phenalene with one and two indole units were also prominent in the spectrum. Satellite peaks corresponding to hydrogenation and oxidation products are also present. Their presence indicates a multitude of redox reactions that accompany the coupling.

INTRODUCTION

Storage of diesel fuels often results in the formation of deposits that cause problems with filtration and pumping of the fuels. Furthermore, some soluble gum is also formed that subsequently forms deposits on the hot engine parts causing additional problems. Numerous tests have been developed to predict the tendency of a fuel to form deposits.(1) Often, these tests require stressing the fuel at elevated temperatures, and the relevancy of such tests to storage conditions is not clear. Studies have also been conducted with dopants (2, 3), but again it is unclear whether the deposits formed in the presence of the dopant are the same as those formed under storage. An improved chemical understanding of the nature and causes of deposit formation is clearly needed. Chemical characterization of the sediments is valuable, because the agents reponsible for their formation may be present at extremely low concentration in the fuel, but will necessarily be concentrated in the sediments.

We have previously shown that pyrolysis–field ionization mass spectrometry (Py–FIMS) is very useful in characterizing the deposits formed during storage of fuels.(4,5) We have found that there are a few patterns that repeat in the spectra for sediments from a variety of sources and that the filtered sediments and adherent insoluble gums are very similar in chemical nature with the sediments being enriched in the benzologs of the components in the gum. Peaks due to alkyl indoles are prominent in these spectra, and clusters of peaks corresponding to dimers and higher oligomers are also evident. In accord with the mechanism proposed by Hiley and Pedley (6), most of the prominent peaks in these spectra can be ascribed to the coupling products of phenalenone with one, two, three, or four alkylindole moieties. However, the peaks due to alkylphenalenes and phenalenones themselves are not very intense. In order to better understand the coupling mechanisms, we have prepared acid-catalyzed coupling products of indole and phenalenone, and examined it by field ionization mass spectrometry. Our objective was to determine if indeed the coupling product of phenalenone and indole does not give a strong peak signal corresponding to phenalene or phenalenone.

EXPERIMENTAL

Coupling Reaction. Coupling product of indole and phenalenone (perinaphthenone) was prepared by adapting the procedure of Pedley and Hiley (6) for the synthesis of 2-methylindolylphenalene. Approximately 0.66 mmol indole was stirred overnight with an equivalent amount of phenalenone in the presence of *p*-toluenenesulfonic acid (also 0.66 mmol) in methanol. The product was treated with excess potassium bicarbonate and extracted with ether. The mixture of coupling products was recovered by evaporating the ether.

Pyrolysis/Field Ionization Mass Spectrometry (Py/FIMS). The technique of field ionization (FI) consists of passing vapors of the material to be analyzed through a region of intense electric field.(7) This mild technique for ionization results in the formation of only the molecular ions for most compounds, and because the ionization is generally not accompanied with any fragmentation it is particularly useful for analyzing complex mixtures. The FIMS system used in this study has been described elsewhere.(8) It consists of an activated tantalum foil field-ionizer interfaced with a 60° magnetic sector mass analyzer and a PDP 11/23 computer for data acquisition and processing. Approximately 50 μg of the sample is introduced via a heatable direct insertion probe. Mass spectral data of the evolving volatiles are collected by repeatedly scanning the magnet over a preset range while the sample is gradually heated from the initial temperature (sometimes as low -78°C) to approximately 500°C. At the end of the run, the sample holder is retrieved and

weighed to determine the fraction that was devolatilized during the analysis. All the samples examined in this study were essentially 100% devolatilized during analysis. For a given sample, many spectra are collected, each representing a certain range of temperature. The individual spectra are added to obtain a spectrum of the total volatiles and produce a thermal evolution profile of total volatiles as well as of any given mass peak.

RESULTS AND DISCUSSION

The FI-mass spectrum of the coupling product of indole (117 Da) and phenalenone (180 Da) is shown in Figure 1. This spectrum represents the sum of sixteen spectra (each comprising eight scans) collected during the heat up from ambient to 500°C. Because field ionization is generally not accompanied by fragmentation, the multitude of peaks in this spectrum corresponds to either multitude of compounds in the product, or extensive fragmentation due to pyrolysis in the FIMS probe. It is therefore instructive to examine the mass spectral data as a function of the probe temperature.

The spectrum of species that evolved almost immediately upon introduction of the probe into the inlet is shown in Figure 2a. This first set of peaks are at 117 Da (indole) and at 165, 166 (phenalenyl radical, and phenalene), and at 180 and 182 (phenalenone and dihydrophenalenone). The dihydrophenalenone peak is substiantially more intense than that due to the parent phenalenone. A possible explanation is that the phenalenone underwent coupling, but the dihydro analog, which cannot undergo Michael addition, survived. Surprisingly, there were also peaks at 195 and 196 Da. The peak at 196 is most likely the methyl enol ether of the dihydrophenalenone, which was probably formed because the coupling was conducted in methanol as solvent. The peak at 195 Da is corresponding stable radical. The stability of the phenalenyl system is well recognized, and it is noteworthy that the radical species were seen with both phenalene and the enol ether; the latter being also capable of forming a phenalenyl radical with the loss of a hydrogen.

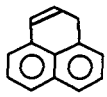

Phenalene (166)

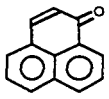

Phenalenone (180)

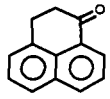

Dihydrophenalenone (182)

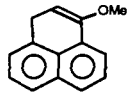

Dihydrophenalenone-enol methyl ether (196)

The fact that phenalene and dihydrophenalenone evolved at almost ambient temperatures suggests that they were present in the product mixture and were not a result of some thermal cracking of coupling products. This result further reinforces the facility with which phenalenone systems can undergo redox reactions (disproportionations), and lead to a multitude of products.

Upon warming the sample, the intensity of the peaks due to indole and phenalene and its analogs decreases, and a new set of peaks centered around 300 Da begins to evolve. They correspond to the coupling products of one phenalene and one indole residues. A representative spectrum is shown in Figure 2b. The simple coupling product of phenalenone and indole has a molecular weight of 295 (180 + 117 -2 = 295). Indeed, the peak at 295 is the most intense peak in the spectra acquired between 120 and 240°C, as well as in the sum spectrum (Figure 1). This peak is also accompanied by phenalene and the dihydrophenalenone analogs at 281 and 297 Da respectively. There is also a peak at 311, which is most likely due to the methyl ether of the corresponding enol. As before, strong peaks due to the phenalenyl radicals are present for the phenalene and the enol ether analogs of the coupling product. The coupling product is also accompanied by a dihydro derivative of the phenalene analog at 283 Da.

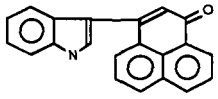

Indolenylphenalenone
(295)

A similar pattern peaks around 410 Da for the bisindolenylphenalenones emerges as the sample is further heated to above 200°C (figure 2c). For the trisindolenylphenalenones, which also evolve in the 200 to 300°C range, however the expected peak at 325 Da (180 + 3 × 117 - 6) is not present to any significant extent. The peaks due to other analogs are present in reasonable intensity.

In the case of fuel sediments, similar peaks have been observed in their FI mass spectra.(5) However, we were not sure whether the products were present as simple oligomers or whether the oligomers were a result of thermal fragmentation of a polymer. Results obtained here show that the vaporization of the dimers and trimers in the FIMS probe occurs around 200 to 250°C. This temperature range corresponds well with the temperature at which these species evolved from the fuel sediments. Hence, we believe that, in the fuel sediments too, the dimers and trimers are present as such.

As mentioned above, the peak due to indole evolved at almost ambient temperatures. This peak was present in the spectra collected up to about 80°C, and was due to indole trapped in the product. The indole peak again appeared above about 180°C along with the evolution of coupling products.

This result suggests that at these temperatures, some of the coupling products do fragment to liberate indole fragments.

CONCLUSION

We have prepared an acid-catalyzed coupling product from the reaction of indole with phenalenone and analyzed it by FIMS. The mass spectrum shows the presence of the expected indolenylphenalenone, bisindolenylphenalenone, trisindolenylphenalenone, and so on. It also shows peak corresponding to redox derivatives and methyl ethers. The temperature resolved mass spectral data are consistent with simple evaporation of the oligomers and not due to thermal fragmentation.

REFERENCES

1. See, for example, **2nd International Conference on Long Term Storage Stabilities of Liquid Fuels, Conference Proceedings**, Southwest Research Institute, October 1986.
2. F. R. Mayo and B. Y. Lan, *I & E. C. Prod. Res. & Dev.* **1986**, *25*, 333.
3. (a) J. V. Cooney, E. J. Beal, and R. N. Hazlett, *Preprints, Am. Chem. Soc., Div. Petro. Chem.* **1983**, *28*, 1139.

   (b) J. V. Cooney, E. J. Beal, and B. D. Beaver, *Preprints, Am. Chem Soc., Div. Fuel Chem.* **1985**, *30*(2), 303.
4. R. Malhotra and G. A. St.John, **2nd International Conference on Long Term Storage Stabilities of Liquid Fuels, Conference Proceedings**, Southwest Research Institute, October 1986, p. 327.
5. R. Malhotra and G. A. St.John, **3rd International Conference on Stability and Handling of Liquid Fuels, Conference Proceedings**, The Institute of Petroleum, London, September 1988, p. 525.
6. J. F. Pedley and R. W. Hiley, **3rd International Conference on Stability and Handling of Liquid Fuels, Conference Proceedings**, The Institute of Petroleum, London, September 1988, p. 510.
7. H. D. Beckey, **Field Ionization Mass Spectrometry**, Pergamon Press, Elmsford, N.Y., 1971.
8. G. A. St.John, S. E. Buttrill, Jr., and M. Anbar, in **Organic Chemistry of Coal**, J. Larsen, Editor, A.C.S. Symposium Series 71, Washington, DC, 1978, p. 223.

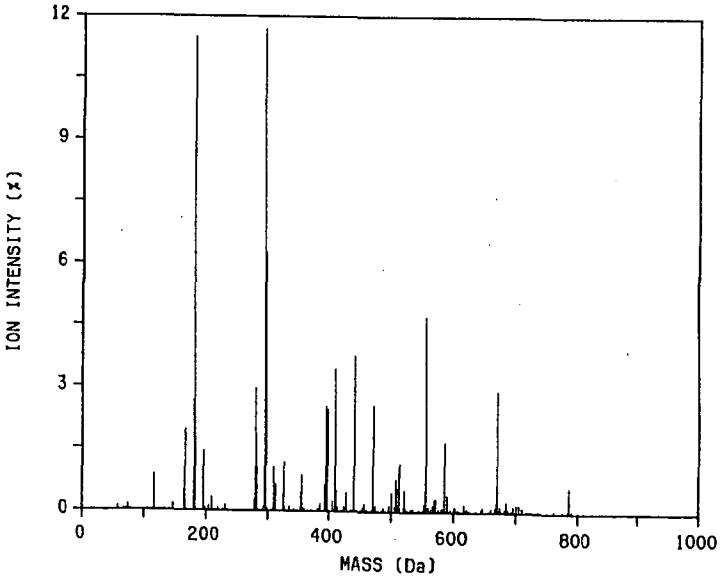

Figure 1. FI mass spectrum of the total volatiles from phenalenone-indole coupling product collected from 30 to 500°C.

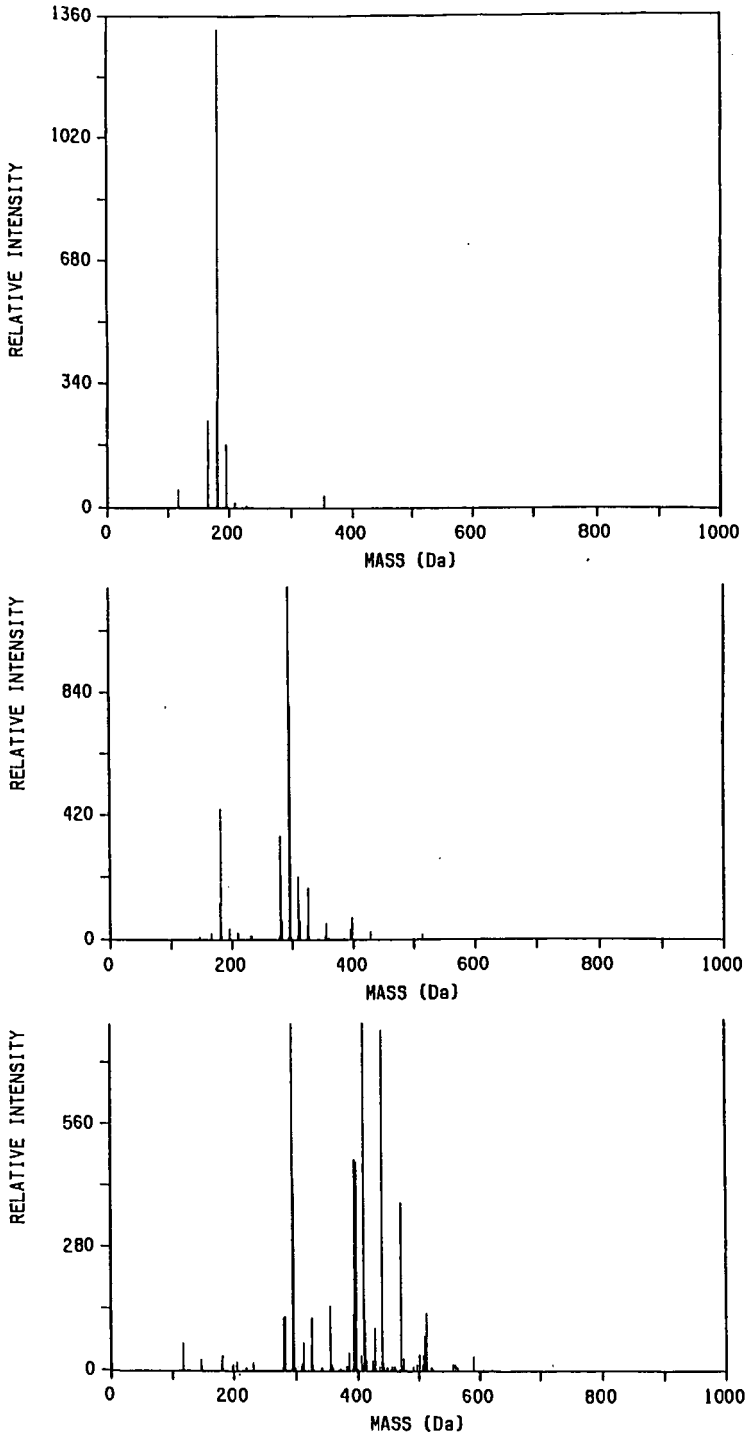

Figure 2. FI mass spectrum of the volatiles from the phenalenone-indole coupling evolving in the temperatures ranges (a) 46651°C (b) 148 to 165°C, and (c) 211 to 238°C.

CHARACTERIZATION OF SOLUBLE MACROMOLECULAR OXIDATIVELY REACTIVE SPECIES (SMORS) FROM MIDDLE DISTILLATE DIESEL FUELS: THEIR ORIGIN AND ROLE IN INSTABILITY

Dennis R. Hardy and Margaret A. Wechter*
Navy Technology Center for Safety and Survivability
U.S. Naval Research Laboratory
Washington, D.C. 20375-5000
*and The University of Massachusetts Dartmouth
N. Dartmouth, MA 02747

INTRODUCTION In diesel fuels which are oxidatively unstable and at least 6 months old, it has been shown that a solid phase can be isolated from the filtered fuels by methanol extraction followed by precipitation with hexane. The weight of this material is directly proprotional to the amount of sludge which forms by both accelerated storage stability tests and by continued field aging of the fuels. We have suggested that the presence of this extraction induced precipitate (EIP) or fuel Soluble, Macromolecular, Oxidatively Reactive Species (SMORS) in these fuels thus accounts for the production of thermally induced precipitate (TIP) or insoluble sediment during oxidative aging of diesel fuels.[1,2,3] In this paper the acronym EIP will be used in place of SMORS in most cases.

This paper describes and summarizes the characterization studies performed to date on the EIP from representative fuels which are all greater than 6 months past production. The origin and apparent role of SMORS in sediment formation in diesel fuels is discussed.

EXPERIMENTAL All procedures for filtering fuels, and for extraction and precipitation steps used in isolating the EIP from fuels have been described in detail elsewhere.[1,2]

GC analysis was performed on samples dissolved in methanol using a Hewlett-Packard Model 5890 GC equipped with flame ionization detector and HP Model 3392 integrator. A 50-m methylated silicone (nonpolar) capillary column was used for separation. Experimental conditions included an inlet temperature of 280 °C, a split ratio of 22:1 and a column temperature program between 100 °C and 280 °C. A 1-min initial hold at 100 °C was used; the temperature was then ramped at 5 °C/min to 280 °C and then held at that temperature for 10 minutes.

The field ionization mass spectral (FIMS) system used for this work has been described elsewhere.[4,5] At the end of each run, the sample holder is retrieved and weighed to determine the fraction that was volatilized during the pyrolysis.

Low voltage electron impact, high resolution mass spectrometry was used to determine the exact masses of several of the key fragment ions, when the EIP was introduced by pyrolysis (identical to the FIMS sample introduction).

Elemental analyses and molecular weight determinations by vapor pressure osmometry were provided by commercial laboratories. All elements including oxygen (but not sulfur) were determined by combustion and not by difference.

All blended stocks used were prepared in the laboratory as 80/20 straight run/LCO mixtures (v/v). Blends were always filtered before extraction. The straight run fuel used was a water-white, clear stock obtained from the same refinery that furnished LCO-3. All fuels and blends are described in earlier papers in this series[1,2,3] and a consistent fuel code has been continued.

RESULTS AND DISCUSSION **Elemental Analyses/Molecular Weights by Vapor Pressure Osmometry.** Table 1 summarizes the elemental analysis data (CHON) obtained for solids (EIP) extracted from 3 light cycle oils (LCOs) and 5 blends. Data are as received and not normalized to 100%. The elemental analysis results for 20% LCO/80% SR EIP from blends is shown in the bottom half of Table 1. Here it is interesting to compare the blends to the LCO's. In general the EIP from blends have somewhat higher oxygen and lower carbon content indicating that EIP from blends is more polar than from LCO's. If higher polarity equates to higher chemical reactivity, then this finding supports the long-known fact that blending reactive LCO's with non-reactive SR streams does not usually dilute the sludge forming tendencies in a direct ratio. With very reactive LCO's, dilution by as much as 70%

SR sometimes has no effect on reducing sludge formation amounts in the resulting blends.[6] It is noteworthy that these blends are made up immediately before the EIP is isolated for elemental analysis and thus the chemical changes in elemental analysis are due to the blending process itself and not any subsequent aging of LCO EIP in the resulting blend.

Table 2 presents a summary of the blend data from Table 1 for EIP which is normalized to 100% in order to determine an empirical formula. Data for typical average elemental analyses of TIP or sediment is given also.[7] The trend for blend EIP to contain more oxygen is continued in the TIP and this is reflected in the average empirical formula which contains an additional CH_2 + H_2O compared with typical EIP.

Included in Table 3 are molecular weight data obtained by vapor pressure osmometry. Note that these data are quite consistent with the molecular weight data obtained by size-exclusion chromatography (570 vs 600-900) considering errors inherent in, in particular single point VPO determinations and in size-exclusion data for molecular weights <1000 Da. for molecular shapes which are likely to be quite different from those of the standards used.

Gas Chromatography. When EIP samples are isolated from the methanol extract and then re-dissolved in methanol they may be subjected to analysis by GC. The dissolved EIP gave surprisingly simple chromatograms with no major peaks that would correspond with any of the moieties commonly thought to be precursors to instability. This led to the conclusion that the methanol fraction contained the presence of higher molecular weight species which were not eluted under the standard experimental GC conditions employed. This also demonstrates very clearly that the EIP does not contain any entrapped fuel species. This is an important fact in the subsequent interpretation of the PYR/FIMS data.

Pyrolysis/Field Ionization Mass Spectrometry (PYR/FIMS). Two representative EIP samples were chosen for PYR/FIMS analysis. These were LCO-3 and LCO-5. The EIP were isolated as a solid powder and then completely dissolved in toluene in order to introduce a homogeneous sample into the glass capillary for pyrolysis field ionization MS. Most of the toluene was removed by evaporation and then the remaining solid sample of EIP was heated at a controlled rate up to 500° C in the high vacuum source region of the MS. Subsequent weighing of the capillary tube revealed that essentially 100% by weight of the EIP had been pyrolyzed and volatilized by this procedure. Identical analyses of TIP/sludge generally show that less than 60% of the sample is consumed after pyrolysis leaving considerable char in the sample tube.

Representative data for LCO-3 are shown in Table 4. Residual toluene solvent is not shown in the figure but volatilized between approximately 30 and 125° C. Since no other ions up to 300 daltons were seen in this region it can be concluded that the original EIP samples were essentially free of entrapped fuel. In addition, as noted above, GC analysis of EIP which are re-dissolved in methanol reveal no entrapped fuel components.

The total ion mass chromatograms for the pyrolysis FIMS are quite complex. This underscores the tremendous amount of pyrolysis that the EIP samples are undergoing. At the same time it is noteworthy that the entire sample is volatilized/pyrolyzed in a fairly narrow range from 175 to 375° C. The calculated number average molecular weight of the LCO-5 EIP by this process is 582 daltons and the calculated weight average molecular weight is 687. This is in fairly good agreement for the VPO determined molecular weight of this sample (see Table 3).

Due to the complexity of presenting the data in the form of mass pyrograms for subsequent interpretation, an alternative approach has been taken. About half of the total ion current of the mass pyrogram is contained in a number of series of homologous ions separated by 14 dalton increments. These homologous ion series have been arbitrarily assigned a mass identification number, usually one of the lowest mass ions in a particular series. In the case of data for Table 4 only the most intense ion in a particular series was used to generate the temperature profile. In the case of data for Table 5 the sum of all the ions in a particularly identified ion series was determined. The mass intensity values in all cases have been taken from normalized spectra. In addition, the base peaks for all three spectra (in ion counts) were very close in intensity. For this reason the ion counts were not converted to percent relative abundance as is normally done but instead are converted to a normalized ion count. At this point it is possible to attempt a more detailed analysis of the nature of the EIP sample as revealed by the mass pyrogram in Table 4. The 9 ion series identified account

for the 9 most intense sets of masses. Most of the mass peaks in Table 4 are pyrolysis fragments of the high molecular weight EIP. This is supported by the fact that the major series below 300 daltons continue to form over the entire temperature range between 90 and 360° C. As the temperature of the pyrolysis increases the pyrolyzate fragments of higher molecular weight begin to appear (between 300 and 600 daltons) up to temperatures of 400° C.

As conjectured in an earlier paper in this series[1], one of the two possible alternative origins of EIP is that a fuel soluble macromolecular species (possibly porphyrinic in nature) is carried over into the fluid catalytic cracker by the feed stock and ends up in the product blending stream. This macromolecular species could then further oxidize (making it more polar and soluble in methanol, at which point it is EIP). Finally further oxidation and condensation reactions with reactive fuel monomers precipitates the final product insoluble sediment or sludge.

Since the above conjecture rests upon a geochemical/processing origin one would then expect that the EIP from various sources would be somewhat similar at least in gross structural features. The PYR/FIMS data for the two LCOs given in Table 5 strongly indicates that this alternative origin for EIP is probably not correct. Although there are some strong similarities in the three EIP samples such as the mass series at 131 and 309, there exist major dissimilarities. In addition to this, a common geochemical origin for EIP would be porphyrinic in nature and the PYR/FIMS fragments of such an EIP moiety would result in significant amounts of pyrrolic species evolved below 300 daltons and these do not occur.

The traditional explanation for the origin of TIP/sludge or sediment postulates reactive monomeric fuel components which oxidize and condense to form larger and more polar and less fuel soluble species. The fact that the EIP species must themselves further oxidize and condense to form TIP/sludge means that we now have a probe of some intermediate stage in sludge formation from reactive fuel monomers which is itself a simpler species compositionally and is much more amenable to analysis. In fact, the EIP themselves are simply produced by reactive fuel monomeric species. This last statement suggests that the detailed chemical nature of the EIP and the sediment itself must be quite fuel dependent and the data in Table 5 support this very clearly.

This information together with the fact that the PYR/FIMS data clearly support the elemental analysis data of the EIP which implicates nitrogen and oxygen containing compounds underscores the need to continue to determine the precursors of EIP in the original fuel. The fact that EIP are formed from reactive fuel monomers implies that freshly refined LCO's will not initially have EIP present and this is the subject of our current investigations. If an LCO or LCO blend has formed as little as 20 mg/L of EIP, then the LCO itself is probably of little use in studies designed to determine the compositional precursors of either EIP or TIP/sludge. It is for this reason that many very carefully performed studies to date have not been able to pinpoint the real precursors of sludge formation. Certainly if an LCO contains high total nitrogen or indoles content it also contains the real precursors to sludge. These indicators, however, are not able to be directly or quantitatively linked to any given fuel's sludge forming tendency.

<u>CONCLUSIONS</u> All of the EIP samples analyzed for this work were from fuels which had already developed EIP, i.e., they were at least 6 months old since production. Molecular weights from VPO and PYR/FIMS were all consistent in the range of 650 to 1000 daltons. The EIP have proven to be considerably easier to analyze than the actual sludge which they apparently produce ultimately.

Since it has been shown that the EIP do not arise as a geochemical/processing artifact it can be concluded that they arise from the oxidation and condensation of reactive fuel monomers. Clues as to the nature of these fuel species are found in the elemental analysis and empirical formulas for EIP which indicates much involvement of oxygen and nitrogen. Further information from the high resolution mass spectral empirical formulas and from the PYR/FIMS indicates that nitrogen containing precursors in the fuel with a formula of $C_nH_{2n-9}N$ and C_nH_{2n-15} are involved in the generation of EIP. The 2n-9 class includes such isoelectronic possibilities as indoles, divinyl pyridines and dihydroquinolines. The 2n-15 class includes such isoelectronic possibilities as benzoindoles, phenalidines, divinyl quinolines and carbazoles.

The EIP are more amenable to PYR/FIMS analysis as evidenced by their complete pyrolysis than the more highly oxidized and polar TIP/sludge. Even so, the PYR/FIMS technique subjects the EIP to a tremendous amount of pyrolysis. Because of this the interpretation of pyrolyzate ions to reconstruct the formation of EIP is not possible.

Only freshly refined, unhydrotreated, catalytically cracked LCO material will be suitable for future studies involving the determination of the fuel precursors of EIP and whether the formation of EIP can be inhibited by antioxidant additives. Essentially no work on the determination of fuel precursors to sludge to date has appreciated the importance of this fact. Certainly no work presented to date has verified the initial absence of EIP before beginning a detailed compositional analysis and this is essential. By the time a measurable amount of EIP has formed, it is quite possible that all of the actual precursors to sludge are already well on their way to the dimer/trimer stage and hence no longer amenable to simple GC analysis techniques to monitor their depletion from the fuel.

REFERENCES

(1) Hardy, D.R.; Wechter, M.A. Energy Fuels **1990**, 4, 270.
(2) Wechter, M.A.; Hardy, D.R. Fuel Sci. Technol. Int. **1989**, 7(4), 423.
(3) Wechter, M.A.; Hardy, D.R. In Proceedings of the 4th International Conference on Stability and Handling of Liquid Fuels; Giles, H.N., Ed.: DOE/CONF-911102; U.S. Department of Energy: Washington, D.C. **1992**; 620.
(4) Malhotra, R.; Hazlett, R.N. In Prepr. Pap. Am. Chem. Soc., Div. Fuel Chem. **1990**, 35, 1163.
(5) Malhotra, R.; Hazlett, R.N. In Proceedings of the 4th International Conference on Stability and Handling of Liquid Fuels; Giles, H.N., Ed.: DOE/CONF-911102; U.S. Department of Energy: Washington, DC, **1992**; 518.
(6) Hazlett, R. N., Fuel Sci. Technol. Int. **1988**, 6, 185.
(7) Beal, E.J.; Cooney, J.V.; Hazlett, R.N.; Morris, R.E.; Mushrush, G.W.; Beaver, B.D.; Hardy, D.R. Mechanisms of Syncrude/Synfuel Degradation, Report DOE/BC/10525-16, NTIS, Springfield, VA, **1987**.

Table 1. Elemental Analysis of Selected EIP. Direct determination of CHON.

Fuel Code	Fuel Type	% C	% H	% O	% N	% Total
LCO-2	100% LCO	79.4	6.1	9.9	2.5	97.9
LCO-3	100% LCO	83.2	6.5	4.6	4.8	99.1
LCO-5	100% LCO	84.2	6.7	3.1	5.6	99.6
B-2	20% LCO	75.3	6.1	10.1	4.9	96.4
B-5	20% LCO	79.4	6.3	7.5	3.0	96.2
B-5*	20% LCO	75.2	6.4	9.8	5.5	96.9
B-13	20% LCO	76.5	6.4	9.1	4.9	96.9
B-14	20% LCO	76.5	5.8	10.4	3.3	96.0

*EIP determined after ASTM D5304 stress test.
Fuel Code is: LCO = catalytically cracked light cycle oil
B = blend of 20% LCO + 80% SR v/v

Table 2. Elemental Analysis Averages (normalized to 100%) for a wide range of 20% LCO blends for EIP and Sediment. Empirical formula also computed from these data.

Property	EIP	Sediment/TIP
% Carbon	79.4	75.4
% Hydrogen	6.4	6.9
% Oxygen	9.7	13.7
% Nitrogen	4.5	4.0
Empirical Formula	$C_{21}H_{20}O_2N$	$C_{22}H_{24}O_3N$

Table 3. Molecular Weight Analysis by Vapor Pressure Osmometry (VPO) for selected EIP samples (in Daltons).

Fuel Code	Single Point	Triple Point
LCO-3	513	525
LCO-5	486	679

Table 4. EIP of LCO-3 analyzed by pyrolysis FIMS. Mass ID referred to the major mass in that homologous mass series from the pyrolyzate. As the temperature of the sample is raised from 100 to 400 C the major ion intensities (raw data counts) are summed for that temperature range. (-) indicates a value close to zero ion counts.

Mass ID	Probe/Sample Temperature Range °C						
	90-150	164-201	203-250	254-299	303-355	359-399	SUM
131	1.2	2.8	4.5	2.2	0.6	0.1	11.4
180	4.0	6.5	1.0	-	-	-	11.5
181	1.5	1.1	1.0	0.6	0.3	-	4.5
202	0.7	1.2	0.3	-	-	-	2.2
309	0.3	0.9	3.7	1.5	0.4	-	6.8
438	-	0.4	5.2	6.1	1.5	0.1	13.3
563	-	-	0.7	9.7	12.5	2.1	25.0
580	-	-	3.5	4.2	0.5	0.5	8.9
581	-	-	2.2	3.4	1.0	0.7	7.3
SUM-->	7.7	12.9	22.1	27.7	16.8	3.5	90.9

Table 5. Pyrolysis FIMS comparative analysis of several EIP solids. The major homologous series are identified by a mass which is generally the highest in the series, but not always. Compare these values for the sum of the homologous series for the entire pyrolysis temperature range to the totals for an individual mass given in Table 4. Compound type empirical formulas for the ion series given is from independent high resolution exact mass (to 10^{-4} mass units) data.

Mass Series ID	Empirical Formula	LCO-3	LCO-5
131	C_9H_9N	34	21
156	---	0	20
180	$C_{13}H_{10}N$	28	51
181	$C_{13}H_{11}N$	14	57
202	---	5	24
261	---	0	0
309	$C_{22}H_{15}NO$	19	35
438	$C_{31}H_{22}N_2O$	41	54
563	---	78	9
580	---	25	0
581	---	23	0

STORAGE STABILITY OF DIESEL FUEL PRODUCED FROM BRAZILIAN CRUDE - CHEMICAL MODIFICATION DURING AGEING AND THE EFFECT OF HYDROTREATING ON FUEL STABILITY

Helineia O. Gomes and Rosana C. L. Pereira
PETROBRÁS Research Center - Ilha do Fundão, Quadra 7
Rio de Janeiro, Brazil 21949-900

Keywords: diesel fuel, stability, hydrotreating

INTRODUCTION

The growing need for diesel fuels and developments in refining processes, particularly the increased use of Fluid Catalytic Cracking (FCC), have led refiners to introduce Light Cycle Oil (LCO) in diesel formulations. Unfortunately, the cracking products, which contain chemically unstable species (1,2), induce changes in color and insolubles formation, even when diluted by blending. The insolubles are known to cause operability problems in diesel engines (3).

Degradation mechanisms are complicated and not well understood. It seems that oxidation plays a determining role (4). Acids such as carboxylic, sulfonic and phenolic, produced by oxidation of fuels have been considered to exert a catalytic effect on the quantity of sediment formed (5). It was demonstrated that aromatic compounds and non-basic nitrogen compounds are also involved in sediment formation (6). Pedley et al. (7,8) found that a major source of strongly colored sediments could be the reaction of oxidized products with alkyl indoles, yielding addition products that precipitate under the influence of sulfonic acids, produced by oxidation of thiols.

The nitrogen compounds present in LCO were largely identified (9) and included anilines, alkyl indoles and alkyl carbazoles. It seems that only the alkyl indoles are subject to changes during degradation in storage (10).

A large number of tests have been used to predict stability of middle distillates. The ASTM D 4625 has widespread acceptance for its good correlation with storage at ambient conditions (11). The new accelerated test method, ASTM D 5304, shows excellent correlation with lower temperature tests (12).

The principal processes used to improve fuel stability include hydrotreatment and the use of additives. Schrepfer et al. (13) reported that although hydrotreating is the most effective method of minimizing stability problems, it is also the most costly.

Some characteristics of Marlim crude oil such as high nitrogen content and low middle distillate yield, have led us to anticipate problems on diesel stability with the begining of Marlim oil processing.

The purposes of this study were to estimate the impact on storage stability behaviour of diesel fuels and to evaluate : 1- the effect of the mildest Petrobrás hydrotreatment unit on fuel stability, in particular with respect to non-basic nitrogen compounds; 2- the influence of hydrotreating and the use of additive; 3- the changes in phenalenone, pyrrolic nitrogen, basic nitrogen, mercaptans, alkyl indoles, acidity during ageing at 43 °C for periods of up to 12 weeks.

EXPERIMENTAL

Nine experimental diesel fuel samples were made up from several streams obtained in the Marlim crude processing. Their composition is shown in Table 1. The physico-chemical characteristics of selected samples are shown in Table 2. A total of 20 liters of each component was stored at low temperature under nitrogen blanket to prevent degradation before analyses.

Effect of hydrotreating on fuel stability

Hydrotreating was performed on two feedstocks, a straight run distillate (A2) and a blend (A2/B), in the following operating conditions: LHSV: 1,5 h^{-1} ; Temperature: 320 °C; H_2 Partial pressure: 29 bar. The method ASTM D 5304 (Assessing Distillate Fuel Storage Stability by Oxygen Overpressure) was used to evaluate the effect of hydrotreating on improving fuels stability.The reported total insolubles values are averages of duplicate analyses. Additionally, color determinations were made before and after ageing according to ASTM D 1500.

The "pyrrolic" nitrogen compounds were separated from the samples by HPLC using basic and acidic alumina columns, based on procedures described by Boduszynski (14). The

isolated compounds were identified by GC/MS. The quantification was conducted by GC-FID using carbazole as internal standard.

Kinetics of ageing at 43 °C in air

In order to better understand the mechanisms of sediment formation in fuels produced from Marlim oil, kinetic analyses were performed in the raw LCO (B) and in the three following blends:A1/A2/B; A1/A2/AD-B; A1/HT-(A2/B). An antioxidant containing terciary amines and metal deactivator in its formulation was added to the hot LCO. Storage stability of each fuel sample was assessed by ASTM D 4625 (Distillate Fuel Storage Stability at 43 °C for 12 weeks). The reported total insolubles values are averages of triplicate analyses. Additionally, color determinations were made before and after ageing according to ASTM D 1500.

To follow the kinetics of the blends a total of 1000 ml of each fuel was placed in amber glass bottles of the same volume and the bottles closed with vented screw caps. Six bottles of each fuel were aged concurrently in a dark room at 43 ± 1 °C, in contact with atmospheric air, for periods of up to twelve weeks. After every two weeks, one bottle of each fuel was removed and allowed to cool to ambient temperature. All samples were protected from light before, during and after ageing. The filterable insolubles were determined by vaccum filtration of 300 ml of each aged fuel, through two preweighted cellulose acetate filters (0,8 µm porosity). The filters were then rinsed with isooctane to remove traces of fuel, removed from the filter support assembly, oven dried (90 °C), cooled to ambient temperature in a desiccator and reweighted. The fuel samples were also analysed for color degradation, changes in phenalenone, pyrrolic nitrogen, basic nitrogen, mercaptans, alkyl indoles and total acid number.

The concentration of phenalenone was determined by normal phase HPLC with UV detection and direct injection of the sample, based on procedure described by Marshman (15). Concentrations of phenalenone up to 0,5 mg/l could be determined by this methodology.

The changes in alkyl indoles were monitored using a capillary gas chromatograph (CG) with selective detection by isobutane chemical ionization mass spectrometry (16). The method is based on the fact that the carbazole remains relatively unaffected during ageing, as verified by some authors (10). The evolution of alkyl indoles was then determined through changes in the ratios of alkyl indoles/carbazole peak areas.

RESULTS AND DISCUSSION

Effect of hydrotreating on fuel stability

The effect of hydrotreating on fuel stability assessed by ASTM D 5304 is presented in Table 3. The degrees of hydrodesulfurization (HDS) and hydrodenitrification (HDN) are also indicated. The hydrotreating process improved color stability of both samples, however complete stabilization was not achieved. On the other hand, the A2/B blend was stabilized in terms of insolubles formation.

As can be seen in Table 4, the alkyl indoles were partially removed while the alkyl carbazoles remained in the original levels. Additionally, a decrease in other species such as acids and mercaptans, that are supposed to contribute to degradation, was observed. Based on these results, it is confirmed that alkyl indoles and acidity play an important role on sediment formation and that stabilization of the fuel can be achieved by hydrotreating even at mild severity, without requiring total removal of nitrogen compounds. Under low H_2 partial pressure, the fuel chemical composition is not deeply modified, mainly with regard to nitrogen and aromatic content.

Kinetics of ageing at 43 °C in air

The results related to color changes and total insolubles formation using ASTM D 1500 and ASTM D 4625 are presented in Figures 1 and 2, respectively. The raw LCO (B) is unstable mainly with respect to color degradation. A low formation of insolubles were observed, with the majority of insolubles in the adherent form. This behaviour drastically changed when the raw LCO was added to straight run distillates (A1,A2), as can be seen through the A1/A2/B blend results. In this sample, there was extensive formation of insolubles (mostly filterable insolubles) and color degradation. The contribution of the straight run distillates components in terms of acidity seems to exert a great influence on the sediment formation. From the results of the blend with additive it can be concluded that the antioxidant was ineffective on improving fuel stability. On the other hand, the blend containing hydrotreated components exhibited satisfactory results with total insolubles content of 0,2 mg/100 ml. The color degradation was minimized but was not completely eliminated.

The results obtained from the kinetics of ageing are summarized in Table 5. As can be seen, the phenalenone concentrations increased rapidly during the first two weeks of ageing, levelling off thereafter in the following samples: B, A1/A2/B and A1/A2/AD-B. It is difficult to conclude if this stabilization was a result of the balance between consumption and production of phenalenone during the overall mechanism of sediment formation or was due to occurrence of degradation before the ageing at 43 °C. There appears to be a correlation between color degradation and phenalenone concentration since color degradation also reached the maximum value during the first two weeks. All the samples exhibited decrease in the pyrrolic nitrogen concentration and in the ratio alkyl indoles/carbazole. The decrease agrees with the relationship between the reactivity of the alkyl indoles and the filterable insolubles formation. According to this observation it can be concluded that: 1- the degradation mechanism proposed by Pedley et *al.* seems to be the major source of sediment formation in samples containing LCO, 2- the additive tested was ineffective to prevent phenalene oxidation and the progressive consumption of alkyl indoles. Hydrotreating appears to remove phenalenes since phenalenones were not detected in A1/HT-(A2/B) blend. The decreases in the pyrrolic nitrogen and in the ratio alkyl indoles/carbazole were also verified in a lower extent comparing to the others samples. The mercaptans and the total acid number remained pratically inalterated during the ageing. These observations suggest that exists a correlation between the insoluble formation and the alkyl indoles disappearance and that other *different mechanism* of degradation from the proposed by Pedley takes place. It confirms, as previously demonstrated by some authors (17), that the removal of phenalenes, indoles or acids, will result in a stable fuel.

CONCLUSIONS

On the whole, the experimental fuels obtained from Marlim oil presented poor stability. The addition of light cycle oil in the straight run distillate, to increase the yield of diesel fuel, was not satisfactory inducing higher levels of insolubles and color degradation.

The results of ASTM D 4625 and kinetics study showed that the additive was ineffective on preventing phenalene oxidation and the progressive disappearance of alkyl indoles. Similar levels of insolubles formation and color degradation was verified in the fuel in presence and absence of the additive. In both samples it seems that the major mechanism of degradation was similar to the proposed by Pedley et al..

The hydrotreating, even at mild operating conditions, improved substantially the stability properties of the fuel. Under the tested conditions the hydrodenitrification was not complete, just only partial alkyl indoles elimination has occured. Hydrotreating also appears to remove species that are considered to contribute to the degradation of the fuel, such as, acids, mercaptans and phenalenes. This study suggests that in this case, other mechanisms of degradation are taking place and confirms earlier findings that the major mechanism of fuel degradation depends above all on the composition of the fuel.

REFERENCES

(1) Lee, G.H. and Stavinoha, L.L., "Insoluble Gum Formation in Middle Distillate Fuels" 1st International Conference on Long-term Storage Stability of Liquid Fuels, Tel Aviv, 1983.

(2) Schrepfer, M.W., Arnold, R.J. and Stansky, C.A., "Distillate Stability Ensured by Testing and Treatment" Oil and Gas Journal, Vol 3, pp 79 - 84, 1984.

(3) Halsall, R., "Effects of an Unstable Diesel Fuel on Injector Coking and Vehicle Performance" 2nd International Conference on Storage Stability of Liquid Fuels, San Antonio (Texas), pp 722 - 737, 1986.

(4) Taylor, W.F. and Frankenfeld, J.W., "Chemistry and Mechanism of Distillate Fuel Stability" 2nd International Conference on Storage Stability of Liquid Fuels, San Antonio (Texas), pp 496 - 511, 1986.

(5) Hazlett, R.N. and Power, A.J., "The role of Phenols in Distillate Fuel Stability" 2nd International Conference on Storage Stability of Liquid Fuels, San Antonio (Texas), pp 556 - 569, 1986.

(6) Bhan, O.K., Brinkman, D.W., Green, J.B., Carley, B., "Storage Stability of Marine Diesel Fuel" Fuel, Vol 66, pp 1200 - 1214, 1986.

(7) Pedley, J.F. and Hiley, R.W., "Investigation of 'Sediment Precursors' Present in Cracked Gas Oil" 3rd International Conference on Stability and Handling of Liquid Fuels, London, pp 495 - 509, 1988.

(8) Pedley, J.F. and Hiley, R.W., " Synthesis of 'Sediment Precursor' Compounds and Simulation of Sediment Formation in Cracked Gas Oil Using Model Systems" 3rd International Conference on Stability and Handling of Liquid Fuels, London, pp 510 - 524, 1988.

(9) Dorbon, M. and Bernasconi, C. "Nitrogen Compounds in Light Cycle Oils. Identification Consequences of Ageing" Fuel, Vol 68, pp 1067 - 1074, 1989.

(10) Dorbon, M. and Bernasconi, C., "Storage Stability of Fuels. Identification of Nitrogen Compounds and their Evolution During Ageing in Absence and Presence of Additives" ACS Division of Fuel Chemistry, pp 1135 - 1155, 1990.

(11) Marshman, S.J. "Prediction of Storage Stability of Middle Distillate Fuels Using a Rapid Colorimetric Method" 4th International Conference on Stability and Handling of Liquid Fuels, Orlando, pp 594 - 604, 1991.

(12) Hardy, D.R., Hazlet, R.N. , Beal, E.J. and Burnett, J.C., "Assessing Distillate Fuel Storage Stability by Oxygen Overpressure" Energy Fuels, Vol 3, pp 20 - 24, 1989.

(13) Schrepfer, M.W., R.J. Arnold and C.A. Stansky, "Distillate Stability Ensured by Testing and Treatment" Oil and Gas Journal, Vol 3, pp 79 - 84, 1984.

(14) Boduszynski, M.N., "Composition of Heavy Petroleums. 2. Molecular Characterization" Energy and Fuels, Vol 2(5), pp 597 - 613, 1988.

(15) Marshman, S.J., "Liquid Chromatographic Determination of Phenalenone in Middle Distillate Fuels" Fuel, Vol 69, pp 1558 - 1560, 1990.
(16) Dizidic, I., Balicki, M.D., Rhodes, I.A.L. and Hart, H.V., "Identification and Quantification of Nitrogen and Sulfur Compounds in Catalytically Cracked Heavy Gas Oil by Isobutane/CI GC/MS and GC using Selective Detectors" Journal of Chromatographic Science, Vol 26, pp 236 - 240, 1988.
(17) Marshman, S.J., "Storage Stability of Middle Distillate Fuels: Degradation Chemistry of Catalytically Cracked Gas Oil Blends" 4th International Conference on Stability and Handling of Liquid Fuels, Orlando, pp 489 - 502, 1991.

Table 1 - Composition of the samples

Samples	Composition
A1	100 vol. % straight run distillate
A2	100 vol. % straight run distillate
HT-A2	100 vol. % hydrotreated A2
B	100 vol. % raw catalytically cracked cycle oil (LCO)
A2/B	84 vol. % A2 + 16 vol. % B
HT-(A2/B)	Hydrotreated A2/B
A1/A2/B	36 vol. % A1 + 54 vol. % A2 + 10 vol. % B
A1/A2/AD-B[a]	36 vol. % A1 + 54 vol. % A2 + 10 vol. % AD-B
A1/HT-(A2/B)	36 vol. % A1 + 64 vol. % HT-(A2/B)

a - hot LCO plus additive (terciary amines and metal deactivator)

Table 2 - Physico-chemical characteristics

Characteristics	Method	A1	A2	HT-A2	B	A2/B	HT-(A2/B)
Specific gravity at 20/4 °C	ASTM D 1298	0,8544	0,8940	0,8918	0,9438	0,9060	0,8986
Distillation IBP/EBP, °C	ASTM D 86	217/313	110/402	132/ -	208/314	208/402	230/ -
Color	ASTM D 1500	1,0	2,5	L 1,5	4,0	3,0	1,5
Total acid number, mg KOH/g	ASTM D 974	0,54	1,50	0,02	0,04	1,10	0,04
Sulfur, wt. %	ASTM D 2622	0,33	0,58	0,21	0,70	0,69	0,16
Mercaptans, mg/kg	ASTM D 3227	10	26	7	28	30	8,2
Total nitrogen, mg/kg	ASTM D 4629	110	1100	1000	2000	1200	980
Basic nitrogen, mg/kg	UOP 269	110	515	530	445	470	430
Pyrrolic nitrogen, mg/l	UOP 278	-	18,1	16,7	889	170	99,2
% C aromatic	NMR	-	20,1	21,8	83,8	31,7	27,5

Table 3 - Stability of hydrotreated fuels

Heteroatoms removal	A2	HT-A2	A2/B	HT-A2/B
HDN, %	-	9	-	18
HDS, %	-	64	-	68
Stability test - ASTM D 5304				
ASTM color before test	L 2,5	L 1,5	L 3,5	L 1,5
ASTM color after test	L 8,0	L 3,5	L 8,0	L 3,5
Total insolubles, mg/100 ml	0,7	0,5	8,2	0,6
Pass/Fail criteria (max.)	IT 4,0	mg/100 ml	Color after	3,0

Table 4 - Changes in pyrrolic nitrogen compounds with hydrotreating

Compounds, µg/g	A2	HT-A2	A2/B	HT-(A2/B)
Alkyl indoles	ND[b]	ND	2022	1061
C_0[a]	ND	ND	41	7
C_1	ND	ND	327	82
C_2	ND	ND	722	294
C_3	ND	ND	669	441
C_4	ND	ND	263	237
Alkyl carbazoles	2328	2074	2111	1916
C_0	ND	ND	55	49
C_1	81	66	168	174
C_2	350	313	395	355
C_3	685	615	571	498
C_4	832	750	644	593
C_5	380	330	278	247

a - Subscript designates total number of carbons in alkyl groups.
b - non detected.

Table 5 - Ageing kinetics at 43 °C

Characteristics		B	A1/A2/B	A1/A2/AD-B	A1/HT-(A2/B)
ASTM color	0	L 5,0	L 3,0	L 3,0	L 2,0
	W 2	D 8,0	L 7,5	L 8,0	L 2,5
	E 4	D 8,0	D 8,0	L 8,0	L 3,5
	E 6	D 8,0	D 8,0	D 8,0	L 3,5
	K 8	D 8,0	D 8,0	D 8,0	L 4,0
	S 10	D 8,0	L 8,0	L 8,0	L 3,5
	12	D 8,0	L 8,0	D 8,0	L 3,5
Filterable insolubles, mg/100ml	0	0,4	0,0	0,5	0,2
	W 2	0,2	3,2	3,3	0,3
	E 4	0,7	3,8	4,6	0,1
	E 6	0,9	5,2	5,8	0,5
	K 8	0,4	2,8	1,6	0,0
	S 10	1,1	5,5	2,8	0,5
	12	1,6	6,9	7,8	0,4
Basic nitrogen, mg/kg	0	600	425	380	365
	W 2	525	350	415	330
	E 4	415	370	390	350
	E 6	460	430	425	360
	K 8	400	350	360	300
	S 10	565	360	375	330
	12	550	365	370	320
Pyrrolic nitrogen, mg/l	W 0	737	83,4	87,1	66,8
	E 2	743	71,4	78,8	63,3
	E 4	749	65,3	70,6	65,7
	K 6	696	63,0	64,3	62,4
	S 8	744	59,2	69,1	63,4
	10	680	57,4	60,3	61,2
	12	686	57,1	56,1	59,6
Mercaptans, mg/kg	0	13	17	23	7,5
	W 2	5,0	15	15	7,5
	E 4	5,5	14	14	7,5
	E 6	5,5	11	12	7,5
	K 8	3,0	9,0	9,0	6,0
	S 10	3,0	9,0	9,0	7,0
	12	3,0	8,0	7,0	7,0
Total acid number, mg KOH/g	0	0,01	0,98	0,98	0,20
	W 2	0,02	0,94	0,93	0,18
	E 4	0,02	1,05	1,05	0,18
	E 6	0,02	0,95	0,95	0,19
	K 8	0,02	0,95	0,94	0,17
	S 10	0,02	0,93	0,92	0,20
	12	0,04	0,95	0,94	0,19
Phenalenone, mg/l	0	49,9	5,1	4,3	< 0,5
	W 2	169,4	8,0	9,2	< 0,5
	E 4	269,4	7,4	8,2	< 0,5
	E 6	294,8	7,1	8,1	< 0,5
	K 8	291,7	6,9	7,6	< 0,5
	S 10	296,9	7,0	7,8	< 0,5
	12	285,8	7,0	8,4	< 0,5
Alkyl indoles/ carbazole	0	98,7	48,5	50,3	26,5
	W 2	82,7	39,4	38,3	24,2
	E 4	72,8	37,5	33,5	25,1
	E 6	-	-	-	-
	K 8	77,3	35,2	28,6	22,2
	S 10	-	-	-	-
	12	64,5	32,5	26,4	21,0

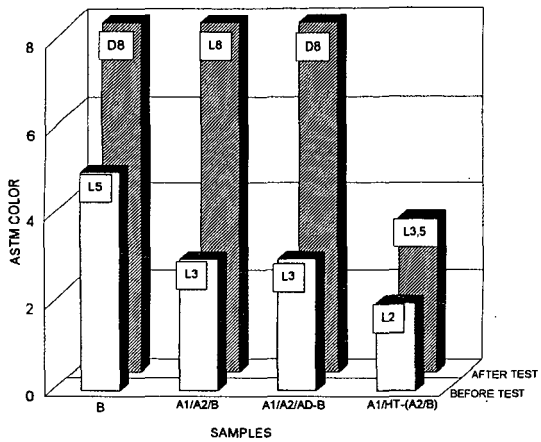

Figure 1 - Results of color changes before and after ASTM D 4625

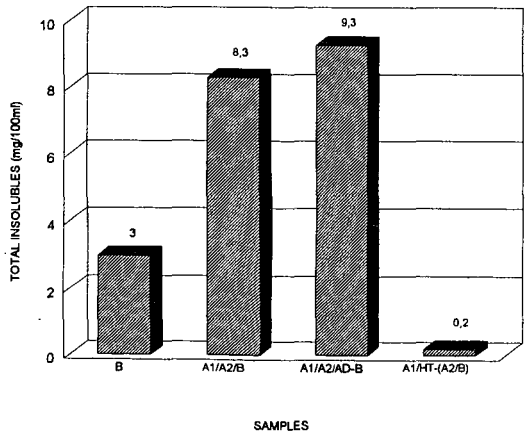

Figure 2 - Results of total insolubles of ASTM D 4625

STUDIES ON THE STABILITY AND SEDIMENT PRECURSORS IN VISBREAKER MIDDLE DISTILLATE.

Yogendra K.Sharma, Hem C.Chandola, Krishna M.Agrawal and Indra D. Singh.

INDIAN INSTITUTE OF PETROLEUM, DEHRADUN 248005 ,INDIA

Keywords : Middle distillate, Stability, FTIR

ABSTRACT

Diesel fuels, particularly those incorporating secondary processed stocks, can degrade during long term storage. The degradation products can cause plugging of fuel filters and blockage of engine components. In the present paper, stability of a middle distillate cut of visbroken product from a refinery unit, before and after extraction with methanol under ambient storage conditions, has been determined. Methanol extraction has been found to reduce the tendency of the fuel to form insolubles significantly and it also separates out sediment precursors. The sediment precursors responsible for the instability of the fuel obtained under different conditions of extraction were characterized for their functional groups by FTIR. Effect of blending the sediment precursors into a typical feed stock on the stability under accelerated aging has also been studied.

INTRODUCTION

Visbreaking is not only used for reducing the viscosity and pour point of heavy fuel oils and residues but also produces relatively cleaner feed stocks for catalytic cracking units. Middle distillates from visbreakers are blended with diesel pool, which enhances the stability problem. Recently Wechter & Hardy [1] and Sharma & Agrawal [2-3] have reported that methanol extraction removes the major portion of sediment precursors in case of light cycle oil (LCO) and total cycle oil (TCO).The present paper reports the stability behaviour of a visbreaker middle distillate from a refinery stream and the effect of methanol extraction, particularly fuel to methanol ratio on the removal of sediment precursors. These sediment precursors have also been characterized using FTIR technique and the effect of different doses of total sediment precursors on sediment formation determined.

EXPERIMENTAL

The storage stability of the visbreaker middle distillate fuel was determined in terms of total insolubles after keeping it for 3,6,and 9 months under ambient conditions.Sediment (insoluble) precursors were separated from the fuel using methanol in sample to solvent ratio 5:1, 5:3, 5:5 and 5:10 by vol,till a neutral (stable) fuel is obtained .The fuel solvent mixture was shaken manually for 10 minutes and was kept over night for separating the fuel and solvent layer.Methanol was recovered from the upper layer by distillation to get the insolubles / sediment precursors (SP1, SP2, SP3 and SP4) as residue. Figure-1 presents the scheme employed for the above extraction.

These residues were characterized by FTIR as thin films obtained from evaporating their solutions in dichloromethane on KBr plates. Different fuels obtained after removing the sediment precursors during consequent extraction were stored under ambient conditions for 7 months and total insolubles were determined. Total sediment precursors SP (SP1+SP2+SP3+SP4) were doped in stable fuel(F4) in different concentrations and their stability was determined by modified UOP-413 accelerated test method (100 psi pressure of oxygen, 4 hours, 100 °C). Physico-chemical properties of visbreaker middle distillate and total sediment precursors were determined using standard IP/ASTM methods.

RESULTS AND DISCUSSION

The physico-chemical properties of fuel and total sediment precursors are

reported in Table- 1 while total insolubles yield under ambient storage conditions are presented in Figure-2. Physico-chemical data of visbroken middle distillate (Table 1) reveals that the fuel is quite unstable due to presence of higher bromine number, sulphur and nitrogen content (more than 50% of nitrogen basic in nature).This trend is supported from the insoluble yield obtained from this fuel under ambient storage for different time intervals, which shows an increasing trend (Figure-2) upto 9months (maximum storage time in the present study).

The elemental composition of total sediment precursors indicate that nitrogen and sulphur containing aromatic structures are predominantly responsible for sediment formation.This is supported by H/C atomic ratio (1.36 as compared to 1.63 in fuel).

Figure-1 shows that the sediment precursors yield is increasing with decreasing fuel to solvent ratio (F/S). It has been observed that with F/S 5:10 ratio (at fourth stage) most of the precursors are extracted out and the fuel becomes practically stable during ambient storage of seven months. This has been confirmed by keeping the fuels (F,F1,F2,F3, and F4) for seven months under ambient storage conditions and determining the yield of insolubles .Total insolubles obtained from different fuel (F1,F2,F3,and F4) under ambient storage of seven months are shown in Figure-3. It has been observed (Figure-3) that total insolubles decreases slowly in F1, F2, and F3, while in F4 the decrease is quite significant and fuel becomes practically stable.

This fuel (F4) has further been doped with different concentrations (1, 3 and 5 % wt/vol) of total sediment precursors (SP) and stability determined by modified UOP-413 accelerated test method. The results obtained are presented in Figure.4, which reveal that the sediment yield increases with increase of sediment precursors added. Further, it is also observed from the Figure-4 that the added precursors are more effective in sediment formation compared to those present in the original fuel.

The FTIR spectra of different precursors (SP1, SP2, SP3 and SP4) are mainly of same nature. The bands at 749, 811 and 875 cm^{-1}(with decreasing relative intensity) are observed in all the precursors, showing the same type of substitution pattern on aromatic ring . The broad OH/NH streching bands around 3300 cm^{-1} and broad carbonyl band at around 1700 cm^{-1} are found to decrease in intensity from SP1 to SP4. The absence of band at 720 cm^{-1} (due to n-paraffinic $(CH_2)_n$, $n \geq 4$) and relatively stronger band at 1456 cm^{-1} due to $-CH_2$ bending indicates the presence of significant concentrations of naphthenic structures in all the precursors.

The study thus indicated that repeated methanol extractions are required for getting the stable fuel from visbreaker middle distillate product.

ACKNOWLEDGEMENT :

The authors are thankful to their colleagues Dr O.S Tyagi & Mr G.M.Bahuguna for providing the IR spectra.

REFERENCES

1. Wechter,M.A. & Hardy,D.R., Fuel Science & Technol, International. **7**, 423, (1989)

2. Sharma, Y.K. & Agrawal, K.M., Fuel **73**, 269 (1994)

3. Sharma, Y.K., Chandola, H.C., Agrawal, K.M. & Singh.I.D., Fuel science & Technol.International (1994) In press.

TABLE- 1 Characteristics of visbreaker middle distillate and total sediment precursors

Visbreaker Middle Distillates		**Total Sediment precursors (SP)**	
Density, D15	0.8617	C, % Wt	85.40
Bromine number	20.7	H, % Wt	9.65
Nitrogen Total, ppm	237.3	S, % Wt	3.46
Sulfur Total,% wt	1.65	N, % Wt	0.36
Nitrogen Basic, ppm	138	O, % Wt	1.23
Carbon residue, %wt	0.04	Nitrogen Basic, ppm	932
C,% wt	83.95	Molecular Weight	274
H,% wt	11.40	Atomic H/C ratio	1.36
Atomic H/C ratio	1.63		
Molecular weight	255		
Boiling range, °C	176-393		

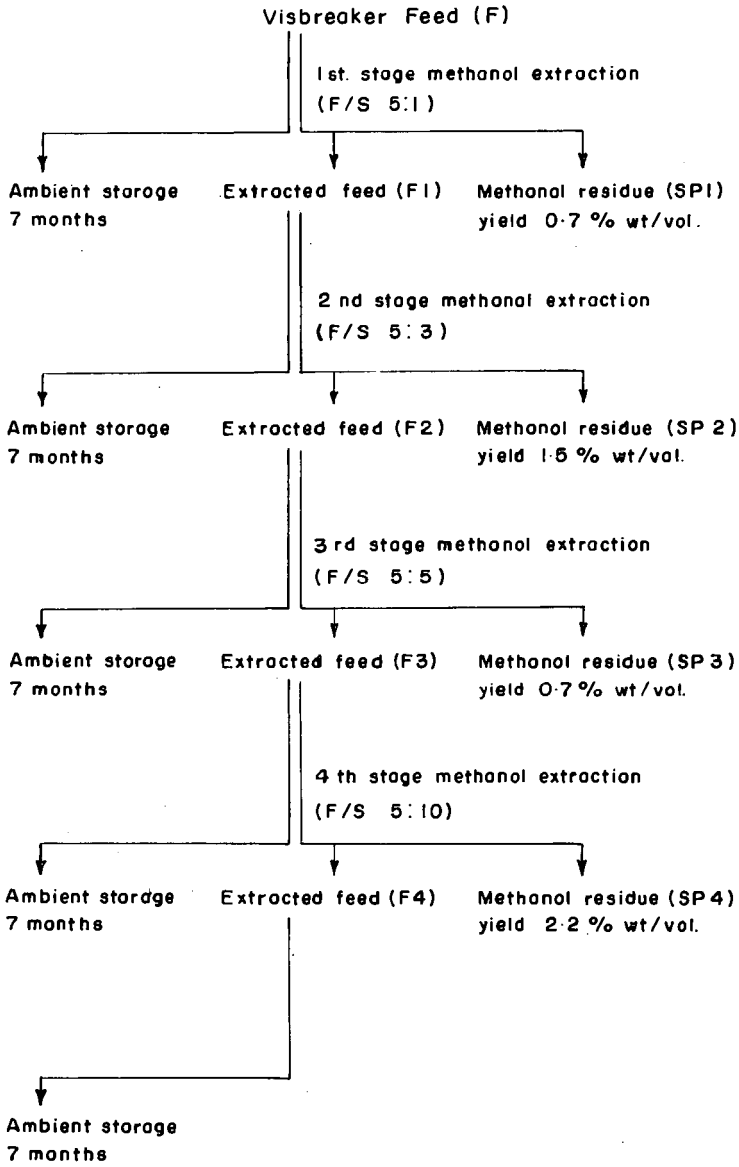

Fig. 1 – Scheme used for the extraction of insolubles / sediment precursors.

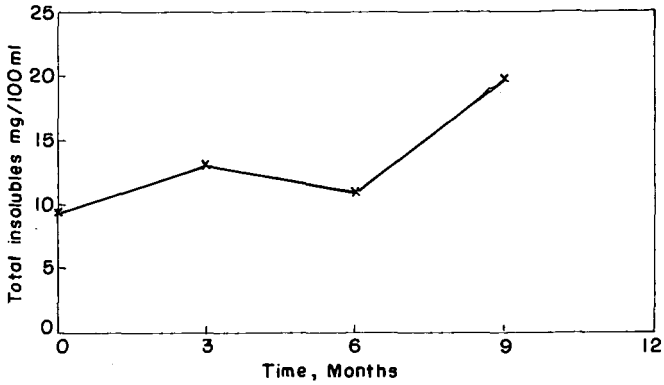

Fig. 2 - Total insolubles Vs time during ambient storage stability of visbroken middle distillate.

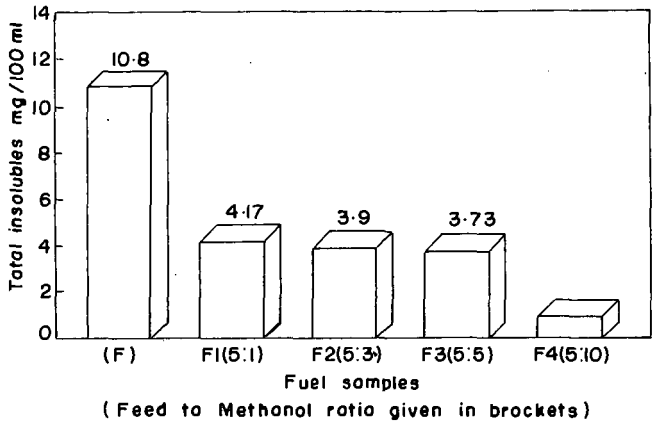

(Feed to Methanol ratio given in brackets)

Fig. 3 - Effect of extraction on ambient storage stability (7 months) of visbroken middle distillate.

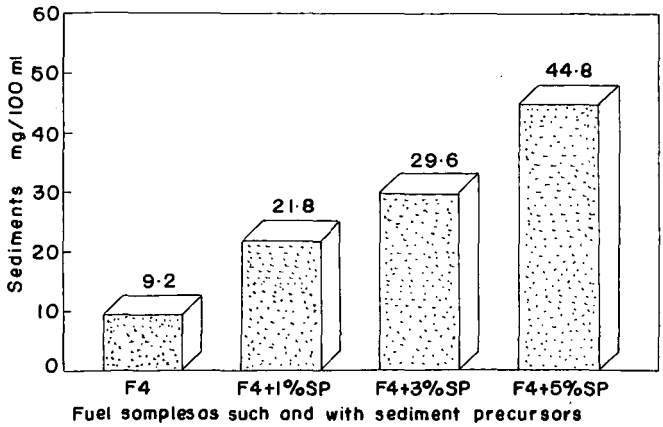

Fig. 4 - Effect of sediment precursors on extracted visbroken middle distillate (UOP-413 MODIFIED)

INSTABILITY OF MIDDLE DISTILLATE FUELS DURING STORAGE AND CHARACTERIZATION OF INSOLUBLES BY FTIR

Yogendra K. Sharma, Indra D. Singh, Dhirendra S. Aswal and Krishna M. Agrawal

Indian Institute of Petroleum, Dehradun - 248 005, India

Keywords : Middle distillates, Stability, FTIR

ABSTRACT

The problem of stability of diesel fuels has become more pronounced in recent years with the increasing use of cracked stocks in the diesel pool. These cracked products induce gum and sediment formation in fuels. In the present paper, the instability of total cycle oil (TCO) derived from FCC operation of Bombay High VGO, under accelerated and ambient storage conditions has been studied with and without additive doping. During ambient storage yield of the insolubles in TCO has been found to decrease after a period of about 18 months which may be attributed to the reformation of fresh oxidised species from insolubles. However during accelerated tests trend of increasing insoluble formation with time is revealed. The qualitative composition of insolubles obtained from ambient storage of additive doped and undoped fuels has been studied by FTIR and the role of additives on the composition of insolubles is discussed.

INTRODUCTION

Diesel fuels, particularly obtained from catalytically cracked stocks, start degradation right from production and on storage degrade to the extent that start giving application problems. The degradation mechanism and additive response depend on fuel composition, temperature, oxygen availability, static and dynamic conditions, storage time and type and size of storage vessels. In the present investigation, the instability of total cycle oil (TCO) derived from FCC stream of a refinery and doped with commercial additives has been studied under accelerated as well as ambient storage conditions. FTIR spectroscopy has been employed to explain the mechanism of additive functioning by comparing the spectra of sediments obtained under different conditions.

EXPERIMENTAL

The total cycle oil (TCO) was doped with 100 ppm of phenol (A1) and amine (A2) types additives. Various accelerated test methods viz modified[1] ASTM D-2274, ASTM D-4625 along with ambient storage tests for 4, 8, 12, 18 and 24 months were performed on TCO as such and doped with additives. FTIR spectra of various insolubles were recorded in absorbance mode on Perkin-Elmer 1760 FTIR spectrometer by making thin films of samples on KBr plates by evaporating their dichloro methane solution.

RESULTS & DISCUSSION

The physico chemical properties of TCO determined by standard ASTM/IP test methods are reported in Table-1. The insoluble yields from TCO as such and doped with additives (TCO+A1, TCO+A2) under modified ASTM D-2274 test conditions are shown in Fig.1, while those obtained with ASTM D-4625 and ambient storage conditions are presented in Figs. 2 & 3 respectively. Typical FTIR spectra of sediments obtained after 18 months and 24 months storage of TCO as such and with additives (TCO + A1 and TCO + A2) are presented in Fig.4.

From Fig.1, it is evident that sediment yield, under accelerated test conditions (dynamic) in the presence of oxygen is reduced significantly after doping with additives due to better additive fuel interaction under these conditions. This reduction is more pronounced in case of amine type additive as compared to phenol type. But in case of

static conditions (ASTM D-4625) as the oxygen availability is limited and agitation is also not there, the overall sediment formation and reduction after doping with additives are relatively small (Fig.2). Incase of ambient storage (Fig.3) sediment formation is low in the begining which increases significantly with time up to 18 months. Here also the reduction in sediment formation after doping with additive is significant. An appreciable reduction in sediments after ambient storage of 18 months in TCO as such as well as in doped with additives is observed (Fig.3). This observed pattern may be due to the formation of fresh oxidized species after 18 months storage. This has further been confirmed from the comparison of FTIR spectra of sediments from TCO, TCO+A1 and TCO+A2 after 18 and 24 months storage (Fig.4).

The appearance of two carbonyl band around 1740 and 1710 cm^{-1} (having comparable intensity) in all the sediments obtained after 24 months reveals that on longer duration, hydrolysis of ester type structures in sediments takes place forming the carboxylic and phenolic structures which are soluble in fuels. Thus the sediment yield is reduced. This is supported by the enhancement of bands at 3270 and 1600 cm^{-1} due to stretching and bending vibrations of OH groups.

FTIR spectroscopy has also been employed to explain the higher effectiveness of amine type additive compared to phenol type in inhibiting the sediment formation. The comparison of FTIR spectra of sediments from TCO, TCO+A1 and TCO+A2 after ambient storage of 18 months (Figs.4 A,B,C) reveals that while there is no appreciable qualitative variation in the spectra of TCO and TCO+A1, the spectrum from TCO+A2 (Fig.4C) is quite different in nature.

The sediment from TCO as such shows an appreciable amount of ester type carbonyl 1740 cm^{-1} (Fig.4A), while this is reduced considerably in sediment from TCO+A2 (Fig.4C). Further, the structures like quinone diamine type which forms during controlling the peroxy radicals also appears in the sediments due to sludge formation during storage. This may probably occur in sediment through polymerisation as per following mechanism of action of amine type additive[2].

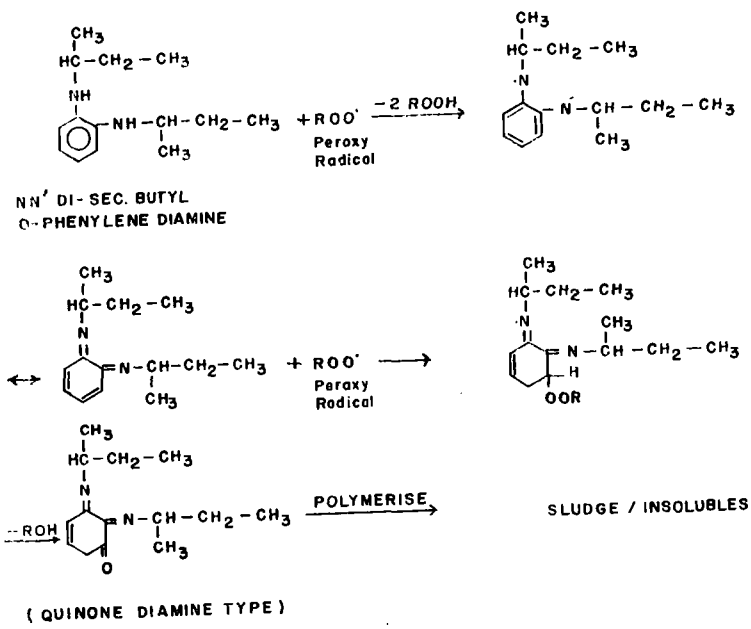

This is also supported from the FTIR spectra of sediment from TCO+A2 (748 cm^{-1} band due to 3-adjacent protons on aromatic rings). The strong and broad adsorptions at 3260 and 1600 cm^{-1} in sediment of TCO+A2 (Fig.4C) as compared to those of TCO and TCO+A1 (Figs.4 A & B) show the dominance of structures containing OH functionalities (phenolic type). Aromatic structures are confirmed by the appearance of 3052 cm^{-1} band (aromatic C-H stretching) and enhanced absorption at 1600 cm^{-1}. Thus, amine type additive is more effective in inhibiting the formation of sediment containing ester type structures during ambient storage of total cycle oil.

REFERENCES

1. Sharma, Y.K. & Agrawal, K.M., Fuel. **73**, 269 (1994).

2. Bownan, D.F., Middleton, B.S. & Ingold, K.K., J.Org.Chem. **34**, 3456 (1969).

Table-1 Characteristics of Total Cycle Oil

Density D15	0.8821
Kinematic viscosity, at 40 ^{0}C, cSt	2.46
Pour point, ^{0}C	18
Molecular weight	177
Maleic anhydride value	5.56
Diene value	1.44
Sulphur, %wt	1.46
Nitrogen, ppm	125
Boiling range, ^{0}C (5-95% vol)	158-441

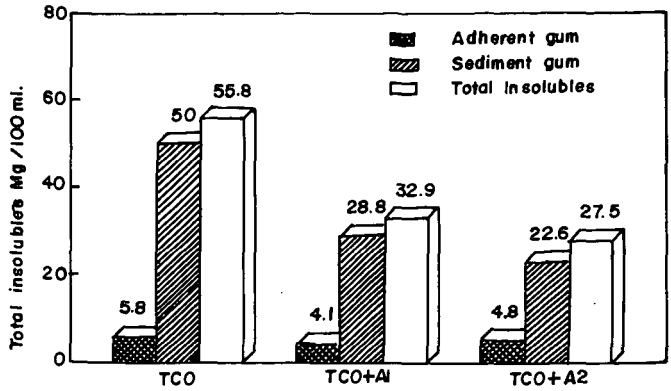

Fig. 1 : Response of Additives in TCO on stability under Modified ASTM D-2274

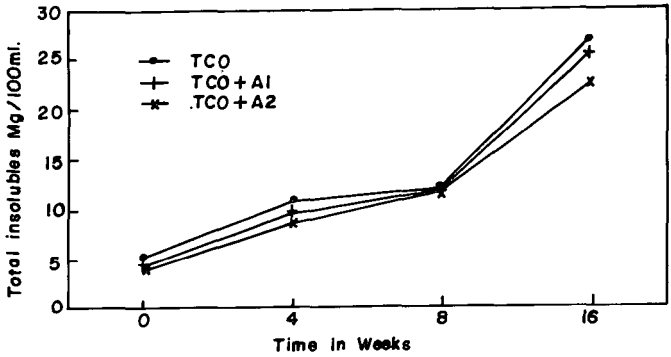

Fig. 2 : Response of Additives in TCO on long storage stability in non vented conditions at 43.3°C

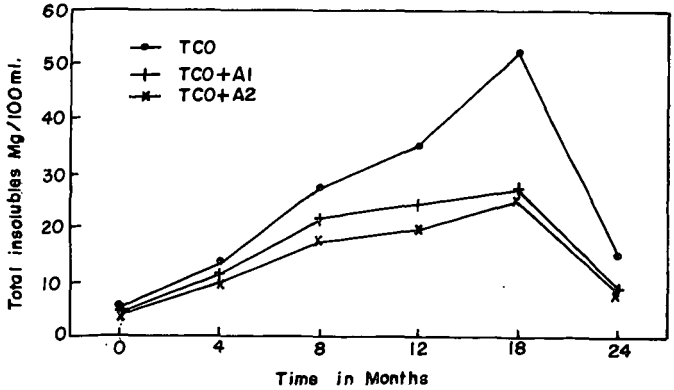

Fig. 3 : Response of Additives in TCO on Ambient storage stability.

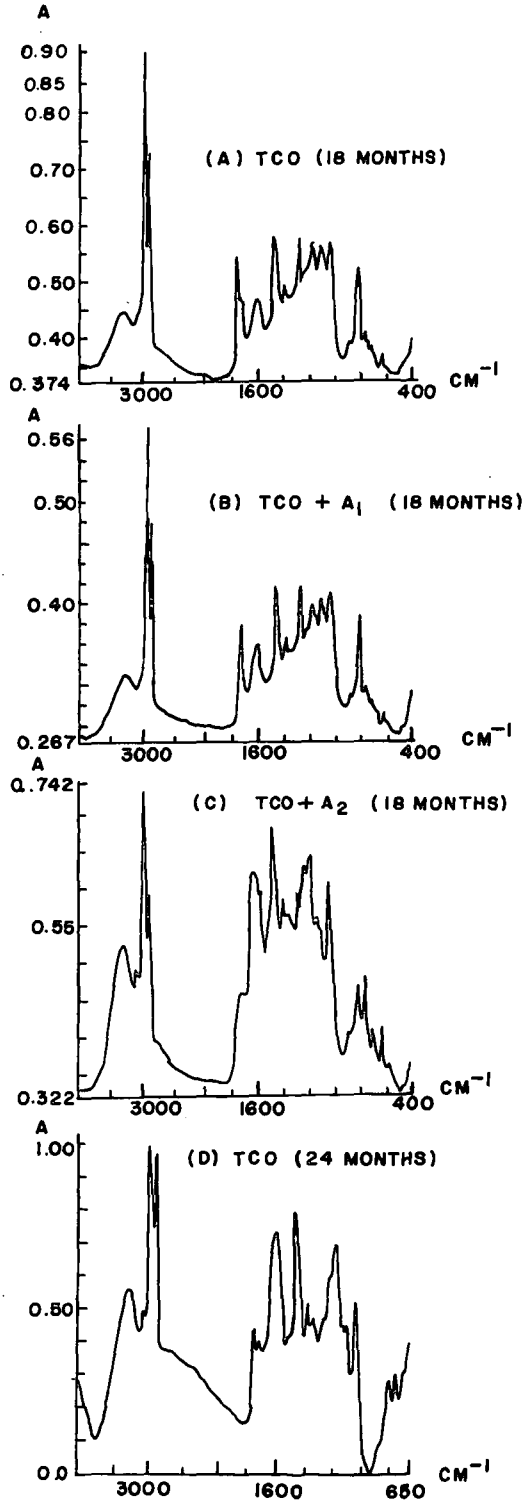

FIG. 4. FTIR SPECTRA OF SEDIMENTS

PREDICTING STABILITY AT THE REFINERY USING SMORS

Margaret A. Wechter* and Dennis R. Hardy
Naval Research Laboratory Code 6180
Washington, D.C. 20375-5000

* and the University of Massachusetts Dartmouth
North Dartmouth, MA 02747

Keywords: SMORS, diesel fuel, storage stability

INTRODUCTION

It has been previously reported[1] that extraction with methanol will improve storage stability characteristics for mid distillate diesel fuel which is at least 6 months old. Moreover, a potential relationship between the methanol soluble, hexane insoluble extractible material and the thermally induced precipitate (TIP) which forms in some fuels under accelerated aging conditions which simulate long term ambient storage, has been suggested.[2,3] Fuel stability is currently assessed through the use of an accelerated aging procedure.[4] However, the procedure or procedures used require substantial commitments of laboratory time and resources and they are necessarily limited to predicting only the relatively short term (1 - 2 years). A predictive stability test which could serve for field use for fuels at least 6 months old, or which would require a sufficiently short turnaround time to make it attractive for procurement use is highly desirable. This is particularly true when circumstances require that the fuels may be stored for very extended periods, such as military fuel reserves.

Fuels which have been aged by six months of ambient storage in the laboratory or field show a very linear relationship between the solids produced by methanol extraction and subsequent precipitation with hexane (EIP - extraction induced precipitate), and solids, or insolubles, formed during the stress, or accelerated aging process (TIP).[3] Thus, for these fuels, the extractibles yields can be used as a predictive test for storage stability. When these aged and thermally stressed fuels are extracted with methanol after filtration for TIP, the yield of extractible solids is typically found to be no more than a few percent higher than the EIP isolated from the unstressed fuel. We propose that, for those cases where the post-stress extractibles (PEIP) yields are about equal to the pre-stress yields (EIP), there is an equilibrium concentration of distributed soluble macromolecular material (which we have previously called SMORS).[2,3,5,6] Examples of fuels which have been aged to this equilibrium condition are found in Table 1 (Code A = aged).

Fuels which are refinery fresh, or are not aged to equilibrium either because they have been stored under non-oxidative conditions (inert atmosphere, freezer conditions) or their ambient storage times are too short, will frequently show very different extractibles yields before and after accelerated aging. Until these fuels are aged to equilibrium there is no consistently useful relationship between EIP and TIP to obviate the need for a stress test. Some examples of pre (EIP) and post (PEIP) stress extractibles yields for some fresh fuels are also found in Table 1 (Code F = fresh).

Because accelerated aging tests for new fuels do not generally permit storage stability prediction beyond a year or so under ambient conditions and because they are not always reliable, we are suggesting that a stress test in combination with a post stress determination of extractibles will serve to better identify fuels which are likely to develop undesirable storage characteristics over time. This test could serve as the basis for deciding which fuels could be safely stored for additional extended periods, and which should be used promptly. We also provide additional experimental evidence to link the extractible material (SMORS) with insoluble sediment formed as a result of ambient storage.

EXPERIMENTAL

The fuels used in this work were refinery fresh fuels which were tested for EIP and TIP (insolubles) as soon as they reached the Laboratory. They included two light cycle oil (LCO) stocks and two straight runs (SR). For experimental purposes, the fuels tested were the two LCOs and 80%/20% blends of the SR/LCO pairs. Designations for the experimental fuels are found in Table 2.

All fuels involved were tested for pre and post stress extractibles (EIP/PEIP) as soon as they were received and at later intervals, ranging between one and nine months, as well. They were tested for insolubles using the 16 hour ASTM D 5304 - 92 procedure at those same times. All fuel aliquots were prefiltered through two thicknesses of 0.8u 47mm nylon filters (MSI, Westboro,MA) using a water aspirator. Aliquots were 100 mL each; separate aliquots were used for the EIP and for the TIP/PEIP determinations. Stress conditions were 16 hrs., 90°C, 690 kPa oxygen overpressure. Post-stress samples were first filtered for TIP, then subjected to extraction for the determination of PEIP.

For the insolubles (TIP) determination: samples were filtered using glass fiber filters and the procedure described in detail elsewhere.[4] For the extractibles determinations: prefiltered aliquots were extracted (separatory funnel; shake 90 sec.) with 40 mL reagent grade methanol. The methanol phase was rotary evaporated for 30 minutes at 58-63°C. After cooling, 50 mL of reagent grade hexane was added to induce precipitation. The resulting precipitate was filtered (nylon filters) and dried at 70°C for at least 20 minutes to remove any traces of hexane before weighing.

An experimental series was performed to test possible effects of a tertiary alkyl amine stabilizer additive on insoluble sediment (TIP) formation and on post stress extractibles (PEIP) formation. The amine additive has been tested in this laboratory and elsewhere and is known to reduce insolubles formation in some fuels.[7] Light cycle oil samples (Fuels B, D) were doped with the additive in varying concentrations (6 - 890 ppm w/v) and tested, along with control samples, using the same procedures previously described for the TIP and PEIP determinations. All samples were run in duplicate and the aliquot size was 100 mL.

RESULTS AND DISCUSSION

Aging (Stress) and Extractibles Testing

Table 3 provides a summary of ambient storage times, pre- and post-stress extractibles levels (EIP and PEIP) and total insolubles/100 mL following the standard 16 hour LPR test (ASTM D 5304 - 92). Fuel A, tested at monthly intervals from 1-3 months passes the LPR test (current pass/fail criterion is 3 mg/100 mL). Pre- and post-stress extractibles levels indicate no tendency for the fuel to degrade over time with respect to insolubles formation and suggest this fuel could be safely stored for extended periods. Fuel B is a light cycle oil and thus might be considered a potential "worst case" fuel. During the time interval between 0 and 3 months of ambient storage the fuel passes the LPR test. The pre-stress extractibles are low, but the post-stress extractibles are increasing to the point where their level suggests that this fuel is not a candidate for long term storage. By 8.5 months of ambient storage LPR insolubles (TIP) and extractibles levels have increased to the point where they support an argument for prompt use. In particular, the post-stress insolubles yield has increased to a level which suggests the fuel is likely to deteriorate badly in the near term. Also EIP and PEIP are beginning to approach equilbrium.

Fuels C and D are an interesting pair; fuel D being a light cycle oil and C a blended fuel comprised of 20% D and 80% straight run stock. Fuel D fails the LPR test badly on initial testing. Moreover, the post-stress extractibles level (41 mg/100 mL) is high and supports the conclusion that this is an unstable fuel. As time passes and the fuel is subjected to ambient storage conditions, the condition of the fuel actually improves as noted by TIP (ASTM D 5304) and PEIP (or post-stress extractibles) levels. Note that this LCO, even at 6 months, is not aged to equilibrium and so pre-stress extractibles levels are not as effective predictors of future behavior as are the post-stress levels. By 12 months of ambient storage the fuel has improved to where it passes the LPR. The PEIP has declined as the pre-stress extractibles level has increased. If the existing extractibles (EIP) are subtracted from the PEIP one obtains a measure of the "aging tendency" during the stress test. For this LCO the trend is toward improvement. The relationship between TIP and PEIP formed during accelerated aging is striking: at 0 months of ambient storage TIP is 8.3 mg/100 mL and PEIP is 40.9 mg/100 mL; at 12 months the numbers have fallen to 1.6 and 13.8 mg respectively.

Fuel D is an unusual LCO in that its storage stability with respect to insolubles formation improves as it ages under ambient conditions. However, if criteria we have proposed for aged LCOs using a 24 hour modification of the LPR stress test (TIP $\geq$ 6 mg/100 mL; extractables $\geq$ 32 mg/100 mL)[3] are adapted to the 16 hr test, predictions for future storage behavior can be made. Based on post-stress extractibles yields (which must be used rather

than pre-stress yields until the fuel is aged to equilibrium) we would predict that, at equilibrium, the pre- and post-stress yields would be roughly equivalent. This fuel is clearly "limited" with respect to the total insolubles it can form during its lifetime prior to use. It apparently forms insolubles rapidly, then levels out to become a rather benign fuel with respect to continued insolubles formation. While this fuel obviously improves with age, it is not a suitable candidate for procurement on the basis of its poor initial extractibles/aging tests. Moreover, even if it were to be held in storage to equilibrium, there would be so much particulate matter suspended in this fuel as to present filtration problems. Thus, this fuel is not a candidate for procurement. Fuel C, the blended stock, is a likely storage candidate on the basis of its extractibles and TIP yields. On the basis of its consistent PEIP and stress test behavior and on its fuel D LCO content, this fuel appears to be a suitable candidate for storage and makes a case for safe storage and use of cracked stock blends.

Effect of Additives

Tables 4 and 5 present results obtained for the two light cycle oils that were tested with the tertiary amine additive (additive #1). Fuel B was also tested using another additive, a hindered phenol (additive #2), for purposes of comparison. Table 4 summarizes additive testing for fuel B. Insolubles (TIP) formation tendency for this fuel is not reduced with either additive. Indeed, it might be argued that TIP increased somewhat on addition of the tertiary amine. PEIP yields for all samples were comparable. Thus, fuel B appears to be one of those fuels that is not affected by tertiary amine additive treatment.

Fuel D, on the other hand, is responsive to additive #1. As was the case with fuel B, additive #2 had no effect on this fuel. Table 5 shows the reduction in insolubles (TIP) that occurs when fuel D is subjected to the 16 hour LPR test after treatment with varying levels of additive #1. A corresponding decrease in PEIP levels is also observed. The fact that additive #1 reduces PEIP levels as it reduces TIP provides additional evidence for a relationship to exist between extractibles levels and the tendency toward insoluble sediment formation in diesel fuels.

Summary

A relationship between extractibles levels before (EIP) and after (PEIP) accelerated aging and insolubles formation tendency has been found to exist in fuels that have not been aged to EIP/PEIP equilibrium. Additional evidence for the relationship between these entities has been provided by the comparable effect of a common stability additive on post stress extractibles and insoluble sediment. Thus, we propose that a combination of the LPR (ASTM D 5304) stress test and methanol extraction of the filtered, stressed fuel with subsequent precipitation of the hexane insoluble fraction, may serve as a basis for a predictive test for storage stability. This test would enable better decisions to be made as regards the candidacy of fuels for long term storage as opposed to their candidacy for prompt usage. Moreover, for cases where storage is required, this test combination might serve as a reasonable basis for procurement.

References

1. Wechter, M. A., and Hardy, D. R. 1989. The Isolation of Precursors Responsible for Insolubles Formation in Mid-Distillate Diesel Fuels. Fuel Science and Technology Intl., 7, 423.

2. Hardy, D. R. and Wechter, M. A. 1990. Insoluble Sediment Formation in Middle-Distillate Diesel Fuel: The Role of Soluble Macromolecular Oxidatively Reactive Species. Energy and Fuels, 4, 270.

3. Wechter, M. A. and Hardy, D. R. 1991. The Use of Soluble Macromolecular Oxidatively Reactive Species (SMORS) to Predict Storage Stability of Mid Distillate Diesel Fuels. Proceedings of the Fourth International Conference on Stability and Handling of Liquid Fuels, U.S. Department of Energy, 4, 620.

4. ASTM D 5304 - 92. Standard Test Method for Assessing Distillate Fuel Storage Stability by Oxygen Overpressure. American Society for Testing and Materials, Annual Book of ASTM Standards, Vol 05.03.

5. Hardy, D. R, and Wechter, M. A. 1990. What are Soluble Macromolecular Oxidatively Reactive Species (SMORS)? Preprints of the Division of Fuel Chemistry, American Chemical Society, 35, 1176.

6. Hardy, D. R. and Wechter, M. A. 1994. Characterization of Soluble Macromolecular Oxidatively Reactive Species (SMORS) from Middle Distillate Diesel Fuels: Their Origin and Role in Instability. Energy and Fuels, In Press.

7. Hazlett, R. N., Hardy, D. R., White, E. W. and Jones-Baer, L. 1985. Assessment of Storage Stability Additives for Naval Distillate Fuel. SAE Technical Paper Series, 851231, Washington, D.C.

Table 1. Weight of Solids Isolated from the Pre- and Post-Stress Hexane-Insoluble Fraction of the Methanol Extracts of Five Aged and Three Fresh Light Cycle Oil Diesel Fuels[a]

fuel code	EIP: mg/100 mL	PEIP: mg/100mL	aged,A or fresh,F
LCO-1	112	116	A
LCO-2	14	17	A
LCO-3	53	63	A
LCO-4	27	40	A
LCO-5	92	114	A
LCO-12	1	14	F
LCO-13	2	101	F
LCO-14	2	58	F

[a]Storage stress test was for 24 h at 90°C and 690 kPa of oxygen.

Table 2. Experimental Fuel Designations.

Fuel	Type	Legend
A	Blend	80% 91-34(SR)+20% 91-35(LCO)
B	LCO	100% 91-35(LCO)
C	Blend	80% 92-1(SR) + 20% 92-2(LCO)
D	LCO	100% 92-2(LCO)

Table 3. Summary of Test Fuel Results

fuel	Months of Storage time (ambient)	TIP (mg/100mL)	EIP (mg/100mL)	PEIP (mg/100mL)
A	0	1.3	0.23	0.16
A	1	0.4	0.05	0.26
A	2	0.8	0.3	2.5
A	3	0.7	0.6	2.5
B	0	1.9	0.29	6.8
B	1	1.3	0.17	7.8
B	2	1.6	0.3	12.5
B	3	1.9	2.3	28.1
B	8.5	2.3	5.0	45.8
B	14	1.4	13	34.6
C	0	1.8	0.09	6.6
C	0.5	2.2	0.15	5.4
C	1.5	2.5	0.7	5.6
D	0	8.3	0.22	41.1
D	0.5	7.6	0.19	40.6
D	1.5	5.2	2.1	28.0
D	6	4.4	7.3	34.9
D	12	1.6	16.2	30

Table 4. Additive studies for fuel B at 8.5 months ambient storage

Sample tested	mg TIP	mg EIP	mg PEIP
Fuel	2.3	5.0	48.8
Fuel + 24ppm #1	3.3	-	39.3
Fuel + 24ppm #2	2.5	-	42.6
Fuel + 24ppm # 1,2	3.2	-	47.2

Table 5. Studies for fuel D at 6 months ambient storage using additive #1.

Sample tested	TIP	EIP	PEIP
Fuel	4.4	7.3	34.6
Fuel + 6ppm	1.3	-	17.5
Fuel + 24ppm	1.1	-	16
Fuel + 890ppm	1.7	-	22.6

A FUEL STABILITY STUDY
FILTERABLE AND ADHERENT INSOLUBLES AS FUNCTIONS OF TIME

Edmund W. White
Naval Surface Warfare Center, Carderock Division
3A Leggett Circle
Annapolis, MD 21402 - 5067

Keywords: Insolubles; Adherents; Filterables

INTRODUCTION

It is generally accepted that the insoluble substances that form in middle distillate fuels in storage are the result of an oxidative coupling of reactive molecules which may be of the same or of different species. It is also generally accepted that the reactive species are to be found among those containing a heteroatom such as nitrogen, sulfur, or oxygen and among unsaturated hydrocarbons. However, the number of reactive compounds is large and the chemical mechanism by which they are converted into insoluble products has not been established despite years of study.

In 1958, Sauer and coworkers(1) postulated the formation of hydroperoxides which then split out water to form aldehydes. The aldehydes then reacted with other peroxides to form peroxyhemiacetals which, in turn, decomposed to form monomeric oxidation products and condensed, esterified products of higher molecular weight. Another hypothesis noted by Taylor and Frankenfeld(2) and by Por (3) is based on a free radical chain mechanism.

From a study of U.K. stocks, Pedley and Hiley(4) have suggested that phenalenes and indoles are the precursors of some fuel sediments. The phenalenes are known to oxidize to form phenalenones which can react by acid catalyzed condensation with indoles to form indolylphenalenes. These then form insoluble products by reaction with acids.

Pedley et al(5) investigated Australian stocks and found that all fuels which proved to be unstable during storage contained both alkylindole and phenalene species. Marshman(6) from a study of research blends made from fresh components obtained from U.K. and European refineries concluded that the stability of a fuel is related to the concentrations of phenalenes and indoles, but the relationship is not straightforward.

ACCELERATED TESTS OF STORAGE STABILITY

Such studies are useful in providing an understanding of the complex chemical mechanism by which sediment is formed. However, the person storing middle distillate fuels is more interested in the rate at which sediments will form. For example, the military and the Strategic Petroleum Reserve, both of which have to store large quantities of fuel, cannot tolerate unstable fuels.

For that reason, a number of test methods have been developed and standardized to provide an indication of the stability of a fuel. ASTM Test Methods D 2274, the accelerated stability procedure, and D5304, oxygen overpressure procedure, are two of the methods. The former has long been a required test in the Navy's distillate fuel specification; the latter is being considered as an alternate or replacement.

In Test Method D2274, which was used in obtaining the data to be presented in this paper, a 350 mL volume of filtered fuel is aged at 95°C for 16 hours while oxygen is bubbled through the fuel at 3 L/h. The fuel is then cooled and insolubles are recovered. Particulates (FI) are recovered by filtration and gums adhering (AI) to the glassware are recovered by solvent washing. The insolubles are weighed and their sum is reported in mg/100 mL as a measure of the fuel's oxidative storage stability.

PROCESS ANALYSIS

The reactions which lead to insolubles formation start as soon as the middle distillate fuel is produced and comes in contact with an oxygen-containing atmosphere. The rate of reaction depends upon the specific fuel system and the materials with which it comes into contact. Copper and some other metals are oxidation catalysts. Rust also has some catalytic properties. Acidic materials can catalyze some of the potential reactions. Consequently, some of the instability reactions may have already occurred prior to laboratory testing of a fuel sample. An early step in the Test Method D2274 procedure is the filtering of the fuel sample to remove an solids that may have formed or that may have entered from other sources.

Let us examine what we think occurs during a D2274 type of testing. First of all, some of the reaction products is bound to be soluble in the fuel, so it is only after the saturation limit is reached that particulates begin to appear in the fuel as filterable insolubles .

Second, during the period required to reach saturation, another rate process is already removing instability products from the fuel. It is an adsorption process, and Fick's law of diffusion defines the rate of diffusion of the instability products to the glassware surface:

$$Q = D(A)(c/t) \qquad (1)$$

Q is the quantity diffusing to the adsorption surface per unit time, D is the diffusion coefficient, A is the area of the glassware wetted by fuel, and c/t is the concentration gradient between the bulk fuel and the surface of the glassware. Thus, while the instability reactions are placing reaction products in solution, the diffusion and adsorption process is removing material from solution and depositing it on the glassware.

Presuming that the reaction process is faster than the rate at which reaction products are removed as adherent insolubles, the solubility limits of the reaction products in the fuel will eventually be reached and the filterable insolubles will begin to precipitate from solution. As long as reaction products are produced at a rate faster than they can be removed by adsorption, excess material will precipitate to add to the quantity of filterable insolubles.

If the concentrations of the reactants is rate controlling, there will be a gradual decrease in the rate of formation of filterable insolubles. However, if reactant concentrations are high, other rate processes may be limiting. For example, the rate at which dissolved oxygen can be replenished from the oxygen which is bubbled through the fuel in Test Method D2274 may be the controlling process. In such cases, the rate of formation of FI would be constant, and a plot of cumulative FI as a function of stress time would be linear, until the concentrations of the reactive fuel components decreases to the point where their concentrations are controlling the rate.

Because the instability reaction products (IRP) in solution will remain constant at the saturation concentration, the rate of formation of adherent insolubles will be constant, i.e. a plot of cumulative AI versus time will be linear. However, once the formation of reaction products drops below the rate just sufficient to maintain saturation, the rate of adherent insolubles formation will begin to decrease, i.e. the slope will decrease and the cumulative AI will approach an asymptotic value.

If both the filterable insolubles and the adherent insolubles approach asymptotic values, the ratio of the two must also approach an asymptotic value.

EXPERIMENTAL PROCEDURE AND RESULTS

The author has previously reported some results obtained when twenty-one fuel stocks were individually stressed in a D2274 procedure using a range of stress times.[7] The time response curves of total insolubles vs. stress time have an S-shape if the period is sufficiently long and the total insolubles level approaches an asymptotic value. The study showed that tests using a single stress time are incapable of fully defining the stability characteristics of a fuel. It was also found that pre-aging a fuel prior to determining its time response curve appeared to affect only the duration of the induction period.

The same twenty-one stocks and the same tests form the basis of this paper, in which we examine the manner in which stress time affects the individual components of total insolubles, i.e. the filterable insolubles (FI) and the adherent insolubles (AI). Properties of the stocks were presented in the earlier paper.

The experimental data tend to support the postulated mechanism. Figures 1 to 4 show the filterable insolubles, the adherent insolubles, and the ratio of filterables to adherents as functions of the time the four fuels were left in the 95°C bath. These illustrations were selected as representative of the twenty one stocks mentioned earlier. Similar curves were obtained with the other fuels.

Although fuels which had data points at five or more times and which had one or more data points representing times of sixty or more hours were preferred, the need to show representative fuels did not always permit such preferences to be honored. In general, the shapes of the curves were not as certain with fewer points or with a smaller range of times.

Figure 1 shows the time response curves for a light cycle oil (LCO). Note the initial linear responses of both the AI and the FI. A rate limiting phenomenon controlling the formation of filterable insolubles below 40 hours of stress is postulated. Above the 40 hour stress point, it appear the concentration of the active components of the fuel are controlling. The AI also exhibit a linear rate response below the 40 hour point, which is consistent with the postulated mechanism. The ratio of FI to AI seems to be approaching an asymptotic value of about 2.

Figure 2 shows the time response curves for a 40/60 volume percent blend of an LCO in a straight run (SR) fraction. The range of times ran only to 46.2 hours but, within that time range, we did obtain six data points. The curves indicates that saturation is not reached until 20 hours have elapsed. The standard 16-hour test would have shown this to be a very stable fuel with very low insolubles whereas, in another 20 hours, it approached its asymptotic level of roughly 3.5 mg/100 mL.

The FI curve shows that the concentrations of active components is controlling, and the AI curve supports the adsorption hypothesis because it is linear. The FI/AI ratio curve seems to be reaching an asymptotic value of about 2.

Figure 3 shows the time response curves for a 30/70 blend of an LCO with an SR fraction. The FI time response curve shows a decreasing rate of FI formation, so the concentrations of active ingredients is postulated as controlling. The AI response curve is again linear, and the ratio curve seems to be approaching an asymptotic value of about 1.

Figure 4 shows the time response curve for a blend of a high sulfur heavy diesel fuel in a CAT 1H fuel. The maximum stress time is 40 hours, but we do have five data points. Linear fits are obtained for both the FI and the AI, and the ratio of the two seems to be reaching an asymptotic value of about 3.5.

FINDINGS AND CONCLUSIONS

1. Formation of FI remains essentially zero until the fuel is saturated with instability reaction products (IRP's). Thereafter, the rate of FI formation may be linear if there is a limiting rate factor such as oxygen supply, or it may decrease as reactive components are depleted.

2. Once a fuel is saturated with IRP's, AI formation is constant until reaction rates are too slow to keep the fuel saturated.

3. After the fuel becomes saturated with IRP's, the FI/AI ratio starts to approach a constant value. Experience indicates this is often about 1 or 2. We have seen no value above 6.

LITERATURE CITED

1. Sauer, R.W. et al, American Chemical Society, Div. Petroleum Chemistry PREPRINTS vol. (#3), p. 95 et seq (1958)

2. Taylor, W.F. and J. W. Frankenfeld, Proceedings 2nd International Conference on Long Term Storage Stabilities of Liquid Fuels, San Antonio, TX, pp. 496 - 511 (1986)

3. Por, N, Stability Properties of Petroleum Products, Chapter 4 and pp. 133 - 134, The Israel Institute of Petroleum and Energy, Tel Aviv, Is. (March 1992)

4. Pedley, J.F. and R. W. Hiley, "Investigation of Sediment Precursors Present in Cracked Gas Oil," Proceedings of 3rd International Conference on Stability and Handling of Liquid Fuels, Institute of Petroleum (host), London, U.K., pp. 495 - 509 (Sept 1988)

5. Pedley, J.F. et al, "The Chemistry of Sediment Formation in Australian Middle Distillate Fuels," American Chemical Society, Division of Fuel Chemistry, Preprints, vol. 35 (#4), pp 1100 - 1107, Washington, DC (August 1990)

6. Marshman, S., "Storage Stability of Middle Distillate Fuels: Degradation Chemistry of Catalytically Cracked Gas Oil Blends," Proceedings, 4th International Conference on Stability and Handling of Liquid Fuels, pp 489 - 502, Orlando, FL (Nov 1991)

7. White, E.W., "A Fuel Stability Study: Total Insolubles as a Function of Time," American Chemical Society, Division of Fuel Chemistry, Preprints vol. 35 (#4), pp. 1184 - 1191, Washington, DC (August 1990)

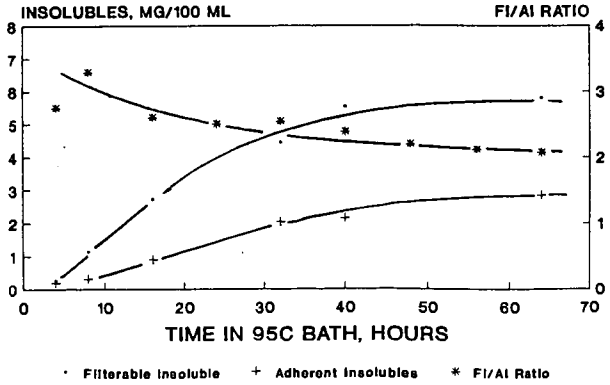

Fig. 1 - Time response curves for a light cycle oil, showing FI, AI, and the FI/AI ratio as functions of time.

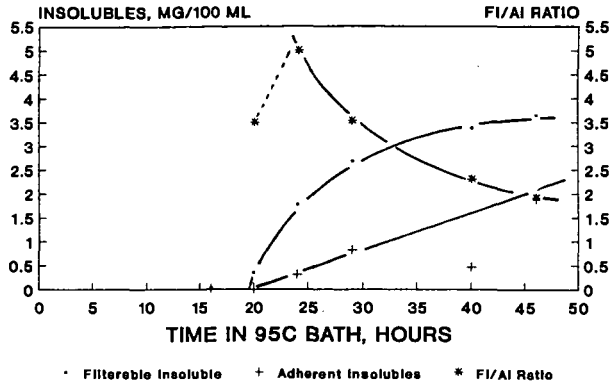

Fig. 2 - Time response curves for a 40/60 volumetric blend of LCO in an SR stock, showing the FI, AI, and FI/AI ratio as functions of stress time.

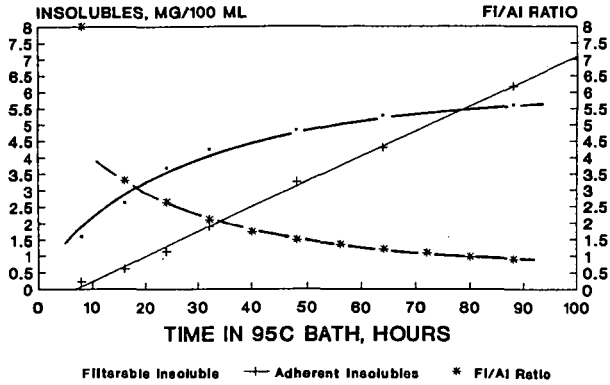

Fig. 3 - Time response curves for a 30/70 blend of a blend of an LCO in an SR stock, showing the FI, AI, and FI/AI ratio as functions of stress time.

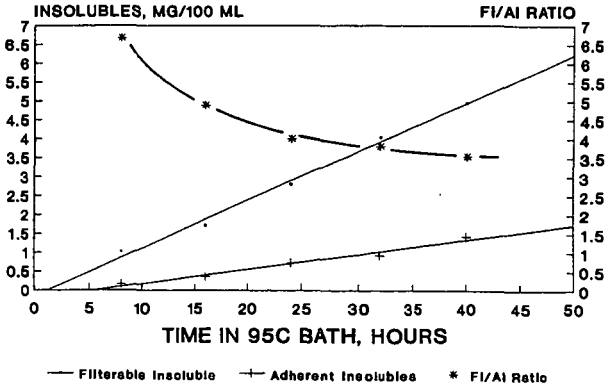

Fig. 4 - Time response curves for a blend of high sulfur, heavy diesel fuel in a CAT 1H fuel, showing the FI, AI, and FI/AI ratio as functions of time.

EFFECTS OF SULFUR COMPOUNDS ON A JP-8 SURROGATE FUEL

William D. Schulz and Ann P. Gillman
Department of Chemistry, Moore Bldg. 337
Eastern Kentucky University
Richmond, KY 40475
(606) 622-1456

Keywords: Jet fuel stability, deposit formation-effects of sulfur compounds, thermal desorbtion/pyrolysis-GC-MS

INTRODUCTION

The thermal stability of military jet fuels is of increasing concern as the fuels must withstand ever increasing loads as the coolant/heat sink for the system of advanced aircraft [1]. Fuels exposed to elevated temperatures and oxygen form soluble and insoluble oxidation products. The formation of insoluble deposits in fuel systems and the resulting possibility of system failure is of particular concern.

Hazlett pointed out the role of phenols and oxidative phenolic coupling in the formation of insoluble deposits under accelerated storage conditions in 1986 [2]. We have observed phenols as the only reactive species in engine augmenter fuel tube and spray ring deposits from a military engine [3]. From the real engine deposits we postulate deposit initiation by oxidative phenolic coupling, followed by condensation to three dimensional aromatic networks as the initial phenolic dimers and oligomers are exposed to more heat energy. In experiments with fuel samples, solid phase extraction of polar compounds were predominately phenolic for non-hydrotreated fuels but not with hydrotreated fuels [4]. The hydrotreated fuels oxidized rapidly and extensively to give alcohols and carbonyl products,including the homologous series of 5-alkyldihydrofuranones. Hydrotreated fuels did not form significant amounts of insoluble solid deposit. Non-hydrotreated fuels oxidized slowly and formed large amounts of insoluble deposits. Heneghan has observed this inverse relationship of deposit formation and "oxidizability" for 20 different fuels as measured by eight separate techniques [5].

Non-hydrotreated fuels are generally high in sulfur relative to hydrotreated fuels. The catalytic effect of sulfuric and sulfonic acids in the decomposition of α-arylhydroperoxides to phenols is well known [6]. Hardy, et. al., observed the effect of several sulfur compounds as anti-peroxidants [7] in fuels and in model systems [8].

If oxidative phenolic coupling is a major mechanism for deposit formation, the effect of sulfur compounds in the production of phenols by decomposition of arylhydroperoxide precursors should significantly increase deposit formation. The relative effects of different classes of sulfur compounds is probably predictable, but the effect of these compounds on phenolic coupling is not known. A previously prepared, 12 component, surrogate fuel [9] presents a test media for doping experiments with representative sulfur compounds from which reaction products of fuel components and sulfur compounds should be easy to follow, compared to complex real fuels.

Aliphatic thiols, thiophenols, thiophenes, benzothiophenes and disulfides are represented by dopant compounds. Gravimetric results of deposit formation, extraction and analysis of polar products by GC-MS and analysis of insoluble solids by step wise thermal desorbtion/pyrolysis-GC-MS gives a fairly complete picture of the oxidation and deposit processes. The information should establish a relationship of structure to deposit tendency for these classes of sulfur compounds. To investigate possible effects of the sulfur compounds in phenolic coupling, 2-propylphenol was added to all samples.

EXPERIMENTAL

Surrogate fuel: Isooctane, 5.0 %; wt./wt., methylcyclohexane, 5.0 %; m-xylene, 5.0 %; cyclooctane, 5.0 %; tetramethylbenzene, 5.0 %; tetralin, 5.0 %; dodecane, 20.0 %; methylnaphthalene, 5.0 %; tetradecane, 15.0 % and hexadecane, 10.0 %, were 99+ % grade purchased from Aldrich.

Dopant compounds: 2-propylphenol, 3,4-dimethylthiophenol, phenylethylmercaptan, dibenzothiophene, phenylsulfide, 2-ethylthiophenol, 2-ethylthiophene and hexanethiol were Aldrich reagent grade. Solvents: acetone, methanol, methylene chloride and toluene were Aldrich reagent or HPLC grade. High purity helium, nitrogen and oxygen gases were used as supplied by Central Kentucky Welding Supply.

Fuel stressing: The flask test apparatus and operation have been described previously [9]. 30.0 mL of surrogate fuel and dopants were stressed in a 50 mL round bottom flask, equipped with a Friedricks condenser with coolant at 0-5 °C and heated with mantles controlled to 175 +/- 2 °C. The fuel was nitrogen purged until temperature equilibrated and oxygen was then sparged into the fuel at 100 mL/min. via 0.53 mm fuzed quartz capillary. Samples were stressed for 24 hours, filtered and washed upon reaching room temperature. Stressed fuel was vacuum filtered with Osmonics® 0.45 silver membrane 47 mm filter. Glassware and filters were washed with heptane. Filtered deposits were washed with acetone. Filters, with acetone insoluble material were dried in vacuum (20-30 torr, 80 °C) 36-48 hours and reweighed. Acetone soluble gums were collected as filtrate, the solvent evaporated with dry nitrogen and weighed.

Solid phase extraction: 1.0 g J & W silica gel SPE cartridges were conditioned with 2 x 5 mL portions of methanol, methanol/acetone, acetone, acetone/heptane and heptane. A 5.0 mL portion of filtered, stressed fuel was extracted and the cartridge washed with 3 x 3 mL of heptane, lightly air dried (2 x 10 mL) and the extract eluted with 3.0 mL methanol. Methanol was evaporated with dry nitrogen, the extract weighed and immediately rediluted to 1.0 mL with methanol.

Analysis: Hewlett Packard 5890 series II GC/5890 MS with 7673A autosampler. MS scanned 35-550 m/z, six minute solvent delay. 1.0 μL splitless injection, 280 °C injection port and transfer line. 50 meter x 0.25 mm x 0.5 μm J & W DB-5 MS column at 30 psi head pressure. Purge time 0.5 min., 2 min. at 60 °C, 2 °C/min. to 250 °C,

10 °C/min. to 280 and 10 min. final hold. Sample samples by thermal desorbtion/pyrolysis with CDS model 1000 Pyroprobe®. Coil probe, 2 x 16 mm quartz tube. Approximately 10 mg of dry sample for sequential thermal desorbtion and pyrolysis at 200, 280, 450, 750 and 1100 °C. Interface at 200 and 280 °C for first two samples, probe fired immediately upon attaining interface temperature. Interface at 325-330 °C for final three pyrolysis runs. Probe fired 99.9 seconds in all cases and GC run started immediately after probe firing. MS scanned 15-550 m/z. GC purge time four minutes. Initial temperature @ -50 °C for six minutes, 10 °C/min. to 50 °C, then three °C/min. to 280 °C and 17.33 min. hold for 110 min. Total run time with the same column as soluble sample runs.

RESULTS & DISCUSSION

The conditions of the flask test in this work (175 °C, 24 hr., 100 mL/min. O_2) represent extremes, short of pyrolytic conditions, for the thermal-oxidative stress of fuel and must be understood to represent no possible real case. If anything, it is a hyper-accelerated storage model. The advantage of the conditions is the production of oxidation products and deposits in quantities amenable to the analytical methods used in a relatively short time.

We have subjected nine samples to thermal oxidative stress under identical conditions: The surrogate fuel, undoped; surrogate + 1.0 % 2-propylphenol; and surrogate + 1.0 % 2-propylphenol with 0.5 % sulfur compound (3,4-dimethylthiophenol, 2-ethylthiophenol, phenylethylmercaptan, hexanethiol, 2-ethylthiophene, dibenzothiophene and phenylsulfide). Soluble oxidation products are represented as silica gel extracts. Fuel insoluble, but acetone soluble solids are gums and acetone insoluble material is called solids. Table 3 is a compilation of the gravimetric data obtained. Relative comparison of these data to that obtained from real fuels [4] suggest that solid formation is the most valid indicator of thermal stability.

Fuels stable to deposit formation and thermally stable by JFTOT, etc., such as JP-7, JPTS, POSF 2747 and the surrogate fuel form substantial amounts of gum but insignificant solids in the flask test. Less stable fuels form less gum but dramatically more solids. The fuels with high gum and extract concentrations can be characterized as "oxidizable" fuels and those with high solids but low gums and extracts as "non-oxidizable". Table 3 shows dibenzothiophene, phenylsulfide and 2-ethylthiophene as dopants that produce "oxidizable" fuels relative to undoped surrogate (JP-8S) or surrogate doped only with 2-propylphenol. The thiophenols and alkyl thiols, 3,4-dimethylthiophenol, 2-ethylthiophenol, phenylethylmercaptan and hexanethiol doped fuels are "non-oxidizable" and form larger amounts of solid deposit. 2-ethylthiophene is somewhat anomalous by gravimetric data as well as chromatographic analysis. This is probably due to extreme oxidative conditions, cleaving the ring to form a sulfonic acid.

Space permits only representative chromatograms and product identification for polar extracts and thermal desorbtion/pyrolysis of solids. The more extreme cases are used. Chromatograms of polar extracts of "oxidizable" fuels are Figure 1a, surrogate, no dopant, 1b, phenylsulfide dopant and Figure 1c, dibenzothiophene dopant. Tables 1a, 1b and 1c are product identification for the corresponding chromatograms. Figures 2a and 2b are chromatograms of "non-oxidizable" fuels, doped with phenylethylmercaptan and 3,4-dimethylthiophenol. Tables 2a and 2b are product identification for these chromatograms.

Comparison of the chromatograms shows a dearth of oxidation products from the fuels doped with the thiol and thiophenol and a proliferation of oxidized species in undoped and fuels doped with phenylsulfide and dibenzothiophene. 2-propylphenol and 2,4,5-trimethylphenol are the most abundant compounds in the extracts of phenylethylmercaptan and 3,4-dimethylthiophenol doped surrogate. The trimethylphenol has to be the product of hydroperoxide decomposition from the 1,2,4,5-tetramethylbenzene (durene), present in the surrogate fuel. The phenols are minor components in the chromatograms of the "oxidizable" fuel extracts. The sulfones of dibenzothiophene and phenylsulfide are found in the respective chromatograms (at about 94 and 88 min. R.T.). The most reasonable interpretation of these observations is that the alkyl and aryl thiols both quickly oxidize to sulfonic acids that catalyze phenol production from α-arylhydroperoxides. Oxidation of aliphatic fuel components is inhibited. The sulfide and thiophene are oxidized to sulfones but essentially do not affect oxidation of fuel components.

Sequential thermal desorbtion/pyrolysis with GC-MS analysis has proven a valuable technique for characterization of insoluble solids, but care must be exercised in interpretation of data. Pyrolysis onset temperature and the result of thermo-synthesis degradation and rearrangements can not be exactly known. Total ion chromatograms for the technique applied to solids formed by the surrogate fuel doped with 2-propylphenol and 3,4-dimethylthiophenol are presented in Figure 3. The temperature sequence the sample is subjected to for separate chromatograms is 200, 280, 450, 750 and 1100 °C. Experience has shown that solid deposits from jet fuels contain high concentrations of absorbed fuel components. These are essentially all desorbed at 200 °C. 280 and 450 °C provide the most useful information for characterizing the solid matrix. At 280 °C, it is assumed that strongly absorbed compounds are desorbed and weak chemical bonds are broken. At 450 °C, we assume pyrolytic decomposition of the polymeric matrix without extensive rearrangement or pyrosynthesis. This is supported by model studies with "Noryl" (poly-2,6-dimethylphenol) polymer [3]. Pyrolysis at 450 °C produced monomeric C_1-C_3 phenols in high abundance and several -O- and -CH_2- linked dimers. The major product was 2,6-dimethylphenol. We assume that this step condenses remaining solid sample and subsequent chromatograms are essentially all from aromatic hydrocarbons.

Figures 4a and 4b through 7a and 7b, are the respective total ion chromatograms obtained from solids of fuels doped with phenylsulfide, dibenzothiophene, phenylethylmercaptan and 3,4-dimethylthiophenol at 280 and 450 °C. These chromatograms support the oxidative phenolic coupling as the mechanism for formation of extensive solid deposits. The chromatograms from the "non-oxidizing" thiophenol and mercaptan doped surrogate are essentially all phenolic and aromatic while the chromatograms of solids from sulfide and thiophene doped fuel show predominately alkenes, alcohols and ketones. The sulfonic acids of phenylethylmercaptan and 3,4-dimethylthiophenol are present in the respective chromatograms, as are the dibenzosulfone and phenylsulfoxide.

The data from this work is consistent with sulfonic acid formation and catalysis of phenol production to result in insoluble solid deposits formed by oxidative phenolic coupling. A consequence of these observations is that it should be relatively simple to devise a method to predict fuel stability (to solid deposit formation) that would be

based on caustic extraction followed by further separation and analysis. Such a method would need to include removal of extractable interferences such as deicer.

The dilemma of stability to peroxidation verses deposition remains. Hydrotreated fuels would seem to solve the deposition problems if engines and fuel transfer systems were "peroxide proof". At present, it seems the solution requires antioxidants that are themselves not deposit promoters.

ACKNOWLEDGMENTS

This work was supported under USAF contract F49620-90-C-09076 and subcontract RI-84470X, contract F33615-92-C-2207 (University of Dayton Research Institute). We especially thank Dr. Mel Roquemore, Bill Harrison, Ellen Stewart, of WL/POSF, and Dr. Dilip Ballal and Dr. Shawn Heneghan of UDRI for contributions and assistance.

REFERENCES

1. Zarbarnick, S. and Grinstead, B.R., Preprints, Division of Petroleum Chemistry, ACS, 39, 51 (1994).

2. Hazlett, R.N. and Power, A.J., Proceedings, 2nd International Conference on Long Term Storage Stabilities of Liquid Fuels, San Antonio, TX, 556 (1986).

3. Schulz, W.D., Preprints, Division of Petroleum Chemistry, ACS, 39, 61 (1994).

4. Schulz, W.D., Preprints, Division of Petroleum Chemistry, ACS, 39, 30 (1994).

5. Heneghan, S.P., Locklear, S.L., Geiger, D.L., Anderson, S.D. and Schulz, W.D., Jet Propulsion, 9, 5 (1993).

6. Seymore, R.B. and Carraher, C.E., "Polymer Chemistry", 3rd Ed., John Wiley & Sons, New York (1991).

7. Watkins, J.M., Mushrush, G.W., Beal, E.J. and Hardy, D.R., Preprints, Division of Petroleum Chemistry, ACS, 34, 832 (1989).

8. Mushrush, G.W., Hazlett, R.N. and Hardy, D.R., Proceedings, 2nd International Conference on Long Term Stability of Liquid Fuels, San Antonio, TX, 512 (1986).

9. Schulz, W.D., Preprints, Division of Petroleum Chemistry, ACS, 31, 383 (1992).

Figure 1a. Total Ion Chromatogram of Solid Phase Extract of JP-8S + 1.0 % 2-propylphenol. 24 Hour Flask Test at 175 °C With Flowing Oxygen.

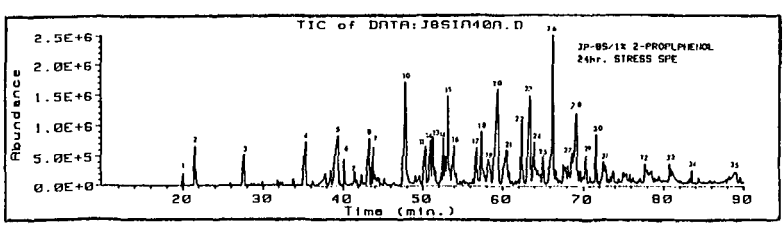

Figure 1b. Total Ion Chromatogram of Solid Phase Extract of JP-8S + 1.0 % 2-propylphenol and 0.5 % Phenylsulfide. 24 Hour Flask Test at 175 °C With Flowing Oxygen.

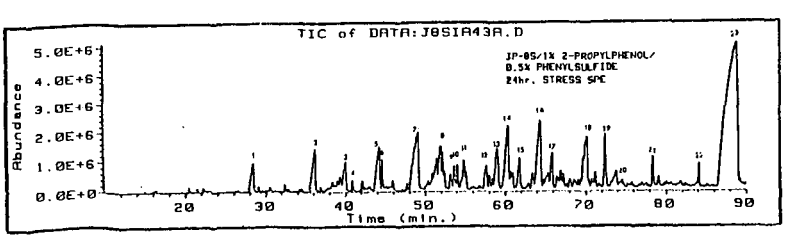

Figure 1c. Total Ion Chromatogram of Solid Phase Extract of JP-8S + 1.0 % 2-propylphenol and 0.5 % Dibenzothiophene. 24 Hour Flask Test at 175 °C With Flowing Oxygen.

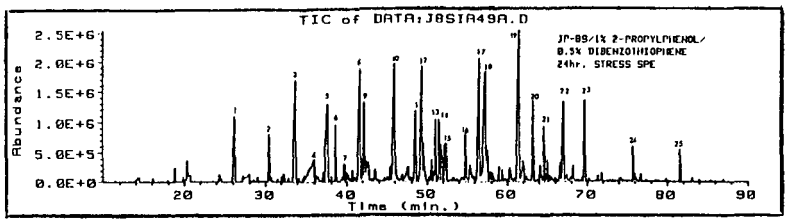

Figure 2a. Total Ion Chromatogram of Solid Phase Extract of JP-8S + 1.0 % 2-propylphenol and 0.5 % Phenylethylmercaptan. 24 Hour Flask Test at 175 °C with Flowing Oxygen.

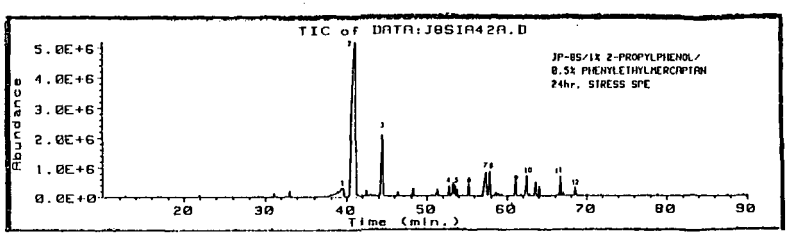

Figure 2b. Total Ion chromatogram of Solid Phase Extract of JP-8S + 1.0 % 2-propylphenol and 0.5 % 3,4-dimethylthiophenol. 24 Hour Flask Test at 175 °C With Flowing Oxygen.

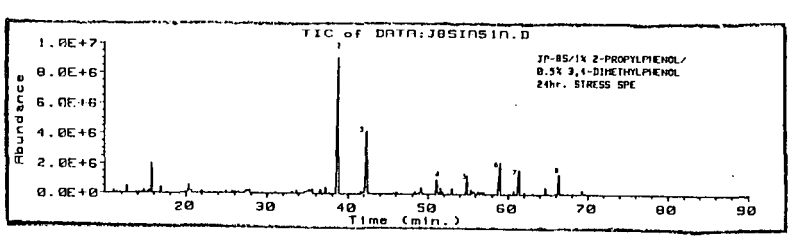

Table 1a. Peak Identification for Figure 1a.

Peak #	Rt (min.)	Compound			
1.	20.06	Methyldihydrofuran	23.	63.53	Propenylbenzodioxole
2.	21.60	Mixed phenol/furanmethanol	24.	64.02	C_6 phenol
3.	27.65	Ethyldihydrofuran	25.	65.15	Heptyldihydrofuran
4.	35.37	Propyldihydrofuran	26.	66.43	Hexadecane/C_7 dihydrofuran mix
5.	39.43	Mixed acid	27.	68.66	Methylnaphthalenol
6.	40.20	2-propylphenol	28.	69.19	Phenylketone
7.	41.56	Aliphatic alcohol	29.	70.39	Substituted cycloketone
8.	43.36	Butyldihydrofuran	30.	71.62	C_8 dihydrofuran
9.	43.87	2,4,5-trimethylphenol	31.	72.64	Substituted naphthalene
10.	47.62	Mixed isobenzofurandione/methyl naphthalene			
11.	50.37	Isobenzofuranone	32.	77.64	C_9 dihydrofuran
12.	51.02	Pentyldihydrofuran	33.	80.78	Substituted aromatic
13.	51.29	Substituted benzene	34.	83.47	C_{10} dihydrofuran
14.	52.60	C_6 phenol	35.	89.03	Substituted aromatic
15.	53.21	Tetradecane			
16.	53.99	Methylisobenzofurandione			
17.	56.80	Benzopyranone			
18.	57.40	Substituted benzopyran			
19.	58.29	Hexyldihydrofuran			
20.	59.47	Naphthalenone			
21.	60.45	Indolediole			
22.	64.02	C_6 phenol?			

Figure 1c. Total Ion Chromatogram of Solid Phase Extract of JP-8S + 1.0 % 2-propylphenol and 0.5 % Dibenzothiophene. 24 Hour Flask Test at 175 °C With Flowing Oxygen.

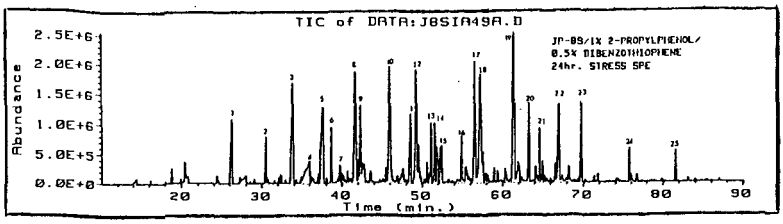

Figure 2a. Total Ion Chromatogram of Solid Phase Extract of JP-8S + 1.0 % 2-propylphenol and 0.5 % Phenylethylmercaptan. 24 Hour Flask Test at 175 °C with Flowing Oxygen.

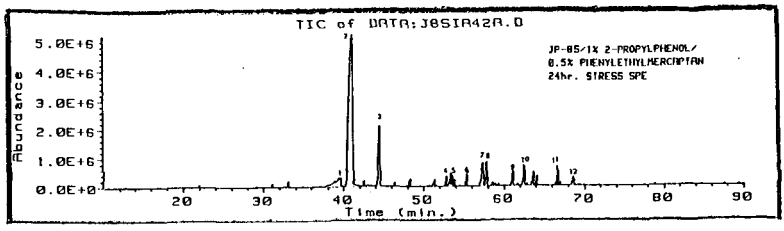

Figure 2b. Total Ion chromatogram of Solid Phase Extract of JP-8S + 1.0 % 2-propylphenol and 0.5 % 3,4-dimethylthiophenol. 24 Hour Flask Test at 175 °C With Flowing Oxygen.

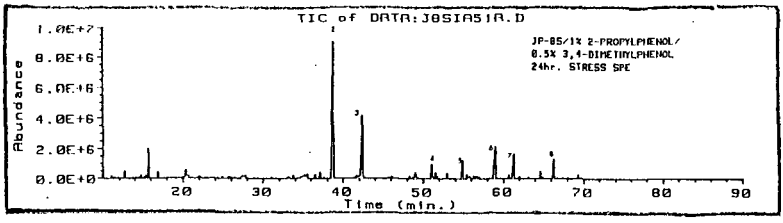

Table 1a. Peak Identification for Figure 1a.

Peak #	Rt (min.)	Compound			
1.	20.06	Methyldihydrofuran	23.	63.53	Propenylbenzodioxole
2.	21.60	Mixed phenol/furanmethanol	24.	64.02	C_6 phenol
3.	27.65	Ethyldihydrofuran	25.	65.15	Heptyldihydrofuran
4.	35.37	Propyldihydrofuran	26.	66.43	Hexadecane/C_7 dihydrofuran mix
5.	39.43	Mixed acid	27.	68.66	Methylnaphthalenol
6.	40.20	2-propylphenol	28.	69.19	Phenylketone
7.	41.56	Aliphatic alcohol	29.	70.39	Substituted cycloketone
8.	43.36	Butyldihydrofuran	30.	71.62	C_8 dihydrofuran
9.	43.87	2,4,5-trimethylphenol	31.	72.64	Substituted naphthalene
10.	47.62	Mixed isobenzofurandione/methyl naphthalene			
11.	50.37	Isobenzofurawone	32.	77.64	C_9 dihydrofuran
12.	51.02	Pentyldihydrofuran	33.	80.78	Substituted aromatic
13.	51.29	Substituted benzene	34.	83.47	C_{10} dihydrofuran
14.	52.60	C_6 phenol	35.	89.03	Substituted aromatic
15.	53.21	Tetradecane			
16.	53.99	Methylisobenzofurandione			
17.	56.80	Benzopyranone			
18.	57.40	Substituted benzopyran			
19.	58.29	Hexyldihydrofuran			
20.	59.47	Naphthalenone			
21.	60.45	Indolediole			
22.	64.02	C_6 phenol?			

Table 1b. Peak Identification for Figure 1b.

Peak #	Rt (min.)	Compound
1.	28.52	Ethyldihydrofuran
2.	36.34	Propyldihydrofuran
3.	40.12	Hexanoic acid
4.	40.97	2-propylphenol
5.	44.37	Butyldihydrofuran
6.	44.72	C_4 dihydrofuran
7.	49.27	Isobenzofurandione
8.	52.13	C_5 dihydrofuran
9.	53.83	Methylbenzofurandione
10.	54.23	Alkaneol
11.	54.99	Methylisobenzofurandione
12.	57.78	Benzopyranone
13.	59.12	Hexyldihydrofuran
14.	60.53	Dihydronaphthalenone
15.	61.94	Phthalate
16.	64.56	Phenylpropenal
17.	66.07	C_7 dihydrofuran
18.	70.27	Substituted cyclokctone
19.	72.52	C_8 dihydrofuran
20.	73.91	Naphthoic acid
21.	78.50	C_9 dihydrofuran
22.	84.25	C_{10} dihydrofuran
23.	88.94	Phenylsulfone

Table 1c. Peak Identification for Figure 1c.

Peak #	Rt (min.)	Compound
1.	26.22	Ethyldihydrofuran
2.	30.49	Diene ?
3.	33.82	Propyldihydrofuran
4.	35.95	Phenylethylethanone
5.	37.55	Carboxylic acid
6.	38.50	2-propylphenol
7.	39.69	Substituted cyclohexanone
8.	41.72	Butyldihydrofuran
9.	42.25	2,4,5-trimethylphenol
10.	46.03	Isobenzofurandione
11.	48.52	Isobenzofurandione
12.	49.29	Butyldihydrofuranone
13.	51.11	Substituted benzofuran
14.	51.52	Substituted alkane
15.	52.42	Pentyldihydrofuran
16.	54.86	Benzopyranone
17.	56.62	Hexyldihydrofuran
18.	57.34	Substituted benzoic acid
19.	61.45	Substituted benzene
20.	63.27	Heptyldihydrofuran
21.	64.57	Alkane
22.	67.02	Substituted ketone
23.	69.73	Octyldihydrofuran
24.	75.77	Nonyldihydrofuran
25.	81.54	Decyldihydrofuran

Table 2a. Peak Identification for Figure 2a.

Peak #	Rt (min.)	Compound
1.	39.42	Substituted benzoic acid
2.	41.18	2-propylphenol
3.	44.50	2,4,5-trimethylphenol
4.	52.75	Dihydronaphthalenone
5.	53.28	3,4-dihydrobenzopyran-2-one
6.	55.22	1,2-dihydroxypropylbenzene
7.	57.37	Benzopyran-2-one
8.	57.84	Substituted benzopyran
9.	61.04	Sub. dihydrobenzopyranone
10.	62.50	C_5 phenol
11.	66.65	Pentadecane
12.	68.60	Methylnaphthalenol

Table 2b. Peak Identification for Figure 2b

Peak #	Rt (min.)	Compound
1.	15.72	Ketone
2.	38.77	2-propylphenol
3.	42.35	2,4,5-trimethylphenol
4.	51.06	Methylbenzofuranone
5.	54.90	Benzopyran-2-one
6.	58.96	Substituted dimethylphenol
7.	61.29	Dimethyl-2,3-dihydroindene-1-one
8.	66.29	Substituted phenol

Table 3. Gravimetric Analysis of Thermally Stressed Fuels

Stress Sample	Gums	Solids	Total	SiOH Extract*
Surrogate + Dopant	Mass % of Fuel			mg/5mL Fuel
1 % 2-propylphenol/0.5 % dibenzothiophene	4.70	0.46	5.00	110.20
1 % 2-propylphenol/0.5 % 2-ethylthiophene	4.13	0.58	4.71	210.20
JP-8S (No dopant)	3.32	0.06	3.38	122.70
1 % 2-propylphenol/0.5 % phenylsulfide	2.43	0.29	2.72	191.50
1 % 2-propylphenol	1.71	0.16	1.87	155.80
1 % 2-propylphenol/0.5 % 2-ethylthiophenol	0.57	0.91	1.48	29.00
1% 2-propylphenol/0.5 % 3,4-dimethylthiophenol	0.38	1.30	1.68	32.00
1 % 2-propylphenol/0.5 % phenylethylmercaptan	0.35	0.46	0.81	34.10
1 % 2-propylphenol/0.5 % hexanethiol	0.29	0.43	0.72	21.60

*SiOH extract: Represents values for "soluble gums".

Figure 3. Sequential Thermal Desorbtion/Pyrolysis Total Ion Chromatograms of Insoluble Solids From JP-8S Doped With Cumene and 3,4-dimethylthiophenol.

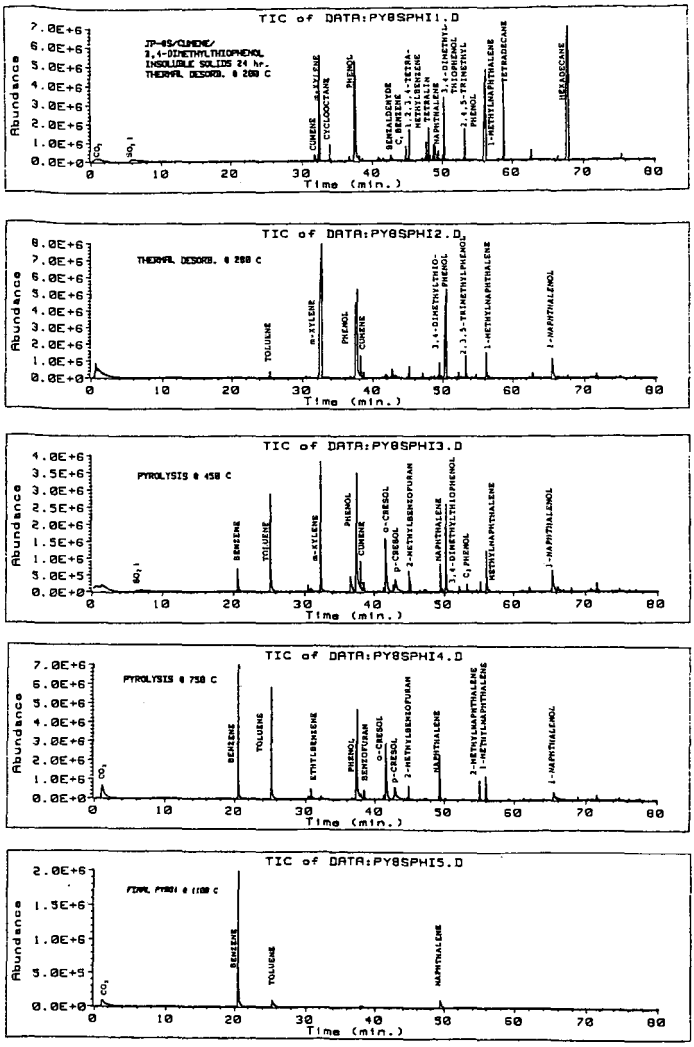

Figures 4a & b. Total Ion Chromatograms of Insoluble Solids From JP-8S + 1.0 % 2-propylphenol and 0.5 % Phenylsulfide. Thermal Desorbtion at 280 °C (a) and Pyrolysis at 450 °C (b).

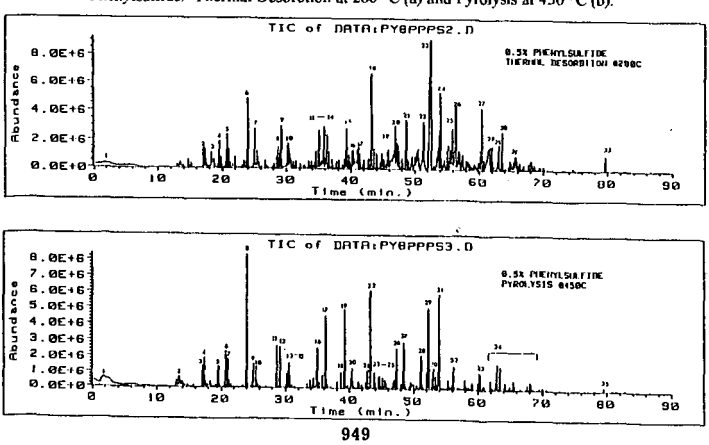

Figures 5a & b. Total Ion Chromatograms of Insoluble Solids From JP-8S + 1.0 % 2-propylphenol and 0.5 % Dibenzothiophene

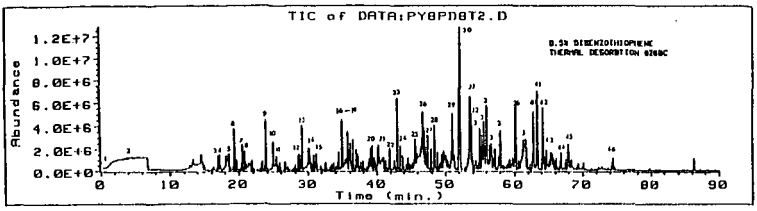

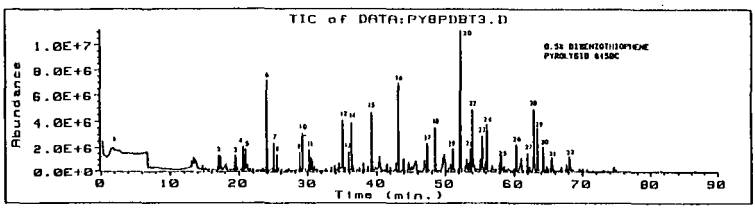

Figures 6 a & b. Thermal Desorbtion @ 280 °C and Pyrolysis @ 450 °C of Solids Formed From JP-8S Doped With 1.0 % 2-propylphenol & 0.5 % Phenylethylmercaptan.

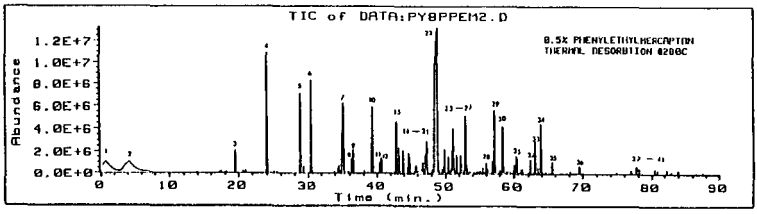

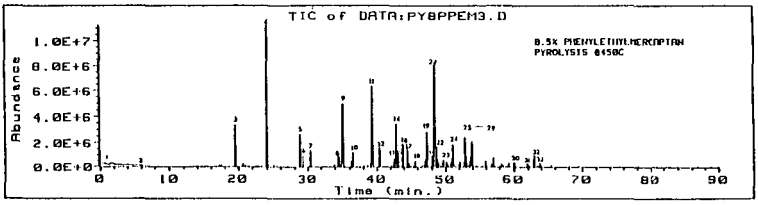

Figures 7 a & b Thermal Desorbtion @ 280 °C and Pyrolysis @ 450 °C of Solids Formed From JP-8S Doped With 1.0 % 2-propylphenol & 0.5 % 3,4-dimethylthiophenol.

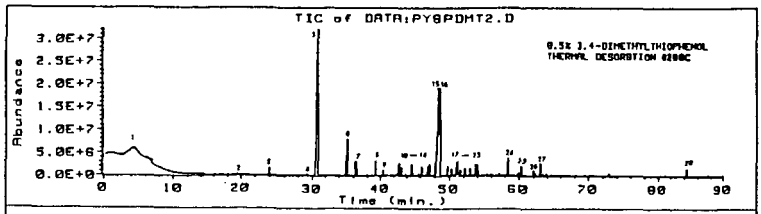

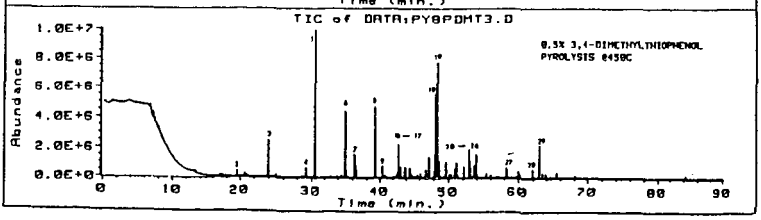

Tables 4 a & b Compound Identification for Figures 4 a & b

Peak #	Rt (min.)	Compound @ 280 °C	Rt (min.)	Compound @ 450 °C
1	1.58	Carbon dioxide	1.72	Carbon dioxide
2.	17.35	Hexane	13.50	Substituted alkane
3	18.29	Hexadiene	17.10	Hexene
4.	19.50	Benzene	17.36	Hexane
5.	23.48	Toluene	19.35	Benzene
6	25.01	Octene	20.66	Heptene
7	28.72	Ethylbenzene	21.00	Heptane
8	29.05	Xylene	24.00	Toluene
9	30.40	Styrene	25.01	Octene
10	33.60	Heptanol	25.42	Octane
11.	35.06	Phenol	28.74	Ethylbenzene
12.	35.84	Decene	29.30	Xylene
13	36.25	Trimethylbenzene	30.19	Substituted heptene
14.	39.29	Propylbenzene	30.49	Xylene
15	40.32	Octanol	30.67	Nonane/xylene mix
16	41.18	Dihydrobenzofuran	35.02	Phenol
17	43.27	C_4 benzene	36.29	Trimethylbenzene
18	44-46.50	Substituted alkanes	38.69	2,3-dihydro-1H-indene
19	46.93	Dodecene	39.29	Cresol
20	48.68	2-propylphenol	40.41	Cresol
21	51.36	Trimethylphenol	42.82	Methylbenzofuran
22.	52.58	2,3-dihydro-1H-indenecene	43.26	1,2,4,5-tetramethylbenzene
23.	54.07	Methylnaphthalene	43.85	2-ethylphenol
24.	55.92	1,1'(1,3-phenylene)bis-ethanone	44.68	C_3 phenol
25	56.45	Isobenzofuranone	45.14	Methyl-1H-indene
26.	60.21	C_4 phenol	47.34	Naphthalene
27	61.50	Trimethylbenzoic acid	48.47	2-propylphenol*
28.	63.06	Naphthalenol	48.47	Trimethylphenol
29	65.71	Tetrahydromethanonaphthalene	51.15	2,3-dihydro-1H-indenecene
30.	79.62	Phenylsulfoxide**	52.23	Methylnaphthalene
31			53.10	Methylnaphthalene
32.			54.03	C_4 benzene
33.			56.21	Substituted phenol
34			62.93-68.13	Naphthalenols
35.			79.58	Phenylsulfoxide**

* Dopant

**Oxidized dopant

Tables 7 a & b Compound Identification for Figures 7 a & b

Peak #	Rt (min.)	Compound @ 280 °C	Rt (min.)	Compound @ 450 °C
1	0-15	Air/sulfur dioxide mix	0-15	Air/sulfur dioxide mix
2.	19.54	Benzene	19.53	Benzene
3	23.96	Toluene	23.95	Toluene
4.	29.23	Ethylbenzene	29.20	Ethylbenzene
5.	30.86	Xylene	30.54	Xylene
6	35.12	Phenol	35.04	Phenol
7	36.34	Trimethylbenzene	36.26	Trimethylbenzene
8	39.28	Cresol	39.30	Cresol
9	40.46	Cresol	40.40	Cresol
10.	43.22	2-methylbenzofuran	42.85	Phenylpropenal
11.	43.75	C_3 benzene	43.21	C_4 benzene
12.	44.73	Dimethylphenol	43.86	Ethylphenol
13	46.24	Dimethylphenol	44.55	C_3 phenol
14	47.37	Naphthalene	44.83	Phenylpropenal
15.	48.46	2,3-dimethylthiophenol*	45.70	Benzaldehyde
16	48.72	2-propylphenol*	46.15	Ethylphenol
17.	49.79	C_4 benzene	47.33	Naphthalene
18.	50.40	C_4 naphthalene	48.23	3,4-dimethylthiophenol*
19	50.95	Substituted benzofuran	48.49	2-propylphenol
20.	51.09	2,4,5-trimethylphenol	48.72	Dimethylbenzofuran
21.	52.98	C_4 phenol	49.67	Cyclooctatrienedione
22.	53.99	Methylnaphthalene	50.80	Dimethylocta-ne
23.	57.18	Substituted aromatic	0.99	Trimethylphenol
24.	58.45	dihydroxypropylbenzene	52.14	2,3-dihydro-1H-indenecene
25.	61.99	2,3-dimethylphenolsulfonic acid**	52.92	C_4 phenol
26.	63.00	Naphthalenol	53.11	Methylnaphthalene
27.	72.88	Substituted aromatic	53.93	Dihydromethanonaphthalene
28.	84.31	Substituted aromatic	61.94	3,4-dimethylphenylsulfonic acid**
29			62.93	Naphthalenol

Tables 5a & b Compound Identification for Figures 5a & b

Peak #	Rt (min.)	Compound @ 280 °C	Rt (min.)	Compound @ 450 °C
1.	0.75	Carbon dioxide	1.20	Carbon dioxide
2.	0.75-7.00	Air	17.07	Hexene
3.	16.88	Hexene	19.47	Benzene
4	17.07	Butanol	20.85	Heptene
5.	18.16	Hexadiene	20.98	Heptane
6.	19.36	Benzene	23.97	Toluene
7.	20.50	Heptene	25.01	Octene
8	20.83	Heptane	25.43	Octane
9.	23.81	Toluene	28.73	m,p-xylene
10.	24.84	Octene	29.23	o-xylene
12.	25.28	Octane	30.43	Styrene
13.	28.39	Ethylbenzene	35.02	Phenol
14.	29.03	Xylene	35.87	Alkene
15.	30.24	Styrene	36.30	1,2,4-trimethylbenzene
16.	30.84	Cyclooctadiene	39.27	o-cresol mixed
17	34.89	Phenol	43.25	1,2,1,5-tetramethylbenzene
18	35.67	Nonene	47.36	Naphthalene
19.	36.08	Trimethylbenzene	48.52	2-propylphenol*
20.	36.46	Decene	51.14	2,3,6-trimethylphenol
21.	39.33	Cyclooctanedienone	52.32	2,3-dihydroindene-1-one
22.	40.13	Mixed alcohol	53.69	1,3-isobenzofurandione
23.	41.89	Mixed diene	54.00	Methylnaphthalene
24	43.03	C_3 benzene	55.52	Isobenzofuranone
25.	43.14	C_4 alkylbenzene	56.25	Diphenylethanone
26.	45.67	Butylcyclopropene	58.23	Ethylbenzylfuran
27	46.77	Dodecenes	61.99	Methylnaphthalenediol
28.	48.42	Mixed alkene	63.03	Naphthalenol
29.	49.23	2-propylphenol*	63.48	Naphthalenol
30.	51.04	C_4 phenol	64.33	C_4 phenol
31.	52.21	2,3-dihydro-1H-indenecene	65.56	Methylnaphthalenol
32	53.66	Isobenzofurandione	68.20	Methylnaphthalenol
33.	53.86	Methylnaphthalene	74.62	Dimethylnaphthalenol
34	55.02	Indene-1H-diene		
35.	55.67	Phenylethylene bis ethanone		
36.	56.15	Isobenzofuranone		
37	56.54	Tetradecene		
38.	58.13	Benzofuran		
39	60.19	C^3 benzene		
40.	62.15	Dihydromphthalenone		
41.	62.84	Naphthalenol		
42.	63.44	Naphthalenol		
43.	64.27	Mixed isobenzofurandione		
44	64.50-67.00	Alkane/aromatic mix		
45.	68.00	C_4 benzene		
46	74.43	Naphthalene/alkene mix		
	86.27	Dibenzosulfone**		

Tables 6 a & b Compound Identification for Figures 6 a & b.

Peak #	Rt (min.)	Compound @ 280 °C	Rt (min.)	Compound @ 450 °C
1	0.70	Carbon dioxide	0.40	Carbon dioxide
2.	4.32	Sulfur dioxide	4.55	Sulfur dioxide
3.	19.55	Benzene	19.54	Benzene
4	23.91	Toluene	24.01	Toluene
5.	28.75	Ethylbenzene	28.70	Ethylbenzene
6	30.42	Styrene	29.16	Xylene
7.	35.15	Phenol	30.37	Styrene
8	36.21	Trimethylbenzene	34.45	Benzaldehyde
9	36.45	Benzofuran	35.07	Phenol
10.	39.33	Cresol	36.40	Benzofuran
11.	40.42	Cresol	39.33	Cresol
12	42.82	Methylbenzofuran	40.39	Cresol
13.	43.17	1,2,4,5-tetramethylbenzene	42.49	Dimethylphenol
14	43.28	Benzenethanol	42.84	Methylbenzofuran
15.	43.82	2-ethylphenol	43.14	Ethylbenzene
16.	44.66	dimethylphenol	43.80	Ethylphenol
17.	44.82	Dihydromethylbenzofuran	44.51	Dimethylphenol
18.	45.74	Hydroxyphenylethanone	45.66	2-hydroxyphenylethanone
19	46.79	Phenylethylmercaptan*	47.31	Azulene
20	47.14	Benzenedial	48.03	Isopropylbenzaldehyde
21	47.33	Naphthalene	48.48	2-propylphenol*
22.	48.80	2-propylphenol*	48.66	Dimethylbenzofuran
23.	49.84	Substituted aromatic acid	51.05	C_2 phenol
24	50.89	Dihydromethylbenzofuran	52.63	2,3-dihydro-1H-indenecene
25.	51.10	2,4,5-trimethylphenol	52.96	C_3 phenol
26.	52.29	2,3-dihydro-1H-indenecene	53.05	Methylnaphthalene
27	52.96	C_4 phenol	55.89	Propylbenzaldehyde
28.	55.42	Methylbenzoxybenzaldehyde	57.08	2-thiophene
29.	57.24	2-thiophene	59.28	Methoxypropenylphenol
30.	58.46	Dihydroxypropylbenzene	59.99	Dimethylnaphthalene
31.	60.34	Substituted benzene	61.83	Phenylethylsulfonic acid**
32.	62.98	Naphthalenol	62.86	Methylnaphthalenol
33	63.86	2-thiophene	63.80	Dihydromethoxynaphthalene
34.	65.53	Anthracene		
35.	69.54	Methylidibenzofuran		
36	77.15	Substituted methoxybenzene		
37.	80.40	Substituted phenylether		
38.	80.88	2-thiophene		
39.	82.29	Substituted aromatic		
40	83.92	Substituted anthracene		
41.				
42.				

SURFACE FOULING: SHORT- VS. LONG -TERM TESTS

E. Grant Jones and Walter J. Balster
Systems Research Laboratories, Inc.
A Division of Calspan Corporation
2800 Indian Ripple Road
Dayton, OH 45440-3696

Keywords: Autoxidation, Autocatalysis, Surface Fouling

INTRODUCTION

Problems associated with surface fouling of fuel lines, nozzles, and heat exchangers caused by thermo-oxidative stressing of aviation fuel have been documented.[1] With enhanced aircraft performance, heat loads from both the airframe and the engine that must be dissipated via the fuel become greater. The resultant additional fuel degradation exacerbates aircraft system failures. Since the extent of surface fouling depends strongly upon the particular aviation fuel, it is important to be able to assess each fuel in a simple accelerated laboratory test for simulating the thermo-oxidative stress experienced in aircraft fuel lines.

In the present study a simple dynamic test is employed, whereby the fuel is stressed under well-defined chemical-oxidation conditions that are near-isothermal. Quantification of surface and filtered insolubles provides an objective evaluation of fuel behavior at each temperature. In addition, the dependence of deposition rate upon stress duration provides a temporal profile of the reaction. The general laboratory goal is to evaluate fuel at several temperatures in an attempt to simulate thermo-oxidative stress but not the fluid-dynamic conditions in aircraft. These results can then be used to calibrate Computational-Fluid-Dynamics (CFD) models[2] for calculating fouling under the diverse temperature and fuel-flow conditions that are found within aircraft but are difficult to achieve experimentally with small-scale rigs.

The present investigation has involved fouling of heated stainless-steel surfaces caused by a particular Jet-A aviation fuel designated POSF-2827. Although this is a representative fuel that meets USAF specifications, it has a propensity for fouling heated surfaces at low temperatures, making it an ideal candidate for experimental study.[3] Recent results were reported from this laboratory on surface deposition on stainless-steel surfaces as a function of stress duration for fuel flowing through a heat exchanger at 185°C under near-isothermal conditions.[4,5] These results indicated that deposition arises from a bulk-formed species designated a surface-deposition precursor, P, and that deposition is complete within 10 min of stressing inside 0.125-in-o.d. stainless-steel tubing. Deposition over the temperature range 155-225°C was found to occur during a time interval that correlates with the measured time for oxygen consumption.[6,7] The experimental test time in these prior experiments was set at 6 hr to ensure measurable deposits yet maintain surface fouling predominantly on the steel rather than on previously deposited surfaces.

The goal of the current study was to compare deposition in short-term (6-hr) tests with that in long-term tests where most of the deposition occurs on previously deposited surfaces. Results reported here show that the average surface fouling rates measured during extended test times differ from those measured during a 6-hr test. Since the bulk-fuel/wall temperature is held constant during the course of these experiments as a result of the low flow rate, deposits serve only to change the surface layer without influencing the bulk temperature of the fuel.

As the test time is extended, the deposition-rate-versus-stress-duration profile broadens, the maximum is reduced, and its location shifts to longer stress duration. These observations made at 155 and 185°C are shown to arise from a transition in the rate of oxygen loss as a result of surface fouling and a reduction in adherence to a fouled surface. The implications of these findings with respect to inherent surface fouling within aviation fuel systems are discussed.

EXPERIMENTAL

POSF-2827 fuel has a JFTOT breakpoint of 266°C and a sulfur level of 0.079% (w/w). This fuel falls into a category described by Kendall and Mills[8] where the presence of sulfur compounds tends to inhibit oxidation but at the expense of increased insoluble formation.[3]

Data were collected using the Near-Isothermal Flowing Test Rig (NIFTR) which has been described previously.[4,5] The advantage of the NIFTR experiment is the ability to measure deposition rates and dissolved oxygen as a function of reaction time at a fixed temperature. For each selected fuel-flow rate, the reaction time or stress duration is determined by tube dimensions and location along the tube axis. In the present experiment deposits were collected on 0.125-in.-o.d., 0.085-in.-i.d. commercial stainless-steel (304) tubing. The standard heated section was 32 in.; however, for test times longer than 6 hr, the spatial distribution of the deposition broadened and the complete profile could not be collected on a single pass through the heat exchanger. Three approaches were taken: 1) only the limited profile was collected on a single pass, 2) the fuel was passed back through a second tube within the NIFTR to double the path length, and 3) the fuel-flow rate was reduced to extend the stress duration accordingly within a single pass. It is important to distinguish stress duration from experimental test time in dynamic isothermal experiments. Stress duration is the reaction time at temperature, and the experimental test time (along with the fuel-flow rate) determines the total quantity of fuel passed through the system. The total fuel ranged from 25 to 1035 mL. Dissolved oxygen was measured in separate experiments using the entire tube as a reaction region, with stress time being varied by changing the fuel-flow rate.

Deposition rates at 185 and 155°C are based on the quantity of carbon in the deposits determined from surface-carbon burnoff (LECO RC-412) of 2-in. sections cut from the 32-in. heated tube. Rate is expressed in units of micrograms of carbon per unit volume of tube section per unit test time which is equivalent to micrograms of carbon per unit stress time within a tube section per unit volume of fuel passed through the system.[5] In each case the fuel is saturated with respect to air, with oxygen being measured as 64 ppm (w/w).[9]

RESULTS AND DISCUSSION

Deposition. The measured deposition rate averaged for 6, 24, 30, 32, 48, and 69 hr is shown in Figure 1 as a function of stress duration at 185°C for a fixed fuel-flow rate of 0.25 mL/min. The following observations describe the changes in surface deposition with extension of integration time: 1) the profile broadens with significant tailing; 2) the maximum in the deposition rate is reduced; and 3) the center of the deposition peak shifts to slightly longer stress times. Also, the profiles appear to approach a common shape at the longest experimental times. Extended reaction time in the 30- and 69-hr experiments was afforded by a second pass through the heat exchanger. Results of similar experiments at 155°C are presented in Figure 2. The same trends are observed; however, the reaction time frame is extended to permit completion of the deposition processes at lower temperature.

Note that when comparing rates averaged over different experimental times, the baseline drops as the experimental time is increased. Background carbon which is independent of experimental test time has not been subtracted, and its impact is reduced in the longer-term averages.

The major difference between 6-hr tests and those of much longer duration is the nature of the surface. Initially the deposition occurs on cleaned stainless-steel tube surfaces. As the experimental time is extended, the surface gradually makes a transition to a completely carbonaceous-coated one. Deposition should be constant after complete coverage of the stainless-steel surfaces; for example, after the 48-hr test at 185°C, the surface density at the maximum is 90 $\mu g\ cm^{-2}$. The maximum deposition rate per unit area is 1.1 $\mu g\ cm^{-2}$ per hour of experiment. The observed variation in deposition is related to surface changes, and the major factor will be shown to be the rate of oxygen consumption.

Oxygen Loss. The residual dissolved oxygen for this fuel has been reported as a function of reaction time in stainless-steel tubes.[5] Accelerated oxygen consumption observed at higher conversion was attributed to autocatalysis. Figure 3 shows the oxygen loss at 185°C measured using 1) a 32-in. cleaned stainless-steel tube,[5] 2) a tube that previously had been coated with carbonaceous deposits containing 0.27 mg of carbon, and 3) a tube coated with the same deposits containing 1.5 mg of carbon. The initial rates are similar. Autocatalysis causes the rapid increase in rate at higher conversion in the cleaned tube; however, this appears to be a surface-related phenomenon that is no longer observed when the surface becomes coated with deposits. Rates measured with the coated tubes remain constant, indicating a predominantly zeroth-order or oxygen-non-limited reaction.[4] After 8-9 min all of the oxygen is converted, and the source of the deposits (namely, P) can no longer be maintained. This

time corresponds to the location of the maximum in the shifted deposition profile at 185°C. Similarly, oxygen loss measured at 155°C (Figure 4) shows the same trend.

If the stainless-steel tubing is viewed as the norm, then deposits perturb the oxygen consumption by eliminating autocatalysis. If the coated (passivated) tubing is viewed as the norm--an alternative and preferable view--then the stainless steel perturbs the oxygen consumption by providing active catalytic sites which, at higher conversion, lead to an increased oxygen reaction rate. Deposition in short-term (6-hr) tests over the temperature range 155-225°C correlates with oxygen loss measured in cleaned stainless-steel tubes;[6] similarly, deposition in long-term tests is expected to correlate with oxygen loss measured using tubes that have been passivated by deposits. The higher deposition rate observed in 6-hr experiments results from the oxygen loss that occurs during surface-induced autocatalysis. The reduction in surface deposition rate, the broadening of the deposition profile, and the shift in the maximum in the long-term experiments are manifestations of the slower, constant rate of oxygen loss.

The deposition profiles in long-term tests have tails that extend well beyond the region of 100% oxygen conversion. For example, at 185°C, despite complete oxygen depletion at 9 min, the deposition continues beyond 17 min. This is interpreted as reduced surface adherence of P.

Implications. Autocatalysis has been attributed to thermal dissociation of an oxidation product such as hydroperoxide.[5] The present results indicate that autocatalytic effects in POSF-2827 fuel are caused by a surface-induced reaction of an oxidation product involving active sites on stainless steel. Carbonaceous deposits remove active sites, thereby eliminating autocatalysis.

Carbon-burnoff techniques generally require the use of cleaned surfaces for minimizing background. Based upon the current findings, when surface-induced autocatalysis occurs, the maximum deposition and the oxygen reaction rates will be faster in short-term experiments that are carried to high conversion. Fuel evaluation in this laboratory is predicated on accelerated short-term tests that stress the fuel to complete oxygen conversion. In rating fuels, a deposition-rate criterion has not been applied; instead a total integrated quantity of deposit, i.e. the area under the deposition profile in units of micrograms/milliliter, has been used.

Catalytic effects of metals dissolved in fuels, in particular, copper from copper tubing as in Naval applications, can reduce fuel thermal stability, even at low concentrations.[1] Kendall and Mills[8] observed this effect in flask tests, and Morris and Turner[10] observed it in expanded JFTOT experiments. Conceivably, the role of dissolved copper in catalyzing oxygen loss is analogous to the role of stainless-steel walls in what has been termed surface-induced autocatalysis.

Fuel-evaluation techniques such as the JFTOT and Hot Liquid Process Simulator (HLPS) which make use of clean aluminum and stainless-steel surfaces, respectively, would be expected to be sensitive to the nature of the surface and also the manner in which oxygen is consumed. For example, Clark et al.[11] have reported that a metal deactivator (MDA) functions optimally on clean metal surfaces; however, once a lacquer layer has formed, MDA does not reduce deposition. The vulnerability of JFTOT results in short-term tests has been discussed by Clark and Bishop.[12] The initial surface-passivation effects of MDA may mask problems detectable only during extended time periods. In view of the current results, the short-term benefit of MDA may be surface passivation which prevents autocatalysis. The reduced deposition would then be explained in terms of MDA slowing oxygen consumption rather than hindering adherence to the surface. In recent studies the DuPont fuel additive JFA-5 which contains the MDA, N,N'-disalicylidene-1,2-propanediamine, has been found to eliminate autocatalytic oxygen loss in POSF-2827 fuel.[13]

CONCLUSIONS

The dependence of the surface deposition rate of POSF-2827 fuel on isothermal stress duration at 155 and 185°C has been found to be a function of the experimental test time. In short-term (6-hr) tests, initial deposition is governed by the autocatalytic consumption of oxygen. For long-term (~ 70-hr) tests during which the initial stainless-steel surface becomes covered with deposits, the deposition profile changes to one governed by a slower loss of oxygen.

Oxygen loss in cleaned stainless-steel tubes is enhanced at high conversion as a result of surface-induced autocatalysis. After deposits have completely covered the stainless-steel surfaces, active sites necessary for autocatalysis are removed.

ACKNOWLEDGMENTS

This work was supported by Wright Laboratory, Aero Propulsion and Power Directorate, Wright-Patterson Air Force Base, Ohio, under USAF Contract No. F33615-90-C-2033. The authors would like to thank Mr. Tim Gootee for conducting the surface-carbon analyses, Mrs. Marian Whitaker for editorial assistance, and Dr. James M. Pickard for valuable discussions.

REFERENCES

1. Hazlett, R. N. *Thermal Oxidation Stability of Aviation Turbine Fuels*, ASTM Monograph 1; American Society for Testing and Materials: Philadelphia, 1991.
2. Katta, V. R., Jones, E. G. and Roquemore, W. M. "Development of Global-Chemistry Model for Jet-Fuel Thermal Stability Based on Observations from Static and Flowing Experiments," Paper No. PEP-19, Presented at the 81st AGARD Symposium on Fuels and Combustion Technology for Advanced Aircraft Engines, May 10-14,1993, Colliferro, Italy.
3. Jones, E. G., Balster, W. J. and Anderson, S. D. *Prepr. - Am. Chem. Soc., Div. Petroleum Chem.* **1992**, *37(2)*, 393-402.
4. Jones, E. G., Balster, W. J. and Post, M. E. "Degradation of a Jet-A Fuel in a Single-Pass Heat Exchanger," ASME Paper No. 93-GT-334, Presented at the 38th International Gas Turbine and Aeroengine Congress and Exposition, May 24-27, 1993, Cincinnati, OH. To be published in *Trans. ASME*.
5. Jones, E. G. and Balster, W. J. *Energy Fuels* **1993**, *7*, 968-977.
6. Jones, E. G. and Balster, W. J. *Prepr.-Am Chem. Soc., Div. Petroleum Chem.* **1994**, *39(1)*,78-81.
7. Jones, E. G., Balster, W. J. and Pickard, J. M. "Effect of Temperature in the Formation of Jet-Fuel Insolubles," Submitted to *Energy Fuels*.
8. Kendall, D. R. and Mills, J. S. *I&EC Prod R&D* **1986,** *25*, 360-366.
9. Striebich, R. C. and Rubey, W. A. *Prepr.-Am Chem. Soc., Div. Petroleum Chem.* **1994**, *39(1)*, 47-50.
10. Morris, R. E. and Turner, N. H. *Fuel Sci. Tech. Int.* **1990**, 8, 327.
11. Clark, R. H., Delargy, K. M. and Heins, R. J. *Prepr.-Am. Chem. Soc., Div. Fuel Chem.* **1990**, *35(4)*, 1223-1232.
12. Clark, R. H. and Bishop, G. H. "Measure of Fuel Thermal Stability - Which Answer is Correct?" *Aviation Fuel: Thermal Stability Requirements. ASTM STP 1138*, P. W. Kirklin and P. David, Eds.; American Society for Testing and Materials: Philadelphia, 1992.
13. Jones, E. G., Balster, W. J. and Goss, L. P. "Application of JFA-5 as an Anti-Fouling Additive in a Jet-A Aviation Fuel," In preparation.

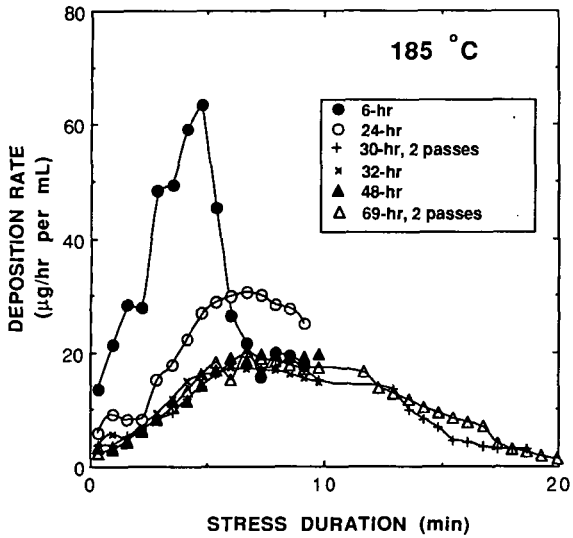

Fig 1. Deposition Rate vs. Stress Duration for POSF-2827 Fuel at 185°C for a Series of Experimental Test Times Measured with a Fuel-Flow Rate of 0.25 mL/min.

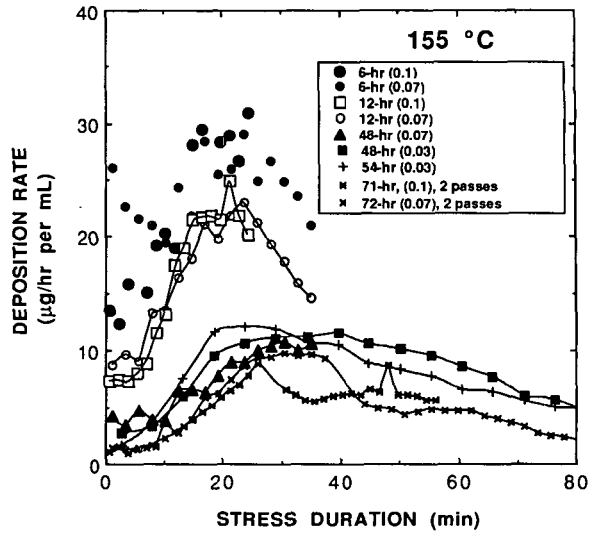

Fig 2. Deposition Rate vs. Stress Duration for POSF-2827 Fuel at 155°C for a Series of Experimental Test Times.

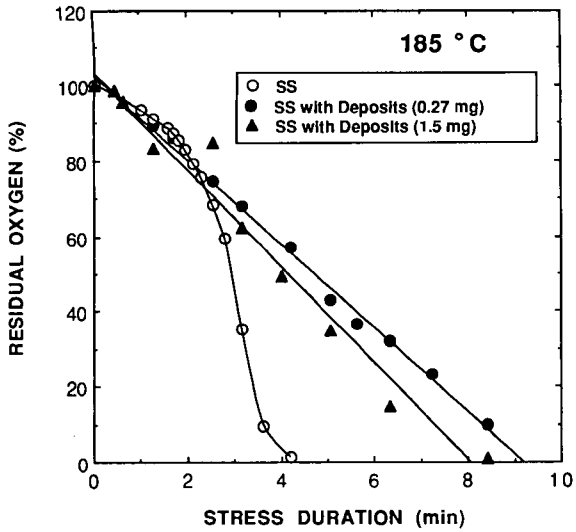

Fig 3. Residual Dissolved Oxygen vs. Stress Duration for POSF-2827 Fuel at 185°C. Measurements Made in 1) Cleaned Stainless-Steel Tubing, 2) Tubing Pre-deposited with 0.27 mg of Insolubles, and 3) Tubing Pre-deposited with 1.5 mg of Insolubles.

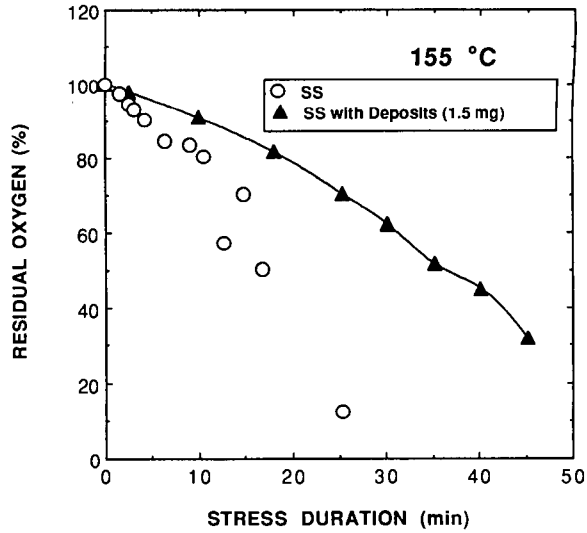

Fig 4. Residual Dissolved Oxygen vs. Stress Duration for POSF-2827 Fuel at 155°C. Measurements Made in 1) Cleaned Stainless-Steel Tubing and 2) Tubing Pre-deposited with 1.5 mg of Insolubles.

THERMAL STABILITY OF DIESEL FUELS BY QUANTITATIVE GRAVIMETRIC JFTOT

Erna J. Beal and Dennis R. Hardy
Naval Research Laboratory, Code 6180
Washington, DC 20375-5000

Keywords: Thermal stability; diesel fuel; gravimetry

INTRODUCTION

The current worldwide standard test method for assessing thermal stability of jet turbine aviation fuels is the ASTM D3241 method. This method generates a visual tube deposit rating which is not quantitative, but assumes that very dark colors equate to unstable fuels. The tube rating is coded against color standards and the darkest color is usually said to fail a fuel for use in jet turbine engines/fuel systems. The method also generates a semi-quantitataive filter pressure drop. The pressure drop is so semi-quantitative that it also is afforded a pass/fail criterion for fuel acceptance in jet aircraft.

In 1991, we described the construction of a test device which duplicated all of the experimentally important parameters of the D3241 method but which substituted a weighable 302 stainless steel (s/s) foil strip for the bulky tube, so that direct weighing of thermal surface deposits could be made.[1] In addition, the nominal 17 micron (dutch weave) s/s filter of the D3241 was substituted with a nylon membrane 0.8 micron filter which was also capable of direct weighing of the fuel entrained solids generated by the test.

In subsequent papers, the use of this device for generating a large data base of results based on aviation fuels from many different refinery processes and many different geographic/crude sources was described.[2,3] In addition this new device, dubbed the gravimetric jet fuel total oxidation tester (JFTOT) after the original ASTM D3241 device, was also used to assess quantitatively the effects of temperature, pressure, and fuel flow in addition to the effects of dissolved metals and various fuel additives.

Now that a reasonable data base for jet turbine fuels has been established regarding the deposit yields for s/s strip deposit weight and filterable deposit weight it was of interest to see how the gravimetric JFTOT would respond to mid distillate diesel type fuels. A suite of 7 fuels which were similar to number 2 diesel fuels and met all the additional criteria of NATO F-76 (US Navy) diesel fuel were selected for the test matrix. These fuels had originally been selected for a separate study involving long term ambient storage stability and thus were chosen in an attempt to span as wide a range of fuel properties as possible and still meet the specification requirements for military use.

EXPERIMENTAL

The precision flow device consists of a reciprocating single piston HPLC pump which is connected to the fuel reservoir at atmospheric pressure on the suction side and to a high pressure filter holder containing a 0.8 micron Nylon 66 pre-filter on the high pressure side. The fuel then flows through a heated section which is maintained at the chosen test temperature by the thermostated block heater. This heated section contains the pre-weighed s/s strip (weighed to the nearest 0.001 mg on a microbalance) which is held in position by the strip holder which is assembled into the s/s tube. The fuel flows through this heated section which has a surface to volume ratio of 17 cm^{-1} at 3.0 ml/min and a residence time of 6 seconds. The fuel is cooled to room temperature and exits through a back pressure valve maintained at 3.4 MPa (500 psi) into a clean glass container.

The effluent fuel is immediately vacuum filtered through a pre-weighed 0.8 micron Nylon 66 filter (weighed to the nearest 0.01 mg for the 47mm filters and to the nearest 0.001mg for the 13mm filters). At the end of the timed test, the strip assembly is removed from the block heater and allowed to cool, while maintaining fuel flow, for about 10 minutes. The foil strip is then removed, rinsed with hexane and allowed to dry, along with the rinsed fuel filter, for approximately 1 hour at 70°C. After equilibration to room temperature the strip and filter are weighed. The increases in weights are reported in mg/L. Exact details of the weighing technique and examples are given in previously published papers.[1,2,3]

RESULTS

Seven recent production diesel fuels were tested with the Gravimetric JFTOT using the standard conditions of 260°C for 2.5 hours at a fuel flow of 3.0 mL/min at a pressure of 500 psi. The results are shown in Table I.

Figure 1 gives the ranking for the filterable deposit weights with a range from 0.9 mgs/L to 23.8 mg/L. For comparison the weight of filterable solids for n-tetradecane is indicated in this figure by a solid line and the maximum and minimum filterable solids weight for jet fuels tested to date is indicated by dashed lines.

The ranking of the s/s foil strip surface deposit weights are given in Figure 2. In this figure the solid line indicates the strip surface deposit weight for n-tetradecane and the dashed lines indicate the maximum and minimum strip surface weights for jet fuels tested to date.

DISCUSSION AND CONCLUSIONS

The dashed lines in Figures 1 and 2 show the maximum and minimum values of the jet turbine fuels used to generate the data base in the last 4 years. Jet fuel average strip weights (in Figure 2) range between 0.02 and 0.20 mg/L with a number average of about 0.08 mg/L and a worldwide volume weighted average of about 0.04 mg/L. These fuels represent a very high percentage of the huge volume of jet fuels currently used worldwide and thus form a significant set of values against which to compare any and all future jet fuel batches.

The jet fuel average filterable solids weights (dashed lines in Figure 1) range between 0.5 and 5.0 mg/L with a number average of about 1.5 mg/L and a worldwide volume weighted average of about 0.8 mg/L.

Table 1 shows the data generated by the gravimetric JFTOT device for 7 representative diesel fuels from the US. The yield of the two types of solid deposit mesured are given in mg/L of fuel for both the strip weight and the filterable solids weight. It is interesting to note that even with this very small number of fuels the gravimetric JFTOT is capable of easily distinguishing between fuels as to their tendency to form solids under the conditions of this particular test. Strip weights range between 0.00 and 0.32 mg/L with an average weight of about 0.12 mg/L. Filterable deposit weights range between 1.0 and 24.0 mg/L with an average weight of about 12 mg/L.

For the large jet fuel data base it has been pointed out already that the filterable deposit weight is always about 10 to 20 times the strip deposit weight for any given fuel. This effect appears to be even more pronounced with the diesel fuels where the filterable deposit weights appear to be about 100 times heavier than the strip deposit weights for any given fuel.

In order to compare the 7 diesel fuels with the jet fuel data base for thermal stability the data in Table 1 are arranged into strip weights in Figure 2 and filter deposit weights in Figure 1. In Figure 2 it can be readily seen that most of the diesel fuels exhibit very good thermal stability with respect to the strip deposit weights for the jet fuel data base. Only fuel B exceeds the heaviest jet deposit weights. If this part of the test can be interpreted as the tendency of a fuel to form insulating lacquer deposits on aircraft heat exchangers, then clearly many diesel fuels are as "stable" as jet fuels in this regard.

The filterable data are shown in Figure 1, where a somewhat different picture can be seen. In this case, two of the fuels (D and E) are very good with respect to the jet fuel data base. On the other hand, two of the diesels are very "thermally unstable" (B and C) when compared to the jet fuel data base, and 3 of the diesels are "marginal" (A, F and G) being somewhat higher than the highest weights obtained for jet fuel in the past 4 years.

If the filterable weight data (or strip plus filter weight data) are used to assess the overall thermal stability performance in any given fuel, then only about a third of the diesel fuels could be deemed thermally stable when compared to typical thermally stable jet fuels. It should be noted that although it is tempting to use the data in this way and call the filterable deposit the material when might cause filter blockage, flow control valve sticking and nozzle fouling/clogging, no attempt has yet been made to validate this kind of correlation.

One should also note in Figures 1 and 2 the solid line which is given for the pure component n-tetradecane in the gravimetric JFTOT. This data can be used in two ways. First, it can serve as a "solvent blank" for both filterable and strip deposit weights for jet fuels. If used in this way it is apparent that most production jet fuels worldwide are very thermally stable indeed to the JFTOT test conditions. Secondly, it can serve as a solvent blank for the diesel fuels, in which case some of the current production diesel fuels are also very thermally stable.

These results indicate that the gravimetric JFTOT is a useful concept for ranking diesel fuels for their thermal stability. The diesels ranged from quite low (better than jet) to quite high (an order of magnitude greater than jet fuel) in their overall deposit forming tendencies. This type of information can be used in two possible ways. First, if gravimetric JFTOT data can be correlated to such phenomena as diesel engine injector fouling, it could be used to assess any given diesel fuels thermal stability for the intended diesel engine application.

Second, and more provocative, this type of information on diesel fuels could be used by commercial or in some cases by military aircraft operators to assess the thermal stability application for aircraft use. This would be subject to a given diesel fuel's suitability in all other aspects in addition to thermal stability. Various additional areas where diesel fuel might be limited would be the higher viscosity and higher freeze point/cloud point of diesel fuel which would then preclude its use as aircraft fuel. The obvious advantage especially to long distance aircraft would be the extended range possible with the usually higher density diesel fuel in volume limited aircraft.

REFERENCES

(1) Hardy, D. R., Beal, E. J. and Burnett, J. C., "Development of a Jet Fuel Thermal Stability Flow Device which Employs Direct Gravimetric Analysis of Both Surface and Fuel Insoluble Deposits," in Aviation Fuel Thermal Stability Requirements ASTM STP 1138, Perry W. Kirklin and Peter David, Eds., American Society for Testing and Materials, Philadelphia, PA, 1991.

(2) Beal, E. J., Hardy, D. R. and Burnett, J. C., "Results of a Jet Fuel Thermal Stability Flow Device which Employs Direct Gravimetric Analysis of Both Surface and Fuel Insoluble Deposits," in Proceedings of the 4th International Conference on Stability and Handling of Liquid Fuels, Orlando, FL, November 19-22, 1991.

(3) Beal, E. J. and Hardy, D. R., "The Effect of Temperature on Jet Fuel Thermal Stability Defined by Direct Gravimetric Analysis of both Surface and Fuel Insoluble Deposits," Preprints of the Division of Petroleum Chemistry, ACS, Volume 39, Number 1, page 82, February 1994.

Table I. Insolubles Formed From Diesel Fuels After Gravimetric Testing. All weights in mg/L of fuel. Test conditions of 260°C, 3.0 mL/min for 2.5 hours

Fuel	s/s Strip Weight	Filter Weight	Total Weight
A	0.23	13.6	13.83
B	0.32	23.8	24.12
C	0.16	21.1	21.26
D	0.01	0.9	0.91
E	0.02	1.8	1.82
F	0.00	8.2	8.20
G	0.08	14.8	14.88

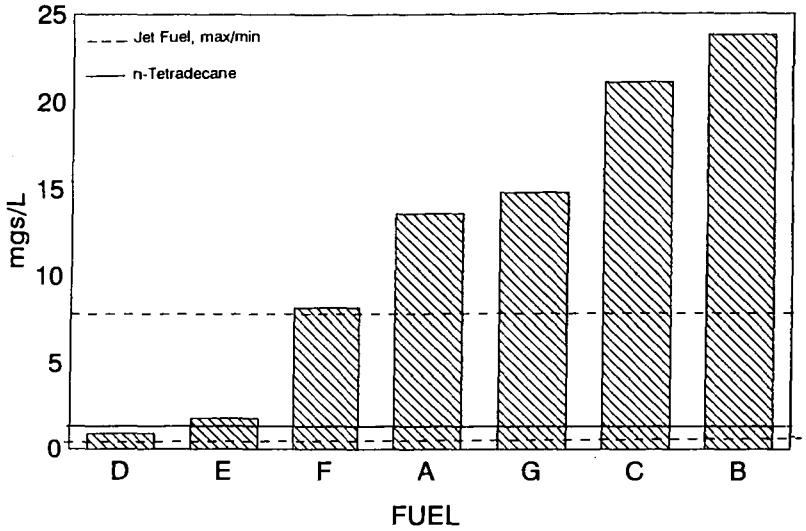

Figure 1 - Gravimetric JFTOT Filter Weights
Seven Diesel Fuels

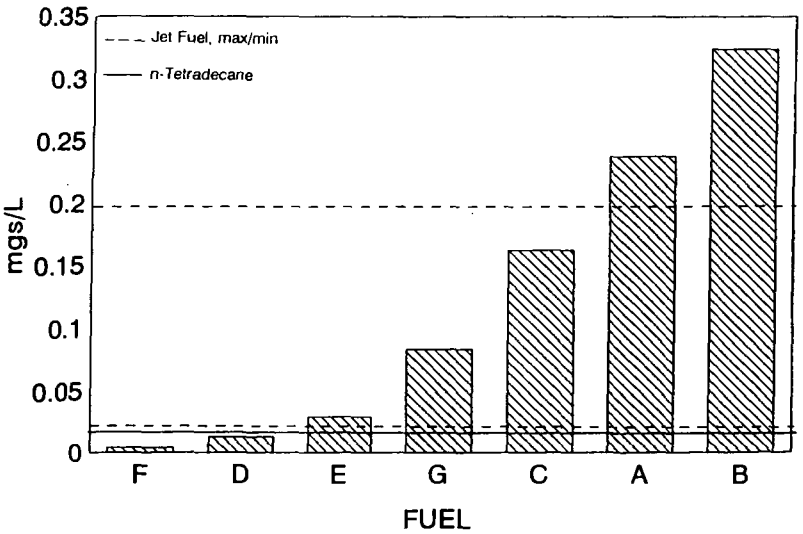

Figure 2 - Gravimetric JFTOT S/S Strip Weights
Seven Diesel Fuels